New physics in rare b-decays : theoretical constraints and phenomenological consequences

Martín Novoa-Brunet

université
PARIS-SACLAY

New physics in rare b-decays: theoretical constraints and phenomenological consequences

Nouvelle physique dans les désintégrations rares du quark b : contraintes théoriques et conséquences phénoménologiques

Thèse de doctorat de l'Université Paris-Saclay

École doctorale n° 567, Particules, Hadrons, Énergie, Noyau, Instrumentation, Imagerie, Cosmos et Simulation (PHENIICS)
Spécialité de doctorat: Physique des particules
Unité de recherche: Université Paris-Saclay, CNRS, IJCLab,91405, Orsay, France
Référent: : Faculté des sciences d'Orsay

Thèse présentée et soutenue à Paris-Saclay, le 29 Septembre 2021, par

Martín NOVOA-BRUNET

Composition du jury:

Asmâa ABADA Professeure, Université Paris-Saclay, CNRS, IJCLab, 91405 Orsay, France	Présidente
Fulvia DE FAZIO Primo Ricercatore INFN (Directrice de Recherche), Bari, Italy	Rapportrice & Examinatrice
Danny VAN DYK Junior Fellow (Chargé de Recherche), Technische Universität München, Garching, Germany	Rapporteur & Examinateur
Eli BEN-HAIM Professeur, Sorbonne Université, CNRS, LPNHE, Paris, France	Examinateur
Aoife BHARUCHA Chargée de Recherche, Aix Marseille Univ, Université de Toulon, CNRS, CPT, Marseille, France	Examinatrice
Svjetlana FAJFER Professeure, Department of Physics, University of Ljubljana, Ljubljana, Slovenia	Examinatrice

Direction de la thèse:

Sébastien DESCOTES-GENON Directeur de Recherche, Université Paris-Saclay, CNRS, IJCLab, 91405 Orsay, France	Directeur de thèse

Thèse de doctorat

NNT : 2021UPASP095

A mis queridos padres

Contents

Acknowledgements

Undertaking a project such as a PhD cannot be done alone, it requires people to guide and support you throughout its duration and I am thankful to have had many of them.

First of all, I would like to thank Sébastien Descotes-Genon, who not only gave me the opportunity to do a PhD under his wing, but did so with dedication and concern. At first I was afraid that you being the director of LPT might be a problem. However, this never felt like a problem or a burden, you were always there when I had a question or needed your guidance, and despite having little time available, you were always willing to find the time to discuss with me and pass on your knowledge and passion for physics. At the end of this journey, I am absolutely certain that it was the right choice to do my PhD with you and I am happy to have made this decision and even though it is the end of this stage, I look forward to continue working with you. Thank you Sébastien.

Secondly, I want to show my appreciation for all the people I collaborated with during these three years, who were fundamental in this process. My dear LHCb collaborators, Yasmine Ahmis, Carla Marin Benito and Marie-Hélène Schune, who were always cheerful and happy to discuss. My dear Slovenian colleagues Svjetlana Fajfer and Jernej F. Kamenik, always bringing new ideas and, brilliantly and efficiently, developing them. My dear zoom colleague K. Keri Vos, it was a pleasure working with you and even more finally meeting you in person this last month, I am pretty sure that we will keep on working together for a long time. And finally my ~~Spanish~~ Catalan colleagues, Marcel Algueró, Bernat Capdevila and Joaquim Matias, always passionate about their work. In particular, I would like to thank Quim Matias, who I felt, for a large part of my PhD, like a second advisor. I greatly appreciate the passion and enthusiasm you have always shown. I would also like to thank Marcel Algueró, who lived the process of doing a PhD with me and was my equal during these years. It has been a pleasure working with you all, and it will be a pleasure to keep on doing it.

I want to also thank the members of my PhD Jury, who took the time to read my work and evaluate me, thank you Aoife, Asmâa, Danny, Eli, Fulvia and Svjetlana. I chose all of you because you are figures I personally respect and look up to in the field. I look forward to the possibility of working with all of you in the future.

My fellow colleagues of LPT and friends, I cannot help but say that you have made the last three years wonderful. Marco, Rahul and Liam, thanks for making me enjoy so much those first months at LPT. Florian and Nicolas, my big brothers of LPT, I am so happy to have shared the two years you were at LPT with you, I only wish you would have stayed longer. Nicolas, I have not forgotten I have to visit you in Okinawa! Timmy, we started this together when doing our internship 3 years ago, and now we finish it together. I will miss you enormously and I know you also will. I wish you the best in Russia and I am pretty sure we will keep on seeing a lot of each other. Lydia, thank you for always having room for me in your office and a nice a comforting conversation, I will deeply miss not working next to you. Eli, thank you for always bringing your knowledge and your humour and always being available to help with any doubt I or anybody would have. I will never forget when we asked you to give a course on Cluster algebras and 2 days later you were practically ready to present it. I will miss that dedication of yours. I still do not understand how you were planning to put that hat on whatever you were planning to put it on, but I hope you managed! Thomas, the one who always has a smile on his face, it is hard not to be happy and cheerful when you are in the room, keep on being who you are and come and visit me in Italy. Doudoune, my love, I will miss you (and your couscous), I hope I will see you in Italy. Mika, my favorite Marseillais, thank you for all of the good times looking for mushrooms or enjoying one of your homemade beers, I will miss you. Fiorentino, thank you for those always constructive discussions and although it took sometime, for your friendship which I truly appreciate. Amaury, I have always admired the passion you show when you talk about physics, about politics or basically about anything you love, keep on showing it as you might keep on inspiring people. My dear Gio and my dear (broken) Victor, you gave me some amazing laughs and moments to remember, I hope we will see more of those.

Giulia and Christina, you deserve your own paragraph as you were both my pillars during my PhD and this I will never forget. Giulia, my dear officemate, you were my companion during this trip, the Sam to my Frodo (Timmy will be jealous that you get the LOTR reference), and I could not have asked for a better one. We went through many times I will never forget, we ate, we laughed, we cried and many others, from our trip in the northern lands to our weeks in the winter of Florence. Christina, my lifeline, without you I would have drowned

in this journey. You believed in me when I did not, you pushed me, and you dedicated your time and effort to help me get there. I am sincerely grateful to both of you.

Marie, je te remercie beaucoup pour toute ton aide, ta disponibilité et toutes les bonnes conversations pour lesquelles tu as toujours trouvé du temps. Gastien, thank you for always inspiring me and showing me which kind of researcher I want to be. Asmaa, Damir and Olcyr thank you for all of the discussions and guidance.

I would like to thank not only those who supported me during the writing of my manuscript or during the development of my thesis, but I also think it is important to thank all those who helped me to get to this point. I think this process started when I left for France, and at this moment, when I am only a few days away from leaving this country, I remember all those who supported me.

Le agradezco a Juan La Rivera, por el apoyo y la motivación para venir a Francia que siempre me brindó, lamento no haberle agradecido más cuando tuve la oportunidad. Agradezco tambien a los profesores que encontré durante mis años en Chile y me llevaron a seguir este camino, Pedro Ayala, Rafael Benguria, Luis Dissett, Claudio Fernández, Wolfgang Rivera y muchos otros. Mis mejores amigos de la infancia Water, Mati, Antar y Catiure, siempre estuvieron incondicionalmente presentes cuando los necesitaba y siempre me reciben con los brazos abiertos cuando estoy de vuelta, se los agradezco enormemente. Mencion especial a Catiure por siempre releer todo lo que escribia en ingles y volver a escribirlo entero porque claramente no se escribir. Greco y Pipin, les agradezco por tantas sopaipillas y noches de trabajo, sin las cuales nunca habria logrado entrar a Polytechnique. Ale, muchas gracias por apoyarme y acompañarme, por muy dificil que fuera, en mi partida a Francia. Mis amigos de la universidad, Javito, Miguel, Maca, Caro, Vero, Greco, Vicho, Nacho y muchos más, les agradezco por siempre hacerme reir y subirme el animo, siempre estar felices de compartir una buena cerveza o un delicioso terremoto para recordarme todo lo bueno que me perdia por estar lejos de Chile. Paula, te agradezco por ser la mejor amiga que alguien podria desear, por estar siempre ahí para apoyarme incluso cuando tu lo necesitabas más que yo. Siempre has tenido y siempre tendras un lugar especial en mi corazón.

Nachito, has sido como un hermano para mi todo este tiempo, te voy a extrañar enormemente, muchas gracias. Mag, tu m'as accompagné et soutenu inconditionnellement pendant une grande partie de mon doctorat, je t'en serai toujours reconnaissant. Domi, Romain, Ambre et Louis, merci pour m'accueillir comme une partie de votre famille quand j'en ai eu besoin. Obrigado queridos, Nahasin, Pops, Glorinha e Loula, por fazerem do ano do meu Mestre um dos melhores da minha vida e por me fazerem querer ficar para sempre em Paris. Sentirei sempre sua falta. Alvarito, Felipito y Nilito, los colocs de mi corazon, muchas gracias por tanto tiempo y tantas cosas compartidas, volvian cada uno de mis dias un poco mas felices.

Finalmente, me gustaria agradecer a mi familia, mis padres, mi hermana Carolina, mi hermano Camilo y mi Cuca, por siempre apoyarme incondicionalmente en este camino. Sin ustedes nunca habría llegado aqui, los amo mucho.

Introduction

The current situation in particle physics is quite peculiar. For many years, experimentalists have been on the lookout for what could be the next step in determining the fundamental constituents of matter and their interactions. This search for the next step has been done having certain guidelines from experiment about what to look for (in terms of energy and processes), as the observed phenomena were not well explained with the already known particles and interactions. This was the case for instance for Deep Inelastic Scattering probing the theory of strong interactions and supporting the physical existence of quarks and gluons, later on, looked for in jet events in e^+e^- collisions. Similarly, Flavour Changing Neutral Currents provided a test for the structure of electroweak interactions and an indication for vector bosons that were, later on, looked for through direct production in $p\bar{p}$ collisions. However, since the discovery of the Higgs boson in 2012, the Standard Model is now "complete", meaning that it is very well understood and well tested in all scales and sectors, making the next step unclear.

Several reasons lead us to believe that the Standard Model is not the final answer, the most obvious one being that gravity is not explained by it and it cannot be easily reconciled with it. This implies the breakdown of the Standard Model and General Relativity at least when energies close to the Planck mass are reached. However, several more subtle problems of the Standard Model and indications of New Physics exist which will suggest that we can expect to find new particles at a lower scale. For instance, some of these hints are related to astrophysical and cosmological observations, which suggest the existence of Dark Matter without which the formation and dynamics of large scale structures (galaxies, clusters) cannot be explained in a satisfying way. Additionally, new sources of CP-violation are required to explain the baryon asymmetry needed to explain cosmological data which is much larger than the one predicted by the Standard Model. Furthermore, if no new particles are present close to the electroweak scale, high levels of fine-tuning are required to explain the mass of the Higgs boson, which is often referred to as the Hierarchy problem.

Unfortunately, no new particles have yet been found by direct search at the Large Hadron Collider, which indicates that the energy of these new particles might be too high or their couplings to SM particles might be too weak to be detected by current experiments. Furthermore, these particles should in principle appear in indirect searches if these are precise enough since they would induce quantum corrections to the SM predictions of many processes. In fact, indirect searches at lower energies predicted in the past the existence of heavier particles, for instance, the charm quark was predicted by the Glashow-Iliopoulos-Maiani mechanism in kaon mixing, and the top quark mass was also constrained by $B - \bar{B}$ mixing.

The next step may be difficult to identify currently, but there are a few experimental clues worth considering. This is in particular the case of the so-called b-quark anomalies (or flavour anomalies), which are one of the few deviations from SM predictions that have been observed. These anomalies, affecting two different transitions $b \to c\ell\bar{\nu}$ and $b \to s\ell^+\ell^-$, started with the measurement of an excess in the $B \to D^*\tau\bar{\nu}$ branching fraction by BaBar in 2012 and with the measurement of deviations in the angular observables of $B \to K^*\mu^+\mu^-$ by LHCb in 2013, since then triggering an intense activity both in the theory community and in several experimental collaborations. Nowadays, these deviations arise in a series of observables measured both at the B-factories Belle and BaBar, and at the Large Hadron Collider experiments, LHCb, CMS and ATLAS showing fairly consistent deviations in b-hadron semileptonic decays.

The most robust of these deviations are found in the Lepton Flavour Universality Ratios, $R_{D^{(*)}}$ which compare the branching fraction of $B \to D^{(*)}\ell\bar{\nu}$ for τ and light leptons and $R_{K^{(*)}}$ which compare the branching fraction of $B \to K^{(*)}\ell^+\ell^-$ for muons and electrons, presenting tensions of over 3σ on both sides. Further deviations have been observed for the branching fractions and angular observables of several decay modes with different New Physics sensitivity leading to an overall picture of Lepton Flavour Violating New Physics affecting these decays.

Global analyses of the observables of both of these transitions have been performed in the model-independent framework of Effective Field Theories, showing a coherence between the different observables studied and a trend suggesting the presence of Lepton Flavour Universality Violating New physics with vector-like couplings, however leaving room for other types of couplings. In fact, some simplified models can explain these anomalies

(either separately or together), generally include new vector bosons, scalar leptoquarks, or vector leptoquarks. These simplified models however require to be embedded into a wider ultraviolet-complete model, opening the possibility for a new sector to be experimentally explored.

In this manuscript, we will discuss the current situation of the flavour anomalies and we will propose new benchmarks to test the anomalies both in $b \to c\ell\bar{\nu}$ and $b \to s\ell^+\ell^-$ and also in related modes. We will see that several New Physics scenarios are possible with current data, especially since certain directions in the space of parameters are only loosely constrained by data. We would like then to narrow down the possibilities by finding new modes and new observables that probe different directions in the parameter space enabling us to disentangle the different New Physics scenarios. Additionally, these new modes have different theoretical and experimental systematics, allowing for cross-checks of the current explanations. We can also consider other decay processes (involving other quarks and/or other leptons) which are connected with these anomalies in many specific New Physics models and which are thus worth investigating experimentally as they may exhibit further deviations.

In Part I we will introduce the main concepts and tools that are required to describe b-quark semileptonic decays. These decays are fairly complex as they involve both the Electroweak interaction and Quantum Chromodynamics which require different treatments. This complexity requires a separation of the different energy scales of the problem through the factorisation of these processes and the introduction of several Effective Field Theories which allow us to understand these decays. This effective approach additionally allows for a model-independent approach for New Physics analyses which is fundamental for the study of the flavour anomalies.

In Part II we will discuss in detail the current flavour anomalies; the different observables that can be measured, their main theoretical uncertainties, and their current experimental determinations. Furthermore, we will perform a global fit to the parameters of the Effective Field Theory obtaining a model-independent study of the possible New Physics behind these anomalies. We will then discuss specific New Physics models which could be responsible for these anomalies as they can be easily connected with the model-independent analysis.

In Part III we will present new benchmarks to study the $b \to s\ell^+\ell^-$ transition, both in the currently measured mode $B \to K\ell^+\ell^-$ through a time-dependent analysis that relies on the $B - \bar{B}$ and $K - \bar{K}$ mixing and in the new baryonic mode $\Lambda_b \to \Lambda^*\ell^+\ell^-$ through a full angular analysis of this mode. These results provide interesting observables that could constrain the complex structure of the possible NP behind the anomalies.

In Part IV we will similarly present new benchmarks to study the $b \to c\ell\bar{\nu}$ transition. In the one case, we consider the angular distribution of $B \to D^*\ell\bar{\nu}$ and we propose interesting cross-checks of experimental measurements of angular observables and different ways to probe New Physics relying on symmetries of the angular distribution. In the other case, we provide new ways of probing the inclusive Lepton Flavour Universality ratios $R(X)_{\tau\ell}$ through the direct use of $\Upsilon(4S)$ decays, which as opposed to previous methods is done through a truly inclusive method.

In Part V we will discuss the possible connections of the b-anomalies with other closely related modes under fairly general assumptions, namely the neutrino modes $b \to s\nu\bar{\nu}$ and $s \to d\nu\bar{\nu}$; and the non-leptonic mode $B_{d(s)} \to K^{*0}\bar{K}^{*0}$. In the first case we get bounds for these modes through simple principles of Minimal Flavour Violation and in the second we find a new potential anomaly in hadronic modes.

We will finally conclude this manuscript by giving an outlook of directions that these anomalies might take in the future, new results that might help to disentangle them, and studies helping to make this picture even more robust.

Part I

Theoretical framework

Chapter 1

The Standard Model

The Standard Model (SM) of particle physics [1–4] is the theory used to describe and classify all known elementary particles and three of the four the interactions in between them, the electromagnetic, weak and strong interactions. In the SM, the first of these interactions, which can be described by the theory of quantum electrodynamics (QED), unifies with the weak interaction and together they can be described by the electroweak (EW) theory. The remaining interaction can be described through the theory of Quantum Chromodynamics (QCD). These theories are constructed under the paradigm of a Quantum Field Theory (QFT), which allows the combination of quantum mechanics and special relativity, where particles appear as excitations of the quantum fields.

1.1 The Standard Model and its gauge structure

The elementary particles that compose the SM are shown in Fig. 1.1 together with their quantum numbers. These particles can be divided according to their spin into bosons (integer spin) and fermions (half integer spin). Spin 1 bosons are the carriers of the three different forces[1], gluons (g) carry the strong force, photons (γ) carry the electromagnetic force, the weak force is carried by the $W^{\pm}$ and Z bosons, while the spin 0 Higgs boson (H) is the excitation of the Higgs doublet field, whose non vanishing vacuum expectation value is responsible for the electroweak symmetry breaking. On the fermionic side we have quarks, which interact through all three forces, and leptons, which are blind to the strong force (and also to the electromagnetic force in the case of neutrinos). The fermions of the SM are organised in a 3-fold family structure, with a mass hierarchy between the families as shown in Fig. 1.1. Each of these families or generations contains two flavours for each fermion, for instance, the first generation is composed of the u and d quarks.

It is worth mentioning at this stage that, due to the confinement occurring in QCD (described in Section 1.4), quarks are not be observed freely. Hadrons, which are composed of quarks and gluons, are the actual physical states that we observe.

The SM is constructed upon symmetries under the gauge group

$$G_{\mathrm{SM}}^{\mathrm{gauge}} = \mathrm{SU}(3)_C \times \mathrm{SU}(2)_L \times \mathrm{U}(1)_Y \tag{1.1}$$

where each gauge group corresponds to a different gauge symmetry, or invariance under local transformations. Each of these symmetries is related to a different gauge interaction. The strong interaction for $\mathrm{SU}(3)_C$, the weak interaction for $\mathrm{SU}(2)_L$ and "hypercharge" interaction for $\mathrm{U}(1)_Y$ [2].

The SM Lagrangian can be divided in 4 parts

$$\mathcal{L}_{\mathrm{SM}} = \mathcal{L}_{\mathrm{gauge}} + \mathcal{L}_{\mathrm{fermion}} + \mathcal{L}_{\mathrm{Higgs}} + \mathcal{L}_{\mathrm{Yukawa}} \,, \tag{1.2}$$

The first term corresponds to the kinematic term for the gauge fields

$$\mathcal{L}_{\mathrm{gauge}} = -\frac{1}{4}\sum_{A} F^a_{\mu\nu} F^{a\,\mu\nu} \,, \qquad F^a_{\mu\nu} = \partial_\mu A^a_\nu - \partial_\nu A^a_\mu + g f^{abc} A^b_\mu A^c_\nu \,, \tag{1.3}$$

where the sum is over the SM gauge fields; the gluon fields $\mathcal{A}^a_\mu$ $(a = 1, ..., 8)$, related to $\mathrm{SU}(3)_C$ gauge symmetry, and the electroweak gauge bosons $\vec{W}_\mu$ (3 components) and B_μ before the symmetry breaking, which are

[1] The fourth interaction missing in the SM is the gravitational force, the carrier of which would be the graviton. While a theory of quantum gravity is yet not established, if we assume it can be treated as a QFT at low energies in the context of an effective field theory, it shows no actual impact at the energies considered here.

[2] The weak and hypercharge interactions are usually grouped and called the electroweak interaction.

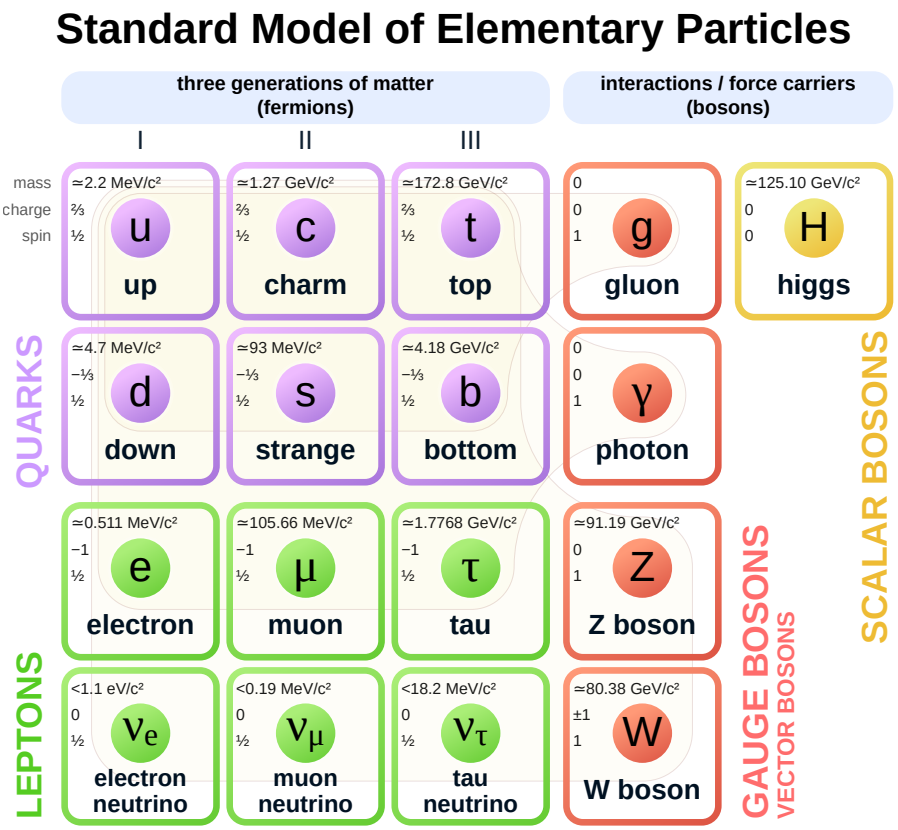

Figure 1.1: Schematic of the Standard Model after the electro-weak symmetry breaking. In the columns from left to right, 1^{st},2^{nd} and 3^{rd} generation of fermions, gauge bosons and lastly the Higgs Boson. On the top left of each box it can be seen the mass the electric charge and the spin of each particle. It is interesting to notice the mass hierarchy of the fermions, with masses ranging from less than 1.1 eV for the neutrinos, to the top mass of around 172.8 GeV, more than 10^11 times larger. Adapted from Ref. [5], with updated values for the masses [6].

respectively related to the $\mathrm{SU}(2)_L$ and $\mathrm{U}(1)_Y$ gauge symmetries. For each of the gauge fields A^a_ν, $F^a_{\mu\nu}$ is the field strength tensor, g is the coupling constant for the interaction in question (g_s, g and g' for $\mathcal{A}^a_\mu$, $\vec{W}_\mu$ and B_μ respectively) and f^{abc} are the structure constants of the gauge group in question (0 in the case of $U(1)_Y$).

The second term in Eq. (1.2) corresponds to the kinematic term for the fermion fields, and their coupling to the gauge bosons which is obtained through the minimal coupling prescription (i.e. $\partial \to D$)

$$\mathcal{L}_{\text{fermion}} = \sum_{\psi,I} \bar{\psi}^I (i\not{D}) \psi^I \,, \tag{1.4}$$

where $I = 1, 2, 3$ is the the flavour index and $\psi = L_L$, Q_L, ℓ_R, u_R, d_R are the left-handed and right-handed fermion fields[3]. They transform under $\mathrm{SU}(2)_L$ respectively as doublets and singlets

$$L_L = \begin{pmatrix} \nu_L \\ \ell_L \end{pmatrix}, \qquad Q_L = \begin{pmatrix} u_L \\ d_L \end{pmatrix}, \qquad \ell_R, \qquad u_R, \qquad d_R \,, \tag{1.5}$$

where we omit the flavour index I. The covariant derivative depends on the quantum numbers of the field ψ in question and it takes the following form

$$D^\mu = \partial^\mu - i g_s T^a_\psi \mathcal{A}^{a\,\mu} - i g \vec{\tau}_\psi \cdot \vec{W}^\mu - i g' \frac{Y_\psi}{2} B^\mu \,, \tag{1.6}$$

where $(T^a_\psi, \vec{\tau}_\psi, Y_\psi)$ are the $G^{\text{gauge}}_{\text{SM}}$ generators for the field ψ, presented in Table 1.1 related to its quantum numbers. The third term in Eq. (1.2) corresponds to the kinematic term for the Higgs doublet Φ and the Higgs

Matter	$G^{\text{gauge}}_{\text{SM}}$		T^a_ψ	$\vec{\tau}_\psi$	Y_ψ	$G_{\mathcal{F}}$	$\mathcal{B}$	$\mathcal{L}$
Q_L	$(\mathbf{3},\mathbf{2})_{+1/3}$	:	$+\lambda^a/2$	$\vec{\sigma}/2$	$+1/3$	$(\mathbf{3},\mathbf{1},\mathbf{1},\mathbf{1},\mathbf{1})$	$1/3$	0
$u^\dagger_R$	$(\mathbf{3},\mathbf{1})_{-4/3}$	:	$-\lambda^a/2$	0	$-4/3$	$(\mathbf{1},\mathbf{3},\mathbf{1},\mathbf{1},\mathbf{1})$	$-1/3$	0
$d^\dagger_R$	$(\mathbf{3},\mathbf{1})_{+2/3}$	:	$-\lambda^a/2$	0	$+2/3$	$(\mathbf{1},\mathbf{1},\mathbf{3},\mathbf{1},\mathbf{1})$	$-1/3$	0
L_L	$(\mathbf{1},\mathbf{2})_{-1}$	:	0	$\vec{\sigma}/2$	-1	$(\mathbf{1},\mathbf{1},\mathbf{1},\mathbf{3},\mathbf{1})$	0	1
$\ell^\dagger_R$	$(\mathbf{1},\mathbf{1})_{+2}$	:	0	0	$+2$	$(\mathbf{1},\mathbf{1},\mathbf{1},\mathbf{1},\mathbf{3})$	0	-1
Φ	$(\mathbf{1},\mathbf{2})_{+1}$	:	0	$\vec{\sigma}/2$	$+1$	$(\mathbf{1},\mathbf{1},\mathbf{1},\mathbf{1},\mathbf{1})$	0	0

Table 1.1: Quantum numbers and $G^{\text{gauge}}_{\text{SM}}$ generators of the fermion fields of the SM and the Higgs doublet Φ. From left to right, the fermion field, the representation of the field under the SM gauge group $G^{\text{gauge}}_{\text{SM}}$, the $\mathrm{SU}(3)_C$ generator T^a_ψ, the $\mathrm{SU}(2)_L$ generator $\vec{\tau}_\psi$, the weak hypercharge Y_ψ, the representation of the field under the flavour symmetry group $G_{\mathcal{F}}$, the baryon number $\mathcal{B}$ and lastly the lepton number $\mathcal{L}$. λ^a are the Gell-Mann matrices and $\vec{\sigma}$ the Pauli matrices. The electric charge is defined as $Q = \tau_3 + Y/2$ where τ_3 is the weak isospin ($+1/2$ for upper component of the $\mathrm{SU}(2)_L$ doublet, $-1/2$ for the lower component and 0 for the singlets). Modified version of Table 1.1 in Ref. [7]

potential $V(\Phi)$ (which we will discuss in Section 1.2)

$$\mathcal{L}_{\text{Higgs}} = (D_\mu \Phi)^\dagger (D^\mu \Phi) - V(\Phi) \,. \tag{1.7}$$

One can notice that the covariant derivatives are actually independent of the family of the fermions. In other words, the gauge, fermion and Higgs sectors of the Lagrangian are invariant under independent global unitary transformations among different families of each of the 5 fermion fields

$$G_{\mathcal{F}} \equiv \mathrm{U}(3)^5 = \mathrm{U}(3)_{Q_L} \times \mathrm{U}(3)_{u_R} \times \mathrm{U}(3)_{d_R} \times \mathrm{U}(3)_{L_L} \times \mathrm{U}(3)_{\ell_R} \,, \tag{1.8}$$

where there is one U(3) group symmetry for each fermion field which transform as $\mathbf{3}$ under their respective $U(3)$ as shown in Table 1.1. This symmetry is not fully realized in the SM as it is broken explicitly (and exclusively) by the couplings of the fermion fields to the Higgs doublet Φ (i.e. the Yukawa couplings), present in the last term of Eq. (1.2)

$$\mathcal{L}_{\text{Yukawa}} = -Y_u^{IJ} \bar{Q}^I_L i\sigma_2 \Phi^* u^J_R - Y_d^{IJ} \bar{Q}^I_L \Phi d^J_R - Y_e^{IJ} \bar{L}^I_L \Phi e^J_R + h.c. \,, \tag{1.9}$$

where Y_f^{IJ} are 3×3 matrices, called the Yukawa matrices. This breaking of $G_{\mathcal{F}}$ gives rise to a SM flavour structure, which is characterized by the different fermion masses and the quark mixing which we will discuss in Section 1.2.2.

[3] In this manuscript, we consider no right-handed neutrinos ν_R and neutrino masses are neglected.

Two important symmetries of the SM worth mentioning, which are not imposed but appear as a consequence of gauge symmetry and the choice of charges of the fermion fields, are baryon number ($\mathcal{B}$) and lepton number ($\mathcal{L}_\ell$) conservation. Indeed, thanks to gauge invariance, the SM respects an accidental global symmetry under

$$G_{\rm SM}^{\rm global} = \mathrm{U}(1)_{\mathcal{B}} \times \mathrm{U}(1)_{\mathcal{L}_e} \times \mathrm{U}(1)_{\mathcal{L}_\mu} \times \mathrm{U}(1)_{\mathcal{L}_\tau} \tag{1.10}$$

where $\mathrm{U}(1)_{\mathcal{B}}$ is the baryon number symmetry and $\mathrm{U}(1)_{\mathcal{L}_{e,\mu,\tau}}$ are the lepton number symmetries associated with each lepton flavour. The baryon and lepton numbers of an outgoing or incoming state are defined as

$$\mathcal{B} = \frac{1}{3}(n_q - n_{\bar{q}})\,, \qquad \mathcal{L}_\ell = (n_\ell - n_{\bar{\ell}})\,, \tag{1.11}$$

where n_q and $n_{\bar{q}}$ correspond to the number of quarks and antiquarks in the state respectively, and n_ℓ and $n_{\bar{\ell}}$ corresponds to the number of leptons and anti-leptons of flavour ℓ in the state. The total lepton number $\mathcal{L} = \mathcal{L}_e + \mathcal{L}_\mu + \mathcal{L}_\tau$ is then also a symmetry of the SM. All of these numbers are conserved in the SM with massless neutrinos, but flavour specific lepton number conservation is violated when neutrino masses and mixing are introduced in the SM. For practical purposes of the discussion we will neglect this, since lepton flavour violation through neutrino mixing is not strong enough to affect the modes that are studied and discussed in this manuscript (at least with the current experimental sensitivity).

1.2 Electroweak Symmetry Breaking

1.2.1 The Higgs Mechanism

The gauge symmetry group of the Standard Model $G_{\rm SM}^{\rm gauge}$, or more precisely the $\mathrm{SU}(2)_L \times \mathrm{U}(1)_Y$ symmetry, does not allow for mass terms for the fermions and weak gauge bosons in the Lagrangian. In other words, in a theory in which this symmetry is fully realized all matter is massless. This is of course, incompatible with experience, reason why this $\mathrm{SU}(2)_L$ group needs to be somewhat broken. This is solved by having a spontaneously broken symmetry through the addition of a self-interacting complex scalar $\mathrm{SU}(2)_L$ doublet, the Higgs doublet (Φ). This spontaneous symmetry breaking is done through the presence of the Higgs potential given by

$$V(\Phi) = m^2\Phi^\dagger\Phi + \lambda(\Phi^\dagger\Phi)^2\,, \qquad \Phi \equiv \frac{1}{\sqrt{2}}\begin{pmatrix}\sqrt{2}\phi^+ \\ \phi^0 + ia^0\end{pmatrix}\,, \tag{1.12}$$

where ϕ^+ is the complex charged component of the Higgs doublet and ϕ^0 and a^0 are respectively the CP -even and CP -odd neutral components. When the mass term takes negative values (i.e. $m^2 < 0$), the vacuum expectation value (vev) of the Higgs doublet will be different from 0, and can always be brought, through $\mathrm{SU}(2)_L$ rotations, to the following form

$$\langle\Phi\rangle = \frac{1}{\sqrt{2}}\begin{pmatrix}0 \\ v\end{pmatrix} \tag{1.13}$$

where $v = \frac{|m|}{\sqrt{\lambda}} = 246.22\,\mathrm{GeV}$ [6]. This will induce the spontaneous symmetry breaking of the SM gauge group $G_{\rm SM}^{\rm gauge}$ defined in Eq. (1.1) into $\mathrm{SU}(3)_C \times \mathrm{U}(1)_{\rm em}$. Although the Lagrangian of the SM is invariant under $G_{\rm SM}^{\rm gauge}$ the ground state is not. One can parametrise the Φ field, in a fully general way, as [8]

$$\Phi = e^{i\vec{\pi}(x)\cdot\vec{\tau}}\frac{1}{\sqrt{2}}\begin{pmatrix}0 \\ v + H(x)\end{pmatrix} \tag{1.14}$$

with four real fields $H(x)$, $\vec{\pi}(x)$ each corresponding to one of the four degrees of freedom of the Higgs Doublet. The first one, the field $H(x)$ is a gauge-invariant fluctuation of the vacuum state and corresponds to the physical Higgs field.

The three remaining degrees of freedom are not gauge invariant, and thanks to the local $\mathrm{SU}(2)_L$ gauge invariance of the Lagrangian, by choosing the unitarity gauge [9], one can "rotate away" the $\vec{\pi}(x)$ fields.

For a global symmetry, the spontaneous symmetry breaking would give rise to massless states (Goldstone theorem), but in the case of a local (gauge) symmetry this gives masses to gauge bosons through the Higgs mechanism [10–15]. From the four generators of the $\mathrm{SU}(2)_L \times \mathrm{U}(1)_Y$ gauge symmetry, three are spontaneously broken, which will grant a mass to three (Z, $W^\pm$) of the four physical EW gauge bosons; three degrees of freedom of the Higgs doublet ($\vec{\pi}(x)$) will now correspond to the longitudinal polarisation of the massive gauge fields. The remaining $\mathrm{U}(1)_{\rm em}$ symmetry is associated to the fourth unbroken generator and the corresponding gauge field, the photon (γ), which will thus remain massless. The masses of the Higgs and the gauge bosons, at

tree level, are given in the following

$$m_H = \sqrt{2\lambda} v \,, \tag{1.15}$$

$$m_W = \frac{gv}{2} = \frac{ev}{2\sin\theta_W} \,, \tag{1.16}$$

$$m_Z = \sqrt{g^2 + g'^2}\frac{v}{2} = \frac{ev}{2\cos\theta_W \sin\theta_W} \,, \tag{1.17}$$

$$m_\gamma = 0 \,, \tag{1.18}$$

where $e = g\sin\theta_W$ is the positron electric charge and $\theta_W = \tan^{-1}(g'/g)$ is the weak mixing angle.

The interaction Lagrangian between the fermions and the gauge fields after the symmetry breaking takes the following form

$$\begin{aligned}\mathcal{L}_{\text{int}} = &-\frac{g}{2\sqrt{2}} \sum_{\Psi = Q_L, L_L} \bar{\Psi}\gamma^\mu(1-\gamma^5)(\tau^+ W_\mu^+ + \tau^- W_\mu^-)\Psi \\ &- \sum_\psi e Q_\psi \bar{\psi}\gamma^\mu \psi A_\mu + \frac{g}{2\cos\theta_W}\bar{\psi}\gamma^\mu(g_V^\psi - g_A^\psi\gamma^5)\psi Z_\mu \,,\end{aligned} \tag{1.19}$$

where $\psi = L_L$, Q_L, ℓ_R, u_R, d_R and $\tau^\pm = \tau_1 \pm i\tau_2$ is the isospin raising (lowering) operator. Furthermore the axial and vector Z couplings are

$$g_V^\psi = \tau_{3\,\psi} - 2Q_\psi \sin^2\theta_W \,, \tag{1.20}$$

$$g_A^\psi = \tau_{3\,\psi} \,, \tag{1.21}$$

where $\tau_{3\,\psi}$ and Q_ψ the weak isospin and the electrical charge of the fermion ψ as given in Table 1.1

The electroweak symmetry breaking will also generate a mass term and an interaction with the Higgs field H for fermions through the Yukawa interactions, with the Lagrangian taking the following form

$$\mathcal{L}_{\text{SM}} \supset -\frac{v}{\sqrt{2}}\left(\bar{u}_R^I Y_u^{IJ} u_L^J + \bar{d}_R^I Y_d^{IJ} d_L^J + \bar{e}_R^I Y_e^{IJ} e_L^J\right)\left(1 + \frac{H}{v}\right) + h.c. \,, \tag{1.22}$$

where the Yukawa couplings are a priori, non diagonal matrices. It is important to mention that the electroweak symmetry breaking does not provide an explanation of the underlying reason for the, rather unnatural, large variety of fermion masses of the standard model, or an explanation of the mixing between them. It merely transfers the large number of free parameters that are the fermion masses and mixing parameters into the Yukawa couplings.

However it does provide us with interesting predictions that can be tested. First of all, the existence of the Higgs boson, whose mass was first indirectly constrained by global electroweak fits at the Large Electron Positron Collider (LEP) at CERN, and it was latter discovered at the CMS and ATLAS experiments at the Large Hadron Collider (LHC) at CERN . Secondly, the properties of the Higgs field and its interaction with other SM particles. Particularly interesting are the tests of the Higgs couplings to fermions and EW bosons, which are expected to be directly proportional to the particles masses. This prediction as been tested at CMS and ATLAS as shown in Fig. 1.3. Lastly, the consistency of the Electroweak global fits as shown in Fig. 1.4, which show that the SM provides an excellent overall description of the physics at least around the EW scale.

Moreover, New Physics (NP) searches at the LHC have not yet found additional heavy degrees of freedom through direct searches at the CMS and ATLAS experiments. The bounds for the masses of new hypothetical particles, depending on their couplings, starts to approach the TeV scale as shown in Fig. 1.2.

This lack of discovery of new particles through direct searches has lead us to look for NP through indirect searches in processes which could be mediated by NP particles. One of these processes, in which we will focus because of their sensitivity to new physics, are the flavour changing currents which we will discuss in Section 1.3. With that end in mind, we will now discuss the flavour structure of the SM after the electroweak breaking in more detail.

1.2.2 Cabibbo-Kobayashi-Maskawa Matrix

As mentioned before, fermionic matter is organized in a 3-fold family structure both for the lepton side and the quark side. This family structure will come together with an EW structure for all fermions and a color structure for quarks. Fermions will organize in $\text{SU}(2)_L$ doublets and singlets. The left-handed fermion fields of each family transform as doublets while the right-handed ones as singlets

$$L_L = \begin{pmatrix}\nu_L \\ \ell_L^-\end{pmatrix}, \qquad Q_L^{\text{EW}} = \begin{pmatrix}u_L^{\text{EW}} \\ d_L^{\text{EW}}\end{pmatrix}, \qquad \ell_R^-, \qquad u_R^{\text{EW}}, \qquad d_R^{\text{EW}}, \tag{1.23}$$

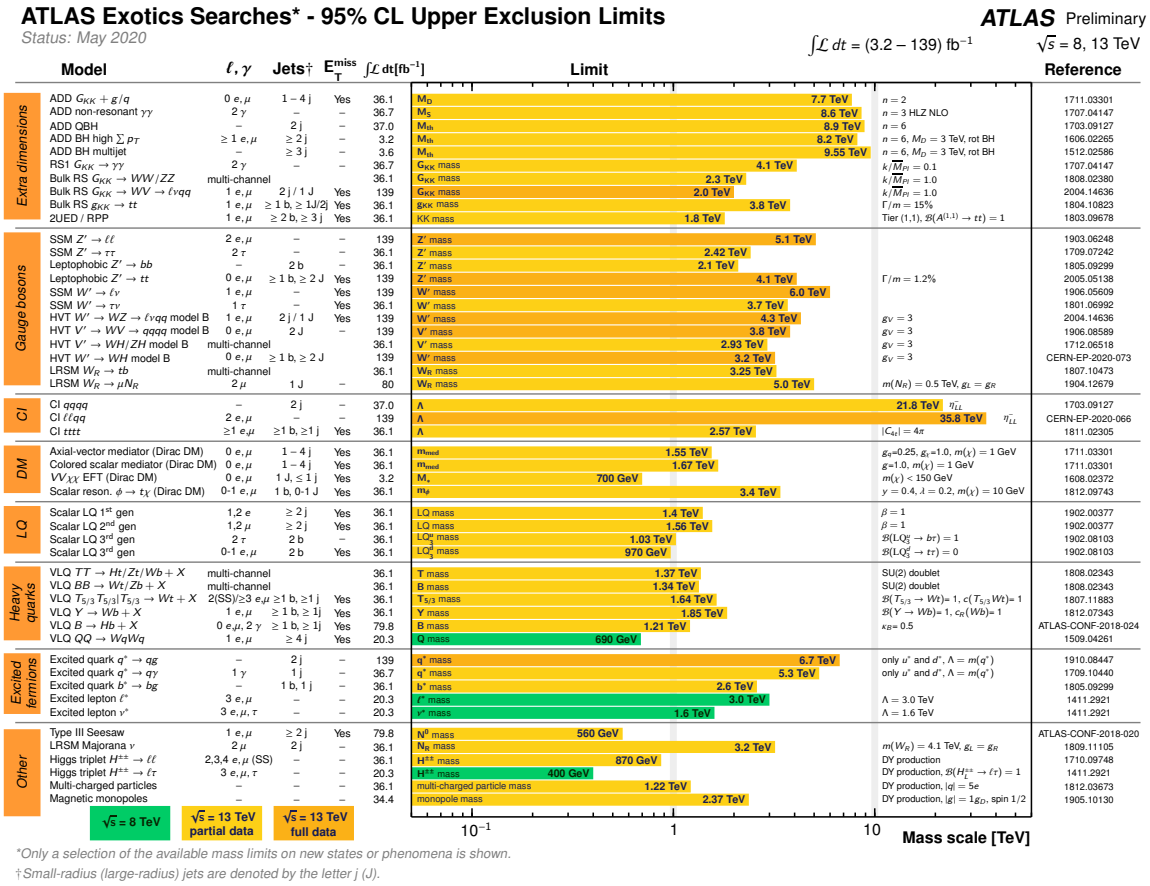

Figure 1.2: Summary plot for NP searches at the ATLAS detector [16] at the LHC. The current bound for most NP particles is around or higher than 1 TeV. Similar results are obtained from the CMS detector[17].

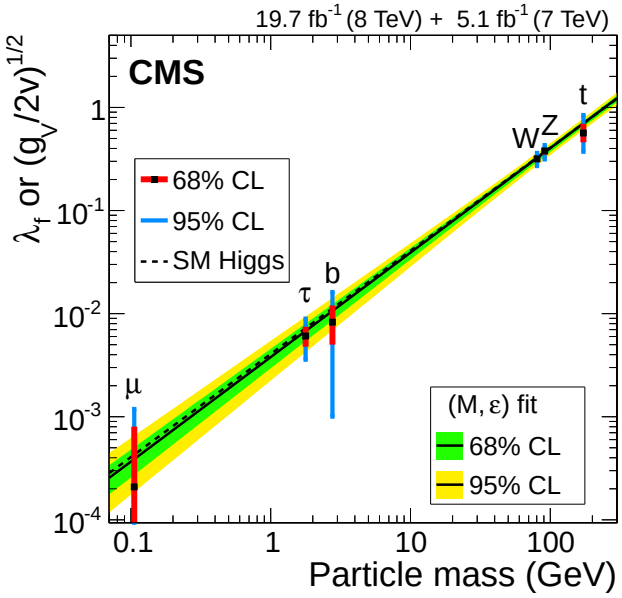

Figure 1.3: Fits to the Higgs-X couplings as a function of the X particle mass performed by the CMS Collaboration [18]. In the case of the fermions the Yukawa couplings Y_f are shown and in the case for the gauge bosons the square root of the coupling normalized by twice the vev of the Higgs $\sqrt{\frac{g_V}{2v}}$ is shown.

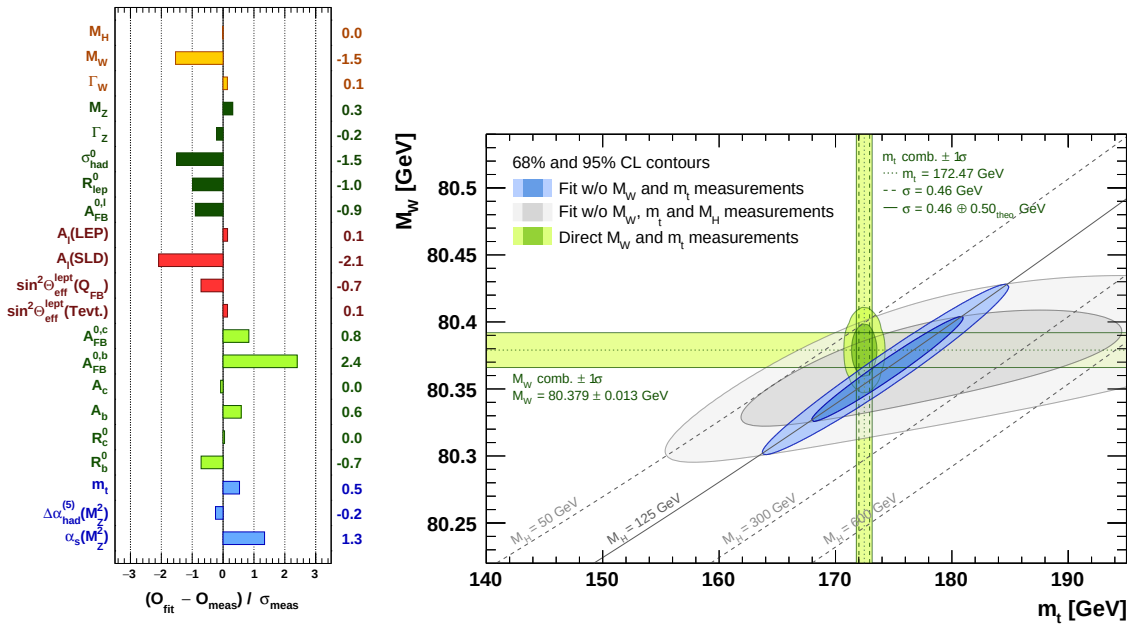

Figure 1.4: On the left, pulls for all of the observables of the Electroweak Global Fits. On the right, consistency of the direct measurement of m_W, t and the results of the Electroweak Global Fits for them. Taken from Ref. [19].

where we add the EW subscript to emphasize that they are written in the EW basis. Then, after the EW breaking the Lagrangian for the quark sector takes the following form[4]

$$\mathcal{L}_{\rm SM} \supset -\frac{v}{\sqrt{2}}(\overline{d}^{\rm EW}_{Li} Y^d_{ij} d^{\rm EW}_{Rj} + \overline{u}^{\rm EW}_{Li} Y^u_{ij} u^{\rm EW}_{Rj}) - \frac{g}{\sqrt{2}} \overline{u}^{\rm EW}_{Li} \gamma^\mu W^-_\mu d^{\rm EW}_{Li} + \text{h.c.} \tag{1.24}$$

where Y^f with $f = u, d$ are the Yukawa matrices. These matrices are both at the origin of the quarks masses and mixing. Then the fermion mass eigenstates can be obtained through the diagonalisation of the Yukawa matrices through a singular value decomposition by four unitary matrices $V^f_{L(R)}$

$$M_f = \frac{v}{2} V^f_L Y_f V^{f\dagger}_R \,, \qquad f = u, d, e \,, \tag{1.25}$$

where M^f are diagonal matrices in flavour space and we also include the lepton ones.

We can then perform a change of basis to define $d_{L(R)i}$ and $u_{L(R)i}$, the mass eigenstates

$$\overline{d}_{Li} \equiv (V^{d\dagger}_L)_{ij} \overline{d}^{\rm EW}_{Lj} \,, \qquad d_{Ri} \equiv (V^d_R)_{ij} d^{\rm EW}_{Rj} \,, \tag{1.26}$$

$$\overline{u}_{Li} \equiv (V^{u\dagger}_L)_{ij} \overline{u}^{\rm EW}_{Lj} \,, \qquad u_{Ri} \equiv (V^u_R)_{ij} u^{\rm EW}_{Rj} \,. \tag{1.27}$$

The quark sector of the SM Lagrangian in the mass basis takes the following form

$$\mathcal{L}_{\rm SM} \supset -\overline{d}_{Li} M^d_{ij} d_{Rj} + \overline{d}_{Li} M^u_{ij} u_{Rj} - \frac{g}{\sqrt{2}} \overline{u}_{Li} \gamma^\mu W^-_\mu \underbrace{(V^u_L V^{d\dagger}_L)_{ij}}_{V_{\rm CKM}} d_{Lj} + \text{h.c.} \tag{1.28}$$

where we identify $V_{\rm CKM}$, the Cabibbo-Kobayashi-Maskawa (CKM) Matrix. Since there is an ambiguity in the definition of the original $\mathrm{SU}(2)_L$ doublets due to flavour symmetry, one could have performed a rotation of the doublet beforehand and define the left handed mass eigenstates as Q_L

$$d_{Li} \equiv d^{\rm EW}_{Lj}, u_{Li} \equiv (V^\dagger_{\rm CKM})_{ij} u^{\rm EW}_{Lj} \tag{1.29}$$

This is the most common way of defining the mass eigenstates since it only involves the CKM matrix and not the unitary matrices V^f_L and we will use it from now on.

The interactions vertices in Eq. (1.28) are represented in Fig. 1.5 and they have important consequences. Since the rotations for u-type and d-type quarks are different, a mixing is induced between the different families.

[4] We focus here only on the mass term and the weak charged current since they are the relevant elements to understand the flavour mixing.

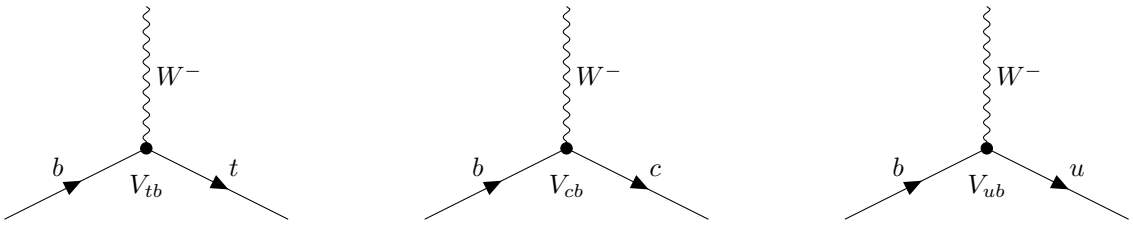

Figure 1.5: Interaction vertices of the W boson after the EW breaking showing the family mixing. Each vertex is accompanied of a CKM factor.

This mixing is mediated by the W bosons through charged currents, which after this rotation, not only change the flavour of the quarks, but they connect quarks from the different families.

In the case of the Z boson and the photon, since their interactions only include one type of quark (either u-type or d-type), they are independent of the choice of basis. For instance, if we explicitly perform the change of basis to the Q_L photon coupling in Eq. (1.19)

$$\begin{aligned} Q_{Q_L}\overline{Q}_L\gamma^\mu Q_L A_\mu = &+ 2/3\overline{u}_L^{\rm EW}\gamma^\mu u_L^{\rm EW}A_\mu - 1/3\overline{d}_L^{\rm EW}\gamma^\mu d_L^{\rm EW}A_\mu \\ &+ 2/3\overline{u}_L\gamma^\mu \underbrace{V_{\rm CKM}V_{\rm CKM}^\dagger}_{\rm I_{3\times 3}} u_L A_\mu - 1/3\overline{d}_L\gamma^\mu d_L A_\mu\,. \end{aligned} \tag{1.30}$$

Because of this, in the SM there are no tree-level flavour changing neutral currents.

The CKM matrix encodes all the information related to the mixing of the different quark families in the SM [5]. We will usually write as follows

$$V_{\rm CKM} \equiv V_L^u V_L^{d\dagger} = \begin{pmatrix} V_{ud} & V_{us} & V_{ub} \\ V_{cd} & V_{cs} & V_{cb} \\ V_{td} & V_{ts} & V_{tb} \end{pmatrix}. \tag{1.31}$$

Since $V_{\rm CKM}$ is the product of unitary matrices it is itself unitary

$$V_{\rm CKM}V_{\rm CKM}^\dagger = {\rm I}_{3\times 3}\,, \tag{1.32}$$

and it can be parametrised by only three mixing angles and a CP-violating phase [20], through the redefinition of the global phases of the quark fields.

Several different parametrisations exist in the literature for the CKM matrix, we will use two of them.

Standard Parametrisation

This parametrisation [21] is obtained by the product of three (complex) rotation matrices, characterized by the mixing angles between each generation θ_{12}, θ_{13} and θ_{23}, and one overall CP-Violating phase δ.

$$\begin{aligned} V_{\rm CKM} &= \begin{pmatrix} 1 & 0 & 0 \\ 0 & c_{23} & s_{23} \\ 0 & -s_{23} & c_{23} \end{pmatrix} \begin{pmatrix} c_{13} & 0 & s_{13}e^{-i\delta} \\ 0 & 1 & 0 \\ -s_{13}e^{i\delta} & 0 & c_{13} \end{pmatrix} \begin{pmatrix} c_{12} & s_{12} & 0 \\ -s_{12} & c_{12} & 0 \\ 0 & 0 & 1 \end{pmatrix} \\ &= \begin{pmatrix} c_{12}c_{13} & s_{12}c_{13} & s_{13}e^{-i\delta} \\ -s_{12}c_{23} - c_{12}s_{23}s_{13}e^{i\delta} & c_{12}c_{23} - s_{12}s_{23}s_{13}e^{i\delta} & s_{23}c_{13} \\ s_{12}s_{23} - c_{12}c_{23}s_{13}e^{i\delta} & -c_{12}s_{23} - s_{12}c_{23}s_{13}e^{i\delta} & c_{23}c_{13} \end{pmatrix} \end{aligned} \tag{1.33}$$

where $c_{ij} = \cos\theta_{ij}$, $s_{ij} = \sin\theta_{ij}$ for $i < j = 1, 2, 3$. This parametrisation strictly satisfies the unitarity relation in Eq. (1.32).

[5] In the case of the leptons, due to the absence of right handed neutrinos in the SM, the diagonalization of Y_e is not an issue. However, in the case of massive ν, a similar matrix to the CKM exists for the case of lepton (neutrino) mixing called Pontecorvo-Maki-Nakagawa-Sakata (PMNS) Matrix, although the nature of this matrix is not strictly defined as it depends on the nature of neutrino masses (i.e. whether neutrinos are Dirac or Majorana particles). In this manuscript we will always work on the approximation where we neglect the effects coming from neutrino masses and thus mixing.

Wolfenstein Parametrisation

The Wolfenstein parametrisation [22] is an alternative parametrisation for V_{CKM} which exploits the empirical hierarchy[6] of the CKM elements $s_{13} \ll s_{23} \ll s_{12} \ll 1$. This parametrisation was originally introduced as a Taylor expansion in $\lambda = V_{us} \sim 0.225$ to order $\mathcal{O}(\lambda^4)$ [22] taking the following form

$$V_{\text{CKM}} = \begin{pmatrix} 1-\lambda^2/2 & \lambda & A\lambda^3(\rho - i\eta) \\ -\lambda & 1-\lambda^2/2 & A\lambda^2 \\ A\lambda^3(1-\rho-i\eta) & -A\lambda^2 & 1 \end{pmatrix} + \mathcal{O}(\lambda^4). \tag{1.34}$$

One of the issues of this parametrisation is that the definition of the parameters λ, A, ρ, η is ambiguous after order $\mathcal{O}(\lambda^4)$ and unitarity is only ensured to this order. One possible extension of this parametrisation that preserves the unitarity relation in Eq. (1.32) to all orders was then introduced by Ref. [23], where the following definitions are given to all orders in λ

$$s_{12} = \lambda, \tag{1.35}$$

$$s_{23} = A\lambda^2, \tag{1.36}$$

$$s_{13}e^{-i\delta} = A\lambda^3(\rho - i\eta) = \frac{A\lambda^3(\bar{\rho} + i\bar{\eta})\sqrt{1 - A^2\lambda^4}}{\sqrt{1-\lambda^2}(1 - A^2\lambda^4(\bar{\rho} + i\bar{\eta}))}. \tag{1.37}$$

where $\bar{\rho}$ and $\bar{\eta}$ are phase convention independent and defined as $\bar{\rho} + i\bar{\eta} = -\frac{V_{ud}V_{ub}^*}{V_{cd}V_{cb}^*}$. Under this parametrisation, the expansion up to order $\mathcal{O}(\lambda^9)$ can be found in Ref. [24].

The unitarity triangle

The CKM unitarity relation in Eq. (1.32) leads to the following explicit relations

$$\sum_{m=u,c,t} V_{mj}V_{ml}^* = \delta_{jl} \quad \text{with} \quad j,l \in \{d,s,b\}\,, \tag{1.38}$$

$$\sum_{n=d,s,b} V_{in}V_{kn}^* = \delta_{ik} \quad \text{with} \quad i,k \in \{u,c,t\}\,, \tag{1.39}$$

of which the 6 non-diagonal terms (i.e. the vanishing components) can be represented as triangles of the same area in the complex plane. Their area corresponds to half of J, the Jarlskog invariant [25], defined by

$$\text{Im}[V_{ij}V_{kl}V_{il}^*V_{kj}^*] = J\sum_{m,n}\epsilon_{ikm}\epsilon_{jln}\,. \tag{1.40}$$

The most commonly used of these triangles is the $b \to d$ unitarity triangle shown in Fig. 1.6, where the unitarity relation is normalised by $V_{cb}V_{cd}^*$, giving

$$\frac{V_{ud}V_{ub}^*}{V_{cd}V_{cb}^*} + \frac{V_{td}V_{tb}^*}{V_{cd}V_{cb}^*} + 1 = 0\,. \tag{1.41}$$

Useful definitions

We define the following combinations of CKM parameters since they will be used repeatedly throughout the manuscript.

$$\lambda_U^{(q)} \equiv V_{Ub}V_{Uq}^*\,, \tag{1.42}$$

$$\beta_s \equiv \arg\left(-\frac{V_{ts}V_{tb}^*}{V_{cs}V_{cb}^*}\right) = -\arg\left(-\frac{\lambda_t^{(s)}}{\lambda_c^{(s)}}\right), \tag{1.43}$$

$$\beta_d \equiv \beta \equiv \arg\left(-\frac{V_{cd}V_{cb}^*}{V_{td}V_{tb}^*}\right) = -\arg\left(-\frac{\lambda_c^{(d)}}{\lambda_t^{(d)}}\right), \tag{1.44}$$

for $U = u,c,t$ and $q = d,s$ [7]. It is important to note that, $\lambda_c^{(q)}$ for both $q = d,s$ is real to a very good approximation, i.e the imaginary part is suppressed compared to the real part by $\mathcal{O}(\lambda^4)$ and $\mathcal{O}(\lambda^6)$ respectively.

[6] This hierarchy comes solely out of experimental measurements and in the SM there is nothing that enforces it.

[7] One should be careful with this definition since, often in the literature, $V_{Ud}V_{Us}^*$ is also referred to as λ_U.

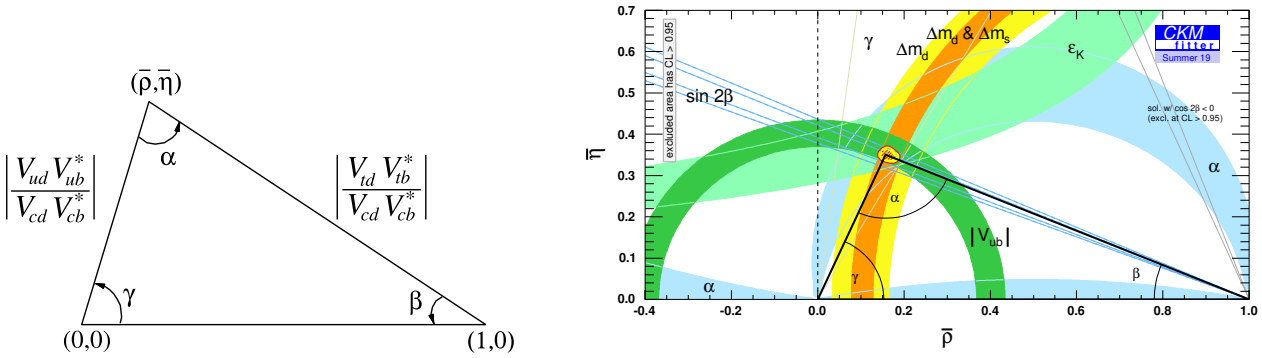

Figure 1.6: On the left a sketch from Ref. [6] showing the $b \to d$ unitarity triangle and the definition of its sides and vertices. The angles of the triangle α, β, γ are commonly used to parametrise the phases of the CKM elements. On the right, the experimental constraints on the values of the CKM parameters of this unitarity triangle [24].

These implies that $\beta_{d,s}$ are to a good approximation, the mixing angles present in $b \to s$ transitions, which we will discuss in more detail later.

Using the definitions in Eq. (1.42) the V_{Ub} unitarity relations can be written in the following form

$$\lambda_u^{(q)} + \lambda_c^{(q)} + \lambda_t^{(q)} = 0\,. \tag{1.45}$$

1.3 Flavour changing currents in the SM

As mentioned in the previous section, since the discovery of the Higgs Boson, no new particles have been found through direct searches. However, powerful tests of the SM, and indirect probes of NP, can be obtained by studying transitions from one flavour to another.

Flavour changing charged currents

In the SM any Flavour changing process will be mediated by a W boson, either if it is on a tree level or at higher orders. These tree level currents are often referred to as *Flavour Changing Charged Currents* (FCCC) as they are mediated by the exchange of a charged gauge boson (see Fig. 1.7). On the quark side, they will manifest as transition between up-type and down-type quarks and on the lepton sector between charged leptons and neutrinos. Due to the misalignment of the electroweak basis and the mass basis for the quark fields, these transitions will be able to change quark flavours and they will carry a CKM element in each vertex. On the other side, if we neglect neutrino masses, there is no misalignment for the lepton sector and lepton flavour is expected to be conserved by them. Furthermore the electroweak couplings of leptons are universal in the Standard Model which is usually referred to as *Lepton Flavour Universality* (LFU). In the SM, the violation of LFU happens only through kinematic/mass effects.

Generally we can distinguish between 3 kinds of decays happening through Flavour changing charged currents: fully leptonic decays like $\mu \to e\bar{\nu}_e\nu_\mu$, semileptonic decays like $B \to D\ell\bar{\nu}_\ell$ and non-leptonic decays like $B \to D\pi$.

The first group of processes like $\tau \to \nu_\tau e\nu_e$, $\tau \to \nu_\tau \mu\nu_\mu$ and $\mu \to \nu_\mu e\nu_e$ are natural processes to test LFU and they have been extensively tested, together with leptonic gauge boson decays and leptonic decays of light pseudoscalar mesons [26].

The second group of decays, semileptonic decays, are not only good test of LFU, but in general, good probes of the SM. The CKM matrix and its consistence, can by tested by semileptonic decays through the extraction of the CKM parameters, and the SM predictions can be tested by the measurement of their branching fractions and angular observables. Furthermore, even if in the SM they probe the same vertex as the fully-leptonic modes, in scenarios of new physics, they can probe SM deviations coming from other kind of particles (for example leptoquarks which we will discuss later).

Their amplitude will come accompanied by one CKM element and it will factorise into a leptonic and hadronic

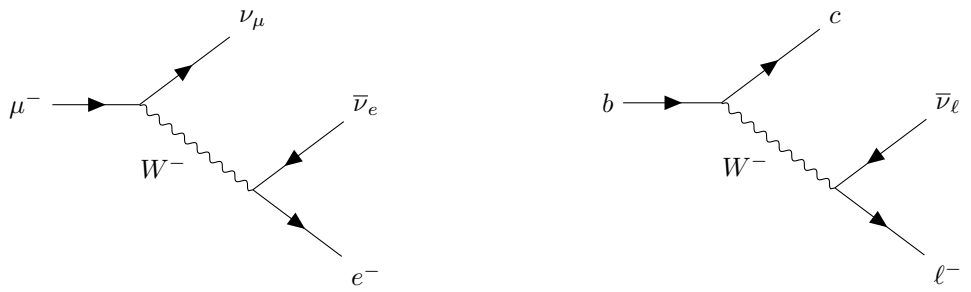

Figure 1.7: Diagrams contributing to FCCCs in the leptonic and semileptonic cases.

part, for instance for $B \to D\ell\bar{\nu}$

$$\begin{aligned}\mathcal{M}(B \to D\ell\bar{\nu}) =& 4\frac{G_F}{\sqrt{2}} V_{cb} \langle D\ell\bar{\nu}|\bar{c}\gamma_\mu P_L b \bar{\ell}\gamma^\mu P_L \nu|B\rangle \\ & 4\frac{G_F}{\sqrt{2}} V_{cb} \langle \ell\bar{\nu}|\bar{\ell}\gamma^\mu P_L \nu|0\rangle \quad \underbrace{\langle D|\bar{c}\gamma_\mu P_L b|B\rangle}_{\text{Hadronic Matrix Element}}\end{aligned} \tag{1.46}$$

where $P_L = \frac{1-\gamma_5}{2}$ and G_F is the Fermi constant.

The third group of decays, non-leptonic decays, no longer probe LFU as there are no leptons involved in the process and, due to non-pertubative QCD effects, require a more complex treatment.

Flavour Changing Neutral Currents

Other decays, that are in some ways more attractive, are the decays through *Flavour Changing Neutral Currents* (FCNCs). We can distinguish in between three different types: radiative, semileptonic and non leptonic (purely leptonic currents are not flavour changing). FCNC semileptonic decays, often referred to as *semileptonic rare decays*, correspond for instance to the $B \to K\ell^+\ell^-$ decay, and the radiative decays to $B \to K^*\gamma$. The non leptonic currents can be further divided into $\Delta F = 2$ and $\Delta F = 1$. The first ones, correspond to decays in which the change is in flavour is of two units, for instance, $B - \bar{B}$ mixing. In the second ones, the flavour changes by only one unit, for instance, the $B \to K\pi$ decay.

FCNCs are loop suppressed in the SM since they do not appear at tree level as already discussed in the previous section. The semileptonic ones, at first order, happen through the penguin and box diagrams shown in Fig. 1.8. Compared to FCCCs, the rates of FCNCs are certainly small (the suppression is of the order of 10^{-5} when comparing $B \to D\ell\nu$ with $B \to K\ell\ell$ [6]), making them more complex to detect. However, in the case of charged leptons, their decay products are easier to detect since the lack of neutrinos (i.e. missing energy) makes these modes cleaner and gives them a higher experimental efficiency. In the case of semileptonic FCNCs into neutrinos, this is however not longer the case, making these decays experimentally challenging.

This makes these decays rather interesting since they could happen at the tree level in some New Physics models, giving them a good sensitivity to possible New Physics.

These decays experience a further suppression than the loop suppression due to CKM unitarity, first proposed by Glashow, Iliopoulos and Maiani in Ref. [27] and usually referred to as the GIM mechanism. In order to simplify the picture, we will not do the full computation of the FCNCs but rather explain the idea behind. When computing the amplitude for an FCNC, for example $b \to s\ell\ell$ as shown in Fig. 1.8, the loop integration over the u type quark loop and the two W insertions give the following

$$\mathcal{M}(b \to s\ell\ell) \propto I = \sum_{i=u,c,t} V_{ib}V_{is}^* F(x_i) \,, \qquad \text{with } x_i = \frac{m_i^2}{m_W^2} \,, \tag{1.47}$$

where F(x) is a function describing the dependence on the internal up-type quark masses resulting from the loop integral calculation including QCD corrections.

For low quark masses this function has the following behaviour [28]

$$F(x) \sim x\ln(x) \,, \quad \text{for} \quad x \ll 1 \,, \tag{1.48}$$

and

$$F(x_c)/F(x_t) \approx \mathcal{O}(10^{-3}) \,, \tag{1.49}$$

	$2^{\text{nd}}/3^{\text{rd}}$ gen		$1^{\text{st}}/3^{\text{rd}}$ gen	
	CKM	Loop	CKM	Loop
$b \to s$	~ 1	$\mathcal{O}(10^{-3})$	$\sim 2 \times 10^{-2}$	$\mathcal{O}(10^{-8})$
$b \to d$	~ 1	$\mathcal{O}(10^{-3})$	~ 0.4	$\mathcal{O}(10^{-8})$
$s \to d$	$\sim 6 \times 10^2$	$\mathcal{O}(10^{-3})$	$\sim 6 \times 10^2$	$\mathcal{O}(10^{-8})$
$c \to u$	$\sim 10^3$	$\mathcal{O}(10^{-3})$	$\sim 10^3$	$\mathcal{O}(10^{-5})$

Table 1.2: We show the weights for the CKM suppression and the quark mass loop suppression for each of the semileptonic FCNCs depending on the quark that runs on the loop (1^{st} or 2^{nd} generation) and normalised to the 3^{rd} generation weight (top or bottom depending on the FNCN) for comparison. For instance, for the $b \to s$ transition, the first column compares the charm quark vs the top quark running on the loop and the second column compares the up with the top. On the left of the first column we show $\left|\frac{V_{cb}V_{cs}}{V_{tb}V_{ts}}\right|$ and on the right $\frac{F(x_c)}{F(x_t)}$ where F is the function in Eq. (1.47).

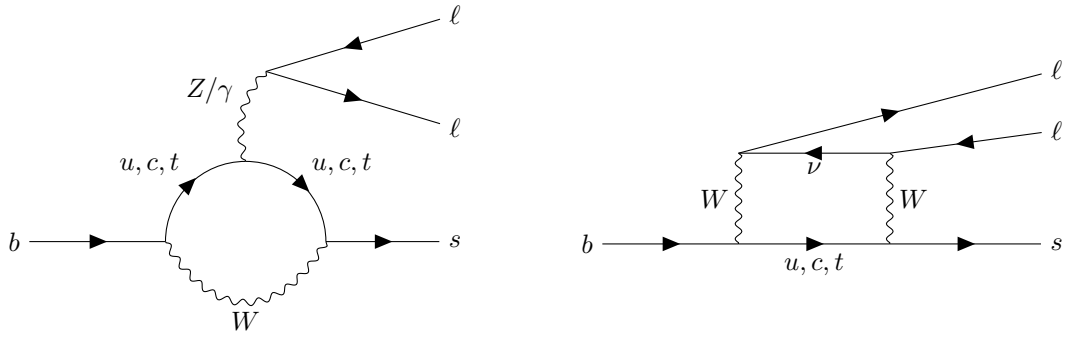

Figure 1.8: Diagrams contributing to the $b \to s\ell^+\ell^-$ FCNC transition in the SM.

which is often referred to as the hard GIM suppression. Then, using the CKM unitarity relation $V_{tb}V_{ts}^* = -V_{cb}V_{cs}^* - V_{ub}V_{us}^*$ we can write Eq. (1.47) as

$$I = -V_{cb}V_{cs}^* \left(F\left(x_t\right) - F\left(x_c\right)\right) - V_{ub}V_{us}^* \left(F\left(x_t\right) - F\left(x_u\right)\right) . \tag{1.50}$$

and using $m_{u,c} \ll m_W$ together with the relations above

$$I \approx V_{tb}V_{ts}^* F\left(x_t\right) . \tag{1.51}$$

This makes the t quark the main contribution in the FCNC loop for $b \to s$ decays with a CKM suppression of $|V_{tb}V_{ts}| \approx 0.04$.

In the case of $b \to d$ decays the hierarchy is similar, but they are further suppressed by CKM since $|V_{tb}V_{td}| \approx 0.009$.

In the case of $s \to d$ decays, this is no longer true because of the $|V_{cs}V_{cd}| \approx |V_{us}V_{ud}| \approx 0.2 \gg |V_{ts}V_{td}| \approx 0.0004$, and the CKM suppression compensates for the value of $F(x_c)$ suppression shown in Eq. (1.49) making the charm contribution of a similar order to the top contribution.

Lastly in the case of $c \to u$, the situation is similar to $s \to d$ and $|V_{cs}V_{us}| \approx |V_{cd}V_{ud}| \approx 0.2 \gg |V_{cb}V_{cu}| \approx 0.00015$, making the strange quark the main contribution. In Table 1.2 we show the CKM suppression and the suppression due to the value of F for each of the FCNCs and each of the loop quarks.

The CKM suppression, on one side is a problem, since these decays get lower decay rates. On the other hand, the fact that the main contribution is expected to be the one from the top quark in $b \to s/d$ is actually positive since the top quark loop is not expected to be dominated by long-distance QCD effects. In the case of $s \to d$ and $c \to u$, this is no longer the case, where the dominance of charm and strange quarks makes these modes very complicated to predict accurately.

As we have seen, flavour changing currents are interesting test of the SM model, and furthermore, interesting probes of NP. However, in order to discuss this transition in detail, we need to discuss some other elements first. The first of these, is the fact that quark transitions do not happen free, they happen through QCD bound-states called hadrons which make the prediction of this decays slightly more challenging. With this in mind we will now discuss the theory of QCD, already introduced at the beginning of the chapter, in further detail.

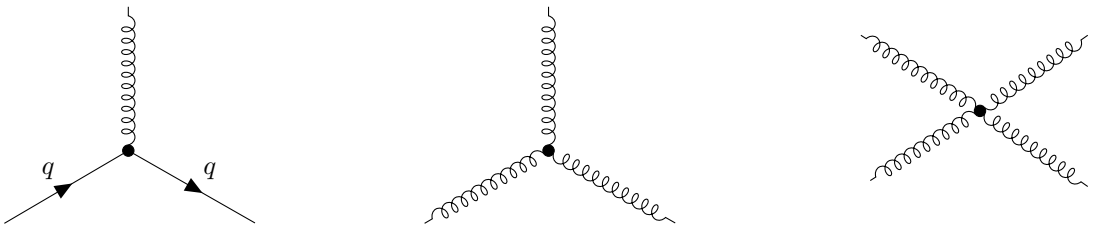

Figure 1.9: Interaction vertices from QCD, from left to right, the quark-gluon vertex, the 3-gluon vertex and the 4-gluon vertex.

1.4 Quantum Chromodynamics

QCD is a gauge field theory that describes the strong interactions between quarks and antiquarks with gluons. It is a non-abelian gauge theory with the $\mathrm{SU}(3)_C$ group, where C stands for colour, as its gauge or symmetry group. Quarks transform under the fundamental representation of $\mathrm{SU}(3)_C$, whereas gluons transform under the adjoint representation.

The expanded QCD Lagrangian reads

$$\begin{aligned}\mathcal{L}_{QCD} = &-\frac{1}{4}(\partial_\mu \mathcal{A}^a_\nu - \partial_\nu \mathcal{A}^a_\mu)(\partial^\mu \mathcal{A}^{a\nu} - \partial^\nu \mathcal{A}^{a\mu}) + \bar{q}_\alpha (i\partial\!\!\!/ - m_q) q_\alpha \\ &- g_s \bar{q}_\alpha T^a_{\alpha\beta} \gamma^\mu q_\beta \mathcal{A}^a_\mu + \frac{g_s}{2} f^{abc}(\partial_\mu \mathcal{A}^a_\nu - \partial_\nu \mathcal{A}^a_\mu)\mathcal{A}^{b\mu}\mathcal{A}^{c\nu} \\ &- \frac{g_s^2}{4} f^{abe} f^{cde} \mathcal{A}^a_\mu \mathcal{A}^b_\nu \mathcal{A}^{c\mu} \mathcal{A}^{d\nu}\end{aligned} \tag{1.52}$$

where we omit the part relative to ghosts and the sum over the possible flavours $q = u, d, s, c, b, t$. We implicitly sum over the Lorentz indices μ, ν and the colour indices α, β, a, the first two running from 1 to $N_C = 3$, the number of colours, and the last one from 1 to $(N_C^2 - 1) = 8$. The $T^a_{\alpha\beta}$ are 3×3 matrices corresponding to the generators of $\mathrm{SU}(3)_C$ and the commutator of them

$$[T^a, T^b] = i f^{abc} T^c \,, \tag{1.53}$$

is given by the structure constants f^{abc} of $\mathrm{SU}(3)_C$.

The terms in the first line of Eq. (1.52) correspond to the dynamics of the gluons fields and the quark fields. The terms in the second line give rise to two interaction vertices of QCD, the quark-gluon vertex and the 3-gluon interaction, while the last line corresponds to the 4-gluon interaction, all shown in Fig. 1.9.

For practical purposes we will refer to $\alpha_s = \frac{g_s^2}{4\pi}$ as the strong coupling constant (as opposed to g_s), since it is the relevant quantity when computing physical processes.

It is important to emphasize that gluons will only interact with coloured particles (i.e. themselves and the quark fields), leaving all of the other SM particles free of QCD interactions. This will be important in the following as it helps to factorize QCD interaction in some EW decays.

In the following, we will not give a detailed description of QCD as it is not the objective of this manuscript, but we will discuss some elements that are important for the following chapters. Indeed, several important issues like the gauge transformation of the fields, the gauge fixing conditions and the quantization of the quark and gluon fields (and the auxiliary ghost fields) will not be discussed, however they can be found in many textbooks and reviews like Refs. [29, 30].

1.4.1 Renormalisation and running of the QCD coupling constant

Similarly to QED, QCD is a renormalisable theory, meaning that the ultraviolet (UV) divergences, appearing in higher-order loop diagrams of the theory perturbation, can all be absorbed into a redefinition of the theory's fields and parameters; in this case, a redefinition of the normalisation of the quark q^α and gluon $\mathcal{A}^a_\mu$ fields, of the coupling constant α_s and of the quark masses m_q. In order to absorb the UV divergences, one requires a regularisation and a renormalisation schemes, both of which can be chosen depending on the calculation at hand. The most common ones are *dimensional regularisation* and the *modified minimal subtraction* scheme ($\overline{\mathrm{MS}}$), which we use in this manuscript unless explicitly mentioned. The relevant divergences induced by the loops are logarithmic, so that after regularisation and renormalisation, the residual contributions of the loop diagrams (to a fixed order) will introduce a logarithmic dependence on a new arbitrary scale μ called the renormalisation scale. This will manifest in a scale dependence of the renormalised coupling "constant" $\alpha_s(\mu)$, of the renormalised quark masses ($m_q(\mu)$) and several other objects that will, to the same fixed order, cancel the logarithmic dependence

of the amplitudes on the renormalisation scale introduced by the loop diagrams. This leads to predictions for observables that are, in principle, independent of the renormalisation scale[8].

This is often referred to as the "running" of the coupling constant and quark masses.

The scale dependence of the coupling constant is given by the β-function of QCD

$$\beta(\alpha_s(\mu)) = \mu \frac{d\alpha_s(\mu)}{\mu}\,, \tag{1.54}$$

defining the *Renormalisation Group Equation* (RGE). The β-function can be expand in power of α_s in the following way

$$\beta(\alpha_s(\mu)) = -2\alpha_s \sum_{n=0}^{\infty} \beta_n \left(\frac{\alpha_s}{4\pi}\right)^{n+1}\,. \tag{1.55}$$

To the first order in this expansion, the RGE solution is given by the Gross-Wilczek-Politzer [31, 32] formula, which relates $\alpha_s(\mu)$ at two different scales:

$$\alpha_s(\mu) = \frac{\alpha_s(\mu_0)}{1 + \frac{\alpha_s(\mu_0)}{4\pi}\beta_0 \ln\frac{\mu^2}{\mu_0^2}}\,, \qquad \beta_0 = 11 - \frac{2}{3}N_f > 0\,. \tag{1.56}$$

The first term in β_0 comes from the gluonic self-interaction and the second from the quark gluon interaction, being $N_f \leq 6$ the number of active quark flavours[9].

To obtain a value of $\alpha_s(\mu)$ at a given scale μ through Eq. (1.56), one requires the value of the coupling constant at a set scale. The value of reference that is more commonly used, coming from Z decays, can be found in Ref. [6] and corresponds to

$$\alpha_s(m_Z) = 0.1179 \pm 0.0010\,. \tag{1.57}$$

One should notice that Eq. (1.56) does not only include the corrections of order $\mathcal{O}(\alpha_s(\mu_0))$ to $\alpha_s(\mu)$, in fact, by performing a Taylor expansion of Eq. (1.56), we find

$$\alpha_s(\mu) = \alpha_s(\mu_0)\left(1 - \frac{\alpha_s(\mu_0)}{4\pi}\beta_0 \ln\frac{\mu^2}{\mu_0^2} + \left(\frac{\alpha_s(\mu_0)}{4\pi}\beta_0 \ln\frac{\mu^2}{\mu_0^2}\right)^2 - ...\right)\,, \tag{1.58}$$

where we have an infinite series on $\left(\frac{\alpha_s(\mu_0)}{4\pi}\beta_0 \ln\frac{\mu^2}{\mu_0^2}\right)$. If $\mu \sim \mu_0$ we can truncate this series and keep only the $\mathcal{O}(\alpha_s)$ term. However, if the difference in between μ and μ_0 is large enough, truncation is no longer an option, since the expansion parameter becomes larger than 1.

This logarithmic dependency, residual of the loop induced divergences, needs to be taken into account to all orders in α_s, or more precisely, all orders in $\left(\frac{\alpha_s(\mu_0)}{16\pi}\beta_0 \ln\frac{\mu^2}{\mu_0^2}\right)^n$ need to be included. Luckily, this is exactly what is done through the resolution of the RGE given in Eq. (1.54). We will then say that the solution in Eq. (1.56), is given to leading logarithm or leading-log order (LL). This differs from the leading order expression (LO) where only $\mathcal{O}(\alpha_s)$ are taken into consideration. The next to leading-log (NLL) order will correspond to $\alpha_s(\mu_0)\left(\frac{\alpha_s(\mu_0)}{16\pi}\beta_0 \ln\frac{\mu^2}{\mu_0^2}\right)^n$.

Until now, the decision of working at the scale μ rather than the scale at which is extracted (for instance m_Z), might seem unjustified given that the amplitudes are in theory independent of the choice of factorisation scale. However, when computing the amplitude of a specific process with a characteristic scale E, logarithms of the kind $\left(\alpha_s \ln\left(\frac{\mu}{E}\right)\right)^n$ will appear to all orders in n. When computing this amplitude to a fix order on α_s, these logarithms will cancel to that fix order on α_s but not to all orders in $\left(\alpha_s \ln\left(\frac{\mu}{E}\right)\right)$.

For instance for a process with characteristic scale around m_b and a renormalisation scale $\mu = m_Z$ these logarithms are considerably big $\left(\alpha_s \ln\left(\frac{m_Z}{m_b}\right)\right) \sim \mathcal{O}(1)$ putting in risk the perturbative expansion.

By choosing the renormalisation scale to be close to the characteristic scale $\mu \sim E$, one avoids the presence of large logarithms of the form $\ln\left(\frac{\mu}{E}\right)$ in the amplitude , by shifting them into $\ln\left(\frac{\mu}{\mu_0}\right)$. However, as discussed above, these second sets of logarithms, through the use of the RGE, are ressumed to all orders to all orders in $\mathcal{O}((\alpha_s \ln[\mu])^n)$. This perturbative treatment, where we take into account the RGE evolution to get rid of large logarithms, is called the *Renormalisation Group Improved Perturbation Theory* and it is a fundamental tool for the perturbative treatment of QFTs.

[8] More precisely, the observables will be independent of the renormalisation scale up to the order of perturbation theory in which the computation is performed.

[9] This corresponds to the number of quarks that have a mass lower than the scales taken into account, and are thus accounted for in the loops. Depending on the renormalisation scheme, this might require a matching procedure when crossing a quark mass (which is the case of the $\overline{\text{MS}}$ scheme).

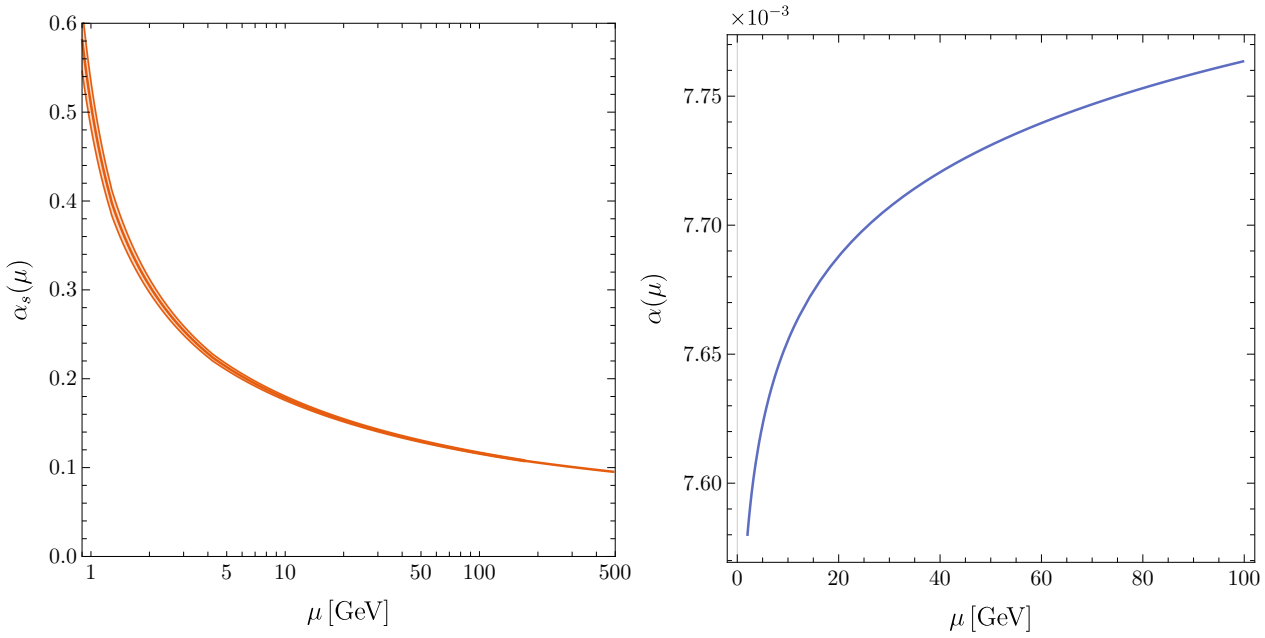

Figure 1.10: Running coupling constants on the $\overline{\text{MS}}$ scheme computed in perturbation theory as a function of the renormalisation scale μ. On the left the strong coupling constant $\alpha_s(\mu)$ and on the right the electromagnetic one $\alpha(\mu)$.

One fundamental aspect of QCD is that, with the number of quark flavours of the SM, β_0 takes a positive value. This gives QCD a peculiar running of its coupling constant. The coupling constant grows (decreases) logarithmically as we go to lower (higher) energies, in other words the strong interaction grows stronger (weaker) at longer (shorter) distances. This behaviour is opposed to the one of the QED coupling constant as it can be seen in Fig. 1.10. Furthermore $\alpha_s(\mu)$ asymptotically vanishes when $\mu \to \infty$. This is often referred to as the phenomenon of "asymptotic freedom" of QCD, implying that at high energies, quarks and gluons act as free particles.

On the other end, when a value of $\mu = \Lambda_{\text{QCD}}$, defined by the condition

$$\frac{\alpha_s(\mu_0)}{4\pi}\beta_0 \ln \frac{\Lambda^2_{\text{QCD}}}{\mu_0^2} = -1\,, \tag{1.59}$$

is reached, the coupling constant diverges. This means that, since the coupling constant is actually the perturbation parameter of the theory, when going to low enough energies ($\mu \sim \Lambda_{\text{QCD}}$) the coupling constant grows too large to have a perturbative treatment of the theory, entering the so-called non-perturbative regime.

The Λ_{QCD} scale allows us to classify quarks (together with hadrons) in two categories: light quarks, where $m_q < \Lambda_{\text{QCD}}$, corresponding to the u, d and s quarks and heavy quarks where $m_q > \Lambda_{\text{QCD}}$, corresponding to the c, b and t quark. This classification is not purely arbitrary, since the Λ_{QCD} scale is the relevant scale in QCD, and will dictate the behaviour of the hadrons at hand. In practice, this allows us to define different effective field theories, that we will discuss later, to treat these two different types of quarks. The top quark is sometimes also refereed as a super-heavy quark, because of its extremely heavy mass and because of its extremely short lifetime.

In the low energy QCD regime we require to use different, non-perturbative, methods to understand QCD. The most common and powerful of them is lattice QCD, consisting of a discrete numerical treatment of QCD which we will further discuss in Section 1.6. In Fig. 1.11 we can see the quark-antiquark static potential computed on the lattice as a function of the distance.

The linear growth of this potential with the distance yields another consequence of QCD, the phenomenon of "colour confinement" [34], which implies that at low energies coloured-charged particles such as quark and gluons cannot be directly observed as free coloured states but rather as colourless (white) bound-states. [10]

These white bound-states are called hadrons and they can be divided into two kinds depending on their spin and baryon number; mesons, which have integer spin (i.e. they are bosons) and baryon number 0; and baryons which have half integer spin (i.e. they are fermions) and baryon number 1. Leaving exotic states [11] aside, mesons

[10] One can see that the quark masses, are not actually observables of the theory, due to confinement, which allows the quark mass to have a scale dependence as shown in Eq. (1.62).

[11] Exotic white-bound states, can correspond, for example, to pentaquarks (3 quarks 2 antiquarks), tetraquarks (2 quarks 2 antiquarks) and glueballs (purely gluonic white state).

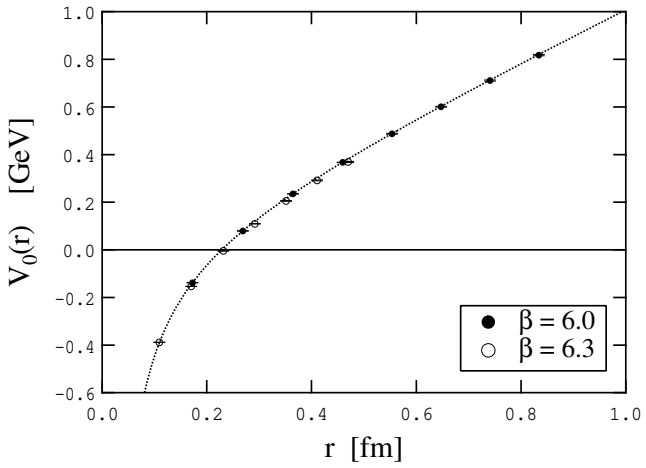

Figure 1.11: Lattice QCD determination of the static quark-antiquark potential from Ref. [33].

are composed of a quark-antiquark pair, while baryons are composed of three quarks (or three antiquarks). They can be composed of quarks of all families with the exception of the t quark which, because of its high mass, decays before being able to hadronise (the lifetime of the top quark is about a twentieth of the hadronisation time scale). The full zoology of hadron states can be found in Ref. [6], together with their characteristics.

The renormalised quark masses $m_q(\mu)$ at two different scales will be related by the following RGE

$$\mu \frac{dm_q(\mu)}{\mu} = \gamma_m(\alpha_s(\mu)) m_q(\mu)\,, \tag{1.60}$$

where $\gamma_m(\alpha_s(\mu))$ is the quark mass anomalous dimensions which we expand in power of α_s

$$\gamma_m(\alpha_s(\mu)) = \sum_{n=0}^{\infty} \gamma_m^n \left(\frac{\alpha_s}{4\pi}\right)^{n+1} \tag{1.61}$$

similarly to the β-function for α_s. At leading-log, the solution of the RGE above is given by the following formula:

$$m_q(\mu) = m_q(\mu_0) \left(\frac{\alpha_s(\mu)}{\alpha_s(\mu_0)}\right)^{-\frac{\gamma_m^0}{2\beta_0}} \tag{1.62}$$

where $\gamma_m^0 = -6C_F = -8$. The presence of large logarithms can be also made explicit for the quark mass by replacing $\alpha_s(\mu)$ by its leading-log expression and expanding Eq. (1.62)

$$\begin{aligned} m_q(\mu) &= m_q(\mu_0) \left(1 + \frac{\alpha_s(\mu_0)}{4\pi}\beta_0 \ln\frac{\mu^2}{\mu_0^2}\right)^{\frac{\gamma_m^0}{2\beta_0}} \\ &= m_q(\mu_0) \left(1 + \frac{\gamma_m^0}{2}\frac{\alpha_s(\mu_0)}{4\pi}\ln\frac{\mu^2}{\mu_0^2} + \frac{\gamma_m^0(\gamma_m^0 - 2\beta_0)}{8}\left[\frac{\alpha_s(\mu_0)}{4\pi}\ln\frac{\mu^2}{\mu_0^2}\right]^2 + \dots\right) \end{aligned} \tag{1.63}$$

1.5 Non-perturbative inputs: Hadronic Form factors and decay constants

As discussed in the previous section, QCD cannot be treated in a fully perturbative way, which means that we need to separate the parts that can be computed perturbatively and the parts that cannot. In the case of weak hadron decays, as shown in Eq. (1.46), the amplitude will sometimes be factorised into a hadronic matrix element with a corresponding current insertion, the gauge boson propagator, and the gauge boson decay. This process of factorisation will generally require the parametrisation of the non-perturbative elements of QCD. These correspond to hadronic matrix elements of different currents, with hadrons or the vacuum as external states computed within QCD. We will discuss three kinds of non pertubative inputs illustrated in Figs. 1.12 and 1.15: decay constants, hadron form factors, and distribution amplitudes. A very complete review on non-perturbative elements in QCD is given in Ref. [35] from which we will borrow some elements.

1.5.1 Meson decay constants

A quantity that we will often encounter are the meson decay constants, they correspond to the parametrisation of the local matrix element of the transition between a meson and the vacuum through a certain current. For a pseudoscalar meson P composed of a quark antiquark pair ($P = (\bar{q}_1, q_2)$), the decay constant f_P is defined through the matrix element of the axial current between a P-meson of 4-momentum p_μ and the vacuum [6] in the following form

$$\langle 0|\bar{q}_1(0)\gamma^\mu\gamma^5 q_2(0)|P(p)\rangle = ip_\mu f_P\,. \tag{1.64}$$

Interestingly, the pseudoscalar meson decay constant is a scale independent quantity, this is, for instant, consistent to the fact that f_π, the pion decay constant, determines the width of the pion, which being an observable quantity, needs to be independent of the renormalisation scale.

Equivalently to the pseudoscalar case, the longitudinal $f_{V,\parallel}$ and transverse $f_{V,\perp}$ decay constants of a vector meson ($V = (\bar{q}_1, q_2)$) of 4-momentum k_μ, polarization vector ε and mass m_V are defined as [36]

$$\langle 0|\bar{q}_1\gamma_\mu q_2|V(k,\varepsilon)\rangle = -if_{V,\parallel}m_V\varepsilon^*_\mu\,, \tag{1.65}$$

$$\langle 0|\bar{q}_1\sigma_{\mu\nu} q_2|V(k,\varepsilon)\rangle = f_{V,\perp}(\mu)(k_\mu\varepsilon^*_\nu - k_\nu\varepsilon^*_\mu)\,, \tag{1.66}$$

where in this case, the transverse decay constant is no longer a scale independent quantity and depends on the scale μ, which usually will be taken as a hadronic factorisation scale. The scale dependence of $f_{V,\perp}$ at leading order is given by

$$f_{V,\perp}(\mu) = f_{V,\perp}(\mu_0)\left(\frac{\alpha_s(\mu)}{\alpha_s(\mu_0)}\right)^{\frac{C_F}{\beta_0}} \tag{1.67}$$

where $C_F = (N_C^2 - 1)/(2N_C) = 8/6$.

Decay constant can be thought as the "wavefunction overlap" of the valence quark and the antiquark, or as a measurement of how probable it is for these quarks to annihilate through the correspondent current. They will appear, for instance, in the description of processes like $B_s \to \mu^+\mu^-$ where the quark anti-quark pair annihilate into an axial current or in non-leptonic decays in the framework of QCD factorisation [37].

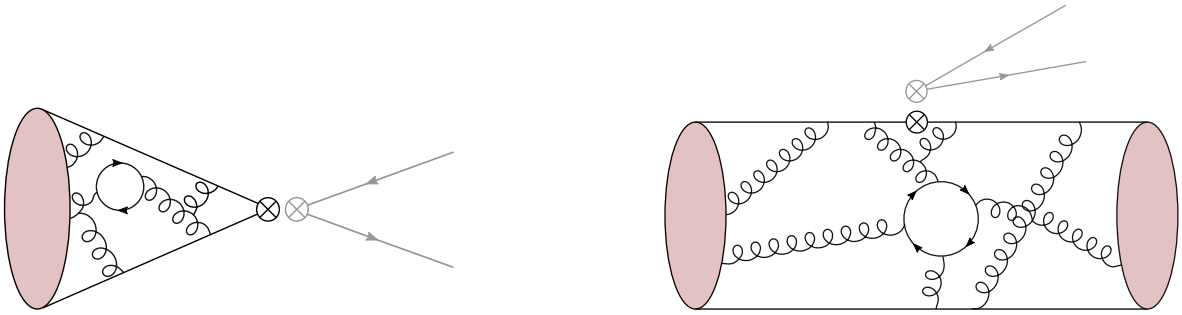

Figure 1.12: Schematics representing different non-perturbative elements. On the left, decay constant of a meson connected to a fermion pair in grey through the current insertion. On the right, form factors of a meson connected to a fermion pair in grey through the current insertion.

1.5.2 Hadron Form factors

Hadron form factors correspond to the parametrisation of the local matrix element of a transition between two hadrons through a certain current. Given a transition between an initial state hadron H_1 and a final state hadron H_2 of 4-momenta p_μ and k_μ respectively, through a current $\mathcal{J}$, we can parametrise its matrix element as

$$\langle H_2(k)|\mathcal{J}(0)|H_1(p)\rangle = \sum_i f_i^{\mathcal{J}}(q^2)K_i\,, \qquad i = 1, ..., n\,, \tag{1.68}$$

where each K_i is a kinematical Lorentz structure which together form a basis of all the allowed Lorentz structures, and $f_i^{\mathcal{J}}$ are the hadron form factors of this transition. These are scalar functions of q^2 (where $q_\mu = p_\mu - k_\mu$ is the momentum transfer), which essentially depend on how the momentum is distributed between the hadron's constituents. The Lorentz structures available depend on the spin and parity of the hadrons involved and on the current at hand. The amount of form factors grows with the spin, as more structures, like the polarization vector, become available.

We will now look explicitly at the form-factor's parametrisations relevant in heavy to light hadron transitions, as these are the matrix elements we encounter in the rest of the manuscript.

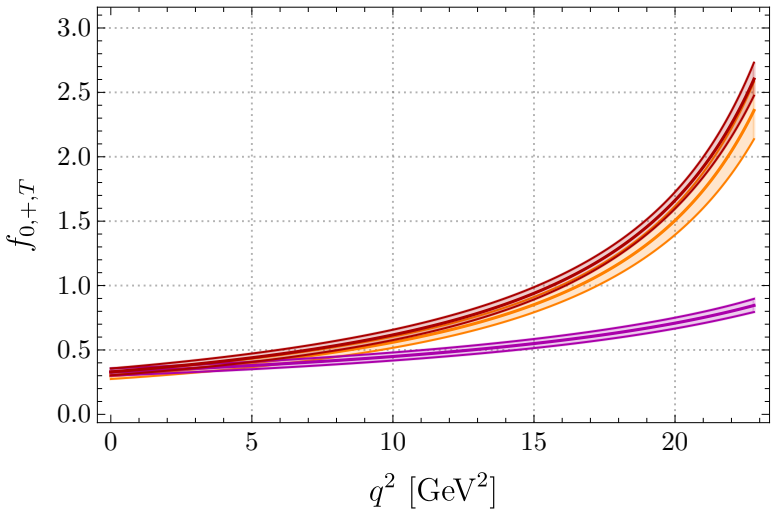

Figure 1.13: $B \to K$ form factors coming from Ref. [39] obtained using light-cone sum rules and Lattice QCD (see Section 1.6). The purple, red and orange curves correspond to the $f_0(q^2)$, $f_+(q^2)$, $f_T(q^2)$ form factors respectively.

$B \to P(S)$ form factors

We will start by considering the form factors for a $\bar{B}$-meson ($b\,\bar{q}'$) of 4-momentum p_μ decaying into a pseudoscalar meson P ($q\,\bar{q}'$) of 4-momentum k_μ . The relevant currents that respect parity are $\mathcal{J} = \bar{q}b$, $\bar{q}\gamma^\mu b$, $\bar{q}\sigma^{\mu\nu}q_\nu b$, respectively the scalar, vector and tensor currents.

In the case of the vector and tensor current which contain one Lorentz index the available structures are only the 4-momenta of both mesons, p_μ and k_μ[12]. In the case of the scalar current the only option is to have a purely scalar function.

In order to simplify the expressions of the decay amplitudes, some kinematical factors are added, leading to the following expressions for the $B \to P$ form factors [38]

$$\langle P(k)|\bar{q}\gamma^\mu b|\bar{B}(p)\rangle = f_+(q^2)\left[p^\mu + k^\mu - \frac{m_B^2 - m_P^2}{q^2}q^\mu\right] + f_0(q^2)\frac{m_B^2 - m_P^2}{q^2}q^\mu\,, \tag{1.69}$$

$$\langle P(k)|\bar{q}\sigma^{\mu\nu}q_\nu b|\bar{B}(p)\rangle = \frac{if_T(q^2)}{m_B + m_P}\left[q^2(p^\mu + k^\mu) - (m_B^2 - m_P^2)q^\mu\right]\,, \tag{1.70}$$

for the vector and tensor form factors, where m_B and m_P are the masses of the $\bar{B}$-meson and the pseudoscalar meson respectively. In the case of the scalar matrix element, through the application of the equations of motion of the quark fields to Eq. (1.69), one obtains the following relation

$$\langle P(k)|\bar{q}b|\bar{B}(p)\rangle = \frac{m_B^2 - m_P^2}{m_b - m_q}f_0(q^2)\,, \tag{1.71}$$

where m_b and m_q are the masses of the quarks in the current. With this parametrisation, the matrix elements defined in Eq. (1.69) apparently exhibits an unphysical singularity at $q^2 = 0$, which is removed by the identity

$$f_+(q^2 = 0) = f_0(q^2 = 0)\,. \tag{1.72}$$

For illustration, the three form factors for the $B \to K$ transition are shown in Fig. 1.13.

Equivalently, in the case of the decay of a $\bar{B}$-meson into a scalar meson S, the form factors are defined in the following way

$$\langle S(k)|\bar{q}\gamma^\mu\gamma_5 b|\bar{B}(p)\rangle = -i\left[f_+(q^2)\left(p^\mu + k^\mu - \frac{m_B^2 - m_S^2}{q^2}q^\mu\right) + f_0(q^2)\frac{m_B^2 - m_S^2}{q^2}q^\mu\right]\,, \tag{1.73}$$

$$\langle S(k)|\bar{q}\sigma^{\mu\nu}\gamma_5 q_\nu b|\bar{B}(p)\rangle = -\frac{f_T(q^2)}{m_B + m_S}\left[q^2(p^\mu + k^\mu) - (m_B^2 - m_S^2)q^\mu\right]\,, \tag{1.74}$$

$$\langle S(k)|\bar{q}\gamma_5 b|\bar{B}(p)\rangle = -i\frac{m_B^2 - m_S^2}{m_b - m_q}f_0(q^2)\,. \tag{1.75}$$

for the axial, pseudotensor and pseudoscalar currents respectively.

[12] For the tensor current, there is actually only one form factor due to the antisymmetric nature of the $\sigma^{\mu\nu}$ tensor, leading to the following constraint $\langle P(k)|\bar{q}\sigma^{\mu\nu}q_\nu b|\bar{B}(p)\rangle q_\mu = 0$.

$B \to V$ form factors

As mentioned before, in the case of a $\bar{B}$-meson decaying into a vector meson V, the situation gets slightly more complex since also the polarization vector ε_μ of the vector meson is available, and contractions with the Levi-Civita symbol[13] are now possible. The vector and axial form factors for the $B \to V$ transition are thus defined as

$$\langle V(k,\varepsilon^*)|\bar{q}\gamma^\mu b|\bar{B}(p)\rangle = \frac{2iV(q^2)}{m_B+m_V}\epsilon^{\mu\nu\rho\sigma}\varepsilon^*_\nu p'_\rho p_\sigma\,, \tag{1.76}$$

$$\begin{aligned}\langle V(k,\varepsilon^*)|\bar{q}\gamma^\mu\gamma_5 b|\bar{B}(p)\rangle =& 2m_V A_0(q^2)\frac{\varepsilon^*\cdot q}{q^2}q^\mu + (m_B+m_V)A_1(q^2)\left[\varepsilon^{*\mu} - \frac{\varepsilon^*\cdot q}{q^2}q^\mu\right]\\ &- A_2(q^2)\frac{\varepsilon^*\cdot q}{m_B+m_V}\left[p^\mu + k^\mu - \frac{m_B^2-m_V^2}{q^2}q^\mu\right]\,,\end{aligned} \tag{1.77}$$

and the tensor and pseudotensor as [14]

$$\langle V(k,\varepsilon^*)|\bar{q}\sigma^{\mu\nu}q_\nu b|\bar{B}(p)\rangle = 2T_1(q^2)\epsilon^{\mu\nu\rho\sigma}\varepsilon^*_\nu p_\rho p'_\sigma\,, \tag{1.79}$$

$$\begin{aligned}\langle V(k,\varepsilon^*)|\bar{q}\sigma^{\mu\nu}\gamma_5 q_\nu b|\bar{B}(p)\rangle =& -iT_2(q^2)\left[(m_B^2-m_V^2)\varepsilon^{*\mu} - (\varepsilon^*\cdot q)(p^\mu+k^\mu)\right]\\ &- iT_3(q^2)(\varepsilon^*\cdot q)\left[q^\mu - \frac{q^2}{m_B^2-m_V^2}(p^\mu+k^\mu)\right]\,,\end{aligned} \tag{1.80}$$

where m_V is the mass of the vector meson.

These form factors are related at $q^2=0$, on one side to remove the unphysical apparent singularity in Eq. (1.77) and on other hand due to the algebraic relation between $\sigma^{\mu\nu}$ and $\sigma^{\mu\nu}\gamma_5$, which leads to the following relations

$$A_0(q^2=0) = A_3(q^2=0)\,, \qquad T_1(q^2=0) = T_2(q^2=0)\,, \tag{1.81}$$

where

$$A_3(q^2) = \frac{m_B+m_V}{2m_V}A_1(q^2) - \frac{m_B-m_V}{2m_V}A_2(q^2)\,. \tag{1.82}$$

This seemingly complicated parametrisation is not purely arbitrary; its objective is to simplify the expressions appearing when computing the amplitude for the process. More precisely, they simplify the *helicity amplitudes*, which correspond to projections of the matrix elements in states of given helicity. We will discuss this further when applying this method to the $\Lambda_b \to \Lambda^*\ell^+\ell^-$ decay in Chapter 5.

Baryon form factors

One cannot only define form factors in the case of meson transitions but also, in the case of baryons. As opposed to mesons which have integer spins, baryons have half-integer spins. This means that even the lowest spin baryon (spin 1/2) already has a more complicated spin structure than the lowest spin mesons (spin 0). This shows up in the need of bispinors to characterise the external baryon states and the additional Dirac structures that come with them.

Let us consider the simplest case, a transition from a spin 1/2 baryon B_i of 4-momentum p_μ to a spin 1/2 baryon B_f of 4-momentum k_μ. These baryons will be described by two bispinors $\bar{u}_{B_f}(k)$, $u_{B_i}(p)$ which satisfy the Dirac equations

$$(\not{p} - m_{B_i})u_{B_i}(p) = 0\,, \qquad \bar{u}_{B_f}(k)(\not{k} - m_{B_f}) = 0\,. \tag{1.83}$$

The 4-vectors constructed from two bispinors will take the general form $\bar{u}_{B_f}(k)V^\mu u_{B_i}(p)$ where

$$V^\mu = \gamma^\mu, p^\mu, k^\mu\,. \tag{1.84}$$

All the other possible combinations of contracted 4-momentum with gamma matrices like

$$\gamma^\mu\not{p}, \gamma^\mu\not{k}, p^\mu\not{p}, \dots\,, \tag{1.85}$$

[13] The sign convention for the Levi-Civita symbol is such that $\epsilon^{0123} = -\epsilon_{0123} = -1$.

[14] Although the proper definition of the tensor and pseudotensor form factors should involve the $\langle V(k,\varepsilon^*)|\bar{q}\sigma^{\mu\nu}(\gamma_5)b|\bar{B}(p)\rangle$ matrix elements, due to the algebraic relation

$$\sigma^{\mu\nu}\gamma_5 = \frac{i}{2}\sigma_{\alpha\beta}\epsilon^{\alpha\beta\mu\nu}\,, \tag{1.78}$$

there is only 3 independent form factors which can be equivalently defined using the $\langle V(k,\varepsilon^*)|\bar{q}\sigma^{\mu\nu}(\gamma_5)q_\nu b|\bar{B}(p)\rangle$ matrix elements.

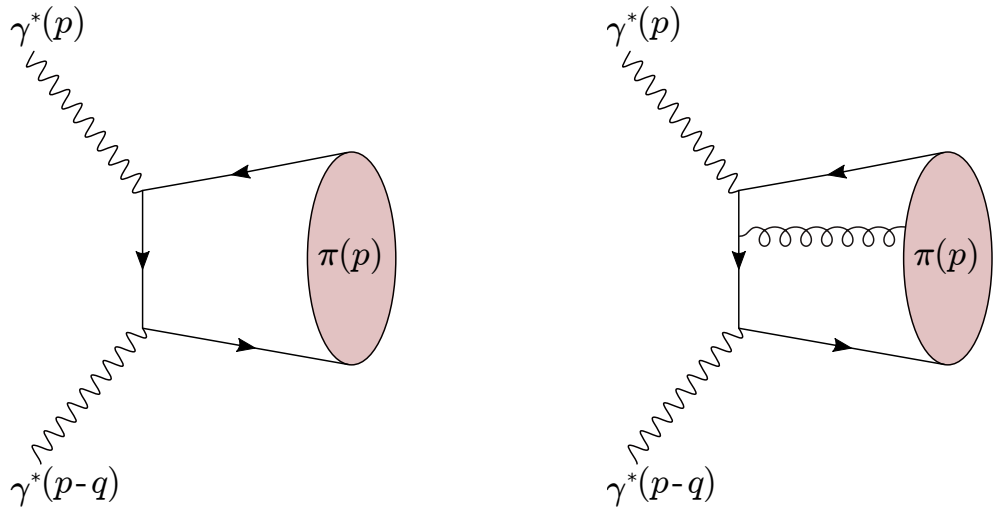

Figure 1.14: Diagrams for the fusion of two virtual photons into a neutral pion. On the left, first order in the twist expansion. On the right, corrections of twist-3.

when sandwiched between the bispinors, will reduce to one of the V^μ 4-vectors and mass factors of the external states thanks to the Dirac equations of B_i and B_f.

Then, for instance the vector form factors for the transition described above can be simply parametrized in the following way

$$\langle B_f(k)|\gamma^\mu|B_i(p)\rangle = \bar{u}_{B_f}(k)\left[\gamma^\mu F_1(q^2) + p^\mu F_2(q^2) + k^\mu F_3(q^2)\right] u_{B_i}(p)\,. \tag{1.86}$$

In the case of baryon form factors, there exist more than one parametrisation that is often used. For example in the case of the nucleon form factors one commonly used parametrisation can be found in many textbooks like Ref. [29], and in the case of $\Lambda_b \to \Lambda$ decays the most common parametrisation is given in Ref. [40]. As in the case of $B \to V$, one will prefer helicity based parametrisations like the one in Ref. [40], which will prove useful to project the amplitudes into states of given helicity.

In the case of a transition involving higher spin states, we will require the introduction of generalized Rarita-Schwinger (RS) spinor tensors [41] and new Lorentz invariant structures. For instance, one of the form factor parametrisation for decays of spin 1/2 baryons to spin 3/2 and spin 5/2 is given in [42]. The case of spin 3/2 baryons will be discussed in more detail in Chapter 5.

1.5.3 Distribution amplitudes

While meson decay constants are related to the probability of finding both valence quarks in the same space-time point, distribution amplitudes (DAs) are their generalisation in the case of non-local matrix elements. For light mesons, they are related to the probability of finding a set of partons with a given collinear momenta in an energetic meson (see Fig. 1.15). Since DAs are slightly more complicated objects, we will start by giving an example of a process in which they play a role, to then explain the framework where they appear, which is the light cone operator product expansion. We will closely follow Ref. [35].

Let us consider the process shown in Fig. 1.14, of a fusion of two virtual photons of four-momenta q and $(p-q)$ (where $q^2 < 0$ and $(p-q)^2 < 0$) into a neutral pion of four-momentum p

$$\gamma^*(q)\gamma^*(p-q) \to \pi^0(p)\,. \tag{1.87}$$

The amplitude for this process, which appears in the $e^+e^- \to \pi^0 e^+ e^-$ electromagnetic scattering, is given by

$$\mathcal{M}_{\mu\nu}(p,q) = \frac{4\pi\alpha_{\rm em}}{(p-q)^2 q^2} \times i \int d^4x e^{-iq\cdot x}\langle 0|T\{j^{\rm em}_\mu(x) j^{\rm em}_\nu(0)\}|\pi^0(p)\rangle\,, \tag{1.88}$$

where T is the time ordered product and $j^{\rm em}_\mu(x) = \sum_q Q_q \bar{q}(x)\gamma_\mu q(x)$ is the electromagnetic current. We will focus on the hadronic non-local matrix element

$$i \int d^4x e^{-iq\cdot x}\langle 0|T\{j^{\rm em}_\mu(x) j^{\rm em}_\nu(0)\}|\pi^0(p)\rangle\,. \tag{1.89}$$

The integral in Eq. (1.89) will be dominated by the regions where $q\cdot x \lesssim \mathcal{O}(1)$ and outside of this region fast oscillations will suppress the integrand. In the case of large (and different) photon virtualities, this region will

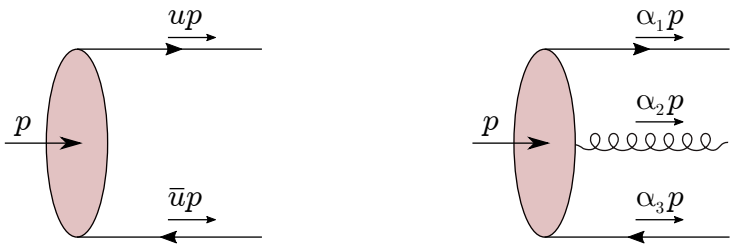

Figure 1.15: Schematics representing different meson distribution amplitudes. On the left, the twist-2 quark-antiquark DA, p is the momentum of the meson, and $0 < u < 1$ and $\bar{u} = 1 - u$ are the momentum fractions of each parton. On the right, the twist three quark-gluon-antiquark DA where in here the momentum is divided in 3 partons and the momentum fractions are such that $\sum_i \alpha_i = 1$ and $0 < \alpha_i < 1$.

correspond to the light-cone region $x^2 \sim 0$. This phenomenon is called light-cone dominance [43–46] and we will thus focus on the amplitudes of light-cone dominated processes. In these processes, we can neglect the transverse momenta of the partons and just consider their collinear components.

The phenomenon of light-cone dominance will allow us to construct an expansion of non-local matrix elements near the light-cone, called the *light-cone expansion*, in terms of hadron light-cone DAs. For instance, near the light-cone, the time ordered product in Eq. (1.89) can be expanded in

$$T\{j^{\text{em}}_\mu(x) j^{\text{em}}_\nu(0)\} = \sum_{t=t_{\min}}^{\infty} [\mathcal{C}_t(x)\mathcal{O}_t(x,0)]_{\mu\nu} \tag{1.90}$$

an infinite series of non local operators $\mathcal{O}_t(x,0)$ composed of the parton fields multiplied by a coefficient function $\mathcal{C}_t(x^2)$.[15] Due to large virtualities, the $\mathcal{C}_t(x^2)$ coefficients can be computed in terms of perturbative QCD and, due to the light cone dominance, the series is expected to be convergent. Its important to mention two differences that the light-cone OPE has with respect to a regular local OPE. First, the operators of the expansion are not local operators and second, the index t (i.e. the expansion order) is not simply the dimension of the operator as it is in a local operator, but rather its twist.

The twist (t) of an operator can be understood [16] as the difference between the dimension and spin of the operator $t = d - s$. In the light-cone expansion, twist determines the relevance of an operator, lower twist operators will be the most relevant operators.

The sandwiched bilocal operators $\langle 0|\mathcal{O}_t(x,0)|\pi^0(p)\rangle$ can be expressed through the light cone DAs. The light-cone DAs of a meson correspond to the Fourier Transform of the vacuum-to-meson matrix elements expanded on the light-cone (i.e. $x^2 \to 0$). For example, in the case of a pseudoscalar meson P ($q\bar{q}'$) and the $\gamma^\mu\gamma^5$ current, we can define the $\varphi_P(u)$ DA through the following relation

$$\langle 0|\bar{q}(x_1)\gamma^\mu\gamma^5[x_1,x_2]q'(x_2)|P(p)\rangle_{x^2\to 0} = -ip^\mu f_P \int_0^1 du\, e^{iu(p\cdot x_1)+i\bar{u}(p\cdot x_2)}\varphi_P(u)\,, \tag{1.91}$$

where $\bar{u} \equiv 1 - u$ and $x_{1,2} = \xi_{1,2}x$ being $\xi_{1,2}$ arbitrary numbers such that x_1 and x_2 are collinear.

The gauge link appearing in Eq. (1.91), which we will now omit for simplicity, is defined as

$$[x,y] = P\left\{\exp\left[i\int_0^1 du\,(x-y)_\mu \mathcal{A}^\mu(ux+(1-u)y)\right]\right\}\,, \tag{1.92}$$

where P is the path-ordering operation (see for example [29, 35]).

In the $x_1 = x_2 = 0$ limit the matrix element in Eq. (1.91) is reduced to the meson decay constant f_P, implying the following normalisation

$$\int_0^1 du\,\varphi_P(u) = 1\,. \tag{1.93}$$

This function $\varphi_P(u)$ is called the *twist-2 light-cone distribution amplitude* of the P meson. Twist-2 is the first order in the light-cone expansion and the only DA of twist-2 is the one given in Eq. (1.91).

[15] The Lorentz indices in Eq. (1.90) are on the parenthesis as they can distribute in between the operators and the coefficients which are not necessarily simple scalar coefficients.

[16] The full definition is slightly more complicated and the determination of the twist of an arbitrary operator is not straightforward in every case. A systematic light-cone expansion of the quark and gluon fields in the transverse and longitudinal components is needed (see Refs. [47, 48]).

The next order in the light-cone expansion is twist-3, where the quark-antiquark DAs (ϕ^p_{3P}, ϕ^σ_{3P}) are defined as it follows

$$\langle 0|\bar{q}(x_1)i\gamma^5 q'(x_2)|P(p)\rangle_{x^2\to 0} = f_P\mu_P \int_0^1 du\, e^{iu(p\cdot x_1)+i\bar{u}(p\cdot x_2)}\phi^p_{3P}(u)\,, \tag{1.94}$$

$$\begin{aligned}\langle 0|\bar{q}(x_1)\sigma^{\mu\nu}\gamma^5 q'(x_2)|P(p)\rangle_{x^2\to 0} = i\,[p^\mu(x_1-x_2)_\nu - p^\nu(x_1-x_2)_\mu] \\ \times \frac{f_P\mu_P}{6}\int_0^1 du\, e^{iu(p\cdot x_1)+i\bar{u}(p\cdot x_2)}\phi^\sigma_{3P}(u)\,,\end{aligned} \tag{1.95}$$

where

$$\mu_P = \frac{m_P^2}{m_q + m_{q'}}\,. \tag{1.96}$$

Starting from twist-3 multi-parton DAs can be defined, for instance, at twist 3 the first quark-gluon-antiquark DAs shown in Fig. 1.15 appears. At higher twist, one can systematically include more partons in the DAs. A detailed study on higher twist DAs for pseudoscalar mesons can be found in Ref. [49].

In the case of vector mesons we can in a similar way define the light-cone DAs which, like in the case of the vector decay constants, will take a slightly more complicated shape due to the spin structure (i.e. the presence of the polarition vector). Their definitions until twist-4 can be, for instance, found in Refs. [47, 48, 50, 51].

Light-cone distribution amplitudes have also been generalized to the case of baryons, more details can be found in Refs. [52, 53].

Going back to the simpler case, the twist-2 light-cone distribution amplitude $\varphi_P(u)$ is expected to have a scale dependence on the renormalisation scale μ. It turns out that $\varphi_P(u)$ does not have a simple multiplicative renormalisation with a correspondent anomalous dimension like the quark masses. Luckily, one can do a polynomial expansion of $\varphi_P(u)$ whose coefficients have a simple multiplicative renormalisation at the one-loop renormalisation level[17]. This polynomial expansion takes the following form

$$\varphi_P(u) = 6u\bar{u}\left[1 + \sum_n a_n^P(\mu)C_n^{3/2}(u-\bar{u})\right]\,, \tag{1.97}$$

where $C_n^{3/2}(u-\bar{u})$ are the *Gegenbauer polynomials* and $a_n^P(\mu)$ are the *Gegenbauer moments* of the DA. The one-loop running of the Gegenbauer moments is given by

$$a_n^P(\mu) = a_n^P(\mu_0)\left(\frac{\alpha_s(\mu)}{\alpha_s(\mu_0)}\right)^{\frac{\gamma_n}{\beta_0}} \tag{1.98}$$

where β_0 is defined in Eq. (1.56) and $\gamma_1 = \frac{32}{9}$, $\gamma_2 = \frac{50}{9}$ [35]. In the case of the pion only the even Gegenbauer moments are non vanishing due to the isospin symmetry, in which limit the following relation holds

$$\varphi_\pi(u) = \varphi_\pi(\bar{u})\,, \tag{1.99}$$

leading to a symmetric DA as opposed to the kaon DA, both shown in Fig. 1.16 following the determinations of Refs. [49, 55].

1.6 Non perturbative QCD methods

There are several methods used to treat QCD in the non-perturbative regime and to describe the bound states of quarks and gluons, which are the incoming and outgoing states of the theory at low energies. These methods can be used to compute the hadronic inputs discussed in the previous section and, in general, each of them works on specific kinematical regions.

1.6.1 Quark Models

Probably the first of these methods to be developed were the *Quark Models*[56–58]. These are phenomenological wave function models based mainly on quantum mechanics, which in general cannot be systematically derived from QCD, but they take some ingredients from QCD and/or data. Many different quark models exist, however they usually bear some common ingredients: a confining interaction like a harmonic oscillator potential , different

[17] This expansion is actually inspired by the conformal symmetry [54] in which this expansion always has a simple multiplicative renormalisation, remarkably this still holds for the one-loop renormalisation in QCD

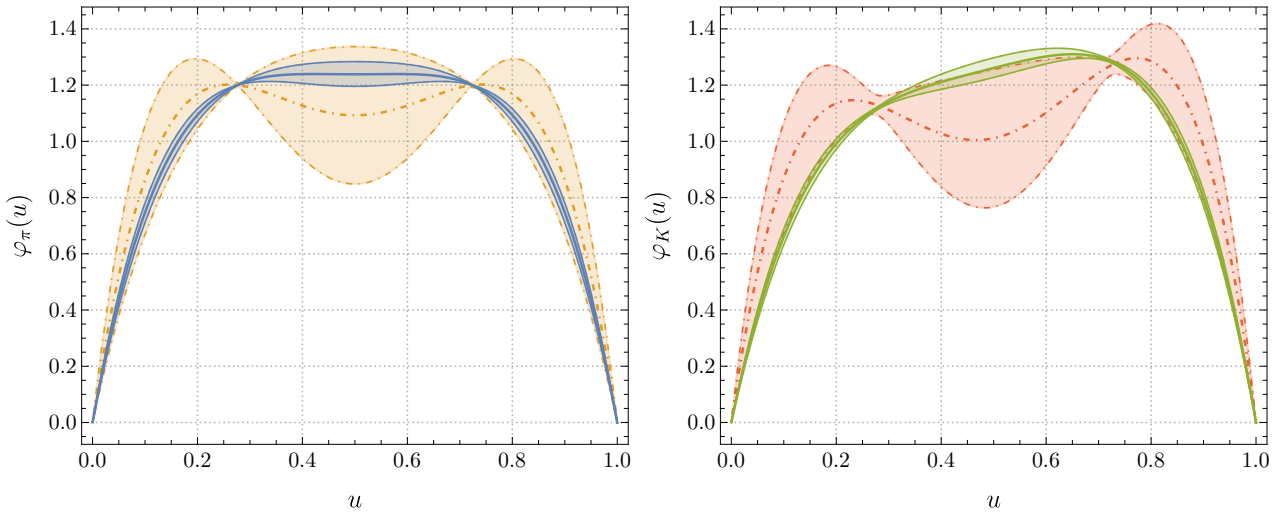

Figure 1.16: On the left (right) we show the twist-2 DA for the pion (kaon) at 2 GeV. The solid blue (green) line corresponds to the Lattice results from Ref. [55] and the dot-dashed orange (red) line corresponds to QCD sum rules results coming from Ref. [49].

types of spin-dependent interactions such as the hyperfine and spin-orbit interactions and of course the different quark masses. Usually the parameters of these elements are then fitted to either the experimental spectrum of hadron states. They have been mainly used to predict the hadron spectrum, however they can also be used to obtain hadronic quantities describing the meson dynamics such as form factors. Even though precision cannot be expected from them, they provide an overall understanding when no more precise option is available.

1.6.2 Lattice QCD

One of the most successful of the non-perturbative methods is Lattice QCD (LQCD) [59–62] which corresponds to a numerical evaluation of the path integral that defines QCD on a discrete finite volume Euclidean space-time lattice. The main limitation of LQCD, although not the only one, is the computational power needed to obtain precise results. Another limitation is the quantities that are accessible on the lattice; since we work on an Euclidean space-time, correlators need to be extrapolated to the Minkowskian region, which can sometimes prove impossible due to the analytic structure of the correlator.

The main applications of LQCD are the predictions of the hadron spectrum, the computation of the strong decay constant, quark masses, decay constants, bag parameters and form factors. Calculations of more complex correlators (i.e. involving multiple hadrons) are still facing computational limitations that might however be solved in the near future due to increasing computational power and conceptual limitations that may (or may not) be solved in the future.

In general, LQCD results come with two kinds of errors, a statistical error related to the use of Monte Carlo technique to perform the integration over the lattice, and a systematic error due to the continuum extrapolation, the infinite volume extrapolation and the use of "unphysical" quark masses. The first of these systematic errors is related to the *lattice spacing* (a) which sets the "granularity" of the discretisation and acts as a cut-off for the momenta ($1/a$). Physical results are obtained in the limit that the lattice spacing goes to zero, which is done trough a process of extrapolation. Discretisation errors are expected to be larger when large energy scales are involved. The second of these errors arises because LQCD calculations need to be carried out in finite volume "space-time-boxes". These are treated by performing calculations in multiple volumes and for large enough volumes are usually exponentially suppressed.

The last of these errors is related to the use of lower values for the quark masses (or equivalently the pion mass) since performing the lattice computations at physical masses is usually more resource consuming. However in the case of light quarks, due to the evolution of computational resources in the last decade, computations are often performed close to physical pion masses, reducing enough these kind of errors to make them sub-leading.

Computations on the lattice require also to carry out the renormalisation of the lattice QCD results (which is more complicated than in the continuum due to the breakdown of Lorentz-Poincaré symmetry). Another limitation is that of the accessible range : the size of the volume and the lattice spacing means that we cannot access all kinematic configurations. In general, we can only simulate "slow-moving" hadrons, leading typically to result in low-recoil configurations.

1.6.3 Sum Rules

Another highly successful non-perturbative technique, or rather family of techniques, are the sum rules based methods. These were first developed in Ref. [63], where they introduced the method of *QCD Sum Rules* often called SVZ Sum Rules for the names of their authors Shifman, Vainshtein and Zakharov. The basic principle for all Sum Rules is the same, first we construct a correlation function that we can extract in a given kinematic region, then we consider it in a different kinematic region where we can apply some sort of operator product expansion (OPE). Short- and long-distance interactions are separated, having a part computed in perturbative QCD and another part which is parametrised in terms of universal quantities, which are the vacuum condensates describing the non-perturbative structure of QCD vacuum. The two representations are then matched using a dispersion integral obtained thanks to the analytic structure of the correlator. This allows us to express non perturbative quantities in term of the OPE of the correlator which involve a simpler set of universal quantities (vacuum condensates).

Another version of these sum rules correspond to the *Light-Cone Sum Rules* (LCSR) [64–66]. The philosophy is similar to that of QCD sum rules, but it is applied in a different kinematic regime [18], corresponding to the case of an energetic meson in the final state. The non-perturbative quantities appearing are not vacuum condensates but light-cone wave functions of increasing twist, being more adapted to the kinematics of exclusive processes with large momentum transfer. Light-cone sum rules have been applied to many exclusive processes, and more recently to heavy-to-light meson processes, which will make them an important source of information for us.

1.6.4 Effective Theory methods

Another tool to tackle QCD in the non-perturbative regime is provided by Effective Field Theories of QCD. We will describe some of them in more detail in the last part of Chapter 2, but a few comments are in order here.

Theses approaches are not able to compute fully QCD matrix elements. However, they allow for a breakdown of the matrix elements into simpler non-perturbative blocks through a systematic expansion on small parameters. The simplified blocks will still require a "truly" non-perturbative treatment. However, important information of the relations in between different non-perturbative elements will be obtained from these theories.

The small expansion parameter, specific of each effective theory, and the theory itself will generally depend on the kinematics of the decays in question. For instance, one of these theories, which will be used to describe light hadrons at low energies, is *Chiral Perturbation Theory* (ChPT) [69]. It corresponds to an expansion around the chiral limit. The parameters of the expansion are quark masses and hadron momenta, in the region where they are small compared to the scale of chiral symmetry breaking.

Two theories that will be of used in the following are the Heavy quark effective theory (HQET) [70, 71] and the Soft collinear effective theory (SCET) [72–76]. We will discuss both of them in more detail in Section 2.5. The first one corresponds to an effective theory in the heavy quark limit (i.e. an expansion on $1/m_Q$), where gluon interactions are soft with respect to the heavy quark masses. It works well for heavy hadron decays in regions where the momentum transfer is large. The second one corresponds to an effective theory in which interactions are either soft (with respect to the fermion masses) or collinear to a preferred direction. It is also used in the context of heavy hadrons, but in regions in which the momentum transfer is small, since the parameter of expansion of the theory corresponds the inverse of it.

1.6.5 Comments

In this manuscript we will work in the context of heavy hadron decays and as a consequence of this and its kinematics we will mainly use results coming from LQCD, LCSR, HQET and SCET.

Due to the finite volume of the lattice form factors results will be more precise in the region where the momentum transfer is large, usually called low recoil regions as the final state hadron moves slowly away from the decaying hadron (see Fig. 2.5). Because of this, LQCD results will usually be complemented by other methods like LCSR (see Fig. 1.13), which provide precise results at the region of small momentum transfer, usually called large recoil region.

As we will see in the next chapter, HQET and SCET will relate different form factors up to corrections of a small parameter, in the low- and large-recoil regions respectively, providing a powerful cross-check of LQCD and Sum Rules results.

When none of these methods are available, we will turn to quark models.

[18] Sum rules can also be applied in other theories than QCD, which is the case of SCET sum rules [67, 68], in which the light-cone sum rules are written already in the framework of an effective theory of QCD called Soft-Collinear Effective Theory, which we describe in Section 2.5.2.

1.7 Summary

We started this chapter by introducing the Standard Model and discussing the breakdown of the electroweak symmetry. One of the consequences of the electroweak breaking is the mixing among different generations. We re-expressed electroweak interactions taking into account this mixing, and we discussed the status of flavour-changing currents in this context. In the case of charged currents, we discussed briefly the structure and impact of the generation-mixing matrices, focusing on the CKM quark-mixing matrix which is well constrained through various experimental tests. In the case of neutral currents, we saw that there is no mixing among generations in the Standard Model and that they are generated only at loop level. This indicates that both transitions are interesting tests of the SM. We then discussed the potential as NP probes and tests of the SM of these currents which will be at the center of the following chapters. We then discussed important details of QCD and the non perturbative elements of it, which will play an important role in the study of flavour changing currents. This indicates that flavour-changing transitions involving both quarks and leptons can provide a very interesting environment to test the SM, as they may be tested in various hadronic environments with a reasonable theoretical control of non-perturbative QCD effects. Moreover, the universality of couplings in the SM can be probed in particular through tests of Lepton Flavour Universality. In the following chapter, we will set the theoretical framework to study flavour changing currents in heavy hadron decays, which corresponds to the framework of effective field theories.

Chapter 2

Flavour Physics and its different energy scales

Throughout this manuscript we will study the weak decays of heavy hadrons. It is then important to understand the energy scales related to the process in hand will occur. The main two transitions that we will be studying are $b \to s\ell^+\ell^-$ and $b \to c\ell\bar{\nu}$. There are 3 different energy scales that are relevant for this kind of processes, which are represented in Fig. 2.1. First of all, the characteristic energy scale of the process in hand which will correspond to our renormalisation scale $\mu = m_b$. Secondly the Electroweak scale ($\mu_{\rm EW}$) which corresponds to the mass scale of the mediator of the interaction in play, the W boson. And lastly, the QCD scale ($\Lambda_{\rm QCD}$) at which hadronisation will occur and at which QCD becomes a non-perturbative theory. These energy scales are roughly of the following size

$$\mathcal{O}(\Lambda_{\rm QCD}) \sim 0.2\,\text{GeV}, \qquad \mathcal{O}(m_b) \sim 4\,\text{GeV}, \qquad \mathcal{O}(\mu_{\rm EW}) \sim 80\,\text{GeV}. \tag{2.1}$$

An extra high energy scale ($\Lambda_{\rm NP}$) can also be taken into account corresponding to the energy scale in which NP could appear and we will assume this scale to be higher than $\mu_{\rm EW}$ since direct searches at the LHC have not yet found new degrees of freedom pushing NP to 1 TeV or more (see Fig. 1.2). This defines an energy hierarchy

$$\Lambda_{\rm QCD} \ll m_b \ll \mu_{\rm EW} \ll \Lambda_{\rm NP} \tag{2.2}$$

that will allow us to separate/factorise the processes that are happening at each of these scales. One of the main reasons to require this factorisation is the the confinement of QCD, which cannot be treated perturbatively at low energies.Another important reason to factorise the processes, is the need to avoid large logarithms of the different scales in hand through the use of RGE improved perturbation theory. In order to do this we will work in the framework of effective field theories which will take advantage of of the natural energy hierarchy.

2.1 Effective Field Theories

Effective Field Theories (EFTs) are a fundamental tool in the study of multi-scale QFTs. Let us consider a QFT which has a high energy scale M (for instance the mass of a heavy field) which we want to describe at a lower energy scale E such that $E \ll M$. One can define a cut-off scale μ, such that $E \ll \mu < M$, which can be used to divide the fields into high energy modes and low energy modes. While low energy modes are the relevant external states at the energy scale E, the high energy modes do not propagate on long distances, they only appear as virtual particles and can be "removed" from the theory. This is done by performing the path integral over these modes, usually referred as "integrating them out" (A more detailed explanation of this procedure can be for instance found in Refs. [77, 78]). However, this leads to a theory which is non-local on scales $\Delta x^\mu \sim \frac{1}{M}$ because of the fluctuations of the high energy modes. Nonetheless, the resulting non-local theory can be expanded, in powers of $1/M$, into a theory of local operators $\mathcal{O}_i$, containing only the low-energy modes of the effective theory. This expansion is described by an effective Lagrangian

$$\mathcal{L}_{eff} = \sum_i \frac{1}{M^{d_i-4}} \mathcal{C}_i(\mu)\mathcal{O}_i(\mu)\,, \tag{2.3}$$

where each operator comes accompanied by a coefficient $\mathcal{C}_i$, coming from the short-distance dynamics that has been integrated out, usually referred as a Wilson coefficient and a power of M^{d_i-4} determined by the mass dimension of the operator $[\mathcal{O}_i] = d_i$ such that the Wilson coefficients are dimensionless. Thus, one can hope that

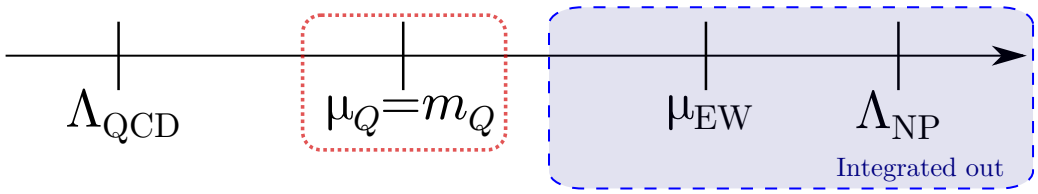

Figure 2.1: Different scales present in flavour physics.

the Wilson coefficients are of $\mathcal{O}(1)$. The theory described by Eq. (2.3) is independent of the value of the scale μ to be chosen. Due to quantum effects, the value of the Wilson coefficients depend logarithmically on μ and their dependence (encoded in anomalous dimensions) can be determined through RGE like in the case of QCD.

At low energy, the contribution of each operator $\mathcal{O}_i$ to an observable is expected to scale as

$$\left(\frac{E}{M}\right)^{d_i-4} = \begin{cases} \gg 1 & \text{if} \quad d_i < 4\,, \\ \mathcal{O}(1) & \text{if} \quad d_i = 4\,, \\ \ll 1 & \text{if} \quad d_i > 4\,, \end{cases} \tag{2.4}$$

hence, the relevance of the operator at low energies is determined by its dimension and a systematic expansion on $\frac{E}{M}$ can be performed by the truncating the series in Eq. (2.3) at a given operator dimension. At each dimension the number of operators is finite.

At this point, the EFT can be interpreted in two different approaches, a top-down and a bottom-up. In the first one, the full theory including the high energy modes is known and we can derive the value of the Wilson coefficients from the it, allowing us to treat low energy processes in a simpler theory. In the second one, the high energy modes of the full theory are unknown but its structure at low energies is fully determined at a given order in $\frac{E}{M}$ by the allowed local operators which include only the low energy modes and that respect the symmetries of the theory.

Different EFTs are interesting at different regions of Fig. 2.1

- When $\mu_{\rm EW} < \mu < \Lambda_{\rm NP}$, the adequate framework is the Standard Model Effective Field Theory (SMEFT) which is constructed with the fields of the Standard Model as "light" degrees of freedom and considers operators that preserve the symmetries of the SM[1].However, since we do not work in this framework, we will not go into any further details.

- When $m_b < \mu < \mu_{\rm EW}$, the appropriate EFT is the Weak Effective Theory (WET) that we will present in the following section. This EFT is used to describe the decays of heavy hadrons, and it is sometimes complemented by the SMEFT in order to connect different modes.

- When $\Lambda_{\rm QCD} < \mu < m_b$, EFTs of strongly interacting heavy quarks can be used, we will describe in Section 2.5.

This framework is often used also in the context of heavy hadron decays as it allows to connect different decay modes and can be of course matched to the WET. However, since we do not work in this framework, we will not go into any further details.

Other EFTs which profit of the large mass of heavy quarks will also have a place in the description of heavy hadron decays and will be thus discussed in the following section (Section 2.5).

2.2 WET: Weak Effective Theory

The best suited framework to describe heavy hadron weak decays at the scale $\mu = m_Q$ is the Weak Effective Theory (WET), also called the Weak Effective Hamiltonian (WEH) [28, 79]. Since the top quark and the $W^\pm$, Z and Higgs bosons are highly massive with respect to the hadron mass, i.e. $m_{\rm Had} \ll m_{W^\pm,Z,H,t}$ the heavy degrees of freedom related to them can be integrated out and reduced to two sets of scale dependents objects: a set of local effective operators $\mathcal{O}_i(\mu)$ and a set of Wilson coefficients $\mathcal{C}_i(\mu)$ as shown diagrammatically in Fig. 2.2 in the case of Fermi Theory.

This set of local operators can be classified by their dimension $d_i = [\mathcal{O}_i]$. We will restrict ourselves to the first order in the local operator expansion, thus we truncate this expansion at $d_i = 6$.

[1]One could of course expect to find NP particles that violate the symmetries of the SM. However, if new particles where to appear at an energy scale close to the EW scale and strongly violate these symmetries, hints of violations of these symmetries would have been already seen. In any case, an EFT of this kind needs to be accompanied by a search of violations of the SM symmetries.

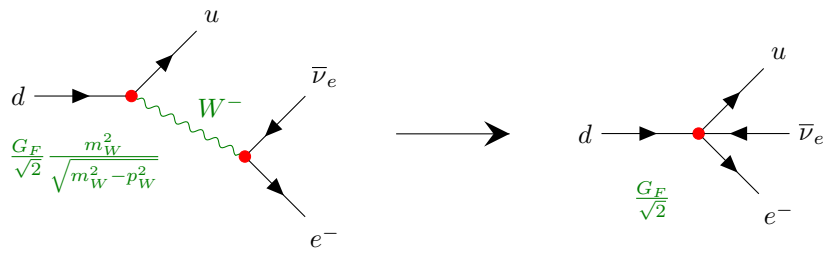

Figure 2.2: EW vs Fermi theory, the W boson does not propagate at the energies of interest. Then the W coupling and expansion of its propagator on $1/M_W$ leads to Fermi constant which acts as Wilson coefficient containing parameters of the underlying theory (couplings and mass).

This leads to the following effective hamiltonian[2]

$$\mathcal{H}_{\text{eff}} = \sum_i \mathcal{C}_i(\mu)\mathcal{O}_i(\mu)\,, \tag{2.5}$$

where the normalisation in Eq. (2.5) is arbitrary and can change depending on the convention and the process in hand, here it is absorbed in the $\mathcal{C}_i$ (making the Wilson coefficients dimensionful). However, the normalisation will in general contain G_F making the Wilson coefficients dimensionless and the relevant elements of the CKM matrix involved in the transition.

The arbitrary scale μ appearing in Eq. (2.5) plays two different roles in the effective theory. On one side, μ plays the role of a renormalisation scale, on the other side, the role of a factorisation scale to differentiate in between the low and high energy modes.

Then, for example, the amplitude for a transition between two states $A \to B$ at first order in the WET formalism will read

$$\mathcal{M}(A \to B) = \langle B|\mathcal{H}_{\text{eff}}|A\rangle = \sum_i \mathcal{C}_i(\mu)\langle B|\mathcal{O}_i|A\rangle(\mu)\,. \tag{2.6}$$

We can thus separate the computation of the amplitude on two parts: A first part related to, obtaining $\langle B|\mathcal{O}_i|A\rangle(\mu_Q)$ through non perturbative methods (cf. Sections 1.5 and 1.6), and a second one related to the computation of the Wilson coefficients $\mathcal{C}_i(\mu)$.

In decay processes A corresponds to a single-particle state, however B is a multi-particle state making slightly more complex to obtain $\langle B|\mathcal{O}_i|A\rangle(\mu_Q)$. We will usually face decays of a single hadron into multi-particle states composed either purely from hadrons or also containing leptons or photons. Often, one will perform an additional step of factorisation of the $\langle B|\mathcal{O}_i|A\rangle(\mu_Q)$ matrix element, in order to reduce it into the simple structures discussed in Section 1.5. This additional factorisation might prove challenging in some transitions like non-leptonic decays, or (up to now) impossible for final states containing many hadrons. We will discuss this further in Sections 2.6 and 2.8.

The computation of the Wilson coefficients is done in two steps: A first step of computing the Wilson coefficient at a high scale (μ_{EW}), and a second step of running the Wilson coefficient to a low scale (μ_b).

The first step is done through a process called matching, in which we will "match" the amplitudes in the full theory (SM) and the effective theory (WET).This process is at an arbitrary matching scale μ that we choose to be the electroweak scale μ_{EW} in order to avoid that logarithms of the form $\ln(M_W/\mu)$ become large. More precisely, the matching consist in computing the amplitudes for several processes, first in the full theory and then the effective theory and "choose" the value of the Wilson coefficients that make these amplitudes equal. The choice of processes is such that all Wilson coefficients are determined after the matching. Since the Wilson coefficients contain the short-distance dynamic, one can simply compute the "non-physical" amplitudes at the quark level to perform the matching. Typically, the exchange of a heavy particle of mass M with coupling g mediating the interaction represented at low energies by a four-fermion operator will have a typical contribution g^2/M^2 to the Wilson coefficient at the matching scale. This matching processes, initially performed at the tree level, can be systematically performed at higher loop orders. More details about the matching procedure in the WET can be found in Ref. [28].

The computation of the Wilson coefficients running is done through the renormalisation of the WET, which we will now discuss.

[2]The convention to use an effective Hamiltonian instead of an effective Lagrangian ($\mathcal{L}_{\text{eff}} = -\mathcal{H}_{\text{eff}}$) is purely historical.

2.2.1 Renormalisation of the WET

The renormalisation of the effective theory has many similarities to the renormalisation of QCD, but some new aspects that were not discussed in Section 1.4 appear, namely the mixing in between different operators through running.

In order to discuss this, let us look at the renormalisation group evolution of a complete set [3] of n local operators $\{\mathcal{O}_i\}_{i=1,\dots,n}$. Due to the renormalisation scale invariance of the amplitudes

$$\frac{d\mathcal{M}}{d\ln\mu} = \frac{d}{d\ln\mu}\sum_i \mathcal{C}_i(\mu)\,\langle\mathcal{O}_i(\mu)\rangle = 0\,. \tag{2.7}$$

The running of the operators

$$\frac{d}{d\ln\mu}\,\langle\mathcal{O}_i(\mu)\rangle = -\sum_j \gamma_{ij}(\mu)\,\langle\mathcal{O}_j(\mu)\rangle\ , \quad i=1,\dots,n\,, \tag{2.8}$$

is given by the *anomalous dimension matrix* $\gamma_{ij}(\mu)$, which is obtained from the coefficient of the $1/\epsilon$ pole term in the renormalisation factors of the local operators (see for example Refs. [28, 30, 80]). Reexpressing Eq. (2.8) in matrix form

$$\frac{d}{d\ln\mu}\,\langle\boldsymbol{\mathcal{O}}(\mu)\rangle = -\gamma(\mu)\,\langle\boldsymbol{\mathcal{O}}(\mu)\rangle\ , \tag{2.9}$$

we obtain the following relation

$$\frac{d}{d\ln\mu}\boldsymbol{\mathcal{C}}(\mu) = \gamma^T(\mu)\boldsymbol{\mathcal{C}}(\mu)\,, \tag{2.10}$$

for the Wilson coefficients. This implies that if γ is not a diagonal matrix, which is in general the case, there will be a mixing in between different operators. Then, for instance, a Wilson coefficient that vanishes at a certain scale, can get a non-vanishing value at a different scale.

The general solution to Eq. (2.10) can be found in Ref. [80] and, at leading order, we obtain a

$$\boldsymbol{\mathcal{C}}(\mu) \approx \exp\left[-\frac{\gamma_0^T}{2\beta_0}\ln\frac{\alpha_s(\mu)}{\alpha_s(\mu_{\rm EW})}\right]\boldsymbol{\mathcal{C}}(\mu_{\rm EW}) \tag{2.11}$$

which, for the simple case of a single operator $\mathcal{O}$, takes the same form as the quark mass running in Eq. (1.62), and can be thus written as

$$\mathcal{C}(\mu) \approx \left(\frac{\alpha_s(\mu)}{\alpha_s(\mu_{\rm EW})}\right)^{-\frac{\gamma_0}{2\beta_0}}\mathcal{C}(\mu_{\rm EW})\,. \tag{2.12}$$

The decision of working in an effective field theory at the characteristic scale μ and performing the matching at a high scale $\mu_{\rm EW}$ rather than working directly at the electroweak scale or the low scale is justified in a similar way to the choice of renormalisation scale in QCD. Any of these two choice will generate large logarithms that would not be accounted for.

This can be seen explicitly by replacing $\frac{\alpha_s(\mu)}{\alpha_s(\mu_{\rm EW})}$ in Eq. (2.12) by the leading-log expression given in Eq. (1.56)

$$\mathcal{C}(\alpha_s(\mu)) \approx \left(1+\frac{\alpha_s(\mu)}{4\pi}\beta_0\ln\frac{\mu_{\rm EW}^2}{\mu^2}\right)^{-\frac{\gamma_0}{2\beta_0}}\mathcal{C}(\alpha_s(\mu_{\rm EW}))\,. \tag{2.13}$$

and then expanding this expression

$$\mathcal{C}(\alpha_s(\mu)) \approx \left(1-\frac{\gamma_0}{2}\frac{\alpha_s(\mu)}{4\pi}\ln\frac{\mu_{\rm EW}^2}{\mu^2}+\frac{\gamma_0(\gamma_0+2\beta)}{8}\left(\frac{\alpha_s(\mu)}{4\pi}\ln\frac{\mu_{\rm EW}^2}{\mu^2}\right)^2+\dots\right)\mathcal{C}(\alpha_s(\mu_{\rm EW}))\,. \tag{2.14}$$

If one were to perform the NLO matching at the low scale μ, only the first two terms Eq. (2.14) will be taken into account, and all the other terms (which as discussed in the previous chapter are $\mathcal{O}(1)$) would be neglected. Fortunately, performing the matching at high-scale plus the leading order RGE allows for the resummation of leading logarithms to all orders , as explicitly shown in Eq. (2.14).

It is maybe important to mention one small detail regarding the running of the effective theory. When discussing the running above, we assumed that the scale μ was somewhere in between the electroweak scale $\mu_{\rm EW}$ and the mass of the b-quark m_b. However, one might want to consider processes in which the characteristic

[3] Here, by complete we mean that the running does not produce mixing with operators external to the set. For instance, this is the case of operators of the same dimension, for which dimensional regularization ensures independent runnings between different dimension operators [80].

energy is below m_b, like in the case of c-meson and light meson decays. This will require an intermediate step when changing the number of active flavours N_f, or in other words when crossing one of the quark masses. For instance, for values of $\mu \sim m_c$ we have $N_f = 4$ (i.e. the u, d, s and c quarks) and the relevant effective theory will have the b-quark integrated out. This will then also require a matching of both theories at the quark mass creating a series of WET with different number of active quark flavours.

2.2.2 Extending the Weak Effective Hamiltonian to NP

One of the benefits of the EFT framework is how easily NP contributions can be taken into consideration. As discussed at the beginning of the chapter, if one considers NP appearing at a scale higher than the EFT's matching scale, NP particles do not appear as external states in the EFT and they "do not propagate" (i.e. their interactions can be approximated through local operators). This means that they can be integrated out together with the rest of the full theory and expanded in a tower of local operators. Then NP can be taken into account in a model-independent way by adding a NP contribution to each Wilson coefficient. However, this is only valid when the NP in hand generates the same long-distance structures present in the SM. In order to include all possible NP contributions, one needs to add all the allowed operators at a given dimension which have the "low energy" SM fields as external states. In general, we will thus extend the Hamiltonian in Eq. (2.5) into

$$\mathcal{H}_{\text{eff}} = \sum_{i \in I} \mathcal{C}_i(\mu)\mathcal{O}_i(\mu) + \sum_{j \in J} \mathcal{C}_j^{\text{NP}}(\mu)\mathcal{O}_j^{\text{NP}}(\mu)\,, \tag{2.15}$$

where the set I corresponds to the indices of the local operators to which have SM-like structures and the set J corresponds to the indices of the EFT operators which appear purely through NP operators. The Wilson coefficients $\mathcal{C}_i$ = in the first set of operators is composed by both a SM and NP contributions such that $\mathcal{C}_i = \mathcal{C}_i^{\text{SM}} + \mathcal{C}_i^{\text{NP}}$.

Low-energy experiments will allow us to constrain the Wilson coefficients at the low scale. In general, one can run these constraints up to a high scale of New Physics and determine in this way the potential models that could match these constraints. If the NP contributions to Wilson coefficients are due to the exchange of a particle, the contributions read typically as $g_{\text{NP}}^2/\Lambda_{\text{NP}}^2$. Depending on the assumptions made on the size of the NP couplings (of order 1, suppressed or proportional to SM couplings due to symmetry arguments), this allows one to determine the typical mass scale of the (lightest) NP heavy degrees of freedom contributing to the Wilson coefficients.

This has been done for neutral-meson mixing [81] and can be done for other processes. In the following, we will illustrate this for $b \to c\ell\bar{\nu}$ and $b \to s\ell^+\ell^-$ processes.

2.3 $\Delta B = 1$, $\Delta C = 1$ WET for the $b \to c\ell\bar{\nu}$ transition

Assuming that there are no light right-handed neutrinos, the effective Hamiltonian for the $b \to c\ell\bar{\nu}$ transition takes the following form:

$$\begin{aligned} H_{\text{eff}} = \sqrt{2}G_F V_{cb} \big[&(1+g_V)(\bar{c}\gamma_\mu b)(\bar{\ell}_L\gamma^\mu\nu_L) + (-1+g_A)(\bar{c}\gamma_\mu\gamma_5 b)(\bar{\ell}_L\gamma^\mu\nu_L) \\ &+ g_S(\bar{c}b)(\bar{\ell}_R\nu_L) + g_P(\bar{c}\gamma_5 b)(\bar{\ell}_R\nu_L) \\ &+ g_T(\bar{c}\sigma_{\mu\nu}b)(\bar{\ell}_R\sigma^{\mu\nu}\nu_L) + g_{T5}(\bar{c}\sigma_{\mu\nu}\gamma_5 b)(\bar{\ell}_R\sigma^{\mu\nu}\nu_L)\big] + \text{h.c.} \end{aligned} \tag{2.16}$$

One may also use the equivalent notation of Refs. [82, 83]

$$\begin{aligned} H_{\text{eff}} = 4\frac{G_F}{\sqrt{2}}V_{cb} \big[&(1+g_{V_L})(\bar{c}_L\gamma_\mu b_L)(\bar{\ell}_L\gamma^\mu\nu_L) + g_{V_R}(\bar{c}_R\gamma_\mu b_R)(\bar{\ell}_L\gamma^\mu\nu_L) \\ &+ g_{S_L}(\bar{c}_R b_L)(\bar{\ell}_R\nu_L) + g_{S_R}(\bar{c}_L b_R)(\bar{\ell}_R\nu_L) + g_{T_L}(\bar{c}_R\sigma_{\mu\nu}b_L)(\bar{\ell}_R\sigma^{\mu\nu}\nu_L)\big] + \text{h.c.} \end{aligned} \tag{2.17}$$

with the corresponding effective coefficients

$$g_{V,\,A} = g_{V_R} \pm g_{V_L}\,, \qquad g_{S,\,P} = g_{S_R} \pm g_{S_L}\,, \qquad g_T = -g_{T5} = g_{T_L}\,. \tag{2.18}$$

The SM tree level contribution (Fermi Theory) is recovered by taking all the effective coefficients $g_{V,\,A,\,S,\,P,\,T,\,T5}$ to 0. Up to electroweak corrections, the renormalisation of the operators in Eqs. (2.16) and (2.17) can be found in Ref. [84].

2.4 $\Delta B = 1$, $\Delta S = 1$ WET for $b \to s$ transitions

When applying the EFT formalism described before to $b \to s$ transitions the WET takes the following form:[4]

$$\mathcal{H}_{\text{eff}} = \frac{4G_F}{\sqrt{2}}\Bigg[\lambda_c^{(s)}(\mathcal{C}_1^c(\mu)\mathcal{O}_1^c + \mathcal{C}_2^c(\mu)\mathcal{O}_2^c) + \lambda_u^{(s)}(\mathcal{C}_1^u(\mu)\mathcal{O}_1^u + \mathcal{C}_2^u(\mu)\mathcal{O}_2^u) - \lambda_t^{(s)}\sum_{i\in I}\mathcal{C}_i(\mu)\mathcal{O}_i\Bigg], \tag{2.19}$$

where $\lambda_q^{(s)} = V_{qb}V_{qs}^*$ as defined in Eq. (1.42) and $I = \{3, 4, 5, 6, 7, 8, 9, 10, 7\gamma, 8g, 9\ell, 10\ell\}$. The local operators present in the SM , which come from the non local high energy structures shown in Fig. 2.3, are the following:

Current-Current operators:

$$\mathcal{O}_1^q = [\bar{q}_\alpha P_L b_\beta][\bar{s}_\beta P_L q_\alpha] \tag{2.20}$$
$$\mathcal{O}_2^q = [\bar{q}_\alpha P_L b_\alpha][\bar{s}_\beta P_L q_\beta]\,, \tag{2.21}$$

QCD Penguins:

$$\mathcal{O}_3 = [\bar{s}_\alpha P_L b_\alpha]\sum_{\substack{q=u,d,\\ s,c,b}}[\bar{q}_\beta P_L q_\beta]\,, \tag{2.22}$$
$$\mathcal{O}_4 = [\bar{s}_\alpha P_L b_\beta]\sum_{\substack{q=u,d,\\ s,c,b}}[\bar{q}_\beta P_L q_\alpha]\,, \tag{2.23}$$
$$\mathcal{O}_5 = [\bar{s}_\alpha P_L b_\alpha]\sum_{\substack{q=u,d,\\ s,c,b}}[\bar{q}_\beta P_R q_\beta]\,, \tag{2.24}$$
$$\mathcal{O}_6 = [\bar{s}_\alpha P_L b_\beta]\sum_{\substack{q=u,d,\\ s,c,b}}[\bar{q}_\beta P_R q_\alpha]\,, \tag{2.25}$$

EW Penguins:

$$\mathcal{O}_7 = \frac{3}{2}[\bar{s}_\alpha P_L b_\alpha]\sum_{\substack{q=u,d,\\ s,c,b}}e_q[\bar{q}_\beta P_R q_\beta]\,, \tag{2.26}$$
$$\mathcal{O}_8 = \frac{3}{2}[\bar{s}_\alpha P_L b_\beta]\sum_{\substack{q=u,d,\\ s,c,b}}e_q[\bar{q}_\beta P_R q_\alpha]\,, \tag{2.27}$$
$$\mathcal{O}_9 = \frac{3}{2}[\bar{s}_\alpha P_L b_\alpha]\sum_{\substack{q=u,d,\\ s,c,b}}e_q[\bar{q}_\beta P_L q_\beta]\,, \tag{2.28}$$
$$\mathcal{O}_{10} = \frac{3}{2}[\bar{s}_\alpha P_L b_\beta]\sum_{\substack{q=u,d,\\ s,c,b}}e_q[\bar{q}_\beta P_L q_\alpha]\,, \tag{2.29}$$

Electromagnetic dipole and chromomagnetic penguin operators:

$$\mathcal{O}_{7\gamma} = \frac{e}{16\pi^2}m_b[\bar{s}_\alpha\sigma^{\mu\nu}P_R b_\alpha]F_{\mu\nu}\,, \tag{2.30}$$
$$\mathcal{O}_{8g} = \frac{g}{16\pi^2}m_b[\bar{s}_\alpha\sigma^{\mu\nu}P_R T^a_{\alpha\beta}b_\beta]G^a_{\mu\nu}\,, \tag{2.31}$$

[4] In several references[28, 30], the normalisation does not include the factor 4 in the numerator, this is compensated by the preference for the left and right handed projectors $P_{L,R}$ defined in Eq. (2.34) instead of the $V \pm A$ structures, i.e. $1 \pm \gamma_5$, in the definition of the Wilson operators. Then the normalisation of the Wilson coefficients is the same.

SM Wilson Coefficients (at $\mu = 4.8$ GeV)									
$\mathcal{C}_1$	$\mathcal{C}_2$	$\mathcal{C}_3$	$\mathcal{C}_4$	$\mathcal{C}_5$	$\mathcal{C}_6$	$\mathcal{C}_{7\gamma}^{\text{eff}}$	$\mathcal{C}_{8g}^{\text{eff}}$	$\mathcal{C}_{9\ell}$	$\mathcal{C}_{10\ell}$
−0.2632	1.0111	−0.0055	−0.0806	0.0004	0.0009	−0.2923	−0.1663	4.0749	−4.3085

Table 2.1: Values for the SM Wilson Coefficients at NNLO coming from Ref. [87]. In the case of the electromagnetic dipole and the chromomagnetic penguin operators we give the value of the effective Wilson coefficients $\mathcal{C}_{7\gamma,8g}^{\text{eff}}$ discussed in Section 2.7. The value for both $\mathcal{C}_{1,2}^{c}$ and $\mathcal{C}_{1,2}^{u}$ is the same in the SM so we omit the index c and u. The values for the EW penguin operators can be found in Table 10.A.1 at NLO.

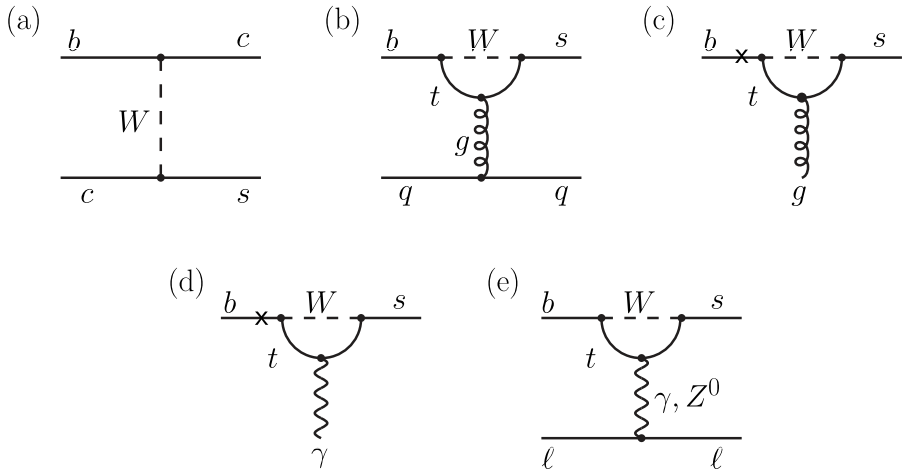

Figure 2.3: SM diagrams contributing to $b \to s$ transitions. Adapted from Ref. [88].

Semileptonic operators:

$$\mathcal{O}_{9\ell} = \frac{e^2}{16\pi^2}[\bar{s}_\alpha \gamma_\mu P_L b_\alpha][\bar{\ell}\gamma^\mu \ell]\,, \tag{2.32}$$

$$\mathcal{O}_{10\ell} = \frac{e^2}{16\pi^2}[\bar{s}_\alpha \gamma_\mu P_L b_\alpha][\bar{\ell}\gamma^\mu \gamma_5 \ell]\,, \tag{2.33}$$

where

$$P_{L,R} = (1 \mp \gamma_5)/2 \tag{2.34}$$

and $m_b \equiv \overline{m}_b(\overline{m}_b)$ denotes the running b quark mass in the $\overline{\text{MS}}$ scheme.

In the SM, regarding the 4-quark operators, $\mathcal{C}_2^c = \mathcal{C}_2^u$ is the largest coefficient and it corresponds to the colour-allowed tree-level contribution from the W exchange, whereas $\mathcal{C}_1^c = \mathcal{C}_1^u$ is colour suppressed. QCD-penguin operators are numerically suppressed, and the electroweak operators even more so.

A similar weak effective theory can be written for the $b \to d$ transition by performing the trivial replacement $s \to d$. Neglecting the difference of mass between the d and s quarks, the SM values of the Wilson coefficients are identical in both cases. Whenever the distinction is necessary, we will add a d or s subscript in the operators and Wilson coefficients.

We work in the naive dimensional regularisation (NDR) and $\overline{\text{MS}}$ schemes, for which the parameters of the running of the operators of the WET (i.e. the anomalous dimension matrix and the evolution matrix) can be found in Refs. [28, 30] and electroweak corrections to them can be found in Refs. [85, 86]. The values for the SM Wilson coefficients can be found in Table 2.1.

NP contributions could either modify the value of the short-distance Wilson coefficients $\mathcal{C}_i$, or make other operators contribute in a significant manner, such as the chirality-flipped operators O_i' or other operators (scalar, pseudoscalar, tensor). Since the list of NP operators that can affect any $b \to s$ transition is quite long, we will only present the ones relevant for the transitions that we will discuss in the following chapters.

2.4.1 NP in semileptonic and radiative $b \to s$ decays

When working on either radiative or semi-leptonic decays we generally neglect small corrections proportional to $\lambda_u^{(s)}$ in the SM [5], since they are strongly CKM suppressed as discussed in Section 1.3 as well as EW penguins

[5] This corresponds to doing the replacement $\lambda_c^{(s)}\mathcal{O}_i^c \to -\lambda_t^{(s)}\mathcal{O}_i^c = (\lambda_c^{(s)} + \lambda_u^{(s)})\mathcal{O}_i^c$ and $\lambda_u^{(s)}\mathcal{O}_i^u \to 0$ to Eq. (2.19).

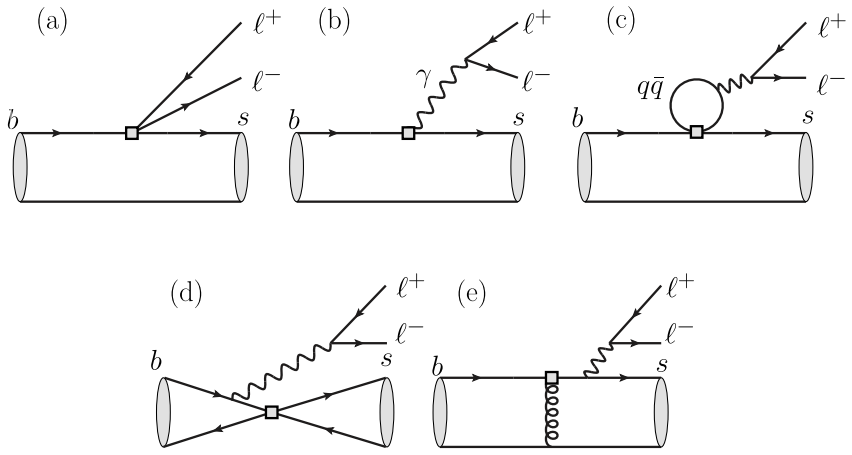

Figure 2.4: Diagrams of the Weak Effective Theory contributions to $b \to s\ell^+\ell^-$. These diagrams are obtained through contractions of the diagrams in Fig. 2.3. Adapted from Ref. [88].

which have small Wilson coefficients. We will also consider NP structures not present in the SM. Then the effective Hamiltonian will take the following form:

$$\mathcal{H}_{\text{eff}} = -\frac{4G_F}{\sqrt{2}}\lambda_t^{(s)} \sum_{i\in I} \mathcal{C}_i(\mu)\mathcal{O}_i, \tag{2.35}$$

Where $I = \{1c, 2c, 3, 4, 5, 6, 7^{(\prime)}\gamma, 8g, 9^{(\prime)}\ell, 10^{(\prime)}\ell, S^{(\prime)}\ell, P^{(\prime)}\ell, T^{(\prime)}\ell\}$ and $i = 1c(2c)$ refers to $\mathcal{O}^c_{1(2)}$. The main diagrams contributing to the $b \to s\ell^+\ell^-$ transition are shown in Fig. 2.4. The Scalar, Pseudoscalar, Tensor and Chirally flipped SM operators are defined in the following way:

Chirally flipped SM operators:

$$\mathcal{O}_{7'\gamma} = \frac{e}{16\pi^2} m_b [\bar{s}_\alpha \sigma^{\mu\nu} P_L b_\alpha] F_{\mu\nu}\,, \tag{2.36}$$

$$\mathcal{O}_{9'\ell} = \frac{e^2}{16\pi^2} [\bar{s}_\alpha \gamma_\mu P_R b_\alpha][\bar{\ell}\gamma^\mu \ell]\,, \tag{2.37}$$

$$\mathcal{O}_{10'\ell} = \frac{e^2}{16\pi^2} [\bar{s}_\alpha \gamma_\mu P_R b_\alpha][\bar{\ell}\gamma^\mu \gamma_5 \ell]\,, \tag{2.38}$$

Tensor and (Pseudo)Scalar Semileptonic operators:

$$\mathcal{O}_{S^{(\prime)}\ell} = \frac{e^2}{16\pi^2} [\bar{s}_\alpha P_{R(L)} b_\alpha][\bar{\ell}\ell]\,, \tag{2.39}$$

$$\mathcal{O}_{P^{(\prime)}\ell} = \frac{e^2}{16\pi^2} [\bar{s}_\alpha P_{R(L)} b_\alpha][\bar{\ell}\gamma_5 \ell], \tag{2.40}$$

$$\mathcal{O}_{T^{(\prime)}\ell} = \frac{e^2}{16\pi^2} [\bar{s}_\alpha \sigma_{\mu\nu} P_{R(L)} b_\alpha][\bar{\ell}\sigma^{\mu\nu} \ell], \tag{2.41}$$

Since for semileptonic decays we do not consider the electroweak penguin operators $\mathcal{O}_{7-10}$ we will often omit the index γ in the radiative operator and the index ℓ in semileptonic operators. However, the ℓ index will only be omitted if the context is clear enough to determine whether we consider a generic lepton or a specific case like $\ell = \mu$.

2.4.2 NP in non-leptonic $b \to s$ decays

In the case of non-leptonic decays, we will consider only NP entering the Wilson coefficients associated with the SM operators $\mathcal{O}_i$ or the chirally-flipped ones $\tilde{\mathcal{O}}_i$ as defined in Ref. [89] by exchanging P_L and P_R in the all quark bilinears constituting the operators.

Chirally flipped Current-Current operators:

$$\tilde{\mathcal{O}}_1^q = [\bar{q}_\alpha P_R b_\beta][\bar{s}_\beta P_R q_\alpha] \tag{2.42}$$

$$\tilde{\mathcal{O}}_2^q = [\bar{q}_\alpha P_R b_\alpha][\bar{s}_\beta P_R q_\beta]\,, \tag{2.43}$$

Chirally flipped QCD Penguins:

$$\tilde{\mathcal{O}}_3 = [\bar{s}_\alpha P_R b_\alpha] \sum_{\substack{q=u,d,\\ s,c,b}} [\bar{q}_\beta P_R q_\beta]\,, \tag{2.44}$$

$$\tilde{\mathcal{O}}_4 = [\bar{s}_\alpha P_R b_\beta] \sum_{\substack{q=u,d,\\ s,c,b}} [\bar{q}_\beta P_R q_\alpha]\,, \tag{2.45}$$

$$\tilde{\mathcal{O}}_5 = [\bar{s}_\alpha P_R b_\alpha] \sum_{\substack{q=u,d,\\ s,c,b}} [\bar{q}_\beta P_L q_\beta]\,, \tag{2.46}$$

$$\tilde{\mathcal{O}}_6 = [\bar{s}_\alpha P_R b_\beta] \sum_{\substack{q=u,d,\\ s,c,b}} [\bar{q}_\beta P_L q_\alpha]\,, \tag{2.47}$$

Chirally flipped EW Penguins:

$$\tilde{\mathcal{O}}_7 = \frac{3}{2}[\bar{s}_\alpha P_R b_\alpha] \sum_{\substack{q=u,d,\\ s,c,b}} e_q[\bar{q}_\beta P_L q_\beta]\,, \tag{2.48}$$

$$\tilde{\mathcal{O}}_8 = \frac{3}{2}[\bar{s}_\alpha P_R b_\beta] \sum_{\substack{q=u,d,\\ s,c,b}} e_q[\bar{q}_\beta P_L q_\alpha]\,, \tag{2.49}$$

$$\tilde{\mathcal{O}}_9 = \frac{3}{2}[\bar{s}_\alpha P_R b_\alpha] \sum_{\substack{q=u,d,\\ s,c,b}} e_q[\bar{q}_\beta P_R q_\beta]\,, \tag{2.50}$$

$$\tilde{\mathcal{O}}_{10} = \frac{3}{2}[\bar{s}_\alpha P_R b_\beta] \sum_{\substack{q=u,d,\\ s,c,b}} e_q[\bar{q}_\beta P_R q_\alpha]\,, \tag{2.51}$$

Chirally flipped Chromomagnetic Penguin:

$$\tilde{\mathcal{O}}_{8g} = \frac{g}{16\pi^2} m_b[\bar{s}_\alpha \sigma^{\mu\nu} P_L T^a_{\alpha\beta} b_\beta] G^a_{\mu\nu}\,, \tag{2.52}$$

2.5 Effective theories of QCD in the Heavy Quark Limit

In the previous sections we made use of the energy hierarchy shown in Fig. 2.1 in order to write an effective theory for Weak Hadron Decays. However, there is still a part of this energy hierarchy that we have not used. In the case of heavy-quark systems, the hierarchy $m_Q \gg \Lambda_{\text{QCD}}$ provides another natural separation scale. On one hand, heavy hadrons are composed of a heavy quark of mass m_Q, on the other hand, the hadronisation process occur at scales around Λ_{QCD}.

This will allow us to perform an expansion on $\frac{1}{m_Q}$ which at its first order will correspond to the *Heavy Quark Limit* ($m_Q \to \infty$) However, the separation of scales is slightly less trivial than before. Since the heavy quark is an external state of the decays that we are interested in, we cannot simply integrate it out. Nonetheless, not all of the degrees of freedom of the heavy quark are relevant in these decays. In fact, we can actually separate the heavy quark into its hard and soft degrees of freedom and integrate out the former together with the hard gluons. These procedure can be done in two different kinematical regimes schematically shown in Fig. 2.5.

The first one, corresponds to processes where all incoming and outgoing particles have limited energy. In this case all of the degrees of freedom of the process (other than the heavy quark) are soft. For example, in the case of semileptonic heavy hadron decays, this corresponds to the situation where the hadronic decay products are not boosted with respect to the heavy hadron (low-recoil of the emitted hadron), which is consistent with the zone of high lepton invariant mass ($q^2 \approx q^2_{\text{max}}$). In this regime we can construct an effective theory of soft interactions of the heavy quark called Heavy Quark Effective Theory (HQET).

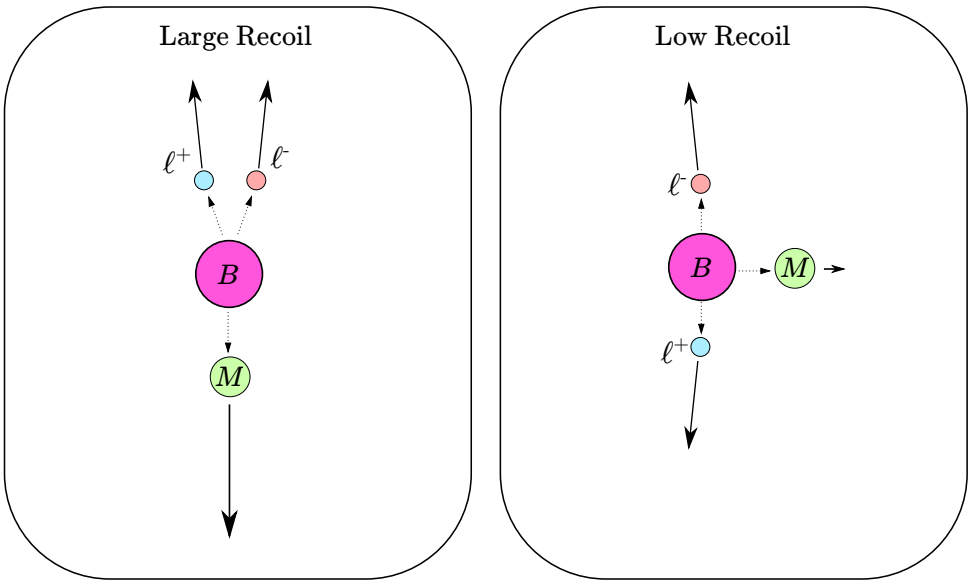

Figure 2.5: Schematical view of a semileptonic B-meson decay in two different kinematical regimes, the large and low recoil limits. In the first one (left) the emmited hadron is highly energetic in the B-meson rest frame, in the second one (right) the emmited hadron is almost at rest in the B-meson rest frame.

The second regime, corresponds to processes where all incoming and outgoing particles are either soft or very energetic (i.e. they have almost light-like 4-momenta). In this case, not only soft degrees of freedoms are present but also collinear degrees of freedom. Giving the same example as above, this corresponds to the situation when the hadronic decay products are highly boosted with respect to the heavy hadron (large-recoil of the emitted hadron), which is consistent with the zone of low lepton invariant mass ($q^2 \approx 0$). In this second regime we can construct an effective theory of soft and collinear interactions of the heavy quark called Soft Collinear Effective Theory (SCET).

In both of these frameworks it will be important to have a clear distinction or treatment of heavy and light quarks. Light quarks will correspond to the quarks whose mass vanishes in the heavy quark limit and heavy quarks to the ones whose masses are taken to infinity. In order to make a distinction in between different heavy quarks, in the Heavy Quark limit, the ratio of masses of two heavy quarks will stay fixed (in practice m_c/m_b stays fixed when the charm quark is treated as heavy).

2.5.1 Heavy Quark Effective Theory

We start by considering a heavy hadron of momentum p_H and mass m_H which contains a heavy quark interacting through soft gluons with a soft light-quark. Since a softly interacting heavy quark is nearly on-shell its momentum can be decomposed in the following way

$$p_Q^\mu = m_Q v^\mu + k^\mu \tag{2.53}$$

where v is the 4-velocity of the heavy hadron $v = \frac{p_H}{m_H}$ ($v^2 = 1$) and $k \ll m_Q v$ is the residual momentum of the heavy quark [6]. Changes on the residual momentum, resulting from the soft interaction of the heavy quark with the light components of the hadron, are such that $\Delta k \sim \Lambda_{\text{QCD}} \ll m_Q v$. In this near on-shell setting, the heavy quark spinor $Q(x)$ can be decomposed into two large and two small components

$$h_v(x) = e^{i m_Q v\cdot x} \frac{1+\not{v}}{2} Q(x)\,, \tag{2.54}$$

$$H_v(x) = e^{i m_Q v\cdot x} \frac{1-\not{v}}{2} Q(x)\,, \tag{2.55}$$

such that

$$Q(x) = e^{-i m_Q v\cdot x} \left[h_v(x) + H_v(x)\right]\,. \tag{2.56}$$

These components follow the projection relations

$$\not{v} h_v(x) = h_v(x)\,, \tag{2.57}$$

$$\not{v} H_v(x) = -H_v(x)\,, \tag{2.58}$$

[6] This requires to be placed in a reference frame where $v = \mathcal{O}(1)$

leading to the following Lagrangian for the kinetic fermion term [90]

$$\begin{aligned}\mathcal{L}_Q &= \bar{Q}(i\not{D} - m_Q)Q \\ &= \bar{h}_v iv\cdot D h_v - \bar{H}_v(-iv\cdot D - 2m_Q)H_v + \dots\end{aligned} \tag{2.59}$$

where the ellipsis stands for interaction terms between both components. The Lagrangian above can be interpreted as, the kinetic term of a massless fermion h_v and of a fermion H_v of mass $2m_Q$. This separation of the heavy quark spinor corresponds then to the separation of the "light" and "heavy" degrees of freedom. We will therefore, integrate out the "heavy" field H_v (and the hard gluons), leaving only the "light" field h_v as a degree of freedom of the theory.

This leads to the HQET Lagrangian

$$\mathcal{L}_{\text{HQET}} = \bar{h}_v iv\cdot D_s h_v + \mathcal{O}\left(\frac{\Lambda_{\text{QCD}}}{m_Q}, \alpha_s\right) \tag{2.60}$$

where the covariant derivative $iD_s^\mu = i\partial^\mu + g_s A_s^\mu$ contains only the soft gluon field, we omit the light quark and soft gluons kinetic terms and we only show the leading order term in $\mathcal{O}\left(\frac{\Lambda_{\text{QCD}}}{m_Q}, \alpha_s\right)$. This theory is relevant only if the dynamics of the heavy meson is dominated by the soft component h_v of the heavy quark, which occurs when the interactions with the heavy quarks occur only through soft gluons. At leading order in $\mathcal{O}\left(\frac{\Lambda_{\text{QCD}}}{m_Q}\right)$ this Lagrangian shows a SU($2n_Q$) spin-flavour symmetry, where n_Q is the number of heavy quarks described. This can be interpreted as the fact that QCD properties of heavy hadron are independent of the spin and flavour [78]. For instance, in the heavy quark limit, the properties of different heavy mesons (i.e. B, B^*, D, D^*) will be related.

Moreover, in the heavy quark limit, different QCD quark currents can be related though the heavy quark spin symmetry featured in HQET. This has important consequences on the structure of the heavy hadron decays, more precisely, it yields important relations between the form factors that parametrise the different matrix elements of these transitions. This will relate either form factors involving different heavy hadrons or different form factors involving the same heavy hadron.

For instance, in the case of heavy-to-heavy transitions, the form factors for the $B \to D^{(*)}$ transition introduced in Section 1.5 reduce to a single form factor $\xi(v\cdot v')$, called the Isgur-Wise function [91–93].

In the case of heavy-to-light form factors, relations in between the form factors coming from HQET only hold in the low recoil limit. These relations take the following form in the case of $B \to P$ [94, 95]

$$f_T(q^2) = \frac{m_B(m_B + m_P)}{q^2} f_+(q^2) + \mathcal{O}\left(\frac{\Lambda_{\text{QCD}}}{m_b}, \alpha_s\right), \tag{2.61}$$

$$f_0(q^2) = 0 + \mathcal{O}\left(\frac{\Lambda_{\text{QCD}}}{m_b}, \alpha_s\right), \tag{2.62}$$

which in the low recoil region ($q^2 \sim (m_B - m_P)^2$) leads to $f_T(q^2)/f_+(q^2) \approx 1$ as it can be appreciated in Fig. 2.6 for $B \to K$.

In the case of $B \to V$ form factors, where V is a light meson, the following relations are obtained [94, 97, 98]

$$\begin{aligned}T_1(q^2) &= V(q^2) + \mathcal{O}\left(\frac{\Lambda_{\text{QCD}}}{m_b}, \alpha_s\right), \\ T_2(q^2) &= A_1(q^2) + \mathcal{O}\left(\frac{\Lambda_{\text{QCD}}}{m_b}, \alpha_s\right), \\ T_3(q^2) &= A_2(q^2)\frac{m_B^2}{q^2} + \mathcal{O}\left(\frac{\Lambda_{\text{QCD}}}{m_b}, \alpha_s\right).\end{aligned} \tag{2.63}$$

Unfortunately, the flavour spin symmetry is only preserved at leading order and it will be broken by operators arising at next to leading order $\mathcal{O}\left(\frac{\Lambda_{\text{QCD}}}{m_Q}\right)$ in Eq. (2.60). However, improved relations can be obtained at higher orders on $\mathcal{O}\left(\frac{\Lambda_{\text{QCD}}}{m_b}\right)$, by the inclusion of subleading HQET form factors. In the case of heavy-to-light form factors these corrections can be found in [95, 97–100].

In general, the HQET framework will allow us to obtain similar Isgur-Wise relations for all Heavy Hadron decays (mesons and baryons), leading to slightly different results whether we consider Heavy to Heavy form factors or Heavy to Light Form Factors.

These relations of course are a good approximation at the low recoil region, where HQET is valid, but they break down out of these region. Similar relations can be obtained at the large recoil limit, in the framework of Soft Collinear Effective Theory which we will now discuss.

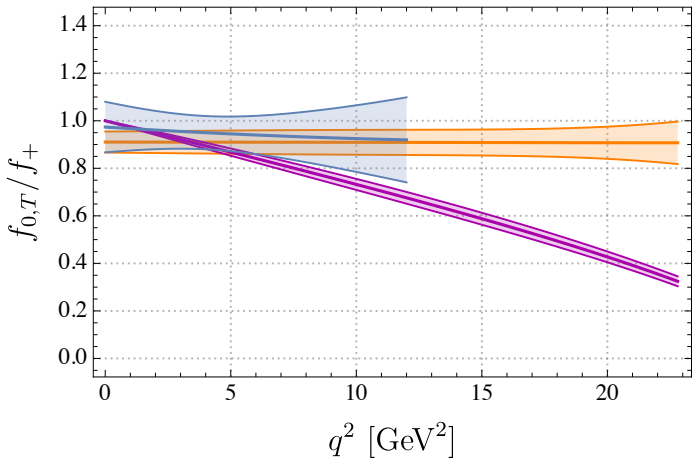

Figure 2.6: f_0/f_+ (purple) and f_T/f_+ (orange) form factors ratios for $B \to K$ with a lattice QCD and LCSR combination from Ref. [39] and f_T/f_+ (blue) coming from Ref. [96]. The HQET and SCET behaviours in Eqs. (2.61) and (2.74) can be appreciated. In the low recoil region $f_T(q^2)/f_+(q^2) \approx 1$ and $f_0(q^2)/f_+(q^2) \approx 0$, while in the large recoil region $f_T(q^2)/f_+(q^2) \approx f_0(q^2)/f_+(q^2) \approx 1$

2.5.2 Soft Collinear Effective Theory

In the previous section, we studied the HQET used to describe the behaviour of heavy hadrons in the low recoil limit.

Heavy to light hadron decays can be treated exclusively with HQET only when the four-momenta of the light degrees of freedom are small compared to m_Q. A natural factorisation of these process arises due to the clear energy separation, $m_Q \ll \Lambda_{\rm QCD}$, between the heavy hadrons and the soft light degrees of freedom.

However, when looking at regions of the phase space in which the light hadrons decay products are highly energetic (i.e. large recoil), this energy separation becomes more complicated. For example, in the case of semileptonic FCNCs B-decays the energy of the light meson E at low dilepton invariant masses is of order $\mathcal{O}(m_b)$. In this situation, the light hadron that we want to describe has almost collinear quarks and antiquarks inside. These can interact through collinear gluons (which can also be seen as partons of the energetic light mesons) which are "highly energetic". Then, the energetic gluon cannot be absorbed in a short-distance contribution , since it interacts with the energetic quarks inside the emitted hadrons. We want then to know if in this context there is still a separation/factorisation in the interaction of the various types of gluons with soft and collinear quarks.

First attempts to develop a theory for these highly energetic processes lead to the Large Energy Effective Theory (LEET) [101, 102], which describes the interaction of very energetic quarks with soft gluons. However, this theory did not include the important degrees of freedom, namely the collinear gluons, which entailed the failure to reproduce the IR behaviour of QCD[75, 76, 103, 104] at the loop level. The inclusion of these collinear degrees of freedom together with the soft degrees of freedom lead to the development of the Soft Collinear Effective Theory (SCET) [72–76]. There exist two formulations or "versions" of SCET, SCET$_{\rm I}$ and SCET$_{\rm II}$, which depend on the level of off-shellness allowed for the various degrees of freedom. The first one is commonly used for the study of jets, where SCET had great success. In the case of heavy to light transitions, both versions are used. We will focus on the latter and briefly describe it, for which we borrow some elements of Refs. [105–107].

Although SCET was conceived to study heavy to light transitions, it has found applications on many other fields, namely jet physics. Let us consider a semileptonic decay of a B-meson like $B \to K\ell\ell$ in the large recoil limit ($q^2 \approx 0$). It is convenient to work in the B-meson rest frame and choose the K three-momentum $\vec{k}$ in the z-direction. We can then define two light-like vectors $n^\mu = (1,0,0,1)$, pointing in the direction of the outgoing meson, and $\bar{n}^\mu = (1,0,0,-1)$, pointing in the opposite direction. These vectors satisfy $n^2 = \bar{n}^2 = 0$ and $n \cdot \bar{n} = 2$. Then the kaon momentum can be written as

$$k^\mu = E n^\mu + \mathcal{O}\left(\frac{m_K^2}{4E}\right) \tag{2.64}$$

where $E = \frac{m_B^2 + m_K^2 - q^2}{2m_B} = \mathcal{O}(m_B)$ is the energy of the K meson. The momentum k^μ is then almost light-like, up to $\mathcal{O}(\frac{\Lambda_{\rm QCD}^2}{E})$ corrections. In the two-parton picture of the meson state, the final state quark and antiquark

outgoing momenta $k^\mu_{1,2}$ hadronised into the light-meson can be written as

$$k^\mu_{1,2} = x_{1,2} E n^\mu \pm k^\mu_\perp + \mathcal{O}\left(\frac{m_K^2}{4E}\right) \tag{2.65}$$

where $x_{1,2}$ are the longitudinal momentum fractions (such that $x_1 + x_2 = 1$) and the transverse momentum $k^\mu_\perp$ is of order $\mathcal{O}(\Lambda_{\rm QCD})$

It is convenient, in order to account for the different scaling on E of the momenta components to systematically decompose the 4-vectors in the light-cone basis defined by n^μ and $\bar n^\mu$. The light-cone decomposition of an arbitrary 4-vector p^μ reads

$$p^\mu = (n\cdot p)\,\frac{\bar n^\mu}{2} + (\bar n\cdot p)\,\frac{n^\mu}{2} + p^\mu_\perp \equiv p^\mu_+ + p^\mu_- + p^\mu_\perp\,, \tag{2.66}$$

where $p_\perp \cdot n = p_\perp \cdot \bar n = 0$. We will then represent the scaling of a momenta or a field as the scaling properties of the components $(n\cdot p, \bar n\cdot p, p_\perp)$. In general, the relevant expansion parameter in SCET is $\lambda = \Lambda_{\rm QCD}/E$ and, for instance, the scaling on this parameter of the kaon momenta is $k^\mu \sim E(1,\lambda^2,\lambda^2)$ and in the case of the final state quark and antiquark momenta defined above it is $k^\mu_{1,2} \sim E(1,\lambda^2,\lambda)$.

The relevant degrees of freedom of the external hadronic state in SCET are the soft, collinear or soft-collinear degrees of freedom. More precisely they are classified by the scaling of the relevant momenta: soft momenta $p^\mu_s \sim E(\lambda,\lambda,\lambda)$, collinear momenta $p^\mu_c \sim E(\lambda^2,1,\lambda)$ and soft collinear-momenta $p^\mu_{sc} \sim E(\lambda^2,\lambda,\lambda)$.

In the case of the effective-theory fields, they are separated into: h soft heavy quark, q_s soft light quark, A^μ_s soft gluon, ξ collinear quarks, and A^μ_c collinear gluon.

Here we use the identity $n\cdot\bar n = 2$ to decompose the Dirac field ψ_c of a collinear quark into two 2-component spinors

$$\xi = \frac{\not n \not{\bar n}}{4}\psi_c\,, \quad \text{and} \quad \eta = \frac{\not{\bar n}\not n}{4}\psi_c\,, \tag{2.67}$$

where $\psi_c = \xi + \eta$ and the components of η are suppressed with respect to those of ξ by a factor λ and are integrated out in the construction of the SCET.

Fields that are both soft and collinear need to be taken into account as well, having soft-collinear quark θ and the soft collinear gluons A^μ_{sc}. The latter are usually referred to as gluon "messenger fields" since they have couplings to both soft and collinear fields. A similar decomposition to the one done for collinear fields is performed for the Dirac field ψ_{sc} of a soft-collinear quark, leaving only the $\theta = \frac{\not n\not{\bar n}}{4}\psi_{sc}$ field after having integrated out the suppressed components.

The two-component spinor that describe the collinear and soft-collinear quark fields fulfil $\not n\,\xi = 0$ and $\not n\,\theta = 0$, similarly to the heavy-quark field described in the previous section, which fulfils $\not v\, h = h$.

The SCET Lagrangian can be split up as

$$\mathcal{L}_{\rm SCET} = \mathcal{L}_s + \mathcal{L}_c + \mathcal{L}_{sc} + \mathcal{L}^{(0)}_{\rm int} + \dots\,, \tag{2.68}$$

where the dots represent power-suppressed interactions. The first three terms correspond respectively to the kinetic terms of soft, collinear and soft-collinear fields respectively and can be written, omitting purely gluonic terms, as

$$\mathcal{L}_s = \bar q_s\, i \not D_s\, q_s + \bar h i v\cdot D_s\, h\,, \tag{2.69}$$

$$\mathcal{L}_c = \bar\xi\,\frac{\not{\bar n}}{2}\, in\cdot D_c\,\xi - \bar\xi\, i\not D_{c\perp}\,\frac{\not{\bar n}}{2}\,\frac{1}{i\bar n\cdot D_c}\, i\not D_{c\perp}\,\xi\,, \tag{2.70}$$

$$\mathcal{L}_{sc} = \bar\theta\,\frac{\not{\bar n}}{2}\, in\cdot D_{sc}\,\theta - \bar\theta\, i\not D_{sc\perp}\,\frac{\not{\bar n}}{2}\,\frac{1}{i\bar n\cdot D_{sc}}\, i\not D_{sc\perp}\,\theta\,, \tag{2.71}$$

where $iD^\mu_{s,c,sc} \equiv i\partial^\mu + gA^\mu_{s,c,sc}$ is the covariant derivative built using soft, collinear or soft-collinear gauge fields [7].

The leading order interaction term in Eq. (2.68), omitting purely gluonic terms, is given by

$$\begin{aligned}\mathcal{L}^{(0)}_{\rm int}(x) = {}& \bar q_s(x)\,\frac{\not{\bar n}}{2}\, g\bar n\cdot A_{sc}(x_+)\, q_s(x) + \bar h(x)\,\frac{n\cdot v}{2}\, g\bar n\cdot A_{sc}(x_+)\, h(x)\\ & + \bar\xi(x)\,\frac{\not{\bar n}}{2}\, gn\cdot A_{sc}(x_-)\,\xi(x)\,.\end{aligned} \tag{2.72}$$

[7] One can now understand the scaling properties of the effective-theory fields, by the scaling of their momenta and by ensuring that the kinetic terms of the Lagrangian are $\mathcal{O}(1)$. Their scaling is then given by: $h \sim \lambda^{3/2}$ for soft heavy quarks, $q_s \sim \lambda^{3/2}$ for soft light quarks, $A^\mu_s \sim (\lambda,\lambda,\lambda)$ for soft gluons, $\xi \sim \lambda$ for collinear quarks, and $A^\mu_c \sim (\lambda^2,1,\lambda)$ for collinear gluons, $\theta \sim \lambda^2$ for soft-collinear quarks and $A^\mu_{sc} \sim (\lambda^2,\lambda,\lambda^{3/2})$ for soft-collinear gluons.

where due to momentum conservation soft-collinear gluons cannot interact with both collinear and soft quark fields at the same time.

The Lagrangian in Eq. (2.72) shows that not all modes are interacting which other, allowing their separation in (potentially complicated) amplitudes mixing various modes and energy. The redefinition of the fields involving Wilson lines similar to those introduced in Eq. (1.92) allows one to illustrate more explicitly this separation of interactions, providing the grounds for factorisation formulae.

For instance, the heavy to light $B \to K$ form factors be represented by

$$\langle K(k)|\bar{s}\Gamma b|B(p)\rangle = \langle K(En_+)|\bar{\xi}\Gamma h|B(m_b v)\rangle + \mathcal{O}\left(\frac{\Lambda_{\rm QCD}}{m_b}, \alpha_s\right) \tag{2.73}$$

since $E = \mathcal{O}(m_b)$.

This leads to the following relations for the $B \to K$ (or $B \to P$ in general) form factors

$$f_+(q^2) \approx \frac{M}{2E} f_0(q^2) \approx \frac{m_B}{m_B + m_K} f_T(q^2) \approx \xi_P(E) + \mathcal{O}\left(\frac{\Lambda_{\rm QCD}}{m_b}, \alpha_s\right), \tag{2.74}$$

which had been previously derived on the LEET [38, 102]. These relations reduce the pseudoscalar form factors to a a single soft form factor $\xi_P(E)$. Neglecting the light meson mass and at the large-recoil limit ($q^2 = 0$), these relations are reduced to $f_+(0) \approx f_0(0) \approx f_T(0)$ which can be appreciated in Fig. 2.6.

In the case of $B \to V$ form factors, where V is a light meson, the following relations are obtained

$$\frac{m_B}{m_B + m_V} V(q^2) = \frac{m_B + m_V}{2E} A_1(q^2) = T_1(q^2) = \frac{m_B}{2E} T_2(q^2) = \xi_\perp(E), \tag{2.75}$$

$$\frac{m_V}{E} A_0(q^2) = \frac{m_B + m_V}{2E} A_1(q^2) - \frac{m_B - m_V}{m_B} A_2(q^2) = \frac{m_B}{2E} T_2(q^2) - T_3(q^2) = \xi_\parallel(E), \tag{2.76}$$

where the vector form factors are reduced to two soft form factors $\xi_{\perp,\parallel}(E)$. In the case of heavy to heavy form factors (i.e. $b \to c$ decays) the relations reduce to same relations obtained in HQET Ref. [38].

These relations can be then systematically improved through power corrections thanks to the framework of SCET and like for HQET, similar relations can be obtained for all heavy hadrons. For instance, the expressions for the $B \to P(V)$ form factors at next to leading order can be found in Ref. [106]. In the case of baryons, expression for the $\Lambda_b \to \Lambda$ form factors at leading order can be found in Ref. [40].

Determinations of the soft form factors appearing in Eqs. (2.74) and (2.75) have been determined through the use of *SCET sum rules* [40, 67, 68], where the sum rules are directly applied within the Soft-Collinear Effective Theory framework, instead of the light-cone expansion of QCD. These results can be, for instance, compared with the heavy-quark limit of LCSR form factor determinations.

Another natural place to apply SCET, are non-leptonic B-decays into two light mesons. It turns out that this separation allows one to recover results derived in QCD factorisation, expressing the amplitude in terms of a limited number of hadronic inputs, as discussed briefly in Section 2.8

2.6 Factorisation of semi-leptonic decays

When thinking about semi-leptonic decays and, in general, of processes involving quarks, we are interested in being able to separate the contributions from the various energy scales and factorise them. A separation in between the (non-perturbative) QCD part (see Section 1.4) and the EW part (see Section 1.2) is necessary to be able to treat them in different frameworks. If factorisation is possible, we will then be able to use the hadronic non-perturbative inputs discussed in Section 1.5 to compute the amplitude. In this section, we start by discussing the factorisation process in purely leptonic decays to then discuss the factorisation process in semileptonic decays in which we are interested. The situation in non-leptonic decays is more complex and its discussion will be left for later (see Section 2.8).

2.6.1 Factorisation of FCCCs: $b \to c\ell\bar{\nu}$

In order to understand the process of factorisation, we will start by looking at the processes involving leptonic charged electroweak currents, like the muon decay shown in Fig. 1.7. To treat this decay we will use the equivalent of WET for leptonic processes, i.e. the Fermi theory (see Fig. 2.2). The amplitude of this process trivially factorizes (at the leading order in QED) in the following way

$$\begin{aligned} \mathcal{M}(\mu \to e\bar{\nu}_e\nu_\mu) &\propto G_F \langle e\bar{\nu}_e\nu_\mu|\bar{\nu}_\mu\gamma^\alpha(1-\gamma_5)\mu\bar{\nu}_e\gamma^\beta(1-\gamma_5)e|\mu\rangle\,, \\ &\propto G_F \langle \nu_\mu|\bar{\nu}_\mu\gamma^\alpha(1-\gamma_5)\mu|\mu\rangle\langle e\bar{\nu}_e|\bar{\nu}_e\gamma^\beta(1-\gamma_5)e|0\rangle\,. \end{aligned} \tag{2.77}$$

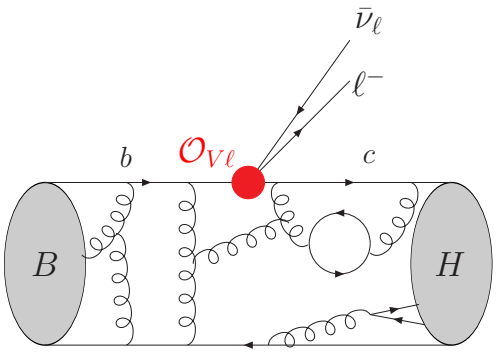

Figure 2.7: Schematic representing the low energy structure of the vectorial contribution in $b \to c\ell\nu$ transitions. Soft gluons coming from the decaying hadron cannot connect to the external lepton legs allowing for the factorisation of these contributions. The picture is similar for all the other operators in Eq. (2.16). Taken from Ref. [26]

This corresponds to the factorisation of the four fermion local operator into two distinct lepton currents. In the case of fully leptonic decays like the one above, this trivial factorisation relies on the fact that this process can be treated in a fully perturbative way and radiative corrections can be accounted for systematically.

A slightly less trivial scenario is the case of charged current semi-leptonic decays like $b \to c\ell\bar{\nu}$ for which a schematic is shown in Fig. 2.7. In this case, QCD is involved, so the decay cannot be treated in a fully perturbative way. However, at tree level, a factorisation of the process is possible in the following way

$$\langle D\ell\nu|\bar{c}\gamma^\mu P_L b\bar{\nu}\gamma^\nu P_L\ell|B\rangle = \underbrace{\langle D|\bar{c}\gamma^\mu P_L b|B\rangle}_{\text{Hadronic matrix element}} \underbrace{\langle \ell\nu|\bar{\nu}\gamma^\nu P_L\ell|0\rangle}_{\text{Leptonic matrix element}} . \tag{2.78}$$

This is because semileptonic operators, as opposed to 4-quark operators, have leptons as external states, and since leptons are blind to coloured interactions, low energy gluons cannot connect the two factorised parts of the process [8].

The leptonic matrix element can be easily computed perturbatively and the hadronic matrix element is the only piece that needs to be treated in a non-perturbative fashion. This hadronic matrix element is parametrised through the form factors described in Section 1.5.

2.6.2 Factorisation of FCNCs: $b \to s\ell^+\ell^-$

In the case of FCCCs, as described in the previous section, factorisation is rather straightforward and does not require much more discussion. Different is the case of FCNCs where the contribution of 4-quark operators are relevant for the transition. We will illustrate this discussion in the $b \to s\ell^+\ell^-$ case.

The amplitude for a semileptonic decay of a b-hadron H_b into a light strange hadron H in the SM can be then written as [108, 109]

$$\begin{aligned}\mathcal{A}(H_b \to H\ell^+\ell^-) \propto \Bigg[\frac{1}{q^2}\Big\{ \mathcal{C}_{7\gamma} 2im_b \langle H|\bar{s}\sigma_{\mu\nu}q^\nu P_R b|H_b\rangle + 16\pi^2 \mathcal{H}_\mu^{H_b\to H}\Big\} \\ + \mathcal{C}_{9\ell}\langle H|\bar{s}\gamma_\mu P_L b|H_b\rangle \Bigg] \bar{u}_\ell\gamma^\mu v_\ell \\ + \mathcal{C}_{10\ell}\langle H|\bar{s}\gamma_\mu P_L b|H_b\rangle \bar{u}_\ell\gamma^\mu\gamma_5 v_\ell \,,\end{aligned} \tag{2.79}$$

where $\mathcal{H}_\mu^{H_b\to H}$ contains the non-local contributions and is defined as

$$\mathcal{H}_\mu^{H_b\to H} \equiv i\int d^4x e^{iq\cdot x}\langle H|T\{j_\mu^{\text{em}}(x), (\mathcal{C}_1\mathcal{O}_{1c} + \mathcal{C}_2\mathcal{O}_{2c})(0)\}|H_b\rangle \tag{2.80}$$

where T is the time ordered product and $j_\mu^{\text{em}}(x) = \sum_q Q_q\bar{q}(x)\gamma_\mu q(x)$ with $q = u, d, s, c, b$ is the electromagnetic current.

[8] Non factorisable contributions could of course appear at loop level, but the loop suppression is enough to neglect the non-resonant contributions compared to the uncertainties of the tree level contribution which are generally dominated by the knowledge of the form factors. In the case of resonant contributions like $B \to D\pi(\to \ell\bar{\nu})$, they could contribute at the 10% order ($\mathcal{B}(B \to D\pi)\mathcal{B}(\pi \to \ell\bar{\nu}) \approx 0.1 \times \mathcal{B}(B \to D\ell\nu)$) but they can be dealt with through experimental cuts.

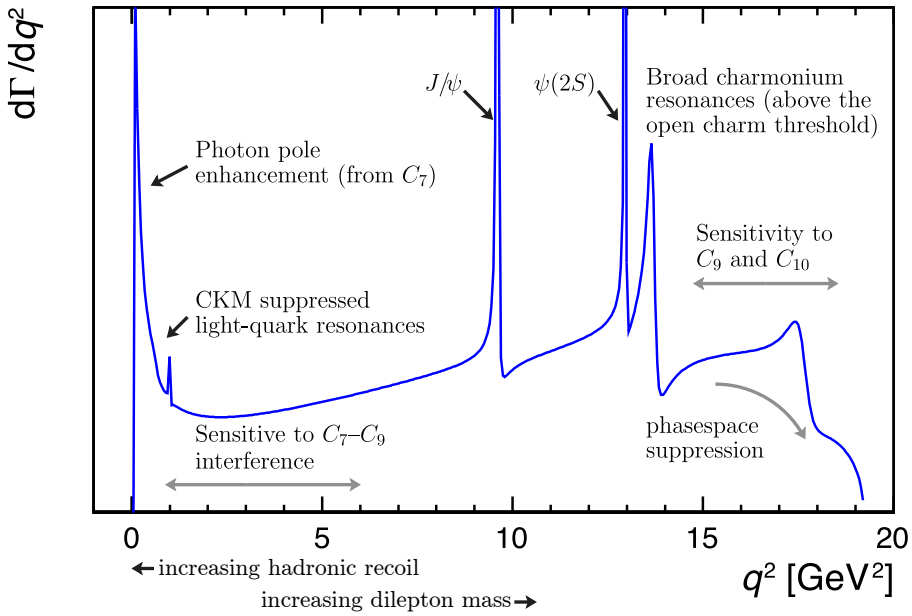

Figure 2.8: Illustration of the dilepton invariant mass squared q^2 dependence of the differential decay rate of $B \to K^* \ell^+ \ell^-$ decays. The different contributions to the decay rate are also illustrated. For $B \to K \ell^+ \ell^+ -$ decays there is no photon pole enhancement due to angular momentum conservation. Adapted from Ref. [88].

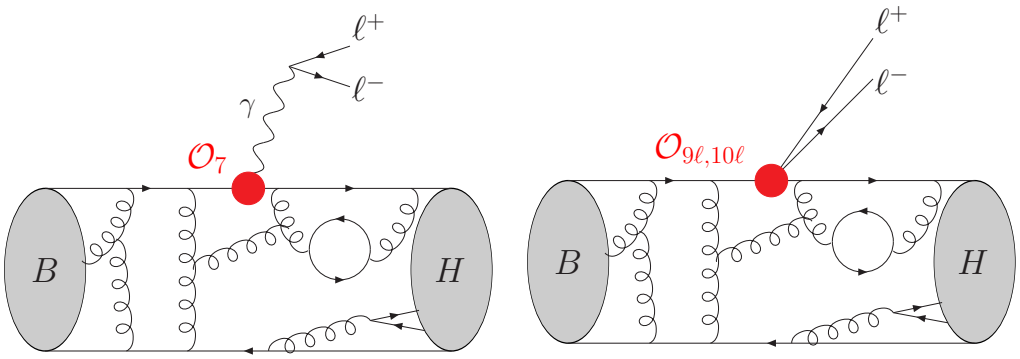

Figure 2.9: Schematic representing the low energy structure of the contributions from semileptonic operators in $b \to s\ell\ell$ transitions. Soft gluons coming from the decaying hadron cannot connect to the photon in $\mathcal{O}_7$ or the external lepton legs in both diagrams, allowing for the factorisation of these contributions. On the left the contribution from $\mathcal{O}_7$ and on the right contributions from $\mathcal{O}_{9\ell,10\ell}$. Taken from Ref. [26]

The main contributions come from the semileptonic and radiative operators $\mathcal{O}_{7\gamma,9\ell,10\ell}$, which are q^2 dependent, having different regions in which they dominate as seen in Fig. 2.8 for $B \to K^* \ell^+ \ell^-$.

The contribution of semi-leptonic operators and from the electromagnetic dipole operator will be easily factorised into a form factor and a leptonic current as shown in Eq. (2.79) and Fig. 2.9, similarly to the situation in FCCCs.

However contributions from non-leptonic operators (i.e. 4-quark and chromomagnetic operators) play also an important role, through photon line insertions, and cannot be neglected. For instance, the relevant diagrams are shown at leading order in Fig. 2.10 and at next-to-leading order in Fig. 2.11.

In Eq. (2.80) we omit the terms containing other operators than the $\mathcal{O}_{1c(2c)}$ operators, since they have the small coefficients in the SM. The contribution of the $\mathcal{O}_{1c(2c)}$ operators is often called "$c\bar{c}$ contribution" or "charm loop effect". As mentioned before, similar contributions from the $u\bar{u}$ are controlled due to their double Cabibbo suppression and $t\bar{t}$ contributions are already accounted for at the level of the matching of the effective theory.

These contributions can be divided into short and long distance contributions. While the former can be easily computed in perturbation theory, the latter are more complicated to estimate.

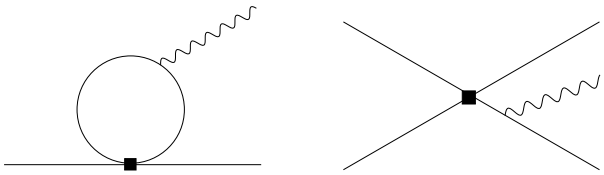

Figure 2.10: Leading order contribution of 4 quark operator to radiative and semileptonic decays. For semileptonic decays the photon line needs to be connected to a lepton pair. Similar diagrams can be obtained by connecting the photon line in other legs of the diagrams.

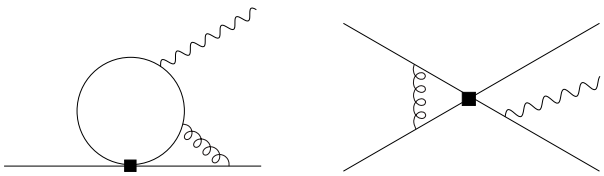

Figure 2.11: Example of diagrams contributing at next-to-leading order to radiative and semileptonic decays through 4 quark operators and the chromomagentic operator. For semileptonic decays the photon line needs to be connected to a lepton pair. Similar diagrams can be obtained by connecting the photon line in other fermion legs of the diagrams.

2.7 Non leptonic operators contributions: Charm-loop effect

2.7.1 Short distance contributions

For radiative decays, the short distance contributions can be expressed as an effective Wilson coefficient $\mathcal{C}_{7\gamma}^{\text{eff}}$ [110] [9]

$$\mathcal{C}_{7\gamma}^{\text{eff}} = \mathcal{C}_{7\gamma} - \frac{1}{3}\mathcal{C}_3 - \frac{4}{9}\mathcal{C}_4 - \frac{20}{3}\mathcal{C}_5 - \frac{80}{9}\mathcal{C}_6 + \mathcal{O}(\alpha_s)\,. \tag{2.81}$$

such that at leading order

$$\mathcal{A}(b \to s\gamma) = -\frac{4G_F}{2}\lambda_t^{(s)} \sum_i \mathcal{C}_i \langle \mathcal{O}_i \rangle = -\frac{4G_F}{2}\lambda_t^{(s)} \mathcal{C}_{7\gamma}^{\text{eff}} \langle \mathcal{O}_{7\gamma} \rangle\ . \tag{2.82}$$

Similarly for semileptonic decays, these short distance contributions can be included into an effective Wilson coefficients $\mathcal{C}_{9\ell}^{\text{eff}}(q^2)$ [28, 97, 111]. At leading order, these contributions are perturbatively computed leading to the process independent expression

$$\mathcal{C}_{9\ell}^{\text{eff}}(q^2) = \mathcal{C}_{9\ell} + Y(q^2) \tag{2.83}$$

where $Y(q^2)$ can be for instance found in Ref. [111].

Subleading short distance contributions can been taken into consideration at the large recoil in a similar framework to QCD factorisation (which we will later discuss in Section 2.8). These corrections are however process dependent, which is expressed on their dependence on the LCDA of the mesons [111]. In the case of $B \to V\ell\ell$, they can be found in Ref. [111].

2.7.2 Long distance contributions

In the case of long-distance contributions, external legs of 4-quark operators can be connected via soft-gluons to the decaying hadron. More precisely soft gluons coming from the decaying hadron can connect to the $c\bar{c}$ loop shown in Fig. 2.12. Long distance contributions are q^2 dependent and they depend on the external states (for instance on the helicity).

Near the masses of charmonia (J/Ψ, $\Psi(2S)$, ...), the long distance contribution becomes resonant and it dominates the decay (as shown in Fig. 2.8). Near the poles of the charmonia resonances, NP is expected to be substantially suppressed with respect to SM contributions, allowing these regions to be used for different cross checks. For instance, experimentally they are used to suppress systematic errors and theoretically they are used to have a better understanding of the long distance contributions [109, 112]. When enough phase space is available, the resonances divide the spectrum of the dilepton invariant mass in two regions (see Fig. 2.8): the "low-q^2" region found below the $c\bar{c}$ threshold, i.e. $q^2 \ll 4m_c^2$ ant the "high-q^2" region, in which numerous $c\bar{c}$ resonances are present and one can consider using quark-hadron duality to approximate them using perturbative

[9] One can similarly define $\mathcal{C}_{8g}^{\text{eff}}$

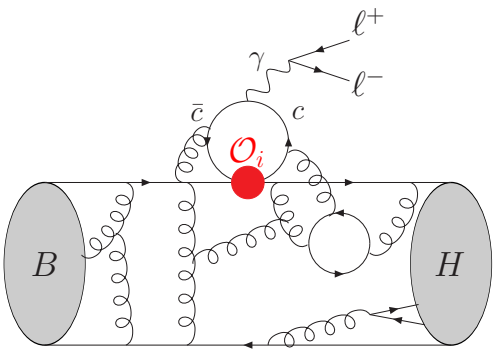

Figure 2.12: Schematic representing the non-local contributions of 4-quark operators in $b \to s\ell\ell$ transitions. Gluons coming from the decaying hadron can connect to the $c\bar{c}$ loop which then decays into a lepton pair through a photon. Similar contributions from the $u\bar{u}$ are controlled due to their double Cabibbo suppression. Taken from Ref. [26]

QCD. Estimations of long-distance contributions in the low-recoil region, which rely on quark-hadron duality, indicate that corrections to the quark level computations are of the order of 10% [113]. This is in line with $\mathcal{O}(\Lambda/m_b)$ suppressed effects, but it should be highlighted that this estimate was obtained only for $B \to K^*\ell^+\ell^-$ branching ratio using a single model of $c\bar{c}$ resonances. This question was also discussed in Ref. [114].

In the large-recoil region, long-distance contributions have been estimated, for $B \to K$, $B \to K^*$ and $B_s \to \phi$, through approaches that use analyticity and dispersion relations [109, 112, 115, 116]. Determinations in this region rely on the light-cone OPE of the non-local operators and they are performed at values of q^2 ensuring a rapid convergence of the expansion ($q^2 \lesssim -1\,\text{GeV}^2$). The matrix elements of the LCOPE are computed through non-perturbative methods, namely through the use of LCSR, and they are then extrapolated to the regions of interest $q^2 > 0$, through dispersion relations and assumptions on the analyticity structure of the correlator $\mathcal{H}_\mu$ defined in Eq. (2.80).

The first determination of the subleading operator of soft gluon emission from the $c\bar{c}$ pair was obtained through LCSR in Ref. [115], where they extrapolate their results to the positive q^2 region through dispersion relations and a resonance model. Further attempts to enhance the extrapolation on q^2 where done in Refs. [109, 112] through the use of experimental data at the J/Ψ and $\Psi(2S)$ poles (turning the extrapolation into an interpolation). Furthermore, the authors of Ref. [109] update the LCSR results of Ref. [115], obtaining results for the subleading corrections two times smaller. They also improve the analytic continuation of the non-local effects and bound the truncated terms of the analytical continuation through the introduction of a new parametrisation of the matrix element.

In general, we will express long distance contributions as an additional contribution to $\mathcal{C}_{9\ell}$

$$\mathcal{C}_{9\ell}^{\text{eff}}(q^2) \to \mathcal{C}_{9\ell}^{\text{eff}}(q^2) + \Delta\mathcal{C}_{9\ell}^{\text{LD}}(q^2) \tag{2.84}$$

where $\Delta\mathcal{C}_{9\ell}^{\text{LD}}(q^2)$ is different for different helicities and external states.

For the $B \to K$ decay, long distance contributions are found to be of around 5% ($\Delta\mathcal{C}_{9\ell}^{\text{LD}}(q^2) \approx 0.05\mathcal{C}_{9\ell}^{\text{eff}}(q^2)$) in Ref. [115], which together with short distance contributions are found to be of around 10% in Ref. [116]. In the case of $B \to K^*$ they are found to be around 20% [115], the difference being mainly caused by the soft-gluon contribution.

In practice, in this thesis, we will have to parametrise this effect in different cases. For global fits of $b \to s\ell^+\ell^-$ data (see Chapter 4), we will follow the same line as in Ref. [108], taking Ref. [115] as an order of magnitude estimate. For the prediction of observables, (Chapters 5 and 6) we will take a rougher estimate of 10% that will be described in detail in the corresponding chapters.

Further discussion on this topic can be found in Refs. [117–137].

2.8 Factorisation of non leptonics decays

Non-leptonic decays, as opposed to semi-leptonic decays, undoubtedly suffer from more intricate QCD effects. Although the underlying weak decay can be easily treated in the effective Hamiltonian framework discussed in the precedent sections, these decays are complicated on account of strong-interaction effects. However, a good understanding of these effects would largely enhance our ability to prove the SM and would be complementary to semi-leptonic decays.

The simplest case of non-leptonic decays, is the case of two-body B-meson decays (like $B \to \pi\pi$). In these decays, the factorization is not evident since low energy gluons, that require a non-perturbative treatment, can connect the two sides of the electroweak decay and prevent us from factorising the amplitude into simpler hadronic inputs.

We will focus in the decays in which the B-meson decays into two light mesons M_1 and M_2.

The amplitude for a $B \to M_1 M_2$ decay can be expressed in terms of the general Weak Effective Hamiltonian as

$$\mathcal{A}(B \to M_1 M_2) = \sum_i \mathcal{C}_i(\mu) \, \langle M_1 M_2 | \mathcal{O}_i | B \rangle(\mu), \tag{2.85}$$

where the computation of these matrix elements is the main theoretical problem.

The framework that we will consider to compute these matrix elements is the one of of QCD factorisation (QCDF) [36, 86, 138, 139], which reduces these matrix elements into perturbative objects that are simpler in structure and/or universal (process independent). Its arguments make extensive use of the heavy-quark limit, similarly to SCET since for non-leptonic decays a large momentum is transferred to at least one of the final-state mesons. Before the development of QCDF, several efforts had been put into obtaining a factorization of this kind of non-leptonic processes, we will start by briefly discussing two of them that are at the origin of QCD factorisation.

The first one is the *naive factorisation* approach [140, 141], in which the matrix element in Eq. (2.85) is simply replaced by the product of two dissociated currents, for instance for a left handed current in $B \to \pi^+\pi^+$

$$\langle \pi^+\pi^- | \bar{u}\gamma^\mu P_L b \bar{d}\gamma^\nu P_L u | \bar{B} \rangle \to \langle \pi^- | \bar{d}\gamma^\nu P_L u | 0 \rangle \langle \pi^+ | \bar{u}\gamma^\mu P_L b) | \bar{B} \rangle \, . \tag{2.86}$$

Here the exchange of gluons with virtualities below $\mu \sim m_b$ between the π^- and the $(\bar{B}\,\pi^+)$ system are assumed to be negligible, assumption which is in general not justified.

The second approach is the *hard-scattering* approach [142, 143], where the decay is assumed to be dominated by hard gluon exchange. In this approach the decay amplitude is simply expressed as a convolution of a hard-scattering factor T with the light-cone distribution amplitudes of the participating mesons Φ_M, for the same example above

$$\langle \pi^+\pi^- | \bar{u}\gamma^\mu P_L b \bar{d}\gamma^\nu P_L u | \bar{B} \rangle \to \int_0^1 d\xi du dv \, \Phi_B(\xi) \, \Phi_\pi(u) \, \Phi_\pi(v) \, T(\xi, u, v; m_b) \, . \tag{2.87}$$

This approach works in processes in which the short-distance dominance is ensured. This is the case for hard processes involving only light hadrons in which soft contributions are powered suppressed. However in the case of heavy-hadron decays, soft contributions are not power suppressed and they are one of the main contributions [138].

2.8.1 QCD Factorisation

In non-leptonic decays the term "factorization" generally refers to the concept of naive factorisation described above. Corrections to this approximation are called "non-factorizable". QCD factorisation makes use of the Heavy Quark Expansion in order to obtain its main general result: in two body decays B-meson decays as the one in Eq. (2.85), these "non-factorisable" corrections are dominated by hard gluon exchanges and the soft contributions that remain in the heavy-quark limit are confined to two body systems $(B - M_1)$ and $(B - M_2)$.

The above result is expressed in terms of a factorisation formula, up to power corrections of order $\mathcal{O}\left(\frac{\Lambda_{\rm QCD}}{m_b}\right)$ [138] which reads

$$\begin{aligned} \langle M_1 M_2 | \mathcal{O}_i | \bar{B} \rangle = & \sum_j F_j^{B\to M_1}(m_2^2) \int_0^1 du \, T_{ij}^I(u) \, \Phi_{M_2}(u) \; + \; (M_1 \leftrightarrow M_2) \\ & + \int_0^1 d\xi du dv \, T_i^{II}(\xi, u, v) \, \Phi_B(\xi) \, \Phi_{M_1}(v) \, \Phi_{M_2}(u) \, , \end{aligned} \tag{2.88}$$

where $m_{1,2}$ corresponds to the mass of the $M_{1,2}$ meson. When M_2 cannot absorb the spectator quark the $(M_1 \leftrightarrow M_2)$ term is absent. Three different class of elements appear in the above formulas: the form factors for the $B \to M$ transition $F_j^{B\to M}$, the light-cone distribution amplitudes for the three mesons $\Phi_B(\xi)$, $\Phi_{M_1}(v)$, $\Phi_{M_2}(u)$, and the hard-scattering kernels $T_{ij}^I(u)$, $T_i^{II}(\xi, u, v)$.

The first and the second classes have been discussed in Section 1.5 with the exceptions of the B-meson light cone DAs which require a special treatment due to the the heavy nature of the meson. In principle, the B-meson has no preferred direction (contrary to the light mesons), however the final states have naturally light-like directions which define the relevant direction for the definition of the B-meson light cone DAs (we refer the

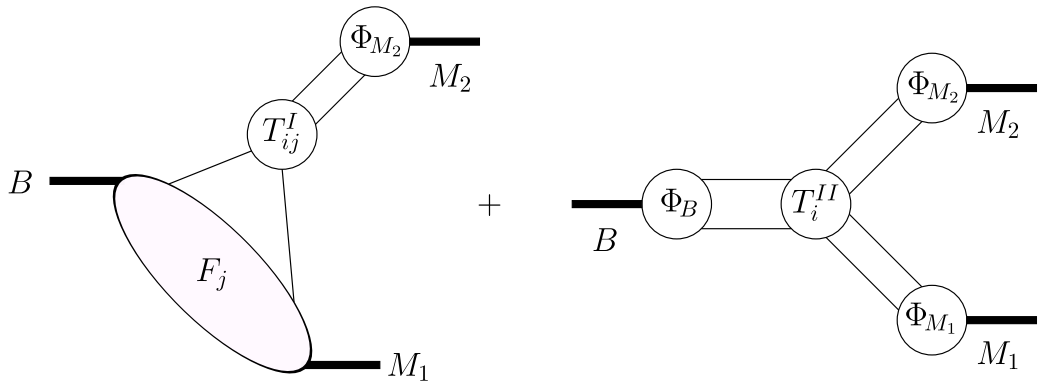

Figure 2.13: Graphical representation of the factorisation formula in Eq. (2.88). The $(M_1 \leftrightarrow M_2)$ is not shown [138].

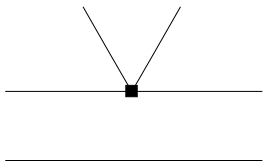

Figure 2.14: Leading order contribution to the hard scattering kernel $T_{ij}^I(u)$.

reader to Ref. [138] for more details). The last class of elements, the hard-scattering kernels $T_{ij}^I(u)$, $T_i^{II}(\xi, u, v)$ are perturbatively calculable functions.

We will refrain from giving explicit expressions for the hard-scattering kernels and their corrections, for which we refer the reader to Refs. [37, 138, 144]. However, we will qualitatively discuss the different topologies of the contributing diagrams, a more detailed explanation of the arguments given here can be found in Ref. [138].

The main contribution ($\mathcal{O}(1)$) to the hard scattering kernel comes from the diagram in Fig. 2.14 and goes into $T_{ij}^I(u)$. When neglecting all $\mathcal{O}\left(\alpha_s, \frac{\Lambda_{\text{QCD}}}{m_b}\right)$ corrections, the hard scattering kernel is then only given by this diagram, which will be u-independent and will reduce Eq. (2.88) to the naive factorisation result given in Eq. (2.86).

The diagrams in Fig. 2.15 correspond to factorisable contributions which can be separated into a hard and a soft part, taken into consideration in the matching and the non-pertubative inputs respectively.

The $\mathcal{O}(\alpha_s)$ corrections to the hard-scattering kernels, correspond to "non factorisable" contributions. In the case of these contributions it is fundamental that in the heavy quark limit, the soft part of them are suppressed.

There are two groups of "non factorisable" diagrams contributing to $T_{ij}^I(u)$, the vertex correction diagrams shown in Fig. 2.16 and the penguin and chromomagnetic diagrams shown in Fig. 2.17. The "non factorisable" diagrams contributing to $T_{ij}^{II}(\xi, u, v)$ can also be divide in two groups, the spectator interactions shown in Fig. 2.18 and the weak annihilation diagrams shown in Fig. 2.19.

Higher order α_s corrections to the hard scattering kernels have been computed in Ref. [144] and higher orders in $\frac{\Lambda_{\text{QCD}}}{m_b}$ have been computed in Ref. [37]. One comment about this higher order corrections is required and it is regarding to particular situations in which these corrections contain infrared divergences. Hard-gluon exchanges with the spectator quark and weak annihilation feature $1/m_b$-suppressed contributions exhibiting infrared divergences related to the endpoint of the meson twist-3 light-cone distribution amplitudes. These divergences put in risk the factorisation if not treated, however they are expected to be of the order $\ln(m_b/\Lambda_{\text{QCD}})$. We will thus parametrise them, by two, a priori external state dependent, coefficients X_H and X_A [37], representing the uncertainty over these terms. The first one characterises the divergences arising from the spectator interaction

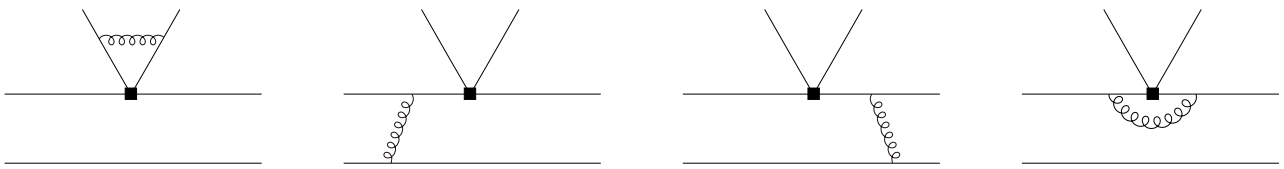

Figure 2.15: Next to leading order corrections which are already accounted for in the DAs and the form factors. They will thus not contribute to the hard scattering kernels.

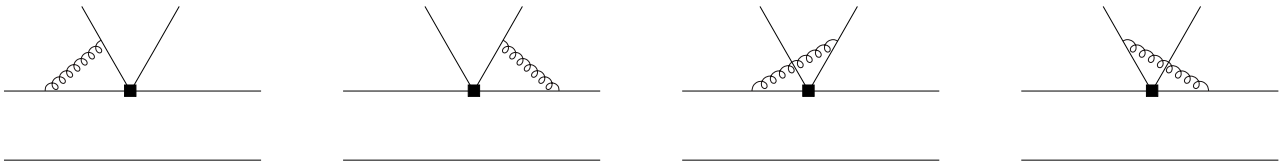

Figure 2.16: "Non factorisable" vertex corrections which contribute to the $T_{ij}^{I}(u)$ hard-scattering kernel.

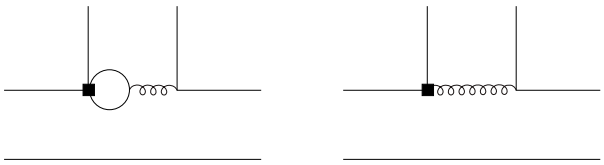

Figure 2.17: Penguin contribution on the left and the chromomagnetic operator contribution on the right, both of which contribute to the $T_{ij}^{I}(u)$ hard-scattering kernel.

diagrams and the second one from annihilation diagrams. In this thesis we will model them in the same manner as in Ref. [37]. We take the following parametrisation, assuming $X_{H,A}$ to be universal for all channels:

$$X_{H,A} = (1 + \rho_{H,A} e^{i\varphi_{H,A}}) \ln\left(\frac{m_B}{\Lambda_h}\right). \tag{2.89}$$

where $\Lambda_h = 0.5\,\text{GeV}$. We take $\rho_{H,A} \in [0,1]$ and $\varphi_{H,A} \in [0, 2\pi]$ with flat distributions. This translates into assigning a 100% uncertainty to the magnitude of such corrections.

A comment regarding the treatment of non-leptonic decays in general might be important. At the base of the QCDF treatment is the fact that the decay products of the B-meson are highly energetic, which bares certain similarities with the SCET framework. In fact, these results have been studied in the SCET framework, leading to similar results to the ones obtained in QCDF, leading to a reinterpretation of QCDF in terms of SCET [144–148].

2.8.2 $B \to PP$, $B \to PV$ and $B \to VV$

One important point that we have not mentioned yet, is the dependence on the spin nature of the mesons in hand. The results of QCDF will differ slightly in the case of them pseudoscalar mesons or vector mesons. In the case of $B \to PP$ and $B \to PV$ decays, an in-depth analysis can be found in Ref. [37], in the case of $B \to VV$ one can refer to Refs. [89, 139, 149].

The first two cases are rather straight forward since in the first (S-wave) both meson have spin 0 and on the second (P-wave) the helicity of the vector meson is fixed by the spin of the B and P mesons. However, in the case of $B \to VV$ decays different helicities are allowed for the vector mesons. We will know discuss the relative scaling of these amplitudes which will be relevant in Chapter 10.

The decay amplitude of a B-meson decay into two light vector mesons can decomposed into three scalar amplitudes $S_{1,2,3}$

$$\mathcal{A}_{B\to V_1V_2} = i\eta^{*\mu}\varepsilon^{*\nu}\left(S_1\, g_{\mu\nu} - S_2\,\frac{p_\mu p_\nu}{m_B^2} + S_3\, i\epsilon\mu\nu\rho\sigma\,\frac{p_1^\rho p_2^\sigma}{p_1\cdot p_2}\right). \tag{2.90}$$

where p, p_1 and p_2 are the four momenta of the B-meson and the 2 vector mesons V_1 and V_2 respectively, m_B, m_1 and m_2 their masses and η^* and ε^* the polarization vectors of the vector mesons. These amplitude can be

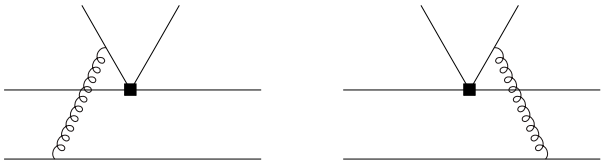

Figure 2.18: "Non factorisable" spectator corrections contributing to the $T_i^{II}(\xi, u, v)$ hard-scattering kernel.

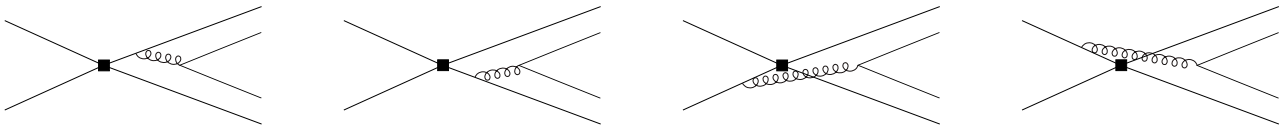

Figure 2.19: Annihilation contribtuions to the $T_i^{II}(\xi, u, v)$ hard-scattering kernel.

more simply described in a basis of definite helicity for the final states

$$\begin{aligned} \mathcal{A}_0 &= \mathcal{A}(B \to V_1(p_1, \eta_0^*) V_2(p_2, \varepsilon_0^*)) = \frac{i m_B^2}{2 m_1 m_2} \left(S_1 - \frac{S_2}{2} \right) \\ \mathcal{A}_\pm &= \mathcal{A}(B \to V_1(p_1, \eta_\pm^*) V_2(p_2, \varepsilon_\pm^*)) = i \, (S_1 \mp S_3). \end{aligned} \tag{2.91}$$

where, in the B meson rest frame, p_1 is chosen to be directed in the positive z-direction and since both vector mesons have large momenta p_2 is collinear with p_1 up to $\frac{m_{1,2}}{m_b}$ corrections. In this frame the polarisation four-vectors are given by $\varepsilon_\pm^\mu = \eta_\mp^\mu = (0, \pm 1, i, 0)/\sqrt{2}$, and $\epsilon_0^\mu = p_2^\mu / m_2$, $\eta_0^\mu = p_1^\mu / m_1$.

A naive factorisation analysis indicates a hierarchy of helicity amplitudes [139]

$$\mathcal{A}_0 : \mathcal{A}_+ : \mathcal{A}_- = 1 : \frac{\Lambda_{\text{QCD}}}{m_b} : \left(\frac{\Lambda_{\text{QCD}}}{m_b} \right)^2 \tag{2.92}$$

for B-meson decays, which means that only $\mathcal{A}_0$ (longitudinal polarisation) can be predicted meaningfully in QCD factorisation. This structure is due to the left-handedness of weak interactions and to the fact that helicity is conserved in short-distance QCD interactions [28]. In the case of $\bar{B}$-meson decays the $\mathcal{A}_+$ and $\mathcal{A}_-$ are exchanged.

Part II

The flavour anomalies: experimental status and global fits

Chapter 3

Flavour Anomalies and NP models

In the recent years several hints of a tension with respect to Standard Model expectations have appeared concerning two different classes of b-quark semileptonic decays. These series of hints of NP, usually referred as the flavour anomalies or the b-anomalies, have appeared both in the charged and neutral current semileptonic b-decays. On the one hand, charged-current $b \to c\ell\bar{\nu}$ transitions have exhibited deviations in observables comparing $\ell = \tau$ and lighter leptons ($\ell = \mu, e$) showing hints of Lepton Flavour Universality Violation (LFUV). On the other hand, neutral current $b \to s\ell^+\ell^-$ transition have similarly shown deviations in LFUV observables comparing muons and electrons, but also a consistent pattern of deviations in branching fractions and angular observables in the case of muons.

In this chapter, we will present the different accessible observables on these modes, discussing their theoretical predictions and the existing experimental results for them. In Section 3.1 we start by discussing the $b \to c\ell\bar{\nu}$ observables and its theoretical predictions including branching fractions, angular observables and Lepton Flavour Universality (LFU) ratios. We then present the available experimental results and an overview of the current results of global fits performed on current data in the EFT framework discussed in the previous chapter. We will follow this by a similar discussion in for the $b \to s\ell^+\ell^-$ transition in Section 3.2 where we will also discuss the use of optimized angular observables in order to suppress hadronic uncertainties. Unlike the case of $b \to c\ell\bar{\nu}$, we will not discuss global fits for the $b \to s\ell^+\ell^-$ transition in this chapter, since we will dedicate a full chapter to this transition (see Chapter 4). We will finish this chapter in Section 3.3, by a overview of several NP models that can potentially account for these deviations, both in the charged and neutral currents.

3.1 The $b \to c\ell\bar{\nu}$ flavour anomalies

3.1.1 Theoretical predictions in $b \to c\ell\bar{\nu}$

We will discuss now the main elements that go into the theoretical predictions of $b \to c\ell\bar{\nu}$ modes and their cleanness. We will mainly focus on the $B \to D^{(*)}\ell\bar{\nu}$ modes, as they are the most experimentally accessible modes, and since the treatment of the other meson modes like $B_c \to J/\Psi\tau\bar{\nu}$ and $B_s \to D_s^{(*)}\ell\bar{\nu}$ is similar. Some other modes, like the baryonic modes $\Lambda_b \to \Lambda_c\ell\bar{\nu}$ or the purely leptonic $B_c \to \ell\bar{\nu}$, which might be also accessed in the future, will then be briefly discussed.

Branching Fractions and LFU ratios

The branching fractions of $b \to c\ell\bar{\nu}$ modes depend mainly on two elements, the form factors for the specific mode and the CKM element V_{cb} introduced in Section 1.2.2.

- The $B \to D$ transition, similarly to $B_s \to D_s$, is described by 3 form factors $f_{0,+,T}$ (defined in Eqs. (1.69) and (1.70)) and the $B \to D^*$ transition, similarly to $B_s \to D_s^*$ and $B_c \to J/\Psi$, is described by 7 form factors V, $A_{0,1,2}$ and $T_{1,2,3}$ (defined in Eqs. (1.76), (1.77), (1.79) and (1.80)). However, the $B_{(s)} \to D_{(s)}^{(*)}$ form factors possess an interesting property, as they are all related through HQET and reduced to a single form factor $\xi(v \cdot v')$, called the Isgur-Wise function [91, 92] (see Section 2.5.1), in the Heavy Quark Limit ($m_b, m_c \to \infty$). Corrections to this limit have been computed in Ref. [150] for $B \to D^{(*)}$, where corrections to order $\mathcal{O}(\alpha_s, \frac{1}{m_b}, \frac{1}{m_c^2})$ are taken into consideration. The parameters (non-perturbative HQET elements) of this expansions are then obtained through the use of a combination of Lattice QCD, LCSR, QCDSR and unitarity bounds [150] and indicate a good convergence of the Heavy Quark Expansion.

LFU Ratio	SM Prediction	Observation	Tension
R_D	0.299(3)[158]	0.340(30)[158]	1.4σ
R_{D^*}	0.258(5)[158]	0.295(14)[158]	2.5σ
$R_{J/\Psi}$	0.2582(38)[159]	0.71(26)[160]	1.8σ
R_{D_s}	0.2993(46)[161]	-	-
$R_{D_s^*}$	0.2442(86) [162]	-	-
R_{Λ_c}	0.333(13)[163, 164]	-	-

Table 3.1: We show the SM prediction, experimental values and the individual tensions of several LFU ratios in $b \to c\ell\bar{\nu}$ as defined in Eq. (3.1). For the SM prediction of $R_{D^{(*)}}$ we quote the value from [158], however results from Refs. [150, 165] suggest slightly lower values and reduced uncertainties for R_{D^*} which enhance further the tension with the experimental measurement.

- The second main element entering the branching fractions is the CKM element V_{cb} [6, 151]. The treatment of this element is not trivial, as its main exclusive determinations come from processes with light leptons, i.e. from the $B \to D^{(*)}\ell\bar{\nu}$ decays with $\ell = \mu, e$. Furthermore, a historical tension has existed between the exclusive and inclusive V_{cb} determinations. This tension is still an open subject, however some elements might lead to believe that this tension is related to an underestimation of the systematic errors of these determinations (both theoretical and experimental) rather than NP. Several studies on the possible NP explanations of this tension exist in the literature [152–155], however, the latest results on the angular distributions of $B \to D^*\ell\bar{\nu}$ imply that simple NP explanations do not improve significantly the agreement between in inclusive and exclusive determinations of V_{cb} [155]. Furthermore, the most recent determination of the $B \to D^{(*)}$ form factors [150] suggest a higher value for the exclusive determination of V_{cb}, which is both compatible with the V_{cb} inclusive determination and previous exclusive determinations. We will thus assume that no NP is present in the light lepton $b \to c\ell\bar{\nu}$ modes [1], so that NP will be discussed at the level of the heavy mode $b \to c\tau\bar{\nu}_\tau$.

The branching fractions for the light leptons cannot be used for NP searches, but we may exploit the light lepton modes as a normalisation to get rid of V_{cb} by defining the *LFU ratios*

$$R_{H_c} = \frac{\Gamma(H_b \to H_c\tau\bar{\nu}_\tau)}{\Gamma(H_b \to H_c\ell\bar{\nu}_\ell)} \qquad \ell \in \{e, \mu\}\,, \tag{3.1}$$

for any $H_b \to H_c\tau\bar{\nu}_\tau$ mode. The numerator and denominator can be expressed very simply as sums of (squared moduli of) amplitudes. Using the weak effective Hamiltonian approach of Section 2.3, these amplitudes are linear combinations of Wilson coefficients and form factors (coming from hadronic matrix elements). The ratios R_{H_c} are interesting probes of LFUV and are very precisely predicted (to the percent level) in the SM, as shown in Table 3.1. This is due to the cancellation to a certain extent of the hadronic uncertainties from the form factors, which are correlated as shown by the HQET relations at leading order in Section 2.5.1

Angular Observables

Angular observables correspond to the observables that can be measured by looking at the angular distribution of the particles involved in the decay. At the theoretical level, they correspond to interferences between the amplitudes describing the decay, of the form $\mathrm{Re}[AB^*]$ or $\mathrm{Im}[AB^*]$, where A and B are linear combinations of Wilson coefficients and form factors.

As an example we will discuss the differential decay width of $B \to D\ell\bar{\nu}$ which is defined by 3 q^2-dependent

[1] Interestingly, a recent study [156] found discrepancies between the muon and electron mode forward backward asymmetry in $B \to D^*\ell\bar{\nu}$ at the level of 4σ by a reanalysis of Belle data [157], which could invalidate this hypothesis. However this might be related to inconsistencies found in the correlation matrices of the data published by Belle, so no conclusions should be drawn before further studies of the data are performed.

angular coefficients

$$\frac{d^2\Gamma}{dq^2 d\cos\theta_\ell} = a_{\theta_\ell}(q^2) + b_{\theta_\ell}(q^2)\cos\theta_\ell + c_{\theta_\ell}(q^2)\cos^2\theta_\ell\,, \tag{3.2}$$

$$a_{\theta_\ell}(q^2) = \mathcal{N}\left[\left|\tilde{h}_0^-\right|^2 + \frac{m_\ell^2}{q^2}\left|\tilde{h}_t\right|^2\right]\,, \tag{3.3}$$

$$b_{\theta_\ell}(q^2) = 2\mathcal{N}\frac{m_\ell^2}{q^2}\mathrm{Re}\left[\tilde{h}_0^+\tilde{h}_t^*\right]\,, \tag{3.4}$$

$$a_{\theta_\ell}(q^2) = \mathcal{N}\left[\left|\tilde{h}_0^-\right|^2 - \frac{m_\ell^2}{q^2}\left|\tilde{h}_0^+\right|^2\right]\,, \tag{3.5}$$

where $\mathcal{N}$ is a q^2 dependent normalisation, containing the phase space and the CKM matrixelement, and θ_ℓ is the angle of the charged lepton in its rest frame with respect to the direction of the D meson in the B rest frame (both the normalisation $\mathcal{N}$ and the explicit definition of θ_ℓ can be found for instance in Ref. [166]). The three amplitudes $\tilde{h}_0^+$, $\tilde{h}_0^-$, $\tilde{h}_t$, usually called the *helicity amplitudes* of the decay, are linear combinations of Wilson coefficients and form factors as mentioned above and they can be found in Ref. [166]. For instance, the first of them is given by

$$\tilde{h}_0^+(q^2) = (1+g_V)\sqrt{\frac{\lambda_{BD}(q^2)}{q^2}}f_+(q^2) + 2\frac{\sqrt{q^2}}{m_\ell}(g_T - g_{T5})\frac{\sqrt{\lambda_{BD}(q^2)}}{m_B+m_D}f_T(q^2)\,, \tag{3.6}$$

where $\lambda_{BD}(q^2) = m_B^4 + m_D^4 + q^4 - 2(m_B^2 m_D^2 + m_B^2 q^2 + m_D^2 q^2)$, illustrating the fact that the amplitudes are linear combinations of Wilson coefficients and form factors.

These angular coefficients can be recast into easily accessible quantities, the differential decay width $\frac{d\Gamma}{dq^2}(q^2)$ plus two other q^2 dependent observables: the forward backward asymmetry $A_{\mathrm{FB}}(q^2) = \frac{b(q^2)}{d\Gamma/dq^2(q^2)}$ and a "convexity" coefficient $A_{\pi/3} = \frac{c(q^2)}{2d\Gamma/dq^2(q^2)}$ [167]. In the case in which the polarization of the τ can be measured, more angular observables can be built taking into account this polarisation, and for instance, the polarisation asymmetry $A_{\lambda_\ell}(q^2)$ can also provide interesting information.

The angular observables are generally normalised to the branching fraction of the decay which in the case of $b \to c\ell\bar{\nu}$ decays makes them particularly interesting. Due to the existence of HQET relations reducing the form factors to a single function at leading order, one can see that hadronic uncertainties from the form factors are suppressed in A_{FB} and $A_{\pi/3}$ since the function ξ cancels in the heavy-quark limit, in a similar fashion to LFU ratios leading to uncertainties as low as a few percent [166] depending on the mode.

In the case of $B \to D^*\ell\bar{\nu}$ [166–168], the decay has a richer structure due to the higher spin of the D^* meson. The differential decay width is in this case defined by twelve q^2-dependent angular coefficients normalised to the branching fraction (described in detail in Chapter 7), including the longitudinal D^* polarisation $F_L^{D^*}$ and the lepton polarisation $P_\tau^{D^*}$. A similar cancellation of the function ξ occurs for these observables as in the case of $B \to D$.

Other modes

Other modes involving the $b \to c\ell\bar{\nu}$ transition than the above mentioned $B \to D^{(*)}\ell\bar{\nu}$ can also be studied. For instance, the $B_c \to J/\Psi\ell\bar{\nu}$ form factors have been studied on the lattice in Ref. [159] and the $B_s \to D_s^{(*)}\ell\bar{\nu}$ form factors in Refs. [161, 162], however these studies are less advanced than the ones in $B \to D^{(*)}$. Theoretical studies of the baryonic modes $\Lambda_b \to \Lambda_c^{(*)}\ell\bar{\nu}$ have been carried out in Refs. [163, 164, 169, 170], which would complement the results on the meson side if measured.

In the case of $B_c \to \ell\bar{\nu}$, the only observable is the branching ratio, with an accurate prediction depending on a single hadronic input, the B_c meson decay constant f_{B_c}. Predictions for the SM branching fraction of this decay based on the latest lattice QCD results [171, 172] for f_{B_c} can be found in Ref. [173] leading to a value slightly smaller than 2% a relative uncertainty at the 5% level.

3.1.2 Experimental results in $b \to c\ell\bar{\nu}$

We will now discuss the different observables experimentally accessible in $b \to c\tau\bar{\nu}_\tau$, of which an overview is shown in Table 3.2.

Observables	$\mathcal{B}\,\ell = \tau$	R	Angular Observables
$B \to D\ell\bar{\nu}$	✓	✓	✗
$B \to D^*\ell\bar{\nu}$	✓	✓	✓†
$B_c \to J/\Psi\ell\bar{\nu}$	✗	✓	✗
$B_c \to \ell\bar{\nu}$	✓‡	✗	✗
$B_s \to D_s\ell\bar{\nu}$	✗	✗	✗
$B_s \to D_s^*\ell\bar{\nu}$	✗	✗	✗
$\Lambda_b \to \Lambda_c\ell\bar{\nu}$	✗	✗	✗

Table 3.2: Observables experimentally available in $b \to c\ell\bar{\nu}$ modes. †: Only the Longitudinal D^* polarization F_L and the τ polarization P_τ are available. ‡: Although this decay has not been yet measured, constraints on its branching fraction exist, coming from the B_c lifetime.

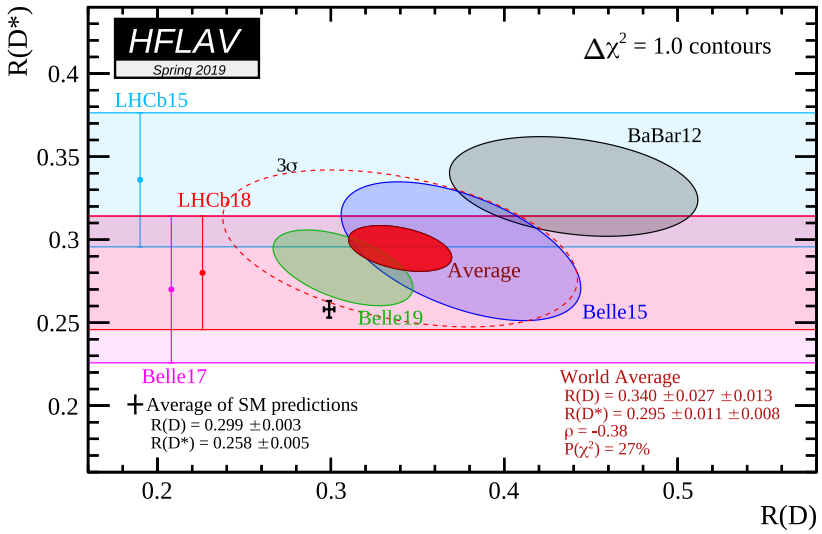

Figure 3.1: Combination of $(R(D), R(D^*))$ results showing a tension with the SM predictions of 3.1σ [158].

LFU Ratios

The LFU ratios $R(H_c)$ defined in Eq. (3.1) have been of huge interest in the past few years as a number of experiments have observed hints of LFUV in several of them [158, 174–182], with enhancements of the τ branching fractions with respect to the light lepton ones. Their experimental measurements can be found in Table 3.1. The Heavy Flavour Averaging Group (HFLAV) [158] currently reports a combined tension of $\sim 3.1\sigma$ for R_D and R_{D^*} (see Fig. 3.1), with some of the latest SM predictions reaching a tension of 3.8σ [150, 165] due to slightly lower values for $R_{D^*}^{SM}$ and reduced uncertainties. A related 1.8σ tension has also been reported in the $B_c \to J/\psi\ell\bar{\nu}$ decay branching ratio [160]. No measurement on the baryon side has been reported yet.

Other Observables

Currently none of the angular observables of $B \to D\tau\nu$ have been measured and only two of the twelve angular observables available have been experimentally measured for $B \to D^*\tau\bar{\nu}_\tau$; on one side, the lepton polarization (P_τ) for $B \to D^*\tau\bar{\nu}$ was measured to be compatible with the SM at $< 1\sigma$ [178, 179] and, on the other side, the longitudinal polarization (F_L) was measured to be compatible with SM at 1.7σ [183]. Experimentally, the reconstruction of this angular distribution is not straightforward because the neutrino is not detected, however a method for an unbiased measure of these observables has been proposed in Ref. [184].

On the side of $B_c \to \tau\bar{\nu}$, the branching ratio is not measured yet, but it cannot be larger than 100% and thus a bound is obtained through the B_c^- lifetime [185]. This can be further constraint by considering the branching fractions for B_c that have been already measured. Conservative estimates of this bound yield a value of $\mathcal{B}(B_c \to \tau\bar{\nu}) \lesssim 30\%$[186] and up to $\mathcal{B}(B_c \to \tau\bar{\nu}) \lesssim 10\%$ with more liberal approaches. This bound has been fundamental to constrain NP global fits as we will see now.

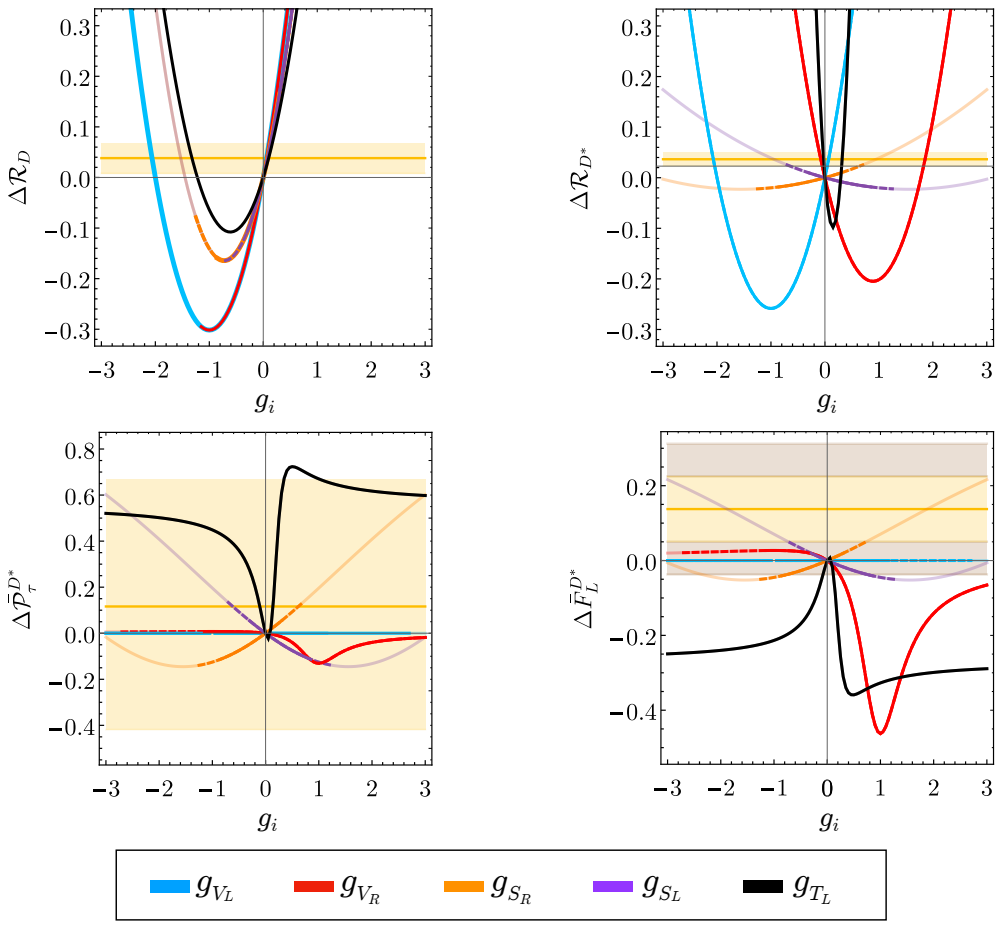

Figure 3.2: Dependence of the R_D, R_{D^*}, $P_\tau^{D^*}$ and $F_L^{D^*}$ observables on the individual variation of each Wilson coefficients of the effective Hamiltonian of $b \to c\ell\bar{\nu}$. The horizontal bands (orange, gray) correspond the $1\sigma/2\sigma$ ranges for the deviations observed with respect to SM expectations. The solid (dashed) lines show the parameter space allowed by the constraint $\mathcal{B}(B_c \to \tau\bar{\nu}) < 10\%(30\%)$, whereas the faint lines show the predictions without taking into account this constraint. Adapted from Ref. [187]

3.1.3 Global Fits

Noticeably, the amount of observables available in the $b \to c\ell\bar{\nu}$ transition is not overwhelming. In fact, a whole family of angular observables for $B \to D^*\tau\bar{\nu}$ decays are yet to be measured which could provide a hold on the nature of the possible NP behind the deviations on the LFU ratios [156, 166, 188, 189]. However, the current constraints already provide some insight on the NP explanations allowed.

Global fits to the Wilson coefficients of the $b \to c\tau\bar{\nu}_\tau$ WET (see Eqs. (2.16) and (2.17)) have been performed by several groups [82, 83, 165, 166, 187], generally favouring a NP contribution through a real g_{V_L} for $b \to c\tau\bar{\nu}_\tau$ (see Fig. 3.4), as it allows one to modify the tauonic branching ratios involved in R_D and R_{D^*} by the same amount without altering the angular observables nor exhibiting any tension with the loose bounds on the B_c lifetime as it can be seen in Figs. 3.2 and 3.3. Of course, an enhancement of $F_L^{D^*}$ would be desirable as it would reduce the tension with the relatively high value, compared to the SM prediction, measured by Belle. However this appears difficult to accommodate in simple NP scenarios (with a main real NP contribution in a single Wilson coefficient) while respecting the B_c lifetime constraint as shown in Figs. 3.2 to 3.4.

For real contributions, scenarios based purely on scalar and pseudoscalar contributions exhibit some tension with the B_c lifetime as their contributions are enhanced compared to the helicity-suppressed contribution from the SM. The tension depends on the relative size of the contribution allowed for $B_c \to \tau\bar{\nu}_\tau$ in the total lifetime, which requires the pseudoscalar contribution to be somewhat small [185, 186, 190]. Similarly, real tensor contributions are disfavoured, as they tend to drastically lower the longitudinal polarisation of the D^* meson compared to the SM [166], when the first measurement from the Belle experiment indicated a value higher than SM expectations [183]. If g_{V_L} is allowed as well as contributions of other operators, the former is the largest NP contribution and the other operators (scalar, pseudoscalar, tensors) are subleading [82, 83, 166]. Other constraints on $b \to c\tau\bar{\nu}_\tau$ come from direct searches at LHC involving mono-τ jets [191]. The corresponding bounds are again much tighter on tensor operators than on vector or scalar operators.

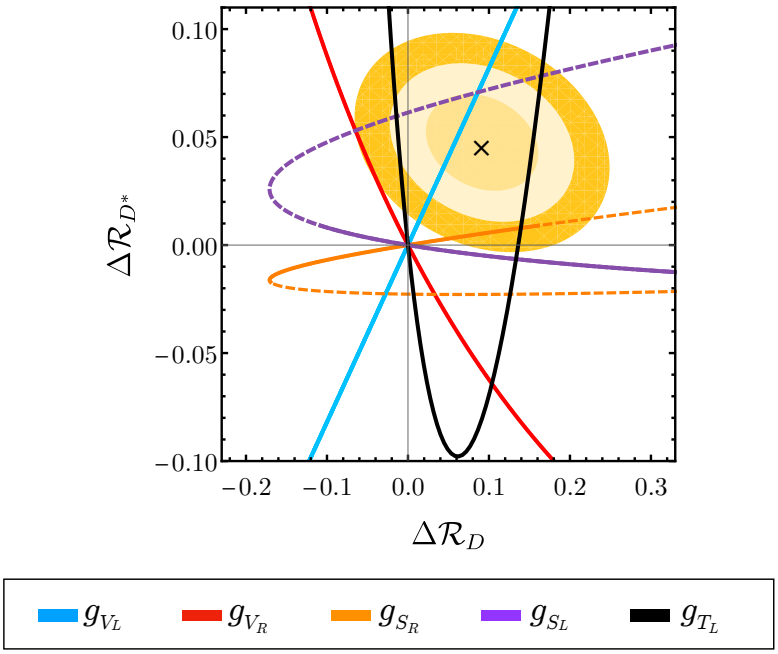

Figure 3.3: Values of R_D and R_{D^*} by including New physics in each of the Wilson coefficients in the $b \to c\ell\bar{\nu}$ global fit. The orange ellipses correspond the 1σ, 2σ and 3σ ranges for the deviations observed with respect to SM expectations. The solid lines show the parameter space allowed by the constraint $\mathcal{B}(B_c \to \tau\bar{\nu}) < 10\%$, whereas the dashed lines show the predictions without taking into account this constraint. Adapted from Ref. [165]

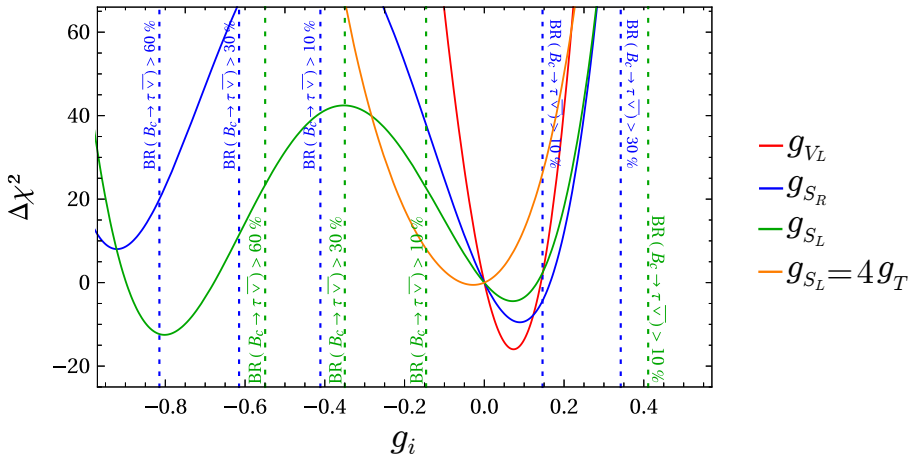

Figure 3.4: $\Delta\chi^2$ for the different 1D global fit of the $b \to c\ell\bar{\nu}$ transition performed in Ref. [83], different $\mathcal{B}(B_c \to \tau\bar{\nu})$ constraints for the scalar scenarios are shown by the dashed lines. Adapted from Ref. [83].

Turning now to scenarios with complex coefficients, some allow large imaginary parts [82, 83, 166], with a similar hierarchy of scenarios as in the real case. However, one must take into account that such large imaginary parts are allowed due to the limited number of observables. Additional observables, in particular CP asymmetries, could bring a dramatic modification of the landscape of the allowed scenarios, restricting the possible size of imaginary parts and the applicability of scenarios currently viable severely. Indeed some of the NP scenarios favour large imaginary parts so that there are no interferences between the SM and NP contributions, which add up in quadrature only (see for instance the scenario of a purely imaginary g_{S_L} discussed in Ref. [192]). Restricting the size of these imaginary parts would enhance the interferences between SM and NP parts and would restrict the viability of the NP models where these interferences are negative.

This trend is confirmed by model-dependent analyses which we will discuss in Section 3.3.

3.2 The $b \to s\ell^+\ell^-$ flavour anomalies

3.2.1 Theoretical predictions in $b \to s\ell^+\ell^-$

Similarly to the last section, we will discuss now the main elements that go into the theoretical predictions of $b \to s\ell^+\ell^-$ modes and the cleanest observables available. We will first focus on the branching fractions and the LFU ratios, and then discuss the angular observables available. We will discuss several different modes, starting with the $B \to K^{(*)}\ell^+\ell^-$ and $B_s \to \phi\ell^+\ell^-$ modes then discussing the baryonic mode $\Lambda_b \to \Lambda\ell^+\ell^-$ which offers a different theoretical and experimental environment. Finally we will briefly discuss the purely leptonic $B_s \to \ell^+\ell^-$ and the radiative modes $B \to K^*\gamma$, $B_s \to \phi\gamma$ and $B \to X_s\gamma$. Due to the difficulties of τ reconstruction, experimental results for $b \to s\tau^+\tau^-$ decays are not yet available (although there are existent bounds), so we will focus on $b \to s\mu^+\mu^-$ and $b \to se^+e^-$ decays.

As discussed in Chapter 2, the amplitude of $b \to s\ell^+\ell^-$ is determined by 4 main elements: a CKM factor, the short-distance Wilson coefficients (potentially containing NP contributions), the hadronic form factors for the corresponding hadron states and a non-factorisable contribution.

- Contrary to $b \to c\ell\bar{\nu}$, since $b \to s\ell^+\ell^-$ transition is a loop suppressed transition, the V_{tb} and V_{ts} CKM elements present in it are not constrained through $b \to s\ell^+\ell^-$, but through other processes measured in more detail and better understood theoretically ($V_{tb}V_{ts}^*$ is determined mainly from B_s meson mixing). However, if NP is present, it may interfere also with the processes used for the determination of CKM matrix elements. For instance, a NP model contributing to $\Delta F = 1$ transitions like $b \to s\ell^+\ell^-$ is very likely to also contribute to $\Delta F = 2$ transitions (i.e. $B_s - \bar{B}_s$ mixing). However, since no inconsistency has been found in global CKM fits within the SM (see Ref. [151]), we may assume that shifts due to NP in $\Delta F = 2$ are either small or have SM-like flavour structure [2] and that they are thus not a major issue for the separation between CKM determination and NP searches.

- The Wilson coefficients are systematically computed in the SM and in NP models without posing a main issue (see Chapter 2). As discussed before, the main contributions in the SM come from $\mathcal{C}_{7\gamma}$, $\mathcal{C}_{9\ell}$, $\mathcal{C}_{10\ell}$ and their respective influence in the different q^2 regions is shown in Fig. 2.8.

- Form factors are determined through the same methods as in $b \to c\ell\bar{\nu}$ with varying precision depending on the mode at hand and the kinematic region considered, usually being an important source of uncertainty, reason why one would like to suppress their contributions. As opposed to the situation in $b \to c\ell\bar{\nu}$, the form factors describing the $b \to s\ell^+\ell^-$ transition, do not in general reduce to a single form factor like the Isgur-Wise function. However, as we discussed in Section 2.5, in the low- and large-recoil limits, relations between the form factors can be derived up to $\mathcal{O}(\Lambda_{\rm QCD}/m_b)$ corrections.

- Non-factorisable contributions (related to charm loops) are an extra issue of this transition, they are computed perturbatively to LO, i.e. up to $\mathcal{O}(\alpha_s, \Lambda_{\rm QCD}/m_b)$ corrections which are harder to compute and their uncertainties harder to estimate. Soft gluon corrections to non-factorisable contributions have been determined in Refs. [109, 112, 115, 116] $B \to K^*\ell^+\ell^-$ mode together with the $B \to K\ell^+\ell^-$ and $B_s \to \phi\ell^+\ell^-$ modes as discussed in Section 2.7. Non-factorisable contributions also become large in the regions where the invariant dilepton mass q^2 is close to $c\bar{c}$ resonances like the J/Ψ or the $\Psi(2S)$ as shown in Fig. 2.8. These regions are harder to predict and are dominated by non-perturbative QCD, reason why we will refrain to use them for studying possible NP, but we can still exploit these regions to cross-check our understanding of the QCD dynamics at work. For instance, they are used to extrapolate results of non-factorisable contributions from LCSR to the region of interest of the invariant mass [109, 112]. On the experimental side they are also used as normalisations to calibrate the assessment of systematic uncertainties and cross-check the selection of the events.

[2] This is usually referred to as a Minimal Flavour Violation structure, which we will discuss at the end of this chapter.

LFU Ratio	SM Prediction	Observation	Tension
$R_K^{[1.1,6]}$	1.00(1)	$0.846^{+0.06}_{-0.06}$	2.5σ
$R_{K^*}^{[0.045,1.1]}$	0.92(2)	$0.66^{+0.11}_{-0.08}$	2.1σ
$R_{K^*}^{[1.1,6]}$	1.00(1)	$0.69^{+0.12}_{-0.09}$	2.4σ
$R_{pK}^{[0.1,6]}$	$0.99^{\dagger}$	$0.85^{+0.14}_{-0.13}$	1σ

Table 3.3: We show the SM prediction [204, 205], experimental values and the individual tensions of several LFU ratios in $b \to s\ell^+\ell^-$ as defined in Eq. (3.7) for two different bins of q^2. Experimental values come from the LHCb collaboration [206, 207] as they are the most precise results to date. †: Naive estimation including only the phase space.

Because of the above, several observables in which hadronic contributions are suppressed have been developed, which we will discuss below. The aim of this section is only to provide an overview of the observables considered and we will not yet discuss the global fits to the $b \to s\ell^+\ell^-$ transition, since the next chapter, will be fully devoted to the $b \to s\ell^+\ell^-$ global fit, and will provide more detail on these anomalies.

Branching fractions and LFU Ratios

In principle, branching fractions are the less clean observables available, since hadronic contributions are not suppressed. However there has been big efforts in the last few years to extract the form factors corresponding to these branching fractions more precisely and to estimate the non-factorisable contributions as discussed in the previous chapter. This has lead to relatively precise (30% uncertainty) theoretical predictions for several modes which are of the same order as the current experimental uncertainties, which can be seen for instance in Table 4.A.1 where we show the SM predictions and the experimental measurement for several of these branching fractions.

The simplest semileptonic exclusive $b \to s\ell^+\ell^-$ decay corresponds to the $B \to K\ell^+\ell^-$ decay, it is described by 3 form factors which have been determined through Lattice QCD and LCSR in Refs. [39, 96, 193, 194]. Due to its large phase space, extending largely above the first $c\bar{c}$ resonances, the $B \to K\ell^+\ell^-$ decay provides a good probe of the $b \to s\ell^+\ell^-$ transition in the low-recoil region, allowing for an integration over multiple $c\bar{c}$ resonances which is required for the validity of the quark-hadron duality argument discussed in Section 2.7. The $B \to K^*\ell^+\ell^-$ and $B_s \to \phi\ell^+\ell^-$ modes are more complicated and involve 7 form factors which have also been determined in different kinematic ranges through Lattice QCD and LCSR in Refs. [39, 109, 195].

It is also interesting to consider $b \to s\ell^+\ell^-$ hadronic decays involving baryons instead of mesons. Indeed LHCb provides information on decays not only of mesons but also of baryons containing a quark b, in particular Λ_b decays, which might in principle be produced in polarized states. The theoretical analysis of these decays does not stand at the same level as for meson decays (in particular for the determination of the form factors and the estimation of charm-loop contributions) but it can provide interesting cross checks of the results obtained in the meson sector. A first step in this direction has been attempted through the study of the decay $\Lambda_b \to \Lambda(\to N\pi)\mu^+\mu^-$ which has been investigated in Refs. [196–202]. Determinations for the 8 $\Lambda_b \to \Lambda$ form factors have been obtained on the lattice in Ref. [203] and through SCET sum rules in Ref. [40].

In a similar way to $b \to c\ell\bar{\nu}$, the ratio of branching fractions

$$R_{H_s} = \frac{\Gamma(H_b \to H_s\mu^+\mu^-)}{\Gamma(H_b \to H_s e^+e^-)} \tag{3.7}$$

will be a very interesting observable. In this case, we not only get rid of the CKM factor but of practically all SM uncertainties. Since LFU is conserved in the SM up to corrections of the lepton masses, these ratios will be 1 up to kinematic corrections of order $\mathcal{O}(m_\mu/\sqrt{q^2})$ which are however computable to a very good accuracy as show in Table 3.3, leading to accuracies on the percent level. This makes the R_{H_s} ratios extremely clean probes of LFUV NP.

One decay in which the situation is slightly different for the branching fraction, is the purely leptonic mode $B_s \to \ell^+\ell^-$. In this decay, similarly to $B_c \to \ell\bar{\nu}$, the hadronic uncertainties of the branching fraction are reduced since it depends on a single hadronic parameter, the B_s decay constant f_{B_s}. Recent estimations [208, 209] for the branching fraction of this decays suggest a value of

$$\mathcal{B}(B_s \to \mu^+\mu^-)_{\rm SM} = (3.6 \pm 0.17) \times 10^{-9} \tag{3.8}$$

Contrary to $B_c \to \ell\bar{\nu}$ and thanks to $B_s - \bar{B}_s$ mixing, an extra observable can be defined for this mode corresponding to the $B_s \to \ell^+\ell^-$ effective lifetime discussed in Ref. [210]. One interest feature of purely leptonic

$b \to s\ell^+\ell^-$ modes is that they are helicity suppressed in the SM, suppression which could be lifted in NP scenarios with new (pseudo)scalar particles, making them good probes for these kind of NP.

The branching fractions of the exclusive radiative modes $\mathcal{B}(B \to K^*\gamma)$, $\mathcal{B}(B_s \to \phi\gamma)$ and inclusive radiative mode $\mathcal{B}(B \to X_s\gamma)$ are important observables that constrain the contribution from the electromagnetic dipole operator and its chirally flipped partner ($\mathcal{O}_{7\gamma}$ and $\mathcal{O}_{7'\gamma}$). The exclusive modes however suffer from large hadronic uncertainties, making the inclusive radiative mode $\mathcal{B}(B \to X_s\gamma)$, the most constraining mode as it can be seen in Fig. 3.8. The most accurate predictions to date for this mode Ref. [211]. A general discussion of the theoretical prediction and the constraints on NP coming from radiative modes can be found in Ref. [212].

Angular distributions and optimized observables

Unlike $b \to c\ell\bar{\nu}$, in $b \to s\ell^+\ell^-$ angular observables normalised to the branching ratio do not have a natural suppression of hadronic uncertainties, as they depend on several form factors which cannot always be correlated using EFTs of QCD (HQET or SCET). Indeed, depending on the spins of the hadrons involved, different relations between the form factors can be obtained in the low- and large-recoil regions, as can be illustrated by considering $B \to K$ versus $B \to K^*$. In the case of $B \to K$, all form factors are reduced to a single form factor at leading order ($\mathcal{O}(\Lambda_{\rm QCD}/m_b)$) in both limits, although in a different way for f_0 in both limits (see Section 2.5). These makes all angular observables normalised to the branching ratio optimized in both limits in the sense that both numerator and denominator of these observables involve a single form factor, which cancels, up to $\mathcal{O}(\Lambda_{\rm QCD}/m_b)$ corrections (typically of order 10%). However this is no longer the case for $B \to K^*$ in which full QCD form factors only reduce to two different form factors ($\xi_{\perp,\parallel}$, see Eq. (2.75)) in SCET, i.e. in the large-recoil limit, and into four independent form factors in HQET, i.e. in the low-recoil limit. One has then to carefully design specific ratios of angular observables involving only subsets of these form factors. In these ratios, called "optimized observables", the soft form factors defined in the EFT cancel in the heavy-quark limit, leaving $\mathcal{O}(\Lambda_{\rm QCD}/m_b)$ corrections which are again, typically at the order of 10%.

The angular distribution of $B \to K\ell^+\ell^-$ is described by 3 angular observables [213]: the differential decay width itself $d\Gamma/dq^2$, the forward backward asymmetry $A_{\rm FB}$ and lastly F_H. $A_{\rm FB}$ vanishes in the SM, making it a good null test, and F_H is suppressed by the lepton mass. Since we are dealing with the light lepton modes, the polarisation of the leptons is not easily experimentally accessed as it is in the case of $b \to c\tau\bar{\nu}_\tau$.

In the case of $B \to K^*\ell^+\ell^-$ and $B_s \to \phi\ell^+\ell^-$ the angular distribution is described by 12 angular observables that reduce to 9 in the massless lepton limit including the so "optimized observables" P_i and P_i' introduced in Refs. [87, 214]. The P_i observables are designed to suppress the LO hadronic uncertainties both in the low- and large-recoil limits and the P_i' observables have the advantage of being experimentally cleaner, while being optimized at large-recoil, however at low-recoil [215, 216] their cleanness requires further assumptions [87]. Furthermore, observables to compare the muon and electron decays, called Q_i, have been defined based on the P_i observables, by taking the differences in between the two modes ($Q_i = P_i^\mu - P_i^e$) [136]. These observables are thus optimised LFUV angular observables, with an interesting sensitivity to NP effects.

The treatment of the neutral modes like $B_d \to K^0\ell^+\ell^-$, $B_d \to K^{*0}\ell^+\ell^-$ and $B_s \to \phi\ell^+\ell^-$ is slightly different than the charged modes due to neutral meson mixing.

For instance, in the case of $B_d \to K^0\ell^+\ell^-$ both the B_d and $\bar{B}_d$ mesons can decay into any of the two kaon CP-eigenstates $K_{S,L}$ making the decay non self-tagging [3].

Contrary to the pseudoscalar meson mode, the vector meson mode $B \to K^{*0}\ell^+\ell^-$ can be self-tagging or not [217] depending on the decay of the K^{*0} (self-tagging : $K^\pm\pi^\mp$ or not self-tagging : $K_S\pi^0$) since there is no mixing of K^{*0}.

The description of the the $B_s \to \phi\ell^+\ell^-$ decay is similar to $B \to K^{*0}\ell^+\ell^-$ with the small caveat that this decay is not self-tagging (since ϕ is a $s\bar{s}$ state) [217].

For the non-self-tagging modes we can consider two possibilities :

- Take into account the $B - \bar{B}$ mixing, by performing a time dependent analysis leading to new observables at the price of requiring higher statistics and a good experimental ability to analyse the time evolution of the B-meson.
- Ignore the mixing by integrating over time and performing an average over B and $\bar{B}$. Because of the obligation of choosing a singular angle convention for both B and $\bar{B}$, some angular observables will correspond to CP averages while others will be CP asymmetries, finally obtaining only half of the observables that can be accessed in the self-tagging case.

We will discuss this further in Chapter 6.

[3] A neutral B-decay is said to be self-tagging when one can know whether the decaying state is a B or a $\bar{B}$ by its decay products. In the charged case ($B^+ \to K^+\ell^+\ell^-$), this is possible by looking at the charge of the K meson. However in the case of the neutral B decay, since both B and $\bar{B}$ decay into $K_{S,L}$ the distinction between B and $\bar{B}$ becomes impossible.

Modes/Observables	$\mathcal{B}\,\ell = \mu$	R	Angular Observables $\ell = \mu$	Angular Observables $\ell = e$
$B \to K\ell^+\ell^-$	✓	✓	✓	✗
$B \to K^*\ell^+\ell^-$	✓	✓	✓	✓†
$B_s \to \phi\ell^+\ell^-$	✓	✗	✓	✗
$B_s \to \ell^+\ell^-$	✓	✗	-	-
$\Lambda_b \to \Lambda\ell^+\ell^-$	✓	✗	✓	✗
$\Lambda_b \to pK\ell^+\ell^-$	✓	✓	✗‡	✗‡

Table 3.4: Observables experimentally available in $b \to s\ell^+\ell^-$ modes. †: Only a fraction of these observables are measured. ‡: The measurement of angular observables of the $\Lambda_b \to pK\ell^+\ell^-$ directly would not provide any relevant information as the contribution of multiple Λ resonances is involved.

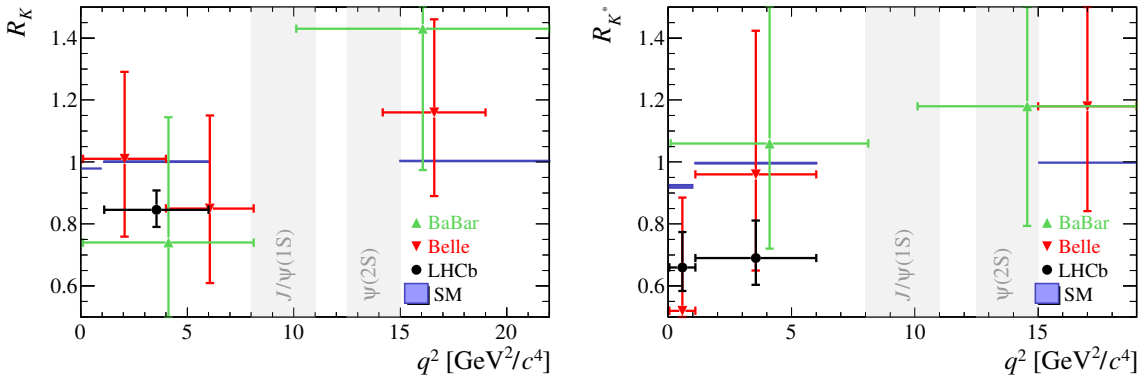

Figure 3.5: Measured values of the R_K (left) and R_{K^*} (right) LFU ratios by the LHCb [206, 207], Belle [219, 220] and BaBar [221] collaborations. Taken from Ref. [222].

The angular distribution of the $\Lambda_b \to \Lambda(\to N\pi)\mu^+\mu^-$ decay is given by 10 angular observables, through which we can define a single optimized observable in the low-recoil limit [197]. However, in the case large recoil limit, any ratio of angular observables is optimized thanks to SCET relations between the form factors, which reduce all 8 form factors into a single soft form factor [197]. The possible polarisation of the Λ_b baryon, could allow for an even richer angular distribution [201], however, measurement of the Λ_b polarisation at LHCb shows values compatible with 0 [218].

3.2.2 Experimental results in $b \to s\ell^+\ell^-$

We will now present the main experimental results available in the $b \to s\ell^+\ell^-$ transition. The amount of $b \to s\ell^+\ell^-$ observables currently available is rather large compared to $b \to c\ell\bar{\nu}$. In the case of the $b \to s\ell^+\ell^-$ transition, all angular observables are binned according to the dilepton invariant mass q^2, and not integrated over the full q^2 range, in order to avoid the region of the lighter charmonium resonances. Moreover, the large amount of data currently available, allows one to separate the observables in several q^2 bins in order to have a hold on the q^2 dependence of this observables. An overview of the observables available in the $b \to s\ell^+\ell^-$ transition is shown in Table 3.4 and the measured values of the majority of them can be found in Appendix 4.A together with their theoretical predictions.

LFU ratios

We start this discussion with the LFU ratios R_{H_s} defined in Eq. (3.7), in which notable deviations from the SM predictions have appeared over the past few years. The LFU ratios R_K and R_{K^*}

$$R_{K^{(*)}} = \frac{\mathcal{B}(B \to K^{(*)}\mu^+\mu^-)}{\mathcal{B}(B \to K^{(*)}e^+e^-)}, \tag{3.9}$$

have been measured by the LHCb, Belle and BaBar collaborations as shown in Fig. 3.5. The most precise of these results, obtained for two different q^2 bins ($[0.045, 1.1]$ and $[1.1, 6]$ GeV^2), come from the LHCb collaboration and they are largely dominated by statistical uncertainties. They show individual tensions with the SM predictions ranging from 2.1σ to 2.5σ as shown in Table 3.3, showing all a tendency towards lower branching fractions

for muons compared to electrons. These measurements correspond to one of the main flavour anomalies in $b \to s\ell^+\ell^-$ decays and without a doubt, the cleanest of them.

Recently, the LHCb experiment has also measured the ratio R_{pK^-}

$$R_{pK^-} = \frac{\mathcal{B}(\Lambda_b \to pK^-\mu^+\mu^-)}{\mathcal{B}(\Lambda_b \to pK^-e^+e^-)} \tag{3.10}$$

for a squared dilepton invariant mass, q^2, between 0.1 and 6 GeV$^2/c^4$ and a pK^- invariant mass below 2.6 GeV/c^2 [223]. This result, shown in Table 3.3, is compatible with SM expectations, but it suggests a suppression of $\mathcal{B}(\Lambda_b \to pK^-\mu^+\mu^-)$ compared $\mathcal{B}(\Lambda_b \to pK^-e^+e^-)$, similarly to R_K and R_{K^*}. However, the interpretation of this result would require a precise theoretical knowledge of the various excited Λ states contributing in this large pK^- region (hadronic form factors, interference patterns). A deeper understanding could be achieved by focusing on a single of these resonances as an intermediate state, which we will discuss further in Chapter 5.

Differential decay width

The differential decay width for exclusive semileptonic $b \to s\ell^+\ell^-$ decays has been measured for several modes which we show in Fig. 3.6, the most precise measurements coming from the LHCb collaboration. These modes show a tension with the SM prediction in several bins of the branching fraction with values going from 1σ to as high as 3.6σ

The first of these modes is the $B \to K\mu^+\mu^-$ mode, for which the LHCb measurements [224] show consistently lower values than the SM prediction of the branching fraction at the large-recoil region. The first low q^2 bin is compatible with the SM, suggesting a SM-like $\mathcal{C}_{7\gamma}$ contribution whereas the low value of the other bins suggest a possible NP contribution to $\mathcal{C}_{9\mu}$. The measurement of the $B \to K^*\mu^+\mu^-$ branching fraction also lie slightly below the SM predictions in the low q^2 region, however still compatible with the SM with tensions only slightly higher than 1σ.

In the case of $B_s \to \phi\mu^+\mu^-$, its differential decay width has been measured [225] to be lower than the SM expectations in the low q^2 region, following the trend of $B \to K\mu^+\mu^-$ and showing the highest tension with the SM prediction, reaching a value of 3.6σ in the q^2-region between 1.1 and 6.0 GeV^2.

The $\Lambda_b \to \Lambda(\to N\pi)\mu^+\mu^-$ differential decay width was measured by the LHCb collaboration in Ref. [226] . There seems to be a trend for the branching ratio to be lower than the SM expectations at large-Λ recoil and larger at low-Λ recoil (although compatible within errors). It is important to mention that these results are to be carefully interpreted, since the normalisation used in Ref. [226] relies on the measurement of $f(b \to \Lambda_b)$, which presented some issues due to a strong dependence on the b-quark transverse momentum and the production processes. This issue is discussed in Ref. [227] where also a corrected approach is presented. The corrected differential decay width for this mode is shown in Fig. 3.6 suggesting a deviation at low-recoil.

The $B_s \to \mu^+\mu^-$ branching fraction and effective lifetime have been measured by the LHCb, CMS, and ATLAS collaborations. The joint measurement [233] for the branching fraction is shown in Fig. 3.7 together with the current limits on the $B \to \mu^+\mu^-$ branching fraction. These results correspond to a branching fraction of

$$\mathcal{B}(B_s \to \mu^+\mu^-)_{\text{exp}} = 2.69^{+0.37}_{-0.35} \times 10^{-9} \tag{3.11}$$

which shows a tension of 2.2σ[4] with the SM prediction in Eq. (3.8).

The branching fractions for the exclusive radiative modes $B \to K^*\gamma$, $B_s \to \phi\gamma$ have been measured by the BaBar [234], Belle [235, 236] and LHCb [237] collaborations, showing results compatible with the SM predictions. The world average for the inclusive mode $B \to X_s\gamma$, which is also compatible with its SM prediction, can be found in Ref. [158]. The constraints on the $\mathcal{C}_{7\gamma}$ Wilson coefficient derived from the radiative modes can be seen in Fig. 3.8.

Angular observables

The angular distribution of the $B \to K\mu^+\mu^-$ decay have been analysed by several collaborations, with the most precise results coming from LHCb [238]. These measurements do not show deviations from the SM expectations.

The most precise measurements of the angular observables of the $B \to K^*\mu^+\mu^-$ mode come from the LHCb collaboration [239, 240]. While most of the observables are compatible with their SM predictions, the optimised observable P_5' shows consistent deviations from the SM predictions for both the charged and neutral modes (i.e. $B^+ \to K^{*+}\mu^+\mu^-$ and $B^0 \to K^{*0}\mu^+\mu^-$) as shown in Fig. 3.9. In the case of the charged mode, deviations

[4] This tension is however mainly driven the results from the ATLAS collaboration which are in slight tension with the LHCb and CMS results. Furthermore, even though the ATLAS collaboration has not yet found evidence for the $B^0 \to \mu^+\mu^-$ decay, they include the fit result of the $B^0 \to \mu^+\mu^-$ branching fraction (which takes a negative unphysical central value in the fit) into the combination, which has a large weight in the tension of the average with the SM.

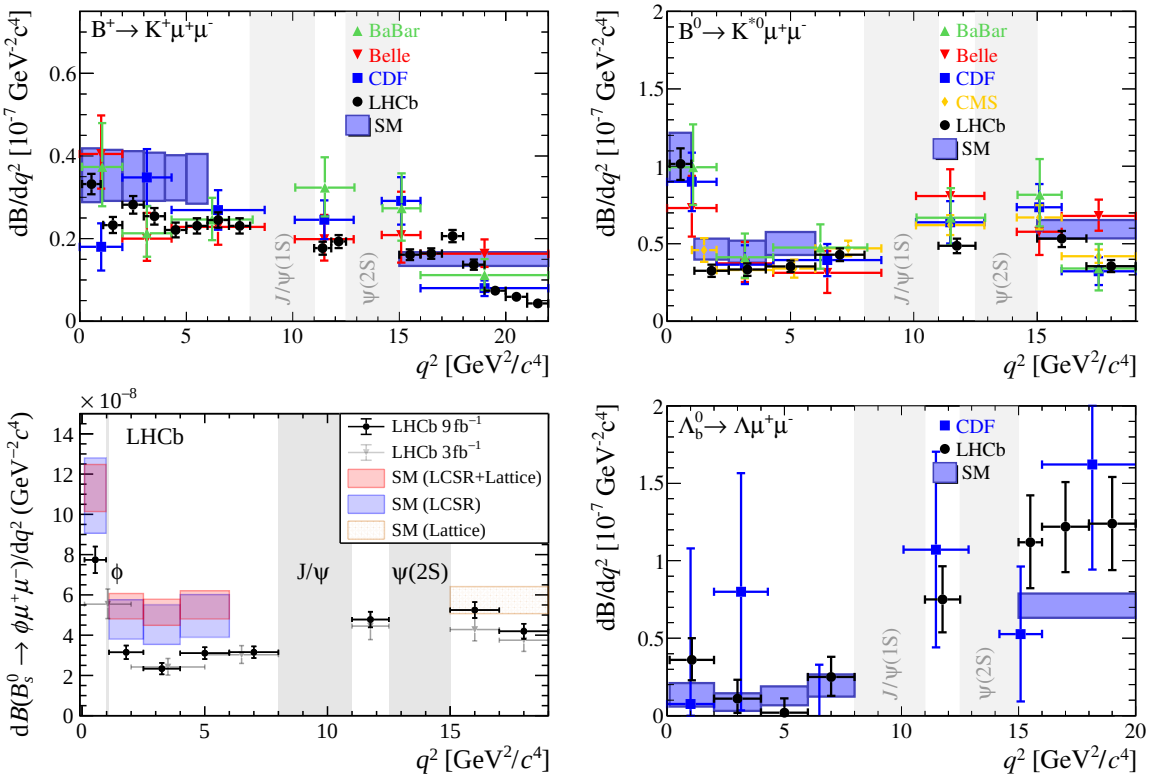

Figure 3.6: SM predictions and measurements of the differential branching fraction of the exclusive semileptonic $b \to s\mu^+\mu^-$ modes in several bins of the invariant dilepton mass q^2. From left to right and top to bottom, $B^+ \to K^+\mu^+\mu^-$, $B^0 \to K^{*0}\mu^+\mu^-$, $B_s \to \phi\mu^+\mu^-$ and $\Lambda_b \to \Lambda(\to N\pi)\mu^+\mu^-$ as measured by the LHCb [224–226, 228, 229], CMS [230], Belle [231], BaBar [221] and CDF [232] collaborations. Taken from Refs. [222, 225].

have been also found in the P_2 optimised observable. When a 1D fit is performed to the angular observables allowing for real NP contributions to $\mathcal{C}_{9\mu}$, a tension of 3.1σ and 3.4σ is found for the charged and neutral modes respectively.

Angular observables for the $B \to K^* e^+ e^-$ mode have been also been measured, in the low q^2 region by LHCb [241] [5]. However, only a reduced amount of them has been obtained due to the lower efficiency of LHCb to measure electrons (compared to muons).

The $P'_{4,5}$ observables have been also measured by Belle [242] for both the muon and electron modes shown some deviations for the muon mode for $P'_{5\mu}$ similarly to LHCb. From these observable they have extracted for the first time the LFU angular observables $Q'_{4,5}$ showing the same deviations that appear in $P'_{5\mu}$ when comparing them with the extremely accurate SM predictions for these observables.

The LHCb collaboration has recently updated the angular analysis for the $B_s \to \phi\mu^+\mu^-$ mode [229, 243, 244], where they perform a time integrated angular analysis. They measure the CP-averaged angular observables F_L and $S_{3,4,7}$ and the CP-asymmetries $A_{\rm FB}^{\rm CP}$ and $A_{5,8,9}$ obtaining results compatible with the SM.

The $\Lambda_b \to \Lambda(\to N\pi)\mu^+\mu^-$ angular observables were measured by the LHCb collaboration in Refs. [226, 247]. The measured angular observables at low-Λ recoil did not indicate any deviation from the SM expectations and they are compatible with a non-polarized Λ_b.[6] These angular observables seemed to be deviating to unphysical regions (incompatible with value of the $\Lambda \to p\pi^-$ asymmetry parameter at the moment), however this was fixed by the newly updated measurement of the $\Lambda \to p\pi^-$ asymmetry parameter by the BESIII collaboration [248][7]. After this is taken into consideration, these angular observables show no significant deviations from their SM expectations.

[5] These low q^2 region have been used to constraint the electromagnetic dipole operator and its chirally flipped partner ($\mathcal{O}_{7\gamma}$ and $\mathcal{O}_{7'\gamma}$) as shown in Fig. 4.13.

[6] One should be careful that the results for the forward-backward asymmetries presented in Ref. [226] contain a mistake, the reported value correspond to the CP-asymmetry of these observables instead of the CP-average, this is corrected in Ref. [247].

[7] A discussion on this issue can be found in Ref. [227]

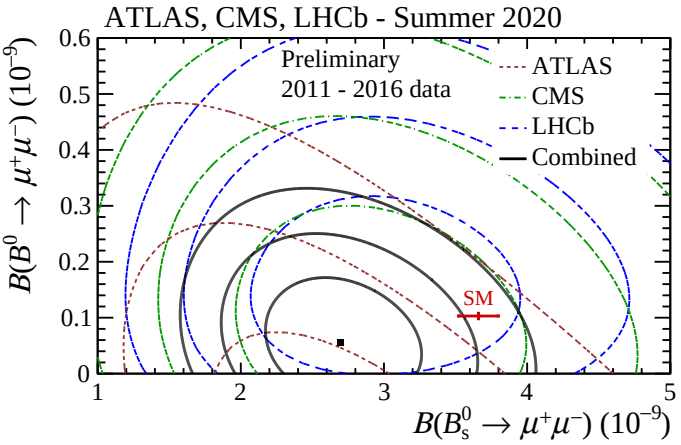

Figure 3.7: SM predictions and measurements of the branching fraction of the $B_s \to \mu^+\mu^-$ and $B \to \mu^+\mu^-$ modes as measured by the LHCb, CMS, and ATLAS collaborations [233].

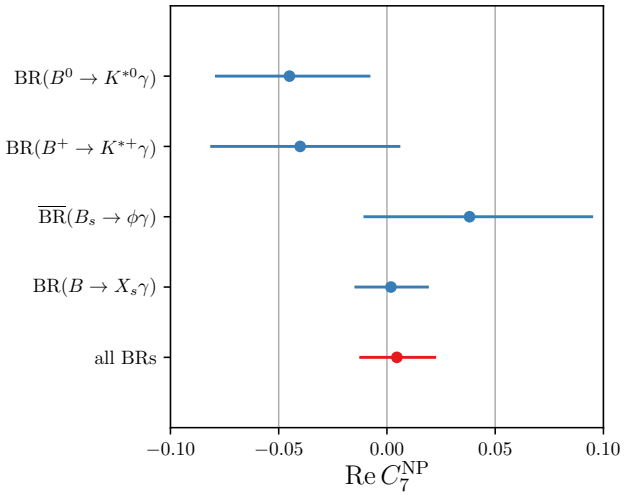

Figure 3.8: Constraints on $\mathrm{Re}[\mathcal{C}_{7\gamma}]$ coming from the branching fractions of the radiative $b \to s$ modes. Taken from Ref. [212].

3.3 NP explanations for the b-anomalies

We will know briefly discuss some of the simple NP models that can explain the observed flavour anomalies. We will not present here a full zoology of models, but rather discuss the most common explanations through "simple models" that have arisen in the past and their status with current data. Here, "simple" refers to models involving a small amount of mediators (usually one) coupling only to the relevant fermions. For instance, one can imagine a new neutral vector boson (Z') which has only bsZ' and $\mu\mu Z'$ vertices in order to explain the $b \to s\ell^+\ell^-$ anomalies (see Fig. 3.10).

Having such an ad hoc and simple model can seem unappealing and would be in many cases UV incomplete, however this kind of particles could be embedded into a larger model, being these only the lightest degrees of freedom of a new sector beyond the SM. Regarding the flavour structure, a coupling only to the fermions involved in the anomalies seems also unappealing and in a general model one would like to consider a complete favour structure for the couplings between the various families.

Tight bounds on specific NP models are often obtained from flavour observables (in particular neutral meson mixing such as $K - \bar{K}$ [7]) in the case where the flavour structure of the theory exhibits no hierarchical structure. On the contrary, models with a SM-like flavour structure might face less severe constraints. Moreover, in the context of the anomalies, the SM Yukawa couplings already have a flavour structure which is only of order 1 for the third generation, so NP models which bear the same flavour structure could likely have large effects on $b \to s\ell^+\ell^-$ and $b \to c\ell\bar{\nu}$. Such a hierarchy is also important since the NP involved must provide 10-20% corrections to a tree-level SM process for $b \to c\tau\bar{\nu}_\tau$, but to a loop-level SM process for $b \to s\mu^+\mu^-$, which are rather different in size.

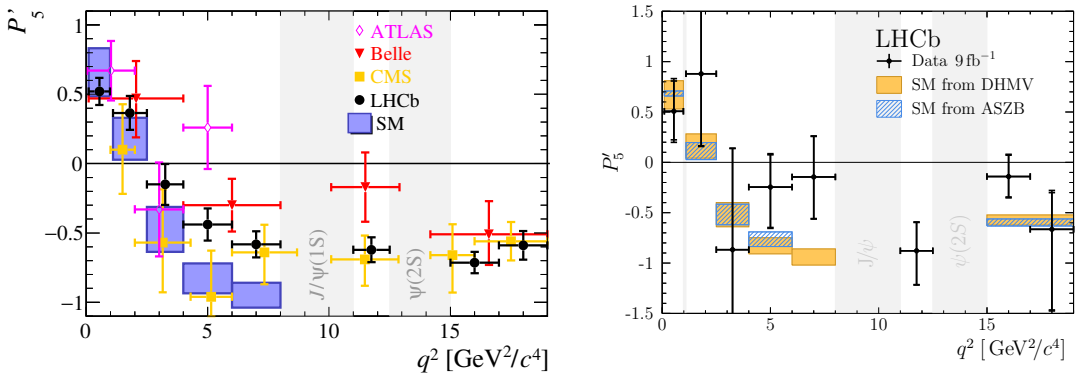

Figure 3.9: SM predictions and measurements of the P_5' optimised angular observable for the $B^0 \to K^{*0}\mu^+\mu^-$ (left) and $B^+ \to K^{*+}\mu^+\mu^-$ (right) decays as measured by the Belle [242], LHCb [239, 240], CMS [245], and ATLAS [246] collaborations. Taken from Refs. [222, 240].

Figure 3.10: Typical diagram of the $b \to s\ell\ell$ transition through a simple Z' (left) and a vector leptoquark (right) NP mediators.

Having this in mind we will first discuss the simple models (with simple couplings) that could generate the flavour anomalies and then discuss more general flavour structures that could be behind these models, allowing us to understand how they would appear in different modes like $b \to d$, $b \to u$, $s \to d$, etc.

3.3.1 Simple EFT connections

In order to discuss NP that connect both the $b \to c\ell\bar{\nu}$ and $b \to s\ell^+\ell^-$ sectors, it is natural to consider an EFT framework that respects the SM symmetries in a similar approach to SMEFT.

As discussed in Section 3.1.3, a good solution to the $b \to c\ell\bar{\nu}$ anomalies is through the addition of left handed vector currents (i.e. g_{V_L}). Furthermore, in the case of $b \to s\ell^+\ell^-$ (as we will discuss in the next chapter), the anomalies observed can also be explained through the addition of left handed vector currents where we have $\mathcal{C}_{9\mu} = -\mathcal{C}_{10\mu}$.

Since both LFU deviations are well explained by a NP vector contribution to left-handed fermions, Ref. [249] studies the effective Lagrangian [249–251]

$$\mathcal{L}_{\text{eff.}} = \mathcal{L}_{\text{SM}} - \frac{1}{v^2}\lambda^q_{ij}\lambda^\ell_{\alpha\beta}\left[C_T\left(\bar{Q}^i_L\gamma_\mu\sigma^a Q^i_L\right)\left(\bar{L}^\alpha_L\gamma^\mu\sigma^a L^\beta_L\right) + C_S\left(\bar{Q}^i_L\gamma_\mu Q^i_L\right)\left(\bar{L}^\alpha_L\gamma^\mu L^\beta_L\right)\right], \tag{3.12}$$

as an intermediate step in between the concrete NP models and the WET framework. The Lagrangian above, which respect the $SU(2)_L$ gauge symmetry, is written in the down-quark and charged lepton mass basis (see Section 1.2)

$$Q^i_L = (V^{\text{CKM}*}_{ji}u^j_L, d^i_L)^T, \qquad L^\alpha_L = (\nu^\alpha_L, \ell^\alpha_L)^T, \tag{3.13}$$

and the flavour structure of the NP is contained in λ^q_{ij} and $\lambda^\ell_{\alpha\beta}$ which are fixed in Ref. [249] on the basis of a U(2) flavour symmetry to account for the hierarchy of couplings between the third generation and the lighter ones.

This Lagrangian is of course not general and will not include all models that could explains the anomalies. However, it gives a simple framework in which one can easily test some NP scenarios that can properly describe data on $b \to c\ell\bar{\nu}$ and $b \to s\ell^+\ell^-$. Different mediators may lead to the operators shown in Eq. (3.12): colour-singlet vectors B'_μ and $\vec{W}'_\mu$, colour-triplet scalars S_1 and S_3 and colour-triplet vectors U^μ_1 and U^μ_3.

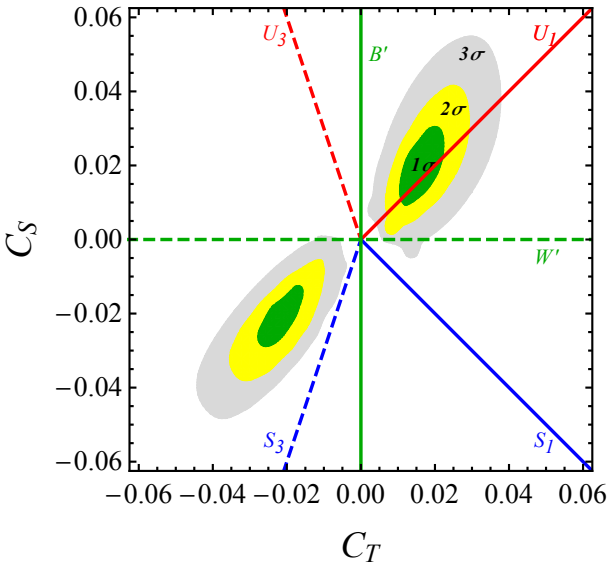

Figure 3.11: Fit to semi-leptonic and purely leptonic observables related to the $b \to s\ell^+\ell^-$ and $b \to c\ell\bar{\nu}$ transition (see Table 1 of Ref. [249]). The green, yellow and gray regions correspond to the 1σ, 2σ and 3σ regions respectively. The lines show the correlations among triplet and singlet operators in single-mediator models. Colour-less vectors are shown in green, coloured scalars in blue, while coloured vectors in red. Electroweak singlet mediators are shown with the solid lines while triplets with dashed lines. Taken from Ref. [249].

Through a simple flavour structure [249] given both by the SM flavour hierarchy and the hints of LFUV one can study the possible solutions to the anomalies in the $C_S - C_T$ plane as shown in Fig. 3.11 [8], where the allowed regions for (C_S, C_T) are displayed. The fitness of single mediator models can then be simply studied by matching them to the EFT in Eq. (3.12)

3.3.2 Simple models

The EFT analysis shown before indicates that one or two mediators leading to left-handed vector operators are sufficient to explain the deviations observed. More generally, one can think of either colourless or coloured mediators to generate the NP contributions to WET operators. In the case of coloured particles, leptoquarks are favoured and more flexible in terms of couplings to different fermion generations, compared to massive gauge mediators. In the case of colourless particles, heavy vector bosons are favoured and may come from additional SU(2) or U(1) gauge symmetries, although one could also consider additional scalar bosons coming, for instance, from Two-Higgs-doublet models (2HDMs) [252]. We will discuss some examples of such theories, without trying to be exhaustive.

Leptoquarks

Leptoquarks are coloured-triplet bosons which carry a lepton and baryon numbers, having couplings that allow a decay into leptons and quarks (see Fig. 3.10). They can be classified by their quantum numbers into six different types of representations [253]: three scalar (S_1, R_2, S_3) and three vector (U_1, V_2, U_3) leptoquarks. They differ by their $\mathrm{SU}(2)_L$ representations, where S_1 and U_1 are singlets, R_2 and V_2 are doublets and S_3 and U_3 are triplets, with all of them being triplets under $\mathrm{SU}(3)_C$. These type of particles naturally appear in some UV complete models like composite Higgs models [254, 255], the Pati-Salam model [256] and supersymmetric models with R-parity violation[257].

We will focus only in some of them as not all are capable of explaining $R_{K^{(*)}}$ and $R_{D^{(*)}}$ as shown in Table 3.5.

The vector U_1 leptoquark, coupled to the left-handed quark and lepton currents, as it can be seen in Fig. 3.11, is the best candidate for explaining the flavour anomalies as it can explain both the $b \to s\ell^+\ell^-$ and $b \to c\ell\bar{\nu}$ anomalies and it does not yield tree level contribution to neutral meson mixing and to $B \to K^*\nu\nu$. However, the addition of a vector leptoquark requires a UV completion to yield a consistent theory and the loop-level contributions to neutral meson mixing depend strongly on this UV completion [249, 258].

[8] Since the publication of Ref. [249], some of the numerical inputs have changed (for instance the deviation of R_D and R_{D^*} has slightly decreased), which should lead to an overall better fit of the data, but the overall conclusions concerning single mediators should not be modified.

Model	$R_{K^{(*)}}$	$R_{D^{(*)}}$	$R_{K^{(*)}}$ & $R_{D^{(*)}}$
S_3 $(\bar{\mathbf{3}}, \mathbf{3}, 1/3)$	✓	✗	✗
S_1 $(\bar{\mathbf{3}}, \mathbf{1}, 1/3)$	✗	✓	✗
R_2 $(\mathbf{3}, \mathbf{2}, 7/6)$	✗	✓	✗
U_1 $(\mathbf{3}, \mathbf{1}, 2/3)$	✓	✓	✓
U_3 $(\mathbf{3}, \mathbf{3}, 2/3)$	✓	✗	✗

Table 3.5: Summary of the leptoquark models which can accommodate $R_{K^{(*)}}$ (first column), $R_{D^{(*)}}$ (second column), and both $R_{K^{(*)}}$ and $R_{D^{(*)}}$ (third column), without being in conflict with existing constraints. Taken from Ref. [258].

Additionally, the best scalar leptoquark solution for explaining the $b \to s\ell^+\ell^-$ deviations is the S_3 leptoquark, which however cannot accommodate the $b \to c\ell\bar{\nu}$ anomalies [258]. Nonetheless, the combination of it with the S_1 scalar leptoquark (which yields a contribution to g_{V_L} and $g_{S_L} = -4g_T$) is often cited in the literature [249, 258] as they can together accommodate for the anomalies in both sectors (This can be seen in Fig. 3.11 as the combination of both leptoquarks can span the $C_S - C_T$ plane). A second possibility is the combination with the R_2 scalar leptoquark which yields a contribution to $b \to c\ell\bar{\nu}$ through $g_{S_L} = 4g_T$ which can explain the values of $R_{D^{(*)}}$ through complex couplings [259].

Vector bosons

One can consider different types of new vector bosons, in particular singlets B' and triplets $\vec{W}'$, which appear in several NP models such as 331 models [260–262], SU(2) × SU(2) × U(1) models [263] and models where the difference $L_\mu - L_\tau$ is promoted into a gauge symmetry [264]. Singlets could only explain the $b \to s\ell^+\ell^-$ anomalies while triplets can contribute at tree level to $b \to c\ell\bar{\nu}$ through the charged $W'^{\pm}$ and to $b \to s\ell^+\ell^-$ through the neutral component (i.e. the Z').

However, these vector bosons would also contribute to four-quark and four-lepton operators. A particular constraining process for the four quark operators is given by $B_{(s)} - \bar{B}_{(s)}$ mixing, as illustrated for instance in Ref. [249]. Additionally, bounds from high p_T tau lepton searches and bounds to the $\tau \to 3\mu$ branching fraction at the LHC [265, 266] also strongly constrain these models as they constrain $b \to c\tau\bar{\nu}_\tau$ operators. In the case of single B' or $\vec{W}'$ mediators with the flavour structure of Ref. [249], the regions of the parameter space that respect the high energy bounds lead to large values for the mixing which overwhelmingly exceed the experimental constraints and vice versa.

This can be solved by strongly fine tuning (10^{-4}) the parameters to avoid neutral meson mixing or through the addition of additional interaction terms with the Higgs which can relax the high energy bounds at the cost of some milder tuning [249].

Two-Higgs-doublet models

Two-Higgs-doublet models are simple NP models in which a second scalar $\mathrm{SU}(2)_L$ doublet is added to the SM, leading to the addition of a neutral CP-even scalar H_0, a neutral CP-odd scalar A_0 and a charged scalar $H^\pm$. This addition comes with a whole new family of Yukawa couplings and in order to restrain the number of new parameters and also to prevent from the appearance of FCNC at tree level it is common to assume a specific pattern of Yukawa couplings. Under these assumptions, four types of 2HDMs are usually studied, called Type I, II, X (Lepton Specific) and Z (Flipped) 2HDM [252]. One of the benefits (and sometimes also their doom) of some of the 2HDMs (like the type II) is that they have few parameters, making them very predictive models.

In the case of the $b \to c\ell\bar{\nu}$ it could be possible to consider a charged scalar mediating this decay at the tree level, however this explanation is not currently favoured by global fits [82, 83, 165, 166, 187] and suffers from constraints due to the B_c lifetime [186] and high p_T tau lepton searches at LHC [265, 266].

In the case of $b \to s\ell^+\ell^-$ a possible contribution from additional scalars would be through a neutral scalar which could have a tree level contribution to $b \to s\ell^+\ell^-$. However this is not preferred by the global fits which do not favour scalar contributions [267] and it is strongly constrained by $B_s - \bar{B}_s$ mixing as a neutral scalar would also produce a tree level contribution to the mixing. Another option, is an explanation through a loop contribution of a charged scalar to this decay [268, 269]. However, without the inclusion of heavy right-handed

neutrinos, this only allows for sizeable contributions through penguin diagrams which are LFU. Only through the addition of right-handed neutrinos, a charged scalar can provide, through a box diagram, sizeable LFUV contributions to $b \to s\ell^+\ell^-$.

In conclusion, 2HDMs suffer from strong experimental constraints, and thus struggle to explain both $b \to s\ell^+\ell^-$ and $b \to c\ell\bar{\nu}$ anomalies.

3.3.3 Flavour structure and MFV

As discussed at the beginning of this section, models where the NP degrees of freedom couple only to a few specific fields chosen to accommodate the deviations observed are not a very appealing explanation. The complete absence of some couplings which are not forbidden in principle but could contradict earlier experimental measurements is not very natural. One would expect NP degrees of freedom to have a rich flavour structure. On the other hand, one can notice that the deviations appear in b-decays into quarks of the second generation and leptons of the second or third generation, whereas lighter quarks and leptons do not seem affected at the same extent. This could support the existence of a flavour hierarchy among the NP couplings and we would like to provide these models with a more elaborate flavour hierarchy of couplings, in order to see how different generations may be involved through NP interactions.

As discussed in Chapter 1, the SM itself, partially respects a flavour symmetry under the flavour group

$$G_\mathcal{F} \equiv \mathrm{U}(3)^5 = \mathrm{U}(3)_{Q_L} \times \mathrm{U}(3)_{u_R} \times \mathrm{U}(3)_{d_R} \times \mathrm{U}(3)_{L_L} \times \mathrm{U}(3)_{\ell_R}\,, \tag{3.14}$$

discussed in Section 1.1. This flavour symmetry is only broken by the Yukawa couplings, which define the SM hierarchy of flavour.

One could in principle consider two options for the NP new degrees of freedom:

1. They have a new arbitrary flavour structure which has a different origin from the SM.
2. They have a flavour structure which is similar to the SM hierarchy or at least has a similar origin to the flavour hierarchy of the SM.

The first option presents several problems. On one side, an arbitrary flavour structure would have a strong effect in flavour observables that are well constrained by experimental measurements, like neutral meson mixing, pushing the energy scale of NP to high values ($\gtrsim 10^2 - 10^4$ TeV [7, 270]). On the other side, a new arbitrary flavour structure would introduce multiple sources of CP violation, since the complex phases involved in this new structure cannot be absorbed at the same time as the SM complex phases into the redefinition of the fields. This would spoil the consistency shown by the fits determining the CKM matrix (seeSection 1.2.2.) by providing inconsistent information on the amount of CP-violation encoded in the unitarity triangle. The concept of NP having a very similar flavour structure to the SM is thus supported by the very stringent is quite logical considering the stringent tests that the SM has passed until now. So this arbitrary structure, is somewhat bounded to be aligned with the SM one, with only small departures from it being allowed.

The second option is a more minimalistic approach, in which no new source of flavour symmetry violation is introduced. This approach, is generally refereed as Minimal Flavour Violation (MFV)[250, 270]. The principle behind MFV starts by restoring the flavour symmetry of the SM under $G_\mathcal{F}$. This is done by promoting the Yukawa couplings to spurions, or in other words by treating them as fields with the proper transformation properties such that the SM Lagrangian is invariant under $G_\mathcal{F}$. The transformation required for the Yukawa fields is given by

$$Y_u \sim (\bar{\mathbf{3}}, \bar{\mathbf{3}}, \mathbf{1}, \mathbf{1}, \mathbf{1})_{G_\mathcal{F}}: \quad Y_u \xrightarrow{G_\mathcal{F}} g^\dagger_{Q_L} Y_u g^\dagger_{u_R}\,, \tag{3.15}$$

$$Y_d \sim (\bar{\mathbf{3}}, \mathbf{1}, \bar{\mathbf{3}}, \mathbf{1}, \mathbf{1})_{G_\mathcal{F}}: \quad Y_d \xrightarrow{G_\mathcal{F}} g^\dagger_{Q_L} Y_d g^\dagger_{d_R}\,, \tag{3.16}$$

$$Y_e \sim (\mathbf{1}, \mathbf{1}, \mathbf{1}, \bar{\mathbf{3}}, \bar{\mathbf{3}})_{G_\mathcal{F}}: \quad Y_e \xrightarrow{G_\mathcal{F}} g^\dagger_{L_L} Y_e g^\dagger_{e_R}\,, \tag{3.17}$$

where $g_X \in \mathrm{U}(3)_X$.

Then the flavour structure can be recovered by setting the fields to the "physical" values (sometimes referred as "freezing the fields") corresponding to SM Yukawa couplings

$$vY_u \to M_u V_{\mathrm{CKM}} \qquad vY_d \to M_d \qquad vY_e \to M_e \tag{3.18}$$

The interest of this approach, is that one can create new operators invariant under $G_\mathcal{F}$ which involve the spurions and would lead to a flavour structure compatible with the breaking of $G_\mathcal{F}$ within the SM upon freezing of the fields. We will focus on the flavour structure of the quark sector, as MFV cannot yield a flavour structure on the lepton sector without first defining a mass mechanism for neutrinos.

In the language of spurions that we have just discussed, MFV can be defined by two principle or conditions:

- First, flavour couplings need to be invariant under $G_\mathcal{F}$ with the only flavour structure coming from the freezing of the Yukawa spurions. This requirement does not yield only the flavour structure of operators already present in the SM : however this flavour structure needs to be written as a polynomial of the allowed spurions. For instance for an operator involving the quark bilinear $C^{ij}\bar{d}^i_R\gamma^\mu d^j_R$, the flavour coupling coefficient C^{ij} needs to transform as $C \xrightarrow{G_\mathcal{F}} g^\dagger_{d_R} C g_{d_R}$ and can thus be written as

$$C = f(Y_u, Y_d) = z_1 \mathrm{I}_{3\times 3} + z_2 Y_d Y_d^\dagger + z_3 Y_d Y_u^\dagger Y_u Y_d^\dagger + z_4 Y_d Y_u Y_u^\dagger Y_d^\dagger + \dots . \tag{3.19}$$

  Nonetheless, without a further assumption, this idea is not very interesting as polynomials of the Yukawa spurions can span the full flavour space.

- This leads to the second condition which is that all coefficients z_i that appear in these polynomials have to be natural (i.e. $\lesssim \mathcal{O}(1)$), which will avoid interaction terms that are largely misaligned with SM flavour structure.

These conditions however leaves us with an infinite series of polynomials on the Yukawa couplings, that can be treated in two different ways, yielding two different realisation of MFV. Let us rewrite the polynomial expansion on the Yukawa expansion in Eq. (3.19) by introducing two parameters $\epsilon_{u,d}$ such that $C = f(\epsilon_u Y_u, \epsilon_d Y_d)$ and assume that all coefficients z are of order $\mathcal{O}(1)$ such the convergence of the expansion is given by the values of $\epsilon_{u,d}$. This kind of expansion could be for instance motivated by the conception that the spurions could be actual dynamical fields that acquire a non vanishing vacuum expectation value through a dynamical process (similar to the case of electroweak symmetry breaking), in which every addition of extra fields $Y_{u,d}$ would come accompanied by a coupling constant related to $\epsilon_{u,d}$. In this case we have two options:

- The first option is that $\epsilon_{u,d} \ll 1$ in which case only first order terms in spurions are relevant. This realisation of MFV is called *linear MFV* as it keeps only the first order terms (which are not necessarily linear in the spurions). This would correspond, for instance, to taking only z_1 and z_2 in Eq. (3.19).

- The second option is that $\epsilon_{u,d} \sim \mathcal{O}(1)$ and the expansion cannot be truncated. In this case all order terms are relevant, however this is only due to the size of the top and bottom Yukawa couplings $y_{t,b}$ ($\sim \mathcal{O}(1)$ for y_t), which dominate the flavour breaking. An approach to deal with MFV in this case was proposed in [270], where they separate the flavour breaking into two different parts. First a breaking of the quark sector of $G_\mathcal{F}$ into

$$\mathcal{H} = \mathrm{U}(2)_{Q_L} \times \mathrm{U}(2)_{u_R} \times \mathrm{U}(2)_{d_R} \times \mathrm{U}(1)^3 \tag{3.20}$$

  where the light quark fields (u, d, s, c) still preserve a U(2) [9]. This subgroup is then broken by (smaller) terms responsible for flavour symmetry breaking for the the first and second generations. This structure of breaking allows one to treat these two stages differently and perform a expansion on the small parameters of the Yukawa matrices related to the light quarks, while keeping the expansion to all orders in the large Yukawas. This realisation of MFV is called *General Minimal Flavour Violation* (GMFV) or Non-linear MFV (NLMFV) [270] as the breaking from $G_\mathcal{F}$ to $\mathcal{H}$ is parametrised in a non-linear fashion, whereas the breakdown of $\mathcal{H}$ can be described in a linear way. As can be guessed from their names, GMFV keeps more terms in the spurion expansion than LMFV.

3.4 Conclusion

The flavour anomalies observed in semileptonic B meson decays constitute one of the most promising hints of New Physics (NP) found at LHC and B-Factories. Although global fits to the $b \to c\ell\bar{\nu}$ transition show a certain preference for vector currents, the present constraints are not sufficient to determine the nature of the NP that could be behind these anomalies. In the case of $b \to s\ell^+\ell^-$, more experimental measurements are available, however the theoretical predictions suffer from slightly bigger uncertainties. Furthermore, the complex phases of the Wilson coefficients describing the $b \to s\ell^+\ell^-$ transition are not yet well constrained. It is thus particularly important to probe these transitions (both $b \to c\ell\bar{\nu}$ and $b \to s\ell^+\ell^-$) with a higher experimental and theoretical accuracy, but also to provide new modes and observables constraining NP scenarios in different ways.

We discussed the NP models that could be at the source of the b-anomalies, finding that simple models can explain each of the b-anomalies, but that the discussion of a full flavour structure for the models discussed is slightly more difficult.

[9] This structuration of flavour breaking in two steps, conserving first a U(2) symmetry and then breaking this second symmetry has also been used in NP models out of the context of MFV in order to constrain their flavour structure even extending this formalism to the lepton sector [271–273].

In the next chapter we will discuss in detail the global fit of the Wilson coefficients describing the $b \to s\ell^+\ell^-$ to better understand the NP that might be behind these anomalies through an EFT framework. In the following chapters, we will propose new ways of testing the b-anomalies, starting by new modes and observables that will help better understand the $b \to s\ell^+\ell^-$ transition to then discuss interesting new ways to probe the $b \to c\ell\bar{\nu}$ transition.

Chapter 4

Global analysis of $b \to s\ell^+\ell^-$

Since the first works showing a deviation from the SM in the $B \to K^*\mu^+\mu^-$ angular observables measured by LHCb [274], there has been a growing evidence of experimental deviations (as discussed in Chapter 3) and a parallel theoretical discussion of the possible sources of these deviations. In particular, global fits to $b \to s\ell^+\ell^-$ data have tried to identify if the deviations exhibit a consistency compatible with simple NP scenarios within an EFT framework.

In this chapter we present a discussion of the status of such a global analysis of the $b \to s\ell^+\ell^-$ transition [1] . The results presented here follow closely Ref. [275] and correspond to the latest update to Refs. [108, 132, 134, 135].

First, we describe the main experimental results and the main elements of the theoretical predictions required to perform this analysis. In Section 4.1 we discuss the observables that compose the different fits. In Section 4.2 we present the theoretical inputs required to predict the SM values as well as an analysis of the main uncertainties and the choices that we make in order to estimate them in a conservative fashion. In Section 4.3 we discuss the SM and NP Wilson coefficients that are the most relevant to these transitions, which correspond to $\mathcal{C}_{7^{(\prime)}}$,$\mathcal{C}_{9^{(\prime)}}$ and $\mathcal{C}_{10^{(\prime)}}$. We then briefly describe in Section 4.4 the statistical framework used, the treatment of both experimental and theoretical uncertainties and how confidence regions for the Wilson coefficients are obtained.

We continue by presenting the results of the global fits, their statistical significance and the new emerging patterns of NP spanned by the effective operators driven by data within two different types of NP scenarios. First, following Ref. [135] we assume in Section 4.5.1 that NP affects only muons and is thus purely Lepton-Flavour Universality Violating (LFUV). In Section 4.5.2 we follow the complementary approach discussed in Ref. [134], where we consider the consequences of removing the frequently made hypothesis that NP is purely LFUV. We then explore the implications of allowing both LFU and LFUV NP contributions to the Wilson coefficients $\mathcal{C}_{9^{(\prime)}}$ and $\mathcal{C}_{10^{(\prime)}}$.

In Section 4.6.1 we discuss the favoured scenarios of the global fits and some of models that motivate them and can explain the b-anomalies complementing Section 3.3. In Section 4.6.2, we focus on a particular scenario (scenario 8) which can, within an EFT framework, link the flavour anomalies in $b \to s\ell^+\ell^-$ and $b \to c\ell\nu$ processes. Some models that motivate the different fit scenarios in Sections 4.5.1 and 4.5.2 and can explain the b-anomalies are discussed briefly in Section 4.6.1 complementing Section 3.3.

In Section 4.7 we discuss the results of other groups performing global fits to $b \to s\ell^+\ell^-$ data and compare these results to ours. Finally, we sum up our results in Section 4.8 and we conclude this chapter by commenting on the impact that new measurements could have on our analysis. An appendix (Appendix 4.A) is devoted to include the list of observables included in the fit (Table 4.A.1) and an exhaustive list of the 1D patterns and their bfps.

4.1 Experimental inputs

The experimental results on these modes have been discussed in the previous chapter and they have been measured mainly by the LHCb, CMS, ATLAS, Belle and BaBar collaborations. In the fits, we will compare the experimental results for $B \to K^{(*)}\ell^+\ell^-$, $B_s \to \phi\ell^+\ell^-$, $B \to K^{(*)}\gamma$, $B_s \to \phi\gamma$ and $B_s \to \mu^+\mu^-$ with their theoretical predictions in terms of the WET. For each of these modes we include the branching fractions, LFU

[1] The radiative mode $b \to s\gamma$ is also taken into account in order to constrain $\mathcal{C}_{7^{(\prime)}}$. We consider only the semileptonic and radiative modes, as opposed to all of $b \to s$ transitions, because, as discussed in the previous chapters, in these modes we can benefit from factorisation and from the knowledge on form factors to get accurate predictions. In purely hadronic modes factorisation is far more complicated, QCD Factorisation (Section 2.8) can be used to predict these modes, but its accuracy is far from the one of the semileptonic and radiative modes. An example will be given in Chapter 10.

Observables included in the Global Fit "LFUV "			
R_K [LHCb]	SM	Experiment [277]	Pull
[1.1, 6.]	1.00 ± 0.00	0.85 ± 0.04	$+3.5$
R_K [Belle]	SM	Experiment [220]	Pull
[1., 6.]	1.00 ± 0.00	1.03 ± 0.28	-0.1
[14.18, 22.9]	1.00 ± 0.00	1.16 ± 0.30	-0.5
R_{K^*} [LHCb]	SM	Experiment [207]	Pull
[0.045, 1.1]	0.91 ± 0.02	0.66 ± 0.11	$+2.2$
[1.1, 6.]	1.00 ± 0.01	0.69 ± 0.12	$+2.6$
R_{K^*} [Belle]	SM	Experiment [219]	Pull
[0.045, 1.1]	0.92 ± 0.03	0.52 ± 0.36	$+1.1$
[1.1, 6.]	1.00 ± 0.01	0.96 ± 0.46	$+0.1$
[15., 19.]	1.00 ± 0.00	1.18 ± 0.53	-0.3
$Q_4'(B \to K^*)$ [Belle]	SM	Experiment [242]	Pull
[0.1, 4.]	0.03 ± 0.01	1.46 ± 1.39	-1.0
[4., 8.]	0.00 ± 0.00	-0.90 ± 0.80	$+1.1$
[14.18, 19.]	0.00 ± 0	-0.08 ± 1.14	$+0.1$
$Q_5'(B \to K^*)$ [Belle]	SM	Experiment [242]	Pull
[0.1, 4.]	-0.02 ± 0.01	-0.10 ± 0.62	$+0.1$
[4., 8.]	-0.00 ± 0.00	0.50 ± 0.42	-1.2
[14.18, 19.]	-0.00 ± 0.00	0.78 ± 0.51	-1.5
$10^5 \times B(B^0 \to K^{*0}\gamma)$ [PDG]	SM	Experiment [6]	Pull
	4.65 ± 5.41	4.18 ± 0.25	$+0.1$
$10^5 \times B(B^+ \to K^{*+}\gamma)$ [PDG]	SM	Experiment [6]	Pull
	4.62 ± 5.59	3.92 ± 0.22	$+0.1$
$10^5 \times B(B_s \to \phi\gamma)$ [PDG]	SM	Experiment [6]	Pull
	4.86 ± 1.29	3.40 ± 0.40	$+1.1$

Table 4.1: List of observables included in the fit "LFUV", with their SM prediction, experimental measurements and the pull of this measurement. The sign of the pull value represents whether the observable theoretical prediction is above (+) or below (−) the experimental measurement.

ratios and angular observables [2] discussed in the previous chapter. We consider only CP-averaged quantities (and accordingly we will not consider scenarios with CP-violating NP). The following measured experimental results are excluded from this fit and will be included in the future: all the results on the baryonic b-decays [223, 226, 247], the latest measurement of $B \to K^*\mu^+\mu^-$ from CMS [276], and the latest updates of LHCb on the $B_s \to \phi\mu^+\mu^-$ mode [225, 243].

We will consider two different sets of observables:

- On one side, we will perform a fit with all of the observables coming from the modes mentioned above. We call this the "All" fit, and the full list of the 246 observables included in this fit is given in Table 4.A.1.
- On the other side, we will consider a reduced amount of observables, which have two interesting properties. First, they are tests of Lepton Flavour Universality (LFU) and secondly, they have reduced uncertainties in the SM since they come only from Lepton Flavour Universality Violation (LFUV). The list of the 22 observables included in this fit, to which we will refer as the "LFUV" fit, is given in Table 4.1.

We will consider only Gaussian uncertainties, as discussed in Section 4.4. In the case of asymmetric uncertainties (such as R_K), in order to be conservative, we symmetrise the uncertainties by taking the largest uncertainty.

[2] Our treatment for the Belle observables within the global fit follows the same strategy as described in Ref. [135] for $Q_{4,5} = P'_{4\mu,5\mu} - P'_{4e,5e}$ which were isospin averaged and where we introduced a nuisance parameter accounting for the relative weight of each isospin component.

4.2 Important aspects of the theoretical predictions

4.2.1 Choice of the form factors

We now discuss the explicit choice of form factors that enter into our predictions for different $b \to s\ell^+\ell^-$ observables. We start with the $B \to K$ mode, for which we use the form factors from Ref. [115] at large-recoil and the purely lattice results from Ref. [193] at low-recoil. In the case of $B \to K^*$ we use the results from Ref. [115] at large-recoil and the purely lattice results from Ref. [195] at low-recoil, while for $B_s \to \phi$ we use the results from Ref. [278] at large-recoil and the purely lattice results from Ref. [195] at low-recoil.

The form factors obtained through LCSR (see Section 1.6) we consider include two different types of LCSR: in the case of Ref. [278] the expansion is chosen so that the form factors are either written in terms of the light-meson DA while in the case of Refs. [39, 109, 115] they are written in terms of the B-meson DA. The two LCSR differ through the initial correlator and the kinematics chosen to perform the light-cone expansion. We prefer to use B-meson DA to be more conservative as they have larger uncertainties than the results in terms of the light-meson DA.

A more recent determination of these form factors through LCSR with B-meson DA has been performed on Refs. [39, 109], that we have not used yet, however we plan to include them in future works. In Refs. [39, 109, 278] LCSR at low q^2 are combined with lattice results at high q^2. Results are compatible with each other, bearing however different uncertainties.

4.2.2 Form factors at large-recoil

Form factors are one of the main theoretical inputs that go into the prediction of branching fractions and angular observables. While in the branching fractions the uncertainties of the form factors contribute directly to the theoretical predictions, in angular observables, or more precisely in the optimized angular observables, the form factors are cancelling in the heavy quark limit so that their contribution to the hadronic uncertainties of optimised observables is suppressed. It is thus important to verify that the results obtained either from LQCD or from LCSR, respect the relations that are expected from HQET and SCET that we have discussed in Section 2.5 up to corrections in agreement with the $\mathcal{O}(\alpha_s, \Lambda_{\rm QCD}/m_b)$ suppression. This can be explicitly verified by using a different parametrisation of the form factors highlighting the power corrections to the large-recoil limit. Two different types of factorisable corrections will affect the soft form factors defined in SCET

$$F(q^2) = F^{\infty}(\xi_\perp(q^2), \xi_\parallel(q^2)) + \Delta F^{\alpha_s}(q^2) + \Delta F^{\Lambda}(q^2) \tag{4.1}$$

where $F^{\infty}(\xi_\perp(q^2), \xi_\parallel(q^2))$ represents the correspondent soft form factor combination (see Section 2.5.2), $\Delta F^{\alpha_s}(q^2)$ and $\Delta F^{\Lambda}(q^2)$ represent the factorisable α_s and $\Lambda_{\rm QCD}/m_b$ corrections to the leading order respectively. While the former can be computed in QCDF [38], the latter cannot. We thus parametrise them as an expansion in $\frac{q^2}{m_B^2}$ following Ref. [279]

$$\Delta F^{\Lambda}(q^2) = a_F + b_F \frac{q^2}{m_B^2} + c_F \left(\frac{q^2}{m_B^2}\right)^2 + \dots \tag{4.2}$$

These contributions are important to take into account, since the symmetries that protect the optimised observables are broken by this corrections making them the main source of hadronic uncertainties related to the form factors for the optimised observables.

The definition of the soft form factors is a priori arbitrary since one can make variations of $\mathcal{O}(\alpha_s, \frac{q^2}{m_B^2})$ to its definition. The choice of the soft form factor definition is done by fixing the soft form factor to be equal to a certain combination of the full form factors to all orders and this defines a choice of scheme for the soft form factors. Within a certain scheme, one can fit the values of the a_F, b_F, c_F defined above for each of the form factors. One can thus check that the size of the coefficients are in agreement with SCET expectations.

In the past, there were doubts that some choices of scheme could lead to large uncertainties [279, 280] but it turned out to be due to choices of schemes enhancing artificially the uncertainties [137]. We choose the following scheme

$$\xi_\perp(q^2) \equiv \frac{m_B}{m_B + m_V} V(q^2) \tag{4.3}$$

$$\xi_\parallel(q^2) \equiv \frac{m_B + m_V}{2E} A_1(q^2) - \frac{m_B - m_V}{m_B} A_2(q^2) \tag{4.4}$$

where these coefficients have their expected values in SCET leading to a typical 10% correction from power corrections at large recoil. More details and the numerical values that the power corrections take in our analysis, can be found in Ref. [137].

4.2.3 Non-local hadronic contributions at large-recoil

The treatment of non-local contributions used in this global analysis is based on the discussion in Refs. [108, 137], where more details can be found. As discussed in Section 2.7, non-local contributions can be split into hard and soft gluon contributions.

Hard gluon contributions

The contributions from non-local contributions can already be analysed in terms of QCD factorisation, which goes beyond the perturbative QCD contributions by considering additional hard-gluon exchanges. In Refs. [111, 281] the matrix element $\langle K^*\gamma^*|\mathcal{H}_{\rm eff}|B\rangle$ is decomposed in terms of three hadronic form factors $\mathcal{T}_i(q^2)$, which reduce to only two in SCET. These hadronic form factors are re-expressed in terms of Wilson coefficients, soft form factors ($\xi_{\parallel,\perp}$), light-cone sum rules and hard-scattering kernels using QCD factorisation [281]

$$\mathcal{T}_a^{(i)} = \xi_a\, C_a^{(i)} + \frac{\pi^2}{N_c}\frac{f_B f_a}{M_B}\,\Xi_a \sum_{\pm}\int \frac{d\omega}{\omega}\,\Phi_{B,\pm}(\omega)\int_0^1 du\;\phi_a(u)\,T_{a,\pm}^{(i)}(u,\omega). \tag{4.5}$$

and correspond at leading-order in α_s to the perturbative correction induced by the function $Y(q^2)$ introduced in Eq. (2.83).

We could have considered these results directly to take into account $\mathcal{O}(\alpha_s)$ corrections only to these formulae. We have however to take also into account $\mathcal{O}(1/m_b)$ corrections coming from power-suppressed effects (soft gluons, higher-twist DA effects...). We can modify this expression to enlarge the uncertainties focusing on the contributions affecting $c\bar{c}$ contributions. In each of the amplitudes, we single out the hadronic contribution that is not related to the radiative Wilson coefficients by taking the limit $\mathcal{T}_i^{\rm had} = \mathcal{T}_i|_{\mathcal{C}_{7^{(\prime)}}\to 0}$. In order to be conservative, we multiply each of the hadronic amplitudes with a complex q^2-dependent factor such that

$$\mathcal{T}_i^{\rm had} \to \big(1 + r_i(q^2)\big)\mathcal{T}_i^{\rm had}\,, \tag{4.6}$$

where

$$r_i(s) = r_i^a e^{i\phi_i^a} + r_i^b e^{i\phi_i^b}(s/m_B^2) + r_i^c e^{i\phi_i^c}(s/m_B^2)^2\,. \tag{4.7}$$

We define the central values as the ones with $r_i(s) \equiv 0$, and estimate the uncertainties from non-factorizable power corrections by varying $r_i^{a,b,c} \in [0, 0.1]$ and $\phi_i^{a,b,c} \in [-\pi, \pi]$ independently, corresponding to a $\sim 10\%$ correction with an arbitrary phase modifying the QCD factorisation results to take into account soft-gluon contributions.

Soft gluon contributions

We have already treated the hard-gluon contributions, and modify it to include power-suppressed effects that include soft-gluon contributions. However, as there have been many interrogations on our ability to properly assess the size of soft-gluon contributions to $c\bar{c}$ loops at low q^2 [119, 123, 127, 282], we will add a further source of theoretical uncertainty (admittedly with the risk of overestimating the theoretical uncertainties attached to this effect). In order to take into account soft-gluons from a different source than QCD factorisation, we make use of the non-local contribution $\mathcal{H}$ in Eq. (2.80) which can be estimated in LCSR at q^2 slightly negative [109, 115]. One has then to perform the extrapolation to the physical low-q^2 region using either a model [115] or experimental data [109, 112]. For $B \to K^*\ell^+\ell^-$ we will take the results of Ref. [115], subtract the hard-gluon contribution at LO and parametrise the remaining contribution $\Delta\mathcal{C}_{9\ell}^{\rm LD}(q^2)$ defined in Eq. (2.84) as done in Ref. [108]. We then consider three different helicity dependent parametrisations

$$\delta\mathcal{C}_{9\ell}^{\rm LD,0}(q^2) = \frac{a^0 + b^0(q^2+s_0)(c^0-q^2)}{(q^2+s_0)(c^0-q^2)} \tag{4.8}$$

$$\delta\mathcal{C}_{9\ell}^{\rm LD,\parallel}(q^2) = \frac{a^\parallel + b^\parallel q^2(c^\parallel-q^2)}{q^2(c^\parallel-q^2)} \tag{4.9}$$

$$\delta\mathcal{C}_{9\ell}^{\rm LD,\perp}(q^2) = \frac{a^\perp + b^\perp q^2(c^\perp-q^2)}{q^2(c^\perp-q^2)} \tag{4.10}$$

corresponding to the contributions to the longitudinal amplitude $\mathcal{A}_0$ and the 2 transverse amplitudes respectively $\mathcal{A}_{\parallel,perp}$ which we are shown in Fig. 4.1. The a^i, b^i and c^i parameters are tuned to cover the results from Ref. [115] and we set $s_0 = 1\,\text{GeV}$ in the longitudinal contribution which does not exhibit a pole at $q^2 = 0$ [108].

It is important to mention that the soft-gluon contribution computed in Ref. [115] induces a positive contribution to $\mathcal{C}_{9\ell}^{\rm eff}$ whose effect is to further enhance the anomaly. Ref. [109] has reassessed the LCSR evaluation

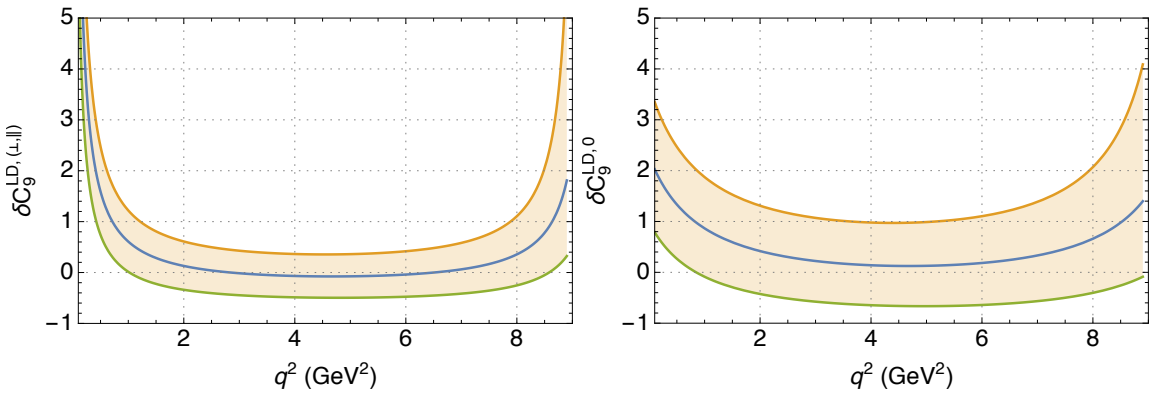

Figure 4.1: Parametrisation of $c\bar{c}$ contributions defined in Eq. (4.8) for transverse (left) and longitudinal (right) of $B \to K^* \ell^+ \ell^-$ amplitudes. Taken from Ref. [108]

of Ref. [115] using the complete set of higher-twist B-meson LCDAs.. The results from Ref. [109] a significantly smaller contribution than Ref. [115] at $q^2 < 0$, however the effect of the extrapolation at low q^2 still has to be discussed fully to determine the final impact of the soft-gluon contribution. In order to be conservative, we consider the results obtained in Ref. [115] as an order of magnitude estimation by introducing three independent parameters $s_i = 0 \pm 1$ with $i = 0, \parallel, \perp$, such that

$$\Delta \mathcal{C}_{9\ell}^{\mathrm{LD}}(q^2) \to s_i \delta \mathcal{C}_{9\ell}^{\mathrm{LD},i}(q^2)\,. \tag{4.11}$$

In the case of $B_s \to \phi \ell^+ \ell^-$, long distance contributions will be treated in the same way as $B \to K^* \ell^+ \ell^-$, however with independent parameters, meaning that we consider no correlation between long distance contributions between these modes.

In the case of $B \to K \ell^+ \ell^-$, these contributions are neglected since they are found to be small [109, 115, 116] compared to our main uncertainties.

4.2.4 Form factors and non local contributions at low-recoil

In the low-recoil region, one could in principle perform a similar expansionof the form factors in terms of an OPE and HQET, however we refrain from this and we simply use the full lattice form factors [195]. However, non-local contributions still need to be taken into account, in fact this region is afflicted by the presence of $c\bar{c}$ resonances structure, which prevents us from taking small bins. However when observables are integrated into a large energy ranges, quark-hadron duality is a good approximation. In Refs. [97, 113] a quantitative estimate of duality violation is given, showing an impact of a few percent at the level of the branching ratio (estimated to 5% Ref. [97] or 2% in Ref. [113]) when integrating over a large energy range with a dependency on the exact position where the bin ends. These estimations are however unavoidably model dependent and it remains to be determined if these estimates hold in the case of the angular observables. Nonetheless, we add a contribution of $\mathcal{O}(10\%)$ (with an arbitrary phase) to the term proportional to $\mathcal{C}_{9\ell}^{\mathrm{eff}}$ for each transversity amplitude of the different transitions, in order to take into account effects of duality violation.

4.3 Relevant operators

In our fits, we will discuss the $b \to s\ell^+\ell^-$ and $b \to s\gamma$ transitions on the WET framework introduced in Section 2.4 at the relevant scale ($\mu_b = 4.8\,\mathrm{GeV}$) and we allow for NP to appear only on vector and axial semileptonic operators ($\mathcal{C}_{9^{(\prime)}\ell}, \mathcal{C}_{10^{(\prime)}\ell}$) and the electromagnetic dipole operator ($\mathcal{C}_{7^{(\prime)}\ell}$).

We will not consider NP on the 4-quark operators $\mathcal{O}_{1-6}$ or on the gluon magnetic penguin $\mathcal{O}_{8g}$ for the following reasons:

- They only appear as loop suppressed contributions, which in practice implies that the amount of NP required to explain the deviations seen in $b \to s\mu^+\mu^-$ through C_{1-6} is of the order of their SM value.
- They would appear as LFU contributions which do not allow to explain the LFUV deviations seen in $R_{K^{(*)}}$.
- They would be hard to distinguish from hadronic uncertainties or in other words, they would only appear in observables that are sensitive to hadronic uncertainties.

The reader is referred to Refs. [114, 283] for the potential room left for NP in 4-quark operators, as well as Chapter 10.

In the case of (pseudo)scalar contributions C_S and C_P, they are fairly constrained by $B_s \to \mu\mu$ and they do not ameliorate substantially the tensions present in the $b \to s\ell^+\ell^-$ transition. In the case of (pseudo)tensors, the same is true regarding the tensions present and because of the running a (pseudo)tensor contribution at the NP scale will generate a (pseudo)scalar contribution suffering the same constraints through $B_s \to \mu\mu$. As will be discussed in Section 4.7, other groups have tried to include these contributions without finding the need for NP contributions to these Wilson coefficients.

4.4 Statistical framework

We will know describe briefly the method used to fit the experimental data. We perform this analysis in a frequentist framework and we treat theoretical and experimental uncertainties in the same way (i.e. we treat theoretical inputs and experimental measurements on the same footing, taking them as random variables). We follow the method of maximum likelihood (ML) in the Gaussian approximation. A more detailed explanation of this method is given in the Statistics review in Sec. 40 of Ref. [6].

4.4.1 Observables, predictions and measurements

We consider a set of observables (measurable quantities) $\boldsymbol{O} = O_1, ..., O_{n_{\rm obs}}$, where $n_{\rm obs}$ is the number of observables included in the fit. This set of observables corresponds to a set of random variables. Each of these observables has an experimental value and a theoretical prediction. We denote $\boldsymbol{O}_i^{exp}$ the central values of the experimental measurements. The theoretical predictions ($\boldsymbol{O}^{th}(\boldsymbol{\nu}, \boldsymbol{\mathcal{C}})$) are functions of two set of parameters:

- First, the NP contributions to the Wilson coefficients $\boldsymbol{\mathcal{C}}$. Our objective is to estimate this set of parameters [3], which we will do through the maximum likelihood method.
- Secondly, the nuisance parameters $\boldsymbol{\nu}$, which correspond to any input of the theoretical predictions: the masses of the particles, the SM values of the Wilson coefficients, the form factor parameters, etc. For simplicity, the nuisance parameters will be treated as random variables. In other words, each one of this parameters has an associated distribution, which in general will simply correspond to a normal distribution. We denote $\text{pdf}_{\boldsymbol{\nu}}$ the multivariate probability distribution function for the nuisance parameters. We then denote the mean of the theoretical predictions for a given value of the Wilson coefficients as

$$\boldsymbol{O}^{th}(\boldsymbol{\mathcal{C}}) \equiv \mathbb{E}\left[\boldsymbol{O}^{th}(\boldsymbol{\nu}, \boldsymbol{\mathcal{C}}) \middle| \boldsymbol{\mathcal{C}}\right] = \int d\boldsymbol{u} \boldsymbol{O}^{th}(\boldsymbol{u}, \boldsymbol{\mathcal{C}}) \text{pdf}_{\boldsymbol{\nu}}(\boldsymbol{u})\,. \tag{4.12}$$

The set of observables $\boldsymbol{O}$ is then distributed under an a priori unknown distribution of which the central value is given by $\boldsymbol{O}^{th}(\boldsymbol{\mathcal{C}})$ and depends on the Wilson coefficients $\boldsymbol{\mathcal{C}}$. In the Gaussian approximation, the distribution of the set $\boldsymbol{O}$, is given by a multinormal distribution centered at $\boldsymbol{O}^{th}(\boldsymbol{\mathcal{C}})$ where the covariance matrix is defined as

$$\text{Cov} \equiv \text{Cov}^{th} + \text{Cov}^{exp}\,. \tag{4.13}$$

The covariance in between experimental measurements is given in (Cov^{exp}) where the measurements are assumed uncorrelated when the values are not quoted. The theoretical covariance matrix Cov^{th} is obtained through Monte Carlo sampling of the nuisance parameters $\boldsymbol{\nu}$ [4].

The *likelihood function* $\mathcal{L}(\boldsymbol{\mathcal{C}})$ assesses how well a hypothesis for the theoretical distribution of the observables can explain data for given values of the unknown parameters. In this case the unknown parameters are the Wilson coefficients of which the likelihood is a function. More precisely the likelihood corresponds to the probability of obtaining the measurements $\boldsymbol{O}_i^{exp}$ for a given set of $\boldsymbol{\mathcal{C}}$. In the Gaussian approximation the likelihood function is simply given by the χ^2-statistic defined as

$$\chi^2(\boldsymbol{\mathcal{C}}) = \sum_{i=1}^{n_{\rm obs}} \sum_{j=1}^{n_{\rm obs}} (O_i^{th}(\boldsymbol{\mathcal{C}}) - O_i^{exp}) \text{Cov}_{ij}^{-1} (O_j^{th}(\boldsymbol{\mathcal{C}}) - O_j^{exp})\,, \tag{4.14}$$

[3] In the literature [6, 284] the parameters to be estimated are usually denoted as θ and their estimators as $\hat{\theta}$. Since in our case these parameters always correspond to the NP contributions to the Wilson coefficients, we will systematically call these parameters $\boldsymbol{\mathcal{C}}$ and their estimators $\hat{\boldsymbol{\mathcal{C}}}$

[4] For numerical purposes we will assume the Covariance matrix to be independent of the parameters $\boldsymbol{\mathcal{C}}$ (or relatively flat). This assumption is of course violated for some observables, but it will allow us to obtain a fit in a reasonable time. We will then verify if this assumption is reasonable by redoing the fit, using the Covariance matrix at the bfps for the NP Wilson coefficients $\boldsymbol{\mathcal{C}}$, and comparing the new best fit points with the ones previously obtained. For the practical applications considered here, it has been checked for several different fits and with different theoretical and statistical approaches by various groups.

where Cov^{-1} is the inverse of the full covariance matrix defined above and with the following relation defined the likelihood $\mathcal{L}$ from χ^2

$$-2\ln\mathcal{L}(\boldsymbol{\mathcal{C}}) + \text{constant} = \chi^2(\boldsymbol{\mathcal{C}})\,. \tag{4.15}$$

4.4.2 Goodness of fit

We would like to use this likelihood to estimate the parameters of the theory, however this only makes sense when the theory considered can actually describe the data. In order to do this we need to test the *goodness of fit*, in other words, how accurately can the model being tested (i.e. the hypothesis) predict data. For this one looks at the $\chi^2_{\mathrm{min}} = \min_{\boldsymbol{\mathcal{C}}} \chi^2(\boldsymbol{\mathcal{C}})$ value , which is expected to be distributed as a χ^2 distribution with n_{dof} degrees of freedom, where the number of degrees of freedom of the fit is defined as

$$n_{\mathrm{dof}} = n_{\mathrm{obs}} - n_{\mathrm{pars}}\,, \tag{4.16}$$

and n_{pars} corresponds to the "fit dimension", i.e. the number of parameters that are being estimated. This assumes the fact that the observables have a similar sensitivity to all parameters, and that the linear (Gaussian) approximation is appropriate to deal with this problem (Wilks' theorem [285]). In the case of a hypothesis which does not depend on any parameter (like the SM hypothesis in this framework) we simply take $n_{\mathrm{pars}} = 0$. If the model provides a good fit, one would expect a χ^2_{min} value close to n_{dof}. A value smaller than this does not mean that the model does not provide a good fit, but it might suggest an over-estimation of the errors. A value much larger than this suggests that the hypothesis should be doubted. In order to do this one usually quotes the significance level (p-value), which corresponds to the probability of obtaining a worse χ^2 value than the value obtained from the fit, assuming that the hypothesis is true. It is defined as

$$p = 1 - \mathrm{CDF}_{\chi^2(n_{\mathrm{dof}})}(\chi^2_{\mathrm{min}}) \tag{4.17}$$

where $\mathrm{CDF}_{\chi^2(n_{\mathrm{dof}})}$ is the cumulative distribution function of the χ^2 distribution with n_{dof} degrees of freedom. This p-value is then what should be used as a criterion to decide when one should disregard a model to explain the data. A high χ^2 (i.e. a low p-value) indicates that a statistical fluctuation leading to the data observed is rather unlikely within the hypothesis assumed, and it can thus be considered as an indication against this hypothesis.

4.4.3 Comparing different hypotheses

In addition to the goodness of fit, one might want to test not only the compatibility of one hypothesis and the data, but also how different hypothesis compare and if one explains significantly better the data than another. To this end, we will use a statistical tool usually referred to as Pull which measures how much better a hypothesis fares compared to another one in explaining the data.

For two different parametric nested hypotheses H_0 and H_1 where $H_0 \subset H_1$ (i.e. H_0 is part of the family of parametrisations that H_1 describes) we refer to the minimum values of the χ^2 statistic for each hypothesis as $\chi^2_{\mathrm{min},H_0}$ and $\chi^2_{\mathrm{min},H_1}$. The Pull between the two hypotheses is directly related to the difference $\Delta\chi^2_{H_0,H_1} = \chi^2_{\mathrm{min},H_0} - \chi^2_{\mathrm{min},H_1}$ in the linear (Gaussian) approximation. This difference follows a χ^2 distribution with

$$n_{\mathrm{dof}} = n^{H_0}_{\mathrm{dof}} - n^{H_1}_{\mathrm{dof}} \tag{4.18}$$

degrees of freedom.

It is common to present the Pull in units of Gaussian standard deviations "σ". Then, the Pull of hypothesis H_1 over H_0 is defined as

$$\mathrm{Pull}_{H_0,H_1} \equiv -\mathrm{CDF}^{-1}_{\mathcal{N}(0,1)}\left(\frac{1 - \mathrm{CDF}_{\chi^2(n_{\mathrm{dof}})}\left(\Delta\chi^2_{H_0,H_1}\right)}{2}\right)\,, \tag{4.19}$$

where $\mathrm{CDF}_{\chi^2(n_{\mathrm{dof}})}$ is the Cumulative Distribution Function of a χ^2-distribution with n_{dof} degrees of freedom, $\mathrm{CDF}^{-1}_{\mathcal{N}(0,1)}$ the inverse of the Cumulative Distribution Function of the Normal distribution with $(\mu,\sigma) = (0,1)$.

The hypothesis H_0, is commonly referred as the null hypothesis and when it corresponds to the SM, we refer to the Pull as "$\mathrm{Pull}_{\mathrm{SM}}$" .

4.4.4 Pull for experimental data

For each experimental observable a Pull is also defined to quantify its deviation from the SM prediction, the interpretation of this value is slightly different. When considering the Pull of an observable we do not compare two different hypotheses, but rather compare two different datasets. This can be done in two different ways which aim at measuring different things:

Observable	SM	Experiment	Pull
R_K $[1.1, 6.0]$ [LHCb]	$+1.00 \pm 0.00$	$+0.85 \pm 0.04$ [277]	$+3.5$
$P_5'(B^0 \to K^{*0}\mu\mu)$ $[6.0, 8.0]$ [LHCb]	-0.94 ± 0.08	-0.58 ± 0.09 [287]	-2.9
$P_2(B^+ \to K^{*+}\mu\mu)$ $[6.0, 8.0]$ [LHCb]	-0.38 ± 0.06	$+0.06 \pm 0.14$ [240]	-2.9
$10^7 \times B(B^0 \to K^{*0}\mu\mu)$ $[15.0, 19.0]$ [LHCb]	$+2.46 \pm 0.21$	$+1.74 \pm 0.14$ [228]	$+2.8$
$P_4'(B^0 \to K^{*0}\mu\mu)$ $[4.0, 6.0]$ [ATLAS]	$+0.82 \pm 0.16$	-1.28 ± 0.75 [246]	$+2.7$
$P_2(B^0 \to K^{*0}\mu\mu)$ $[0.1, 0.98]$ [LHCb]	$+0.12 \pm 0.02$	$+0.00 \pm 0.04$ [287]	$+2.7$
$P_5'(B^0 \to K^{*0}\mu\mu)$ $[4.0, 6.0]$ [LHCb]	-0.82 ± 0.08	-0.44 ± 0.12 [287]	-2.7
$P_5'(B^0 \to K^{*0}\mu\mu)$ $[4.0, 6.0]$ [ATLAS]	-0.82 ± 0.08	$+0.26 \pm 0.39$ [246]	-2.7
$10^7 \times B(B^+ \to K^{*+}\mu\mu)$ $[15.0, 19.0]$ [LHCb]	$+2.65 \pm 0.23$	$+1.60 \pm 0.32$ [224]	$+2.7$
$P_5'(B \to K^*\mu\mu)$ $[4.0, 8.0]$ [Belle]	-0.89 ± 0.08	-0.03 ± 0.32 [242]	-2.6
R_{K^*} $[1.1, 6.0]$ [LHCb]	$+1.00 \pm 0.01$	$+0.69 \pm 0.12$ [207]	$+2.6$
$10^7 \times B(B_s \to \phi\mu\mu)$ $[15.0, 18.8]$ [LHCb]	$+2.26 \pm 0.15$	$+1.62 \pm 0.20$ [229]	$+2.5$

Table 4.2: Observables included in the fit with a pull > 2.5. This table is an extract of Table 4.A.1. The sign of the pull value represents whether the observable theoretical prediction is above $(+)$ or below $(-)$ the experimental measurement.

- First, by defining the Pull of a observable on its own. For instance for an observable O, a theoretical prediction O^{th} with a standard deviation σ and a experimental observation O^{exp} the pull is defined as

$$\text{Pull}_{\text{exp}} \equiv -\text{CDF}^{-1}_{\mathcal{N}(0,1)}\left(\frac{1-\text{CDF}_{\chi^2(1)}\left(\left(\frac{O^{\text{exp}}-O^{\text{th}}}{\sigma}\right)^2\right)}{2}\right) = \left|\frac{O^{\text{exp}}-O^{\text{th}}}{\sigma}\right| . \tag{4.20}$$

  This pull defines simply the tension of the observable with the SM, but not how it affects the fit.

- Secondly, by defining the Pull of the observable as a part of the full dataset of a fit. This is done by comparing the χ^2_{min} value when the measurement of this observable is included and when it is not, similarly to Eq. (4.19). This measures the tension between the observable at hand and both the SM prediction and the other observables. It represents thus the influence that the observable has on a fit, rather than the tension with the SM as opposed to the first definition. Certain subtleties exist in this definition and they are for instance discussed in Ref. [286].

Both of these definitions are similar when observables are not correlated, but different when they are. The value of the Pull_{exp} for each observable of the fit (with the first definition) is given in Table 4.A.1 and an extract of the observables with the highest Pulls is given in Table 4.2. One can see that R_K and R_{K^*} exhibit deviations, but also some optimised angular observables, in particular P_5' and P_2, as well as a few branching ratios both at low and high q^2.

4.4.5 Estimation of parameters

The maximum likelihood method is used to find the best estimators of the theory parameters $\boldsymbol{\mathcal{C}}$ for a set of experimental measurements $\boldsymbol{O}_i^{exp}$.

In order to estimate $\boldsymbol{\mathcal{C}}$ we maximize the likelihood, obtaining the so called ML estimators of $\boldsymbol{\mathcal{C}}$, which we simply refer as the best fit points (bfps). The ML estimators ($\hat{\boldsymbol{\mathcal{C}}}$) are defined as

$$\hat{\boldsymbol{\mathcal{C}}} \equiv \text{argmax}\left(\ln \mathcal{L}(\boldsymbol{\mathcal{C}})\right) . \tag{4.21}$$

In practice it is the $\chi^2(\boldsymbol{\mathcal{C}})$ function that we will minimize as this is by construction equivalent to maximizing the likelihood. This is also referred in the literature (for example Sec. 40.2.3 of Ref. [6]) as the method of least squares (LS). Then we obtain the bfps of $\boldsymbol{\mathcal{C}}$ through the LS method, where the LS estimators, equivalent to the ML estimators, are defined as

$$\hat{\boldsymbol{\mathcal{C}}} \equiv \text{argmin}\left(\chi^2(\boldsymbol{\mathcal{C}})\right) , \qquad \chi^2_{\text{min}} = \chi^2(\hat{\boldsymbol{\mathcal{C}}}) \tag{4.22}$$

However, it is not sufficient to determine the bfps we require also to asses the errors and correlations of our bfps estimation which we will due through the definition of confidence regions.

The information on the error and correlation of the bfps is contained in the likelihood function and it we extract it by the determination of confidence intervals (CI) or confidence regions (CR), for multidimensional estimators, which correspond to a geometrical way of understanding the uncertainty on the estimators $\hat{\boldsymbol{\mathcal{C}}}$.

nσ	$1-\gamma$	Q_α					
		$n=1$	$n=2$	$n=3$	$n=4$	$n=5$	$n=6$
1σ	0.683	1.0	2.3	3.5	4.7	5.9	7.0
2σ	0.955	4.0	6.2	8.0	9.7	11.3	12.8
3σ	0.997	9.0	11.8	14.2	16.3	18.2	20.1
4σ	0.99994	16.0	19.3	22.1	24.5	26.8	28.9
5σ	0.9999994	25.0	28.7	31.8	34.6	37.1	39.5

Table 4.3: Quantiles of the χ^2 distribution $Q_{\gamma;n} = CDF^{-1}_{\chi^2(n)}(1-\gamma)$ for different confidence levels $1-\gamma$ and for different number of fitted parameters n. The choice of values of $1-\gamma$ is such that they are equivalent to the usually quoted "σ tensions".

In general, a confidence region is constructed to contain the true value of the parameter with a certain probability, usually called *coverage probability*. In the case of 1D regions, we will say that a CI $[\hat{\mathcal{C}}-\delta_-, \hat{\mathcal{C}}+\delta_+]$ is central when the probability of the true value being out of the CI is evenly distributed between the external regions (i.e $]\infty, \hat{\mathcal{C}}-\delta_-]$ and $[\hat{\mathcal{C}}+\delta_+, \infty[$).

In the case of a Gaussian estimator, a central confidence interval $[\hat{\mathcal{C}}-\delta_-, \hat{\mathcal{C}}+\delta_+]$ can by determined through the following relations

$$\ln \mathcal{L}(\hat{\mathcal{C}}^{+\delta_+}_{-\delta_-}) = \ln \mathcal{L}_{\max} - \frac{Q_{\gamma;1}}{2}\,, \tag{4.23}$$

$$\chi^2(\hat{\mathcal{C}}^{+\delta_+}_{-\delta_-}) = \chi^2_{\min} + Q_{\gamma;1}\,, \tag{4.24}$$

where Q^n_γ corresponds to the quantiles of the χ^2 distribution

$$Q_{\gamma;n} = \mathrm{CDF}_{\chi^2(n)}(1-\gamma)\,, \tag{4.25}$$

which can be found for certain values of $1-\gamma$ in Table 4.3. In the case of a non-Gaussian estimator, in the large sample limit, the above definitions will also hold. We will thus generalize this definition for a n-dimensional confidence region as the points $\boldsymbol{\mathcal{C}}$ for which

$$\ln \mathcal{L}(\boldsymbol{\mathcal{C}}) \geq \ln \mathcal{L}_{\max} - \frac{Q_{\gamma;n}}{2}\,, \tag{4.26}$$

$$\chi^2(\boldsymbol{\mathcal{C}}) \leq \chi^2_{\min} + Q_{\gamma;n}\,. \tag{4.27}$$

These regions will have in general a complicated geometry, but in the large sample limit they will approach an n-dimensional hyper-ellipsoid, in which the covariance matrix is encoded. An example of this can be seen in the ($\mathcal{C}^{\rm NP}_{9\mu}$ vs $\mathcal{C}_{9'\mu}$) plot in Fig. 4.3 where even though the confidence regions for single experiments (i.e. Belle, CMS and ATLAS) do not have an ellipse shape, the LHCb and "All" fit do resemble more to an ellipse since the number of samples is higher. We will in general refer to this confidence intervals/regions by their coverage probability in terms of standard deviations (i.e. the size of the interval in standard deviations for a similar coverage probability in the Gaussian case), so we will, as shown in Table 4.3 refer to a 68.3% confidence interval as a 1σ interval/region and so on.

4.5 Fit results

As can be seen in the previous section, the global fits considered require the minimisation of a likelihood and an analysis of the shape of this likelihood around this minimum, in a multi-dimensional space spanned by the NP contributions to Wilson coefficients. This is done through a proprietary code developed over the years in Refs. [108, 132, 134, 135, 275]. Results from alternative codes will be discussed in Section 4.7.

4.5.1 Global fits in presence of LFUV NP

We start by considering the fits for NP scenarios which affect muon modes only. Tables 4.4 to 4.6 and Figs. 4.2 and 4.3 show the resulting bfps and the confidence regions for the most significant NP hypotheses based on fits to the full set of data ("All", 246 observables) or restricted to quantities assessing LFUV ("LFUV", 22 observables). The hierarchy of the results with all of the current data is similar to the one in Ref. [132] with slightly higher Pulls, while the SM hypothesis p-value is notably reduced to 1.1% for the fit "All" and 1.4% for the fit LFUV (around 2.5σ).

The different NP hypotheses are either motivated by NP models (see Sections 3.3 and 4.6.1) or by the data itself. The most prominent 1D scenarios (Table 4.4) correspond to a contribution to $\mathcal{C}_{9\mu}^{\rm NP}$ which can come accompanied by contributions to $\mathcal{C}_{10\mu}^{\rm NP}$, $\mathcal{C}_{9'\mu}$. The scenarios with the biggest significance have Pulls of $6-7\sigma$ for the "All" fit while for the "LFUV" fit they are around 4σ. A few comments are in order:

1. The scenario $\mathcal{C}_{9\mu}^{\rm NP}$ has the largest p-value in the "All" fit while $\mathcal{C}_{9\mu}^{\rm NP} = -\mathcal{C}_{10\mu}^{\rm NP}$ has the largest p-value in the LFUV fit, a difference which can be solved through the introduction of LFU NP (see Ref. [134] and Section 4.5.2).

2. The scenario $\mathcal{C}_{9\mu}^{\rm NP} = -\mathcal{C}_{9'\mu}$, has a reduced relative significance in the "LFUV" fit compared to the "All" fit since it favours a SM-like value of $R_K^{[1.1,6]}$ [133, 134].

3. The best-fit point for the all scenarios shown are 1-*sigma* compatible for the "All" and LFUV fits.

4. The scenario with only $\mathcal{C}_{10\mu}^{\rm NP}$ has a relatively low Pull in the "All" fit (compared to the highest Pulls) of only 4.5σ level while for the LFUV fit it has a strong Pull of 4.5σ.

5. As amply discussed since Ref. [288] a significant NP contribution to $\mathcal{C}_{9\mu}^{\rm NP}$ (around 1/4 of the SM contribution) is required in all favoured NP scenarios.

	All				LFUV			
1D Hyp.	Best fit	$1\ \sigma/2\ \sigma$	$\text{Pull}_{\rm SM}$	p-value	Best fit	$1\ \sigma/\ 2\ \sigma$	$\text{Pull}_{\rm SM}$	p-value
$\mathcal{C}_{9\mu}^{\rm NP}$	-1.06	$[-1.20,-0.91]$ $[-1.34,-0.76]$	7.0	39.5 %	-0.82	$[-1.06,-0.60]$ $[-1.32,-0.39]$	4.0	36.0 %
$\mathcal{C}_{9\mu}^{\rm NP} = -\mathcal{C}_{10\mu}^{\rm NP}$	-0.44	$[-0.52,-0.37]$ $[-0.60,-0.29]$	6.2	22.8 %	-0.37	$[-0.46,-0.29]$ $[-0.55,-0.21]$	4.6	68.0 %
$\mathcal{C}_{9\mu}^{\rm NP} = -\mathcal{C}_{9'\mu}$	-1.11	$[-1.25,-0.96]$ $[-1.39,-0.80]$	6.5	28.0 %	-1.61	$[-2.13,-0.96]$ $[-2.54,-0.41]$	3.0	9.3 %

Table 4.4: Most prominent 1D patterns of NP in $b \to s\mu^+\mu^-$. $\text{Pull}_{\rm SM}$ is quoted in units of standard deviation. The p-value of the SM hypothesis is 1.1% for the fit "All" and 1.4% for the fit LFUV.

	All			LFUV		
2D Hyp.	Best fit	$\text{Pull}_{\rm SM}$	p-value	Best fit	$\text{Pull}_{\rm SM}$	p-value
$(\mathcal{C}_{9\mu}^{\rm NP}, \mathcal{C}_{10\mu}^{\rm NP})$	$(-1.00,+0.11)$	6.8	39.4 %	$(-0.12,+0.54)$	4.3	65.6 %
$(\mathcal{C}_{9\mu}^{\rm NP}, \mathcal{C}_{7'})$	$(-1.06,+0.00)$	6.7	37.8 %	$(-0.82,-0.03)$	3.7	32.6 %
$(\mathcal{C}_{9\mu}^{\rm NP}, \mathcal{C}_{9'\mu})$	$(-1.22,+0.56)$	7.2	49.8 %	$(-1.80,+1.12)$	4.1	53.6 %
$(\mathcal{C}_{9\mu}^{\rm NP}, \mathcal{C}_{10'\mu})$	$(-1.26,-0.35)$	7.4	55.9 %	$(-1.82,-0.59)$	4.7	84.1 %
Hyp. 1	$(-1.21,+0.28)$	7.2	48.6 %	$(-1.62,+0.30)$	4.1	55.5 %
Hyp. 2	$(-1.11,+0.09)$	6.3	28.8 %	$(-1.95,+0.25)$	3.4	22.5 %
Hyp. 3	$(-0.44,+0.03)$	5.9	21.4 %	$(-0.37,-0.15)$	4.3	64.6 %
Hyp. 4	$(-0.48,+0.11)$	6.0	24.0 %	$(-0.46,+0.15)$	4.5	74.5 %
Hyp. 5	$(-1.26,+0.25)$	7.4	55.8 %	$(-2.08,+0.51)$	4.7	86.0 %

Table 4.5: Most prominent 2D patterns of NP in $b \to s\mu^+\mu^-$. The last five rows correspond to Hypothesis 1: $(\mathcal{C}_{9\mu}^{\rm NP} = -\mathcal{C}_{9'\mu}, \mathcal{C}_{10\mu}^{\rm NP} = \mathcal{C}_{10'\mu})$, 2: $(\mathcal{C}_{9\mu}^{\rm NP} = -\mathcal{C}_{9'\mu}, \mathcal{C}_{10\mu}^{\rm NP} = -\mathcal{C}_{10'\mu})$, 3: $(\mathcal{C}_{9\mu}^{\rm NP} = -\mathcal{C}_{10\mu}^{\rm NP}, \mathcal{C}_{9'\mu} = \mathcal{C}_{10'\mu})$, 4: $(\mathcal{C}_{9\mu}^{\rm NP} = -\mathcal{C}_{10\mu}^{\rm NP}, \mathcal{C}_{9'\mu} = -\mathcal{C}_{10'\mu})$ and 5: $(\mathcal{C}_{9\mu}^{\rm NP}, \mathcal{C}_{9'\mu} = -\mathcal{C}_{10'\mu})$.

	$\mathcal{C}_7^{\rm NP}$	$\mathcal{C}_{9\mu}^{\rm NP}$	$\mathcal{C}_{10\mu}^{\rm NP}$	$\mathcal{C}_{7'}$	$\mathcal{C}_{9'\mu}$	$\mathcal{C}_{10'\mu}$
Best fit	+0.01	-1.21	+0.15	+0.01	+0.37	-0.21
$1\ \sigma$	$[-0.02,+0.04]$	$[-1.38,-1.01]$	$[+0.00,+0.34]$	$[-0.02,+0.03]$	$[-0.12,+0.80]$	$[-0.42,+0.02]$
$2\ \sigma$	$[-0.04,+0.06]$	$[-1.52,-0.83]$	$[-0.11,+0.49]$	$[-0.03,+0.05]$	$[-0.51,+1.12]$	$[-0.60,0.23]$

Table 4.6: 1 and 2 σ confidence intervals for the NP contributions to Wilson coefficients in the 6D hypothesis allowing for NP in $b \to s\mu^+\mu^-$ operators dominant in the SM and their chirally-flipped counterparts, for the fit "All". The $\text{Pull}_{\rm SM}$ is 6.6σ and the p-value is 49.9%.

$\alpha_{0\mu}$	$\alpha_{1\mu}$	$\alpha_{2\mu}$	$\alpha_{3\mu}$	$\alpha_{4\mu}$	$\alpha_{5\mu}$	$\alpha_{6\mu}$	$\alpha_{7\mu}$	$\alpha_{8\mu}$	$\alpha_{9\mu}$	$\alpha_{10\mu}$
4.00	0.92	0.12	0.92	0.12	0.24	-1.06	0.12	-1.06	0.12	0.25
α_{0e}	α_{1e}	α_{2e}	α_{3e}	α_{4e}	α_{5e}	α_{6e}	α_{7e}	α_{8e}	α_{9e}	α_{10e}
3.99	0.92	0.12	0.92	0.12	0.24	-1.05	0.12	-1.05	0.12	0.24

Table 4.7: Coefficients for the polynomial parameterisation of the numerator and denominator of $R_K^{[1.1,6]}$ in the vicinity of the SM point.

Scenario		Best-fit point	1 σ	2 σ	Pull_{SM}	p-value
Scenario 5	$\mathcal{C}_{9\mu}^{\text{V}}$	-0.67	$[-1.12, -0.24]$	$[-1.58, +0.18]$	6.6	38.6 %
	$\mathcal{C}_{10\mu}^{\text{V}}$	$+0.42$	$[+0.01, +0.77]$	$[-0.54, +1.08]$		
	$\mathcal{C}_{9}^{\text{U}} = \mathcal{C}_{10}^{\text{U}}$	-0.31	$[-0.68, +0.17]$	$[-0.97, +0.65]$		
Scenario 6	$\mathcal{C}_{9\mu}^{\text{V}} = -\mathcal{C}_{10\mu}^{\text{V}}$	-0.52	$[-0.60, -0.44]$	$[-0.68, -0.36]$	6.8	40.1 %
	$\mathcal{C}_{9}^{\text{U}} = \mathcal{C}_{10}^{\text{U}}$	-0.41	$[-0.54, -0.28]$	$[-0.66, -0.15]$		
Scenario 7	$\mathcal{C}_{9\mu}^{\text{V}}$	-0.76	$[-1.00, -0.52]$	$[-1.25, -0.30]$	6.9	41.7 %
	$\mathcal{C}_{9}^{\text{U}}$	-0.39	$[-0.68, -0.09]$	$[-0.94, +0.19]$		
Scenario 8	$\mathcal{C}_{9\mu}^{\text{V}} = -\mathcal{C}_{10\mu}^{\text{V}}$	-0.30	$[-0.39, -0.21]$	$[-0.47, -0.13]$	7.3	53.8 %
	$\mathcal{C}_{9}^{\text{U}}$	-0.92	$[-1.10, -0.72]$	$[-1.27, -0.51]$		
Scenario 9	$\mathcal{C}_{9\mu}^{\text{V}} = -\mathcal{C}_{10\mu}^{\text{V}}$	-0.51	$[-0.64, -0.39]$	$[-0.77, -0.28]$	6.0	24.2 %
	$\mathcal{C}_{10}^{\text{U}}$	-0.27	$[-0.49, -0.05]$	$[-0.69, +0.16]$		
Scenario 10	$\mathcal{C}_{9\mu}^{\text{V}}$	-1.02	$[-1.18, -0.85]$	$[-1.32, -0.68]$	6.9	42.8 %
	$\mathcal{C}_{10}^{\text{U}}$	$+0.27$	$[+0.11, +0.44]$	$[-0.04, +0.60]$		
Scenario 11	$\mathcal{C}_{9\mu}^{\text{V}}$	-1.12	$[-1.28, -0.95]$	$[-1.43, -0.78]$	7.1	48.4 %
	$\mathcal{C}_{10'}^{\text{U}}$	-0.31	$[-0.46, -0.15]$	$[-0.60, -0.01]$		
Scenario 12	$\mathcal{C}_{9'\mu}^{\text{V}}$	-0.22	$[-0.37, -0.06]$	$[-0.51, +0.09]$	2.7	2.3 %
	$\mathcal{C}_{10}^{\text{U}}$	$+0.46$	$[+0.29, +0.64]$	$[+0.13, +0.82]$		
Scenario 13	$\mathcal{C}_{9\mu}^{\text{V}}$	-1.22	$[-1.37, -1.05]$	$[-1.50, -0.87]$	7.0	52.6 %
	$\mathcal{C}_{9'\mu}^{\text{V}}$	$+0.59$	$[+0.31, +0.84]$	$[+0.03, +1.04]$		
	$\mathcal{C}_{10}^{\text{U}}$	$+0.27$	$[+0.07, +0.48]$	$[-0.13, +0.69]$		
	$\mathcal{C}_{10'}^{\text{U}}$	-0.04	$[-0.23, +0.16]$	$[-0.43, +0.37]$		

Table 4.8: Most prominent patterns for LFU and LFUV NP contributions from Fit "All". Scenarios 5 to 8 were introduced in Ref. [134]. Scenarios 9 (motivated by 2HDMs [269]) and 10 to 13 (motivated by Z' models with vector-like quarks [289]) were introduced in Ref. [132].

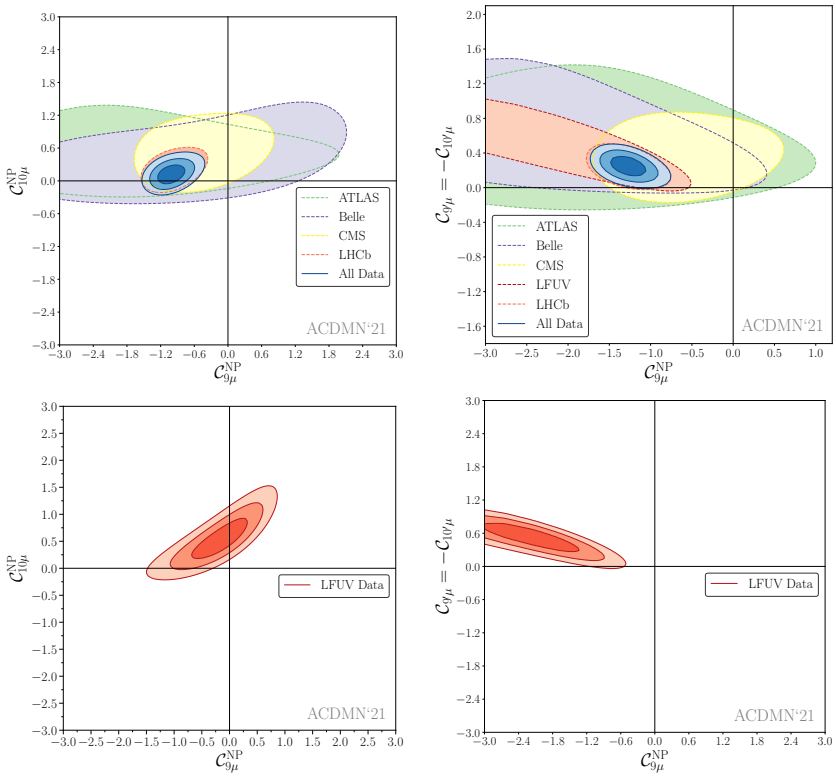

Figure 4.2: From left to right: Allowed regions in the $(\mathcal{C}^{\rm NP}_{9\mu}, \mathcal{C}^{\rm NP}_{10\mu})$ and $(\mathcal{C}^{\rm NP}_{9\mu}, \mathcal{C}_{9'\mu} = -\mathcal{C}_{10'\mu})$ planes for the corresponding 2D hypotheses, using all available data (fit "All") upper row or LFUV fit lower row. Dashed lines represent the 3 σ regions while the solid lines represent 1, 2 and 3 σ regions.

Concerning the 2D scenarios collected in Table 4.5, a similar picture to the 1D scenarios arises. Small contributions to RHC seem slightly favoured ($\mathcal{C}_{9'\mu} > 0, \mathcal{C}_{10'\mu} < 0$)[5]. Indeed, these RHC contributions tend to increase the value of $R_K^{[1.1,6]}$ while $\mathcal{C}^{\rm NP}_{9\mu} < 0$ tend to decrease it as can be seen from the explicit expression of $R_K^{[1.1,6]} = A_\mu/A_e$ where the numerator and the denominator can be given by an approximate polynomial parametrisation near the SM point

$$\begin{aligned} A_\ell = \alpha_{0\ell} + \alpha_{1\ell}\,\mathcal{C}^{\rm NP}_{9\ell} + \alpha_{2\ell}\,\left(\mathcal{C}^{\rm NP}_{9\ell}\right)^2 + \alpha_{3\ell}\,\mathcal{C}_{9'\ell} + \alpha_{4\ell}\,\left(\mathcal{C}_{9'\ell}\right)^2 + \alpha_{5\ell}\,\mathcal{C}^{\rm NP}_{9\ell}\mathcal{C}_{9'\ell} \\ + \alpha_{6\ell}\,\mathcal{C}^{\rm NP}_{10\ell} + \alpha_{7\ell}\,\left(\mathcal{C}^{\rm NP}_{10\ell}\right)^2 + \alpha_{8\ell}\,\mathcal{C}_{10'\ell} + \alpha_{9\ell}\,\left(\mathcal{C}_{10'\ell}\right)^2 + \alpha_{10\ell}\,\mathcal{C}^{\rm NP}_{10\ell}\mathcal{C}_{10'\ell} \end{aligned} \tag{4.28}$$

with the coefficients provided in Table 4.7 (for linearised expressions, see Refs. [134, 290]).

The comparison between Hyps. 4 and 5 shows that the scenario $\mathcal{C}_{9'\mu} = -\mathcal{C}_{10'\mu}$ (left-handed lepton coupling for right-handed quarks) prefers to be associated with $\mathcal{C}^{\rm NP}_{9\mu}$ (vector lepton coupling for left-handed quarks) rather than $\mathcal{C}^{\rm NP}_{9\mu} = -\mathcal{C}^{\rm NP}_{10\mu}$ (left-handed lepton coupling for left-handed quarks). Finally, no significant changes are observed in the 6D fit compared to previous results [132, 135], except for the slight increase in the $\text{Pull}_{\rm SM}$, see Table 4.6.

One can see that the main Wilson coefficient deviating in the 6D fit is $\mathcal{C}_{9\mu}$ with a deviation well over 3σ while the other Wilson coefficients are all compatible at the 1σ level with their SM value being $\mathcal{C}_{10\mu}$ and $\mathcal{C}_{10'\mu}$ the ones more distant from their prediction. This in agreement with the scenarios already discussed, where the main NP contribution is $\mathcal{C}_{9\mu}$.

4.5.2 Global fits in presence of LFUV and LFU NP

We turn to scenarios that allow also for the presence of LFU NP [132–134] (in addition to LFUV contributions to muons only), leading to the value of the Wilson coefficients

$$\mathcal{C}_{ie} = \mathcal{C}_i^{\rm U}\,, \qquad \mathcal{C}_{i\mu} = \mathcal{C}_i^{\rm U} + \mathcal{C}_i^{\rm V}\,. \tag{4.29}$$

[5] Interestingly, these small contributions also reduce slightly the mild tension between P_5' at large and low recoils pointed out in Ref. [133] compared to the scenario with only $\mathcal{C}^{\rm NP}_{9\mu}$.

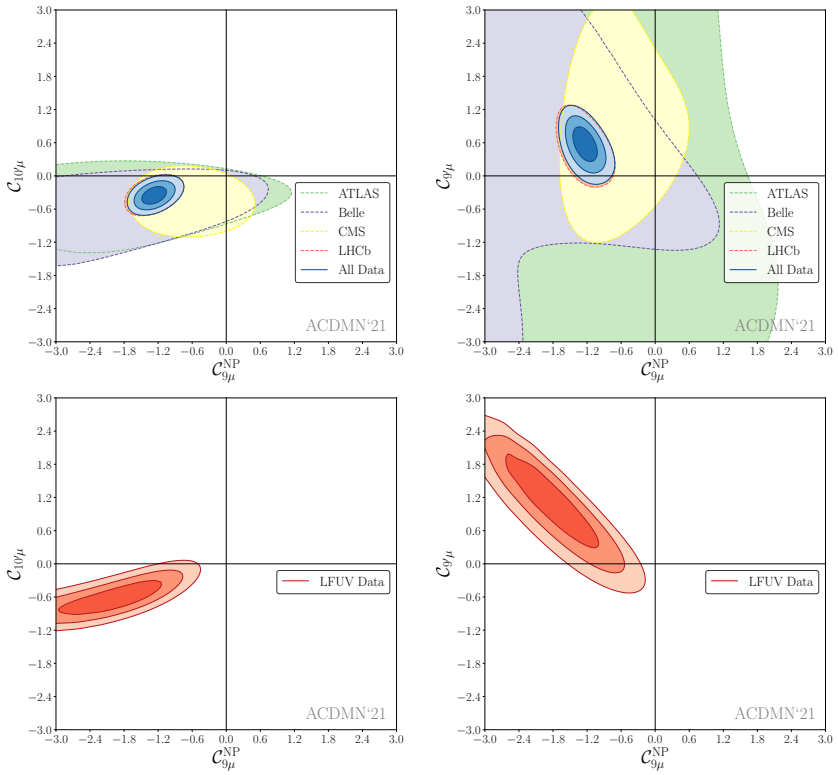

Figure 4.3: From left to right: Allowed regions in the $(\mathcal{C}_{9\mu}^{\rm NP}, \mathcal{C}_{10'\mu})$ and $(\mathcal{C}_{9\mu}^{\rm NP}, \mathcal{C}_{9'\mu})$ planes for the corresponding 2D hypotheses, using all available data (fit "All") upper row or LFUV fit lower row. Dashed lines represent the 3 σ regions while the solid lines represent 1, 2 and 3 σ regions.

(with $i = 9, 10$) for $b \to s e^+ e^-$ and $b \to s \mu^+ \mu^-$ transitions respectively.

In many NP models, a universal contribution could be expected through the mixing of NP operators with the SM ones via electromagnetic (radiative) corrections [291] as shown in Fig. 4.10 in the case of a U_1 leptoquark.

The results for different scenarios including both lepton flavour universal and violating contributions are presented in Table 4.8 and the allowed regions in Fig. 4.4. Concerning new directions in parameter space we allow for RHC, motivated by the results of Section 4.5.1, and focus on scenarios that could be fairly easily obtained in simple NP models.

With the updated experimental inputs, we confirm earlier results [132, 134] that a LFUV left-handed lepton coupling structure (corresponding to $\mathcal{C}_9^{\rm V} = -\mathcal{C}_{10}^{\rm V}$ and preferred from a model-building point of view) yields a better description of data with the addition of LFU-NP in the coefficients $\mathcal{C}_{9,10}$, as shown by the scenarios 6,8 in Table 4.8 with p-values larger than 40%.

The comparison of scenarios 10 and 12 illustrates that $\mathcal{C}_{9\mu}^{\rm V}$ plays an important role in LFU NP scenarios and cannot be swapped for its chirally-flipped counterpart without consequences.

4.5.3 Hadronic contributions to $c\bar{c}$ versus NP

Clearly, in all viable NP scenarios presented above, $\mathcal{C}_{9\mu}^{\rm NP}$ plays a very significant role. For quite some time it has been under discussion [119, 123, 127, 282] that the flavour anomalies, specially since they can be explained by a change on $\mathcal{C}_9$ (through which the charm-loop contributes), could have an origin of purely hadronic effects that might not be as well understood as we think. In these works, they considered only $B \to K^* \mu^+ \mu^-$ and they included a set of 9 (18) independent parameters to parametrise each of the 3 different helicity hadronic contributions through an order 2 (complex) polynomial in q^2, which are then fitted from data, either within the SM or together with NP contributions to Wilson coefficients. The inclusion of such a large set of parameters inevitably allows more freedom in the agreement between the data and the SM expectations. In Ref. [127], the authors argued that large higher-order coefficients were found for some of their fits, which could not be mimicked by NP changes in $\mathcal{C}_7^N P$ and $\mathcal{C}_{9\mu}^N P$. They considered this as an indication that large non-local contributions were needed to explain the data. However, the fits used to obtain such large effects were criticised in Ref. [205] and confirmed in Refs. [119, 123] as using an improprer parametrisation and exploiting only part of the experimental and theoretical information available. The consideration of alternative, more complete, fits did not indicate any

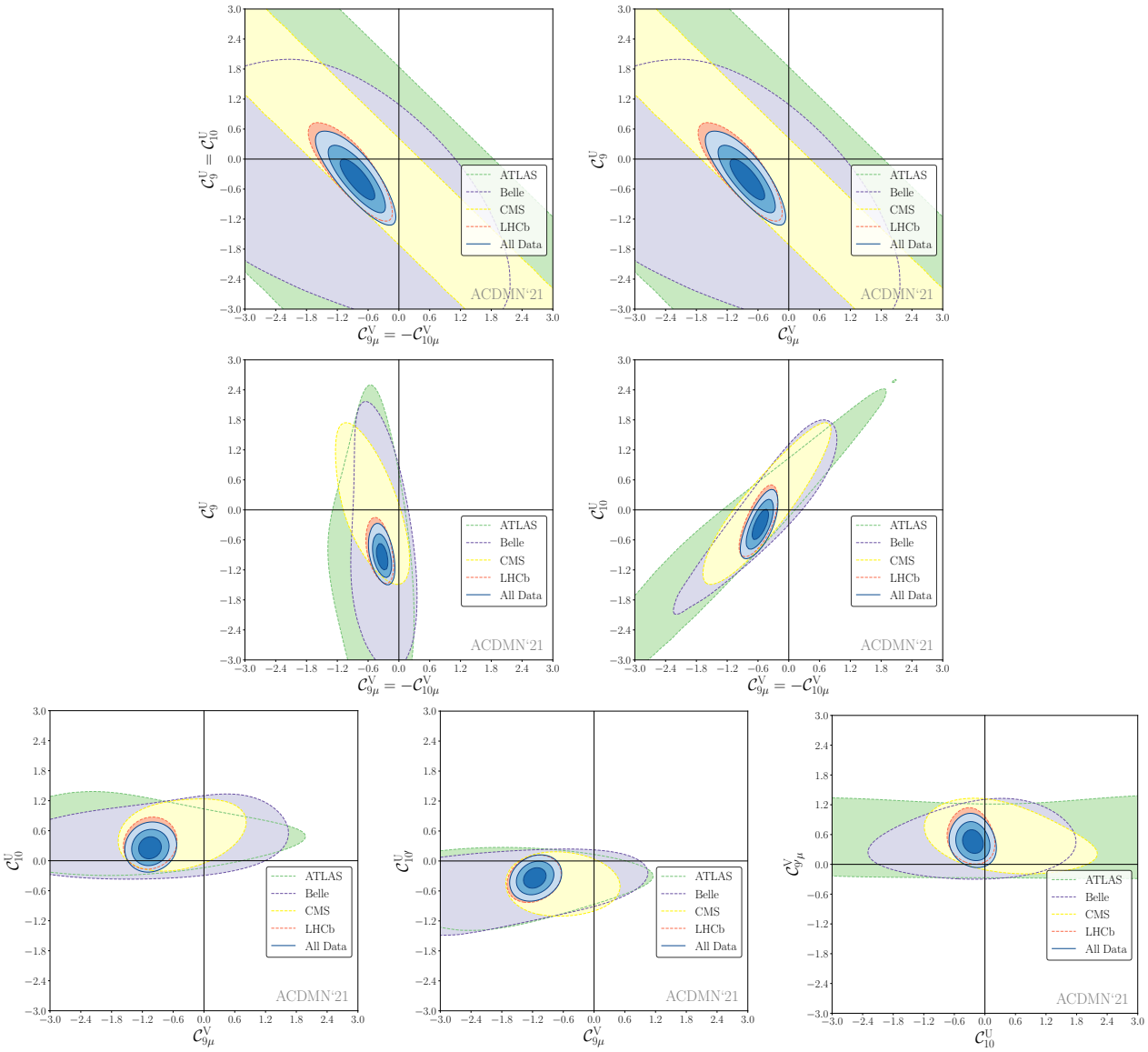

Figure 4.4: From left to right : Allowed regions for the 2D scenarios presented in Table 4.8. Scenarios 6 and 7 on the upper row, 8 and 9 in the middle row and 10 to 12 in the bottom row using all available data (fit "All"). Dashed lines represent the 3 σ regions while the solid lines represent 1, 2 and 3 σ regions.

strong q^2 dependence that could be attributed to a hadronic effect, and the size of the parameters are in perfect agreement with the parametrisations used in the literature for non-local effects, up to a constant contribution to $\mathcal{C}_{9\mu}^{N}P$.

Furthermore a comparison of different determinations of the hadronic uncertainties [292] for the branching fraction and the P_5' optimised observable for the $B \to K^*\mu^+\mu^-$ decays is displayed in Fig. 4.6, showing a good agreement between the different determinations.

The discussion has naturally changed after the measurements of R_K and R_{K^*} have hinted at LFUV NP, since their measured value cannot be explained by hadronic contributions which are LFU. Nonetheless, one could think that the universal contribution to $\mathcal{C}_9^U$ discussed before could still have a hadronic origin. However, these hadronic contributions, would be expected to yield a q^2 dependent $\mathcal{C}_9^U$ contribution. This possibility was analysed in Ref. [132] showing no signs of q^2-dependence for binned determinations of $\mathcal{C}_9^U$ (see Fig. 4.5). Nonetheless, the binning of the data to compute $\mathcal{C}_9^U$ reduces the sensitivity of the fit and could still hide some slight q^2 dependence, however the result shown in Fig. 4.5 suggests that hadronic contributions do not drive alone this contribution.

At this stage, we have thus no indication from the fits that the non-local contributions from $c\bar{c}$ loop are not well controlled theoretically. Naturally, a better theoretical control of this effect will be needed to exploit fully the data as more and more precise information will be gathered from the LHCb and Belle II experiments, see Refs. [109, 112] for progress in this direction.

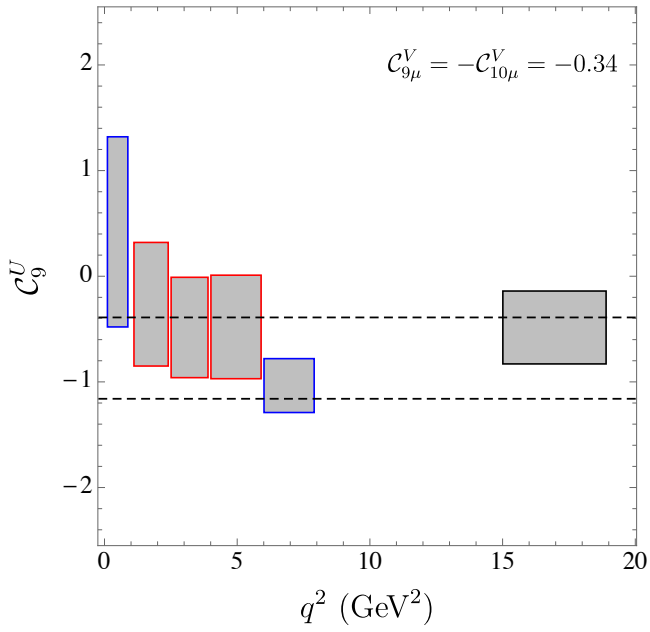

Figure 4.5: Determination of the $\mathcal{C}_9^U$ Wilson coefficient, setting the LFUV coefficients $\mathcal{C}_{9\mu}^V = -\mathcal{C}_{10\mu}^V$ to their values at the best-fit point of the All fit, in a bin-by-bin fit using only LHCb data on optimized observables, branching ratios and radiative decays. Each box correspond to the 1σ confidence interval obtained in this bin. The band corresponds to the 2σ interval obtained from the fit of the NP hypothesis to the All data set. This exercise was done with an earlier set of data (in Ref. [132]), but are not any indications that this could change much with the current set of data.

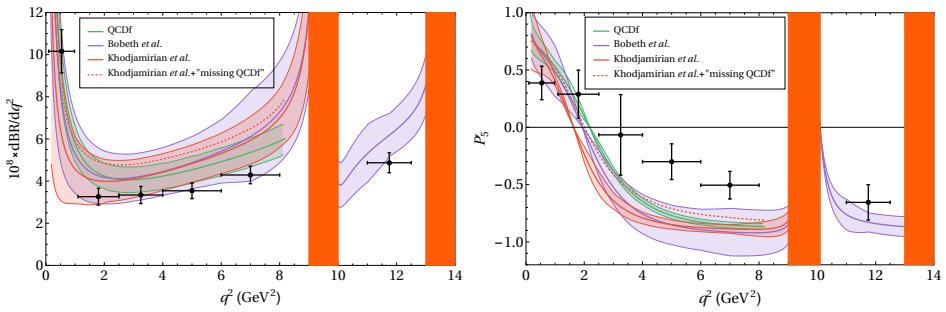

Figure 4.6: Comparison between the different determinations of hadronic uncertainties [38, 112, 115, 281] for the branching fraction and the P_5' optimised observable in the $B \to K^* \mu^+ \mu^-$ mode. Taken from Ref. [292]

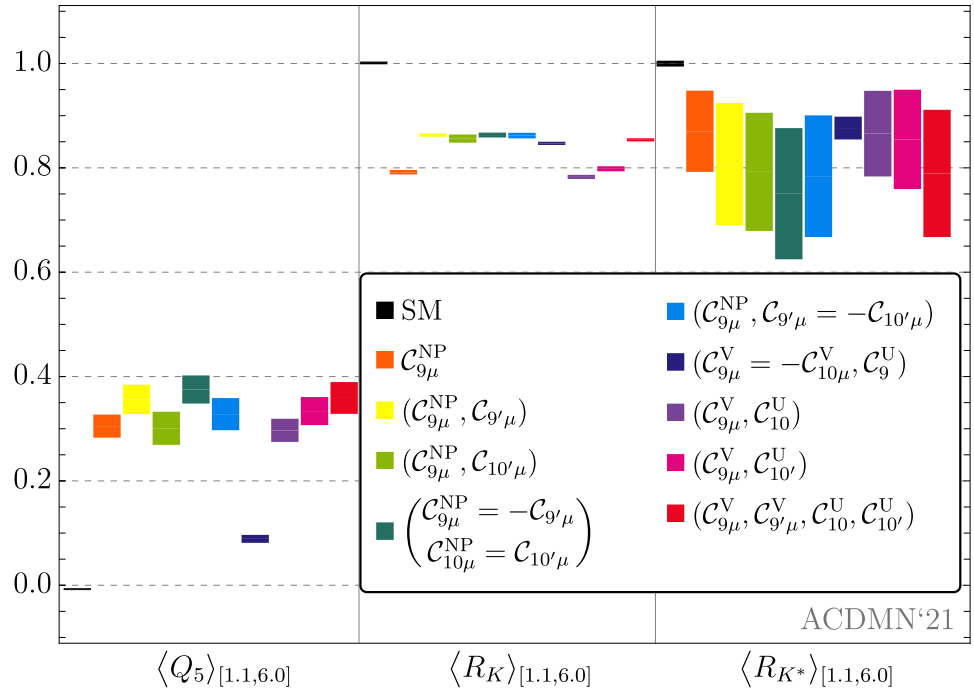

Figure 4.7: Values of $\langle Q_5 \rangle_{[1.1,6]}$, $\langle R_K \rangle_{[1.1,6]}$, $\langle R_{K^*} \rangle_{[1.1,6]}$ in the SM and nine different scenarios: SM (black), $\mathcal{C}^{\rm NP}_{9\mu}$ (orange), $(\mathcal{C}^{\rm NP}_{9\mu}, \mathcal{C}_{9'\mu})$ (yellow), $(\mathcal{C}^{\rm NP}_{9\mu}, \mathcal{C}_{10'\mu})$ (light green), $(\mathcal{C}^{\rm NP}_{9\mu} = -\mathcal{C}_{9'\mu}, \mathcal{C}^{\rm NP}_{10\mu} = \mathcal{C}_{10'\mu})$ (dark green), $(\mathcal{C}^{\rm NP}_{9\mu}, \mathcal{C}_{9'\mu} = -\mathcal{C}_{10'\mu})$ (light blue), $(\mathcal{C}^{\rm V}_{9\mu} = -\mathcal{C}^{\rm V}_{10\mu}, \mathcal{C}^{\rm U}_{9})$ (dark blue), $(\mathcal{C}^{\rm V}_{9\mu}, \mathcal{C}^{\rm U}_{10})$ (purple), $(\mathcal{C}^{\rm V}_{9\mu}, \mathcal{C}^{\rm U}_{10'})$ (pink), $(\mathcal{C}^{\rm V}_{9\mu}, \mathcal{C}^{\rm V}_{9'\mu}, \mathcal{C}^{\rm U}_{10}, \mathcal{C}^{\rm U}_{10'})$ (red). The boxes correspond to the predictions of the 1 σ regions at the b.f.p. value of the Wilson coefficients in each of the scenarios for the fit to the "All" data set.

4.6 Interpretations

4.6.1 Favoured scenarios and connection with NP explanations

Several scenarios ($\mathcal{C}^{\rm NP}_{9\mu}$, $\mathcal{C}^{\rm NP}_{9\mu} = -\mathcal{C}^{\rm NP}_{10\mu}$, ($\mathcal{C}^{\rm NP}_{9\mu}$, $\mathcal{C}^{\rm NP}_{9'\mu} = -\mathcal{C}^{\rm NP}_{10\mu}$), ($\mathcal{C}^{V}_{9} = -\mathcal{C}^{V}_{10}$,$\mathcal{C}^{U}_{9\mu}$)) exhibit a significant improvement in the description of the data compared to the SM. Fig. 4.7 shows the predictions for the observables Q_5, R_K and R_{K^*} in several of these scenarios. The large uncertainties for R_{K^*} in most NP scenarios come from the presence of three different helicity amplitudes involving different combinations of form factors: if the $SU(2)_L$ symmetry of the SM is respected, one amplitude dominates leading to reduced uncertainties for the prediction of R_{K^*}, but in other cases, the presence of several helicity amplitudes leads to larger uncertainties. Fig. 4.9a illustrates the importance of R_K and P'_5 in highlighting the favoured scenarios compared to others considered in the previous section.

In Fig. 4.8 we show the impact of the favoured NP scenarios on the observable P'_5. The $\mathcal{C}^{\rm NP}_{9\mu}$ scenario, the scenario 8 and Hyp. 5 cluster together showing a good agreement with the experimental measurement, while the $\mathcal{C}^{\rm NP}_{9\mu} = -\mathcal{C}^{\rm NP}_{10\mu}$ and $\mathcal{C}^{\rm NP}_{10\mu}$ scenarios cluster close to the SM predictions, showing no relief of the tension present in P'_5 with respect to the SM.

One can also notice that Q_5 is able to separate three cases of interest: the SM, the scenario 8 ($\mathcal{C}^{\rm U}_{9}$,$\mathcal{C}^{\rm V}_{9\mu} = -\mathcal{C}^{\rm V}_{10\mu}$), and the scenarios with right-handed couplings and a large negative contribution to $\mathcal{C}_{9\mu}$. It will be thus very interesting to see if Belle II can obtain further information on Q_5.

With the updated data, little change is observed among the preferred 2D NP models discussed in Section 3.3. Nevertheless, with an $R_K^{[1.1,6]}$ value closer to one, scenarios with right-handed currents (RHC), namely $(\mathcal{C}^{\rm NP}_{9\mu}, \mathcal{C}_{9'\mu})$ and $(\mathcal{C}^{\rm NP}_{9\mu}, \mathcal{C}_{10'\mu})$, seem to emerge. The first scenario is naturally generated in a Z' model with opposite couplings to right-handed and left-handed quarks and was proposed in Ref. [264] within the context of a gauged $L_\mu - L_\tau$ symmetry with vector-like quarks.

Scenario 8, which exhibits one of the most significant Pulls with respect to the SM, can actually be realized via off-shell photon penguins [291] in a leptoquark model explaining also $b \to c\tau\bar{\nu}_\tau$ data (we will return to this point in Section 4.6.2).

The scenarios 9–13 are characterized by a $\mathcal{C}^{\rm U}_{10^{(\prime)}}$ contribution. This arises naturally in models with modified Z couplings (to a good approximation $\mathcal{C}^{\rm U}_{9^{(\prime)}}$ can be neglected). The pattern of scenario 9 occurs in Two-Higgs-Doublet

models where this flavour universal effect can be supplemented by a $\mathcal{C}_9^{\rm V} = -\mathcal{C}_{10}^{\rm V}$ effect [269].

In case of scenarios 11 to 13, one can invoke models with vector-like quarks where modified Z couplings are even induced at tree level. The LFU effect in $\mathcal{C}_{10^{(\prime)}}^{\rm U}$ can be accompanied by a $\mathcal{C}_{9,10^{(\prime)}}^{\rm V}$ effect from Z' exchange [289]. Vector-like quarks with the quantum numbers of right-handed down quarks (left-handed quarks doublets) generate effect in $\mathcal{C}_{10}^{\rm U}$ and $\mathcal{C}_{9'}^{\rm V}$ ($\mathcal{C}_{10^{(\prime)}}^{\rm U}$ and $\mathcal{C}_{9}^{\rm V}$) for a Z' boson with vector couplings to muons [289].

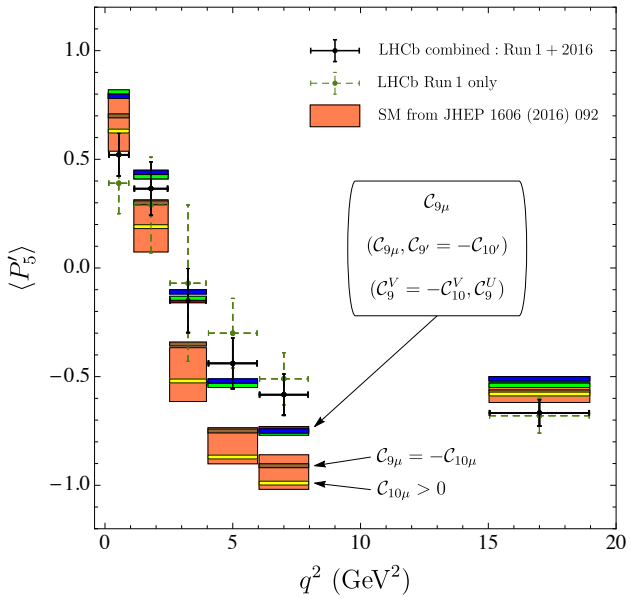

Figure 4.8: Impact of favoured NP scenarios on the observable P_5'. Only central values for the NP scenarios are displayed. The most interesting scenarios cluster together while traditional scenarios like $\mathcal{C}_{9\mu}^{\rm NP} = -\mathcal{C}_{10\mu}^{\rm NP}$ or the scenario $\mathcal{C}_{10\mu}^{\rm NP}$ considered in Ref. [128] fail to explain this anomaly.

4.6.2 Model-independent connection to $b \to c\ell\bar{\nu}$

In complement with the above EFT analysis, we focus now on the NP interpretation of scenario 8. Indeed, this scenario allows for a model-independent connection between the anomalies in $b \to s\ell^+\ell^-$ and those in $b \to c\tau\nu$, which are at the 3.1σ level [158].

Such a correlation arises in the SMEFT scenario where $C_S = C_T$ expressed in terms of the Lagrangian introduced in Eq. (3.12). This scenario stems naturally from models with an $SU(2)$ singlet vector leptoquark [265, 293, 294] (see Section 3.3). The operator involving-third generation leptons ($\lambda_{32}^q \lambda_{\tau\tau}^\ell$) explains $R_{D^{(*)}}$ and the one involving the second generation ($\lambda_{32}^q \lambda_{\mu\mu}^\ell$) gives a LFUV effect in $b \to s\mu^+\mu^-$ processes. The constraint from $b \to c\tau\nu$ and $SU(2)_L$ invariance leads generally to large contributions to the operator $\bar{s}\gamma^\mu P_L b \bar{\tau}\gamma_\mu P_L \tau$, which enhances $b \to s\tau^+\tau^-$ processes [295], but also mixes it into $\mathcal{O}_9$ generating a $\mathcal{C}_9^{\rm U}$ contribution at $\mu = m_b$ [291] as shown in Fig. 4.10 [6].

Therefore, scenario 8 is reproduced in this setup with an additional correlation between $\mathcal{C}_9^{\rm U}$ and $R_{D^{(*)}}$. Assuming a generic flavour structure so that small CKM elements can be neglected [291, 295], we get

$$\mathcal{C}_9^{\rm U} \approx 7.5 \left(1 - \sqrt{\frac{R_{D^{(*)}}}{R_{D^{(*)}\rm SM}}}\right)\left(1 + \frac{\log(\Lambda^2/(1\text{TeV}^2))}{10.5}\right). \tag{4.30}$$

where Λ is the typical scale of NP involved. Realizations of this scenario in specific NP models yield also an effect in $\mathcal{C}_7$ generally [291]. However, since this effect is model dependent (and in fact small in some UV complete models [298, 299]), we neglect it here.

We show the global fit of Scenario 8 without and with the additional input on $R_{D^{(*)}}$ from Ref. [158] in Fig. 4.9b, taking the scale $\Lambda = 2$ TeV. The best-fit point for $(\mathcal{C}_9^{\rm U}, \mathcal{C}_{9\mu}^{\rm V} = -\mathcal{C}_{10\mu}^{\rm V})$ is $(-0.74, -0.36)$, with 1-σ intervals $[-0.86, -0.61]$ and $[-0.43, -0.28]$ respectively. The agreement among all data is very good, shown by the fact that the scenario 8 supplemented with $R_{D^{(*)}}$ exhibits a Pull with respect to the SM of 8.1 σ and p-value

[6] Note that not all models addressing the charged and neutral current anomalies simultaneously have an anarchic flavour structure. In fact, in the case of models with a flavour structure that does not produce tree level FCNC [296, 297], one does not find large effects in $b \to s\tau^+\tau^-$ or $\mathcal{C}_9^{\rm U}$.

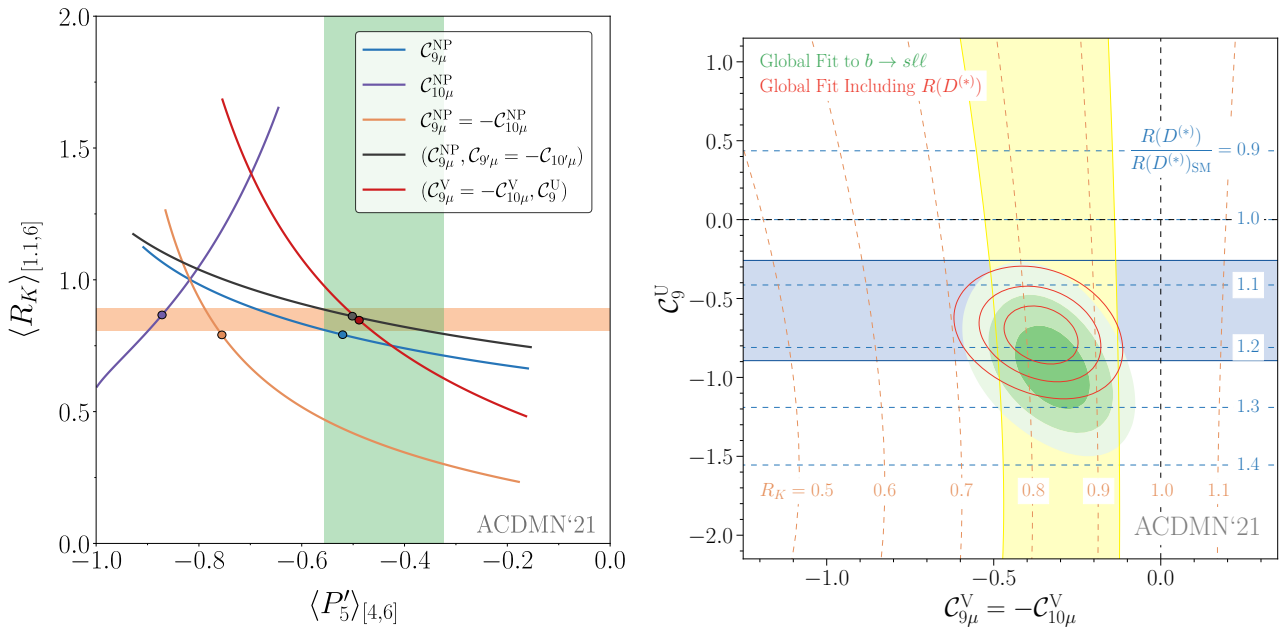

(a) (b)

Figure 4.9: Left: $\langle R_K \rangle_{[1.1,6]}$ versus $\langle P_5' \rangle_{[4,6]}$ in five different scenarios: $\mathcal{C}_{9\mu}^{\rm NP}$ (blue), $\mathcal{C}_{9\mu}^{\rm NP} = -\mathcal{C}_{10\mu}^{\rm NP}$ (orange), and $(\mathcal{C}_{9\mu}^{\rm V} = -\mathcal{C}_{10\mu}^{\rm V}, \mathcal{C}_9^{\rm U})$ (red), $(\mathcal{C}_{9\mu}^{\rm NP}, \mathcal{C}_{9'\mu}^{\rm NP} = -\mathcal{C}_{10'\mu}^{\rm NP})$ (black), and $\mathcal{C}_{10\mu}^{\rm NP}$ (purple). The curves correspond only to the predictions for central values. In the 2D scenarios (red and black) the Wilson coefficient on the right (i.e. $\mathcal{C}_9^{\rm U}$ and $\mathcal{C}_{9'\mu}^{\rm NP} = -\mathcal{C}_{10'\mu}^{\rm NP}$) is set to its bfp value. The current experimental values from the LHCb collaboration are also indicated (orange horizontal and green vertical bands respectively). The dots correspond to the b.f.p. values of the corresponding scenario for the fit to the "All" data set. Right: Preferred regions at the 1, 2 and 3 σ level (green) in the $(\mathcal{C}_{9\mu}^{\rm V} = -\mathcal{C}_{10\mu}^{\rm V}, \mathcal{C}_9^{\rm U})$ plane from $b \to s\ell^+\ell^-$ data. The red contour lines show the corresponding regions once $R_{D^{(*)}}$ is included in the fit (for $\Lambda = 2$ TeV). The horizontal blue (vertical yellow) band is consistent with $R_{D^{(*)}}$ (R_K) at the $2\,\sigma$ level and the contour lines show the predicted values for these ratios.

of 51.4%. An even better agreement could be reached if $R_{D^{(*)}}$ is slightly further away from the SM expectations, or if the scale of New Physics is increased.

4.7 Comparison with other works

4.7.1 Global fits by other groups

We will now discuss some of the other results available in the literature and how they compare with our results.

We start by looking at the results of the analysis performed in Ref. [267] through a similar frequentist approach using the open-source software flavio [300]. Compared to our results, they use the form factors from Ref. [278] for both $B \to K^*$ and $B_s \to \phi$ and use a simple polynomial order-of-magnitude estimate for the $c\bar{c}$ contributions. In spite of these differences their fit shows similar overall results to the ones discussed above. One difference, is that they generally obtain reduced tensions compared to ours. This reduction is mainly driven by the fact that they don not include bins of $q^2 > 6\,\text{GeV}^2$ which show certain tension with the SM. This is also responsible for the slight difference in hierarchy regarding $\mathcal{C}_{9\mu}$ vs $\mathcal{C}_{9\mu} = -\mathcal{C}_{10\mu}$ where in Ref. [267] the $\mathcal{C}_{9\mu} = -\mathcal{C}_{10\mu}$ scenario has the highest pull and in our fits the $\mathcal{C}_{9\mu}$ scenario shows the highest pull. This can more clearly be understood when comparing the bfps and confidence regions in the 2D fits $(\mathcal{C}_{9\mu}, \mathcal{C}_{10\mu})$ as shown in Fig. 4.11. Two interesting points about the results in Ref. [267] are that:

- First, they also test the inclusion of scalar currents, finding as expected, that they cannot relieve the tension with experimental measurements.

- Secondly, they have tested whether the dependence of the covariance matrix on the Wilson coefficients has an effect on the results of the fits and include for some of the observables experimental non-Gaussianities in their likelihood, showing that this does not significantly affect the results. This confirms that our approximation of computing the covariance matrix only once at the SM is valid.

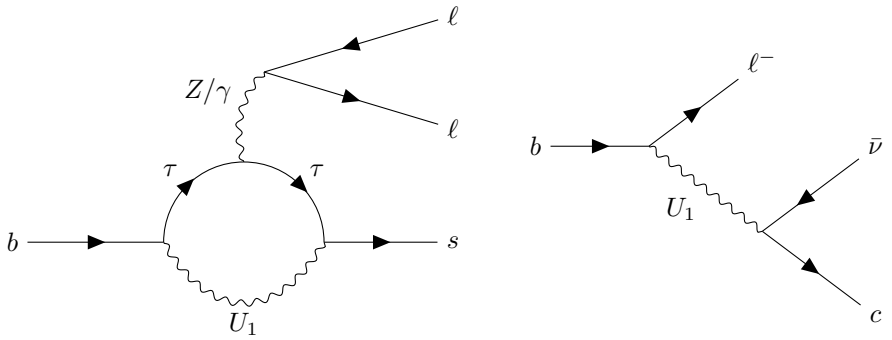

Figure 4.10: Universal contribution to $b \to s\ell^+\ell^-$ (left) from a U_1 leptoquark through the same vertex that induces the $b \to c\ell\bar{\nu}$ anomalies (right).

Results in Ref. [301] present a good agreement with our results and even better agreement with results in Ref. [267]. However the compatibility between results in Refs. [267, 301] is not surprising since both fits are performed using the same python package (flavio [300]).

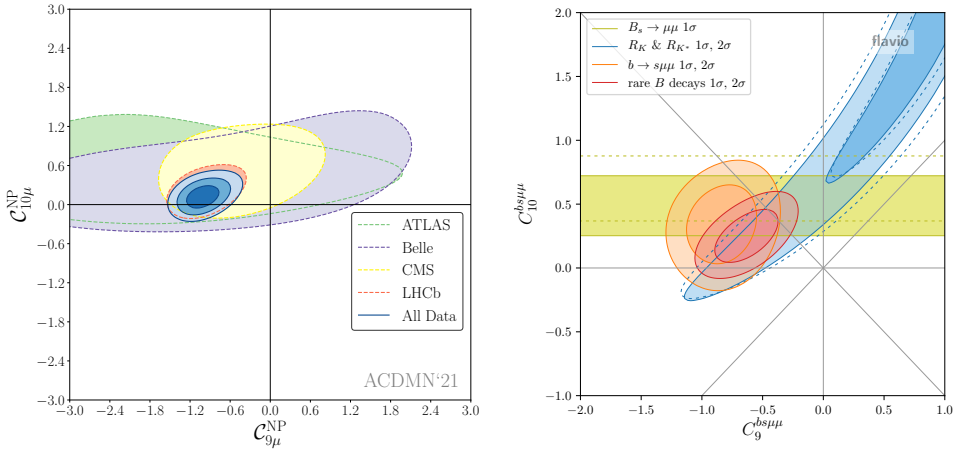

Figure 4.11: Comparison of the allowed regions in the $(\mathcal{C}^{\rm NP}_{9\mu}, \mathcal{C}^{\rm NP}_{10\mu})$ plane obtained by us (left) and the one in Ref. [267] (right). Details on the left plot can be found in Fig. 4.2 and of the right one in the original work [267].

The analysis performed in Ref. [302] is performed using the FlavBit module of the GAMBIT package, with which they obtain the likelihoods both with a frequentist and bayesian approaches, dealing practically identical results. They use the form factors from Ref. [278] for both $B \to K^*$ and $B_s \to \phi$ similarly to Ref. [267], and non local hadronic contributions are included as power corrections with coefficients treated as uncorrelated complex nuisance parameters. This analysis yields a 3D confidence region in the $(\mathcal{C}^{\rm NP}_{7\mu}, \mathcal{C}^{\rm NP}_{9\mu}, \mathcal{C}^{\rm NP}_{10\mu})$. However, they find the $\mathcal{C}^{\rm NP}_{7\mu}$ and $\mathcal{C}^{\rm NP}_{10\mu}$ coefficients to be small and compatible with SM hypothesis. Although we do not perform a 3D fit to these coefficients, this result can be compared to our $\mathcal{C}^{\rm NP}_{9\mu}$ 1D fit and the $(\mathcal{C}^{\rm NP}_{7\mu}, \mathcal{C}^{\rm NP}_{9\mu})$ and $(\mathcal{C}^{\rm NP}_{9\mu}, \mathcal{C}^{\rm NP}_{10\mu})$ 2D fits, showing compatible results with Ref. [302].

The possibility of complex Wilson coefficients has been studied in Refs. [267, 303], finding a large room allowed for imaginary parts in them as show in Fig. 4.12 for the case of a complex $\mathcal{C}^{\rm NP}_{9\mu}$ coefficient. This is mainly due to the small amount of observables available testing CP violation in the $b \to s\ell^+\ell^-$ transition.

In addition to global fits, it is interesting to recall more specific studies :

- A Bayesian study of the full angular distribution of the $\Lambda_b \to \Lambda(\to p\pi^-)\mu^+\mu^-$ decay measured by the LHCb collaboration [247] was performed in Ref. [227] using the EOS software [304]. Here they updated the results from Ref. [305] including the newly updated measurement of the $\Lambda \to p\pi^-$ asymmetry parameter by the BESIII collaboration [248], an extension of the results presented in Ref. [226], and lattice inputs for the $\Lambda_b \to \Lambda(1116)$ form factors [203]. Due to the large uncertainties present in the LHCb results, this studies favours both the SM and the best fit points $(\mathcal{C}^{\rm NP}_{9\mu}, \mathcal{C}^{\rm NP}_{10\mu})$ obtained above and in similar works.

- A analysis of the possibility of NP in the electromagnetic dipole operator and its chirally flipped counterpart

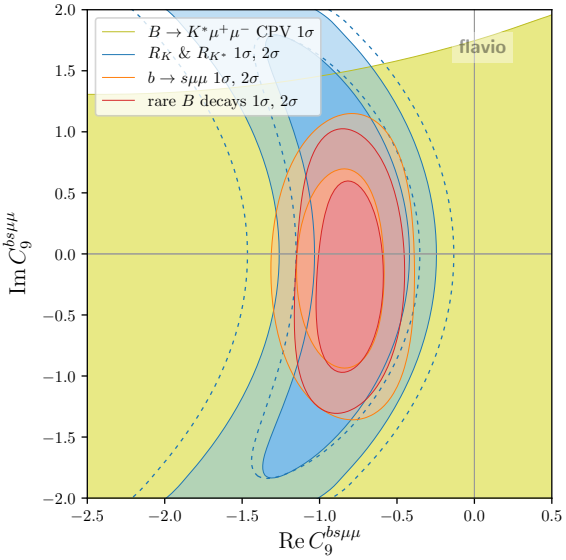

Figure 4.12: Allowed regions for a complex $\mathcal{C}_{9\mu}^{\mathrm{NP}}$ coefficient in the $b \to s\ell^+\ell^-$ transition as computed in Ref. [267].

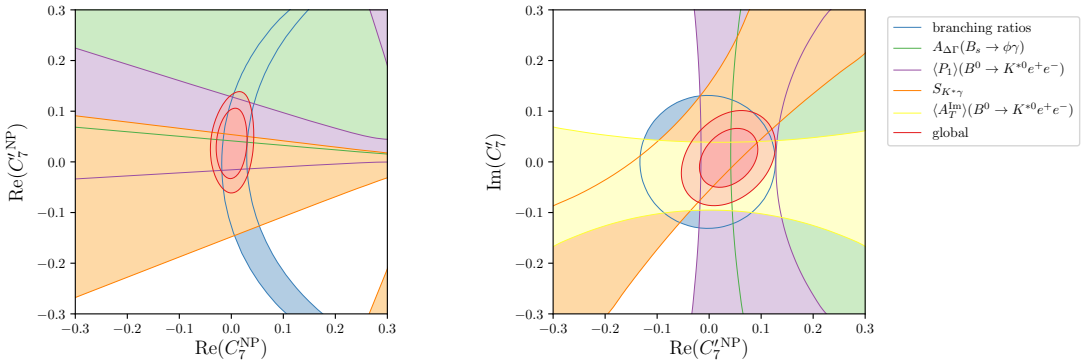

Figure 4.13: Constraints on $\mathcal{C}_7^{\mathrm{NP}}$ and $\mathcal{C}_{7'}^{\mathrm{NP}}$ from $b \to s\gamma$ observables and the low q^2 bin of $b \to se^+e^-$ angular analyses. Taken from Ref. [212]

$\mathcal{C}_7^{\mathrm{NP}}$ and $\mathcal{C}_{7'}^{\mathrm{NP}}$ was performed in Ref. [212] showing no signs for NP in these operators (see Fig. 4.13). This analysis was performed using the flavio [300] and the HEPfit [306] open-source software.

4.7.2 Statistical interpretation of the p-values

One comment should be said regarding the significance of the p-values and the pulls given in this chapter for each of the different fits. All our fits, the statistical interpretation of these statistical parameters and the possibility to reject (or not) specific scenarios (including the SM) are done within some specific assumptions.

In 1D fits, pulls assess how well the WET can explain data compared to the SM under the assumption of the presence of NP contribution to a single Wilson coefficient. Similarly in the case of multidimensional fits, they asses this under the assumption of the presence of NP contributions to several Wilson coefficients. In both cases, we restrict NP to a specific subset of Wilson coefficients.

These are of course not the most general assumptions, reason why its significance cannot be treated as a statistical indicator assessing the need of NP to describe the $b \to s\ell^+\ell^-$ anomalies. One option to this would be to perform a multidimensional fit that includes all possible NP contributions discussed in Section 2.4 However this significance still needs to be treated carefully.

First of all, our scenarios are defined within the context of an EFT, which already considers certain assumptions; for instance, the absence of light degrees of freedom and the omission of higher dimension operators. Nonetheless, the estimation of the $b \to s\ell^+\ell^-$ significance of the flavour anomalies given these assumptions remains undoubtedly interesting.

Secondly, before we assumed the fact that all observables have a similar sensitivity to all parameters, and that the linear approximation is appropriate to deal with this problem (Wilks' theorem [285]). However, as

pointed out in Ref. [307], the set of observables is not "fully sensitive" to all Wilson coefficients. This exactly the reason why one may prefer to consider NP only in a subset of Wilson coefficients rather than allowing all of them to receive NP contributions. If the latter is allowed, the true number of degrees of freedom needs to be reassessed through Monte-Carlo sampling to take into account the different sensitivity to the observables. This can be seen in Figure 2 of Ref. [307] where they show that the difference $\chi^2_{\text{min}} - \chi^2_{\text{SM}}$ of the hypothesis tested does not distribute like a χ^2 distribution with n_{pars} degrees of freedom as defined in Eq. (4.19) but rather a smaller number of effective degrees of freedom due to the lack of sensitivity to these parameters. For 9 (5) Wilson coefficients the effective degrees of freedom is as low as 5.6 (3.3) in Ref. [307]. This effect can thus only enhance a naive estimation of a global significance in the linear approximation, as we compute the pull by interpreting the difference of χ^2_{min} with too many "apparent" degrees of freedom, when we should use a much lower "effective" number of degrees of freedom.

Let us add that this effect should be investigated in more detail, since Ref. [307] considers only a limited subset of observables and samples and it treats the $c\bar{c}$ contribution as a constant nuisance parameter common to all decays. A more complete study could help to understand better this effect and disentangle the effect of the various hypotheses considered in Ref. [307] so that we could interpret the statistical significance of the p-values and the pulls of these global fits more accurately.

4.8 Conclusion

In this chapter we presented a global analysis of the $b \to s\ell^+\ell^-$ transitions experimental data and the so called b-anomalies in terms of the WET introduced in Section 2.4.We discussed the various elements entering the theoretical predictions for the modes considered and the procedure used to assess various NP hypotheses and constrain their parameters, i.e. NP contributions to Wilson coefficients of the WET.

Our results show that NP can explain the $b \to s\ell^+\ell^-$ anomalies, where NP contributions to the Wilson coefficients of the muon mode are required to explain the data. Lepton-flavour universal contributions (or NP contributions in the electron mode), although not required, are allowed. The results discussed in this chapter reaffirm the viability of the NP models discussed in Section 3.3.

Furthermore, several scenarios can explain the data being $\mathcal{C}^{\text{NP}}_{9\mu}$, $\mathcal{C}^{\text{NP}}_{9\mu} = -\mathcal{C}^{\text{NP}}_{10\mu}$, ($\mathcal{C}^{\text{NP}}_{9\mu}$, $\mathcal{C}^{\text{NP}}_{9'\mu} = -\mathcal{C}^{\text{NP}}_{10\mu}$) and ($\mathcal{C}^{V}_{9} = -\mathcal{C}^{V}_{10}$,$\mathcal{C}^{U}_{9\mu}$) the favoured ones. One common feature of this scenarios is the presence in all of them of a significant NP contribution to $\mathcal{C}^{\text{NP}}_{9\mu}$ (around 1/4 of the SM contribution).

Our results are compatible with the results of several other groups [267, 301–303] with the tensions varying slightly. This agreement is remarkable given that other groups have different approaches regarding the statistical framework (bayesian vs frequentist), non-local contributions, form factors and the experimental data taken into consideration.

One would ideally like to disentangle the different NP scenarios in order to find a single NP solution. However, current data does not yet allow us to disentangle all of the possible scenarios, this is partially because the most precise observables are sensitive to the same combinations of Wilson coefficients and the observables that could disentangle this are not yet precise enough. The study of new observables and the measurement of already proposed observables which have not yet been measured could help the situation . We discuss the different observables that can help this disentangling of NP being P'_5, Q'_5 and R_K complementary in this task in the case of real Wilson coefficients.

Clearly additional modes and observables would be useful to make progress here. On one hand, baryon modes are not very much represented although they are accessible at LHCb, and we will study some of their rare decays in Chapter 5. Further observables would also be needed to properly study the possibility of complex Wilson coefficients. Indeed, imaginary parts of Wilson coefficients are still only loosely constrained as shown in Refs. [267, 303], so the measurement of new observables to constrain this complex phases (like the ones we will discuss in Chapter 6) is fundamental to understand the structure of the NP that could be behind the flavour anomalies.

Appendices

4.A Observables included and exhaustive results of the global fits

Observables included in the Global Fit "All"			
$10^7 \times B(B^+ \to K^+\mu\mu)$ [LHCb]	SM	Experiment [224]	Pull
$[0.1, 0.98]$	0.32 ± 0.10	0.29 ± 0.02	$+0.3$
$[1.1, 2.]$	0.33 ± 0.10	0.21 ± 0.02	$+1.2$
$[2., 3.]$	0.36 ± 0.11	0.28 ± 0.02	$+0.7$
$[3., 4.]$	0.36 ± 0.11	0.25 ± 0.02	$+0.9$
$[4., 5.]$	0.35 ± 0.12	0.22 ± 0.02	$+1.1$
$[5., 6.]$	0.35 ± 0.12	0.23 ± 0.02	$+1.0$
$[6., 7.]$	0.35 ± 0.12	0.25 ± 0.02	$+0.8$
$[7., 8.]$	0.35 ± 0.13	0.23 ± 0.02	$+0.9$
$[15., 22.]$	1.00 ± 0.13	0.85 ± 0.05	$+1.1$
$10^7 \times B(B^+ \to K^+\mu\mu)$ [Belle]	SM	Experiment [220]	Pull
$[1., 6.]$	1.79 ± 0.56	2.30 ± 0.41	-0.7
$[14.18, 22.9]$	1.21 ± 0.16	1.34 ± 0.24	-0.4
$10^7 \times B(B^0 \to K^0\mu\mu)$ [LHCb]	SM	Experiment [224]	Pull
$[0.1, 2.]$	0.64 ± 0.19	0.23 ± 0.11	$+1.8$
$[2., 4.]$	0.67 ± 0.21	0.37 ± 0.11	$+1.2$
$[4., 6.]$	0.66 ± 0.22	0.35 ± 0.11	$+1.3$
$[6., 8.]$	0.65 ± 0.23	0.54 ± 0.12	$+0.4$
$[15., 22.]$	0.93 ± 0.12	0.67 ± 0.12	$+1.6$
$10^7 \times B(B^0 \to K^0\mu\mu)$ [Belle]	SM	Experiment [220]	Pull
$[1., 6.]$	1.66 ± 0.52	0.62 ± 0.44	$+1.5$
$[14.18, 22.9]$	1.13 ± 0.15	0.98 ± 0.44	$+0.3$
$A_{FB}(B^+ \to K^+\mu\mu)$ [CMS8]	SM	Experiment [308]	Pull
$[1., 2.]$	0 ± 0	0.08 ± 0.23	-0.4
$[2., 4.3]$	0 ± 0	-0.04 ± 0.14	$+0.3$
$[4.3, 8.68]$	0 ± 0	0 ± 0.04	$+0$
$[16., 18.]$	0 ± 0	0.04 ± 0.06	-0.7
$[18., 22.]$	0 ± 0	0.05 ± 0.05	-0.9
$F_H(B^+ \to K^+\mu\mu)$ [CMS8]	SM	Experiment [308]	Pull
$[1., 2.]$	0.05 ± 0.00	0.21 ± 0.49	-0.3
$[2., 4.3]$	0.02 ± 0.00	0.85 ± 0.37	-2.2
$[4.3, 8.68]$	0.01 ± 0.00	0.01 ± 0.04	$+0.0$
$[16., 18.]$	0.01 ± 0.00	0.07 ± 0.10	-0.6
$[18., 22.]$	0.01 ± 0.00	0.10 ± 0.13	-0.7
$F_L(B^0 \to K^{*0}\mu\mu)$ [LHCb]	SM	Experiment [287]	Pull
$[0.1, 0.98]$	0.23 ± 0.25	0.26 ± 0.03	-0.1
$[1.1, 2.5]$	0.68 ± 0.27	0.66 ± 0.05	$+0.1$
$[2.5, 4.]$	0.77 ± 0.23	0.76 ± 0.05	$+0.0$

[4., 6.]	0.71 ± 0.28	0.68 ± 0.04	$+0.1$
[6., 8.]	0.63 ± 0.33	0.65 ± 0.03	-0.0
[15., 19.]	0.34 ± 0.03	0.35 ± 0.02	-0.1
$P_1(B^0 \to K^{*0}\mu\mu)$ [LHCb]	SM	Experiment [287]	Pull
[0.1, 0.98]	0.03 ± 0.08	0.09 ± 0.12	-0.5
[1.1, 2.5]	-0.01 ± 0.06	-0.62 ± 0.30	$+2.0$
[2.5, 4.]	-0.00 ± 0.06	0.17 ± 0.37	-0.4
[4., 6.]	0.02 ± 0.12	0.09 ± 0.24	-0.2
[6., 8.]	0.02 ± 0.14	-0.07 ± 0.21	$+0.4$
[15., 19.]	-0.64 ± 0.05	-0.58 ± 0.10	-0.6
$P_2(B^0 \to K^{*0}\mu\mu)$ [LHCb]	SM	Experiment [287]	Pull
[0.1, 0.98]	0.12 ± 0.02	0.00 ± 0.04	$+2.7$
[1.1, 2.5]	0.44 ± 0.03	0.44 ± 0.10	-0.0
[2.5, 4.]	0.23 ± 0.13	0.19 ± 0.12	$+0.2$
[4., 6.]	-0.19 ± 0.11	-0.11 ± 0.07	-0.6
[6., 8.]	-0.38 ± 0.07	-0.21 ± 0.05	-2.1
[15., 19.]	-0.36 ± 0.02	-0.36 ± 0.02	-0.1
$P_3(B^0 \to K^{*0}\mu\mu)$ [LHCb]	SM	Experiment [287]	Pull
[0.1, 0.98]	-0.00 ± 0.00	-0.07 ± 0.06	$+1.3$
[1.1, 2.5]	0.00 ± 0.01	-0.32 ± 0.15	$+2.2$
[2.5, 4.]	0.00 ± 0.01	-0.05 ± 0.20	$+0.3$
[4., 6.]	0.00 ± 0.01	0.09 ± 0.14	-0.6
[6., 8.]	0.00 ± 0.00	0.07 ± 0.10	-0.6
[15., 19.]	0.00 ± 0.02	-0.05 ± 0.05	$+1.0$
$P_4'(B^0 \to K^{*0}\mu\mu)$ [LHCb]	SM	Experiment [287]	Pull
[0.1, 0.98]	-0.50 ± 0.16	-0.27 ± 0.24	-0.8
[1.1, 2.5]	-0.08 ± 0.16	0.16 ± 0.29	-0.7
[2.5, 4.]	0.52 ± 0.21	0.87 ± 0.35	-0.9
[4., 6.]	0.82 ± 0.16	0.62 ± 0.23	$+0.7$
[6., 8.]	0.93 ± 0.12	1.15 ± 0.19	-1.0
[15., 19.]	1.28 ± 0.02	1.28 ± 0.12	$+0.0$
$P_5'(B^0 \to K^{*0}\mu\mu)$ [LHCb]	SM	Experiment [287]	Pull
[0.1, 0.98]	0.67 ± 0.14	0.52 ± 0.10	$+0.9$
[1.1, 2.5]	0.19 ± 0.12	0.37 ± 0.12	-1.0
[2.5, 4.]	-0.47 ± 0.12	-0.15 ± 0.15	-1.7
[4., 6.]	-0.82 ± 0.08	-0.44 ± 0.12	-2.7
[6., 8.]	-0.94 ± 0.08	-0.58 ± 0.09	-2.9
[15., 19.]	-0.58 ± 0.05	-0.67 ± 0.06	$+1.2$
$P_6'(B^0 \to K^{*0}\mu\mu)$ [LHCb]	SM	Experiment [287]	Pull
[0.1, 0.98]	-0.06 ± 0.02	0.02 ± 0.09	-0.7
[1.1, 2.5]	-0.07 ± 0.03	-0.23 ± 0.13	$+1.2$
[2.5, 4.]	-0.06 ± 0.03	-0.16 ± 0.15	$+0.6$
[4., 6.]	-0.04 ± 0.02	-0.29 ± 0.12	$+2.2$
[6., 8.]	-0.02 ± 0.01	-0.16 ± 0.10	$+1.4$
[15., 19.]	-0.00 ± 0.07	0.07 ± 0.07	-0.8
$P_8'(B^0 \to K^{*0}\mu\mu)$ [LHCb]	SM	Experiment [287]	Pull
[0.1, 0.98]	0.02 ± 0.02	0.01 ± 0.24	$+0.0$
[1.1, 2.5]	0.04 ± 0.03	0.73 ± 0.32	-2.2
[2.5, 4.]	0.05 ± 0.03	-0.07 ± 0.34	$+0.4$
[4., 6.]	0.03 ± 0.02	-0.33 ± 0.25	$+1.4$
[6., 8.]	0.02 ± 0.01	0.26 ± 0.20	-1.2
[15., 19.]	-0.00 ± 0.03	-0.02 ± 0.14	$+0.1$
$F_L(B^0 \to K^{*0}\mu\mu)$ [ATLAS]	SM	Experiment [246]	Pull

$[0.04, 2.]$	0.32 ± 0.29	0.44 ± 0.11	-0.4
$[2., 4.]$	0.76 ± 0.23	0.64 ± 0.12	$+0.5$
$[4., 6.]$	0.71 ± 0.28	0.42 ± 0.18	$+0.9$
$P_1(B^0 \to K^{*0}\mu\mu)$ [ATLAS]	SM	Experiment [246]	Pull
$[0.04, 2.]$	0.02 ± 0.08	-0.05 ± 0.31	$+0.2$
$[2., 4.]$	-0.00 ± 0.05	-0.78 ± 0.61	$+1.3$
$[4., 6.]$	0.02 ± 0.12	0.14 ± 0.50	-0.2
$P_4'(B^0 \to K^{*0}\mu\mu)$ [ATLAS]	SM	Experiment [246]	Pull
$[0.04, 2.]$	-0.36 ± 0.15	-0.62 ± 0.89	$+0.3$
$[2., 4.]$	0.43 ± 0.21	1.52 ± 0.75	-1.4
$[4., 6.]$	0.82 ± 0.16	-1.28 ± 0.75	$+2.7$
$P_5'(B^0 \to K^{*0}\mu\mu)$ [ATLAS]	SM	Experiment [246]	Pull
$[0.04, 2.]$	0.51 ± 0.11	0.67 ± 0.31	-0.5
$[2., 4.]$	-0.36 ± 0.13	-0.33 ± 0.34	-0.1
$[4., 6.]$	-0.82 ± 0.08	0.26 ± 0.39	-2.7
$P_6'(B^0 \to K^{*0}\mu\mu)$ [ATLAS]	SM	Experiment [246]	Pull
$[0.04, 2.]$	-0.06 ± 0.02	-0.18 ± 0.21	$+0.6$
$[2., 4.]$	-0.06 ± 0.03	0.31 ± 0.34	-1.1
$[4., 6.]$	-0.04 ± 0.02	0.06 ± 0.30	-0.3
$P_8'(B^0 \to K^{*0}\mu\mu)$ [ATLAS]	SM	Experiment [246]	Pull
$[0.04, 2.]$	0.03 ± 0.02	0.58 ± 1.03	-0.5
$[2., 4.]$	0.05 ± 0.03	-2.14 ± 1.13	$+1.9$
$[4., 6.]$	0.03 ± 0.02	0.48 ± 0.86	-0.5
$F_L(B^0 \to K^{*0}\mu\mu)$ [CMS8]	SM	Experiment [230]	Pull
$[1., 2.]$	0.63 ± 0.29	0.64 ± 0.12	-0.0
$[2., 4.3]$	0.76 ± 0.24	0.80 ± 0.10	-0.2
$[4.3, 6]$	0.71 ± 0.29	0.62 ± 0.12	$+0.3$
$[6, 8.68]$	0.62 ± 0.33	0.50 ± 0.08	$+0.3$
$[16., 19.]$	0.34 ± 0.03	0.38 ± 0.07	-0.6
$P_1(B^0 \to K^{*0}\mu\mu)$ [CMS8]	SM	Experiment [245]	Pull
$[1., 2.]$	-0.00 ± 0.07	0.12 ± 0.48	-0.2
$[2., 4.3]$	-0.00 ± 0.05	-0.69 ± 0.62	$+1.1$
$[4.3, 6]$	0.02 ± 0.12	0.53 ± 0.38	-1.3
$[6, 8.68]$	0.02 ± 0.14	-0.47 ± 0.31	$+1.4$
$[16., 19.]$	-0.69 ± 0.05	-0.53 ± 0.25	-0.7
$P_5'(B^0 \to K^{*0}\mu\mu)$ [CMS8]	SM	Experiment [245]	Pull
$[1., 2.]$	0.33 ± 0.12	0.10 ± 0.33	$+0.7$
$[2., 4.3]$	-0.41 ± 0.13	-0.57 ± 0.38	$+0.4$
$[4.3, 6]$	-0.84 ± 0.08	-0.96 ± 0.33	$+0.3$
$[6, 8.68]$	-0.95 ± 0.08	-0.64 ± 0.23	-1.3
$[16., 19.]$	-0.53 ± 0.04	-0.56 ± 0.14	$+0.2$
$F_L(B^0 \to K^{*0}\mu\mu)$ [CMS7]	SM	Experiment [309]	Pull
$[1., 2.]$	0.63 ± 0.29	0.60 ± 0.34	$+0.1$
$[2., 4.3]$	0.76 ± 0.24	0.65 ± 0.17	$+0.4$
$[4.3, 8.68]$	0.65 ± 0.32	0.81 ± 0.14	-0.5
$[16., 19.]$	0.34 ± 0.03	0.44 ± 0.08	-1.3
$A_{FB}(B^0 \to K^{*0}\mu\mu)$ [CMS8]	SM	Experiment [230]	Pull
$[1., 2.]$	-0.20 ± 0.19	-0.27 ± 0.41	$+0.2$
$[2., 4.3]$	-0.08 ± 0.08	-0.12 ± 0.18	$+0.2$
$[4.3, 6.]$	0.09 ± 0.12	0.01 ± 0.15	$+0.4$
$[6., 8.68]$	0.22 ± 0.21	0.03 ± 0.10	$+0.8$

[16., 19.]	0.34 ± 0.03	0.35 ± 0.07	-0.1
$A_{FB}(B^0 \to K^{*0}\mu\mu)$ [CMS7]	SM	Experiment [309]	Pull
[1., 2.]	-0.20 ± 0.19	-0.29 ± 0.41	$+0.2$
[2., 4.3]	-0.08 ± 0.08	-0.07 ± 0.20	-0.0
[4.3, 8.68]	0.18 ± 0.19	-0.01 ± 0.11	$+0.9$
[16., 19.]	0.34 ± 0.03	0.41 ± 0.06	-1.1
$10^7 \times B(B^0 \to K^{*0}\mu\mu)$ [LHCb]	SM	Experiment [228]	Pull
[0.1, 0.98]	0.92 ± 0.82	0.89 ± 0.09	$+0.0$
[1.1, 2.5]	0.56 ± 0.36	0.46 ± 0.06	$+0.3$
[2.5, 4.]	0.58 ± 0.41	0.50 ± 0.06	$+0.2$
[4., 6.]	0.91 ± 0.68	0.71 ± 0.07	$+0.3$
[6., 8.]	1.13 ± 0.90	0.86 ± 0.08	$+0.3$
[15., 19.]	2.46 ± 0.21	1.74 ± 0.14	$+2.8$
$10^7 \times B(B^0 \to K^{*0}\mu\mu)$ [CMS8]	SM	Experiment [230]	Pull
[1., 2.]	0.42 ± 0.27	0.46 ± 0.08	-0.1
[2., 4.3]	0.89 ± 0.62	0.76 ± 0.12	$+0.2$
[4.3, 6.]	0.79 ± 0.59	0.58 ± 0.10	$+0.3$
[6., 8.68]	1.57 ± 1.27	1.26 ± 0.13	$+0.2$
[16., 19.]	1.70 ± 0.14	1.26 ± 0.13	$+2.3$
$10^7 \times B(B^0 \to K^{*0}\mu\mu)$ [CMS7]	SM	Experiment [309]	Pull
[1., 2.]	0.42 ± 0.27	0.48 ± 0.15	-0.2
[2., 4.3]	0.89 ± 0.62	0.87 ± 0.18	$+0.0$
[4.3, 8.68]	2.36 ± 1.84	1.62 ± 0.35	$+0.4$
[16., 19.]	1.70 ± 0.14	1.56 ± 0.23	$+0.5$
$F_L(B^+ \to K^{*+}\mu\mu)$ [LHCb]	SM	Experiment [240]	Pull
[0.1, 0.98]	0.24 ± 0.26	0.34 ± 0.12	-0.4
[1.1, 2.5]	0.69 ± 0.27	0.54 ± 0.19	$+0.5$
[2.5, 4.]	0.77 ± 0.23	0.17 ± 0.24	$+1.8$
[4., 6.]	0.72 ± 0.28	0.67 ± 0.14	$+0.1$
[6., 8.]	0.63 ± 0.33	0.39 ± 0.21	$+0.6$
[15., 19.]	0.34 ± 0.03	0.40 ± 0.13	-0.4
$P_1(B^+ \to K^{*+}\mu\mu)$ [LHCb]	SM	Experiment [240]	Pull
[0.1, 0.98]	0.03 ± 0.08	0.44 ± 0.41	-1.0
[1.1, 2.5]	-0.00 ± 0.06	1.60 ± 4.93	-0.3
[2.5, 4.]	0.00 ± 0.06	-0.29 ± 1.45	$+0.2$
[4., 6.]	0.02 ± 0.12	-1.24 ± 1.21	$+1.0$
[6., 8.]	0.02 ± 0.14	-0.78 ± 0.70	$+1.1$
[15., 19.]	-0.64 ± 0.05	-0.70 ± 0.44	$+0.1$
$P_2(B^+ \to K^{*+}\mu\mu)$ [LHCb]	SM	Experiment [240]	Pull
[0.1, 0.98]	0.12 ± 0.02	0.05 ± 0.12	$+0.6$
[1.1, 2.5]	0.44 ± 0.02	0.28 ± 0.45	$+0.4$
[2.5, 4.]	0.21 ± 0.12	-0.03 ± 0.28	$+0.8$
[4., 6.]	-0.20 ± 0.11	0.15 ± 0.21	-1.5
[6., 8.]	-0.38 ± 0.06	0.06 ± 0.14	-2.9
[15., 19.]	-0.36 ± 0.02	-0.34 ± 0.10	-0.2
$P_3(B^+ \to K^{*+}\mu\mu)$ [LHCb]	SM	Experiment [240]	Pull
[0.1, 0.98]	-0.00 ± 0.00	0.42 ± 0.22	-1.9
[1.1, 2.5]	0.00 ± 0.01	0.09 ± 1.01	-0.1
[2.5, 4.]	0.00 ± 0.01	0.45 ± 0.65	-0.7
[4., 6.]	0.00 ± 0.01	0.52 ± 0.83	-0.6
[6., 8.]	0.00 ± 0.00	-0.17 ± 0.34	$+0.5$
[15., 19.]	0.00 ± 0.02	0.07 ± 0.13	-0.5

$P_4'(B^+ \to K^{*+}\mu\mu)$ [LHCb]	SM	Experiment [240]	Pull
$[0.1, 0.98]$	-0.49 ± 0.17	0.18 ± 0.76	-0.9
$[1.1, 2.5]$	-0.07 ± 0.16	-1.16 ± 1.26	$+0.9$
$[2.5, 4.]$	0.53 ± 0.20	1.62 ± 2.20	-0.5
$[4., 6.]$	0.82 ± 0.15	1.58 ± 0.96	-0.8
$[6., 8.]$	0.93 ± 0.11	0.86 ± 0.91	$+0.1$
$[15., 19.]$	1.28 ± 0.02	0.78 ± 0.47	$+1.1$
$P_5'(B^+ \to K^{*+}\mu\mu)$ [LHCb]	SM	Experiment [240]	Pull
$[0.1, 0.98]$	0.67 ± 0.14	0.51 ± 0.32	$+0.4$
$[1.1, 2.5]$	0.16 ± 0.12	0.88 ± 0.72	-1.0
$[2.5, 4.]$	-0.50 ± 0.11	-0.87 ± 1.68	$+0.2$
$[4., 6.]$	-0.84 ± 0.08	-0.25 ± 0.41	-1.4
$[6., 8.]$	-0.95 ± 0.08	-0.15 ± 0.41	-1.9
$[15., 19.]$	-0.58 ± 0.05	-0.24 ± 0.17	-1.9
$P_6'(B^+ \to K^{*+}\mu\mu)$ [LHCb]	SM	Experiment [240]	Pull
$[0.1, 0.98]$	-0.05 ± 0.03	-0.02 ± 0.40	-0.1
$[1.1, 2.5]$	-0.06 ± 0.03	0.25 ± 1.32	-0.2
$[2.5, 4.]$	-0.05 ± 0.03	-0.37 ± 3.91	$+0.1$
$[4., 6.]$	-0.03 ± 0.02	-0.09 ± 0.41	$+0.1$
$[6., 8.]$	-0.02 ± 0.01	-0.74 ± 0.40	$+1.8$
$[15., 19.]$	-0.00 ± 0.07	-0.28 ± 0.19	$+1.3$
$P_8'(B^+ \to K^{*+}\mu\mu)$ [LHCb]	SM	Experiment [240]	Pull
$[0.1, 0.98]$	0.08 ± 0.03	-0.90 ± 1.02	$+1.0$
$[1.1, 2.5]$	0.07 ± 0.03	-0.24 ± 1.52	$+0.2$
$[2.5, 4.]$	0.05 ± 0.03	-0.24 ± 15.80	$+0.0$
$[4., 6.]$	0.03 ± 0.02	0.30 ± 0.97	-0.3
$[6., 8.]$	0.02 ± 0.01	0.78 ± 0.78	-1.0
$[15., 19.]$	-0.00 ± 0.03	0.22 ± 0.38	-0.6
$F_L(B^+ \to K^{*+}\mu\mu)$ [CMS8]	SM	Experiment [276]	Pull
$[1., 8.68]$	0.68 ± 0.30	0.60 ± 0.34	$+0.2$
$[14.18, 19.]$	0.35 ± 0.04	0.55 ± 0.14	-1.4
$A_{FB}(B^+ \to K^{*+}\mu\mu)$ [CMS8]	SM	Experiment [276]	Pull
$[1., 8.68]$	0.08 ± 0.10	-0.14 ± 0.39	$+0.5$
$[14.18, 19.]$	0.37 ± 0.03	0.33 ± 0.12	$+0.3$
$10^7 \times B(B^+ \to K^{*+}\mu\mu)$ [LHCb]	SM	Experiment [224]	Pull
$[0.1, 2.]$	1.40 ± 1.09	1.12 ± 0.27	$+0.3$
$[2., 4.]$	0.84 ± 0.57	1.12 ± 0.32	-0.4
$[4., 6.]$	0.99 ± 0.73	0.50 ± 0.20	$+0.6$
$[6., 8.]$	1.22 ± 0.97	0.66 ± 0.22	$+0.6$
$[15., 19.]$	2.65 ± 0.23	1.60 ± 0.32	$+2.7$
$P_4'(B \to K^*\mu\mu)$ [Belle]	SM	Experiment [242]	Pull
$[0.1, 4.]$	-0.06 ± 0.16	0.76 ± 1.03	-0.8
$[4., 8.]$	0.88 ± 0.13	0.14 ± 0.66	$+1.1$
$[14.18, 19.]$	1.26 ± 0.03	0.20 ± 0.79	$+1.3$
$P_5'(B \to K^*\mu\mu)$ [Belle]	SM	Experiment [242]	Pull
$[0.1, 4.]$	0.16 ± 0.10	0.42 ± 0.41	-0.6
$[4., 8.]$	-0.89 ± 0.08	-0.03 ± 0.32	-2.6
$[14.18, 19.]$	-0.60 ± 0.05	-0.13 ± 0.39	-1.2
$P_1(B_s \to \phi\mu\mu)$ [LHCb]	SM	Experiment [229]	Pull
$[0.1, 2.]$	0.11 ± 0.08	-0.13 ± 0.33	$+0.7$
$[2., 5.]$	-0.10 ± 0.10	-0.38 ± 1.47	$+0.2$
$[5., 8.]$	-0.20 ± 0.11	-0.44 ± 1.27	$+0.2$

[15., 18.8]	-0.69 ± 0.03	-0.25 ± 0.34	-1.3
$P_4'(B_s \to \phi\mu\mu)$ [LHCb]	SM	Experiment [229]	Pull
[0.1, 2.]	-0.29 ± 0.14	-1.35 ± 1.46	$+0.7$
[2., 5.]	0.78 ± 0.12	2.02 ± 1.84	-0.7
[5., 8.]	1.06 ± 0.06	0.40 ± 0.72	$+0.9$
[15., 18.8]	1.30 ± 0.01	0.62 ± 0.49	$+1.4$
$P_6'(B_s \to \phi\mu\mu)$ [LHCb]	SM	Experiment [229]	Pull
[0.1, 2.]	-0.06 ± 0.02	0.10 ± 0.30	-0.5
[2., 5.]	-0.06 ± 0.02	-0.06 ± 0.49	$+0.0$
[5., 8.]	-0.02 ± 0.01	0.08 ± 0.40	-0.2
[15., 18.8]	-0.00 ± 0.07	0.29 ± 0.24	-1.1
$F_L(B_s \to \phi\mu\mu)$ [LHCb]	SM	Experiment [229]	Pull
[0.1, 2.]	0.42 ± 0.09	0.20 ± 0.09	$+1.7$
[2., 5.]	0.77 ± 0.05	0.68 ± 0.16	$+0.6$
[5., 8.]	0.62 ± 0.06	0.54 ± 0.10	$+0.7$
[15., 18.8]	0.36 ± 0.02	0.29 ± 0.07	$+0.9$
$10^7 \times B(B_s \to \phi\mu\mu)$ [LHCb]	SM	Experiment [229]	Pull
[0.1, 2.]	1.60 ± 0.35	1.11 ± 0.16	$+1.3$
[2., 5.]	1.43 ± 0.30	0.77 ± 0.14	$+2.0$
[5., 8.]	1.73 ± 0.36	0.96 ± 0.15	$+2.0$
[15., 18.8]	2.26 ± 0.15	1.62 ± 0.20	$+2.5$
$F_L(B^0 \to K^{*0}ee)$ [LHCb]	SM	Experiment [241]	Pull
[0.0008, 0.257]	0.03 ± 0.06	0.04 ± 0.03	-0.2
$P_1(B^0 \to K^{*0}ee)$ [LHCb]	SM	Experiment [241]	Pull
[0.0008, 0.257]	0.03 ± 0.08	0.11 ± 0.10	-0.6
$P_2(B^0 \to K^{*0}ee)$ [LHCb]	SM	Experiment [241]	Pull
[0.0008, 0.257]	0.01 ± 0.00	0.03 ± 0.04	-0.5
$P_3(B^0 \to K^{*0}ee)$ [LHCb]	SM	Experiment [241]	Pull
[0.0008, 0.257]	-0.00 ± 0.00	0.01 ± 0.05	-0.2
$P_4'(B \to K^*ee)$ [Belle]	SM	Experiment [242]	Pull
[0.1, 4.]	-0.10 ± 0.15	-0.68 ± 0.93	$+0.6$
[4., 8.]	0.88 ± 0.13	1.04 ± 0.48	-0.3
[14.18, 19.]	1.26 ± 0.03	0.30 ± 0.82	$+1.2$
$P_5'(B \to K^*ee)$ [Belle]	SM	Experiment [242]	Pull
[0.1, 4.]	0.18 ± 0.10	0.51 ± 0.47	-0.7
[4., 8.]	-0.89 ± 0.08	-0.52 ± 0.28	-1.3
[14.18, 19.]	-0.60 ± 0.05	-0.91 ± 0.36	$+0.8$
R_K [LHCb]	SM	Experiment [277]	Pull
[1.1, 6.]	1.00 ± 0.00	0.85 ± 0.04	$+3.5$
R_K [Belle]	SM	Experiment [220]	Pull
[1., 6.]	1.00 ± 0.00	1.03 ± 0.28	-0.1
[14.18, 22.9]	1.00 ± 0.00	1.16 ± 0.30	-0.5
R_{K^*} [LHCb]	SM	Experiment [207]	Pull
[0.045, 1.1]	0.91 ± 0.02	0.66 ± 0.11	$+2.2$
[1.1, 6.]	1.00 ± 0.01	0.69 ± 0.12	$+2.6$
R_{K^*} [Belle]	SM	Experiment [219]	Pull
[0.045, 1.1]	0.92 ± 0.03	0.52 ± 0.36	$+1.1$
[1.1, 6.]	1.00 ± 0.01	0.96 ± 0.46	$+0.1$

[15., 19.]	1.00 ± 0.00	1.18 ± 0.53	-0.3
$10^5 \times B(B^0 \to K^{*0}\gamma)$ [PDG]	SM	Experiment [6]	Pull
	4.65 ± 5.41	4.18 ± 0.25	$+0.1$
$10^5 \times B(B^+ \to K^{*+}\gamma)$ [PDG]	SM	Experiment [6]	Pull
	4.62 ± 5.59	3.92 ± 0.22	$+0.1$
$10^5 \times B(B_s \to \phi\gamma)$ [PDG]	SM	Experiment [6]	Pull
	4.86 ± 1.29	3.40 ± 0.40	$+1.1$

Table 4.A.1: List of observables included in the fit "All", with their SM prediction, experimental measurements and the pull of this measurement. The sign of the pull value represents whether the observable theoretical prediction is above (+) or below (−) the experimental measurement.

Coefficient	Best fit	1σ	2σ	Pull_{SM}	p-value (%)
$\mathcal{C}_7^{\text{NP}}$	-0.02	$[-0.04, -0.00]$	$[-0.06, 0.02]$	1.1	1.11
$\mathcal{C}_{9\mu}^{\text{NP}}$	-1.06	$[-1.20, -0.91]$	$[-1.34, -0.76]$	7.0	39.50
$\mathcal{C}_{10\mu}^{\text{NP}}$	0.52	$[0.41, 0.64]$	$[0.29, 0.76]$	4.7	7.72
$\mathcal{C}_{7'}^{\text{NP}}$	-0.00	$[-0.02, 0.01]$	$[-0.04, 0.03]$	0.3	0.98
$\mathcal{C}_{9'}^{\text{NP}}$	-0.17	$[-0.31, -0.03]$	$[-0.45, 0.11]$	1.2	1.14
$\mathcal{C}_{10'}^{\text{NP}}$	0.03	$[-0.07, 0.13]$	$[-0.16, 0.23]$	0.3	0.98
$\mathcal{C}_{9\mu}^{\text{NP}} = \mathcal{C}_{10\mu}^{\text{NP}}$	-0.02	$[-0.15, 0.12]$	$[-0.27, 0.27]$	0.1	0.97
$\mathcal{C}_{9\mu}^{\text{NP}} = -\mathcal{C}_{10\mu}^{\text{NP}}$	-0.44	$[-0.52, -0.37]$	$[-0.60, -0.29]$	6.2	22.78
$\mathcal{C}_{9\mu}^{\text{NP}} = \mathcal{C}_{10'}^{\text{NP}}$	-0.51	$[-0.62, -0.40]$	$[-0.73, -0.29]$	4.7	7.40
$\mathcal{C}_{9'}^{\text{NP}} = \mathcal{C}_{10'}^{\text{NP}}$	-0.10	$[-0.24, 0.04]$	$[-0.37, 0.17]$	0.7	1.03
$\mathcal{C}_{9'}^{\text{NP}} = -\mathcal{C}_{10'}^{\text{NP}}$	-0.05	$[-0.11, 0.01]$	$[-0.17, 0.08]$	0.8	1.03
$\mathcal{C}_{9\mu}^{\text{NP}} = -\mathcal{C}_{9'}^{\text{NP}}$	-1.11	$[-1.25, -0.96]$	$[-1.39, -0.80]$	6.5	27.98
$\mathcal{C}_{9\mu}^{\text{NP}} = -\mathcal{C}_{10\mu}^{\text{NP}} = -\mathcal{C}_{9'}^{\text{NP}} = -\mathcal{C}_{10'}^{\text{NP}}$	-0.42	$[-0.50, -0.34]$	$[-0.59, -0.26]$	5.8	16.55
$\mathcal{C}_{9\mu}^{\text{NP}} = -\mathcal{C}_{10\mu}^{\text{NP}} = \mathcal{C}_{9'}^{\text{NP}} = -\mathcal{C}_{10'}^{\text{NP}}$	-0.18	$[-0.13, -0.13]$	$[-0.09, -0.09]$	4.2	5.37

Table 4.A.2: Exhaustive list of 1D patterns of NP in $b \to s\mu^+\mu^-$ and their bfps for the fit "All". Pull_{SM} is quoted in units of standard deviation.

Coefficient	Best fit	1σ	2σ	Pull_{SM}	p-value (%)
$\mathcal{C}_7^{\text{NP}}$	0.00	$[-0.02, 0.59]$	$[-0.03, 0.59]$	0.2	0.98
$\mathcal{C}_{9\mu}^{\text{NP}}$	-0.82	$[-1.06, -0.60]$	$[-1.32, -0.39]$	4.0	35.99
$\mathcal{C}_{10\mu}^{\text{NP}}$	0.62	$[0.48, 0.77]$	$[0.35, 0.93]$	4.7	70.46
$\mathcal{C}_{7'}^{\text{NP}}$	-0.03	$[-0.08, 0.02]$	$[-0.14, 0.08]$	0.6	1.06
$\mathcal{C}_{9'}^{\text{NP}}$	-0.41	$[-0.60, -0.23]$	$[-0.79, -0.06]$	2.3	4.01
$\mathcal{C}_{10'}^{\text{NP}}$	0.09	$[-0.03, 0.21]$	$[-0.15, 0.33]$	0.7	1.12
$\mathcal{C}_{9\mu}^{\text{NP}} = \mathcal{C}_{10\mu}^{\text{NP}}$	0.47	$[0.29, 0.66]$	$[0.11, 0.85]$	2.6	5.76
$\mathcal{C}_{9\mu}^{\text{NP}} = -\mathcal{C}_{10\mu}^{\text{NP}}$	-0.37	$[-0.46, -0.29]$	$[-0.55, -0.21]$	4.6	67.96
$\mathcal{C}_{9\mu}^{\text{NP}} = \mathcal{C}_{10'}^{\text{NP}}$	-0.37	$[-0.52, -0.21]$	$[-0.68, -0.06]$	2.4	4.43
$\mathcal{C}_{9'}^{\text{NP}} = \mathcal{C}_{10'}^{\text{NP}}$	-0.21	$[-0.37, -0.04]$	$[-0.54, 0.12]$	1.3	1.49
$\mathcal{C}_{9'}^{\text{NP}} = -\mathcal{C}_{10'}^{\text{NP}}$	-0.11	$[-0.19, -0.04]$	$[-0.27, 0.04]$	1.5	1.77
$\mathcal{C}_{9\mu}^{\text{NP}} = -\mathcal{C}_{9'}^{\text{NP}}$	-1.61	$[-2.13, -0.96]$	$[-2.54, -0.41]$	3.0	9.28
$\mathcal{C}_{9\mu}^{\text{NP}} = -\mathcal{C}_{10\mu}^{\text{NP}}$ $= -\mathcal{C}_{9'}^{\text{NP}} = -\mathcal{C}_{10'}^{\text{NP}}$	-0.35	$[-0.44, -0.26]$	$[-0.54, -0.17]$	4.1	38.21
$\mathcal{C}_{9\mu}^{\text{NP}} = -\mathcal{C}_{10\mu}^{\text{NP}}$ $= \mathcal{C}_{9'}^{\text{NP}} = -\mathcal{C}_{10'}^{\text{NP}}$	-0.16	$[-0.11, -0.11]$	$[-0.07, -0.07]$	3.5	18.05

Table 4.A.3: Exhaustive list of 1D patterns of NP in $b \to s\mu^+\mu^-$ and their bfps for the fit "LFUV". Pull_{SM} is quoted in units of standard deviation.

Part III

New benchmarks for $b \to s\ell^+\ell^-$

Chapter 5

Angular analysis of $\Lambda_b \to \Lambda^*(\to pK)\ell^+\ell^-$

As discussed in Chapters 3 and 4, it is of primary interest to confirm and constrain the scenarios of New Physics in $b \to s\ell^+\ell^-$ transitions. On one side, this can be done by sharpening the theoretical predictions and collecting more data for the modes already studied. On the other side, one can study new observables in either totally new modes, or on modes that are not fully studied yet. In this chapter and the following we will do exactly this. We will start in this chapter by discussing the study of observables of the new mode $\Lambda_b \to \Lambda^*(\to pK)\ell^+\ell^-$, and in Chapter 6 we will discuss a time-dependent analysis of $B \to K\ell^+\ell^-$.

As mentioned in Section 3.2 it is of interest to further study the $b \to s\ell^+\ell^-$ transition in other hadronic decays than the mesonic decays which have been deeply studied. An interesting way of doing this consists in investigating Λ_b decays which offer completely different theoretical and experimental environments and can be currently studied at LHCb. A first step in this direction has been attempted through the study of the decay $\Lambda_b \to \Lambda(1116)(\to N\pi)\mu^+\mu^-$ (see Section 3.2).

Another promising possibility consists in looking at decays of the Λ_b baryon into excited Λ states through the decay chain $\Lambda_b \to \Lambda^*(\to pK^-)\ell^+\ell^-$. Due to the higher mass of the excited states, they can decay under strong interaction into pK^- as opposed to the ground state which decays into $p\pi$ under the weak interaction. However, compared to the ground state decay, the interpretation of a measurement of the observables of $\Lambda_b \to \Lambda^*(\to pK^-)\ell^+\ell^-$ over the full pK^- invariant mass (m_{pK^-}) spectrum requires a precise theoretical knowledge of the various excited Λ states contributing to the m_{pK^-} spectrum (hadronic form factors, interference patterns).

Interestingly, the LHCb search for pentaquarks states in $\Lambda_b \to pK^-J/\psi$ provides information on $\Lambda_b \to \Lambda(\to pK^-)\ell^+\ell^-$ for a dilepton invariant mass q^2 around the J/ψ mass, where Λ is any intermediate baryon with the appropriate quantum numbers. As indicated in Fig. 5.1, the dominant contribution comes from $\Lambda(1520)$ ($J^P = 3/2^-$), which is reasonably narrow. For a pK^- invariant mass around 1.5 GeV, there is a contamination coming from two other states, $\Lambda(1405)$ (with a mass below the $N\bar{K}$ threshold, but sufficiently wide to provide a contribution to this decay) and $\Lambda(1600)$. Following the LHCb analysis, these two states contribute at similar levels and they might be discriminated from $\Lambda(1520)$ thanks to their different spin and parity ($J^P = 1/2^\pm$ rather than $3/2^-$) – for instance, this could be implemented through an angular analysis, although this demanding approach would require a significant number of events. This dominance of $\Lambda(1520)$ for a pK^- invariant mass around 1.5 GeV, which has been observed for $q^2 = m^2_{J/\psi}$, may hold for other values of the dilepton invariant mass. For instance, the $\Lambda_b \to pK^-\gamma$ decay has been investigated to learn its potential in determining the polarisation of the photon in the $b \to s\gamma$ transition using polarised Λ_b baryons [310, 311]. These studies involve models for the pK^- invariant mass spectrum where $\Lambda(1520)$ is again prominent, but this time for $q^2 = 0$ (see Fig. 5.2). One may thus hope that for a large range for the dilepton invariant mass q^2, the contribution from $\Lambda(1520)$ remains important. This is confirmed by the m_{pK^-} spectrum in Ref. [223] (see Fig. 5.3) over the q^2 bin $[0.1, 6]\,\text{GeV}^2$. Then the $\Lambda_b \to \Lambda(1520)\ (\to NK)\ell^+\ell^-$ decay should be accessible, from the signal observed in $\Lambda_b \to pK^-\mu^+\mu^-$ [223, 312], and could be studied in detail at LHCb, both for the branching ratio and for the angular observables.

Compared to $\Lambda(1116)$, a decay involving $\Lambda(1520)$ (from now on denoted as Λ^*) feature two main differences: the spin of the intermediate Λ^* state is higher ($J^P = 3/2^-$ rather than $1/2^+$) and the Λ^* decays into pK^- under the strong interaction (rather than into $p\pi$ under the weak interaction). Obviously the same issues exist in both intermediate states concerning the uncertainties on hadronic contributions [205], the determination of form factors and of non-local contributions. Concerning the form factors, a lattice determination of them already exists, but it is constrained to the high-q^2 region (see Refs. [314, 315]); some efforts are still needed to obtain a determination over the whole q^2 range. Form factors could be determined in the large-recoil region through the use of light-cone sum rules [316] or SCET sum rules as done for the ground state intermediate state in Ref. [40],

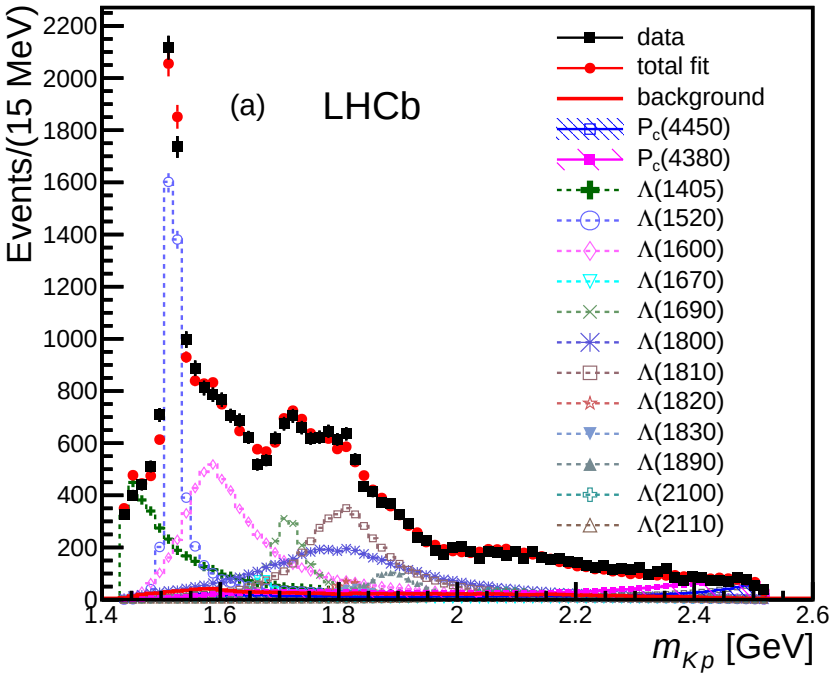

Figure 5.1: Measured m_{pK^-} spectrum for the $\Lambda_b \to pK^- J/\psi$ decay in black (squares) obtained by LHCb's pentaquark searches and shown in Fig. 3 of Ref. [313]. A fit is shown in red (full circles) performed to measure the contribution of each Λ^* resonance and two pentaquark states. Each Λ^* component is also shown where the $\Lambda(1520)$ resonance correspond to the blue dashed curve (empty circles).

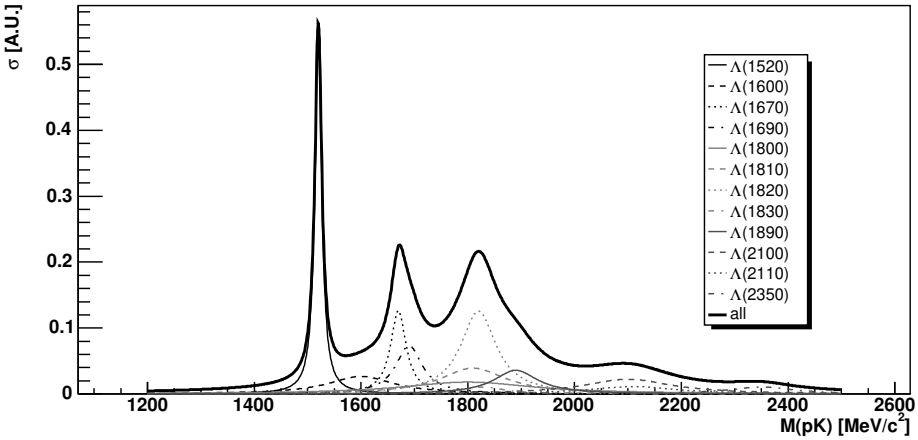

Figure 5.2: Approximate m_{pK^-} spectrum from $\Lambda_b \to pK^-\gamma$ decays, obtained by adding up non-relativistic Breit-Wigner forms presented in Fig. 1 of Ref. [310]. The interference effect are neglected as also is a possible non-resonant contribution. The relative contribution of each resonance is derived from simple kinematic suppression.

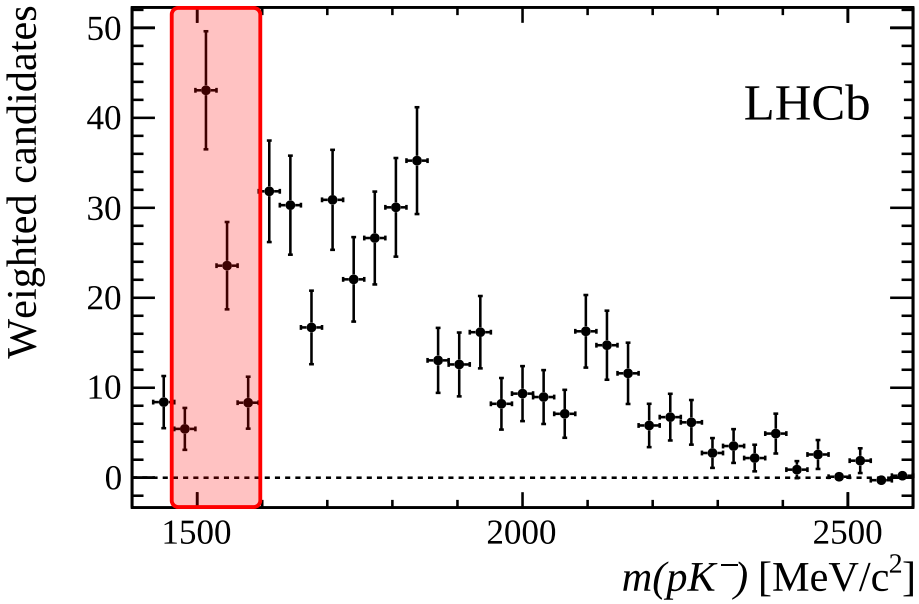

Figure 5.3: m_{pK^-} spectrum, measured by LHCb [223], for the $\Lambda_b \to pK^-\mu^+\mu^-$ decay in the $[0.1, 6.0]\,\text{GeV}^2$ q^2 bin. In red is shown the region corresponding to the $\Lambda(1520)$ resonance. Modified version of Fig. 9 in supplementary material of Ref. [223].

but this has yet to be explored. The question of non-local (charm) contributions could be understood based on data-driven methods similar to Refs. [112, 317], involving light-cone sum rules similar to Refs. [40, 115, 116, 318]. It is thus already interesting to discuss the general structure of this decay and the observables that can be obtained, even before these issues are completely resolved.

This chapter, based on Refs. [319, 320], is organised in the following way. We discuss the specific effective Hamiltonian (see Section 2.4) framework used in this study and the kinematics of $\Lambda_b \to \Lambda^*(\to N\bar{K})\ell^+\ell^-$ with $N\bar{K} = pK^-, n\bar{K}^0$ in Section 5.1. We consider different hadronic inputs for this transition in Section 5.2, namely the $\Lambda_b \to \Lambda^*$ form factors and the description of the $\Lambda^* \to N\bar{K}$ decay. We compute the helicity amplitudes and the angular observables and discuss phenomenology aspects of this decay in Section 5.3, assuming unpolarised Λ_b baryons and neglecting the lepton mass. In Section 5.4, as there is currently no determination of the form factors available from lattice simulations or light-cone sum rules for the whole q^2 range, we perform a first illustration of the sensitivity of some observables to New Physics contributions using hadronic inputs from quark models. We then present in Section 5.5 prospects of an experimental study of this decay at the LHCb experiment in the near future before drawing a few conclusions in Section 5.6. Technical considerations concerning the kinematics and the free solutions in several rest frames as well as cross checks of our results with earlier work are collected in Appendices 5.A to 5.D.

5.1 General framework

As discussed in Section 2.4 it is possible to analyse $b \to s\ell^+\ell^-$ decays using a model-independent approach, namely the effective Hamiltonian Eq. (2.35) where heavy degrees of freedom have been integrated out in short-distance Wilson coefficients $\mathcal{C}_i$, leaving only a set of operators $\mathcal{O}_i$ describing the physics on long distances. In the SM, three operators play a leading role in the discussion, namely the electromagnetic operator $\mathcal{O}_7$ and the semileptonic operators $\mathcal{O}_{9\ell}$ and $\mathcal{O}_{10\ell}$, differing with respect to the chirality of the emitted charged leptons. NP contributions could either modify the value of the short-distance Wilson coefficients $\mathcal{C}_{7,9,10}$, or make other operators contribute in a significant manner, such as the chirality-flipped operators $\mathcal{O}_{7',9',10'}$ defined above, or other operators (scalar, pseudoscalar, tensor). In this study we focus on the effect of SM operators and their chirality-flipped counterparts, although we will discuss the impact of the other SM operators (four-quark operators $\mathcal{O}_{1-6}$ and $\mathcal{O}_{8g}$) briefly in Section 5.3.

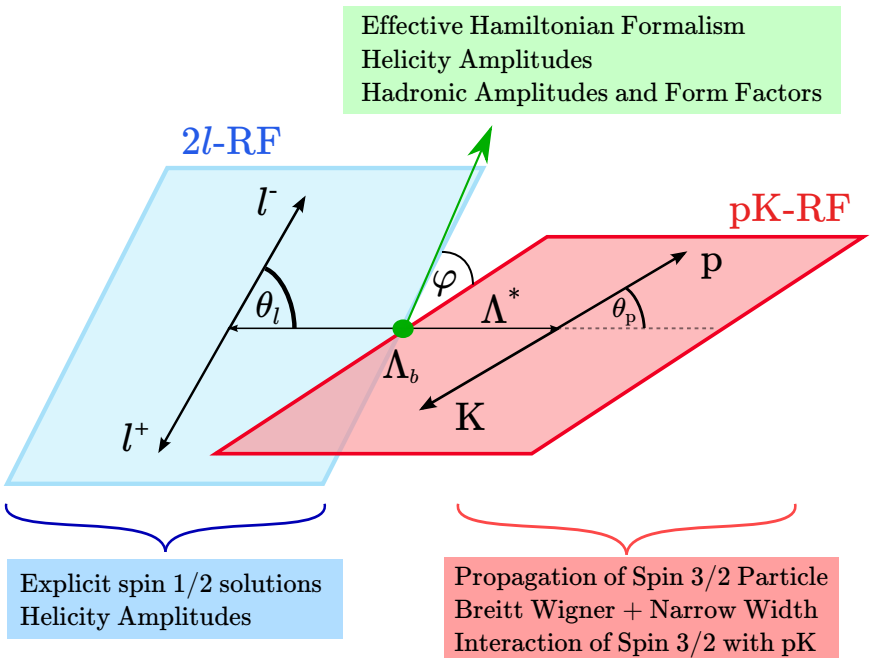

Figure 5.4: Schematics of the kinematics and the treatment of the four-body $\Lambda_b \to \Lambda^*(\to N\bar{K})\ell^+\ell^-$ decay. The angles are defined in the corresponding rest frames, indicated in colours. In green, the parts of the treatment related to the separation of scales. In red, the treatment of the Λ^* propagation and decay. In blue, the treatment of the leptonic amplitudes.

5.1.1 Kinematics

We consider the decay chain with the corresponding momenta for the various particles and their spin projections along the z-axis of the rest frame of the decaying particle

$$\begin{aligned} &\Lambda_b(p, s_{\Lambda_b}) \to \Lambda^*(k, s_{\Lambda^*})\ell^+(q_1)\ell^-(q_2), \\ &\Lambda^*(k, s_{\Lambda^*}) \to N(k_1, s_N)K(k_2) \qquad (N\bar{K} = pK^-, n\bar{K}^0), \end{aligned} \tag{5.1}$$

where we denote $\Lambda^*(1520)$ as Λ^* and we have

$$q^\mu = q_1^\mu + q_2^\mu, \qquad k^\mu = k_1^\mu + k_2^\mu, \qquad p^\mu = q^\mu + k^\mu. \tag{5.2}$$

We can introduce the same kinematics as for semileptonic four-body B-meson decays, leading to four independent variables chosen as the dilepton invariant mass q^2, the angles θ_p and θ_ℓ with respect to the z axis and the angle between the hadronic and leptonic planes ϕ, following the same LHCb conventions as for $\Lambda_b \to \Lambda(\to N\pi)\ell^+\ell^-$ [201, 226, 247] (up to the identifications $\theta_p = \theta_b$ and $\phi = \chi$) recalled in Fig. 5.4. The CP-conjugate mode can also be described using the same formalism, where an appropriate redefinition of the angle ensures that the angular observables will have the same form, up to the complex conjugation of the weak phases [201, 321].

The differential decay rate can be written

$$d\Gamma = \frac{|\mathcal{M}|^2}{2m_{\Lambda_b}} d\Phi_4(p; k_1, k_2, q_1, q_2), \tag{5.3}$$

where the phase space

$$d\Phi_n(P; p_1, \ldots, p_n) = (2\pi)^4 \, \delta^{(4)}(P - \sum_i p_i) \, \prod_i \frac{d^3 p_i}{(2\pi)^3 2E_i}, \tag{5.4}$$

can be decomposed iteratively as [322]

$$\int d\Phi_4 \frac{|\mathcal{M}|^2}{2m_{\Lambda_b}} = \int \frac{dq^2}{2\pi} \frac{dk^2}{2\pi} d\Phi_2(k; k_1, k_2) d\Phi_2(q; q_1, q_2) d\Phi_2(p; q, k) \frac{|\mathcal{M}|^2}{2m_{\Lambda_b}}, \tag{5.5}$$

with the two-body phase space of the form

$$\int d\Phi_2(k; k_1, k_2) X(k; k_1, k_2) = \int \frac{d\Omega_k}{4\pi} \frac{1}{8\pi} \frac{\sqrt{\lambda(k^2, k_1^2, k_2^2)}}{k^2} X(k; k_1, k_2), \tag{5.6}$$

with $d\Omega_k$ the element of integration of the the solid angle for k and the Källén function is

$$\lambda(k^2,k_1^2,k_1^2) = k^4 + k_1^4 + k_2^4 - 2k^2k_1^2 - 2k^2k_2^2 - 2k_1^2k_2^2. \tag{5.7}$$

The re-expression of the two-body phase space differential elements yields

$$\int d\Phi_4 \frac{|\mathcal{M}|^2}{2m_{\Lambda_b}} = \frac{1}{(2\pi)^2(8\pi)^4}\int dk^2\ (\beta_{\Lambda_b}\beta_{N\bar{K}}\beta_\ell)\ (dq^2\ d\cos\theta_\ell\ d\cos\theta_p\ d\phi)\frac{|\mathcal{M}|^2}{2m_{\Lambda_b}}, \tag{5.8}$$

with

$$\beta_{\Lambda_b} = \frac{\sqrt{\lambda(m_{\Lambda_b}^2,k^2,q^2)}}{m_{\Lambda_b}^2}, \qquad \beta_{N\bar{K}} = \frac{\sqrt{\lambda(k^2,m_N^2,m_{\bar{K}}^2)}}{k^2}, \qquad \beta_\ell = \sqrt{1-\frac{4m_\ell^2}{q^2}}. \tag{5.9}$$

5.1.2 Helicity amplitudes

It is well known that such a decay chain is best analysed by performing a decomposition according to helicity amplitudes, as discussed in Ref. [323] and illustrated for $b\to s\ell^+\ell^-$ decays in Ref. [321]. In particular, it proves very useful to introduce a vector basis which can be seen as the polarisation of an intermediate virtual boson decaying into the dilepton pair[1], defined in the dilepton rest frame as

$$\varepsilon^\mu(0) = \begin{pmatrix}0\\0\\0\\1\end{pmatrix}, \quad \varepsilon^\mu(+) = \frac{1}{\sqrt{2}}\begin{pmatrix}0\\-1\\-i\\0\end{pmatrix}, \quad \varepsilon^\mu(-) = \frac{1}{\sqrt{2}}\begin{pmatrix}0\\1\\-i\\0\end{pmatrix}, \quad \varepsilon^\mu(t) = \begin{pmatrix}1\\0\\0\\0\end{pmatrix}. \tag{5.10}$$

in agreement with Ref. [323]. Boosts can be used to define this basis in other reference frames. We can also easily define the scalar and time-like vectors in a general way as

$$\varepsilon^\mu(0) = \frac{e^\mu}{\sqrt{|e^2|}}, \qquad \varepsilon^\mu(t) = \frac{q^\mu}{\sqrt{q^2}}, \qquad e^\mu = p^\mu + k^\mu - \frac{q^\mu}{q^2}(m_{\Lambda_b}^2 - m_{\Lambda^*}^2), \tag{5.11}$$

with $e^2 = -\lambda(m_{\Lambda_b}^2, m_{\Lambda^*}^2, q^2)/q^2$.

We have the completeness and orthogonality relations for $\lambda,\lambda' = t,0,+,-$

$$\varepsilon^{*\mu}(\lambda)\varepsilon_\mu(\lambda') = g_{\lambda\lambda'}, \qquad \sum_{\lambda,\lambda'=t,0,+,-}\varepsilon^{*\mu}(\lambda)\varepsilon^\nu(\lambda')g_{\lambda\lambda'} = g^{\mu\nu}, \tag{5.12}$$

where g is defined as diagonal in the polarisation space, with $g_{tt} = -g_{00} = -g_{++} = -g_{--} = 1$. Assuming factorisation between the hadronic and the leptonic parts, and focusing on operators with a single Lorentz index, we have for the $\Lambda_b\to\Lambda^*\ell^+\ell^-$ part of this decay chain

$$\begin{aligned}\langle\Lambda^*\ell^+\ell^-|O_\mu^H O^{L;\mu}|\Lambda_b\rangle =& \langle\Lambda^*|O_\mu^H|\Lambda_b\rangle g^{\mu\nu}\langle\ell^+\ell^-|O_\nu^L|0\rangle \\ =& \sum_{\lambda=t,0,+,-} g_{\lambda\lambda'}(\varepsilon^{*\mu}(\lambda)\langle\Lambda^*|O_\mu^H|\Lambda_b\rangle)(\varepsilon^\nu(\lambda)\langle\ell^+\ell^-|O_\nu^L|0\rangle) \\ =& \sum_{\lambda=t,0,+,-} g_{\lambda\lambda'}\sum_i f_\lambda^i\ (\bar{u}_{\Lambda^*}^\alpha\varepsilon^{*\mu}(\lambda)\Gamma_{\mu\alpha}^{Hi}u_{\Lambda_b})\ (\bar{u}_{\ell^-}\varepsilon^\nu(\lambda)\Gamma_\nu^L v_{\ell^-}),\end{aligned} \tag{5.13}$$

which defines the hadronic and leptonic helicity amplitudes of interest, where we express the results in terms of the solutions for free fermions u and v (see Appendix 5.A for explicit expressions) and the helicity form factors f_λ^i to be defined in more detail in Section 5.2.

5.1.3 Propagation and decay of Λ^*

Once $\Lambda_b\to\Lambda^*\ell^+\ell^-$ has been described, we still have to include the propagation and the decay of the Λ^* baryon, which has the quantum numbers $J^P = 3/2^-$. This is usually done in the Rarita-Schwinger framework [41], with a field ψ_a^α combining a spinor index a and a vector index α (in the following, the spinor index a will often be kept implicit for simplicity). The corresponding free Lagrangian reads

$$\mathcal{L} = \bar{\psi}_\mu\frac{i}{2}\{\sigma^{\mu\nu},(i\partial\!\!\!/ - m_{\Lambda^*})\}\psi_\nu. \tag{5.14}$$

[1] This interpretation is discussed in detail in Ref. [321], where it is shown to be valid in full generality in the absence of tensor operators in the effective Hamiltonian.

The solutions $u_a^\alpha(k, s_{\Lambda^*})$ obey then the following properties:

$$\not{k} u^\alpha = m_{\Lambda^*} u^\alpha, \qquad \gamma_\alpha u^\alpha = 0, \qquad k_\alpha u^\alpha = 0. \tag{5.15}$$

Following Ref. [324], one can determine the explicit solutions for $s_{\Lambda^*} = -3/2, -1/2, 1/2, 3/2$ as

$$u_a^\alpha(k, s_{\Lambda^*}) = \sum_{\lambda=-1,0,1} \sum_{r=-1/2,1/2} \delta_{\lambda+r,s_{\Lambda^*}} \left\langle 1, \lambda; \frac{1}{2}, r \middle| 1, \frac{1}{2}, \frac{3}{2}, s_{\Lambda^*} \right\rangle \varepsilon_\lambda^\alpha(k) u_a^r(k), \tag{5.16}$$

where $u_a^r(k)$ are regular Dirac spin-1/2 spinors and a similar construction can be found for the anti-fermion solutions. This is used in Appendix 5.A to determine the appropriate solutions of the Λ^* equation of motion in both Λ_b and Λ^* rest frames.

The free propagator derived from Eq. (5.14) reads

$$G^{\mu\nu} = \frac{i(\not{k} + m_{\Lambda^*})\Delta^{\mu\nu}}{k^2 - m_{\Lambda^*}^2}, \qquad \Delta^{\mu\nu} = g^{\mu\nu}\mathrm{Id} - \frac{1}{3}\gamma^\mu\gamma^\nu - \frac{2k^\mu k^\nu}{3m_{\Lambda^*}^2} - \frac{\gamma^\mu k^\nu - \gamma^\nu k^\mu}{3m_{\Lambda^*}}, \tag{5.17}$$

where Id denotes the identity matrix in the Dirac matrix space. We checked that the summation formula expected from general unitarity arguments (see for instance Ref. [325])

$$\sum_{s_{\Lambda^*}=-3/2}^{3/2} u_a^\mu(k, s_{\Lambda^*}) \bar{u}_b^\nu(k, s_{\Lambda^*}) = -(\not{k} + m_{\Lambda^*})\Delta_{ab}^{\mu\nu}, \tag{5.18}$$

is indeed satisfied by the solution Eq. (5.16) given in Appendix 5.A.

One should note that the tensor $\Delta^{\mu\nu}$ involved in the propagator is not the projector on the spin-3/2 component given by

$$P^{\mu\nu} = g^{\mu\nu} - \frac{1}{3}\gamma^\mu\gamma^\nu - \frac{1}{3m_{\Lambda^*}^2}(\not{k}\gamma^\mu k^\nu + k^\mu\gamma^\nu\not{k}). \tag{5.19}$$

By construction, a field of the form ψ_a^α contains both spin-1/2 and spin-3/2 components: only 4 components of the 16-component field ψ_a^α are actually needed to describe the spin-3/2 part. Even though the Rarita-Schwinger construction aims at describing a spin-3/2 object only, it turns out that one cannot modify the kernel in Eq. (5.14) to keep only on the spin-3/2 component of the field, as the projected kernel cannot be inverted [326]. Attempts to enforce the projection at the level of the propagator led to theories with unwanted properties, such as spurious poles affecting higher orders in perturbation theory [327–329]. In practice, the quantisation must be performed with the whole field ψ_a^α, in the presence of constraints that will ensure that only the spin-3/2 component of the field is actually physical [330].

The problem is even made more acute in the case of an interacting spin-3/2 theory, as the interaction term should be compatible with the quantisation of the theory. This led to a significant amount of debate concerning the description of the $\pi N\Delta$ interaction at low energies, which can be used as a template to describe the $KN\Lambda^*$ interaction (the quantum numbers are the same, apart from the opposite parity of the Δ and Λ^* fermions). A first type of effective interaction at low energies was proposed (here translated to the $KN\Lambda^*$ case) [331]

$$\mathcal{L}_1 = g m_{\Lambda^*} \bar{\psi}_\mu (g^{\mu\nu} + a\gamma^\mu\gamma^\nu)\gamma_5 \Psi \partial_\nu \phi + h.c., \tag{5.20}$$

where Ψ denotes the spin-1/2 N field and ϕ the spin-0 K field (coming with a derivative due to the pseudo-Goldstone nature of the kaon), and a is an off-shell parameter that is relevant only for loop computations.

As discussed in Ref. [330], this interaction is simple, but once used to build an interacting theory, it involves not only the physical spin-3/2 components of the Rarita-Schwinger field ψ_μ, but also unphysical spin-1/2 components, leading to problems of causality and to a significant contribution from spin-1/2 background underneath the Λ^* (or Δ) resonance. In Ref. [330], an alternative interaction has been proposed

$$\mathcal{L}_2 = g\varepsilon^{\mu\nu\alpha\beta}(\partial_\mu \bar{\psi}_\nu)\gamma_\alpha \Psi \partial_\beta \phi + h.c. \tag{5.21}$$

This choice is suggested by the invariance of the free massless theory under gauge transformations of ψ_μ: it is compatible with the quantisation of the theory under constraints, and using the projector Eq. (5.19) and the propagator Eq. (5.17), it can be shown easily that it involves only the spin-3/2 part of ψ^α.

Fortunately, we do not have to take sides on this issue here. Indeed, these two choices of interaction term will yield actually the same result for the branching ratio of interest here. This is in agreement with the fact that we use these interactions only for a tree-level interaction with on-shell particles, and it will provide a further cross-check of our results.

5.1.4 Narrow-width approximation

The Λ^* propagation and decay can thus be included in the description Eq. (5.13) as

$$\begin{aligned}\mathcal{M} =&\langle (N\bar{K})_{\Lambda^*}\ell^+\ell^-|O_\mu^H O^{L;\mu}|\Lambda_b\rangle \\ =&i\sum_{\lambda=t,0,+,-}\sum_i\sum_{s_{\Lambda^*}}\bar{u}_N G u_{\Lambda^*}\ \frac{i}{k^2-m_{\Lambda^*}^2}\ (\bar{u}^\alpha_{\Lambda^*}(\varepsilon^{*\mu}_\lambda\Gamma^{Hi}_{\mu\alpha})u_{\Lambda_b})\ f^i_\lambda\ (\bar{u}_{\ell^-}(\varepsilon^\nu_\lambda\Gamma^L_\nu)v_{\ell^-}),\end{aligned} \tag{5.22}$$

where G is a momentum-dependent quantity defined as $\langle NK|\mathcal{L}_i|\Lambda^*\rangle = \bar{u}_N G(k_1,k_2)u_{\Lambda^*}$ from the interaction Lagrangians in Eq. (5.20) or Eq. (5.21). The decay rate can be computed as

$$\int d\Gamma = \int d\Phi_4 \frac{|\overline{\mathcal{M}}|^2}{2m_{\Lambda_b}}, \qquad |\overline{\mathcal{M}}|^2 = \frac{1}{2}\sum_{s_{\Lambda_b}}\sum_{s_N}|\mathcal{M}|^2, \tag{5.23}$$

where we summed over the final spins and averaged over the initial spins, assuming that the Λ_b baryon is produced essentially in an unpolarised way at the LHC [218, 332].

Following Ref. [333], we modify the propagator of the Λ^* baryon to take into account the width of the resonance, but treat it as narrow ($\Gamma_{\Lambda^*} \ll m_{\Lambda^*}$)

$$\begin{aligned}\int d\Phi_4 \frac{|\overline{\mathcal{M}}|^2}{2m_{\Lambda_b}} &= \int d\tilde{\Phi}\ dk^2 \frac{|\overline{\mathcal{N}}|^2}{(k^2-m^2)^2} \\ &\to \int d\tilde{\Phi}\ dk^2 \frac{|\overline{\mathcal{N}}|^2}{(k^2-m^2)^2+(m_{\Lambda^*}\Gamma_{\Lambda^*})^2} \\ &\to \int d\tilde{\Phi}\ dk^2 |\overline{\mathcal{N}}|^2\ \frac{\pi}{m_{\Lambda^*}\Gamma_{\Lambda^*}}\delta(k^2-m_{\Lambda^*}^2) = \int d\tilde{\Phi}|\overline{\mathcal{N}}|^2_{k^2=m^2_{\Lambda^*}}\ \frac{\pi}{m_{\Lambda^*}\Gamma_{\Lambda^*}},\end{aligned} \tag{5.24}$$

where $d\tilde{\Phi}$ describes the phase space without the integration with respect to dk^2 as shown in Eq. (5.8), and $\mathcal{N}$ is defined from the matrix element $\mathcal{M}$ in Eq. (5.22) as

$$\mathcal{N} = (k^2-m_{\Lambda^*}^2)\mathcal{M}. \tag{5.25}$$

Up to a phase space, the branching ratio is the product of three matrix elements corresponding to the helicity amplitude for the leptonic part, the helicity amplitude for the $\Lambda_b \to \Lambda^*$ hadronic part and the matrix element for the $\Lambda^* \to N\bar{K}$ decay. We finally obtain

$$\int d\Gamma = \int dq^2 d\cos\theta_\ell d\cos\theta_p d\phi \frac{1}{2^{15}\pi^5 m_{\Lambda_b} m_{\Lambda^*}\Gamma_{\Lambda^*}}(\beta_{\Lambda_b}\beta_{N\bar{K}}\beta_\ell)|\overline{\mathcal{N}}|^2\Big|_{k^2=m^2_{\Lambda^*}}. \tag{5.26}$$

5.2 Hadronic matrix elements

Since the general framework of the kinematics and helicity amplitudes has been set up, we can turn to the description of the hadronic part of the decay through form factors.

5.2.1 $\Lambda_b \to \Lambda^*$ vector form factors

The hadronic matrix elements can be decomposed using the spinors for Λ_b and Λ^*, and inserting all the possible Dirac structures taking into account the parity and the e.o.m constraints. In the case of the vector form/axial operators, there are four structures, and thus four form factors, once the equations of motion for Λ_b and Λ^* are taken into account [42]. As seen before, they are better defined using helicity form factors [40, 197], which corresponds to choosing combinations of these Dirac matrices so that they are orthogonal to the polarisation

eigenvectors defined in Eq. (5.10). This leads to the following definition

$$\begin{aligned}
\langle \Lambda^* | \bar{s}\gamma^\mu b | \Lambda_b \rangle =& \bar{u}_\alpha(k, s_{\Lambda^*}) \Bigg\{ p^\alpha \Bigg[f_t^V(q^2)(m_{\Lambda_b} - m_{\Lambda^*}) \frac{q^\mu}{q^2} \\
&+ f_0^V(q^2) \frac{m_{\Lambda_b} + m_{\Lambda^*}}{s_+} (p^\mu + k^\mu - \frac{q^\mu}{q^2}(m_{\Lambda_b}^2 - m_{\Lambda^*}^2)) \\
&+ f_\perp^V(q^2)(\gamma^\mu - 2\frac{m_{\Lambda^*}}{s_+} p^\mu - 2\frac{m_{\Lambda_b}}{s_+} k^\mu) \Bigg] \\
&+ f_g^V(q^2) \left[g^{\alpha\mu} + m_{\Lambda^*} \frac{p^\alpha}{s_-} \left(\gamma^\mu - 2\frac{k^\mu}{m_{\Lambda^*}} + 2\frac{m_{\Lambda^*} p^\mu + m_{\Lambda_b} k^\mu}{s_+} \right) \right] \Bigg\} u(p, s_{\Lambda_b}), \\
\langle \Lambda^* | \bar{s}\gamma^\mu \gamma^5 b | \Lambda_b \rangle =& -\bar{u}_\alpha(k, s_{\Lambda^*}) \gamma^5 \Bigg\{ p^\alpha \Bigg[f_t^A(q^2)(m_{\Lambda_b} + m_{\Lambda^*}) \frac{q^\mu}{q^2} \\
&+ f_0^A(q^2) \frac{m_{\Lambda_b} - m_{\Lambda^*}}{s_-} (p^\mu + k^\mu - \frac{q^\mu}{q^2}(m_{\Lambda_b}^2 - m_{\Lambda^*}^2)) \\
&+ f_\perp^A(q^2)(\gamma^\mu + 2\frac{m_{\Lambda^*}}{s_-} p^\mu - 2\frac{m_{\Lambda_b}}{s_-} k^\mu) \Bigg] \\
&+ f_g^A(q^2) \left[g^{\alpha\mu} - m_{\Lambda^*} \frac{p^\alpha}{s_+} \left(\gamma^\mu + 2\frac{k^\mu}{m_{\Lambda^*}} - 2\frac{m_{\Lambda^*} p^\mu - m_{\Lambda_b} k^\mu}{s_-} \right) \right] \Bigg\} u(p, s_{\Lambda_b}).
\end{aligned} \tag{5.27}$$

We have introduced

$$s_\pm = (m_{\Lambda_b} \pm m_{\Lambda^*})^2 - q^2. \tag{5.28}$$

We have used similar normalisations to the $\Lambda_b \to \Lambda(1116)$ form factors chosen in Refs. [40, 197] for $f_t, f_0, f_\perp$ so that in the limit where the three form factors are set to 1, one recovers a point-like behaviour $\bar{u}_\alpha(k, s_{\Lambda^*}) p^\alpha \gamma^\mu (\gamma_5) u(p, s_{\Lambda_b})$. However, in the Λ^* case, a fourth form factor, f_g, arises [42, 334, 335]. Further constraints arise by considering the limit $q^2 \to 0$: since there are no physical states with $\bar{s}b$ quantum numbers and a vanishing mass, the matrix elements cannot exhibit any singularity at $q^2 = 0$, which leads to the constraints in this limit

$$f_t^V(q^2) - f_0^V(q^2) = O(q^2), \qquad f_t^A(q^2) - f_0^A(q^2) = O(q^2), \tag{5.29}$$

$$\begin{aligned}
&f_t^V(q^2) = O(1), \quad f_0^V(q^2) = O(1), \quad f_\perp^V(q^2) = O(1), \quad f_g^V(q^2) = O(1), \\
&f_t^A(q^2) = O(1), \quad f_0^A(q^2) = O(1), \quad f_\perp^A(q^2) = O(1), \quad f_g^A(q^2) = O(1).
\end{aligned} \tag{5.30}$$

Some conditions should also obeyed by the form factors for $q^2 = (m_{\Lambda_b} - m_{\Lambda^*})^2$, where additional s_- factors arise from the normalisation of the free Dirac solutions u and $\bar{u}_\alpha$, see Appendix 5.A. We finally obtain the following constraints in this limit

$$\begin{aligned}
&f_t^V(q^2) = O\left(\tfrac{1}{\sqrt{s_-}}\right), \quad f_0^V(q^2) = O\left(\tfrac{1}{s_-}\right), \quad f_\perp^V(q^2) = O\left(\tfrac{1}{s_-}\right), \quad f_g^V(q^2) = O(1), \\
&f_t^A(q^2) = O\left(\tfrac{1}{s_-}\right), \quad f_0^A(q^2) = O\left(\tfrac{1}{\sqrt{s_-}}\right), \quad f_\perp^A(q^2) = O\left(\tfrac{1}{\sqrt{s_-}}\right), \quad f_g^A(q^2) = O\left(\tfrac{1}{\sqrt{s_-}}\right).
\end{aligned} \tag{5.31}$$

At both endpoints, the conditions indicated above are sufficient to ensure the absence of unphysical poles in the hadronic matrix elements, but obviously, form factors exhibiting less singular behaviours are also acceptable.

The choice of helicity form factors means that the matrix elements for each polarisation correspond to a very simple expression in terms of form factors for the vector part

$$\begin{aligned}
H_t^V(s_{\Lambda_b}, s_{\Lambda^*}) &\equiv \varepsilon_\mu^*(t) \langle \Lambda^*(k, s_{\Lambda^*}) | \bar{s}\gamma^\mu b | \Lambda_b(p, s_{\Lambda_b}) \rangle \\
&= f_t^V(q^2) \frac{m_{\Lambda_b} - m_{\Lambda^*}}{\sqrt{q^2}} \bar{u}_\alpha(k, s_{\Lambda^*}) p^\alpha u(p, s_{\Lambda_b}), \\
H_0^V(s_{\Lambda_b}, s_{\Lambda^*}) &\equiv \varepsilon_\mu^*(0) \langle \Lambda^*(k, s_{\Lambda^*}) | \bar{s}\gamma^\mu b | \Lambda_b(p, s_{\Lambda_b}) \rangle \\
&= -f_0^V(q^2) \frac{m_{\Lambda_b} + m_{\Lambda^*}}{s_+} \sqrt{|e^2|} \bar{u}_\alpha(k, s_{\Lambda^*}) p^\alpha u(p, s_{\Lambda_b}), \\
H_\pm^V(s_{\Lambda_b}, s_{\Lambda^*}) &\equiv \varepsilon_\mu^*(\pm) \langle \Lambda^*(k, s_{\Lambda^*}) | \bar{s}\gamma^\mu b | \Lambda_b(p, s_{\Lambda_b}) \rangle \\
&= \left(f_\perp^V(q^2) + f_g^V(q^2) \frac{m_{\Lambda^*}}{s_-} \right) \bar{u}_\alpha(k, s_{\Lambda^*}) p^\alpha \not{\varepsilon}^*(\pm) u(p, s_{\Lambda_b}) + f_g^V(q^2) \bar{u}_\alpha(k, s_{\Lambda^*}) \varepsilon^{*\alpha}(\pm) u(p, s_{\Lambda_b}),
\end{aligned} \tag{5.32}$$

and for the axial part

$$\begin{aligned}
H_t^A(s_{\Lambda_b}, s_{\Lambda^*}) &\equiv \varepsilon_\mu^*(t)\langle\Lambda^*(k,s_{\Lambda^*})|\bar{s}\gamma^\mu\gamma^5 b|\Lambda_b(p,s_{\Lambda_b})\rangle \\
&= -f_t^A(q^2)\frac{m_{\Lambda_b}+m_{\Lambda^*}}{\sqrt{q^2}}\bar{u}_\alpha(k,s_{\Lambda^*})\gamma^5 p^\alpha u(p,s_{\Lambda_b}), \\
H_0^A(s_{\Lambda_b}, s_{\Lambda^*}) &\equiv \varepsilon_\mu^*(0)\langle\Lambda^*(k,s_{\Lambda^*})|\bar{s}\gamma^\mu\gamma^5 b|\Lambda_b(p,s_{\Lambda_b})\rangle \\
&= f_0^A(q^2)\frac{m_{\Lambda_b}-m_{\Lambda^*}}{s_-}\sqrt{|e^2|}\bar{u}_\alpha(k,s_{\Lambda^*})\gamma^5 p^\alpha u(p,s_{\Lambda_b}), \\
H_\pm^A(s_{\Lambda_b}, s_{\Lambda^*}) &\equiv \varepsilon_\mu^*(\pm)\langle\Lambda^*(k,s_{\Lambda^*})|\bar{s}\gamma^\mu\gamma^5 b|\Lambda_b(p,s_{\Lambda_b})\rangle \\
&= \left(f_\perp^A(q^2) - f_g^A(q^2)\frac{m_{\Lambda^*}}{s_+}\right)\bar{u}_\alpha(k,s_{\Lambda^*})p^\alpha \not{\varepsilon}^*(\pm)\gamma^5 u(p,s_{\Lambda_b}) - f_g^A(q^2)\bar{u}_\alpha(k,s_{\Lambda^*})\varepsilon^{*\alpha}(\pm)\gamma^5 u(p,s_{\Lambda_b}),
\end{aligned} \tag{5.33}$$

where e is the vector defined in Eq. (5.11). Using the expression for the spinor matrix elements given in Appendix 5.A, we obtain for the non-vanishing amplitudes in the vector part

$$\begin{aligned}
H_t^V(+1/2,+1/2) &= H_t^V(-1/2,-1/2) = f_t^V(q^2)\frac{m_{\Lambda_b}-m_{\Lambda^*}}{\sqrt{q^2}}\frac{s_+\sqrt{s_-}}{\sqrt{6}m_{\Lambda^*}}, \\
H_0^V(+1/2,+1/2) &= H_0^V(-1/2,-1/2) = -f_0^V(q^2)\frac{m_{\Lambda_b}+m_{\Lambda^*}}{\sqrt{q^2}}\frac{s_-\sqrt{s_+}}{\sqrt{6}m_{\Lambda^*}}, \\
H_+^V(+1/2,-1/2) &= H_-^V(-1/2,+1/2) = -f_\perp^V(q^2)\frac{s_-\sqrt{s_+}}{\sqrt{3}m_{\Lambda^*}}, \\
H_+^V(-1/2,-3/2) &= H_-^V(+1/2,+3/2) = f_g^V(q^2)\sqrt{s_+},
\end{aligned} \tag{5.34}$$

and for the axial part

$$\begin{aligned}
H_t^A(+1/2,+1/2) &= -H_t^A(-1/2,-1/2) = f_t^A(q^2)\frac{m_{\Lambda_b}+m_{\Lambda^*}}{\sqrt{q^2}}\frac{s_-\sqrt{s_+}}{\sqrt{6}m_{\Lambda^*}}, \\
H_0^A(+1/2,+1/2) &= -H_0^A(-1/2,-1/2) = -f_0^A(q^2)\frac{m_{\Lambda_b}-m_{\Lambda^*}}{\sqrt{q^2}}\frac{s_+\sqrt{s_-}}{\sqrt{6}m_{\Lambda^*}}, \\
H_+^A(+1/2,-1/2) &= -H_-^A(-1/2,+1/2) = f_\perp^A(q^2)\frac{s_+\sqrt{s_-}}{\sqrt{3}m_{\Lambda^*}}, \\
H_+^A(-1/2,-3/2) &= -H_-^A(+1/2,+3/2) = -f_g^A(q^2)\sqrt{s_-}.
\end{aligned} \tag{5.35}$$

5.2.2 $\Lambda_b \to \Lambda^*$ tensor form factors

A similar discussion takes place in the case of the tensor form factors. The relevant matrix elements are the following, once again defined in order to have structures orthogonal to the polarisation vectors Eq. (5.10)

$$\begin{aligned}
\langle\Lambda^*|\bar{s}i\sigma^{\mu\nu}q_\nu b|\Lambda_b\rangle =& -\bar{u}_\alpha(k,s_{\Lambda^*})\Big\{p^\alpha\Big[f_0^T(q^2)\frac{q^2}{s_+}(p^\mu+k^\mu-\frac{q^\mu}{q^2}(m_{\Lambda_b}^2-m_{\Lambda^*}^2)) \\
&+ f_\perp^T(q^2)(m_{\Lambda_b}+m_{\Lambda^*})(\gamma^\mu - 2\frac{m_{\Lambda^*}}{s_+}p^\mu - 2\frac{m_{\Lambda_b}}{s_+}k^\mu)\Big] \\
&+ f_g^T(q^2)\left[g^{\alpha\mu} + m_{\Lambda^*}\frac{p^\alpha}{s_-}\left(\gamma^\mu - 2\frac{k^\mu}{m_{\Lambda^*}} + 2\frac{m_{\Lambda^*}p^\mu + m_{\Lambda_b}k^\mu}{s_+}\right)\right]\Big\}u(p,s_{\Lambda_b}), \\
\langle\Lambda^*|\bar{s}i\sigma^{\mu\nu}\gamma^5 q_\nu b|\Lambda_b\rangle =& -\bar{u}_\alpha(k,s_{\Lambda^*})\gamma^5\Big\{p^\alpha\Big[f_0^{T5}(q^2)\frac{q^2}{s_-}(p^\mu+k^\mu-\frac{q^\mu}{q^2}(m_{\Lambda_b}^2-m_{\Lambda^*}^2)) \\
&+ f_\perp^{T5}(q^2)(m_{\Lambda_b}-m_{\Lambda^*})(\gamma^\mu + 2\frac{m_{\Lambda^*}}{s_-}p^\mu - 2\frac{m_{\Lambda_b}}{s_-}k^\mu)\Big] \\
&+ f_g^{T5}(q^2)\left[g^{\alpha\mu} - m_{\Lambda^*}\frac{p^\alpha}{s_+}\left(\gamma^\mu + 2\frac{k^\mu}{m_{\Lambda^*}} - 2\frac{m_{\Lambda^*}p^\mu - m_{\Lambda_b}k^\mu}{s_-}\right)\right]\Big\}u(p,s_{\Lambda_b}).
\end{aligned} \tag{5.36}$$

We have again used similar normalisations to the $\Lambda_b \to \Lambda(1116)$ form factors chosen in Refs. [40, 197] for f_0, $f_\perp$, so that in the limit where the two form factors are set to 1, one recovers a point-like behaviour. In the Λ^* case, there is again an additional form factor to be taken into account [42, 334, 335].

As in the vector/axial case, the matrix elements cannot exhibit a singularity at $q^2 = 0$ nor $q^2 = (m_{\Lambda_b} - m_{\Lambda^*})^2$, which yields the following constraints for $q^2 \to 0$ (see Appendix 5.C for further detail)

$$\begin{aligned} f_\perp^T(q^2) &= O(1), \quad f_0^T(q^2) = O(1), \quad f_g^T(q^2) = O(1), \\ f_\perp^{T5}(q^2) &= O(1), \quad f_0^{T5}(q^2) = O(1), \quad f_g^{T5}(q^2) = O(1), \end{aligned} \tag{5.37}$$

and the following constraints for $q^2 \to (m_{\Lambda_b} - m_{\Lambda^*})^2$

$$\begin{aligned} f_\perp^T(q^2) &= O\left(\tfrac{1}{s_-}\right), \quad f_0^T(q^2) = O\left(\tfrac{1}{s_-}\right), \quad f_g^T(q^2) = O(1), \\ f_\perp^{T5}(q^2) &= O\left(\tfrac{1}{\sqrt{s_-}}\right), \quad f_0^{T5}(q^2) = O\left(\tfrac{1}{\sqrt{s_-}}\right), \quad f_g^{T5}(q^2) = O\left(\tfrac{1}{\sqrt{s_-}}\right). \end{aligned} \tag{5.38}$$

These conditions are sufficient to ensure the absence of unphysical poles in the hadronic matrix elements, but once again, form factors exhibiting less singular behaviours are also acceptable. Moreover, the equality $\sigma_{\mu\nu}\gamma_5 = i\epsilon_{\mu\nu\rho\sigma}\sigma^{\rho\sigma}/2$ yields the following constraints for the values of the tensor form factors at $q^2 = 0$

$$f_\perp^{T5}(0) = f_\perp^T(0), \qquad f_g^{T5}(0) = f_g^T(0)\frac{m_{\Lambda_b} + m_{\Lambda^*}}{m_{\Lambda_b} - m_{\Lambda^*}}. \tag{5.39}$$

As can be seen by comparing with the previous section, the situation is slightly different from the vector/axial case: there is no form factor corresponding to the time-like polarisation (or q^μ), the normalisation of the Lorentz structures is different, and the resulting constraints at $q^2 = 0$ are different.

This leads to the helicity amplitudes

$$\begin{aligned} H_t^T(s_{\Lambda_b}, s_{\Lambda^*}) &\equiv \varepsilon_\mu^*(t)\langle\Lambda^*(k, s_{\Lambda^*})|\bar{s}i\sigma^{\mu\nu}q_\nu b|\Lambda_b(p, s_{\Lambda_b})\rangle = 0, \\ H_0^T(s_{\Lambda_b}, s_{\Lambda^*}) &\equiv \varepsilon_\mu^*(0)\langle\Lambda^*(k, s_{\Lambda^*})|\bar{s}i\sigma^{\mu\nu}q_\nu b|\Lambda_b(p, s_{\Lambda_b})\rangle \\ &= f_0^T(q^2)\frac{q^2}{s_+}\sqrt{|e^2|}\bar{u}_\alpha(k, s_{\Lambda^*})p^\alpha u(p, s_{\Lambda_b}), \\ H_\pm^T(s_{\Lambda_b}, s_{\Lambda^*}) &\equiv \varepsilon_\mu^*(\pm)\langle\Lambda^*(k, s_{\Lambda^*})|\bar{s}i\sigma^{\mu\nu}q_\nu b|\Lambda_b(p, s_{\Lambda_b})\rangle \\ &= -\left(f_\perp^T(q^2)(m_{\Lambda_b} + m_{\Lambda^*}) + f_g^T(q^2)\frac{m_{\Lambda^*}}{s_-}\right)\bar{u}_\alpha(k, s_{\Lambda^*})p^\alpha \not{\varepsilon}^*(\pm)u(p, s_{\Lambda_b}) \\ &\quad - f_g^T(q^2)\bar{u}_\alpha(k, s_{\Lambda^*})\varepsilon^{*\alpha}(\pm)u(p, s_{\Lambda_b}), \\ H_t^{T5}(s_{\Lambda_b}, s_{\Lambda^*}) &\equiv \varepsilon_\mu^*(t)\langle\Lambda^*(k, s_{\Lambda^*})|\bar{s}i\sigma^{\mu\nu}q_\nu\gamma^5 b|\Lambda_b(p, s_{\Lambda_b})\rangle = 0, \\ H_0^{T5}(s_{\Lambda_b}, s_{\Lambda^*}) &\equiv \varepsilon_\mu^*(0)\langle\Lambda^*(k, s_{\Lambda^*})|\bar{s}i\sigma^{\mu\nu}q_\nu\gamma^5 b|\Lambda_b(p, s_{\Lambda_b})\rangle \\ &= f_0^{T5}(q^2)\frac{q^2}{s_-}\sqrt{|e^2|}\bar{u}_\alpha(k, s_{\Lambda^*})\gamma^5 p^\alpha u(p, s_{\Lambda_b}), \\ H_\pm^{T5}(s_{\Lambda_b}, s_{\Lambda^*}) &\equiv \varepsilon_\mu^*(\pm)\langle\Lambda^*(k, s_{\Lambda^*})|\bar{s}i\sigma^{\mu\nu}q_\nu\gamma^5 b|\Lambda_b(p, s_{\Lambda_b})\rangle \\ &= \left(f_\perp^{T5}(q^2)(m_{\Lambda_b} - m_{\Lambda^*}) - f_g^{T5}(q^2)\frac{m_{\Lambda^*}}{s_+}\right)\bar{u}_\alpha(k, s_{\Lambda^*})p^\alpha \not{\varepsilon}^*(\pm)\gamma^5 u(p, s_{\Lambda_b}) \\ &\quad - f_g^{T5}(q^2)\bar{u}_\alpha(k, s_{\Lambda^*})\varepsilon^{*\alpha}(\pm)\gamma^5 u(p, s_{\Lambda_b}). \end{aligned} \tag{5.40}$$

We recall that e^μ has been defined in Eq. (5.11). As expected, there is no contribution from the time-like polarisation in the case of the tensor form factors. One obtains the following non-vanishing amplitudes

$$\begin{aligned} H_0^T(+1/2, +1/2) &= H_0^T(-1/2, -1/2) = f_0^T(q^2)\sqrt{q^2}\frac{s_-\sqrt{s_+}}{\sqrt{6}m_{\Lambda^*}}, \\ H_+^T(+1/2, -1/2) &= H_-^T(-1/2, +1/2) = f_\perp^T(q^2)(m_{\Lambda_b} + m_{\Lambda^*})\frac{s_-\sqrt{s_+}}{\sqrt{3}m_{\Lambda^*}}, \\ H_+^T(-1/2, -3/2) &= H_-^T(+1/2, +3/2) = -f_g^T(q^2)\sqrt{s_+}, \\ H_0^{T5}(+1/2, +1/2) &= -H_0^{T5}(-1/2, -1/2) = -f_0^{T5}(q^2)\sqrt{q^2}\frac{s_+\sqrt{s_-}}{\sqrt{6}m_{\Lambda^*}}, \\ H_+^{T5}(+1/2, -1/2) &= -H_-^{T5}(-1/2, +1/2) = f_\perp^{T5}(q^2)(m_{\Lambda_b} - m_{\Lambda^*})\frac{s_+\sqrt{s_-}}{\sqrt{3}m_{\Lambda^*}}, \\ H_+^{T5}(-1/2, -3/2) &= -H_-^{T5}(+1/2, +3/2) = -f_g^{T5}(q^2)\sqrt{s_-}. \end{aligned} \tag{5.41}$$

5.2.3 $\Lambda_b \to \Lambda^* \ell^+ \ell^-$ decay amplitudes

Considering the effective Hamiltonian Eq. (2.19) with only contributions from $\mathcal{C}_7, \mathcal{C}_{9\ell}, \mathcal{C}_{10\ell}$ and their chirality-flipped counterparts and neglecting the lepton mass, we obtain the following decomposition:

$$\mathcal{M}(s_{\Lambda_b}, s_{\Lambda^*}) \equiv N_1 \langle \Lambda^*(s_{\Lambda^*}) \ell^+ \ell^- | \sum_i \mathcal{C}_i \mathcal{O}_i | \Lambda_b(s_{\Lambda_b}) \rangle \tag{5.42}$$

$$\begin{aligned}\mathcal{M}(s_{\Lambda_b}, s_{\Lambda^*}) = \frac{N_1}{2} \Bigg\{ \sum_{L(R)} L^\mu_{L(R)} \\ \times \left[H^V_\mu \mathcal{C}^{L(R)}_{9,10,+} - H^A_\mu \mathcal{C}^{L(R)}_{9,10,-} - \frac{2m_b}{q^2} \left\{ H^T_\mu (\mathcal{C}_7 + \mathcal{C}_{7'}) + H^{T5}_\mu (\mathcal{C}_7 - \mathcal{C}_{7'}) \right\} \right] \Bigg\},\end{aligned} \tag{5.43}$$

where the leptonic and hadronic helicity amplitudes read

$$L^\mu_{L(R)} = \bar{u}(k_2, s_{\ell^-}) \gamma^\mu (1 \pm \gamma_5) v(k_1, s_{\ell^+}), \qquad H^X_\mu = \langle \Lambda^* | \bar{s} \Gamma^X_\mu b | \Lambda_b \rangle, \tag{5.44}$$

with the various Dirac matrices $\Gamma^{V(A)}_\mu = \gamma_\mu(\gamma_5)$ and $\Gamma^{T(T5)}_\mu = \sigma_{\mu\nu} q^\nu (\gamma_5)$. The combinations of Wilson coefficients are defined as

$$\mathcal{C}^{L(R)}_{9,10,+} = (\mathcal{C}_{9\ell} \mp \mathcal{C}_{10\ell}) + (\mathcal{C}_{9'\ell} \mp \mathcal{C}_{10'\ell}), \qquad \mathcal{C}^{L(R)}_{9,10,-} = (\mathcal{C}_{9\ell} \mp \mathcal{C}_{10\ell}) - (\mathcal{C}_{9'\ell} \mp \mathcal{C}_{10'\ell}), \tag{5.45}$$

and the normalization reads

$$N_1 = \frac{4 G_F}{\sqrt{2}} V_{tb} V^*_{ts} \frac{\alpha}{4\pi}. \tag{5.46}$$

We can perform the helicity amplitude decomposition discussed in Section 5.1.2, exploiting the expression of the hadronic helicity amplitudes in terms of the form factors described in Section 5.2 and using the explicit solutions of the Dirac equation in Appendix 5.A in order to determine the leptonic helicity amplitudes. The resulting expressions are given in Table 5.1, with the corresponding hadronic transversity amplitudes

$$\begin{aligned}
B^{L(R)}_{\perp 1} &= +\sqrt{2} N \left(\mathcal{C}^{L(R)}_{9,10,+} H^V_+(-1/2, -3/2) - \frac{2m_b (\mathcal{C}_7 + \mathcal{C}_{7'})}{q^2} H^T_+(-1/2, -3/2) \right), \\
B^{L(R)}_{\parallel 1} &= -\sqrt{2} N \left(\mathcal{C}^{L(R)}_{9,10,-} H^A_+(-1/2, -3/2) + \frac{2m_b (\mathcal{C}_7 - \mathcal{C}_{7'})}{q^2} H^{T5}_+(-1/2, -3/2) \right), \\
A^{L(R)}_{\perp 1} &= +\sqrt{2} N \left(\mathcal{C}^{L(R)}_{9,10,+} H^V_+(+1/2, -1/2) - \frac{2m_b (\mathcal{C}_7 + \mathcal{C}_{7'})}{q^2} H^T_+(+1/2, -1/2) \right), \\
A^{L(R)}_{\parallel 1} &= -\sqrt{2} N \left(\mathcal{C}^{L(R)}_{9,10,-} H^A_+(+1/2, -1/2) + \frac{2m_b (\mathcal{C}_7 - \mathcal{C}_{7'})}{q^2} H^{T5}_+(+1/2, -1/2) \right), \\
A^{L(R)}_{\perp 0} &= +\sqrt{2} N \left(\mathcal{C}^{L(R)}_{9,10,+} H^V_0(+1/2, +1/2) - \frac{2m_b (\mathcal{C}_7 + \mathcal{C}_{7'})}{q^2} H^T_0(+1/2, +1/2) \right), \\
A^{L(R)}_{\parallel 0} &= -\sqrt{2} N \left(\mathcal{C}^{L(R)}_{9,10,-} H^A_0(+1/2, +1/2) + \frac{2m_b (\mathcal{C}_7 - \mathcal{C}_{7'})}{q^2} H^{T5}_0(+1/2, +1/2) \right).
\end{aligned} \tag{5.47}$$

The normalisation factor N, related to the 4-body phase space of this decay, is defined as

$$N = N_1 \sqrt{\frac{q^2 \sqrt{\lambda(m^2_{\Lambda_b}, m^2_{\Lambda^*}, q^2)}}{3 \cdot 2^{10} m^3_{\Lambda_b} \pi^3}}. \tag{5.48}$$

We have used the relations Eqs. (5.34), (5.35) and (5.41)) in order to express H_- amplitudes in terms of H_+. We notice that there are no contributions from H_t here: the tensor hadronic amplitudes vanish exactly, whereas the vector/axial hadronic amplitudes are multiplied by the leptonic helicity amplitude $\epsilon^\mu(t) L_{\mu, L(R)}$ which are proportional to $m^2_\ell / \sqrt{q^2}$ (and neglected here) due to the lepton equation of motion.

5.2.4 $\Lambda^* \to N\bar{K}$ decay

The $\Lambda^* \to N\bar{K}$ decay rate[2] can be computed using

$$\Gamma(\Lambda^* \to N\bar{K}) = \frac{\beta_{N\bar{K}}}{16\pi m_{\Lambda^*}} |\overline{\mathcal{M}^{\Lambda^*}}|^2, \tag{5.49}$$

[2] We have not been specific whether we perform the sum over the two isospin states or select only one of them. This has no impact on the computation as long as the same definition is used for $\Lambda^* \to N\bar{K}$ and $\Lambda_b \to \Lambda^*(\to N\bar{K})\ell^+\ell^-$.

s_{Λ_b}	s_{Λ^*}	$\mathcal{M}$
$+\frac{1}{2}$	$+\frac{1}{2}$	$\frac{N_1}{2\sqrt{2}N}\sum_{L(R)}\left[A_{\perp 0}^{L(R)}+A_{\parallel 0}^{L(R)}\right]\bar{u}\not{\epsilon}(0)P_{L(R)}v$
$-\frac{1}{2}$	$-\frac{1}{2}$	$\frac{N_1}{2\sqrt{2}N}\sum_{L(R)}\left[A_{\perp 0}^{L(R)}-A_{\parallel 0}^{L(R)}\right]\bar{u}\not{\epsilon}(0)P_{L(R)}v$
$+\frac{1}{2}$	$-\frac{1}{2}$	$\frac{N_1}{2\sqrt{2}N}\sum_{L(R)}\left[A_{\perp 1}^{L(R)}+A_{\parallel 1}^{L(R)}\right]\bar{u}\not{\epsilon}(+)P_{L(R)}v$
$-\frac{1}{2}$	$+\frac{1}{2}$	$\frac{N_1}{2\sqrt{2}N}\sum_{L(R)}\left[A_{\perp 1}^{L(R)}-A_{\parallel 1}^{L(R)}\right]\bar{u}\not{\epsilon}(-)P_{L(R)}v$
$-\frac{1}{2}$	$-\frac{3}{2}$	$\frac{N_1}{2\sqrt{2}N}\sum_{L(R)}\left[B_{\perp 1}^{L(R)}+B_{\parallel 1}^{L(R)}\right]\bar{u}\not{\epsilon}(+)P_{L(R)}v$
$+\frac{1}{2}$	$+\frac{3}{2}$	$\frac{N_1}{2\sqrt{2}N}\sum_{L(R)}\left[B_{\perp 1}^{L(R)}-B_{\parallel 1}^{L(R)}\right]\bar{u}\not{\epsilon}(-)P_{L(R)}v$

Table 5.1: $\Lambda_b \to \Lambda^*\ell^+\ell^-$ decay amplitudes in terms of hadronic transversity amplitudes

We can consider either of the two interaction terms discussed in Section 5.1.3, corresponding to

$$\begin{aligned}\mathcal{M}_1^{\Lambda^*}(m,s) =& g m_{\Lambda^*} k_2^\mu \bar{u}^s \gamma_5 U_\mu^m,\\ \mathcal{M}_2^{\Lambda^*}(m,s) =& g\varepsilon^{\mu\nu\alpha\beta} k_\mu k_{2\beta} \bar{u}^s \gamma_\alpha U_\nu^m,\end{aligned} \tag{5.50}$$

These two alternative choices for the interaction terms describe the same physical decay for on-shell particles, and we checked explicitly that these two choices are equivalent and lead to the same final results in the following. From Eqs. (5.22) and (5.26), we see that the computation of the $\Lambda_b \to \Lambda^*(\to N\bar{K})\ell^+\ell^-$ decay rate will require the interference terms between matrix elements with different Λ^* polarisations, which can be defined as

$$\Gamma_2(s_{\Lambda^*}^a, s_{\Lambda^*}^b) \equiv \frac{\sqrt{r_+ r_-}}{16\pi m_{\Lambda^*}^3}\sum_{s_N}\mathcal{M}(s_{\Lambda^*}^a, s_N)\mathcal{M}(s_{\Lambda^*}^b, s_N)^*, \tag{5.51}$$

where $r_\pm = (m_{\Lambda^*}^2 \pm m_N^2) - m_{\bar{K}}^2$. The normalisation for Γ_2 in Eq. (5.51) comes from the phase space, which is present both in $\Lambda^* \to N\bar{K}$ and $\Lambda_b \to \Lambda^*(\to N\bar{K})\ell^+\ell^-$. This definition is such that the $\Lambda^* \to N\bar{K}$ decay reads

$$\Gamma(\Lambda^* \to N\bar{K}) = \sum_{s_{\Lambda^*}}\frac{\Gamma_2(s_{\Lambda^*}, s_{\Lambda^*})}{4}. \tag{5.52}$$

Using the explicit expression of the solutions in Appendix 5.A, we obtain

$$\Gamma_2 = \frac{3\mathcal{B}_{\Lambda^*}\Gamma_{\Lambda^*}}{2}\begin{pmatrix} \sin^2(\theta_p) & \frac{e^{-i\phi}\sin(2\theta_p)}{\sqrt{3}} & -\frac{e^{-2i\phi}\sin^2(\theta_p)}{\sqrt{3}} & 0 \\ \frac{e^{i\phi}\sin(2\theta_p)}{\sqrt{3}} & \frac{\cos(2\theta_p)}{2}+\frac{5}{6} & 0 & -\frac{e^{-2i\phi}\sin^2(\theta_p)}{\sqrt{3}} \\ -\frac{e^{2i\phi}\sin^2(\theta_p)}{\sqrt{3}} & 0 & \frac{\cos(2\theta_p)}{2}+\frac{5}{6} & -\frac{e^{-i\phi}\sin(2\theta_p)}{\sqrt{3}} \\ 0 & -\frac{e^{2i\phi}\sin^2(\theta_p)}{\sqrt{3}} & -\frac{e^{i\phi}\sin(2\theta_p)}{\sqrt{3}} & \sin^2(\theta_p) \end{pmatrix}, \tag{5.53}$$

with rows and columns corresponding to values of $s_a, s_b = -3/2, -1/2, 1/2, 3/2$. We denote $\mathcal{B}_{\Lambda^*} \equiv \mathcal{B}(\Lambda^* \to K^- p) = \mathcal{B}(\Lambda^* \to \bar{K}^0 n)$ and Γ_{Λ^*} is the inclusive decay width of the Λ^* baryon.

5.3 Phenomenology

5.3.1 Angular observables

Combining all the above elements, we obtain finally the differential decay rate

$$\begin{aligned} L(q^2,\theta_\ell,\theta_p,\phi) =& \frac{8\pi}{3}\frac{d^4\Gamma}{dq^2 d\cos\theta_\ell d\cos\theta_p d\phi} \\ =& \cos^2\theta_p\left(L_{1c}\cos\theta_\ell + L_{1cc}\cos^2\theta_\ell + L_{1ss}\sin^2\theta_\ell\right) \\ &+ \sin^2\theta_p\left(L_{2c}\cos\theta_\ell + L_{2cc}\cos^2\theta_\ell + L_{2ss}\sin^2\theta_\ell\right) \\ &+ \sin^2\theta_p\left(L_{3ss}\sin^2\theta_\ell\cos^2\phi + L_{4ss}\sin^2\theta_\ell\sin\phi\cos\phi\right) \\ &+ \sin\theta_p\cos\theta_p\cos\phi(L_{5s}\sin\theta_\ell + L_{5sc}\sin\theta_\ell\cos\theta_\ell) \\ &+ \sin\theta_p\cos\theta_p\sin\phi(L_{6s}\sin\theta_\ell + L_{6sc}\sin\theta_\ell\cos\theta_\ell), \end{aligned} \tag{5.54}$$

with the angular coefficients L that are interferences between the various helicity amplitudes defined in Table 5.1:

$$\begin{aligned} L_{1c} =& -2\mathcal{B}_{\Lambda^*}\left(\mathrm{Re}(A^L_{\perp 1}A^{L*}_{\parallel 1}) - (L\leftrightarrow R)\right), \\ L_{1cc} =& \mathcal{B}_{\Lambda^*}\left(\left|A^L_{\parallel 1}\right|^2 + \left|A^L_{\perp 1}\right|^2 + (L\leftrightarrow R)\right), \\ L_{1ss} =& \frac{1}{2}\mathcal{B}_{\Lambda^*}\left(2\left|A^L_{\parallel 0}\right|^2 + 2\left|A^L_{\perp 0}\right|^2 + \left|A^L_{\parallel 1}\right|^2 + \left|A^L_{\perp 1}\right|^2 + (L\leftrightarrow R)\right), \\ L_{2c} =& -\frac{1}{2}\mathcal{B}_{\Lambda^*}\left(\mathrm{Re}(A^L_{\perp 1}A^{L*}_{\parallel 1}) + 3\mathrm{Re}(B^L_{\perp 1}B^{L*}_{\parallel 1}) - (L\leftrightarrow R)\right), \\ L_{2cc} =& \frac{1}{4}\mathcal{B}_{\Lambda^*}\left(\left|A^L_{\parallel 1}\right|^2 + \left|A^L_{\perp 1}\right|^2 + 3\left|B^L_{\parallel 1}\right|^2 + 3\left|B^L_{\perp 1}\right|^2 + (L\leftrightarrow R)\right), \\ L_{2ss} =& \frac{1}{8}\mathcal{B}_{\Lambda^*}\Big[2\left|A^L_{\parallel 0}\right|^2 + \left|A^L_{\parallel 1}\right|^2 + 2\left|A^L_{\perp 0}\right|^2 + \left|A^L_{\perp 1}\right|^2 + 3\left|B^L_{\parallel 1}\right|^2 + 3\left|B^L_{\perp 1}\right|^2 \\ & -2\sqrt{3}\mathrm{Re}(B^L_{\parallel 1}A^{L*}_{\parallel 1}) + 2\sqrt{3}\mathrm{Re}(B^L_{\perp 1}A^{L*}_{\perp 1}) + (L\leftrightarrow R)\Big], \\ L_{3ss} =& \frac{\sqrt{3}}{2}\mathcal{B}_{\Lambda^*}\left(\mathrm{Re}(B^L_{\parallel 1}A^{L*}_{\parallel 1}) - \mathrm{Re}(B^L_{\perp 1}A^{L*}_{\perp 1}) + (L\leftrightarrow R)\right), \\ L_{4ss} =& \frac{\sqrt{3}}{2}\mathcal{B}_{\Lambda^*}\left(\mathrm{Im}(B^L_{\perp 1}A^{L*}_{\parallel 1}) - \mathrm{Im}(B^L_{\parallel 1}A^{L*}_{\perp 1}) + (L\leftrightarrow R)\right), \\ L_{5s} =& \sqrt{\frac{3}{2}}\mathcal{B}_{\Lambda^*}\left(\mathrm{Re}(B^L_{\perp 1}A^{L*}_{\parallel 0}) - \mathrm{Re}(B^L_{\parallel 1}A^{L*}_{\perp 0}) - (L\leftrightarrow R)\right), \\ L_{5sc} =& \sqrt{\frac{3}{2}}\mathcal{B}_{\Lambda^*}\left(-\mathrm{Re}(B^L_{\parallel 1}A^{L*}_{\parallel 0}) + \mathrm{Re}(B^L_{\perp 1}A^{L*}_{\perp 0}) + (L\leftrightarrow R)\right), \\ L_{6s} =& \sqrt{\frac{3}{2}}\mathcal{B}_{\Lambda^*}\left(\mathrm{Im}(B^L_{\parallel 1}A^{L*}_{\parallel 0}) - \mathrm{Im}(B^L_{\perp 1}A^{L*}_{\perp 0}) - (L\leftrightarrow R)\right), \\ L_{6sc} =& -\sqrt{\frac{3}{2}}\mathcal{B}_{\Lambda^*}\left(\mathrm{Im}(B^L_{\perp 1}A^{L*}_{\parallel 0}) - \mathrm{Im}(B^L_{\parallel 1}A^{L*}_{\perp 0}) + (L\leftrightarrow R)\right), \end{aligned} \tag{5.55}$$

where we have neglected the lepton masses[3]. The expressions including the lepton mass can be found in Ref. [336]. The corresponding CP-conjugate mode will involve $\bar{A}$ and $\bar{B}$ amplitudes, where only the weak phases are taken to their opposite, as already discussed in Section 5.1.1.

We provide further cross-checks of these expressions in Appendix 5.B by comparing our results with general expectations from the partial-wave analysis of four-body $b\to s\ell^+\ell^-$ decays [321], and in Appendix 5.C by checking the agreement with the expressions for $\Lambda_b\to\Lambda^*(\to KN)\gamma$ [310, 311].

5.3.2 Derived observables

One can define derived observables using a particular weight ω to integrate the differential decay rate over the whole phase space

$$X[\omega](q^2) \equiv \int \frac{d^4\Gamma}{dq^2 d\cos\theta_\ell d\cos\theta_p d\phi}\omega(q^2,\theta_\ell,\theta_p,\phi)d\cos\theta_\ell d\cos\theta_p d\phi. \tag{5.56}$$

[3] In the framework we consider this angular coefficient are not linearly independent: $L_{2ss} = L_{1ss}/4 + L_{2cc}/2 - L_{1cc}/8 - L_{3ss}/2$

The differential decay width is

$$\begin{aligned}\frac{d\Gamma}{dq^2} &= X[1] = \frac{1}{3}[L_{1cc} + 2L_{1ss} + 2L_{2cc} + 4L_{2ss} + 2L_{3ss}] \\ &= |A^L_{||0}|^2 + |A^L_{\perp 0}|^2 + |A^L_{||1}|^2 + |A^L_{\perp 1}|^2 + |B^L_{||1}|^2 + |B^L_{\perp 1}|^2 + (L \leftrightarrow R),\end{aligned} \tag{5.57}$$

which we can use to normalise the CP-averaged angular observables and the corresponding CP-asymmetries

$$S_i = \frac{L_i + \bar{L}_i}{d(\Gamma + \bar{\Gamma})/dq^2}, \qquad A_i = \frac{L_i - \bar{L}_i}{d(\Gamma + \bar{\Gamma})/dq^2}. \tag{5.58}$$

One can similarly define the transverse and longitudinal polarization of the dilepton system [197]

$$\begin{aligned}F_1 =& X\left[\frac{5\cos\theta_\ell^2 - 1}{d\Gamma/dq^2}\right] = \frac{2(L_{1cc} + 2L_{2cc})}{L_{1cc} + 2(L_{1ss} + L_{2cc} + 2L_{2ss} + L_{3ss})}, \\ F_0 =& 1 - F_1 = 1 - \frac{2(L_{1cc} + 2L_{2cc})}{L_{1cc} + 2(L_{1ss} + L_{2cc} + 2L_{2ss} + L_{3ss})}.\end{aligned} \tag{5.59}$$

One can also define a forward-backward asymmetry with respect to the leptonic scattering angle normalised to the differential rate

$$A^\ell_{FB} = X\left[\frac{\text{sgn}[\cos\theta_\ell]}{d\Gamma/dq^2}\right] = \frac{3(L_{1c} + 2L_{2c})}{2(L_{1cc} + 2(L_{1ss} + L_{2cc} + 2L_{2ss} + L_{3ss}))}. \tag{5.60}$$

Due to the strong decay of the Λ^*, it is no surprise that the analogous asymmetries for the hadronic system vanish

$$A^{\Lambda^*}_{FB} = X\left[\frac{\text{sgn}[\cos\theta_p]}{d\Gamma/dq^2}\right] = 0, \qquad A^{\ell\Lambda^*}_{FB} = X\left[\frac{\text{sgn}[\cos\theta_p\cos\theta_\ell]}{d\Gamma/dq^2}\right] = 0. \tag{5.61}$$

5.3.3 Low- and large-recoil limits

As seen before, the description of this decay involves 8 vector/axial form factors and 6 tensor form factors. This large number of (poorly known) form factors could be tackled by taking the heavy-quark limit $m_b \to \infty$. Two different kinematic situations can be considered: either the outgoing Λ^* baryon is soft (low-recoil limit), where HQET can be applied (see Section 2.5.1), or it is energetic (large-recoil limit), where SCET can be applied Section 2.5.2.

In the low-recoil limit, one can use the heavy-baryon velocity $v^\mu = p^\mu/m_{\Lambda_b}$ to project the the b-quark field onto its large-spinor component $h_v = \not{v} h_v$:

$$\langle \Lambda^*|\bar{s}\Gamma b|\Lambda_b\rangle \to \bar{u}^\alpha_{\Lambda^*} v_\alpha [\zeta_1 + \not{v}\zeta_2]\Gamma u_{\Lambda_b}, \tag{5.62}$$

where Γ is any Dirac matrix, ζ_1 and ζ_2 are the only two form factors that should be present at leading order in α_s and Λ_{QCD}/m_b according to HQET [337]. These two form factors are functions of q^2 or equivalently $v \cdot v'$ (where $v' = k/m_{\Lambda^*}$ is the velocity of the light baryon). We can take the heavy-quark limit (neglecting Λ_{QCD}/m_b contributions) in the definition of the form factors Eqs. (5.27) and (5.36) and identify the results with Eq. (5.62). This is performed (with slightly different definitions of the form factors) in Refs. [40, 197, 338], and the corresponding expressions yield at low recoil:

$$\begin{aligned}f_\perp^V = f_0^V = f_t^A = f_\perp^T = f_0^T =& (\zeta_1 - \zeta_2)/m_{\Lambda_b}, \\ f_\perp^A = f_0^A = f_t^V = f_\perp^{T5} = f_0^{T5} =& (\zeta_1 + \zeta_2)/m_{\Lambda_b}, \\ f_g^V = f_g^A = f_g^T = f_g^{T5} =& 0.\end{aligned} \tag{5.63}$$

It is also possible to perform a similar analysis in the large-recoil limit where SCET holds. Following Refs. [40, 197, 338], one can see that the SCET analysis yields:

$$\langle \Lambda^*|\bar{s}\Gamma b|\Lambda_b\rangle \to \xi \bar{u}^\alpha_{\Lambda^*} v_\alpha \Gamma u_{\Lambda_b}, \tag{5.64}$$

where Γ is any Dirac matrix, ξ is the only form factor that should be present at leading order in α_s and Λ_{QCD}/m_b according to SCET. These form factors are functions of q^2 or equivalently $n_+ \cdot k$ (where n_+ is a light-like vector orthogonal to k). One can see that formally, the expression for SCET Eq. (5.64) will be obtained from the HQET expression Eq. (5.62) by identifying ζ_1 to ξ and setting ζ_2 to 0, leading to the equality at large recoil:

$$f_t^V = f_\perp^V = f_0^V = f_t^A = f_\perp^A = f_0^A = f_\perp^T = f_0^T = f_\perp^{T5} = f_0^{T5} = \xi/m_{\Lambda_b}, \tag{5.65}$$

whereas all f_g form factors vanish also in the large-recoil limit.

The methods used in Refs. [40, 338] could be used to analyse higher-order corrections to these relations (in powers of α_s and $\Lambda_{\rm QCD}/m_b$) but this is out of the scope of the present work. From Eq. (5.47), we see that all the hadronic amplitudes $A_\perp$ involve $\zeta_1 - \zeta_2$, whereas $A_{||}$ involve $\zeta_1 + \zeta_2$. All $B_\perp$ and $B_{||}$ amplitudes, corresponding to transitions to a Λ^* with helicity 3/2, vanish in both limits because they only depend on f_g form factors. In simple words, the heavy-quark limit allows one to consider the angular momentum of the heavy-quark b and that of the light quarks as good quantum numbers to describe the Λ_b state and its transitions. Since the light quarks are in a spin-0 diquark state and the heavy quark carries a spin 1/2, the $b \to s\ell^+\ell^-$ transition can never yield a Λ with a helicity 3/2 in this limit [40, 337].

Using the equalities in Eq. (5.63) (which are also compatible with the equalities in Eq. (5.65)), we obtain

$$\begin{aligned} L_{1c} &\to \alpha(\zeta_1^2 - \zeta_2^2), & L_{2c} &\to \frac{1}{4}L_{1c}, \\ L_{1cc} &\to \alpha'(\zeta_1 - \zeta_2)^2 + \beta'(\zeta_1 + \zeta_2)^2, & L_{2cc} &\to \frac{1}{4}L_{1cc}, \\ L_{1ss} &\to \alpha''(\zeta_1 - \zeta_2)^2 + \beta''(\zeta_1 + \zeta_2)^2, & L_{2ss} &\to \frac{1}{4}L_{1ss}, \end{aligned} \tag{5.66}$$

whereas the rest of the angular observables ($L_{3ss}, L_{4ss}, L_{5s}, L_{5sc}, L_{6s}, L_{6sc}$) vanishes. The α and β coefficients combine Wilson coefficients and kinematic factors. Considering the relations in Eq. (5.66), we can see that we cannot build in a straightforward manner optimised observables similar to the $B \to K^*\ell^+\ell^-$ channel [87, 214] where the form factors will cancel out and non-trivial information on the Wilson coefficients can be obtained (up to $\Lambda_{\rm QCD}/m_b$ and α_s corrections).

In the case of the large-recoil limit, the three independent observables L_{1c}, L_{1cc}, L_{1ss} only depend on ξ. Then the uncertainties coming from the form factors of any ratio of these observables are suppressed by $\Lambda_{\rm QCD}/m_b$. In both HQET and SCET limits, the angular distribution simplifies substantially

$$\frac{8\pi}{3}\frac{d^4\Gamma}{dq^2 d\cos\theta_\ell d\cos\theta_p d\phi} \simeq \frac{1}{4}(1 + 3\cos^2\theta_p)\left(L_{1c}\cos\theta_\ell + L_{1cc}\cos^2\theta_\ell + L_{1ss}\sin^2\theta_\ell\right), \tag{5.67}$$

where all three angular observables are independent. The forward-backward asymmetry becomes:

$$A_{FB}^\ell \simeq \frac{3L_{1c}}{2(L_{1cc} + 2L_{1ss})}. \tag{5.68}$$

In these limits, we notice that the angular distribution Eq. (5.67) factorises into the product of two terms, leaving only a trivial dependence on the angle describing the hadronic final state but a non trivial dependence on the angle describing the leptonic final state.

This discussion leads us not to consider further the possibility of optimised observables and to focus on the normalised CP-averaged angular observables S.

5.4 Numerical Results

We consider now numerical results for the various angular coefficients described above. This should be considered as a preliminary study, as we are going to make several simplifications that should be reassessed carefully if one wants to provide accurate predictions for this decay. We focus on the muon case ($\ell = \mu$ in the following) and on the contributions coming from $\mathcal{O}_{7,9,10,7',9',10'}$.

5.4.1 Form factors

A complete analysis would require a precise knowledge of the 14 form factors described in Section 5.2 and their correlations. A lattice determination of the form factors currently exist, but it is constrained to the high-q^2 region (see Ref. [314]). Several efforts are currently under development to obtain a determination over the full, or at least a larger, q^2 range. On one side, lattice form factors could be extended to a lower q^2 region through the use of the moving-NRQCD action [314, 339]. Also these form factors have been studied further in the HQET limit in Refs. [336, 340] finding some tension in between the lattice determinations in the low-recoil region and the heavy quark expansion based predictions.

Since the full q^2 range results are not available yet, we will present a numerical illustration based on the MCN quark model of Ref. [42], in order to get an idea of the sensitivity of the angular coefficients to different NP scenarios. The form factors obtained through the MCN quark model are shown in Fig. 5.6 in the basis chosen in Sections 5.2.1 and 5.2.2. A comparison between the MCN model and the lattice QCD determination [314] in

the high q^2 region is shown in Fig. 5.5. While they do not perfectly agree, they show reasonable agreement on the q^2 dependence and on the order of magnitude. Let us add that the results of Ref. [42] obey rather well the HQET relations Eq. (5.63), but do not follow the SCET expectations very well Eq. (5.65).

Due to the lack of accurate estimates of the uncertainties for the various hadronic inputs, we present only a very crude estimate of the uncertainties, assuming uncorrelated 10% uncertainties for the $f_{0,\perp,t}$ form factors and uncorrelated 30% uncertainties for the f_g form factors.

5.4.2 Non-local charm-loop contributions

It is important that the contributions of non-leptonic operators, discussed in Section 2.7, are taken into account. Between these, the long-distance contributions of the charm loops are specially difficult to estimate. Contrary to $B \to K^{(*)}\ell^+\ell^-$ decays, where several estimates based on different theoretical approaches are available [109, 112, 115, 116, 126, 205, 292, 317], non-local contributions to baryonic modes are yet to be estimated. They could be tackled by data-driven methods similar to Refs. [112, 317], involving light-cone sum rules similar to Refs. [40, 109, 115, 116, 318], although this is not as simple as extending the results on the meson side, since new issues appear on these modes [341]. On one side, hard spectator interactions have not yet been computed for these modes, and on the other side, baryon LCDA, which start at 3-particle LCDA, are not as well understood as meson LCDA [40].

Since this is a preliminary study, we will content ourselves with obtaining a rough estimate of the size of these contributions. Focusing on the large recoil region first, we will consider an estimate for the charmonium contribution inspired by estimates for $B \to K^{(*)}\ell^+\ell^-$ [109, 112, 115, 116, 205] at large recoil. Their results suggest a contribution of order 10% of $\mathcal{C}_9$ with a moderate dependence on q^2 in the large-recoil region. For instance, in the estimate from light-cone sum-rules of Ref. [116] for $B \to K\ell^+\ell^-$ within $[1, 6]$ GeV^2 , the range of variation remains within:

$$\text{LCSR contrib. for } q^2 \in [1,6]\ \text{GeV}^2 : \text{Re}\ \mathcal{C}_9^{c\bar{c}} = -0.26 \pm 0.10\,, \qquad \text{Im}\ \mathcal{C}_9^{c\bar{c}} = -0.49 \pm 0.27\,. \tag{5.69}$$

These results are similar in size ($\simeq 10\%$) to the expected impact of charmonium resonances at low K-recoil of a few percent based on quark-hadron duality [113]. They are also in line with the dimensional estimates based on the $1/m_b$ suppression of these contributions. These results can be compared with the results obtained by considering only the perturbative part of the $c\bar{c}$ contribution in Eq. (2.83), for instance

$$\begin{aligned} \text{Perturbative contrib. at } q^2 = 1\ \text{GeV}^2 &: \text{Re}\ \mathcal{C}_9^{c\bar{c}} = 0.16, \qquad \text{Im}\ \mathcal{C}_9^{c\bar{c}} = 0.17\,. \\ q^2 = 6\ \text{GeV}^2 &: \text{Re}\ \mathcal{C}_9^{c\bar{c}} = 0.11, \qquad \text{Im}\ \mathcal{C}_9^{c\bar{c}} = 0.17\,. \end{aligned} \tag{5.70}$$

to which we do not attempt to assign a meaningful theoretical uncertainty.

We will thus consider two different approaches,

- An estimate for the SM value of $\mathcal{C}_9$ including the effect of $c\bar{c}$ resonances both at low- and large-recoil:

$$\text{Our estimate}: \ \mathcal{C}_9^{\text{SM}} = \mathcal{C}_9^{\mathcal{H}_{\text{eff}}}(1 + \rho e^{i\phi})\,, \qquad \rho \in [0, 0.1]\,, \qquad \phi \in [0, 2\pi]\,, \tag{5.71}$$

  where $\mathcal{C}_9^{\mathcal{H}_{\text{eff}}}$ corresponds to the Wilson coefficient appearing in Eq. (2.35).

- And a purely perturbative approach where we consider only the factorisable quark-loop contributions including them into the effective Wilson coefficients $\mathcal{C}_7^{\text{eff}}$ and $\mathcal{C}_9^{\text{eff}}(q^2)$ [38, 111] introduced in Eqs. (2.81) and (2.83). This means that we take into account only the charm-loop contributions derived from perturbation theory (taking $m_c = 1.3$ GeV for illustration).

We consider both of these approaches as the first one allows us to estimate the size of theoretical uncertainties and the second one corresponds to the information currently available for the $\Lambda_b \to \Lambda^*\ell^+\ell^-$ decay. Admittedly, this first proposal is only a rough attempt at obtaining at estimating this effect, as it includes no dependence on q^2 nor on the spins of the baryons and its size is guesstimated. However, since no better estimates are yet available, we will content ourselves with this order-of-magnitude estimation of the size of these contributions. Obviously, non of these models hold in the charmonium resonance region, where the $c\bar{c}$ pair becomes resonant and yields contributions that are much larger [114].

An extension of the long distance contribution estimates to the $\Lambda_b \to \Lambda^*(\to pK^-)\ell^+\ell^-$ decay would be highly commendable and it will be needed in the future once measurements are available and can be interpreted within an effective theory approach, but it is clearly out of the scope of the present study. This said, since we want to discuss the potential of experimental measurements, we need to consider at least a rough estimate of the main theoretical uncertainties.

Taking all of this into consideration, the first approach is used in Section 5.5, Table 5.2, and Figs. 5.11 to 5.13 where we try to asses the possible sensitivity of a future study by LHCb and the second approach is used in Figs. 5.7 to 5.10 where we content ourselves with the information currently available for baryonic decays.

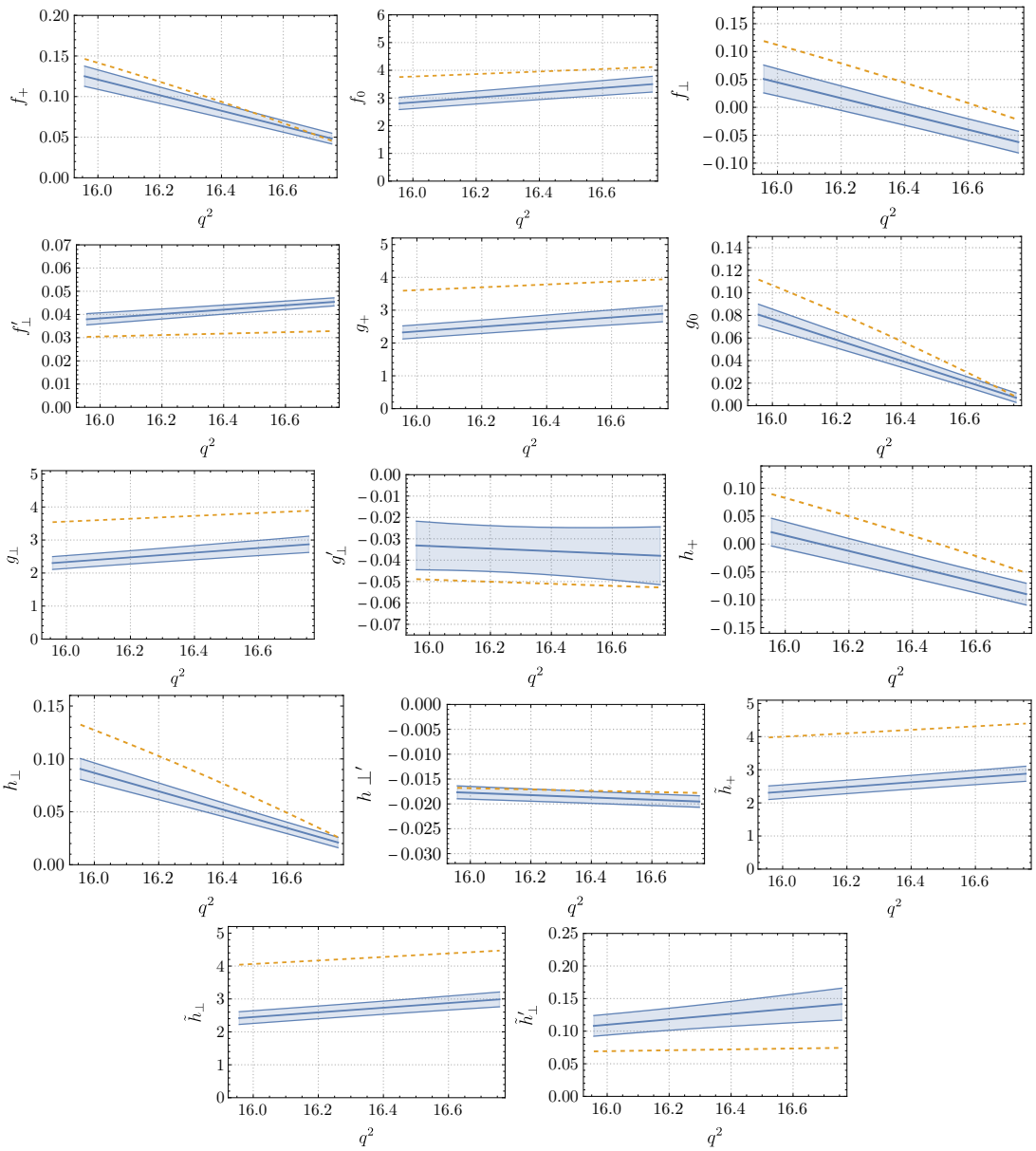

Figure 5.5: Comparison between the MCN model determination [42] and the lattice QCD determination [314] for the form factors of the $\Lambda_b \to \Lambda^*$ transition. For easy comparison, the form factors are shown in the basis of Ref. [314] where the endpoint divergences are removed. The equivalence to the form factors defined in Sections 5.2.1 and 5.2.2 and used throughout this chapter can be found in Appendix A.2 of Ref. [314].

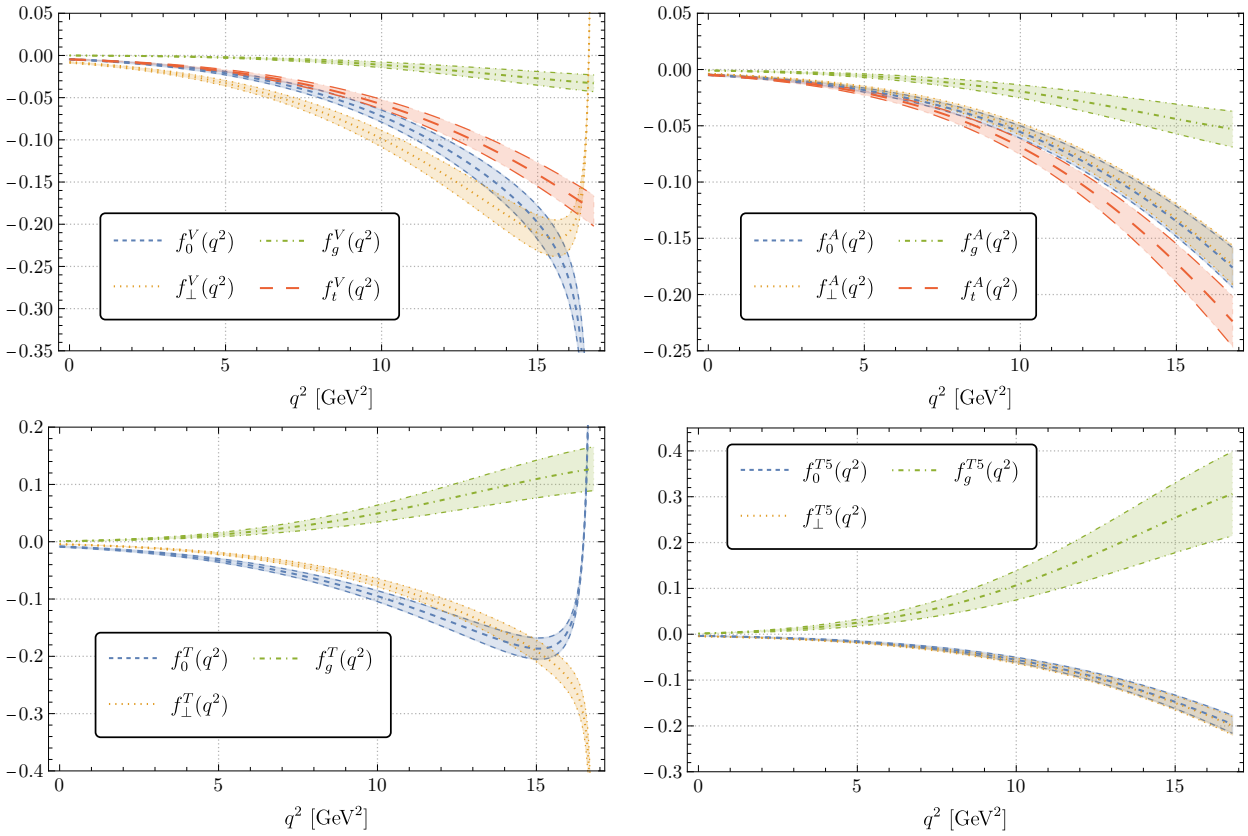

Figure 5.6: Form factors for $\Lambda_b \to \Lambda^*$ on the basis introduced in Sections 5.2.1 and 5.2.2 as a function of q^2 coming from the MCN quark model of Ref. [42]. The vector (axial) form factors are shown on the top left (right), and the tensor (pseudotensor) form factors are shown on the bottom left (right). As an illustration, a 10% uncertainty is considered for all form factors except for f_g where a 30% uncertainty is considered.

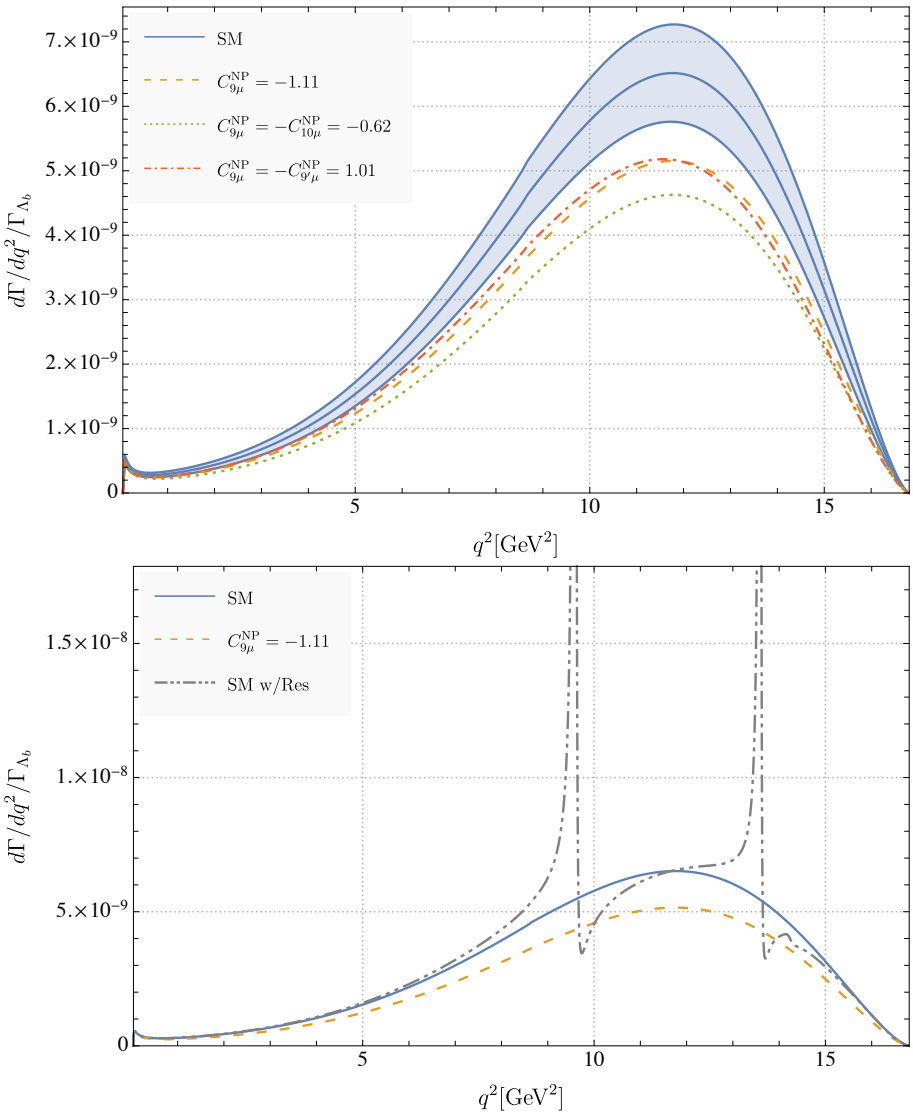

Figure 5.7: Top: Differential decay rate (normalised to the total Λ_b decay width) in the SM case and three NP scenarios. Only short-distance contributions from charm loops are included. Bottom: For illustration only, we also show the effect of a model for charmonium resonances in the SM case [42].

5.4.3 Numerical illustrations

First we show the differential decay rate (normalised to the total Λ_b decay width) and the lepton forward-backward asymmetry as functions of the dilepton invariant mass in Figs. 5.7 and 5.8 in the context of the SM and several NP models inspired by the global fit to $b \to s\ell^+\ell^-$ transitions discussed in Chapter 4: $\mathcal{C}_{9\mu}^{\rm NP} = -1.11$, $\mathcal{C}_{9\mu}^{\rm NP} = -\mathcal{C}_{9'\mu}^{\rm NP} = -0.62$, $\mathcal{C}_{9\mu}^{\rm NP} = -\mathcal{C}_{10\mu}^{\rm NP} = -0.62$. We see that the normalisation of the branching ratio is significantly affected by the presence of NP, while keeping a similar shape in all cases. The lepton forward-backward asymmetry exhibits a zero at large recoil whose position depends on the scenario considered. The mild kink at $q^2 = 4m_c^2$ corresponds to the opening of the $c\bar{c}$ threshold, appearing at the perturbative level as an imaginary part in $\mathcal{C}_9^{\rm eff}(q^2)$ for $q^2 \geq 4m_c^2$.

The corresponding error bar for each observable is shown in the case of the SM predictions, but it is a rather conservative error, as we do not take into account the fact that the various form factors are significantly correlated, as illustrated in both HQET and SCET limits. In order to keep our figures simple to read, we do not show the uncertainties for the various NP models, which are of the same order as in the SM case (see Section 5.5 for more discussion of the uncertainties).

For illustrative purposes, we also show the impact of a naive model of charmonium resonances in the SM case [42], confirming that the impact of charm loops remains quite small below 8 GeV^2 in general, and that the lepton forward-backward asymmetry is much less affected as soon as the resonance region is left. In Figs. 5.7 and 5.8, the window at low recoil between the $\psi(2S)$ resonance (above 15 GeV^2) and the endpoint is rather

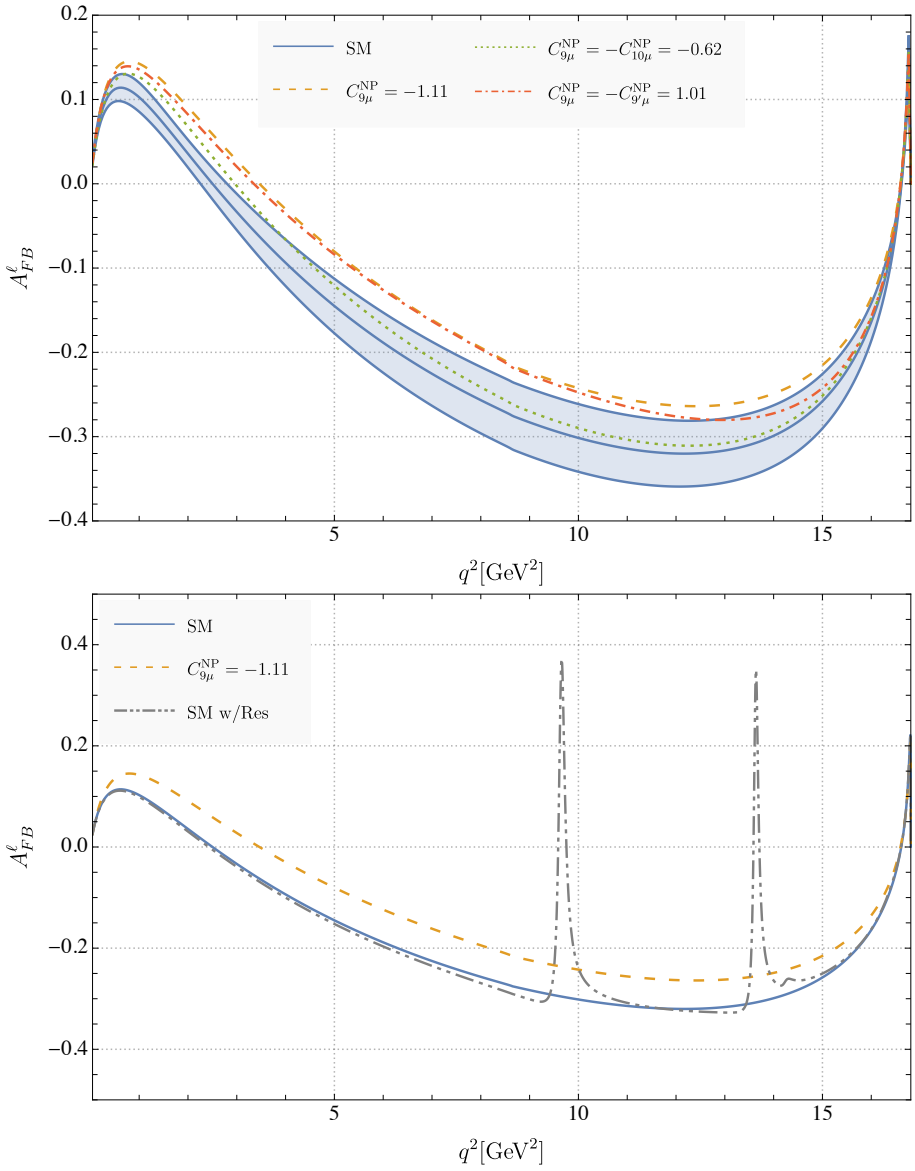

Figure 5.8: Top: A_{FB}^{ℓ} in the SM case and three NP scenarios. Only short-distance contributions from charm loops are include. Bottom: For illustration only, we also show the effect of a model for charmonium resonances in the SM case [42].

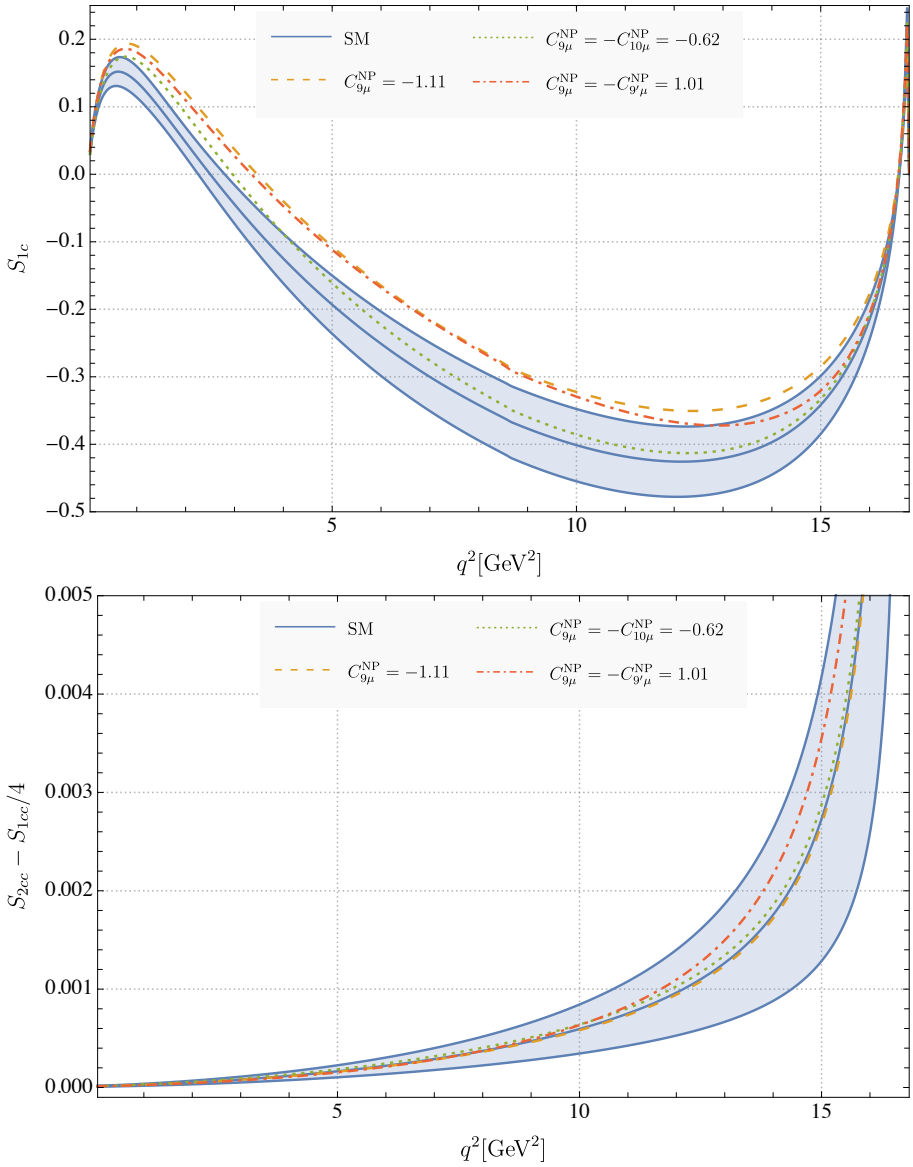

Figure 5.9: Variation of S_{1c} (top) and $S_{2cc} - S_{1cc}/4$ (bottom) with respect to the dilepton invariant mass, in the case of the SM and three NP scenarios.

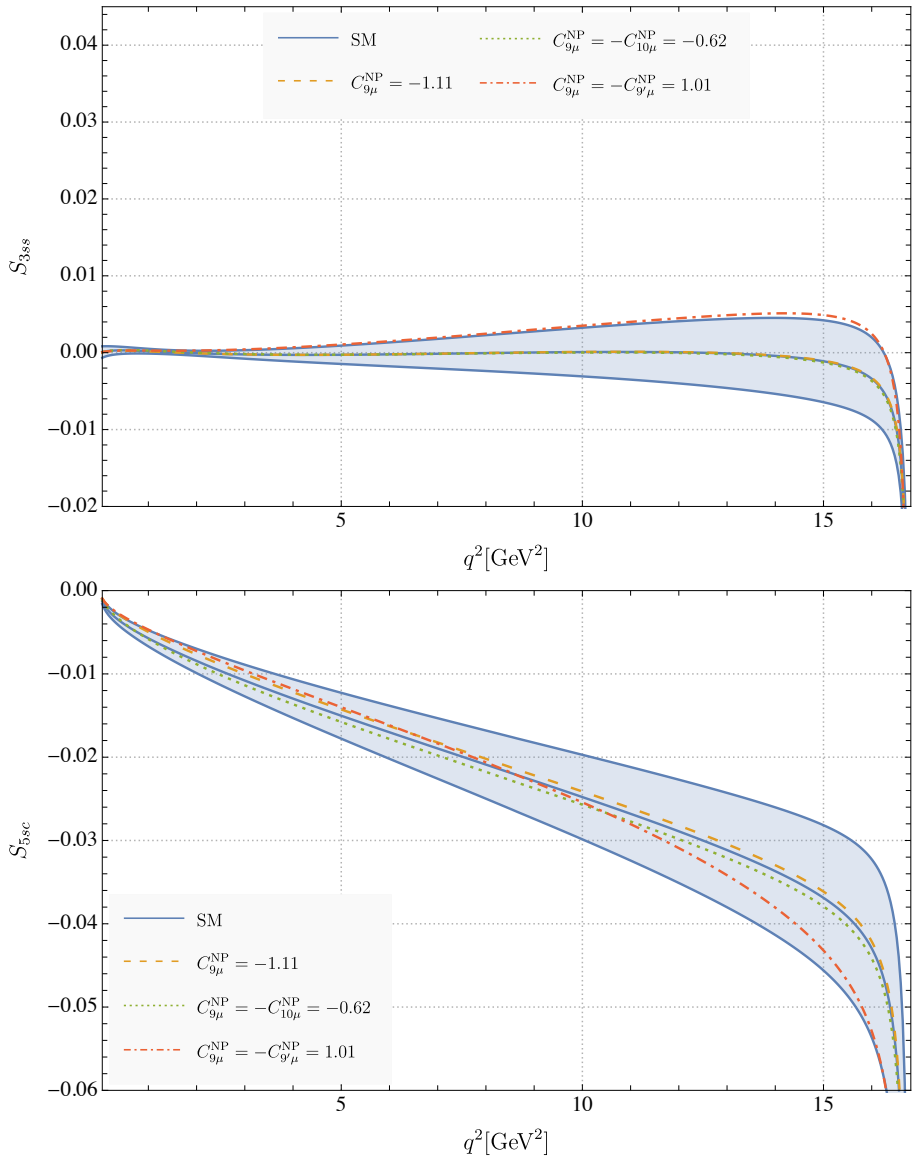

Figure 5.10: Variation of S_{3ss} (top) and S_{5sc} (bottom) with respect to the dilepton invariant mass, in the case of the SM and three NP models.

small, which may affect the application of quark-hadron duality. In the large-recoil region, the main issue is related to non-local contributions from charm loops, which may affect significantly the decay rate but cancels mostly in the lepton forward-backward asymmetry.

We now move to the normalised angular coefficients defined in Eq. (5.58). We do not consider the CP-asymmetries A, or the rates S which involve the imaginary part of the products of amplitudes, as these quantities are very dependent on assumptions about the phase of these amplitudes, and in particular the charm-loop contributions. We show the most interesting remaining observables in Figs. 5.9 and 5.10. We see that these normalised angular coefficients are sensitive to the scenario with right-handed contributions $\mathcal{C}_{9\mu}^{\rm NP} = -\mathcal{C}_{9'\mu}^{\rm NP}$, but the sensitivity is more limited for scenarios with NP contributions in $\mathcal{C}_{9\mu}^{\rm NP}$ only or in $\mathcal{C}_{9\mu}^{\rm NP} = -\mathcal{C}_{10\mu}^{\rm NP}$. S_{1c} exhibits some sensitivity to these scenarios, with a q^2-dependence very similar to A_{FB}^{ℓ} (the two quantities are actually identical in both HQET and SCET limits).

As expected from HQET and SCET expectations, the form factors f_g do not contribute much to the amplitudes apart from the vicinity of the low-recoil endpoint. In particular, B is small compared to the amplitudes A, which explains that most of the angular coefficients have a very similar behaviour, see Eq. (5.66). Moreover, in the SM and in the NP models with no right-handed currents (NP in $\mathcal{C}_{9\mu}^{\rm NP}$ only or in $\mathcal{C}_{10\mu}^{\rm NP} = -\mathcal{C}_{9\mu}^{\rm NP}$), the four dominant amplitudes A are the left-handed ones ($A_{\perp,\parallel}^{L}$), with contributions all proportional to $\mathcal{C}_{9,10,\pm}^{L} = \mathcal{C}_{9\mu} - \mathcal{C}_{10\mu}$. These contributions are all modified in the same proportion in the presence of NP in $\mathcal{C}_{9\mu}$ and/or $\mathcal{C}_{10\mu}$. The dependence on the Wilson coefficients cancels out between the numerator and the denominator of the normalised angular coefficients S_i, which have thus the same q^2-dependence for all these scenarios, as can be seen in Figs. 5.9 and 5.10. This conclusion holds for most of the physical domain, apart from a region at very small q^2 where the photon pole is dominant. Subdominant variations related to the interference between the left-handed contribution $\mathcal{C}_{9,10,\pm}^{L}$ and the other amplitudes (photon pole $\mathcal{C}_7 \pm \mathcal{C}_{7'}$, right-handed contributions $\mathcal{C}_{9,10,\pm}^{R}$) can be seen for S_{1c} and S_{5sc} at large recoil.

On the other hand, the scenario with right-handed contributions $\mathcal{C}_{9\mu}^{\rm NP} = -\mathcal{C}_{9'\mu}^{\rm NP}$ will affect differently $\mathcal{C}_{9,10,+}^{L}$ and $\mathcal{C}_{9,10,+}^{R}$, which are the dominant contributions in the normalised angular coefficients. It is thus not surprising that the q^2-dependence of these coefficients is rather different for this NP scenario with right-handed couplings, as can be seen from the curves in Figs. 5.9 and 5.10 that differ significantly from the SM case.

At the low-recoil endpoint for $q^2 \to (m_{\Lambda_b} - m_{\Lambda^*})^2$, the situation is slightly different and it depends on the behaviour of the form factors. In this region, the model of form factors in Ref. [42] is less singular than requested from Eqs. (5.31) and (5.38). By inspecting Eqs. (5.34), (5.35), (5.41) and (5.47), one can see that only the contributions from f_g^V and f_g^T form factors survive in the various helicity amplitudes, so that the angular coefficients $L_{1c}, L_{2c}, L_{4ss}, L_{5s}, L_{6sc}$ vanish. If we neglect the (very small) contribution from the photon pole (i.e. we take $\mathcal{C}_7, \mathcal{C}_{7'} \to 0$), we obtain the following results for the other observables at the low-recoil endpoint

$$S_{1c} \to 0, \qquad S_{2cc} - S_{1cc}/4 \to 3/8, \qquad S_{3ss} \to -1/4, \qquad S_{5sc} \to -1/2. \tag{5.72}$$

Apart from S_{1c} which vanishes, these values are significantly larger than those obtained over the rest of the physical region. Indeed, as f_g^V and f_g^T are the only non-vanishing contributions, the normalised differential decay rate $d\Gamma/dq^2/N$ (with N defined in Eq. (5.48)) becomes smaller by several orders of magnitudes when $q^2 \to (m_{\Lambda_b} - m_{\Lambda^*})^2$ and enhances the values of $S_{2cc} - S_{1cc}/4$, S_{3ss} and S_{5sc} at that endpoint compared to the rest of the physical range for the dilepton invariant mass.

5.4.4 Comments

Our study is of course very preliminary and should be refined in several ways in order to provide accurate predictions beyond this exploratory work: we have no inputs on the form factors determined from lattice simulations or light-cone sum rules, we have included no correlations among the uncertainties on these form factors even though they are correlated in both SCET and HQET limits. Moreover, we do not attempt a proper assessment of the charmonium contribution. All these issues should be discussed before drawing definite conclusions concerning the sensitivity of these observables to NP contributions. However subsequent studies of this mode [336, 340, 342] have confirmed our expressions and started to work towards a more complete description of this decay.

In Section 5.4, the sensitivity of the angular observables of the $\Lambda_b \to \Lambda^* \ell^+ \ell^-$ decay on hadronic uncertainties and on NP contributions was investigated. Several of them were shown to exhibit sensitivity with respect to NP contributions currently favoured by global fits to the $b \to s\ell^+\ell^-$ data.

Interestingly, the branching ratio for $\Lambda_b \to \Lambda^* \ell^+ \ell^-$ for $\ell = \mu$ decreases for the NP scenarios favoured to explain the deviations observed in the meson sector. This agrees perfectly with the trend shown by the recent LHCb measurement of R_{pK^-} [223]

$$R_{pK^-}^{\rm LHCb} = 0.86^{+0.14}_{0.11} \pm 0.05\,. \tag{5.73}$$

Indeed this measurement involves several intermediate Λ resonances, but with a prominent contribution of the $\Lambda(1520)$ baryon. If one assumes that this measurement is indeed dominated by the contribution of $\Lambda(1520)$ and one neglects long-distance $c\bar{c}$ contributions at large Λ recoil, we can get the measured central value of $R_{pK^-} = 0.86$ for the following three NP points: $C_{9\mu}^{\rm NP} = -0.76$, $C_{9\mu}^{\rm NP} = -C_{10\mu}^{\rm NP} = -0.29$, or $C_{9\mu}^{\rm NP} = -C_{9'\mu}^{\rm NP} = -0.99$ (in each scenario, all the other Wilson Coefficients are purely SM). These points are in remarkable agreement with the results of global fits to $b \to s\ell^+\ell^-$ and $b \to s\gamma$ transitions in B meson decays (see Chapter 4). This exercise is obviously purely illustrative and its significance should not be overstated, but it shows the interest of identifying the fraction due to the $\Lambda(1520)$ excited state in R_{pK^-}, and to measure the angular distribution of the decay $\Lambda_b \to pK^-\ell^-\ell^-$ through this specific baryon intermediate state.

5.5 Prospects for $\Lambda_b \to \Lambda^*(\to pK)\ell^+\ell^-$

In this section we present the prospects of an angular analysis of the $\Lambda_b \to \Lambda^*\ell^+\ell^-$ decay. Using the expected yield in the current dataset collected at the LHCb experiment, as well as the foreseen ones after the LHCb upgrades[4], sensitivity studies are presented to determine the experimental precision on angular observables related to the lepton distribution and their potential to identify New Physics. The forward-backward lepton asymmetry at low dilepton invariant mass is particularly promising. NP scenarios favoured by the current anomalies in $b \to s\ell^+\ell^-$ decays can be distinguished from the SM case with the data collected between the Run 3 and the Upgrade 2 of the LHCb experiment.

The $\Lambda_b \to \Lambda^*\ell^+\ell^-$ decay width and angular coefficients can be conveniently accessed experimentally in bins or regions of q^2. Due to the available phase space in this decay, and avoiding the region dominated by the charmonia resonances, the studies are performed in three regions: $[0.1, 3]$, $[3, 6]$ and $[6, 8.68]$ GeV$^2/c^4$. Additionally, a broader bin covering the central q^2 region, $[1, 6]$ GeV$^2/c^4$, is added to improve the experimental sensitivity in this region and as a more conservative choice regarding $c\bar{c}$ contributions. As a first exercise to grasp the potential of an angular analysis of the $\Lambda_b \to \Lambda^*\ell^+\ell^-$ decay and due to the limited statistics available for this mode, sensitivity studies are performed using the simplified expression of the angular distribution presented in Eq. (5.67) and only CP-averaged observables are considered. We choose the CP-averaged forward-backward asymmetry in the lepton sector, A_{FB}^{ℓ}, and the S_{1cc} coefficient as the observables of interest and fix the normalisation by $\frac{1}{2}L_{1cc} + L_{1ss} = 1$. The SM predictions for these angular observables are extracted in the q^2 bins of interest and shown in Table 5.2, together with the differential decay width. Besides the scenario of uncertainties used in Section 5.4, which we will refer as the "conservative" scenario, the theoretical precision obtained assuming a 5% uncertainty on the form factors due to foreseeable improvements in lattice QCD studies [314] and light cone sum rules is also given, which we refer to as the "liberal scenario". To illustrate the sensitivity of these observables to the effect of NP, the predictions of a scenario with a NP contribution $\mathcal{C}_{9\mu}^{\rm NP} = -1.11$ are also computed.

5.5.1 Experimental simulation

In the recent test of LFU in $\Lambda_b \to pK\ell^+\ell^-$ decays by LHCb [223], around 400 $\Lambda_b \to pK\mu^+\mu^-$ and 100 $\Lambda_b \to pKe^+e^-$ signal events were observed in the q^2 region $[0.1, 6]\,\text{GeV}^2$ and $m(pK^-) < 2600\,\text{MeV}$, in a dataset corresponding to $3\,\text{fb}^{-1}$ recorded at 7 and 8 TeV and $1.7\,\text{fb}^{-1}$ recorded at 13 TeV. The main difference between the muon and electron modes arises from the trigger and selection efficiencies in the experimental study. In the following, we focus on the muon mode due to the larger experimental yields but the results can be directly extrapolated to the electron case by scaling the yields accordingly. LHCb also published the background subtracted invariant mass of the hadronic system for $\Lambda_b \to pK\mu^+\mu^-$ candidates (available in the supplementary material of Ref. [223]), from where we estimate that roughly around 90 events correspond to the $\Lambda_b \to \Lambda^*\mu^+\mu^-$ decay. The LHCb experiment has already recorded a total of $6\,\text{fb}^{-1}$ at 13 TeV and will accumulate a total of 23 and $50\,\text{fb}^{-1}$ after Run 3 and Run 4 of the LHC, respectively. Moreover, it has been proposed to install an upgraded detector to take data during the High-Luminosity phase of the LHC to collect $300\,\text{fb}^{-1}$ [343]. A summary of the completed and planned LHCb running periods is provided in Table 5.3. Table 5.4 collects the estimated yields of $\Lambda_b \to \Lambda^*\mu^+\mu^-$ decays in the different q^2 bins and running periods, extrapolated from the published LHCb data and the SM prediction for the q^2 distribution. These numbers are used to estimate the sensitivity to NP of an angular analysis of this decay mode. For the electron case, fewer events are expected [223], although the trigger-less readout foreseen for LHCb from Run 3 onwards should allow a higher experimental efficiency for this mode.

[4] The definition of the LHCb run periods and upgrades, as well as the size of the collected and expected datasets can be found in Ref. [343].

Observable	[0.1,3]	[3,6]	[6,8.68]	[1,6]
$d\Gamma/dq^2/\Gamma_{\Lambda_b}[10^{-9}]$				
SM	0.397 ± 0.054	1.29 ± 0.18	3.22 ± 0.42	0.95 ± 0.13
SM - 5%	0.397 ± 0.032	1.29 ± 0.11	3.22 ± 0.28	0.95 ± 0.08
NP	0.337 ± 0.042	1.04 ± 0.13	2.58 ± 0.32	0.77 ± 0.10
NP - 5%	0.337 ± 0.023	1.04 ± 0.08	2.58 ± 0.20	0.77 ± 0.06
A_{FB}^{ℓ}				
SM	0.048 ± 0.018	-0.127 ± 0.033	-0.235 ± 0.040	-0.098 ± 0.031
SM - 5%	0.048 ± 0.013	-0.127 ± 0.020	-0.235 ± 0.022	-0.098 ± 0.019
NP	0.098 ± 0.022	-0.059 ± 0.034	-0.166 ± 0.041	-0.031 ± 0.032
NP - 5%	0.098 ± 0.016	-0.059 ± 0.026	-0.166 ± 0.030	-0.031 ± 0.025
S_{1cc}				
SM	0.181 ± 0.031	0.242 ± 0.042	0.361 ± 0.051	0.221 ± 0.038
SM - 5%	0.181 ± 0.019	0.242 ± 0.021	0.361 ± 0.026	0.221 ± 0.020
NP	0.240 ± 0.038	0.263 ± 0.042	0.371 ± 0.050	0.246 ± 0.039
NP - 5%	0.240 ± 0.024	0.263 ± 0.022	0.371 ± 0.026	0.246 ± 0.021

Table 5.2: Theory predictions for A_{FB}^{ℓ} and S_{1cc} in the SM and in a NP model with $\mathcal{C}_{9\mu}^{\rm NP} = -1.11$. As an illustration of the expected precision of the theory predictions, these are given both using "conservative" uncertainties of 10%(30%) for the $f_{0,\perp,t}$ (f_g) form factors and assuming "liberal" uncertainties of 5% for all form factors. In both cases an uncertainty of 10% (see Eq. (5.71)) is included on $\mathcal{C}_{9\mu}^{\rm SM}$ to account for $c\bar{c}$ contributions.

Run period	Run 1 – 2	Run 3	Run 4	Run 5
Start date	2010	2022	2027	2032
End date	2018	2024	2030	2035
Center-of-mass energy	7, 8, 13 TeV	13–14 TeV	14 TeV	14 TeV
Luminosity	9 fb^{-1}	23 fb^{-1}	50 fb^{-1}	300 fb^{-1}

Table 5.3: Completed and planned LHC runs, corresponding start and end dates, center-of-mass pp collision energy and accumulated integrated luminosity expected to be recorded at LHCb.

Angular acceptance

The angular distributions of the $\Lambda_b \to \Lambda^*\mu^+\mu^-$ decay are distorted by the geometrical acceptance of the detector, the trigger and the selection requirements [239]. The shapes of the acceptance have been estimated using a stand-alone fast simulation software called `RapidSim` [344] by applying the LHCb geometrical acceptance and transverse momentum ($p_{\rm T}^2$) requirements, as needed for the track reconstruction and background rejection, on the final-state particles. These are known to be the dominant effects in shaping the acceptance distributions. In particular, the $p_{\rm T}^2$ of the muons is required to be larger than 400 MeV. Using the simplified angular distribution of Eq. (5.54) there is no need to model the angular acceptances of the ϕ and $\cos\theta_p$ variables since they only appear as a common scale factor in the probability density function (PDF).

The $\cos\theta_\ell$ acceptance curve is expected to be symmetric due to the symmetry between the two leptons in the decay with a loss of events for large $|\cos\theta_\ell|$ values due to the muon $p_{\rm T}^2$ requirement. This last characteristic is mainly visible in the low-q^2 region as shown in Appendix 5.D.

Experimental sensitivity

The sensitivity of the differential measurement of the $\Lambda_b \to \Lambda^*\mu^+\mu^-$ decay width and angular observables to NP effects is studied comparing the theoretical predictions for these observables in the SM and the NP scenario to the expected experimental precision. The experimental sensitivity to the decay width is directly extracted from the expected signal yield in each bin given in Table 5.4, assuming poisonian uncertainties on the yields and neglecting the effect of potential backgrounds, which are observed to be very small in this decay mode [223]. One of the main experimental challenges in the selection of $\Lambda_b \to \Lambda^*\ell^+\ell^-$ decays is the contamination from other Λ^* resonances that overlap in the pK^- spectrum with the $\Lambda(1520)$ state. In the amplitude analysis of the related $\Lambda_b \to pKJ/\psi$ mode [313] three other resonances were observed to contribute to the pK^- mass region around the $\Lambda(1520)$ state, namely $\Lambda(1405)$, $\Lambda(1600)$ and $\Lambda(1800)$. However, all these resonances have spin 1/2, in contrast

q^2 bin \ Dataset	9 fb^{-1}	23 fb^{-1}	50 fb^{-1}	300 fb^{-1}
$[0.1, 3]$ GeV^2	50	140	300	1750
$[3, 6]$ GeV^2	150	400	900	5250
$[6, 8.68]$ GeV^2	400	1100	2400	14000
$[1, 6]$ GeV^2	190	510	1140	6650

Table 5.4: Extrapolated $\Lambda_b \to \Lambda^*\mu^+\mu^-$ signal yields in each q^2 bin for the accumulated luminosity expected at LHCb at the end of Run 2, Run 3, Run 4 and HL − LHC.

Observable	9 fb^{-1}	23 fb^{-1}	50 fb^{-1}	300 fb^{-1}
$d\Gamma/dq^2/\Gamma_{\Lambda_b}[10^{-9}]$				
$[0.1, 3]$	0.060	0.036	0.024	0.010
$[3, 6]$	0.106	0.064	0.043	0.018
$[6, 8.68]$	0.176	0.107	0.072	0.030
$[1, 6]$	0.070	0.042	0.029	0.012
A_{FB}^{ℓ}				
$[0.1, 3]$	0.140	0.079	0.053	0.022
$[3, 6]$	0.061	0.037	0.025	0.010
$[6, 8.68]$	0.036	0.022	0.015	0.006
$[1, 6]$	0.058	0.035	0.023	0.010
S_{1cc}				
$[0.1, 3]$	0.241	0.148	0.099	0.041
$[3, 6]$	0.104	0.062	0.041	0.017
$[6, 8.68]$	0.061	0.036	0.024	0.010
$[1, 6]$	0.100	0.060	0.040	0.017

Table 5.5: Estimated experimental uncertainties for the differential decay width, $d\Gamma/dq^2/\Gamma_{\Lambda_b}$ (top), A_{FB}^{ℓ} (middle) and S_{1cc} (bottom) for different data-taking scenarios in the considered q^2 bins in GeV^2.

to the 3/2 spin of $\Lambda(1520)$, which gives place to a different angular distribution that should allow to disentangle them, following a similar strategy to the one used in the angular analysis of $B_d \to K^*\mu^+\mu^-$ to account for the S-wave contribution [287].

The experimental sensitivity to the angular observables is studied with pseudoexperiments. Events are generated according to a PDF that is the product of Eq. (5.67) and the experimental acceptance described above. Distributions of the $\cos\theta_\ell$ variable are generated using both the SM and NP predictions for the angular parameters and are fitted back with the same PDF, letting the A_{FB}^{ℓ} and S_{1cc} parameters float. A large number of experiments is generated for all the q^2 bins and expected signal yields in the different data-taking periods of LHC. The resulting distributions for the parameters, their uncertainties and pull distributions are examined. Small biases on the central values of the parameters in the low and central q^2 bins are observed in the low-statistics scenarios corresponding to the datasets expected in Run 2 and 3 of LHCb. The effect is larger on S_{1cc} and in the SM case but it is always below 20% of the statistical uncertainty and can be added as a systematic to the measurement. The fit uncertainty is checked to provide good coverage in all the cases so it is taken as the experimental sensitivity to the angular observables.

Potential biases arising from the usage of the simplified angular PDF in Eq. (5.67) are checked by generating a large number of pseudoexperiments with the full PDF, Eq. (5.54), and fitting the observables of interest, A_{FB}^{ℓ} and S_{1cc}, with the simplified PDF. At small signal yields no effect can be observed, while a small bias is found, which is less than 10% of the statistical uncertainty, with the events expected during Upgrade 2 of LHCb. This study confirms that Eq. (5.67) is a safe approximation to apply at least until 300 fb^{-1} have been recorded by LHCb.

5.5.2 Comparison with theory

The sensitivity for different accumulated statistics is compared to the theoretical predictions in Figs. 5.11 to 5.13 for the $d\Gamma/dq^2/\Gamma_{\Lambda_b}$, A_{FB}^{ℓ} and S_{1cc} observables, respectively, for the three narrow q^2 bins. The values for all the bins are also reported in Table 5.5, where one can observe the experimental improvement in the broader $[0.1, 6]$ GeV^2 bin. With the conservative theoretical uncertainties the decay width provides little sensitivity to separate the SM from the NP scenario studied. However, with the improved uncertainties on the form factors at

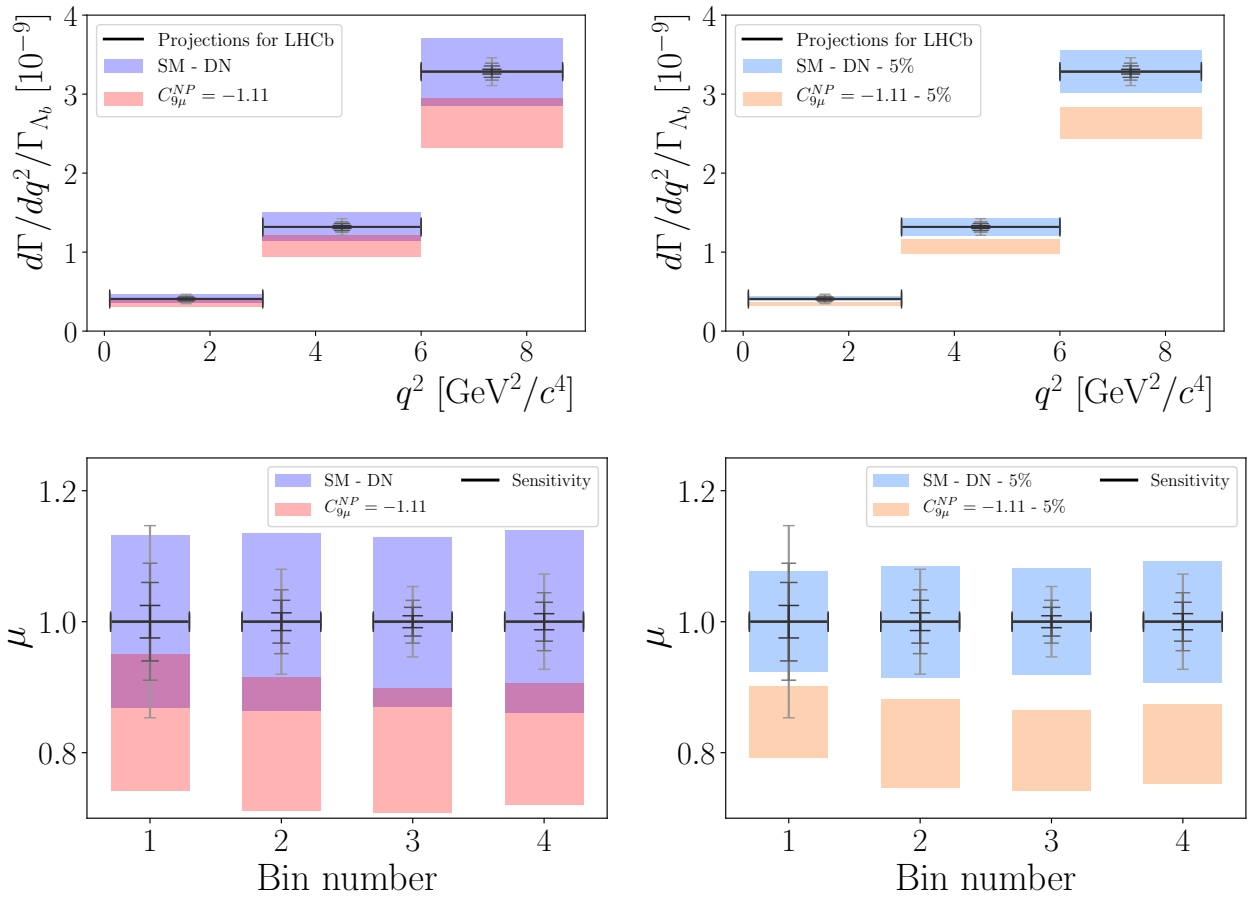

Figure 5.11: Theory predictions for $d\Gamma/dq^2$ in the considered q^2 bins in the SM (blue area) and the NP scenario with $C_{9\mu}^{NP} = -1.11$ (red area), using the nominal theory uncertainties (left) and improved ones with 5% uncertainties on the form factors (right). In both cases an uncertainty of 10% (see Eq. (5.71)) is included on $\mathcal{C}_9$ to account for $c\bar{c}$ contributions. The expected LHCb sensitivity with the full Run 2, Run 3, Run 4 and Upgrade 2 samples is shown by grey-scale markers in increasing sensitivity. The bottom plots show the relative values with respect to the SM prediction in each bin (μ) for all the q^2 bins considered ([0.1, 3],[3, 6],[6, 8.68],[1, 6]).

the level of 5%, one can disentangle with precision the two scenarios in the q^2 bins $[1, 6]$ and $[6, 8.68]\,\text{GeV}^2$. For a better visualisation, the relative values with respect to the SM prediction in each bin are shown in the bottom plots of Fig. 5.11 for all the q^2 bins considered. In this case, the bin number, which follows the order presented in Tables 5.2, 5.4 and 5.5 is used in the x-axis. For the angular observables, while S_{1cc} exhibits a poor sensitivity to NP, A_{FB}^{ℓ} is more promising. In the conservative scenario for theory uncertainties, one could statistically separate the SM and the studied NP model with the data sample collected by LHCb after Upgrade 2. If the theory uncertainties on the form factors can be reduced down to 5%, a good separation is already achieved after Run 3 in the q^2 bins [1, 6] and [6, 8.68] GeV^2.

5.6 Conclusion

The persistent patterns of deviations from SM expectations in $b \to s\mu^+\mu^-$ decays and the hints of violation of lepton-flavour universality between electrons and muons in these modes provide a strong incentive to look for confirmations using other modes with different theoretical and experimental uncertainties. We have investigated the rare decay $\Lambda_b \to \Lambda^*(\to N\bar{K})\ell^+\ell^-$ as a new source of information, in addition to the meson channels already studied at B factories and the LHC. We gave a detailed description of the kinematics of the decay and emphasised the issues related to the propagation and the strong decay of the spin-3/2 Λ^* baryon. We computed the decay rate within the effective Hamiltonian approach, considering only SM and chirality-flipped operators, taking the narrow-width approximation for the Λ^* baryon. The involvement of spin-1/2 and spin-3/2 states yields a fairly complicated differential decay rate which is expressed in terms of 12 angular observables that depend on the dilepton invariant mass q^2. Each observable can be seen as the sum of interference terms among 12 helicity

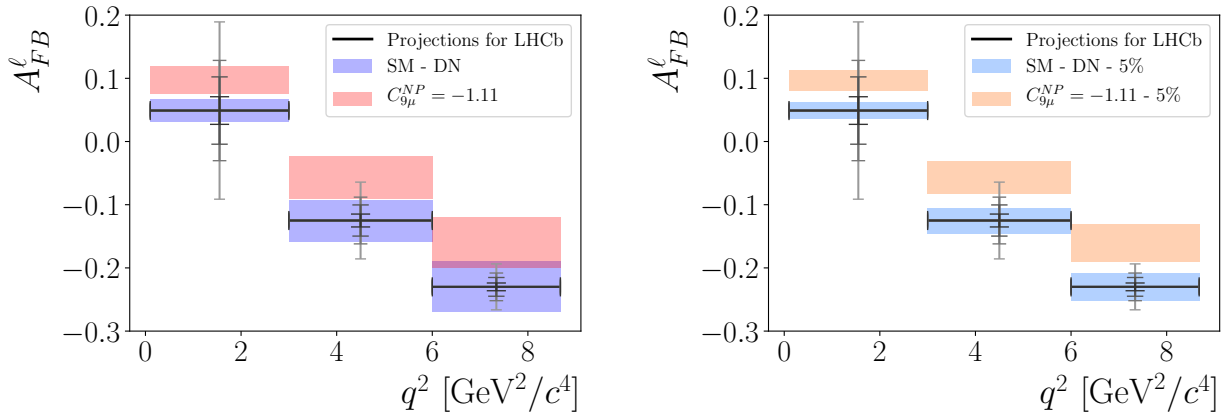

Figure 5.12: Theory predictions for A_{FB}^{ℓ} in the considered q^2 bins in the SM (blue area) and the NP scenario with $C_{9\mu}^{\rm NP} = -1.11$ (red area), using the nominal theory uncertainties (left) and improved ones with 5% uncertainties on the form factors (right). In both cases an uncertainty of 10% (see Eq. (5.71)) is included on $\mathcal{C}_9$ to account for $c\bar{c}$ contributions. The expected LHCb sensitivity with the full Run 2, Run 3, Run 4 and Upgrade 2 samples is shown by the grey-scale markers in increasing sensitivity.

amplitudes, which can be expressed in terms of short-distance Wilson coefficients and hadronic transition form factors defined in a helicity basis. We checked that our result is in agreement with general expectations from the helicity amplitude formalism, and we also checked that our expressions exhibit the expected behaviour in the real-photon limit $q^2 \to 0$ in order to recover the branching ratio for $\Lambda_b \to \Lambda^*\gamma$. We discussed the simplifications arising in the limit of an infinitely heavy b-quark: depending on the kinematics (low or large Λ^* recoil, i.e., large or small q^2), the Heavy Quark Effective Theory and the Soft-Collinear Effective Theory can be used to express all the form factors in terms of 2 or 1 reduced form factors at leading order (i.e up to corrections of order α_s and $\Lambda_{\rm QCD}/m_b$). As there is currently no determination of the form factors over the whole q^2 range available from lattice simulations or light-cone sum rules, we performed a first illustration of the sensitivity of the observables to New Physics contributions using hadronic inputs from quark models. We considered several NP scenarios favoured by the anomalies observed recently in $b \to s\ell^+\ell^-$ decay modes and we compared the results obtained using the whole set of form factors or exploiting the HQET/SCET relations among the form factors. We discussed the phenomenological consequences for some observables. We noticed that the differential decay rate is quite sensitive to the specific NP scenario considered, both at low and large recoils. On the other hand, the angular coefficients normalised to this decay rate show fewer variations. Indeed, in the case of NP scenarios with moderate contributions to $\mathcal{C}_{9\mu}^{\rm NP}$ and/or $\mathcal{C}_{10\mu}^{\rm NP}$, the four numerically significant amplitudes ($A_{\perp,\parallel}^{L}$) are dominated by a single combination of Wilson coefficients which cancel between the numerator and the denominator of the angular coefficients S normalised with respect to the branching ratio. In the very large-recoil region, the interference with the photon pole allows for some discrimination between the NP scenarios for some of the observables. On the other hand, these angular coefficients turn out to be quite sensitive to the presence of right-handed contributions $\mathcal{C}_{9'\mu}^{\rm NP}$ which affect differently the various dominant transversity amplitudes.

We then presented the prospects of angular analyses of $\Lambda_b \to \Lambda^*\ell^+\ell^-$ decays, motivated in particular by recent results on lepton-flavour universality in $\Lambda_b \to pK^-\ell^+\ell^-$ at LHCb. Using the expected yield from the data to be collected at the LHCb experiment in a near future, sensitivity studies were presented to determine the experimental precision on angular observables related to the lepton distribution and their potential to identify New Physics. We studied the impact of acceptance effects on the extraction of these angular observables using published LHCb data together with the fast simulation software `RapidSim`. The lepton forward-backward asymmetry A_{FB}^{ℓ} seems particularly promising: depending on the progress made in reducing the uncertainties on the theory predictions, at some point between Run 3 and Upgrade 2, one could use this observable at low dilepton invariant mass to distinguish between the SM and a scenario with NP contributions to $\mathcal{C}_{9\mu}^{\rm NP}$ supported by the current $b \to s\ell^+\ell^-$ data. We checked that our conclusions were not biased by the significant simplifications of the angular distribution that we proposed based on the heavy-quark limit and supported by phenomenological estimates. The angular distribution then factorises into the product of two terms, i.e. a trivial dependence on the angle describing the hadronic final state and a non trivial dependence on the angle describing the leptonic final state. The three observables can be reexpressed as the branching ratio, the lepton forward-backward asymmetry and a third angular observable S_{1cc}. The first two observables present some sensitivity to NP contributions to the short-distance Wilson coefficient $\mathcal{C}_{9\mu}^{\rm NP}$ for $b \to s\mu^+\mu^-$ transitions.

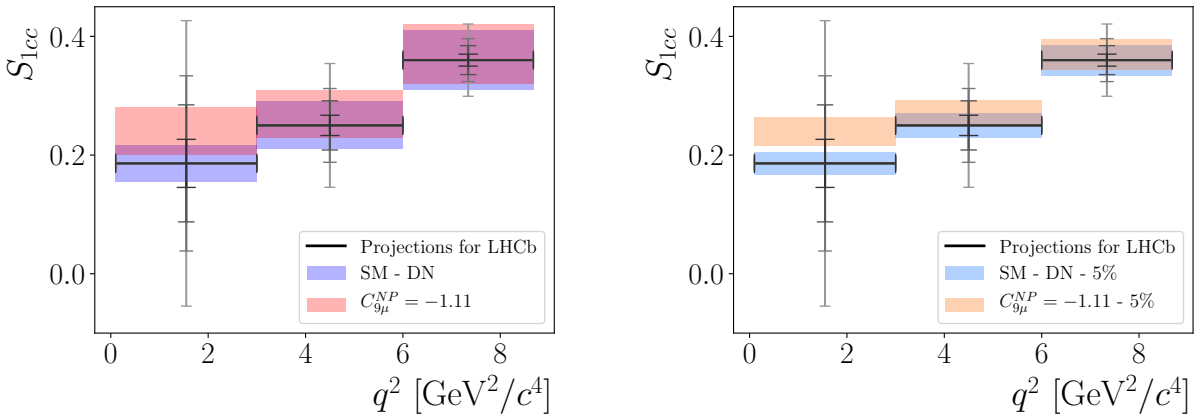

Figure 5.13: Theory predictions for S_{1cc} in the considered q^2 bins in the SM (blue area) and the NP scenario with $C_{9\mu}^{\rm NP} = -1.11$ (red area), using the nominal theory uncertainties (left) and improved ones with 5% uncertainties on the form factors (right). In both cases an uncertainty of 10% (see Eq. (5.71)) is included on $\mathcal{C}_9$ to account for $c\bar{c}$ contributions. The expected LHCb sensitivity with the full Run 2, Run 3, Run 4 and Upgrade 2 samples is shown by the grey-scale markers in increasing sensitivity.

Future experimental information on these observables could thus provide complementary information the on-going search for new physics from $b \to s\ell^+\ell^-$ transitions. However, several issues must be solved before this mode can be competitive compared to $B \to K^{(*)}\ell^+\ell^-$ and even $\Lambda_b \to \Lambda(\to N\pi)\ell^+\ell^-$ decays. Indeed, the theoretical determination of hadronic contributions, local (form factors) and non-local (charm loops) has to be performed accurately. In principle, one could also exploit the polarisation of the initial and final state to build further observables, similarly to Ref. [201] in the $\Lambda_b \to \Lambda\ell^+\ell^-$ case. These aspects should be investigated and solved (partially or fully) in the future. This would open the possibility for a study of $\Lambda_b \to \Lambda^*(\to N\bar{K})\ell^+\ell^-$ at LHC that could complement other modes in the ongoing quest for New Physics in $b \to s\ell^+\ell^-$ transitions.

Appendices

5.A Notation

5.A.1 Kinematics

In agreement with the general analysis in terms of helicity amplitudes [321, 323], we consider the kinematics of the decay in each of the relevant rest frames, which also provides a definition of the angles of interest. In the Λ_b rest frame, we have

$$q^\mu = \begin{pmatrix} \frac{m_{\Lambda_b}^2+q^2-m_{\Lambda^*}^2}{2m_{\Lambda_b}} \\ 0 \\ 0 \\ -\frac{1}{2m_{\Lambda_b}}\sqrt{\lambda(m_{\Lambda_b}^2, m_{\Lambda^*}^2, q^2)} \end{pmatrix}, \qquad k^\mu = \begin{pmatrix} \frac{m_{\Lambda_b}^2+m_{\Lambda^*}^2-q^2}{2m_{\Lambda_b}} \\ 0 \\ 0 \\ \frac{1}{2m_{\Lambda_b}}\sqrt{\lambda(m_{\Lambda_b}^2, m_{\Lambda^*}^2, q^2)} \end{pmatrix}. \tag{5.74}$$

In the dilepton rest frame (where the basis of polarisation vector ε is also defined), we have

$$q_1^\mu = \begin{pmatrix} E_\ell \\ -E_\ell\beta_\ell\sin\theta_\ell \\ 0 \\ -E_\ell\beta_\ell\cos\theta_\ell \end{pmatrix}, \qquad q_2^\mu = \begin{pmatrix} E_\ell \\ E_\ell\beta_\ell\sin\theta_\ell \\ 0 \\ E_\ell\beta_\ell\cos\theta_\ell \end{pmatrix}, \tag{5.75}$$

where

$$E_\ell = \frac{\sqrt{q^2}}{2}, \qquad \beta_\ell = \sqrt{1-\frac{4m_\ell^2}{q^2}}. \tag{5.76}$$

In the Λ^* rest frame we have

$$k_1^\mu = \begin{pmatrix} \frac{m_{\Lambda^*}^2+m_N^2-m_{\bar{K}}^2}{2m_{\Lambda^*}} \\ \frac{m_{\Lambda^*}}{2}\beta_{N\bar{K}}\sin\theta_p\cos\phi \\ \frac{m_{\Lambda^*}}{2}\beta_{N\bar{K}}\sin\theta_p\sin\phi \\ \frac{m_{\Lambda^*}}{2}\beta_{N\bar{K}}\cos\theta_p \end{pmatrix}, \qquad k_2^\mu = \begin{pmatrix} \frac{m_{\Lambda^*}^2+m_{\bar{K}}^2-m_N^2}{2m_{\Lambda^*}} \\ -\frac{m_{\Lambda^*}}{2}\beta_{N\bar{K}}\sin\theta_p\cos\phi \\ -\frac{m_{\Lambda^*}}{2}\beta_{N\bar{K}}\sin\theta_p\sin\phi \\ -\frac{m_{\Lambda^*}}{2}\beta_{N\bar{K}}\cos\theta_p \end{pmatrix}, \tag{5.77}$$

where

$$\beta_{N\bar{K}} = \frac{1}{m_{\Lambda^*}^2}\sqrt{\lambda(m_{\Lambda^*}^2, m_N^2, m_{\bar{K}}^2)}. \tag{5.78}$$

These definitions agree with the LHCb convention for $\Lambda_b \to \Lambda(\to N\pi)\ell^+\ell^-$ [201, 226, 247] (up to the identifications $\theta_p = \theta_b$ and $\phi = \chi$) and they also agree with the LHCb convention for $B \to K^*(\to K\pi)\ell^+\ell^-$ decays [321, 345] up to the identification $\{B^0, K^{*0}, K^+, \pi^-\} \to \{\Lambda_b, \Lambda^*, p, K^-\}$.

5.A.2 Free solutions in the Λ_b rest frame

For the leptons, we can use the well-known expressions for the spin-1/2 case, see for instance Ref. [323] where the application to helicity amplitudes is discussed. We have the following solutions for Λ_b for different values for s_{Λ_b}

$$u_{\Lambda_b}(+1/2) = \begin{pmatrix} \sqrt{2m_{\Lambda_b}} \\ 0 \\ 0 \\ 0 \end{pmatrix}, \qquad u_{\Lambda_b}(-1/2) = \begin{pmatrix} 0 \\ \sqrt{2m_{\Lambda_b}} \\ 0 \\ 0 \end{pmatrix}. \tag{5.79}$$

Following Ref. [324] as discussed in Section 5.1.3, we have the solutions for different values for s_{Λ^*}

$$
\begin{aligned}
u_{\Lambda^*}(-3/2) =& \frac{1}{2\sqrt{m_{\Lambda_b}}} \begin{pmatrix} 0 & 0 & 0 & 0 \\ 0 & \sqrt{s_+} & 0 & -\sqrt{s_-} \\ 0 & -i\sqrt{s_+} & 0 & i\sqrt{s_-} \\ 0 & 0 & 0 & 0 \end{pmatrix}, \\
u_{\Lambda^*}(-1/2) =& \frac{\sqrt{s_- s_+}}{4\sqrt{3} m_{\Lambda_b}^{3/2} m_{\Lambda^*}} \begin{pmatrix} 0 & 2\sqrt{s_+} & 0 & -2\sqrt{s_-} \\ \frac{2m_{\Lambda^*} m_{\Lambda_b}}{\sqrt{s_-}} & 0 & \frac{2m_{\Lambda^*} m_{\Lambda_b}}{\sqrt{s_+}} & 0 \\ -\frac{2im_{\Lambda^*} m_{\Lambda_b}}{\sqrt{s_-}} & 0 & -\frac{2im_{\Lambda^*} m_{\Lambda_b}}{\sqrt{s_+}} & 0 \\ 0 & \frac{s_- + s_+}{\sqrt{s_-}} & 0 & -\frac{s_- + s_+}{\sqrt{s_+}} \end{pmatrix}, \\
u_{\Lambda^*}(+1/2) =& \frac{\sqrt{s_- s_+}}{4\sqrt{3} m_{\Lambda_b}^{3/2} m_{\Lambda^*}} \begin{pmatrix} 2\sqrt{s_+} & 0 & 2\sqrt{s_-} & 0 \\ 0 & -\frac{2m_{\Lambda^*} m_{\Lambda_b}}{\sqrt{s_-}} & 0 & \frac{2m_{\Lambda^*} m_{\Lambda_b}}{\sqrt{s_+}} \\ 0 & -\frac{2im_{\Lambda^*} m_{\Lambda_b}}{\sqrt{s_-}} & 0 & \frac{2im_{\Lambda^*} m_{\Lambda_b}}{\sqrt{s_+}} \\ \frac{s_- + s_+}{\sqrt{s_-}} & 0 & \frac{s_- + s_+}{\sqrt{s_+}} & 0 \end{pmatrix}, \\
u_{\Lambda^*}(+3/2) =& \frac{1}{2\sqrt{m_{\Lambda_b}}} \begin{pmatrix} 0 & 0 & 0 & 0 \\ -\sqrt{s_+} & 0 & -\sqrt{s_-} & 0 \\ -i\sqrt{s_+} & 0 & -i\sqrt{s_-} & 0 \\ 0 & 0 & 0 & 0 \end{pmatrix},
\end{aligned}
\tag{5.80}
$$

where the matrix notation corresponds to the vector and the spinor indices of the solutions $u^{\alpha}_{\Lambda^*,a}$.

5.A.3 Free solutions in the Λ^* rest frame

We have the following solutions for Λ^* for different values for s_{Λ^*}

$$
\begin{aligned}
u_{\Lambda^*}(-3/2) =& \sqrt{m_{\Lambda^*}} \begin{pmatrix} 0 & 0 & 0 & 0 \\ 0 & 1 & 0 & 0 \\ 0 & -i & 0 & 0 \\ 0 & 0 & 0 & 0 \end{pmatrix}, \qquad u_{\Lambda^*}(-1/2) = \sqrt{\frac{m_{\Lambda^*}}{3}} \begin{pmatrix} 0 & 0 & 0 & 0 \\ 1 & 0 & 0 & 0 \\ -i & 0 & 0 & 0 \\ 0 & 2 & 0 & 0 \end{pmatrix}, \\
u_{\Lambda^*}(+1/2) =& \sqrt{\frac{m_{\Lambda^*}}{3}} \begin{pmatrix} 0 & 0 & 0 & 0 \\ 0 & -1 & 0 & 0 \\ 0 & -i & 0 & 0 \\ 2 & 0 & 0 & 0 \end{pmatrix}, \qquad u_{\Lambda^*}(+3/2) = \sqrt{m_{\Lambda^*}} \begin{pmatrix} 0 & 0 & 0 & 0 \\ -1 & 0 & 0 & 0 \\ -i & 0 & 0 & 0 \\ 0 & 0 & 0 & 0 \end{pmatrix}.
\end{aligned}
\tag{5.81}
$$

We have the following solutions for N for different values for s_N

$$
u_N(+1/2) = \frac{1}{\sqrt{2m_{\Lambda^*}}} \begin{pmatrix} \sqrt{r_+}\cos\frac{\theta_p}{2} \\ \sqrt{r_+}\sin\frac{\theta_p}{2} e^{i\phi} \\ \sqrt{r_-}\cos\frac{\theta_p}{2} \\ \sqrt{r_-}\sin\frac{\theta_p}{2} e^{i\phi} \end{pmatrix}, \qquad u_N(-1/2) = \frac{1}{\sqrt{2m_{\Lambda^*}}} \begin{pmatrix} -\sqrt{r_+}\sin\frac{\theta_p}{2} e^{-i\phi} \\ \sqrt{r_+}\cos\frac{\theta_p}{2} \\ \sqrt{r_-}\sin\frac{\theta_p}{2} e^{-i\phi} \\ -\sqrt{r_-}\cos\frac{\theta_p}{2} \end{pmatrix}. \tag{5.82}
$$

5.A.4 Dilepton rest frame

We have the following solutions for ℓ^- for different values for s_{ℓ^-}

$$
u_{\ell^-}(+1/2) = \begin{pmatrix} \sqrt{E_\ell + m_\ell}\cos\frac{\theta_\ell}{2} \\ \sqrt{E_\ell + m_\ell}\sin\frac{\theta_\ell}{2} \\ \sqrt{E_\ell - m_\ell}\cos\frac{\theta_\ell}{2} \\ \sqrt{E_\ell - m_\ell}\sin\frac{\theta_\ell}{2} \end{pmatrix}, \qquad u_{\ell^-}(-1/2) = \begin{pmatrix} -\sqrt{E_\ell + m_\ell}\sin\frac{\theta_\ell}{2} \\ \sqrt{E_\ell + m_\ell}\cos\frac{\theta_\ell}{2} \\ \sqrt{E_\ell - m_\ell}\sin\frac{\theta_\ell}{2} \\ -\sqrt{E_\ell - m_\ell}\cos\frac{\theta_\ell}{2} \end{pmatrix}, \tag{5.83}
$$

and for ℓ^+ for different values for s_{ℓ^+}

$$
v_{\ell^+}(+1/2) = \begin{pmatrix} \sqrt{E_\ell - m_\ell}\cos\frac{\theta_\ell}{2} \\ \sqrt{E_\ell - m_\ell}\sin\frac{\theta_\ell}{2} \\ -\sqrt{E_\ell + m_\ell}\cos\frac{\theta_\ell}{2} \\ -\sqrt{E_\ell + m_\ell}\sin\frac{\theta_\ell}{2} \end{pmatrix}, \qquad v_{\ell^+}(-1/2) = \begin{pmatrix} \sqrt{E_\ell - m_\ell}\sin\frac{\theta_\ell}{2} \\ -\sqrt{E_\ell - m_\ell}\cos\frac{\theta_\ell}{2} \\ \sqrt{E_\ell + m_\ell}\sin\frac{\theta_\ell}{2} \\ -\sqrt{E_\ell + m_\ell}\cos\frac{\theta_\ell}{2} \end{pmatrix}. \tag{5.84}
$$

5.B Cross check of the angular decomposition

The structure of the differential decay rate obtained in Section 5.3.1 can be checked against the general analysis in terms of helicity amplitudes performed in Ref. [321]. Following the arguments presented there, taking into account the spins of the initial, intermediate and final states as well as the absence of spin-2 operators in the effective Hamiltonian, we expect the differential decay rate to be organised as

$$\begin{aligned} L \propto & \text{Re} \sum_{L_{\Lambda^*}=0}^{2J_{\Lambda^*}} \sum_{L_\ell=0}^{2J_\gamma} \sum_{M=0}^{\min(L_{\Lambda^*},L_\ell)} G_M^{L_{\Lambda^*},L_\ell}(q^2)\Omega_M^{L_{\Lambda^*},L_\ell}(\Omega_{\Lambda^*},\Omega_\ell) \\ \propto & \text{Re}[G_0^{0,0}\Omega_0^{0,0} + G_0^{0,1}\Omega_0^{0,1} + G_0^{0,2}\Omega_0^{0,2} \\ & + G_0^{2,0}\Omega_0^{2,0} + G_0^{2,1}\Omega_0^{2,1} + G_1^{2,1}\Omega_1^{2,1} + G_0^{2,2}\Omega_0^{2,2} + G_1^{2,2}\Omega_1^{2,2} + G_2^{2,2}\Omega_2^{2,2}]. \end{aligned} \tag{5.85}$$

The index L_{Λ^*} corresponds to the $N\bar{K}$ system, L_ℓ to the dilepton system, and M to the ϕ-component of both partial waves. In our case we have $J_{\Lambda^*} = 3/2$ and $J_\gamma = 1$, which is the maximal spin of the virtual gauge boson induced by the operators of the effective Hamiltonian in the absence of tensor contributions, as discussed in detail in Ref. [321]. G are angular coefficients depending on the invariant mass of the dilepton pair. The angular functions are given by the product of Wigner D functions

$$\Omega_M^{L_{\Lambda^*},L_\ell}(\Omega_{\Lambda^*},\Omega_\ell) = D^{\Lambda^*}_{M,0}(\phi,\theta_p,-\phi)D^{L_\ell}_{M,0}(0,\theta_\ell,0). \tag{5.86}$$

The second helicity index of both Wigner functions in the angular distribution is zero, i.e. the difference of the helicities of the final-state particles (summed incoherently), and the first index, identical for both Wigner functions, contains the helicities of the internal particles (summed coherently).

Although the sum with respect to L_{Λ^*} in the first line of Eq. (5.85) goes from 0 to $2J_{\Lambda^*}$, the second line of Eq. (5.85) contains only the sum over even values of L_{Λ^*}: this is due to the fact that the decay of the Λ^* baryon is strong and conserves parity, so that it should be invariant under $\theta_p \to \theta_p + \pi$, which eliminates odd-$L_{\Lambda^*}$ partial waves[5]. In addition, some of the Wigner functions are real and L is the real part of the product of these functions with the angular coefficients G, which means that only the following 12 angular coefficients are involved

$$\begin{aligned} \text{Re } G_0^{0,0} \to & \frac{1}{9}(L_{1cc} + 2L_{1ss} + 2L_{2cc} + 4L_{2ss} + 2L_{3ss}), \\ \text{Re } G_0^{0,1} \to & \frac{1}{3}(L_{1c} + 2L_{2c}), \\ \text{Re } G_0^{0,2} \to & \frac{2}{9}(L_{1cc} - L_{1ss} + 2L_{2cc} - 2L_{2ss} - L_{3ss}), \\ \text{Re } G_0^{2,0} \to & \frac{2}{9}(L_{1cc} + 2L_{1ss} - L_{2cc} - 2L_{2ss} - L_{3ss}), \\ \text{Re } G_0^{2,1} \to & \frac{2(L_{1c} - L_{2c})}{3}, \\ \text{Re } G_1^{2,1} \to & \frac{2L_{5s}}{\sqrt{3}}, \qquad \text{Im } G_1^{2,1} \to -\frac{2L_{6s}}{\sqrt{3}}, \\ \text{Re } G_0^{2,2} \to & \frac{2}{9}(2L_{1cc} - 2L_{1ss} - 2L_{2cc} + 2L_{2ss} + L_{3ss}), \\ \text{Re } G_1^{2,2} \to & \frac{2L_{5sc}}{3}, \qquad \text{Im } G_1^{2,2} \to -\frac{2L_{6sc}}{3}, \\ \text{Re } G_2^{2,2} \to & \frac{4L_{3ss}}{3}, \qquad \text{Im } G_2^{2,2} \to -\frac{4L_{4ss}}{3}, \end{aligned} \tag{5.87}$$

where we have indicated the equivalence with the angular coefficients defined in Eq. (5.54).

5.C Connection with $\Lambda_b \to \Lambda^*(\to N\bar{K})\gamma$

5.C.1 Tensor form factors

The expressions for $\Lambda_b \to \Lambda^*(\to N\bar{K})\ell^+\ell^-$ contain a pole at $q^2 = 0$, which is related to the decay $\Lambda_b \to \Lambda^*(\to N\bar{K})\gamma$. The matrix element responsible for the photon contribution to $\Lambda_b \to \Lambda^*\ell^+\ell^-$ will have the structures

[5] Similarly, the decay $B \to K^*(\to K\pi)\ell^+\ell^-$ involves a sum over even values of J_{K^*} in Eq. (28) of Ref. [321] since K^* decays strongly, whereas $\Lambda_b \to \Lambda(\to N\pi)\ell^+\ell^-$ involves a sum over odd and even values of J_Λ in Eq. (E.3) of Ref. [321] as $\Lambda(1150)$ decays weakly. This is related to the P-conserving or violating nature of the decay of the intermediate hadron, and not to the nature of the final state (as stated in Ref. [321]).

$\epsilon^*_\mu M^\mu$ and $\epsilon^*_\mu M^\mu_5$ with

$$M^\mu = \bar{u}_\alpha \Gamma^{\alpha\mu} u, \qquad M^\mu_5 = \bar{u}_\alpha \gamma^5 \Gamma^{\alpha\mu}_5 u, \tag{5.88}$$

with the general form factor decomposition

$$\Gamma^{\alpha\mu}_{(5)} = q^\alpha \gamma^\mu G_1^{(\prime)} + q^\alpha (p+k)^\mu G_2^{(\prime)} + q^\alpha q^\mu G_3^{(\prime)} - g^{\alpha\mu} G_4^{(\prime)}. \tag{5.89}$$

The gauge condition $q_\mu \Gamma^{\alpha\mu}_{(5)} = 0$ implies that

$$\begin{aligned} G_4 &= (m_{\Lambda_b} - m_{\Lambda^*}) G_1 + (m^2_{\Lambda_b} - m^2_{\Lambda^*}) G_2 + q^2 G_3, \\ G'_4 &= (m_{\Lambda_b} + m_{\Lambda^*}) G'_1 + (m^2_{\Lambda_b} - m^2_{\Lambda^*}) G'_2 + q^2 G'_3, \end{aligned} \tag{5.90}$$

leading to the expressions

$$\Gamma^{\alpha\mu} = [q^\alpha \gamma^\mu - g^{\alpha\mu}(m_{\Lambda_b} - m_{\Lambda^*})] G_1 + [q^\alpha (p+k)^\mu - g^{\alpha\mu}(m^2_{\Lambda_b} - m^2_{\Lambda^*})] G_2 + [q^\alpha q^\mu - g^{\alpha\mu} q^2] G_3, \tag{5.91}$$

$$\Gamma^{\alpha\mu}_5 = [q^\alpha \gamma^\mu - g^{\alpha\mu}(m_{\Lambda_b} + m_{\Lambda^*})] G'_1 + [q^\alpha (p+k)^\mu - g^{\alpha\mu}(m^2_{\Lambda_b} - m^2_{\Lambda^*})] G'_2 + [q^\alpha q^\mu - g^{\alpha\mu} q^2] G'_3. \tag{5.92}$$

Focusing on the tensor form factors f_i^T needed for the contribution of $\mathcal{C}_7 + \mathcal{C}_{7'}$ given in Eq. (5.36), we can see that we have the identification

$$G_1 \to -(m_{\Lambda_b} + m_{\Lambda^*}) f_\perp^T - \frac{m_{\Lambda^*}}{s_-} f_g^T, \tag{5.93}$$

$$G_2 \to -\frac{q^2}{s_+} f_0^T + \frac{(m_{\Lambda_b} + m_{\Lambda^*})^2}{s_+} f_\perp^T + \frac{m_{\Lambda_b}(m_{\Lambda_b} + m_{\Lambda^*}) - q^2}{s_+ s_-} f_g^T, \tag{5.94}$$

$$G_3 \to \frac{(m^2_{\Lambda_b} - m^2_{\Lambda^*})}{s_+} [f_0^T - f_\perp^T] - \frac{m^2_{\Lambda_b} + m_{\Lambda_b} m_{\Lambda^*} + 2m^2_{\Lambda^*} - q^2}{s_+ s_-} f_g^T. \tag{5.95}$$

Similarly we have the identification for the pseudotensor form factors f_i^{T5} for $\mathcal{C}_7 - \mathcal{C}_{7'}$

$$G'_1 \to -(m_{\Lambda_b} - m_{\Lambda^*}) f_\perp^{T5} + \frac{m_{\Lambda^*}}{s_+} f_g^{T5}, \tag{5.96}$$

$$G'_2 \to -\frac{q^2}{s_-} f_0^{T5} + \frac{(m_{\Lambda_b} - m_{\Lambda^*})^2}{s_-} f_\perp^{T5} + \frac{m_{\Lambda_b}(m_{\Lambda_b} - m_{\Lambda^*}) - q^2}{s_+ s_-} f_g^{T5}, \tag{5.97}$$

$$G'_3 \to \frac{(m^2_{\Lambda_b} - m^2_{\Lambda^*})}{s_-} [f_0^{T5} - f_\perp^{T5}] - \frac{m^2_{\Lambda_b} - m_{\Lambda_b} m_{\Lambda^*} + 2m^2_{\Lambda^*} - q^2}{s_+ s_-} f_g^{T5}. \tag{5.98}$$

If we want to have three independent form factors $G_1^{(\prime)}$, $G_2^{(\prime)}$, $G_3^{(\prime)}$ with a finite limit at $q^2 \to 0$, it is sufficient to request that $f_\perp^{T(5)}$, $f_0^{T(5)}$, $f_g^{T(5)}$ tend all to a finite value in this limit, see Eq. (5.37). Let us emphasise that these conditions are obtained by considering solely the behaviour of the amplitude at $q^2 \to 0$ in QCD, so that $O(1)$ means $O((q^2)^0)$ here. The SCET limit, though related, is slightly different, taking $q^2 = O(\Lambda^2_{\rm QCD})$, $m_b \to \infty$ and $\Lambda_{\rm QCD}/m_b \to 0$. Eq. (5.65) obtained in the SCET limit shows that the condition for $f_g^{T(5)}$ should be understood as $f_0^{T,T5}(q^2) = O(\Lambda^2_{\rm QCD}/m_b^2)$ then.

Moreover, it is possible to determine relations between some of the tensor form factors at $q^2 = 0$. Indeed, the two matrix elements used in Eq. (5.36) can be obtained from the matrix element $\langle \Lambda^* | \bar{s} i\sigma^{\mu\nu} b | \Lambda_b \rangle$ thanks to the identity $\sigma_{\mu\nu}\gamma_5 = i\epsilon_{\mu\nu\rho\sigma}\sigma^{\rho\sigma}/2$. The latter matrix element can be parametrised in terms of six form factors given in Ref. [42], which can be used to express all the form factors in Eq. (5.36). These relations yield in particular the very simple relationships at $q^2 = 0$

$$G_2 = G'_2, \qquad G_1 = G'_1 - 2m_{\Lambda^*} G'_2, \tag{5.99}$$

leading to the following relations between the form factors in Eq. (5.36)

$$f_\perp^{T5}(0) = f_\perp^T(0), \qquad f_g^{T5}(0) = f_g^T(0) \frac{m_{\Lambda_b} + m_{\Lambda^*}}{m_{\Lambda_b} - m_{\Lambda^*}}, \tag{5.100}$$

5.C.2 Branching ratio

The branching ratio for radiative decay $\Lambda_b \to \Lambda^* \gamma$ is proportional to

$$\lim_{q^2 \to 0} (q^2 \sum_{X=A,B} |X|^2), \tag{5.101}$$

s_{Λ_b}	s_{Λ^*}	$H^{V,A}$	$H^{T,T5}$	A, B
$\pm 1/2$	$\pm 1/2$	$\frac{1}{\sqrt{q^2}}$	$\sqrt{q^2}$	$a\mathcal{C}_{9\ell} + b\mathcal{C}_{10,\ell} + c\mathcal{C}_7$
$\pm 1/2$	$\mp 1/2$	1	1	$\sqrt{q^2}\left[a'\mathcal{C}_{9\ell} + b'\mathcal{C}_{10,\ell} + c'\frac{\mathcal{C}_7}{q^2}\right]$
$\pm 1/2$	$\pm 3/2$	1	1	$\sqrt{q^2}\left[a''\mathcal{C}_{9\ell} + b''\mathcal{C}_{10,\ell} + c''\frac{\mathcal{C}_7}{q^2}\right]$

(5.102)

Table 5.C.1: Behaviour of the amplitudes for $\Lambda_b \to \Lambda^*(\to N\bar{K})\ell^+\ell^-$ in the $q^2 \to 0$ limit in the SM. a, b are generic numbers coming from the kinematics and the form factors.

where the sum goes over the 12 transversity amplitudes in Eq. (5.47). If we consider the transversity amplitudes of interest[6], we see that we have the behaviours given in Table 5.C.1 for $q^2 \to 0$ in the SM. From Table 5.C.1, we can see that the only contributions to the radiative decay comes from the. $\mathcal{C}_7, \mathcal{C}_{7'}$ operators for the transitions $\pm 1/2 \to \mp 1/2$ and $\pm 1/2 \to \pm 3/2$, whereas the branching ratio $\Lambda_b \to \Lambda^*\gamma$ gets no contributions from the transitions $\pm 1/2 \to \mp 1/2$. This situation is naturally reminescent of $B \to K^*\gamma$ [333] that gets contributions from the amplitudes with transverse polarisations, but not from longitudinal polarisation, as can be seen as the level of the transversity amplitudes ($1/q^2$ pole in $A_{\perp,||}$ but not in A_0).

This pattern is in agreement with the general arguments developed in Refs. [310, 311] for $\Lambda_b \to \Lambda^*(\to N\bar{K})\gamma$. We can therefore link our results further with the expressions in Ref. [310]. The latter are given with respect to an arbitrary quantisation axis, which we have identified with the z-axis defined along the Λ^* momentum in the Λ_b rest frame (meaning $\theta_p = 0$ and ϕ_Λ arbitrary, to be integrated over, in the notation of Ref. [310]) and for an arbitrary Λ_b polarisation which we take $P_{\Lambda_b} = 0$, leading to a decay rate proportional to:

$$2[|C_{1/2,1}|^2 + |C_{-1/2,-1}|^2]\cos^2\theta_p + \frac{1}{2}[3|C_{3/2,1}|^2 + 3|C_{-3/2,-1}|^2 + |C_{1/2,1}|^2 + |C_{-1/2,-1}|^2]\sin^2\theta_p. \tag{5.103}$$

We can make contact with our expressions by integrating Eq. (5.54) over θ_ℓ and ϕ, leading to a decay rate proportional to

$$(L_{1cc} + 2L_{1ss})\cos\theta_p^2 + (L_{2cc} + 2L_{2ss} + L_{3ss})\sin\theta_p^2, \tag{5.104}$$

so that it appears that up to a common normalisation we have the identifications

$$\begin{aligned} |C_{1/2,1}|^2 + |C_{-1/2,-1}|^2 &\leftrightarrow |A^L_{||0}|^2 + |A^L_{\perp 0}|^2 + |A^L_{||1}|^2 + |A^L_{\perp 1}|^2 + (L \leftrightarrow R), \\ |C_{3/2,1}|^2 + |C_{-3/2,-1}|^2 &\leftrightarrow |B^L_{||1}|^2 + |B^L_{\perp 1}|^2 + (L \leftrightarrow R), \end{aligned} \tag{5.105}$$

in agreement with the definitions of A and B amplitudes that involve 3/2 and 1/2 Λ^* polarisations respectively.

5.C.3 Matching of the form factors

A final comment is in order concerning the comparison of our formulae with Ref. [311]. There are three form factors contributing to $\epsilon^*_\mu M^\mu$ at $q^2 = 0$. However the computation in Ref. [311] involve only the values of two form factors at $q^2 = 0$. Indeed, the computation of the branching ratio amounts to summing over the physical polarisations, leading to the computation of $M^\mu M^*_\mu$. Since the three tensors involved in M^μ are all transverse with respect to q^μ, one can check that G_1 and G_2, but not G_3, will contribute to the branching ratio $\Lambda_b \to \Lambda^*\gamma$. Comparing the expressions of the matrix elements $\langle\Lambda^*|\bar{s}\sigma_{\mu\nu}q^\nu b|\Lambda_b\rangle$ and $\langle\Lambda^*|\bar{s}\sigma_{\mu\nu}\gamma_5 q^\nu b|\Lambda_b\rangle$ in Eq. (5.36) and in Ref. [311] at $q^2 = 0$, we obtain the relationships

$$\begin{aligned} i\frac{f_1}{2m_{\Lambda_b}} &= -f_\perp^T(0) - f_g^T(0)\frac{m_{\Lambda_b}}{(m_{\Lambda_b} - m_{\Lambda^*})(m_{\Lambda_b}^2 - m_{\Lambda^*}^2)} \\ &= -f_\perp^{T5}(0) - f_g^{T5}(0)\frac{m_{\Lambda_b}}{(m_{\Lambda_b} + m_{\Lambda^*})(m_{\Lambda_b}^2 - m_{\Lambda^*}^2)}, \\ if_2 &= (m_{\Lambda_b} + m_{\Lambda^*})f_\perp^T(0) + f_g^T(0)\frac{m_{\Lambda^*}}{(m_{\Lambda_b} - m_{\Lambda^*})^2} \\ &= (m_{\Lambda_b} + m_{\Lambda^*})f_\perp^{T5}(0) + f_g^{T5}(0)\frac{m_{\Lambda^*}}{m_{\Lambda_b}^2 - m_{\Lambda^*}^2} \end{aligned} \tag{5.106}$$

which agree with the constraints in Eq. (5.100). We thus check that only two constants arise for $\Lambda_b \to pK^-\gamma$, as proposed in Ref. [311]. The identification of f_1, f_2 with the values of the tensor form factors actually yields

[6] The vector/axial form factors are expected to have a finite limit at $q^2 = 0$ with specific linear combinations of $f_t^V, f_\perp^V$ and $f_t^A, f_\perp^A$ expected to vanish, as indicated in Section 5.2.

further cross-checks with this reference in the SCET limit. Using the relations in Eq. (5.65), we see that the contribution proportional to $\tilde{f}_0^T(0)$ can then be neglected, leading to the relation $f_1 = -2f_2 m_{\Lambda_b}/(m_{\Lambda_b} + m_{\Lambda^*})$ given in Ref. [311]. As discussed in this reference, in the same SCET limit, the amplitudes $C_{\pm 3/2,\pm 1/2}$ indeed vanish, since they correspond to $B_{\perp 1}$ and $B_{||1}$, proportional to f_g and f_g^T.

5.D Angular acceptance

The μ^+ and μ^- efficiencies, introduced by the selection requirements discussed in Section 5.5 being the same, give the acceptance shown in Fig. 5.D.1, that can be modelled by an even function of Legendre polynomials:

$$\begin{aligned}\epsilon(\cos\theta_\ell) = \quad & 1 \\ & + c_2/2(3\cos^2\theta_\ell - 1) \\ & + c_4/8(35\cos^4\theta_\ell - 30\cos^2\theta_\ell + 3) \\ & + c_6/16(231\cos^6\theta_\ell - 315\cos^4\theta_\ell + 105\cos^2\theta_\ell - 5).\end{aligned}$$

The parameters c_i are fitted in simulation and used throughout the sensitivity studies.

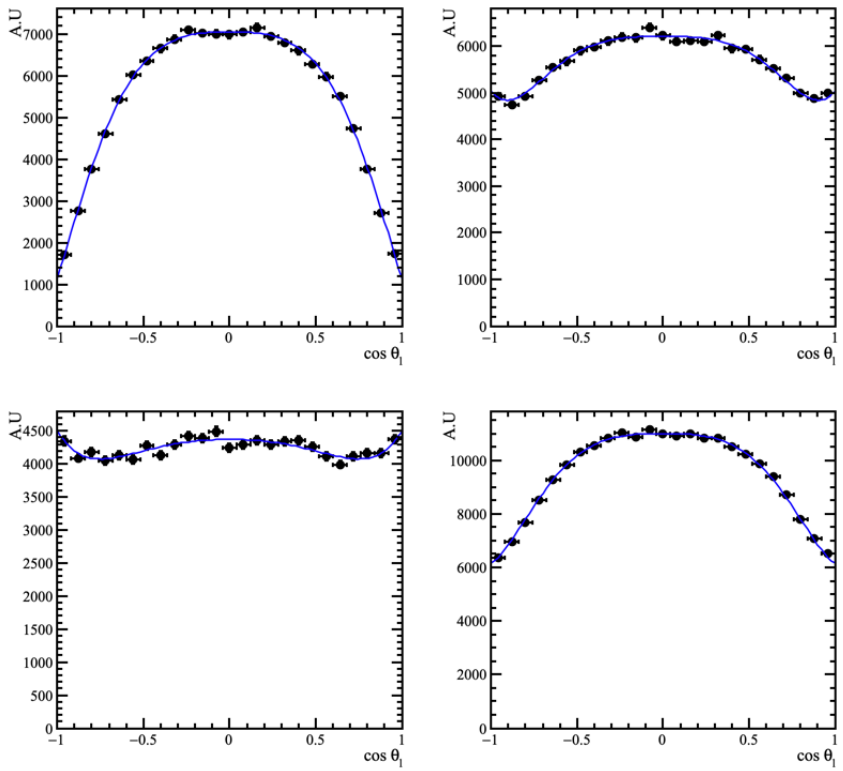

Figure 5.D.1: Acceptance shapes for $\cos\theta_\ell$ for q^2 in $[0.1, 3]$, $[3, 6]$, $[6, 8.68]$, and $[1, 6]\,\text{GeV}^2$ respectively.

Chapter 6

Time-dependent angular analysis of $B_d \to K_S \ell^+ \ell^-$

In addition to investigating hadronic decays not yet measured (like in the prevous chapter), one can probe New Physics in b->sll through additional observables for decays already measured. An interesting way of building new observables has been discussed in Ref. [217] by exploiting neutral B-meson mixing and considering time-dependent observables. This possibility has been discussed in Refs. [217, 346] for light vector resonances into CP eigenstates such as $B_d \to K^{*0}(\to K_S\pi^0)\mu\mu$ and $B_s \to \phi(\to KK)\mu\mu$. The general discussion of CP violation comparing time-integrated and time-dependent observables sheds some light on the interest of the new observables obtained in Ref. [217]: they assess CP violation in the interference between decay and mixing, they contain additional information not present in time-integrated observables (in particular concerning CP-odd "weak" phases) and they are not sensitive to the same hadronic uncertainties. In the context of $B \to K^*\mu\mu$, they lift some of the degeneracies among (time-integrated) angular observables that prevent us from separating the contributions from various helicity amplitudes [214].

In this chapter, based on Ref. [347], we apply the same idea to a final state with a spin-0 meson rather than a spin-1 vector, focusing on the time-dependent analysis of $B_d \to K_S\ell^+\ell^-$ taking into account the time-evolution of the B_d meson and its mixing into $\bar{B}_d$. We discuss the angular conventions required to define the angular observables in a transparent way with respect to CP conjugation. Although our formalism is general, we will consider mainly $B_d \to K_S\mu\mu$ for illustration, since the (time-integrated) angular analysis of this decay has already been performed by LHCb using 3 fb^{-1} of integrated luminosity [238].

The inclusion of time evolution allows us to identify six new observables, out of which three could be accessed from a time-dependent tagged analysis. We also show that these observables could be obtained by time-integrated measurements in a hadronic environment if flavour tagging is available. We provide simple and precise predictions for these observables in the SM and in NP models with real contributions to SM and chirally flipped operators. In these cases, the very simple structure of these observables will allow us to show that they are very well determined and independent of form factors and charm-loop contributions.

As such, these observables will provide robust and powerful cross-checks of the NP scenarios currently favoured by global fits to $b \to s\ell^+\ell^-$ data. In addition, we will discuss the sensitivity of these observables with respect to NP scenarios involving scalar and tensor operators, or CP-violating phases. We will then illustrate how these new observables can provide a benchmark to discriminate among the various NP scenarios in $b \to s\mu^+\mu^-$.

In Section 6.1, we recall the angular analysis of $B \to K\ell^+\ell^-$ without mixing, i.e. the charged case, highlighting the angular convention required to connect CP-conjugate modes and the status of the hadronic inputs needed for the theoretical computation. In Section 6.2, we extend the discussion to the neutral case with mixing, discussing the CP-parity of the final state and deriving the 6 new time-dependent observables that can be measured in principle. In Section 6.3, we focus on three of these new observables which are very precisely determined in the SM and can be used to probe various NP hypotheses (scalar and tensor contributions, NP "weak" phases), before concluding in Section 6.4. In a first appendix, we show that our conclusions are not affected by the choice of a specific model for charm-loop contributions. In a second appendix, we discuss the case of B_s decays into f_0, η or η' mesons showing that similar observables can be defined and computed.

6.1 Angular analysis of $B^\pm \to K^\pm \ell^+\ell^-$

6.1.1 Amplitude analysis

The $b \to s\ell^+\ell^-$ transitions as discussed in Section 2.4 are described by the usual weak effective theory (WET), with SM operators plus (potentially) NP operators with a chirally-flipped, scalar or tensor structure. The main operators of interest for this analysis are $\mathcal{O}_{7^{(\prime)},9^{(\prime)},10^{(\prime)},S^{(\prime)},P^{(\prime)},T^{(\prime)}}$.

Contributions from the semileptonic operators are factorizable and their matrix elements can be written as

$$\langle K\ell^+\ell^-|\mathcal{O}_{\rm sl}|B\rangle = \langle K|\Gamma^A|B\rangle\langle \ell^+\ell^-|\Gamma'_A|0\rangle \ , \tag{6.1}$$

where A denotes a collection of Lorentz indices and Γ, Γ' are Dirac matrices. It is clear that all hadronic, dipole, and semileptonic contributions can be recast as decays of the form

$$B \to KN(\to \ell^+\ell^-) \ , \tag{6.2}$$

where N has the quantum numbers of a boson, whose coupling pattern is determined by the operators arising in the effective Hamiltonian. In the SM, the structure of $\mathcal{O}_7, \mathcal{O}_9, \mathcal{O}_{10}$ shows that N are spin-1 particles, coupling to both left- and right-handed fermions. This is in agreement with the presence of γ^* and Z penguin contributions, but it is also able to reproduce the contribution from box diagrams involving two W bosons and a neutrino ($(V-A)(V-A)$ structure in the SM). In an extension of the SM yielding scalar (tensor) operators, one should add N bosons with spin 0 (spin 2 respectively) [321].

We can exploit Ref. [321] in order to extract information starting with the charged decay. The angular distribution for $B^- \to K^-\ell^+\ell^-$ is

$$\frac{d^2\Gamma(B^- \to K^-\ell^+\ell^-)}{dq^2\, d\cos\theta_\ell} = \bar{G}_0(q^2) + \bar{G}_1(q^2)\cos\theta_\ell + \bar{G}_2(q^2)\frac{1}{2}(3\cos^2\theta_\ell - 1) = \sum_{i=0,1,2} \bar{G}_i(q^2) P_i(\cos\theta_\ell) \tag{6.3}$$

where P_i denotes the i-th Legendre polynomial in terms of the angle θ_ℓ describing the emission of one of the charged leptons (its precise definition will be discussed in the following) and $q = p_B - p_K$ is the momentum transfer. We have

$$\begin{aligned}
\bar{G}_0 =& \frac{4}{3}\left(1 + 2\hat{m}_\ell^2\right)\left|\bar{h}_V\right|^2 + \frac{4}{3}\beta_\ell^2\left|\bar{h}_A\right|^2 + 2\beta_\ell^2\left|\bar{h}_S\right|^2 + 2\left|\bar{h}_P\right|^2 \\
&+ \frac{8}{3}\left(1 + 8\hat{m}_\ell^2\right)\left|\bar{h}_{T_t}\right|^2 + \frac{4}{3}\beta_\ell^2\left|\bar{h}_T\right|^2 + 16\hat{m}_\ell \,\mathrm{Im}\left[\bar{h}_V \bar{h}_{T_t}^*\right] \ , \\
\bar{G}_1 =& -4\beta_\ell\left(2\hat{m}_\ell \,\mathrm{Re}\left[\bar{h}_V \bar{h}_S^*\right] - \mathrm{Im}\left[2\bar{h}_{T_t}\bar{h}_S^* + \sqrt{2}\bar{h}_T \bar{h}_P^*\right]\right) \ , \\
\bar{G}_2 =& -\frac{4\beta_\ell^2}{3}\left(\left|\bar{h}_V\right|^2 + \left|\bar{h}_A\right|^2 - 2\left|\bar{h}_T\right|^2 - 4\left|\bar{h}_{T_t}\right|^2\right) \ ,
\end{aligned} \tag{6.4}$$

where we have used the notation:

$$\hat{m}_\ell = \frac{m_\ell}{\sqrt{q^2}} \ , \qquad \beta_\ell = \sqrt{1 - 4\hat{m}_\ell^2} \ . \tag{6.5}$$

The matrix elements relevant to $\bar{B} \to \bar{K}$ transition yield the following form factors in the standard parametrisation:

$$\begin{aligned}
\langle K^-(p)|\bar{s}\gamma_\mu b|B^-(p_B)\rangle =& (p_B + p)_\mu f_+(q^2) + \frac{m_B^2 - m_K^2}{q^2} q_\mu \left(f_0(q^2) - f_+(q^2)\right) \ , \\
\langle K^-(p)|\bar{s}\sigma_{\mu\nu} b|B^-(p_B)\rangle =& i\left[(p_B + p)_\mu q_\nu - (p_B + p)_\nu q_\mu\right]\frac{f_T(q^2)}{m_B + m_K} \ , \\
\langle K^-(p)|\bar{s} b|B^-(p_B)\rangle =& \frac{m_B^2 - m_K^2}{m_b - m_s} f_0(q^2) \ ,
\end{aligned} \tag{6.6}$$

We find

$$\begin{aligned}
\bar{h}_V =& \mathcal{N} \frac{\sqrt{\lambda_B}}{2\sqrt{q^2}} \left(\frac{2m_b}{m_B + m_K} (\mathcal{C}_7 + \mathcal{C}_{7'}) f_T + (\mathcal{C}_9 + \mathcal{C}_{9'}) f_+ \right) , \\
\bar{h}_A =& \mathcal{N} \frac{\sqrt{\lambda_B}}{2\sqrt{q^2}} (\mathcal{C}_{10} + \mathcal{C}_{10'}) f_+ , \\
\bar{h}_S =& \mathcal{N} \frac{m_B^2 - m_K^2}{2} \left(\frac{(\mathcal{C}_S + \mathcal{C}_{S'})}{m_b - m_s} \right) f_0 , \\
\bar{h}_P =& \mathcal{N} \frac{m_B^2 - m_K^2}{2} \left(\frac{(\mathcal{C}_P + \mathcal{C}_{P'})}{m_b - m_s} + \frac{2m_\ell}{q^2} (\mathcal{C}_{10} + \mathcal{C}_{10'}) \right) f_0 , \\
\bar{h}_T =& - i\mathcal{N} \frac{\sqrt{\lambda_B}}{\sqrt{2}\,(m_B + m_K)} (\mathcal{C}_T - \mathcal{C}_{T'})\, f_T , \\
\bar{h}_{T_t} =& - i\mathcal{N} \frac{\sqrt{\lambda_B}}{2\,(m_B + m_K)} (\mathcal{C}_T + \mathcal{C}_{T'})\, f_T ,
\end{aligned} \tag{6.7}$$

with the normalisation factor $\mathcal{N}$,

$$\mathcal{N} = -\frac{\alpha G_F}{\pi} V_{ts}^* V_{tb} \sqrt{\frac{q^2 \beta_\ell \sqrt{\lambda_B}}{2^{10} \pi^3 m_B^3}} , \tag{6.8}$$

where $\lambda_B \equiv \lambda(m_B^2, m_K^2, q^2)$ (with $\lambda(a,b,c)$ is the Källén-function) is related to the absolute value of the three-momentum of the K^*. Note that the normalisation factor $\mathcal{N}$ disagrees with (the square root of) the normalisation factor of Ref. [321] by a factor $2\sqrt{2}$, but it is in agreement with Refs. [213, 348].

Following Ref. [321], we use the LHCb conventions for the charged case, so that θ_ℓ is defined as the angle between the ℓ^- three-momentum and the opposite of the B^- three-momentum in the dilepton rest frame in the case of $B^- \to K^- \ell^+ \ell^-$, but ℓ^+ and B^+ in the case of $B^+ \to K^+ \ell^+ \ell^-$. With this convention, $d^2\Gamma(B^+ \to K^+ \ell^+ \ell^-)/(dq^2\, d\cos\theta_\ell)$ has the same expression as $d^2\Gamma(B^- \to K^- \ell^+ \ell^-)/(dq^2\, d\cos\theta_\ell)$ above, up to the replacement of the angular coefficients $\bar{G}$ depending on $\bar{h}$ by G depending on h. The h amplitudes are obtained from the $\bar{h}$ amplitudes by performing a complex conjugation of all the weak phases (this applies to $\mathcal{N}$ but also to the weak phases in the Wilson coefficients in the case of CP-violating New Physics). On the other hand, strong phases, in particular those stemming from charm loops generated by the four-quark operators and combining with $\mathcal{C}_9$ in the expressions of the angular observables, are the same in h and $\bar{h}$. If all CP violating effects are neglected, one gets $G_i = \bar{G}_i$.

6.1.2 Hadronic inputs

In order to compute the amplitudes and the angular observables defined above, we need hadronic inputs for $f_{+,0,T}$. We may use the form factors obtained in Ref. [96] (for f_+ and f_T) and Ref. [39] (for f_+, f_0 and f_T). Both perform light-cone sum rules determinations at low q^2, using sum rules based on light-meson and B-meson distribution amplitudes, respectively. The authors of Ref. [39] combine their results with lattice QCD determination at high q^2 (coming from Ref. [349]). The observables built as ratios of angular coefficients G_i depend actually on the ratios of form factors f_0/f_+ and f_T/f_+ shown in Fig. 2.6. It turns out that f_T/f_+ has little q^2-dependence and is very close to 1 within the uncertainties quoted, in agreement with the earlier discussion in Ref. [348] and with the expectations SCET and HQET discussed in Section 2.5. On the other hand f_0/f_+ has a linear dependence on q^2, so that a noticeable q^2 dependence of ratios of angular observables G_i could be the sign of significant scalar/pseudoscalar contributions.

We have not explicitly indicated the contribution from $c\bar{c}$ loops which adds a q^2-dependent contribution to the coefficient $\mathcal{C}_9$, which features both a real and an imaginary part coming from strong phases. Due to the nature of this analysis, we are interested in the effect that possible strong phases can introduce. We will thus, in the following, take the estimate presented in Eq. (5.71) for the SM value of $\mathcal{C}_9$ both at low and large K-recoil. The alternative estimates Eqs. (2.83) and (5.69) will be used only to check that our results depend only very mildly on the model used for charm-loop contribution.

6.1.3 Observables

The angular observables G_i can be recast into more traditional forms. In addition to the decay rate and the forward-backward asymmetry, a third observable can be built from the $B^\pm \to K^\pm \ell^+ \ell^-$ angular analysis [213]. The corresponding CP-averaged observables have the following expressions in terms of the angular coefficients:

$$\Gamma_\ell = G_0 + \bar{G}_0 , \qquad A_{FB}^\ell = \frac{G_1 + \bar{G}_1}{2(G_0 + \bar{G}_0)} , \qquad F_H^\ell = 1 + \frac{G_2 + \bar{G}_2}{G_0 + \bar{G}_0} , \tag{6.9}$$

$B_d \to K_{S(L)}\ell^+\ell^-$ parameters						
$\eta(K_S)$	$\eta(K_L)$	ϕ	$\Delta\Gamma$	$x = \Delta m/\Gamma$	$y = \Delta\Gamma/(2\Gamma)$	$\tau_{B_d}[ps]$
1	-1	-2β	$\simeq 0$	0.769 ± 0.004	0.0005 ± 0.005	1.519 ± 0.004

$B_s \to f_0(\eta,\eta')\ell^+\ell^-$ parameters						
$\eta(f_0)$	$\eta(\eta,\eta')$	ϕ	$\Delta\Gamma$	$x = \Delta m/\Gamma$	$y = \Delta\Gamma/(2\Gamma)$	$\tau_{B_s}[ps]$
1	-1	$2\beta_s$	$\neq 0$	26.81 ± 0.08	0.0675 ± 0.004	1.515 ± 0.004

CKM parameters				
$\sin(-2\beta)$	$\sin(2\beta_s)$	$\mathrm{Re}[V_{ts}]$	$\mathrm{Im}[V_{ts}] \cdot 10^3$	V_{tb}
-0.71 ± 0.01	0.0371 ± 0.0007	-0.0407 ± 0.0004	-0.75 ± 0.02	0.99913 ± 0.00002

λ	A	$\bar\rho$	$\bar\eta$
0.22493 ± 0.00016	0.819 ± 0.010	0.159 ± 0.008	0.351 ± 0.007

Masses [GeV]		
$\bar m_b(m_b)$	$\bar m_s(m_b)$	m_μ
4.18 ± 0.03	0.078 ± 0.007	0.106

Table 6.1: Input parameters used to determine the SM predictions. Decay parameters are from Ref. [6]. The CKM values are obtained from the symmetrised confidence intervals for the Wolfenstein parameters $\lambda, A, \bar\rho, \bar\eta$ given in Ref. [24], while for m_b and m_s we use the $\overline{\rm MS}$ masses at m_b [6]. The SM Wilson coefficients can be found in Table 2.1. The form factors (not recalled here) are taken from Ref. [39].

leading to

$$\frac{d^2\Gamma(B^- \to K^-\ell^+\ell^-)}{dq^2\, d\cos\theta_\ell} + \frac{d^2\Gamma(B^+ \to K^+\ell^+\ell^-)}{dq^2\, d\cos\theta_\ell} = 2\Gamma_\ell \left[\frac{1}{2}F_H^\ell + A_{FB}^\ell \cos\theta_\ell + \frac{3}{4}(1-F_H^\ell)(1-\cos^2\theta_\ell)\right] . \quad (6.10)$$

As can be seen from the above equations, in the absence of tensor and scalar contributions and neglecting $\hat m_\ell$ corrections which are relevant only at very low q^2, one has the simple relations

$$\bar G_0 = -\bar G_2 + 2|\bar h_P|^2 \simeq -\bar G_2\,, \qquad \bar G_1 = 0 \quad (6.11)$$

(and the same for G_i). The observable F_H^ℓ is proportional to $(G_0 + \bar G_0) + (G_2 + \bar G_2)$, and thus probes the first relation in Eq. (6.11). A non-vanishing value of F_H^ℓ can be attributed to NP in tensor and/or scalar contributions. On the other hand, a non-vanishing A_{FB}^ℓ, related to $G_1 + \bar G_1$, probes the second relation in Eq. (6.11) and would be a clear signal of New Physics from scalar or tensor contributions, but we can see from Eq. (6.4) that they should correspond to very large scalar contributions (to beat the m_ℓ-suppressing factors) and/or to (pseudo)tensor and (pseudo)scalar contributions.

One can also think of building CP-violating observables of the form

$$A_i = \frac{G_i - \bar G_i}{G_i + \bar G_i}\,. \quad (6.12)$$

Neglecting again m_ℓ-suppressed contributions, we see that these observables probe differences of the form $|h_X|^2 - |\bar h_X|^2$, which vanish unless both strong and weak phases are present. Assuming that NP contributions do not yield any significant strong phases in the short-distance Wilson coefficients, it can be easily seen that only h_V involves strong phases (due to the $c\bar c$-loops) and thus only the presence of CP-violating NP phases in $\mathcal{C}_{7,7'}$ and $\mathcal{C}_{9,9'}$ can be probed by these observables.

In Appendix 6.A we provide predictions for these observables in the SM and in a few NP scenarios. It is quite clear that they yield rather similar central values in all scenarios, with hadronic uncertainties that are rather large compared to the sensitivity to NP contributions. This makes the NP interpretation of deviations in the measurement of these observables rather challenging.

As a conclusion, the CP-averaged observables built from the angular analysis of $B^+ \to K^+\ell^+\ell^-$ have interesting abilities to probe scalar and tensor NP contributions, but if deviations from the SM are observed, these observables are not sufficient to pin down the actual source of the contributions. The CP asymmetries associated with the same observables probe only the presence of NP phases in a limited subset of Wilson coefficients.

6.2 Angular analysis of $B_d \to K_S \ell^+ \ell^-$

6.2.1 From the charged case to the neutral one

Before analysing the impact of time evolution and mixing, we must first determine how the above formulae must be adapted to the neutral case if mixing were neglected. We must perform the changes in the equations of Section 6.1.1:

$$B^- \to \bar{B}_d\,, \qquad B^+ \to B_d\,, \qquad K^- \to \bar{K}^0\,, \qquad K^+ \to K^0\,. \tag{6.13}$$

We have then to consider the CP-eigenstates rather than the flavour eigenstates for the kaon with the following phase convention:

$$|K^0\rangle \sim d\bar{s}\,, \qquad |\bar{K}^0\rangle \sim s\bar{d}\,, \qquad |K^+\rangle \sim u\bar{s}\,, \qquad |K^-\rangle \sim s\bar{u}\,, \tag{6.14}$$

so that

$$|K_S\rangle \sim \frac{|K^0\rangle + |\bar{K}^0\rangle}{\sqrt{2}}\,, \qquad |K_L\rangle \sim \frac{|K^0\rangle - |\bar{K}^0\rangle}{\sqrt{2}}\,, \tag{6.15}$$

where we have neglected the small amount of CP violation in the kaon system leading to $CP|K^0\rangle = |\bar{K}^0\rangle$ (and similarly $CP|B_d\rangle = |\bar{B}_d\rangle$).

The expressions for $\bar{h}_X(\bar{B}_d \to K_S\ell^+\ell^-)$ and $h_X(B_d \to K_S\ell^+\ell^-)$ are obtained from $\bar{h}_X(\bar{B}_d \to \bar{K}^0\ell^+\ell^-)$ and $h_X(B_d \to K^0\ell^+\ell^-)$ by dividing the normalisation $\mathcal{N}$ by $\sqrt{2}$ in both cases[1]. The latter are equal to the charged amplitudes described in the previous section in the isospin limit, so that we have

$$\bar{h}_X(\bar{B}_d \to K_S\ell^+\ell^-) = \frac{1}{\sqrt{2}}\bar{h}_X(B^- \to K^-\ell^+\ell^-) \qquad h_X(B_d \to K_S\ell^+\ell^-) = \frac{1}{\sqrt{2}}h_X(B^+ \to K^+\ell^+\ell^-) \tag{6.16}$$

Following Ref. [217], the discussion of $B_d \to K_S\ell^+\ell^-$ requires the same convention for both B_d and $\bar{B}_d$, since the decay is not flavour specific. Before taking into account mixing, and following the arguments of Ref. [217] that we will discuss extensively below, we define θ_ℓ as the angle between ℓ^- and K_S (similarly to the case of $B^+ \to K^+\ell^+\ell^-$) for both B_d and $\bar{B}_d$ decays. This yields

$$\frac{d^2\Gamma[B_d \to K_S\ell^+\ell^-]}{ds\; d\cos\theta_\ell} = \sum_i G_i(s)P_i(\cos\theta_\ell)\,, \tag{6.17}$$

$$\frac{d^2\Gamma[\bar{B}_d \to K_S\ell^+\ell^-]}{ds\; d\cos\theta_\ell} = \sum_i \zeta_i\bar{G}_i(s)P_i(\cos\theta_\ell)\,, \tag{6.18}$$

where $\zeta_{0,2} = 1$ and $\zeta_1 = -1$ and the G_i ($\bar{G}_i$) are defined in terms of $h_X(B_d \to K_S)$ ($\bar{h}_X(\bar{B}_d \to K_S)$). In the absence of CP violation, we would have $G_i = \bar{G}_i$.

We stress that Eqs. (6.17) and (6.18) arise just from the identification of kinematics of CP-conjugate decays, and do not rely on any intrinsic CP-parity of the initial or final states involved. We will see now that this choice of conventions is justified by the analysis of the properties of the amplitudes under CP conjugation.

6.2.2 CP-parity of the final state

We now turn to the case of decays into CP eigenstates: $B \to f_{CP}$. In this context, it is useful to define two different angular coefficients $\widetilde{G}_i$, $\bar{G}_i$ which are CP conjugates of G_i:

- the angular coefficients $\widetilde{G}_i$ formed by replacing A_X by $\widetilde{A}_X \equiv A_X(\bar{B}_d \to f_{CP})$ (without CP-conjugation applied on f_{CP}), which appear naturally in the study of time evolution due to mixing, where both B and $\bar{B}$ decay into the same final state f_{CP}.
- the angular coefficients $\bar{G}_i$, obtained by considering $\bar{A}_X \equiv A_X(\bar{B}_d \to \overline{f}_{CP})$ (with CP-conjugation applied to f_{CP}), which can be obtained from A_X by changing the sign of all weak phases, and arise naturally when discussing CP violation from the theoretical point of view.

In the case of interest, we have to consider the transversity amplitudes:

$$\bar{A}_X \equiv A_X(\bar{B} \to \bar{M}\ell^+\ell^-)\,, \quad \widetilde{A}_X \equiv A_X(\bar{B} \to M\ell^+\ell^-)\,, \tag{6.19}$$

where $X = V, A, S, P, T, T_t$, and we have $\bar{A}_X = \bar{h}_X$. These two sets of amplitudes are related by

$$\widetilde{A}_X = \eta_X\bar{A}_X\,, \tag{6.20}$$

[1] For K_L, we would obtain the amplitudes by dividing the normalisation $\mathcal{N}$ by $-\sqrt{2}$ and by $\sqrt{2}$, respectively.

X	$\eta(N)$	$\tau(N)$	η_X
S	1	0	η
P	-1	0	$-\eta$
V	1	1	$-\eta$
A	1	1	$-\eta$
T	-1	1	η
T_t	1	1	$-\eta$

Table 6.2: Quantum numbers and CP-parities associated with the $B \to M\ell^+\ell^-$ transversity amplitudes. We have defined $\eta = \eta(M)$. For $B_d \to K_S\ell^+\ell^-$, we have $\eta = \eta(K_S) = 1$.

where η_X are the CP-parities associated to the different transversity amplitudes. We follow the arguments of Refs. [217, 350] in order to determine the value of η_X. Adapting the arguments of Ref. [350] to the decay $B \to MN$, where M is stable (under the strong interaction) and N decays into the dilepton pair, leads to

$$\eta_X = \eta(M)\eta(N)(-1)^{\tau(N)} , \tag{6.21}$$

where $M = K_S$ here. The assignment of the CP-parity $\eta(N)$ and the transversity $\tau(N)$ requires some discussion.

Concerning the CP-parity $\eta(N)$, we can start from the helicity amplitude analysis performed in Ref. [321], associating the lepton matrix elements $\langle \ell^-(\lambda_1)\ell^+(\lambda_2)|\bar{\ell}\Gamma^X \ell|0\rangle$ to the amplitudes h_X:

$$\Gamma^S = 1, \qquad \Gamma^P = \gamma^5 , \quad \Gamma^V = \gamma^\mu \omega_\mu(\lambda) , \quad \Gamma^A = \gamma^\mu\gamma^5 \omega_\mu(\lambda) , \quad \Gamma^T = \sigma^{\mu\nu}\omega^{1\lambda}_{\mu\nu} , \quad \Gamma^{T_t} = \sigma^{\mu\nu}\omega^{t\lambda}_{\mu\nu} , \tag{6.22}$$

where $\lambda = \lambda_1 - \lambda_2$ (equal to $-1, 0$ or 1). The polarisation vectors $\omega_\mu(\lambda)$ form the usual basis for $\lambda = t, 0, +1, -1$, with $\omega_\mu(t) = q_\mu/\sqrt{q^2}$. The rank-2 polarisation tensors $\omega^{J\lambda}_{\mu\nu}$ are less familiar objects, but they correspond to products of polarisation vectors. On one hand, we have $\omega^{t\lambda}_{\mu\nu} = \omega_\mu(t)\omega_\nu(\lambda)$ and on the other hand $\omega^{1\lambda}_{\mu\nu}$ is a linear combination of products of polarisation vectors $\omega_\mu(\lambda_1)\omega_\nu(\lambda_2)$ with λ_1 and λ_2 being either $0, -1$ or 1, but not timelike. This formulation allows us to determine the parity $\eta(N)$: since we assume that CP-parity is conserved through the decay, we can determine the CP-parity of N through that of the lepton matrix element it couples to, taking into account the sign difference between the time-like polarisation and the space-like polarisations. The corresponding parities of the fermion bilinears with different Dirac matrices can easily be found in the discussion of the Dirac algebra in textbooks on quantum field theory, for instance Ref. [29].

Concerning the transversity $\tau(N)$, we can then use the following two statements: first, the helicity of N is $\lambda(N) = 0$ since both B and M are spin-0 mesons, and second, the antisymmetric structure of the tensor operators means that they are set in a spin-1 representation [321]. We have thus to determine the transversity of the intermediate state N with $\lambda = 0$, with a spin equal either to 0 (scalar, pseudoscalar) or 1 (vector, axial, tensors) and $\lambda = 0$. Following Ref. [350], it is trivial to see that $\tau(N) = 0$ for spin 0. For spin 1, one can see that the $\lambda = 0$ state is a superposition of states with $\tau = +1$ and $\tau = -1$, meaning that one can set $\tau(N) = 1$ for spin 1.

Putting these elements together yields the results collected in Table 6.2, leading to the following CP-parities associated to the different transversity amplitudes

$$\eta_S = \eta_T = \eta(M) = \eta , \qquad \eta_V = \eta_A = \eta_P = \eta_{Tt} = -\eta(M) = -\eta . \tag{6.23}$$

where we have defined $\eta = \eta(M)$. In the $B_d \to K_S\ell^+\ell^-$ case, we have $\eta(M) = \eta(K_S) = 1$.

Coming back to the definition of $\bar{G}_i$, we see that the two types of angular coefficients are related through

$$\widetilde{G}_i = \zeta_i \bar{G}_i . \tag{6.24}$$

The number ζ_i (defined in Section 6.2.1 to perform the identification of the kinematics between CP-conjugate decays) corresponds here to the product of the CP-parities of the amplitudes involved in the interference term G_i, for $i = 0, 1, 2$.

6.2.3 CP-averaged and CP-violating angular observables

We can now check the consistency of the kinematics chosen for CP-conjugate modes in Section 6.2.1. Indeed, since the decay is not flavour specific, an untagged measurement of the differential decay rate (e.g. at LHCb, where the asymmetry production is tiny) yields:

$$\frac{d\Gamma(B_d \to K_S\ell^+\ell^-) + d\Gamma(\bar{B}_d \to K_S\ell^+\ell^-)}{ds\ d\cos\theta_\ell} = \sum_i [G_i + \widetilde{G}_i] P_i(\cos\theta_\ell) = \sum_i [G_i + \zeta_i \bar{G}_i] P_i(\cos\theta_\ell) , \tag{6.25}$$

if we still neglect for the moment the effects of neutral-meson mixing. The difference between the two decay rates (which can be measured only through flavour-tagging) involves:

$$\frac{d\Gamma(B_d \to K_S\ell^+\ell^-) - d\Gamma(\bar{B}_d \to K_S\ell^+\ell^-)}{ds\ d\cos\theta_\ell} = \sum_i [G_i - \widetilde{G}_i] P_i(\cos\theta_\ell) = \sum_i [G_i - \zeta_i \bar{G}_i] P_i(\cos\theta_\ell)\ . \tag{6.26}$$

A slightly counter-intuitive consequence of the identification of the angles between the two CP-conjugates mode is that the CP-asymmetry for G_1 is measured in the CP-averaged rate, and vice-versa. This situation is well known in the case of the angular distribution of other modes that are not self-tagging, such as $B_s \to \phi\ell^+\ell^-$ [217, 229, 346].

We see now that the convention chosen in Eqs. (6.17) and (6.18) for flavour-tagging modes allows one to treat on the same footing the modes with flavour tagging and the modes with final CP-eigenstates, since the same combinations of angular coefficients occur in both cases when one considers the CP-average or the CP-asymmetry in the decay rate.

Let us stress again that this results from a conventional identification between CP-conjugate decays in the case without mixing. This freedom in the angular convention for CP-conjugate flavour-specific modes is not present in the presence of mixing where both decays result in the same final state, which must always be described with the "same" kinematic convention, in the sense of a convention that depends only on the final state, without referring to the flavour of the decaying B meson (see Ref. [217]). The convention chosen in Section 6.2.1 obeys indeed this requirement and it is thus an appropriate choice even in the presence of mixing.

6.2.4 Time-dependent angular distribution of $B \to K_S\ell^+\ell^-$

We can now add the effect of neutral-meson mixing. Indeed, in the case of B decays into CP-eigenstates, where the final state can be produced both by the decay of B or $\bar{B}$ mesons, the mixing and decay processes interfere, inducing a further time dependence in physical amplitudes. These time-dependent amplitudes are given by

$$A_X(t) = A_X(B(t) \to f_{CP}\ell^+\ell^-) = g_+(t)A_X + \frac{q}{p} g_-(t)\widetilde{A}_X\ , \tag{6.27}$$

$$\widetilde{A}_X(t) = A_X(\bar{B}(t) \to f_{CP}\ell^+\ell^-) = \frac{p}{q} g_-(t)A_X + g_+(t)\widetilde{A}_X\ , \tag{6.28}$$

where the absence of the t argument denotes the amplitudes at $t = 0$, i.e. in the absence of mixing, and we have introduced the usual time-evolution functions

$$g_+(t) = e^{-imt}e^{-\Gamma t/2}\left[\cosh\frac{\Delta\Gamma t}{4}\cos\frac{\Delta m t}{2} - i\sinh\frac{\Delta\Gamma t}{4}\sin\frac{\Delta m t}{2}\right]\ , \tag{6.29}$$

$$g_-(t) = e^{-imt}e^{-\Gamma t/2}\left[-\sinh\frac{\Delta\Gamma t}{4}\cos\frac{\Delta m t}{2} + i\cosh\frac{\Delta\Gamma t}{4}\sin\frac{\Delta m t}{2}\right]\ , \tag{6.30}$$

with $\Delta m = M_H - M_L$ and $\Delta\Gamma = \Gamma_L - \Gamma_H$ (detailed definitions can be found in Refs. [351, 352], which must be adapted to our choice concerning CP-conjugation in neutral meson systems: $CP|B_d\rangle = |\bar{B}_d\rangle$ and $CP|K^0\rangle = |\bar{K}^0\rangle$).

In the presence of mixing, the coefficients of the angular distribution also depend on time, as they involve the time-dependent amplitudes given in Eqs. (6.27) and (6.28). This evolution can be simplified by noting that CP violation in $B_q - \bar{B}_q$ mixing is negligible for all practical purposes[2], and we will assume $|q/p| = 1$, introducing the mixing angle ϕ:

$$\frac{q}{p} = e^{i\phi}\ . \tag{6.31}$$

This mixing angle is large in the case of the B_d system but tiny for B_s, see Table 6.1.

The angular coefficients are obtained by replacing time-independent amplitudes with time-dependent ones:

$$G_i(t) = G_i\big(A_X \to A_X(t)\big)\ , \quad \widetilde{G}_i(t) = G_i\big(A_X \to \widetilde{A}_X(t)\big)\ . \tag{6.32}$$

We consider the combinations $G_i(t) \pm \widetilde{G}_i(t)$ appearing in the sum and difference of time-dependent decay rates in Eqs. (6.25) and (6.26). From Eqs. (6.27), (6.28) and (6.32), we get

$$G_i(t) + \widetilde{G}_i(t) = e^{-\Gamma t}\Big[(G_i + \widetilde{G}_i)\cosh(y\Gamma t) - h_i\sinh(y\Gamma t)\Big]\ , \tag{6.33}$$

$$G_i(t) - \widetilde{G}_i(t) = e^{-\Gamma t}\Big[(G_i - \widetilde{G}_i)\cos(x\Gamma t) - s_i\sin(x\Gamma t)\Big]\ , \tag{6.34}$$

[2] The current world averages are $|q/p|_{B_d} = 1.0010 \pm 0.0008$ and $|q/p|_{B_s} = 1.0003 \pm 0.0014$ [6, 158]

where $x \equiv \Delta m/\Gamma$, $y \equiv \Delta\Gamma/(2\Gamma)$, and we have defined a new set of angular coefficients s_i, h_i related to the time-dependent angular distribution. The coefficients G_i, $\widetilde{G}_i$ can be determined from flavour-specific decays.

The expressions for s_i and h_i are

$$\begin{aligned} s_0 =& 2\text{Im}\left[e^{i\phi}\left[\frac{4}{3}\left(1+2\hat{m}_\ell^2\right)\tilde{h}_V h_V^* + \frac{4}{3}\beta_\ell^2 \tilde{h}_A h_A^* + 2\beta_\ell^2 \tilde{h}_S h_S^* + 2\tilde{h}_P h_P^*\right.\right. \\ &\left.\left. + \frac{8}{3}\left(1+8\hat{m}_\ell^2\right)\tilde{h}_{T_t} h_{T_t}^* + \frac{4}{3}\beta_\ell^2 \tilde{h}_T h_T^*\right]\right] - 16\hat{m}_\ell\,\text{Re}\left[e^{i\phi}\tilde{h}_V h_{T_t}^* - e^{-i\phi} h_V \tilde{h}_{T_t}^*\right], \end{aligned} \tag{6.35}$$

$$\begin{aligned} s_1 =& -4\beta_\ell\left(2\hat{m}_\ell \text{Im}\left[e^{i\phi}\tilde{h}_V h_S^* - e^{-i\phi} h_V \tilde{h}_S^*\right]\right. \\ &\left. + \text{Re}\left[e^{i\phi}[2\tilde{h}_{T_t} h_S^* + \sqrt{2}\tilde{h}_T h_P^*] - e^{-i\phi}[2h_{T_t}\tilde{h}_S^* + \sqrt{2}h_T \tilde{h}_P^*]\right]\right), \end{aligned} \tag{6.36}$$

$$s_2 = -\frac{8\beta_\ell^2}{3}\text{Im}\left[e^{i\phi}\left[\tilde{h}_V h_V^* + \tilde{h}_A h_A^* - 2\tilde{h}_T h_T^* - 4\tilde{h}_{T_t} h_{T_t}^*\right]\right], \tag{6.37}$$

and

$$\begin{aligned} h_0 =& 2\text{Re}\left[e^{i\phi}\left[\frac{4}{3}\left(1+2\hat{m}_\ell^2\right)\tilde{h}_V h_V^* + \frac{4}{3}\beta_\ell^2 \tilde{h}_A h_A^* + 2\beta_\ell^2 \tilde{h}_S h_S^* + 2\tilde{h}_P h_P^*\right.\right. \\ &\left.\left. + \frac{8}{3}\left(1+8\hat{m}_\ell^2\right)\tilde{h}_{T_t} h_{T_t}^* + \frac{4}{3}\beta_\ell^2 \tilde{h}_T h_T^*\right]\right] + 16\hat{m}_\ell\,\text{Im}\left[e^{i\phi}\tilde{h}_V h_{T_t}^* + e^{-i\phi} h_V \tilde{h}_{T_t}^*\right], \end{aligned} \tag{6.38}$$

$$\begin{aligned} h_1 =& -4\beta_\ell\left(2\hat{m}_\ell \text{Re}\left[e^{i\phi}\tilde{h}_V h_S^* + e^{-i\phi} h_V \tilde{h}_S^*\right]\right. \\ &\left. - \text{Im}\left[e^{i\phi}[2\tilde{h}_{T_t} h_S^* + \sqrt{2}\tilde{h}_T h_P^*] + e^{-i\phi}[2h_{T_t}\tilde{h}_S^* + \sqrt{2}h_T \tilde{h}_P^*]\right]\right), \end{aligned} \tag{6.39}$$

$$h_2 = -\frac{8\beta_\ell^2}{3}\text{Re}\left[e^{i\phi}\left[\tilde{h}_V h_V^* + \tilde{h}_A h_A^* - 2\tilde{h}_T h_T^* - 4\tilde{h}_{T_t} h_{T_t}^*\right]\right]. \tag{6.40}$$

The time-dependent angular distributions therefore contain potentially new information encoded in the new angular observables s_i and h_i, similarly to the ones derived in Ref. [217] for $B \to K^* \ell^+ \ell^-$ and $B_s \to \phi \ell^+ \ell^-$. These observables measure the interference between B_d-mixing and $B \to K \ell^+ \ell^-$ decay, and they contain therefore additional information compared to the angular observables presented in Section 6.1.3.

Let us stress that these observables are accessible by combining the angular distributions for $B_d(t) \to K_S \ell^+ \ell^-$ and $\bar{B}_d(t) \to K_S \ell^+ \ell^-$, thus requiring flavour tagging. The coefficients h_i seem very difficult to extract, since they are associated with $\sinh(y\Gamma t)$ with y vanishing at the current accuracy. The coefficients s_0 and s_2 are associated with the CP asymmetry of angular coefficients: $G_i - \bar{G}_i$, whereas s_1 is associated with CP-averaged angular coefficients: $G_1 + \bar{G}_1$. The information on New Physics contained in the coefficients s_i will be the focus of the rest of this work.

6.2.5 Time-integrated observables

As discussed in Refs. [217, 353, 354], time integration should be performed differently in the context of hadronic machines and B-factories. The time-dependent expressions in Eqs. (6.33) and (6.34) are written in the case of tagging at a hadronic machine, assuming that the two b-quarks have been produced incoherently, with $t \in [0, \infty)$. In the case of a coherent $B_d \bar{B}_d$ pair produced at a B-factory, one must replace $\exp(-\Gamma t)$ by $\exp(-\Gamma|t|)$ and integrate over $t \in (-\infty, \infty)$ [353]. Interestingly, the integrated versions of CP-violating interference terms are different in both settings, and the measurement at hadronic machines involves an additional term compared to the B-factory case:

$$\langle G_i + \widetilde{G}_i \rangle_{\text{Hadronic}} = \frac{1}{\Gamma}\left[\frac{1}{1-y^2} \times (G_i + \widetilde{G}_i) - \frac{y}{1-y^2} \times h_i\right], \tag{6.41}$$

$$\langle G_i - \widetilde{G}_i \rangle_{\text{Hadronic}} = \frac{1}{\Gamma}\left[\frac{1}{1+x^2} \times (G_i - \widetilde{G}_i) - \frac{x}{1+x^2} \times s_i\right], \tag{6.42}$$

$$\langle G_i + \widetilde{G}_i \rangle_{\text{B-factory}} = \frac{2}{\Gamma}\frac{1}{1-y^2}[G_i + \widetilde{G}_i], \tag{6.43}$$

$$\langle G_i - \widetilde{G}_i \rangle_{\text{B-factory}} = \frac{2}{\Gamma}\frac{1}{1+x^2}[G_i - \widetilde{G}_i]. \tag{6.44}$$

Making contact with experimental measurements requires to consider the total time-integrated decay rate:

$$\left\langle \frac{d(\Gamma + \bar{\Gamma})}{dq^2} \right\rangle = \frac{1}{\Gamma(1-y^2)}\langle \mathcal{I} \rangle, \tag{6.45}$$

$$\langle \mathcal{I} \rangle_{\rm Hadronic} = 2(G_0 + \bar{G}_0 - y\, h_0) \,, \tag{6.46}$$

$$\langle \mathcal{I} \rangle_{\rm B-factory} = 2\langle \mathcal{I} \rangle_{\rm Hadronic}(h=0) \,, \tag{6.47}$$

where $\mathcal{I}$ is the usual normalisation considered in analyses of the angular coefficients. The factor of 2 arising from the time integration in the case of B-factories (correcting a mistake in Ref. [217]) comes from the consideration of entangled $B\bar{B}$ pairs, leading to twice as many possibilities to observe the decay of interest compared to the hadronic case. The normalised time-integrated angular coefficients at hadronic machines or B-factories are therefore:

$$\langle \Sigma_i \rangle_{\rm Hadronic} \equiv \frac{\langle G_i + \widetilde{G}_i \rangle_{\rm Hadronic}}{\langle d(\Gamma+\bar{\Gamma})/dq^2 \rangle_{\rm Hadronic}} = \frac{(G_i + \widetilde{G}_i) - y \times h_i}{\langle \mathcal{I} \rangle_{\rm Hadronic}} \,, \tag{6.48}$$

$$\langle \Sigma_i \rangle_{\rm B-factory} \equiv \frac{\langle G_i + \widetilde{G}_i \rangle_{\rm B-factory}}{\langle d(\Gamma+\bar{\Gamma})/dq^2 \rangle_{\rm B-factory}} = \langle \Sigma_i \rangle_{\rm Hadronic}(h=0) \,, \tag{6.49}$$

$$\langle \Delta_i \rangle_{\rm Hadronic} \equiv \frac{\langle G_i - \widetilde{G}_i \rangle_{\rm Hadronic}}{\langle d(\Gamma+\bar{\Gamma})/dq^2 \rangle_{\rm Hadronic}} = \frac{1-y^2}{1+x^2} \times \frac{(G_i - \widetilde{G}_i) - x \times s_i}{\langle \mathcal{I} \rangle_{\rm Hadronic}} \,, \tag{6.50}$$

$$\langle \Delta_i \rangle_{\rm B-factory} \equiv \frac{\langle G_i - \widetilde{G}_i \rangle_{\rm B-factory}}{\langle d(\Gamma+\bar{\Gamma})/dq^2 \rangle_{\rm B-factory}} = \langle \Delta_i \rangle_{\rm Hadronic}(h=s=0) \,. \tag{6.51}$$

We see that the interpretation of the time-integrated measurements $\langle \Sigma_i \rangle$ from $d\Gamma(B_d \to K_S\ell^+\ell^-) + d\Gamma(\bar{B}_d \to K_S\ell^+\ell^-)$ is straightforward in terms of the angular coefficients at $t=0$. The smallness of y means that h_i will have only a very limited impact. The time-integrated terms $\langle \Delta_i \rangle$ from $d\Gamma(B_d \to K_S\ell^+\ell^-) - d\Gamma(\bar{B}_d \to K_S\ell^+\ell^-)$ are subject to two different effects. On one side, they receive contributions proportional to x corresponding to different combination of interference terms (in the case of a measurement at a hadronic machine). On the other hand, they are multiplied (in all experimental set-ups) by a factor $(1-y^2)/(1+x^2)$.

We see therefore that $\langle \Sigma_i \rangle$ contain essentially the same information as $(G_i + \widetilde{G}_i)$, whereas $\langle \Delta_i \rangle$ have a potentially richer interpretation due to the s_i contribution. This contribution can be separated by comparing the time-integrated difference $d\Gamma(B \to K\ell^+\ell^-) - d\Gamma(\bar{B} \to K\ell^+\ell^-)$ in the case with mixing $(B_d \to K_S\ell^+\ell^-)$ and the case without mixing $(B^+ \to K^+\ell^+\ell^-)$. We have indeed (neglecting y)

$$\langle \Delta_i \rangle^{K_S}_{\rm Hadronic} \equiv \frac{\langle G_i - \widetilde{G}_i \rangle^{K_S}_{\rm Hadronic}}{\langle d(\Gamma+\bar{\Gamma})/dq^2 \rangle^{K_S}_{\rm Hadronic}} = \frac{(G_i - \widetilde{G}_i) - x s_i}{2(1+x^2)(G_0 + \bar{G}_0)} \tag{6.52}$$

leading to

$$\langle \Delta_i \rangle^{K_S}_{\rm Hadronic} = \frac{1}{1+x^2}\langle \Delta_i \rangle^{K^\pm} - \frac{x}{1+x^2}\sigma_i \qquad \sigma_i = \frac{s_i}{2\Gamma_\ell} \qquad i = 0,1,2\,. \tag{6.53}$$

We have [6]

$$\frac{1}{1+x^2} = 0.6284(24)\,, \qquad \frac{x}{1+x^2} = 0.4832(6)\,, \tag{6.54}$$

showing that there is a good sensitivity to σ_i using time-integrated observables. We will show that in the SM and in any NP extension with SM operators and chirally flipped operators, we obtain a very precise prediction for the σ_i. Therefore, also the relation between $\langle \Delta_i \rangle^{K_S}_{\rm Hadronic}$ and $\langle \Delta_i \rangle^{K^\pm}$ can be predicted with high precision which is a very powerful and generic test of the structure of the operators contributing (real, no scalars, no tensors).

Let us add that these time-integrated observables still require a flavour tagging to separate the decays originating from a B_d meson from the ones starting from a $\bar{B}_d$-meson, i.e. $d\Gamma(B_d \to K_S\ell^+\ell^-)$ and $d\Gamma(\bar{B}_d \to K_S\ell^+\ell^-)$. Therefore, this approach enables one to bypass the study of the time dependence, but it still requires initial-state flavour tagging (with the associated effective loss of statistical power).

6.2.6 Extension to other B_d and B_s decays into light spin-0 mesons

Our analysis applies to any $B \to P\ell^+\ell^-$ decay where the initial neutral meson mixes with its antimeson and the final meson P is a (scalar or pseudoscalar) spin-0 CP eigenstate.

Another mode that could be considered is $B_d \to K_L\ell^+\ell^-$. The opposite intrinsic parity of K_L with respect to K_S means that $\widetilde{G}_i = -\zeta_i \bar{G}_i$ and

$$\frac{d\Gamma(B_d \to K_L\ell^+\ell^-) \pm d\Gamma(\bar{B}_d \to K_L\ell^+\ell^-)}{ds\; d\cos\theta_\ell} = \sum_i [G_i \pm \widetilde{G}_i] P_i(\cos\theta_\ell) = \sum_i [G_i \mp \zeta_i \bar{G}_i] P_i(\cos\theta_\ell) \,, \tag{6.55}$$

where the G_i ($\bar{G}_i$) are defined in terms of $h_X(B_d \to K_L)$ ($\bar{h}_X(\bar{B}_d \to K_L)$). In the absence of CP violation, we would have $G_i = -\bar{G}_i$ due to the different normalisation for $h_X(B_d \to K_L)$ and $\bar{h}_X(\bar{B}_d \to K_L)$. The discussion

concerning time-dependent observables is unchanged. We see that the most promising observables $s_{0,1,2}$ can still be accessed through the difference $d\Gamma(B_d \to K_L\ell^+\ell^-) - d\Gamma(\bar{B}_d \to K_L\ell^+\ell^-)$. However, due to the additional experimental difficulties related to the identification of the K_L meson, we will focus on the K_S case in the following.

One can also consider B_s decays. The mixing parameters are different from the B_d case since x is much larger (whereas y is small but not vanishing) and the mixing angle $2\beta_s$ is very small [6]. In this case, the coefficients h_i are difficult to extract, since they are associated with $\sinh(y\Gamma t)$ with y small, but at least not vanishing, meaning that an extraction of h_i is possible in this case. The s_i coefficients are certainly easier to access, but they are different from zero only if there are large NP phases or large tensor contributions, which are not needed in the current global fits to $b \to s\ell^+\ell^-$ transitions (see for instance Ref. [132]).

One may consider $B_s \to f_0(980)\ell^+\ell^-$ with $\eta(f_0) = \eta(K_S) = 1$ and $B_s \to \eta(')\ell^+\ell^-$ with $\eta(\eta(')) = -1$. The determination of the form factors is quite challenging in all three cases, as their exact nature and mixing with other states are not known precisely yet. This translates into a significant spread of results for the form factors. We will thus focus in the following on $B_d \to K_S\mu\mu$ which is better understood from the theory point of view, but we will give a few results for the B_s to f_0, η, η' decays in Appendix 6.B.

6.3 New observables in $B_d \to K_S\mu\mu$ as probes of new physics

6.3.1 Real NP contributions to SM and chirally flipped Wilson coefficients

We will now consider the normalised observables

$$\sigma_i = \frac{s_i}{2(G_0 + \bar{G}_0)} = \frac{s_i}{2\Gamma_\ell}\,, \qquad \rho_i = \frac{s_i}{2(G_i + \bar{G}_i)}\,, \qquad i = 0,1,2\,, \tag{6.56}$$

where the normalisation comes from the CP-averaged decay rate $\Gamma_\ell = G_0 + \bar{G}_0$. We set $y = 0$ and we will neglect the tiny weak phase in $V_{tb}V_{ts}^*$ in the following.

We start by considering scenarios where NP enters only as real shifts to the Wilson coefficients for SM and chirally flipped operators ($\mathcal{C}_{7,7',9,9',10,10'}$). This case includes naturally the SM, but it also covers many NP scenarios currently favoured by global fits to $b \to s\ell^+\ell^-$ data [132]. In this case, we have only contributions from the amplitudes h_V, h_A and h_P. Neglecting the (tiny) weak phase in $V_{tb}V_{ts}^*$, gives $\tilde{h}_{V,A,P} = -h_{V,A,P}$ and $G_i = \bar{G}_i$ $(i = 0,1,2)$.

The s_i observables then become very simple, leading to[3]

$$\rho_0 = \rho_2 = \sigma_0 = -\frac{\sin\phi}{2}\,, \qquad \sigma_1 = 0\,, \qquad \phi = -2\beta\,. \tag{6.57}$$

We stress that these relations neither depend on a specific choice of form factors nor on assumptions made on charm-loop contributions. The only hypothesis required is that NP enters as real contributions to the SM Wilson coefficients. Therefore, a measurement of these observables would constitute a significant cross-check of the NP scenarios currently favoured by global fits to $b \to s\ell^+\ell^-$ data [132]. Moreover, the only parameter with a non-trivial but very small q^2-dependence at the kinematic endpoints is σ_2, such that the relations Eq. (6.57) can be checked by integrating over any kinematic q^2 range. On the other hand, a deviation from these values would constitute a very simple and powerful test of the presence of scalar/tensor operators or that of CP-violating NP phases. We discuss these two cases next.

6.3.2 Real NP contributions including scalar and tensor operators

Considering still real NP contributions, but adding possible scalar and tensor contributions, changes the above situation. The expressions for G_i and s_i can be reduced in the following way (neglecting m_ℓ effects for simplicity):

$$\begin{aligned}
G_0(=\bar{G}_0) &\simeq \frac{4}{3}\left|\bar{h}_V\right|^2 + \frac{4}{3}\left|\bar{h}_A\right|^2 + 2\left|\bar{h}_S\right|^2 + 2\left|\bar{h}_P\right|^2 + \frac{8}{3}\left|\bar{h}_{T_t}\right|^2 + \frac{4}{3}\left|\bar{h}_T\right|^2\,,\\
G_1(=\bar{G}_1) &\simeq 0\,,\\
G_2(=\bar{G}_2) &\simeq -\frac{4}{3}\left(\left|\bar{h}_V\right|^2 + \left|\bar{h}_A\right|^2 - 2\left|\bar{h}_T\right|^2 - 4\left|\bar{h}_{T_t}\right|^2\right)\\
&\simeq -G_0 + 2\left|\bar{h}_S\right|^2 + 2\left|\bar{h}_P\right|^2 + 8\left|\bar{h}_{T_t}\right|^2 + 4\left|\bar{h}_T\right|^2\,,
\end{aligned} \tag{6.58}$$

[3] If we neglect the lepton mass, we have also $\sigma_2 = -\sigma_0$.

leading to

$$\begin{aligned} s_0 &\simeq -2\sin\phi\left(G_0 - 4\left|\bar{h}_S\right|^2 - \frac{16}{3}\left|\bar{h}_{T_t}\right|^2\right), \\ s_1 &\simeq 8\sin\phi\left(-2\mathrm{Im}[\bar{h}_{T_t}]h_S^* + \sqrt{2}\mathrm{Im}[\bar{h}_T]h_P^*\right), \\ s_2 &\simeq -2\sin\phi\left(G_2 - \frac{32}{3}\left|\bar{h}_{T_t}\right|^2\right), \end{aligned} \tag{6.59}$$

Observing how these observables depend on the different scalar, pseudoscalar and tensor contribution allows us to define new observables separating these contributions:

$$R_S \equiv \frac{2}{\sin\phi}(-\sigma_2 + 2\sigma_0) - F_H^\ell + 3 \simeq 16\frac{|\bar{h}_S|^2}{\Gamma_\ell}, \tag{6.60}$$

$$R_{T_t} \equiv \frac{2}{\sin\phi}\sigma_2 + F_H^\ell - 1 \simeq \frac{64}{3}\frac{|\bar{h}_{T_t}|^2}{\Gamma_\ell}. \tag{6.61}$$

These observables could be obtained from a joint study of the charged and neutral $B \to K\ell^+\ell^-$ decays. Neglecting m_ℓ-suppressed contributions, R_S and R_{T_t} allow for a neat separation of the scalar and tensor contributions, contrary to the CP-averaged observables, and in this limit, these two observables must be positive in the absence of NP complex phases.

The combination

$$\begin{aligned} R_W \equiv R_S + 3R_{T_t} &= \frac{4}{\sin\phi}(\sigma_0 + \sigma_2) + 2F_H^\ell \\ &= \frac{2}{\sin\phi\Gamma_\ell}[s_0 + s_2 + \sin\phi(G_0 + \bar{G}_0 + G_2 + \bar{G}_2)] \simeq \frac{16}{\Gamma_\ell}[|\bar{h}_S|^2 + 4|\bar{h}_{T_t}|^2] \end{aligned} \tag{6.62}$$

is also interesting. It vanishes exactly in the limit where $m_\ell = 0$ and $\mathcal{C}_S = \mathcal{C}_P = \mathcal{C}_T = \mathcal{C}_{T_t} = 0$, no matter what the values (real or complex) for $\mathcal{C}_{7,7',9,9',10,10'}$. Indeed, in this limit, $G_0 = -G_2$, $\bar{G}_0 = -\bar{G}_2$ and $s_0 = -s_2$, as can be checked explicitly from Eqs. (6.4), (6.35) and (6.37). One can thus expect that the deviations of R_W from zero should be rather sensitive to the presence of scalar and tensor contributions.

When accounting for m_ℓ and the tiny imaginary part of V_{ts}, these new observables do not vanish any more in the SM. We give their SM values in Table 6.3 over the bin in q^2 from 1 to 6 GeV^2 using the inputs specified in Table 6.1. SM predictions at different values of q^2 or specific bins can easily be obtained using the above equations. We give in Table 6.A.1 the results using alternative models for the charm-loop contribution, showing a very good stability of our results with respect to the change of model, covered by our theoretical uncertainties[4]

The sensitivity to NP scalar and tensor contributions of these observables is

$$\begin{aligned} R_S &= 0.028|\mathcal{C}_S + \mathcal{C}_S|^2, \\ R_{T_t} &= 0.019|\mathcal{C}_T + \mathcal{C}_{T'}|^2, \\ R_W &= 0.028|\mathcal{C}_S + \mathcal{C}_{S'}|^2 + 0.056|\mathcal{C}_T + \mathcal{C}_{T'}|^2. \end{aligned} \tag{6.63}$$

Currently, the bounds on scalar contributions are quite loose. Ref. [120] suggest $|\mathcal{C}_{S\mu}| < 0.1$ and $0 < \mathcal{C}_{S'\mu} < 0.2$ obtained for NP models containing also SM-like and chirally flipped operators with real Wilson coefficients. We are not aware of studies giving bounds on tensor operators, probably due to the fact there are currently no indication of a need for such contributions in global fits.

In order to illustrate the effect of new scalar or tensor contributions, we consider two NP scenarios with $\mathcal{C}_S = 0.2$ and $\mathcal{C}_T = 0.2$, respectively. Although R_S and R_{T_t} are in principle sensitive to scalar and tensor operators, we see that the changes are rather small, as is expected from (6.63). The situation is different for R_W, which is constructed such that it vanishes exactly in the absence of scalar and tensor corrections in the limit $m_\ell = 0$. The SM value is different from zero due to m_ℓ-suppressed corrections, but its value is known very precisely, and it deviates from this value when scalar and/or tensor contributions are present.

Given the accuracy of the theory predictions, it seems thus possible to gain information on scalar and tensor contributions from R_S, R_{T_t} and R_W if they are measured precisely, in complement with the information provided by F_H^ℓ.

[4] Neglected doubly Cabibbo suppressed contributions with relative size of $O(\lambda^2) \simeq 4\%$ are not included in our estimate of the uncertainties, but they do not affect our conclusions concerning the capacity of theses observables to discriminate NP scenarios.

Observable	SM	Scen. 1	Scen. 2	Scen. 3	$C_S = 0.2$	$C_T = 0.2$
σ_0	0.368(5)	0.273(6)	0.402(5)	0.43(1)	0.368(5)	0.368(5)
σ_2	−0.359(5)	−0.266(6)	−0.392(4)	−0.415(9)	−0.359(5)	−0.357(5)
R_S	−0.107(4)	0.69(2)	−0.39(2)	−0.59(9)	−0.105(4)	−0.107(4)
R_{T_t}	0.035(1)	−0.225(8)	0.128(7)	0.19(3)	0.035(1)	0.036(1)
$R_W \times 10^2$	−0.179(8)	1.09(4)	−0.63(4)	−1.0(1)	−0.01(1)	0.04(3)

Table 6.3: Values of the observables in the SM, for the three different scenarios with new complex Wilson coefficients defined in Eq. (6.64) and for the scenarios with $\mathcal{C}_{S(T)} = 0.2$. All quoted values are for $B_d \to K_S \mu\mu$ and are binned in q^2 over $[1, 6]\,\text{GeV}^2$. The inputs are taken from Table 6.1 (neglected doubly Cabibbo-suppressed contributions are not included in our error estimates). A more comprehensive list of results is given in Table 6.A.1. Values for other fixed q^2 values of specific bins can be easily obtained from our expressions.

6.3.3 Complex NP contributions

The equalities in Eq. (6.57) do not hold in the presence of complex NP contributions. In principle, these contributions can be constrained by measuring Γ^ℓ and A_{FB}^ℓ, but their effect in those observables is suppressed by m_ℓ. Besides, such NP effects would show up in the direct CP-asymmetries A_0 and A_2 but due to the interferences between weak and strong phases in those observables the interpretation is less clear. Moreover, as can be seen in Appendix 6.A, hadronic uncertainties are significant for these observables compared to their sensitivity to NP, so that it is difficult to interpret a deviation from the SM expectations[5].

Our new observables s_i correspond to an interference between mixing and decay, and thus are sensitive to NP phases coming from all the amplitudes h_X and all Wilson coefficients. As an illustration of the added power of these observables, we can use Ref. [303] where the following scenarios obtain a good description of the data with the following best-fit points:

$$\begin{aligned}
&\text{Scenario 1}: \quad \mathcal{C}_{9\mu}^{\text{NP}} = -1.12 + i1.00\,, \\
&\text{Scenario 2}: \quad \mathcal{C}_{9\mu}^{\text{NP}} = -1.14 - i0.22\,, \qquad \mathcal{C}_{9'\mu}^{\text{NP}} = 0.40 - i0.38\,, \\
&\text{Scenario 3}: \quad \mathcal{C}_{9\mu}^{\text{NP}} = -1.13 - i0.12\,, \qquad \mathcal{C}_{9'\mu} = 0.52 - i1.80\,, \qquad \mathcal{C}_{10\mu}^{\text{NP}} = 0.41 + i0.13\,,
\end{aligned} \tag{6.64}$$

In these scenarios, we have still $\sigma_1 = \rho_1 = 0$, but the situation is rather different for the cases of $\sigma_{0,2}$. The resulting predictions integrating over the bin in q^2 from 1 to 6 GeV^2 are given in Table 6.3 using in addition the inputs in Table 6.1, i.e. including $m_\ell = m_\mu$ and the imaginary part of V_{ts}. In addition, we give the values for R_S, R_{T_t} and R_W for the three NP scenarios in (6.64). We give in Appendix 6.A the results using alternative models for the charm-loop contribution, showing a very good stability of our results with respect to the change of model. Moreover, our uncertainties cover the small changes in the central values when we consider different models for the $c\bar{c}$ contributions. The values in Table 6.3 serve as an illustration of the sensitivity of our observables to the three new physics scenarios: using our expressions, values for different q^2 ranges can be easily obtained. We point out that the uncertainties in Table 6.3 for σ_0 and σ_2 are fully dominated by the uncertainty on 2β.

We observe that although σ_0 and σ_2 are sensitive to the three NP scenarios, in fact R_S and R_{T_t} are even more sensitive. The deviations of the latter two observables from their SM expectation values allows for a distinction between the three different NP scenarios, even once hadronic uncertainties are taken into account. R_S and R_{T_t} are thus interesting probes for these new weak phases, whereas R_W is still very small in these scenarios (it would vanish in the limit where m_ℓ vanishes).

We emphasize that the above scenarios only serve as a benchmark to indicate the sensitivity of the observables to new phases. Once experimental measurements of these observables are available, performing a more sophisticated NP analysis, including scalar, tensor and complex phases would be interesting.

6.3.4 New physics benchmarking from $B_d \to K_S \mu\mu$

We have seen that a time-dependent angular analysis of $B_d \to K_S \mu\mu$ leads to 6 new observables, measuring CP violation in the interference between decay and mixing. They can be obtained from:

$$\begin{aligned}
&\frac{d\Gamma(B_d(t) \to K_S \ell^+ \ell^-) - d\Gamma(\bar{B}_d(t) \to K_S \ell^+ \ell^-)}{ds\; d\cos\theta_\ell} \\
&\quad = [G_0 - \widetilde{G}_0](t) + [G_1 - \widetilde{G}_1](t)\,\cos\theta_\ell + [G_2 - \widetilde{G}_2](t)\,\frac{1}{2}(3\cos^2\theta_\ell - 1)
\end{aligned} \tag{6.65}$$

[5] It was recently proposed to consider the CP asymmetries in the vincinity of charmonium resonances to enhance their values [355], but the interpretation of a non-vanishing CP-asymmetry in the charmonium region requires a precise knowledge of the strong dynamics of the resonances.

with the time dependence described in Eq. (6.34):

$$G_i(t) - \widetilde{G}_i(t) = e^{-\Gamma t}\Big[(G_i - \widetilde{G}_i)\cos(x\Gamma t) - s_i \sin(x\Gamma t)\Big] \,, \tag{6.66}$$

We also showed that time-integrated angular observables could also provide a good sensitivity on the coefficients $s_{0,1,2}$, by comparing neutral and charged modes at hadronic machines. These observables can be predicted accurately. Depending on the NP scenario, their theoretical predictions have little to no sensitivity to the specific choices for the form factors or the charm-loop contributions.

These three observables can be combined with the usual angular observables for $B \to K\ell^+\ell^-$ to obtain the observables $\sigma_{0,1,2}$, ρ_2 and $R_{S,T_t,W}$ defined in Eqs. (6.56) and (6.60) to (6.62), respectively. These quantities can be computed very precisely theoretically (see Table 6.3). If measured precisely, these observables provide powerful probes for New Physics scenarios:

- Do $\sigma_0, \sigma_1, \rho_2$ obey the simple relations in Eq. (6.57), directly related to B_d-$\bar{B}_d$ mixing?
  If yes, NP enters only the SM and chirally flipped operators $\mathcal{O}_{7(\prime),9(\prime),10(\prime)}$ with real contributions, in agreement with the NP scenarios currently favoured by global fits to $b \to s\ell^+\ell^-$ data.
- Do σ_0, σ_2, R_S and/or R_{T_t} deviate from their SM expectations?
  If yes, it means that NP enters with imaginary contributions, odd under CP-conjugation.
- Does R_W deviate from its SM expectation, but are σ_0, σ_2, R_S and R_{T_t} close to the SM?
  If yes, it means that NP enters through scalar and tensor contributions. Complementary information is then obtained through F_H^ℓ.

We thus see that the time-dependent angular analysis of $B_d \to K_S\mu\mu$ yields interesting observables for the discrimination among NP scenarios, if they can be measured with a sufficient precision[6]. This could be achieved in particular at LHCb, where the time-integrated observables have already been measured [238] and Belle II, following the measurements of branching ratios already performed at Belle [220]. Determining the potential of these two experiments for theses measurements is an interesting question which we leave for future work.

As already been discussed in Section 6.2.6, a similar approach could be used for B_s decays such as $B_s \to f_0\mu\mu$, $B_s \to \eta\mu\mu$, $B_s \to \eta'\mu\mu$. The theoretical determination of the relevant form factor becomes complicated due to the debated structure of these mesons, but we discuss a few results regarding these decays in Appendix 6.B.

6.4 Conclusions

An interesting to probe $b \to s\mu^+\mu^-$ transitions further consists in using neutral-meson mixing and time-dependent analysis in order to define new observables for B_d and B_s decays. This was applied to $B_d \to K^*\mu\mu$ and $B_s \to \phi\mu\mu$ in Ref. [217]. In this chapter, we considered the same idea in the simpler case of $B_d \to K_S\mu\mu$. The charged mode $B^\pm \to K^\pm\mu\mu$ has a much simpler angular structure, with only three observables which provide interesting but limited constraints on scalar and tensor contributions. The hadronic inputs (form factors and charm-loop contributions) are also much more simple to handle and analyse. We discussed the benefits of a time-dependent angular analysis of this mode.

After recalling the formalism in the absence of mixing (charged case), we turned to the neutral case. It required a careful definition of the kinematics of the mode to connect CP-conjugate decays that are now related through B_d mixing into $\bar{B}_d$. A time-dependent angular analysis leads to 6 new observables, measuring CP violation in the interference between decay and mixing. Three of these observables, denoted $s_{0,1,2}$, seem rather promising, and they can also be obtained from time-integrated angular observables by comparing neutral and charged modes at hadronic machines if initial-state flavour tagging is available. These 3 observables $s_{0,1,2}$ have simple expressions in terms of the transversity amplitudes given in Eqs. (6.35) to (6.37). They can be combined with the usual angular observables for $B \to K\ell^+\ell^-$ to obtain the observables $\sigma_{0,1,2}$, ρ_2 and $R_{S,T_t,W}$ defined in Eqs. (6.56) and (6.60) to (6.62).

Very interestingly, we showed that σ_0 and ρ_2 are very precisely known in the Standard Model and in New Physics scenarios with real contributions to SM and chirally-flipped operators. They depend only on the B_d-mixing angle, i.e. the CKM angle β, see Eq. (6.57), and they are valid for any value of the dilepton invariant mass q^2. We stress that these predictions are very robust, as they hold no matter what the assumptions on form factors and charm-loop contributions are. Therefore they constitute very powerful probes of the NP scenarios currently favoured by the global fits to $b \to s\ell^+\ell^-$ data.

We have then investigated two NP cases where these predictions are modified. We showed that R_S, R_T and R_W can probe other NP scenarios, namely scalar and tensor operators (with real contributions) and complex

[6] We have focused the discussion on $B_d \to K_S\mu\mu$ due to the current hints of New Physics in $b \to s\mu^+\mu^-$ transitions, but similar measurements in the electron sector would also be of interest to probe lepton flavour universality.

NP contributions entering with a CP-odd "weak" phase. The sensitivity of these observables to each scenario is different, and the theoretical uncertainties attached to the theoretical predictions are small, which allows us to provide a benchmark of NP scenarios hinging on the measurements of $s_{0,1,2}$. We also briefly discussed similar B_s decay modes such as $B_s \to f_0 \mu\mu$, $B_s \to \eta\mu\mu$ and $B_s \to \eta'\mu\mu$.

In conclusion, the simplicity of the underlying $B \to K\mu\mu$ decay has allowed us to provide a detail analysis of the flavour-tagged time-dependent analysis of $B_d \to K_S\mu\mu$. These new observables provide powerful cross checks of the various NP hypotheses. They may also contribute to global fits to $b \to s\ell^+\ell^-$ in a useful way, providing constraints of a different type on the short-distance physics encoded in Wilson coefficients.

Appendices

6.A Predictions for $B_d \to K_S \mu\mu$ observables in SM and NP scenarios

		SM	Scenario 1	Scenario 2	Scenario 3	$\mathcal{C}_S = 0.2$	$\mathcal{C}_T = 0.2$
$Br \times 10^8$	O.E.	8.4 ± 1.5	6.8 ± 1.2	7.2 ± 1.2	7.4 ± 1.3	8.4 ± 1.5	8.4 ± 1.5
	LCSR	7.9 ± 1.3	6.5 ± 1.0	6.9 ± 1.1	7.0 ± 1.1	7.9 ± 1.3	8.0 ± 1.3
	PQCD	8.6 ± 1.4	7.0 ± 1.1	7.4 ± 1.2	7.6 ± 1.2	8.6 ± 1.4	8.7 ± 1.4
$F_H^\ell \times 10^2$	O.E.	2.48 ± 0.04	2.50 ± 0.04	2.50 ± 0.04	2.48 ± 0.03	2.52 ± 0.04	3.05 ± 0.05
	LCSR	2.49 ± 0.04	2.51 ± 0.04	2.50 ± 0.04	2.48 ± 0.03	2.53 ± 0.04	3.05 ± 0.05
	PQCD	2.49 ± 0.03	2.51 ± 0.04	2.50 ± 0.04	2.48 ± 0.03	2.53 ± 0.03	3.05 ± 0.05
$A_0 \times 10^2$	O.E.	0	0.0 ± 2.3	0.0 ± 1.3	$0. \pm 4.$	0	0
	LCSR	0	3.9 ± 2.1	-2.2 ± 1.2	$-7. \pm 4.$	0	0
	PQCD	0	-1.285 ± 0.005	0.729 ± 0.003	2.27 ± 0.01	0	0
$\sigma_0 \times 10$	O.E.	3.68 ± 0.05	2.73 ± 0.06	4.02 ± 0.05	4.3 ± 0.1	3.68 ± 0.05	3.68 ± 0.05
	LCSR	3.68 ± 0.05	2.77 ± 0.06	3.99 ± 0.04	4.15 ± 0.04	3.68 ± 0.05	3.68 ± 0.05
	PQCD	3.68 ± 0.05	2.73 ± 0.06	4.03 ± 0.04	4.29 ± 0.01	3.68 ± 0.05	3.68 ± 0.05
$\sigma_2 \times 10$	O.E.	-3.59 ± 0.05	-2.66 ± 0.06	-3.92 ± 0.04	-4.15 ± 0.09	-3.59 ± 0.05	-3.57 ± 0.05
	LCSR	-3.59 ± 0.05	-2.69 ± 0.05	-3.89 ± 0.04	-4.05 ± 0.04	-3.59 ± 0.05	-3.57 ± 0.05
	PQCD	-3.59 ± 0.05	-2.66 ± 0.05	-3.92 ± 0.04	-4.18 ± 0.01	-3.59 ± 0.05	-3.57 ± 0.05
$R_S \times 10$	O.E.	-1.07 ± 0.04	6.9 ± 0.2	-3.9 ± 0.2	-5.9 ± 0.9	-1.05 ± 0.04	-1.07 ± 0.04
	LCSR	-1.07 ± 0.04	6.6 ± 0.2	-3.7 ± 0.2	-5.0 ± 0.5	-1.05 ± 0.04	-1.07 ± 0.04
	PQCD	-1.07 ± 0.04	6.9 ± 0.1	-4.0 ± 0.1	-6.2 ± 0.4	-1.05 ± 0.04	-1.07 ± 0.04
$R_{T_t} \times 10$	O.E.	0.35 ± 0.01	-2.25 ± 0.08	1.28 ± 0.07	1.9 ± 0.3	0.35 ± 0.01	0.36 ± 0.01
	LCSR	0.35 ± 0.01	-2.16 ± 0.06	1.21 ± 0.05	1.7 ± 0.2	0.35 ± 0.01	0.36 ± 0.01
	PQCD	0.35 ± 0.01	-2.27 ± 0.05	1.30 ± 0.05	2.0 ± 0.1	0.35 ± 0.01	0.36 ± 0.01
$R_W \times 10^2$	O.E.	-0.179 ± 0.008	1.09 ± 0.04	-0.63 ± 0.04	-1.0 ± 0.1	-0.01 ± 0.01	0.04 ± 0.03
	LCSR	-0.179 ± 0.008	1.05 ± 0.03	-0.60 ± 0.03	-0.83 ± 0.08	0.000 ± 0.009	0.05 ± 0.03
	PQCD	-0.179 ± 0.008	1.10 ± 0.02	-0.65 ± 0.02	-1.01 ± 0.07	-0.013 ± 0.008	0.03 ± 0.03

Table 6.A.1: $B_d \to K_S \mu\mu$ observables integrated from $1 - 6$ GeV^2 for different parametrisations of the $c\bar{c}$ model contribution associated with $\mathcal{C}_9$ (Our Estimate (O.E.), Light-Cone Sum Rules (LCSR), Perturbative QCD (PQCD)). The results are given in the SM case, for several NP scenarios with weak phases (Scenarios 1,2,3) and with contribution to scalar and tensor contributions ($\mathcal{C}_S$,$\mathcal{C}_T$). Neglected doubly Cabibbo-suppressed contributions are not included in our error estimates.

We give in Table 6.A.1 our predictions for the various observables of interest, integrated over the bin [1,6] GeV^2 for the dimuon invariant mass. We compute their values within the SM and several different scenarios of NP, described in Sections 6.3.2 and 6.3.3. We neglect doubly Cabibbo-suppressed contributions with relative size of $O(\lambda^2) \simeq 4\%$, which are not included in our error estimates.

We take into account the various sources of uncertainties (CKM, form factors, charm-loop contributions) and combine them in quadrature. We illustrate the impact of the model used for charm-loop contributions by considering three models described in Section 6.1.2:

- O.E.: Our estimate, corresponding to Eq. (5.71),
- LCSR: A range inspired by the Light-Cone Sum Rule Estimate of Ref. [116], given in Eq. (5.69),
- PQCD: The short-distance charm-loop contribution obtained from perturbative QCD given in Eq. (2.83), without attaching any uncertainty to the result.

As can be seen, our estimate is conservative as far as uncertainties are concerned. These uncertainties cover the central values of the other two models, and they do not hinder the discrimination among different NP scenarios for σ_0, σ_2, R_S, R_{T_t}, R_W.

6.B B_s decays

We can consider $B_s \to f_0(980)\mu\mu$ and $B_s \to \eta^{(\prime)}\mu\mu$ decays following the same formalism as $B_d \to K_{(S,L)}\mu\mu$, up to a few changes:

- the width difference $y \neq 0$ means that it becomes possible in principle to access h_i coefficients,
- the B_s mixing phase is much smaller than in the B_d case and is thus competing with the decay phase from V_{ts},
- the form factors describing these decays are not known as well as for $B \to K$ transitions, due to our limited knowledge of the structure of the f_0, η and η' mesons and their mixing with other states.

The expressions of the relevant form factors and matrix elements for $B_s \to \eta(')$ can be translated directly from the expressions in the $B_d \to K_S$ case described above. The matrix elements relevant to $\bar{B} \to f_0$ transition can be defined as [356]

$$\begin{aligned}
\langle f_0(p)|\bar{s}\gamma_\mu\gamma_5 b|\bar{B}_s(p_B)\rangle &= -i\left[(p_B+p)_\mu f_+(q^2) + \frac{m_{B_s}^2 - m_{f_0}^2}{q^2} q_\mu \left(f_0(q^2) - f_+(q^2)\right)\right], \\
\langle f_0(p)|\bar{s}\sigma_{\mu\nu}\gamma_5 b|\bar{B}_s(p_B)\rangle &= -\left[(p_B+p)_\mu q_\nu - (p_B+p)_\nu q_\mu\right] \frac{f_T(q^2)}{m_{B_s}+m_{f_0}}, \\
\langle f_0(p)|\bar{s}\gamma_5 b|\bar{B}_s(p_B)\rangle &= -i\frac{m_{B_s}^2 - m_{f_0}^2}{m_b - m_s} f_0(q^2),
\end{aligned} \tag{6.67}$$

leading to the amplitudes

$$\begin{aligned}
\bar{h}_V &= i\mathcal{N}\frac{\sqrt{\lambda_{B_s}}}{2\sqrt{q^2}}\left(\frac{2m_b}{m_{B_s}+m_{f_0}}(\mathcal{C}_7 - \mathcal{C}_{7'})f_T + (\mathcal{C}_9 - \mathcal{C}_{9'})f_+\right), \\
\bar{h}_A &= i\mathcal{N}\frac{\sqrt{\lambda_{B_s}}}{2\sqrt{q^2}}(\mathcal{C}_{10} - \mathcal{C}_{10'})f_+, \\
\bar{h}_S &= -i\mathcal{N}\frac{m_{B_s}^2 - m_{f_0}^2}{2}\left(\frac{(\mathcal{C}_S - \mathcal{C}_{S'})}{m_b - m_s}\right) f_0, \\
\bar{h}_P &= -i\mathcal{N}\frac{m_{B_s}^2 - m_{f_0}^2}{2}\left(\frac{(\mathcal{C}_P - \mathcal{C}_{P'})}{m_b - m_s} + \frac{2m_\ell}{q^2}(-\mathcal{C}_{10} + \mathcal{C}_{10'})\right) f_0, \\
\bar{h}_T &= \mathcal{N}\frac{\sqrt{\lambda_{B_s}}}{\sqrt{2}\,(m_{B_s}+m_{f_0})}\,(\mathcal{C}_T + \mathcal{C}_{T'})\,f_T, \\
\bar{h}_{T_t} &= \mathcal{N}\frac{\sqrt{\lambda_{B_s}}}{2\,(m_{B_s}+m_{f_0})}\,(\mathcal{C}_T - \mathcal{C}_{T'})\,f_T,
\end{aligned} \tag{6.68}$$

where $\lambda_{B_s} \equiv \lambda(m_{B_s}^2, m_{f_0}^2, q^2)$. The amplitudes h_X for $B_s \to f_0$ transitions can be obtained from $\bar{h}_X$ by taking the complex conjugate for all weak phases present in the amplitudes. We use the following form factors:

- For $B_s \to \eta$ and $B_s \to \eta'$, we use the updated results of Ref. [357]. In particular, we use updated values [358]
$$\alpha^+_{B_s\eta} = 0.5055 \pm 0.0195\,, \qquad \alpha^+_{B_s\eta'} = 0.4928 \pm 0.0284\,. \tag{6.69}$$
We stress that the values for $\alpha^{0,T}$ in Refs. [357, 358] only include errors from varying b_2. However, currently full errors are not available. Note that also the central value for $\alpha^+_{B_s\eta'}$ in Eq. (6.69) from Ref. [358] differs from that quoted in Ref. [357]. We stress that the $B_s \to \eta$ form factor at $q^2 = 0$, i.e. $f_i(0)$ is negative due to η-η' mixing. We are not aware of other determinations for these form factors.
- For $B_s \to f_0$, we use the Table I of Ref. [356] as a reference. We take their results from Table I ($f_+ = F_1$) with the parametrisation
$$f_i(q^2) = \frac{f_i(0)}{1 - a_i q^2/m_{B_s}^2 + b_i (q^2/m_{B_s}^2)^2}\,, \tag{6.70}$$

	SM	Scenario 1	Scenario 2	Scenario 3	$C_S = 0.2$	$C_T = 0.2$
$Br \times 10^8$	4.8 ± 1.7	3.9 ± 1.4	3.4 ± 1.2	3.3 ± 1.2	4.8 ± 1.7	4.8 ± 1.7
$F_H^\ell \times 10^2$	2.47 ± 0.08	2.48 ± 0.09	2.49 ± 0.10	2.48 ± 0.09	2.51 ± 0.08	3.20 ± 0.26
$A_0 \times 10^2$	0	0.0 ± 2.2	0.0 ± 0.4	$0. \pm 4.$	0	0
$\sigma_0 \times 10^2$	0.00 ± 0.05	-9.65 ± 0.70	-1.45 ± 0.16	-12.7 ± 1.9	0.00 ± 0.05	0.00 ± 0.05
$\sigma_2 \times 10^2$	0.00 ± 0.06	9.46 ± 0.70	1.41 ± 0.15	12.4 ± 1.7	0.00 ± 0.06	0.00 ± 0.06
$\theta_0 \times 10$	-5.00 ± 0.00	-4.61 ± 0.02	-4.989 ± 0.001	-3.70 ± 0.07	-5.00 ± 0.00	-4.997 ± 0.002
$\theta_2 \times 10$	4.876 ± 0.001	4.50 ± 0.02	4.864 ± 0.005	3.61 ± 0.07	4.874 ± 0.004	4.85 ± 0.01

Table 6.B.1: Values of the observables in the SM, for the three different scenarios with new complex Wilson coefficients defined in Eq. (6.64) and for the scenarios with $\mathcal{C}_{S(T)} = 0.2$. All quoted values are for $B_s \to f_0\mu\mu$ and are binned in q^2 over $[1, 6]\,\text{GeV}^2$. The inputs are taken from Table 6.1. Neglected doubly Cabibbo-suppressed contributions are not included in our error estimates.

	SM	Scenario 1	Scenario 2	Scenario 3	$C_S = 0.2$	$C_T = 0.2$
$Br \times 10^8$	7.2 ± 1.2	5.8 ± 1.0	6.2 ± 1.0	6.3 ± 1.1	7.2 ± 1.2	7.2 ± 1.2
$F_H^\ell \times 10^2$	2.59 ± 0.02	2.63 ± 0.03	2.62 ± 0.03	2.57 ± 0.02	2.63 ± 0.03	3.22 ± 0.09
$A_0 \times 10^2$	0	0.0 ± 2.2	0.0 ± 1.2	$0. \pm 4.$	0	0
$\sigma_0 \times 10^2$	0.00 ± 0.05	9.70 ± 0.60	-6.36 ± 0.26	-22.5 ± 0.6	0.00 ± 0.05	0.00 ± 0.05
$\sigma_2 \times 10^2$	0.00 ± 0.05	-9.47 ± 0.60	6.21 ± 0.27	22.0 ± 0.7	0.00 ± 0.05	0.00 ± 0.05
$\theta_0 \times 10$	5.00 ± 0.00	4.62 ± 0.02	4.87 ± 0.01	3.69 ± 0.08	5.00 ± 0.00	5.00 ± 0.00
$\theta_2 \times 10$	-4.871 ± 0.001	-4.49 ± 0.02	-4.74 ± 0.01	-3.59 ± 0.08	-4.869 ± 0.001	-4.844 ± 0.003

Table 6.B.2: Values of the observables in the SM, for the three different scenarios with new complex Wilson coefficients defined in Eq. (6.64) and for the scenarios with $\mathcal{C}_{S(T)} = 0.2$. All quoted values are for $B_s \to \eta\mu\mu$ and are binned in q^2 over $[1, 6]\,\text{GeV}^2$. The inputs are taken from Table 6.1. Neglected doubly Cabibbo-suppressed contributions are not included in our error estimates.

with $i = 0, +, T$. We should however be careful that there is a large spread of the theoretical estimates of these form factors, as illustrated by Table 1 of Ref. [359]. In case of asymmetric errors, we conservatively take the largest.

We can define the normalised angular observables:

$$\sigma_i = \frac{s_i}{2\Gamma_\ell}\,, \qquad \theta_i = \frac{h_i}{2\Gamma_\ell}\,, \tag{6.71}$$

considering also h_i observables since $y \neq 0$. In principle, we could build equivalent quantities to R_S, R_{T_t} and R_W defined in Eqs. (6.60) to (6.62) to isolate scalar and tensor amplitudes, but they would be affected by large uncertainties, as they would require dividing angular observables by $\sin\phi$ where ϕ is the small B_s mixing angle. We will thus consider only σ_i and θ_i, which we provide in the various scenarios of interest in Tables 6.B.1 to 6.B.3 for the three B_s decays, using our estimate (O.E.) for charm loops.

Similarly to the $B_d \to K_S\ell^+\ell^-$ case, we can derive general relations in the case of real NP contributions to SM and chirally flipped Wilson coefficients. The amplitudes h_X can be simplified exactly as in Section 6.3.1. If we take into account the different CKM coefficients (and different CP parities in some cases), we obtain for B_s decays

$$\sigma_0 = \sigma_2 = 0 \qquad \theta_0 = -\theta_2 = -\frac{1}{2}\eta(M)\,, \tag{6.72}$$

up to $O(\lambda^2)$ corrections (were we neglect the lepton mass to obtain the expression of θ_2).

The results illustrate the dependence of the angular observables on the NP scenario and the interest of measuring these quantities. Let us however that one should add to these results an additional theoretical systematic uncertainty reflecting our limited understanding of the form factors for these final states. Moreover, we neglected doubly Cabibbo-suppressed contributions with relative size of $O(\lambda^2) \simeq 4\%$, which are not included in our error estimates.

	SM	Scenario 1	Scenario 2	Scenario 3	$C_S = 0.2$	$C_T = 0.2$
$Br \times 10^8$	9.1 ± 1.9	7.4 ± 1.5	7.8 ± 1.6	8.1 ± 1.7	9.1 ± 1.9	9.2 ± 1.9
$F_H^\ell \times 10^2$	2.64 ± 0.04	2.70 ± 0.04	2.68 ± 0.04	2.63 ± 0.03	2.69 ± 0.04	3.29 ± 0.11
$A_0 \times 10^2$	0	0.0 ± 2.3	0.0 ± 1.3	$0. \pm 4.$	0	0
$\sigma_0 \times 10^2$	0.00 ± 0.05	9.7 ± 0.6	-6.3 ± 0.3	-22.5 ± 0.7	0.00 ± 0.05	0.00 ± 0.05
$\sigma_2 \times 10^2$	0.00 ± 0.05	-9.5 ± 0.6	6.2 ± 0.3	21.9 ± 0.6	0.00 ± 0.05	0.00 ± 0.05
$\theta_0 \times 10$	5.00 ± 0.00	4.62 ± 0.02	4.87 ± 0.01	3.69 ± 0.08	5.00 ± 0.00	5.00 ± 0.00
$\theta_2 \times 10$	-4.868 ± 0.002	-4.49 ± 0.02	-4.74 ± 0.01	-3.59 ± 0.08	-4.867 ± 0.002	-4.841 ± 0.004

Table 6.B.3: Values of the observables in the SM, for the three different scenarios with new complex Wilson coefficients defined in Eq. (6.64) and for the scenarios with $\mathcal{C}_{S(T)} = 0.2$. All quoted values are for $B_s \to \eta' \mu\mu$ and are binned in q^2 over $[1, 6]\,\text{GeV}^2$. The inputs are taken from Table 6.1. Neglected doubly Cabibbo-suppressed contributions are not included in our error estimates.

Part IV

New benchmarks for $b \to c\ell\bar{\nu}$

Chapter 7

Symmetries in $B \to D^* \ell \bar{\nu}$ angular observables

As discussed in Chapter 3, charged-current $b \to c\ell\bar{\nu}$ transitions exhibit deviations in LFUV observables comparing $\ell = \tau$ and lighter leptons. In some of the NP models explaining these deviations, there is a natural connection with the deviations of the $b \to s\ell^+\ell^-$ mode. It is thus interesting to further investigate these deviations. In this chapter and the following, we will propose two different alternate tests for the $b \to c\ell\bar{\nu}$ deviations which might help to elucidate the situation.

The first one of these tests is developed in this chapter, based on Ref. [360], where we apply the formalism of amplitude symmetries to the angular distribution of the decays $B \to D^*\ell\nu$ for $\ell = e, \mu, \tau$. Depending on the NP hypotheses chosen, we will identify a set of symmetries for the massless (electron and muon) and massive (tau) distributions that will lead us to find a set of dependencies or relations among the angular coefficients of the distribution. A similar exercise was done in Refs. [361–363] for the case of the decay mode $B \to K^*\mu\mu$. Here we will follow closely the detailed work in Ref. [361] to use the symmetries of the distribution in order to show that depending on the assumptions of the type of NP at work and the mass of the leptons, not all angular coefficients are independent.

These relations can be used in the case of the $B \to D^*\ell\nu$ decay as a way of cross-checking the consistency of the measurements of angular observables [1], but also to provide orientation on which kind of NP can be responsible for deviations with respect to the SM observed in these observables. For instance, these relations among the observables yield a combination of angular coefficients equivalent to the longitudinal polarisation $F_L^{D^*}$. This can provide a different handle for experimentalists to cross-check the polarisation fraction and confirm or not its high value, which appears difficult to accommodate with NP scenarios. Such a cross-check of the longitudinal D^* polarisation can also be useful if instabilities occur when extracting the p.d.f. of angular observables due to values of $F_L^{D^*}$ beyond physical boundaries for instance [2].

We will provide general expressions for the relations among observables but we will focus mainly on a baseline case without tensor contributions [3] . On the other hand, we will consider the contribution of the pseudoscalar operator that can help to increase $F_L^{D^*}$ and bring it closer to the Belle measurement, as found in Ref. [166]. We will also discuss the simplified case where there are no large NP phases in the Wilson coefficients, i.e. when we assume the coefficients are real or the NP phases are small.

In Section 7.1 we recall the structure of the angular distribution and define the most relevant observables following Ref. [166]. In Section 7.2 we describe the formalism and explain how to count the number of symmetries and dependencies for each particular case and we work out the dependencies in the massless and massive cases, paying special attention to the presence of pseudoscalar operators. In Section 7.3 these dependencies are used to determine $F_L^{D^*}$ (or equivalently $F_T^{D^*}$) in terms of the other observables in various ways and we discuss the impact of binning when using these relations. In Section 7.4 the expected experimental sensitivity of forthcoming experiments is discussed. We give our conclusions in Section 7.5. In Appendix 7.A some details on the derivation of the exact massive dependencies are provided and in Appendix 7.B we give illustrations of the binning effects

[1] An alternative approach is illustrated in Ref. [364] in the case of $B \to \rho(a_1)\ell\nu$ semileptonic decays where the study of specific NP operators extending the SM effective hamiltonian and the large-energy limit of form factors allows one to disentangle the role of the possible new structures in the differential 4-body distribution.

[2] This problem has already occurred in the case of the angular analysis of $B \to K^*\mu^+\mu^-$: the fit to CMS data [365] used to extract P_1, P_5' and F_L altogether from the data has exhibited instabilities that forced the authors of Ref. [365] to include additional information on F_L rather than leave it free in the fit.

[3] For the benchmark points analysed in Ref. [166], the presence of tensor operators decreases the value of $F_L^{D^*}$ for $B \to D^*\tau\nu$ substantially, increasing the discrepancy with the measured value. See Ref. [366] for the impact of tensor operators on R_{D^*} and other observables.

for the relations discussed in this analysis. Finally, in Appendix 7.C we discuss a possible signature of the presence of light right-handed neutrinos in the absence of tensors and imaginary contributions using the different "determinations" of $F_L^{D^*}$.

7.1 $\bar{B} \to D^* \ell \bar{\nu}$ angular distribution

7.1.1 Effective Hamiltonian and angular observables

The angular distribution for $B \to D^* \ell \nu$ has been extensively studied in the literature [184, 188, 367–371]. We base this Chapter on the studies in Ref. [166].

The distribution can be computed in the weak effective Hamiltonian framework using the Hamiltonian in Eq. (2.16) or Eq. (2.17) depending on the basis choice for the operators.

The resulting angular distribution is

$$\begin{aligned}\frac{d^4\Gamma}{dq^2 d\cos\theta_D d\cos\theta_\ell d\chi} = \frac{9}{32\pi}\Big\{ & I_{1c}\cos^2\theta_D + I_{1s}\sin^2\theta_D + \big[I_{2c}\cos^2\theta_D + I_{2s}\sin^2\theta_D\big]\cos 2\theta_\ell \\ & + \big[I_{6c}\cos^2\theta_D + I_{6s}\sin^2\theta_D\big]\cos\theta_\ell + \big[I_3\cos 2\chi + I_9\sin 2\chi\big]\sin^2\theta_\ell \sin^2\theta_D \\ & + \big[I_4\cos\chi + I_8\sin\chi\big]\sin 2\theta_\ell \sin 2\theta_D + \big[I_5\cos\chi + I_7\sin\chi\big]\sin\theta_\ell \sin 2\theta_D \Big\},\end{aligned} \tag{7.1}$$

where the angular coefficients $I_i \equiv I_i(q^2)$ are given in Ref. [166]:

$$I_{1c} = 2N\left[|\tilde{H}_0^-|^2 + \frac{m_\ell^2}{q^2}|\tilde{H}_0^+|^2 + 2\frac{m_\ell^2}{q^2}|\tilde{H}_t|^2\right], \tag{7.2}$$

$$I_{1s} = \frac{N}{2}\left[3\big(|\tilde{H}_+^-|^2 + |\tilde{H}_-^-|^2\big) + \frac{m_\ell^2}{q^2}\big(|\tilde{H}_+^+|^2 + |\tilde{H}_-^+|^2\big)\right], \tag{7.3}$$

$$I_{2c} = 2N\left[-|\tilde{H}_0^-|^2 + \frac{m_\ell^2}{q^2}|\tilde{H}_0^+|^2\right], \tag{7.4}$$

$$I_{2s} = \frac{N}{2}\left[|\tilde{H}_+^-|^2 + |\tilde{H}_-^-|^2 - \frac{m_\ell^2}{q^2}\big(|\tilde{H}_+^+|^2 + |\tilde{H}_-^+|^2\big)\right], \tag{7.5}$$

$$I_3 = -2N\,\mathrm{Re}\left[\tilde{H}_+^-\tilde{H}_-^{-*} - \frac{m_\ell^2}{q^2}\tilde{H}_+^+\tilde{H}_-^{+*}\right] \tag{7.6}$$

$$I_4 = N\,\mathrm{Re}\left[(\tilde{H}_+^- + \tilde{H}_-^-)\tilde{H}_0^{-*} - \frac{m_\ell^2}{q^2}(\tilde{H}_+^+ + \tilde{H}_-^+)\tilde{H}_0^{+*}\right] \tag{7.7}$$

$$I_5 = 2N\,\mathrm{Re}\left[(\tilde{H}_+^- - \tilde{H}_-^-)\tilde{H}_0^{-*} - \frac{m_\ell^2}{q^2}(\tilde{H}_+^+ + \tilde{H}_-^+)\tilde{H}_t^*\right], \tag{7.8}$$

$$I_{6c} = 8N\frac{m_\ell^2}{q^2}\,\mathrm{Re}\big[\tilde{H}_0^+\tilde{H}_t^*\big], \tag{7.9}$$

$$I_{6s} = 2N\big(|\tilde{H}_+^-|^2 - |\tilde{H}_-^-|^2\big) \tag{7.10}$$

$$I_7 = 2N\,\mathrm{Im}\left[(\tilde{H}_+^- + \tilde{H}_-^-)\tilde{H}_0^{-*} - \frac{m_\ell^2}{q^2}(\tilde{H}_+^+ - \tilde{H}_-^+)\tilde{H}_t^*\right], \tag{7.11}$$

$$I_8 = N\,\mathrm{Im}\left[(\tilde{H}_+^- - \tilde{H}_-^-)\tilde{H}_0^{-*} - \frac{m_\ell^2}{q^2}(\tilde{H}_+^+ - \tilde{H}_-^+)\tilde{H}_0^{+*}\right] \tag{7.12}$$

$$I_9 = -2N\,\mathrm{Im}\left[\tilde{H}_+^-\tilde{H}_-^{-*} - \frac{m_\ell^2}{q^2}\tilde{H}_+^+\tilde{H}_-^{+*}\right] \tag{7.13}$$

where N is a normalisation

$$N = \mathcal{B}_{D^*\to D\pi}\frac{G_F^2|V_{cb}|^2}{48(2\pi)^3 m_B^3}q^2\lambda_{BD^*}^{1/2}(q^2)\left(1 - \frac{m_\ell^2}{q^2}\right)^2, \tag{7.14}$$

with $\lambda_{BD^*}(q^2) = m_B^4 + m_{D^*}^4 + q^4 - 2(m_B^2 m_{D^*}^2 + m_B^2 q^2 + m_{D^*}^2 q^2)$ and the amplitudes $\tilde{H}$ correspond to linear combinations of transversity amplitudes for various currents. We can write them in the following way to make the dependence on m_ℓ explicit:

$$\tilde{H}_i^+ = H_i - 2\frac{\sqrt{q^2}}{m_\ell}H_{T,i} \qquad \tilde{H}_i^- = H_i - 2\frac{m_\ell}{\sqrt{q^2}}H_{T,i} \qquad \tilde{H}_t = \frac{\sqrt{q^2}}{m_\ell}\tilde{H}_P \tag{7.15}$$

where $i = 0, +, -$ and H_i correspond to vector and axial currents whereas $H_{T,i}$ correspond to tensor currents, and $\tilde{H}_P$ combines two amplitudes H_t and H_P:

$$\tilde{H}_P = \frac{m_\ell}{\sqrt{q^2}} H_t + H_P \tag{7.16}$$

The H_i amplitudes depend on form factors and on q^2, but not on the lepton mass. In particular, the presence of $1/m_\ell$ in $\tilde{H}_i^+$ means that the discussion of the limit $m_\ell \to 0$ should be considered after expressing all the angular coefficients in terms of H_i.

7.1.2 Observables

Contrary to $B \to K^* \ell\ell$ [87, 214], there are no specific discussions to consider concerning the possibility of optimised observables, since all $B \to D^*$ form factors either vanish or yield the same Isgur-Wise function ξ in the heavy quark limit (see Section 2.5.1), so any ratio of angular observables is appropriate to reduce uncertainties from form factors. We thus take almost the same list as Ref. [166] for the 12 observables that form a basis[4]:

$$O_i = \left\{ A_0, A_3, A_4, A_5, A_{6s}, A_7, A_8, A_9, A_{\rm FB}, R_{A,B}, F_L^{D^*}, d\Gamma/dq^2 \right\} \tag{7.17}$$

Compared to Ref. [166], we do not include the observable A_{λ_ℓ} in this list because it is related to the τ polarisation and requires one coefficient not included in the angular distribution. Instead we must introduce an additional observable (not included in Ref. [166]) so that the numbers of angular coefficients and observables match. We may choose for instance:

$$A_0 = \frac{1}{d\Gamma/dq^2}(I_{1c} + I_{1s}) \tag{7.18}$$

We recall here the definition of the observables defined in Ref. [166] that play an important role in this analysis:

- The differential decay rate
$$\frac{d\Gamma}{dq^2} = \frac{1}{4}(3I_{1c} + 6I_{1s} - I_{2c} - 2I_{2s}) \tag{7.19}$$
- The longitudinal and transverse D^* polarisation decay rates:
$$F_L^{D^*} = \frac{d\Gamma_L/dq^2}{d\Gamma/dq^2} = \frac{1}{d\Gamma/dq^2}\frac{1}{4}(3I_{1c} - I_{2c}) \tag{7.20}$$
$$F_T^{D^*} = 1 - F_L^{D^*} = \frac{d\Gamma_T/dq^2}{d\Gamma/dq^2} = \frac{1}{d\Gamma/dq^2}\frac{1}{2}(3I_{1s} - I_{2s}) \tag{7.21}$$
In order to make a more explicit contact with the integrated longitudinal polarisation we also introduce $\tilde{F}_L^{D^*} = (d\Gamma_L/dq^2)/\Gamma$ and $\tilde{F}_T^{D^*} = (d\Gamma_T/dq^2)/\Gamma$, where $\Gamma = \Gamma(B \to D^* \ell\nu)$ with $\ell = \tau, \mu, e$.
- The ratio $R_{A,B}$ describing the relative weight of the various angular coefficients in the partial differential decay rate with respect to θ_ℓ, in analogy with the longitudinal polarisation fraction
$$R_{A,B}(q^2) = \frac{d\Gamma_A/dq^2}{d\Gamma_B/dq^2} = \frac{1}{2}\frac{(I_{1c} + 2I_{1s} - 3I_{2c} - 6I_{2s})}{(I_{1c} + 2I_{1s} + I_{2c} + 2I_{2s})} \tag{7.22}$$

Eqs. (7.19) to (7.21) are the "standard definitions" of $d\Gamma/dq^2$, $F_L^{D^*}$ and $F_T^{D^*}$ respectively, and they are used to determine these observables with this particular functional dependence of the angular coefficients I.

Similarly to the discussion in Ref. [373], the definition of observables integrated over a bin (or over the whole phase space) requires some care. Experimentally, the measurement yields the integrated angular coefficients $\langle I_k \rangle_\ell$ with the definition[5]

$$\langle X \rangle_\ell = \int_{m_\ell^2}^{(m_B - m_{D^*})^2} dq^2\, X \tag{7.23}$$

where the subscripts ℓ and 0 indicate the massive case (with m_ℓ) and the massless case respectively. We can then define the "standard" integrated longitudinal and transverse polarisations

$$\langle \tilde{F}_L^{D^*} \rangle_\ell = \frac{1}{4\Gamma}\left(3\langle I_{1c}\rangle_\ell - \langle I_{2c}\rangle_\ell\right) \tag{7.24}$$

[4] Further discussions of this differential decay rate can be found in Ref. [372] including CP-violating observables and in Ref. [189] when D^* subsequently decays either to $D\pi$ or to $D\gamma$.

[5] Notice that the definition of $\langle I_i \rangle$ in Ref. [166] is normalised with $\Gamma(B \to D^* \ell\nu)$, while we prefer to keep the dependence on $\Gamma(B \to D^* \ell\nu)$ explicit.

m_ℓ	Tensor ops.	Pseudoscalar op.	Coefficients	Dependencies	Amplitudes	Symmetries
0	No	No	11	6	3	1
0	No	Yes	11	5	4	2
0	Yes	No	11	0	6	1
0	Yes	Yes	12	0	7	2
$\neq 0$	No	No	12	5	4	1
$\neq 0$	No	Yes	12	5	4	1
$\neq 0$	Yes	No	12	0	7	2
$\neq 0$	Yes	Yes	12	0	7	2

Table 7.1: Symmetries and dependencies among the $B \to D^* \ell \nu$ angular observables depending on the mass of the lepton and the contribution of tensor and pseudoscalar operators.

$$\langle \tilde{F}_T^{D^*} \rangle_\ell = \frac{1}{2\Gamma} (3\langle I_{1s} \rangle_\ell - \langle I_{2s} \rangle_\ell) \tag{7.25}$$

The Belle measurement is actually $\langle \tilde{F}_L^{D^*} \rangle_\tau^{\text{Belle}} = 0.60 \pm 0.09$.

At this stage, a brief comment on the possible NP contributions is useful. Most models discussed in Section 3.1.3 that explain the data in $b \to c\ell\nu$ through single-particle exchanges do not generate tensor contributions. The exception to this is the scalar $SU(2)_L$-doublet leptoquark R_2 (as illustrated, for instance, in Ref. [374]) which however generates much larger contributions to g_{S_L} (i.e. g_S and g_P) than to g_{T_L} (i.e. g_T and g_{T5}). This effect is enhanced by the running from the NP scale (1 TeV) down to the m_b scale (reducing the tensor contribution by $\sim 20\%$ and increasing the scalar contribution by $\sim 80\%$), so that scalar contributions are likely to be larger than the tensor contributions if the latter are present [82]. In Refs. [82, 83], a model with a single R_2 leptoquark with complex couplings was shown to have a lower SM-pull than other NP scenarios once the constraint from the B_c lifetime was taken into account. In Ref. [192], a viable model with the R_2 leptoquark was proposed in combination with the S_1 leptoquark, leading to (large real) vector couplings as well as (large imaginary) scalar and (smaller imaginary) tensor couplings.

Although some scenarios might allow for large imaginary contributions, this is mainly due to the limited number of observables currently available that constrain them.

We will thus consider as a baseline scenario that tensor contributions are subleading compared to other operators. We will also consider that the imaginary parts of the amplitudes can be neglected. In the SM as well as in the case of real NP, the only phase comes from the CKM matrix element, and it is actually the same for all the amplitudes. Under our baseline scenario, for instance, the angular coefficients corresponding to imaginary parts ($I_{7,8,9}$) are either small or vanishing, as well as any imaginary contribution. For completeness we will provide full expressions for the relations among the coefficients including these terms (see Appendix 7.A for the general expressions in the massive case).

7.2 Relations among angular coefficients

7.2.1 Symmetries and dependencies

The decay $B \to D^* \ell \nu$ has a rich angular structure, and it is interesting to investigate whether all the angular observables defined in the previous section are independent, following the same steps as in Refs. [214, 361–363] for $B \to K^* \ell\ell$. We can consider the angular coefficients as being bilinears in

$$\begin{aligned} \boldsymbol{A} = \{&\text{Re}[H_0], \text{Im}[H_0], \text{Re}[H_+], \text{Im}[H_+], \text{Re}[H_-], \text{Im}[H_-], \\ &\text{Re}[H_{T,0}], \text{Im}[H_{T,0}], \text{Re}[H_{T,+}], \text{Im}[H_{T,+}], \text{Re}[H_{T,-}], \text{Im}[H_{T,-}], \text{Re}[\tilde{H}_P], \text{Im}[\tilde{H}_P]\} \end{aligned} \tag{7.26}$$

An infinitesimal transformation will be given by

$$\boldsymbol{A}' = \boldsymbol{A} + \boldsymbol{\delta} \tag{7.27}$$

For the infinitesimal transformation to leave the coefficients I unchanged, the vector $\boldsymbol{\delta}$ has to be perpendicular to the hyperplane spanned by the set of gradient vectors $\boldsymbol{\nabla} I_i$ (with the derivatives taken with respect to the various elements of $\boldsymbol{A}$). If the I_i are all independent, the gradient vectors should span the whole space available for the coefficients, i.e. the dimension of the space for the gradient vectors should be identical to the number of angular coefficients.

One can define:

- The number of coefficients n_c, given directly by the angular distribution
- The number of dependencies n_d, given by the difference between the number of angular coefficients I_i and the dimension of the space given by the gradient vectors (provided by the rank of the matrix $M_{ij} = \nabla_i I_j$)
- The number of helicity/transversity amplitudes n_A, leading to $2n_A$ real degrees of freedom
- The number of continuous symmetries n_s explaining the degeneracies among angular coefficients

One has the following relation

$$n_c - n_d = 2n_A - n_s \tag{7.28}$$

which we can investigate in various cases for $B \to D^* \ell\nu$ summarised in Table 7.1.

As discussed above, the assumption of no tensor contributions seems favoured by the current global fits and we will stick to this assumption. In this case it is expected according to Table 7.1 the existence of 5 or 6 relations. The presence or absence of the pseudoscalar operator does not modify the outcome of the analysis and the number of dependencies in the massive case due to Eq. (7.16). However, we find interesting to discuss its effect separately as it was found in Ref. [166] that such a pseudoscalar contribution can help to alleviate the tension in $F_L^{D^*}$ for $B \to D^* \tau\nu$.

We can now explore the dependence relations between angular coefficients, depending on the lepton mass, the presence of pseudoscalar and tensor operators. These relations can be used as a consistency test among the observables if all of these observables are measured in order to check the very general assumptions made to derive them. If these relations are not fulfilled, it means that there is an issue with one or more of the measurements or that some of the underlying assumptions (negligible NP in tensor operator, negligible imaginary parts) are not correct. Such tests are completely independent of any assumption on the details of the NP model or the hadronic inputs.

7.2.2 Massless case with no pseudoscalar operator and no tensor operators

The expressions for the angular observables become in terms of the amplitudes themselves

$$\begin{aligned}
I_{1c} =& 2N \times |H_0|^2 && (7.29)\\
I_{1s} =& \frac{N}{2} \times 3\left[|H_+|^2 + |H_-|^2\right] && (7.30)\\
I_{2c} =& 2N \times (-1)|H_0|^2 && (7.31)\\
I_{2s} =& \frac{N}{2}\left[|H_+|^2 + |H_-|^2\right] && (7.32)\\
I_3 =& -2N \times \mathrm{Re}[H_+ H_-^*] && (7.33)\\
I_4 =& N\left[\mathrm{Re}[H_0 H_+^*] + \mathrm{Re}[H_0 H_-^*]\right] && (7.34)\\
I_5 =& 2N\left[\mathrm{Re}[H_0 H_+^*] - \mathrm{Re}[H_0 H_-^*]\right] && (7.35)\\
I_{6c} =& 0 && (7.36)\\
I_{6s} =& 2N\left[|H_+|^2 - |H_-|^2\right] && (7.37)
\end{aligned}$$

$$\begin{aligned}
I_7 =& 2N\left[-\mathrm{Im}[H_0 H_+^*] - \mathrm{Im}[H_0 H_-^*]\right] && (7.38)\\
I_8 =& N\left[-\mathrm{Im}[H_0 H_+^*] + \mathrm{Im}[H_0 H_-^*]\right] && (7.39)\\
I_9 =& -2N \times \mathrm{Im}[H_+ H_-^*] && (7.40)
\end{aligned}$$

In this case, the only continuous symmetry that can be found is simply

$$H_0 \to e^{i\alpha} H_0\,, \qquad H_- \to e^{i\alpha} H_-\,, \qquad H_+ \to e^{i\alpha} H_+ \tag{7.41}$$

and only 5 of the 11 observables [6] are independent and 6 dependencies are found. Consequently, one can invert the system to determine the value of the real and imaginary parts of the amplitudes in terms of some of the angular coefficients, and re-express the other ones in terms of the same angular coefficients leading to the following relations:

$$I_{1c} = -I_{2c} \tag{7.42}$$

[6] Notice that there are 11 coefficients in this case: $I_{6c} = 0$ and consequently there are 11 observables since A_{FB} and A_{6s} are proportional.

$$I_{1s} = 3I_{2s} \tag{7.43}$$
$$-4I_3 I_{2c} = -4I_4^2 + I_5^2 - I_7^2 + 4I_8^2 \tag{7.44}$$
$$-2I_9 I_{2c} = I_5 I_7 - 4I_4 I_8 \tag{7.45}$$
$$-4I_{2c}\left(\frac{1}{2}I_{6s} + \frac{2}{3}I_{1s}\right) = (2I_4 + I_5)^2 + (I_7 + 2I_8)^2 \tag{7.46}$$
$$-4I_{2c}\left(-\frac{1}{2}I_{6s} + \frac{2}{3}I_{1s}\right) = (-2I_4 + I_5)^2 + (I_7 - 2I_8)^2 \tag{7.47}$$

These relations can be used as a consistency test among the observables if all of these observables are measured, under the hypothesis that we have outlined (negligible lepton mass, negligible pseudoscalar and tensor operators).

Another way of exploiting these equations consists in combining the non-trivial relations Eqs. (7.44) to (7.47) under the assumption that $I_{7,8,9} = 0$ (taking all imaginary parts to be zero). For future use under this assumption we reorganise these equations, allowing us to make contact with the massive ones later on:

$$I_3^2 = \frac{4}{9}I_{1s}^2 - \frac{1}{4}I_{6s}^2 \tag{7.48}$$
$$I_4^2 = -\frac{1}{3}I_{1s}I_{2c} + \frac{1}{2}I_{2c}I_3 \tag{7.49}$$
$$I_5^2 = -\frac{2}{3}I_{2c}(2I_{1s} + 3I_3) \tag{7.50}$$

One of the dependencies disappears once $I_{7,8,9} = 0$ is taken.

7.2.3 Massless case with pseudoscalar operator but no tensor operators

The same relations between angular observables and amplitudes hold as in the previous case, apart from

$$I_{1c} = 2N\left[|H_0|^2 + 2|H_P|^2\right] \tag{7.51}$$

One can see that the two symmetries are

$$H_0 \to e^{i\alpha}H_0\,, \qquad H_- \to e^{i\alpha}H_-\,, \qquad H_+ \to e^{i\alpha}H_+\,, \qquad H_P \to e^{i\beta}H_P\,, \tag{7.52}$$

Again, by inverting the system one can obtain the same relations as in the massless case without pseudoscalar contributions, see Eqs. (7.43) to (7.47), except for Eq. (7.42) which is not fulfilled.

Like in the previous case, these relations can be used as a consistency test among the observables if all of these observables are measured, under the hypothesis that we have outlined (negligible lepton mass, negligible tensor operators).

7.2.4 Massive case with pseudoscalar operator but no tensor operators

The symmetries in the massive case with pseudoscalar operator but no tensors are in principle a simple extension of the analogous massless case. However, obtaining the expression of the dependencies in the massive case is a rather non-trivial task. The absence of tensors implies that there is no distinction between "+" and "-" components of $\tilde{H}_i^+$ and $\tilde{H}_i^-$ (see Eq. (7.15)) and the only surviving symmetry in this case is

$$H_0 \to e^{i\alpha}H_0\,, \quad H_- \to e^{i\alpha}H_-\,, \quad H_+ \to e^{i\alpha}H_+\,, \quad H_t \to e^{i\alpha}H_t\,, \quad H_P \to e^{i\alpha}H_P \tag{7.53}$$

One finds five dependencies in this case, which are identified by solving the system of non-linear equations. The first one is trivial:

$$0 = I_{1s}\left(1 - \frac{m_\ell^2}{q^2}\right) - I_{2s}\left(3 + \frac{m_\ell^2}{q^2}\right) \tag{7.54}$$

and the other exact four non-trivial dependencies are detailed in Appendix 7.A.

We will consider the simplifying case where all Wilson coefficients are real so that $I_{7,8,9}$ and all imaginary contributions can be neglected (see Appendix 7.A for the general case without these assumptions). The remaining four dependencies are then simplified substantially

$$I_3^2 = \left(1 - \frac{m_\ell^2}{q^2}\right)^2\left[\left(\frac{2I_{1s}}{3 + m_\ell^2/q^2}\right)^2 - \frac{I_{6s}^2}{4}\right] \tag{7.55}$$
$$I_4^2 = \frac{I_{2c}(2I_{1s}(m_\ell^2 - q^2) + I_3(m_\ell^2 + 3q^2))}{2(m_\ell^2 + 3q^2)} \tag{7.56}$$

$$I_5^2 = \left[-4I_{2c}I_{6c}I_{6s}(m_\ell^2-q^2)^2(m_\ell^2+3q^2) + I_{6c}^2(m_\ell^2-q^2)^2\left[2I_{1s}(m_\ell^2-q^2)+I_3(m_\ell^2+3q^2)\right]\right.$$
$$\left. -16I_{2c}^2q^4\left[2I_{1s}(-m_\ell^2+q^2)+I_3(m_\ell^2+3q^2)\right]\right] / \left[8I_{2c}(m_\ell^2-q^2)^2(m_\ell^2+3q^2)\right] \quad (7.57)$$

$$I_{6c}^2 = -8m_\ell^2\left[I_{1c}I_{2c}(-m_\ell^2+q^2)+I_{2c}^2(m_\ell^2+q^2)\right] / \left[(m_\ell^2-q^2)^2\right] \quad (7.58)$$

The first three equations above are the generalisation of Eqs. (7.48) to (7.50) in the massive case while the last equation is new: it would vanish in the massless limit with no tensors. These relations can be used as a consistency test among the observables if all of these observables are measured, under the hypothesis that we have outlined (no tensor operators, imaginary contributions negligible).

The last two equations can be combined to get rid of the I_{6c}^2 term and obtain the massive counterpart of Eq. (7.50):

$$I_5^2 = \left[4(m_\ell^2-q^2)^2I_{1s}(m_\ell^2(I_{1c}-I_{2c})-2q^2I_{2c})+2(m_\ell^2+3q^2)(m_\ell^4(I_{1c}-I_{2c})-2q^4I_{2c}\right.$$
$$\left. -m_\ell^2q^2(I_{1c}+I_{2c}))I_3-(m_\ell^2-q^2)^2(m_\ell^2+3q^2)I_{6c}I_{6s}\right] / \left[2(m_\ell^2-q^2)^2(m_\ell^2+3q^2)\right] \quad (7.59)$$

Eq. (7.58) has obviously no counterpart in the massless case, as it vanishes then [7].

7.2.5 Cases with tensor operators

In the massive case with tensors the degeneracy between the $\tilde{H}_i^+$ and $\tilde{H}_i^-$ is broken and two symmetries are identified. The symmetries are better described in terms of the tilde-fields:

$$\tilde{H}_i^- \to e^{i\alpha}\tilde{H}_i^-\,, \qquad \tilde{H}_i^+ \to e^{i\beta}\tilde{H}_i^+\,, \qquad \tilde{H}_t \to e^{i\beta}\tilde{H}_t\,. \quad (7.60)$$

Unfortunately there are no dependencies in this case. The same is true in the massless case.

7.3 Expressions of the D^* polarisation

In the previous section, we have obtained several relationships between the angular coefficients under various hypotheses, assuming that tensor contributions are negligible. In Sections 7.3.2 to 7.3.4, we will provide these exact relationships in their binned form, but the corresponding unbinned versions have exactly the same form.

7.3.1 Massless case without pseudoscalar operator

For completeness we discuss the case with zero mass and no pseudoscalar operator, but still including all imaginary terms. Eqs. (7.42) and (7.43) are trivial. Eqs. (7.44) to (7.47) can be rewritten in terms of observables providing different determinations of $F_L^{D^*}$:

$$\pi A_3 F_L^{D^*} = \frac{2}{9}(A_5^2-A_7^2) - \frac{1}{8}\pi^2(A_4^2-A_8^2) \quad (7.61)$$

$$\pi A_9 F_L^{D^*} = \frac{4}{9}A_5A_7 + \frac{1}{4}\pi^2A_4A_8 \quad (7.62)$$

$$(F_L^{D^*})^2 = \left[\frac{8}{9}(A_5^2+A_7^2) + \frac{1}{2}\pi^2\left(A_4^2+A_8^2\right)\right]R_{A,B} \quad (7.63)$$

$$A_{FB}F_L^{D^*} = \pi\left(A_4A_5 - A_7A_8\right) \quad (7.64)$$

We recall that A_i are defined from the angular observables up to a numerical normalisation given in Ref. [166]. A similar set of expressions can be written for $\tilde{F}_L^{D^*}$, $\tilde{A}_i$ and $\tilde{A}_{FB}$ rather than $F_L^{D^*}$, A_i and A_{FB}, respectively, by substituting the normalization in terms of $d\Gamma/dq^2$ by the integrated decay rate Γ. These expressions can then be binned trivially, however they are rather cumbersome to use. In the following two subsections we will restrict to the case of removing any imaginary contribution corresponding to our baseline scenario that will be relevant to the extraction of $F_L^{D^*}$.

[7] In the massive case, this relation provides access to a sum of two related observables A_{6s} and A_{FB}:

$$2\langle A_{6s}\rangle_\ell + 9\langle A_{\rm FB}\rangle_\ell = \frac{27}{2\sqrt{2}}\frac{1}{\Gamma}\,m_\ell\,\langle\frac{1}{q^2-m_\ell^2}\sqrt{I_{1c}I_{2c}(m_\ell^2-q^2)-I_{2c}^2(m_\ell^2+q^2)}\rangle_\ell$$

7.3.2 Massless case without imaginary contributions

Using Eqs. (7.43) and (7.48) we obtain one of the important results of this chapter:

$$\langle \tilde{F}_T^{D^*} \rangle_0 = \frac{1}{\Gamma} \langle 2\sqrt{I_3^2 + \frac{1}{4} I_{6s}^2} \rangle_0 \qquad \text{where } \langle \tilde{F}_T^{D^*} \rangle_0 = 1 - \langle \tilde{F}_L^{D^*} \rangle_0 \tag{7.65}$$

This relation can be used as a cross-check of the $F_L^{D^*}$ determination in the massless case (without imaginary contributions but allowing for the presence of pseudoscalars).

This expression can be generalised to the case of smaller bins spanning only part of the whole kinematic range, leading to

$$\langle \tilde{F}_T^{D^*} \rangle_0^i = \frac{1}{\Gamma} \langle 2\sqrt{I_3^2 + \frac{1}{4} I_{6s}^2} \rangle_0^i \tag{7.66}$$

where i means that the integral in Eq. (7.23) is taken over the bin i with a narrower $[q^2_{i,\text{min}}, q^2_{i,\text{max}}]$ range [8].

If we restrict further to the case without pseudoscalars (in this case $I_{1c} = -I_{2c}$ is fulfilled), we obtain further expressions using Eqs. (7.49) and (7.50):

$$\langle \tilde{F}_L^{D^*} \rangle_0 = \frac{1}{\Gamma} \langle \frac{I_5^2 - 4 I_4^2}{4 I_3} \rangle_0 \tag{7.67}$$

$$= \frac{1}{\Gamma} \langle R_{A,B} \left(I_3 + \sqrt{4 \frac{I_4^2}{R_{A,B}} + I_3^2} \right) \rangle_0 = \frac{1}{\Gamma} \langle R_{A,B} \left(-I_3 + \sqrt{\frac{I_5^2}{R_{A,B}} + I_3^2} \right) \rangle_0 \tag{7.68}$$

where $R_{A,B}$ is positive and non-vanishing by construction.

7.3.3 Massive case with pseudoscalar operator but without imaginary contributions

In this case, we focus on Eqs. (7.54) to (7.56) to derive equivalences to $F_L^{D^*}$ since Eq. (7.57) is too involved to provide a useful relation to $F_L^{D^*}$. Eqs. (7.54) and (7.55) yield:

$$\langle \tilde{F}_T^{D^*} \rangle_\ell = \frac{1}{\Gamma} \langle \sqrt{(A\, I_3)^2 + \frac{1}{4} (B\, I_{6s})^2} \rangle_\ell \qquad \text{where } \langle \tilde{F}_T^{D^*} \rangle_\ell = 1 - \langle \tilde{F}_L^{D^*} \rangle_\ell \tag{7.69}$$

where we define the auxiliary kinematic quantities (whose value in the massless case is two)

$$A = \frac{m_\ell^2 + 2q^2}{q^2 - m_\ell^2} \qquad B = 2 + \frac{m_\ell^2}{q^2} \tag{7.70}$$

One can write an equivalent equation to Eq. (7.69) for narrower q^2 bins similary to the previous section. In the case of Eq. (7.56) we do not substitute I_{2c}, leading to:

$$\langle \tilde{F}_T^{D^*} \rangle_\ell = 1 - \langle \tilde{F}_L^{D^*} \rangle_\ell = \frac{1}{\Gamma} \langle A \left(I_3 - 2 \frac{{I_4}^2}{I_{2c}} \right) \rangle_\ell \tag{7.71}$$

Relating this equation with the massless case is not straightforward given that in the massless case I_{2c} was substituted (before integrating) in terms of $F_L^{D^*}$ and $R_{A,B}$.

7.3.4 Cases with pseudoscalar operator and imaginary contributions

This corresponds to the most complete expression allowing for the presence of pseudoscalars and also imaginary parts, but no tensors. This can be achieved, as in the previous section, by using I_{1s} and I_{2s} instead of I_{1c} and I_{2c} as a starting point. The corresponding expression in the massless case is:

$$\langle \tilde{F}_T^{D^*} \rangle_0 = \frac{1}{\Gamma} \langle 2\sqrt{I_3^2 + I_9^2 + \frac{1}{4} I_{6s}^2} \rangle_0 \qquad \text{where } \langle \tilde{F}_T^{D^*} \rangle_0 = 1 - \langle \tilde{F}_L^{D^*} \rangle_0 \tag{7.72}$$

and in the massive case

$$\langle \tilde{F}_T^{D^*} \rangle_\ell = \frac{1}{\Gamma} \langle \sqrt{(A\, I_3)^2 + (A\, I_9)^2 + \frac{1}{4} (B\, I_{6s})^2} \rangle_\ell \qquad \text{where } \langle \tilde{F}_T^{D^*} \rangle_\ell = 1 - \langle \tilde{F}_L^{D^*} \rangle_\ell \tag{7.73}$$

[8] Notice that $\langle \tilde{F}_L^{D^*} \rangle_0 + \langle \tilde{F}_T^{D^*} \rangle_0 = 1$ holds because the integration is performed over the whole kinematic range. For the observables $\langle \tilde{F}_L^{D^*} \rangle_0^i$ and $\langle \tilde{F}_T^{D^*} \rangle_0^i$ shown in Figs. 7.1, 7.2, 7.B.1 to 7.B.6 and 7.3, this is no longer the case due to the normalisation of $\tilde{F}_L^{D^*}$ and $\tilde{F}_T^{D^*}$: $\langle \tilde{F}_L^{D^*} \rangle_0^i + \langle \tilde{F}_T^{D^*} \rangle_0^i = \langle d\Gamma/dq^2 \rangle_0^i / \Gamma < 1$. It is trivial to check that a different normalisation for $\tilde{F}_L^{D^*}$ and $\tilde{F}_T^{D^*}$ would only affect the normalisation $1/\Gamma$ appearing in the binned expressions.

Similar expressions can be written for $\langle \tilde{F}_T^{D^*} \rangle_\ell^i$ defined for narrower q^2 bins. These expressions represent the most general relations with the massless and massive polarisation fractions. Compared to the previous case, one can see that the presence of imaginary contributions comes simply from the additional I_9 term in Eqs. (7.72) and (7.73), see also Eq. (7.110) in Appendix 7.A.

Within this more general framework, Eqs. (7.54) and (7.110) yield the following simple relation among the observables defined in Section 7.1.2:

$$\langle x_1 (\tilde{F}_T^{D^*})^2 \rangle_\ell = \langle x_2 \left(\tilde{A}_3^2 + \tilde{A}_9^2 \right) + x_3 \left(\tilde{A}_{6s} \right)^2 \rangle_\ell \tag{7.74}$$

where $\tilde{A}_i$ stands for the observables A_i normalised to Γ rather than $d\Gamma/dq^2$, $x_1 = (m_\ell^2 - q^2)^2$, $x_2 = 4\pi^2 (m_\ell^2 + 2q^2)^2$ and $x_3 = 4 x_1 x_2 / (729 \pi^2 q^4)$ (A_9 vanishes in the absence of large imaginary contributions). This relation implies that the large (small) value of $F_L^{D^*}$ ($F_T^{D^*}$) requires a corresponding suppression in $A_3^2 + A_9^2$, in A_{6s} or both. For this reason it would be particularly interesting to have available predictions in specific models for this couple of observables in case that the unexpectedly large value of this polarisation fraction remains.

7.3.5 Binning

We have obtained these equivalent expressions for $\langle \tilde{F}_L^{D^*} \rangle_\ell$ (or $\langle \tilde{F}_T^{D^*} \rangle_\ell$) assuming that there are no tensors and (in some cases) no large imaginary contributions at short distances. From now on we introduce the notation $\langle \tilde{F}_T^{D^* \, \mathrm{alt}} \rangle_\ell$ (or $\langle \tilde{F}_L^{D^* \, \mathrm{alt}} \rangle_\ell$) to refer to Eq. (7.73) as the coefficient combination equivalent to $F_T^{D^*}$ (or $F_L^{D^*}$) which we refer to as the "alternative determination of $F_T^{D^*}$ (or $F_L^{D^*}$). In the absence of imaginary contributions we will use the notation $\langle \tilde{F}_T^{D^* \, \mathrm{alt}} \rangle_\ell^{I_9=0}$ corresponding to Eq. (7.69). In the massless case we denote $\langle \tilde{F}_T^{D^* \, \mathrm{alt}} \rangle_0$ for Eq. (7.72) and $\langle \tilde{F}_T^{D^* \, \mathrm{alt}} \rangle_0^{I_9=0}$ for Eq. (7.65).

Experimentally we have to consider binned versions of these expressions, which are nonlinear functions of the angular coefficients. Since the binned angular coefficients are the only quantities measured, we should be careful that $f(\langle I_k \rangle_\ell) \neq \langle f(I_k) \rangle_\ell$ when f is non-linear. From an experimental perspective there are two ways to proceed: *i)* measure the coefficients I_3 and I_{6s} of the massless or massive distribution in very small bins in order to reconstruct a q^2 dependence of these functions, so that we can perform the integration in Eq. (7.65) for the massless case or in Eq. (7.69) in the massive case (or their counterparts including imaginary parts Eq. (7.72) and Eq. (7.73)); *ii)* use an unbinned measurement method (as was done for $B \to K^* \mu\mu$ [375]) to determine the q^2 dependence of the coefficients and introduce the obtained expressions inside Eq. (7.65) or Eq. (7.69) as explained above.

Both approaches are however difficult to implement when the statistics is low, and one has to choose between the extraction of the whole angular distribution and the study of the q^2 dependence of simpler observables like the decay rate. Currently, the measurements are integrated over the whole kinematic range, which constitutes a single bin for the analysis.

By comparing with our exact results, we will thus investigate the accuracy of the approximation $f(\langle I_k \rangle_\ell) = \langle f(I_k) \rangle_\ell$, which requires the following transformation on the unbinned expressions:

$$d\Gamma_X/dq^2 \to \langle d\Gamma_X/dq^2 \rangle \qquad I_i \to \langle I_i \rangle \qquad w I_i \to \langle w I_i \rangle \qquad w I_i^2 \to \langle \sqrt{|w|} I_i \rangle^2 \tag{7.75}$$

where w stands for any positive weight depending on m and q^2. This leads to the following "approximate formulae" in the massless case, starting from Eq. (7.72):

$$\langle \tilde{F}_T^{D^* \, \mathrm{alt}} \rangle_0 \simeq \frac{1}{\Gamma} 2 \sqrt{\langle I_3 \rangle_0^2 + \langle I_9 \rangle_0^2 + \frac{1}{4} \langle I_{6s} \rangle_0^2} \tag{7.76}$$

and in the massive case, starting from Eq. (7.73):

$$\langle \tilde{F}_T^{D^* \, \mathrm{alt}} \rangle_\ell \simeq \frac{1}{\Gamma} \sqrt{\langle A \, I_3 \rangle_\ell^2 + \langle A \, I_9 \rangle_\ell^2 + \frac{1}{4} \langle B \, I_{6s} \rangle_\ell^2} \tag{7.77}$$

In the massive case, one should measure the I_i and multiply each event by a numerical factor A for I_3, I_9 and B for I_{6s}.

Similarly, in the absence of imaginary parts, we obtain the approximate binned expression, starting from Eq. (7.69):

$$\langle \tilde{F}_T^{D^* \, \mathrm{alt}} \rangle_\ell^{I_9=0} \simeq \frac{1}{\Gamma} \sqrt{\langle A \, I_3 \rangle_\ell^2 + \frac{1}{4} \langle B \, I_{6s} \rangle_\ell^2} \tag{7.78}$$

and the approximate expression for $\langle \tilde{F}_T^{D^*} \rangle_\ell$ starting from Eq. (7.71)

$$\frac{1}{\Gamma} \langle A \left(I_3 - 2 \frac{{I_4}^2}{I_{2c}} \right) \rangle_\ell \simeq \frac{1}{\Gamma} \left[\langle A I_3 \rangle_\ell - 2 \frac{\langle A I_4 \rangle_\ell^2}{\langle A I_{2c} \rangle_\ell} \right] \tag{7.79}$$

All these expressions have a corresponding expression for $\langle \tilde{F}_T^{D^*} \rangle_\ell^i$ for narrower bins where $\langle \rangle_\ell$ is transformed into $\langle \rangle_\ell^i$ corresponding to the integration over the narrow bin i.

In order to get an idea of the accuracy of these approximate relations, we perform the following numerical exercise. We consider a set of benchmark points corresponding to the global fit best-fit-points of the 1D and 2D NP hypotheses in Refs. [82, 83]. Among the 1D hypotheses, the most favoured one is assuming NP in g_{V_L}, followed by NP in g_{S_R} (see Eq. (2.17)). Specifically we will take for this numerical analysis as benchmark points the best-fit-points of the following four different NP hypotheses (in each case, the remaining couplings are set to zero):

$$(R1): \quad g_{V_L} = 0.07 \tag{7.80}$$
$$(R2): \quad g_{S_R} = 0.09 \tag{7.81}$$
$$(R3): \quad g_{S_L} = 0.07 \tag{7.82}$$
$$(R4): \quad g_{S_L} = 4g_T = -0.03 \tag{7.83}$$

where the values are given at the scale $\mu = 1$ TeV, and we run them down to the scale $\mu = m_b$ [82–84]. For 2D hypotheses, there is a wider range of relevant possibilities, and we select the following ones [9]:

$$(R5): (g_{V_L}, g_{S_L} = -4g_T) = (0.10, -0.04) \tag{7.84}$$
$$(R6) - (R7): (g_{S_R}, g_{S_L}) = (0.21, -0.15) \text{ or } (-0.26, -0.61) \tag{7.85}$$
$$(R8): (g_{V_L}, g_{S_R}) = (0.08, -0.01) \tag{7.86}$$
$$(C0) - (C0)^*: g_{S_L} = 4g_T = -0.06 \pm i\,0.31 \tag{7.87}$$

where once again we run these coefficients down to $\mu = m_b$.

In Ref. [166], a set of benchmark points is determined by considering the best-fit points of different scenarios with one free complex parameter. The resulting 2D benchmark points (in each case, the remaining couplings are set to zero) at the scale $\mu = m_b$ are:

$$(C1): \quad g_{V_L} = 0.07 - i0.16 \tag{7.88}$$
$$(C2): \quad g_{V_R} = -0.01 - i0.39 \tag{7.89}$$
$$(C3): \quad g_{S_L} = 0.29 - i0.67 \tag{7.90}$$
$$(C4): \quad g_{S_R} = 0.19 + i0.08 \tag{7.91}$$
$$(C5): \quad g_T = 0.11 - i0.18 \tag{7.92}$$

Using the operator basis in Eq. (2.16), alternative benchmark points are found to be [10]:

$$(C6): \quad g_V = 0.20 + i0.19 \tag{7.93}$$
$$(C7): \quad g_A = 0.69 + i1.04 \tag{7.94}$$
$$(C8): \quad g_S = 0.17 - i0.16 \tag{7.95}$$
$$(C9): \quad g_P = 0.58 + i0.21 \tag{7.96}$$

In the following we will check the relations given in the previous sections against these benchmark scenarios. We have used the binned approximation of the relations using 6 bins of equal length as shown in Fig. 7.1. On the one hand, this allows us to test the quality of the binned approximation. On the other hand, we can check the impact of the assumptions used in order to derive the various relations: for instance, checking the expressions obtained for real NP contributions in Section 7.3.3 in the case of the scenarios $(C0) - (C9)$ with complex parameters provides an estimate of the impact of realistic NP imaginary contributions on these expressions.

We need to choose a set of form factors to evaluate the hadronic contributions and to be able to test how accurate the relations remain within the binned approximation discussed above, taking into account possible unexpected NP contributions (imaginary parts, tensor contributions). Since our goal is only to check the accuracy of this approximation for the various NP benchmark points it is enough to work using a simplified setting. For this reason, we refrain from using form factors obtained by elaborate combinations of heavy-quark effective theory [91, 92, 376, 377] sum rules and lattice simulations [39, 82, 154, 166, 378–384] and we stick to the simpler quark model in Ref. [385] without attempting to assign uncertainties to these computations.

A sample of the results is shown in Figs. 7.1 to 7.3 to illustrate the accuracy of the determinations from Eq. (7.77), taking into account the contribution from imaginary parts, and Eqs. (7.78) and (7.79), neglecting this

[9] Even though $(C0)$ and $(C0)^*$ are formally different scenarios corresponding to opposite imaginary parts, they yield the same results for our observables which are not sensitive to the sign of the imaginary part.

[10] For completeness, we quote $(C8)$ although this NP scenario has no impact on $B \to D^* \ell \nu$ and is thus equivalent to the SM for our purposes.

contribution. Additional scenarios are considered in Appendix 7.B. In order to be more precise, the relative errors of the approximate binned expression for $\tilde{F}_T^{D^*\,\mathrm{alt}}$ with respect to $\tilde{F}_T^{D^*}$ are given in Tables 7.B.1 and 7.B.2. Let us add that the I_i are integrated with the kinematical weight A or B defined in Eq. (7.70) for the evaluation of the massive expressions whenever needed. We obtain the following results for the benchmark points considered:

- The binned approximation works very well in all cases when testing the relations in the case of scenarios where they are expected to hold. Conversely, when one considers a NP scenario with significant tensor contributions (like $(C0)$ or $(C5)$) in which the relations are not expected to hold, the expressions are off by $\sim 70\%$ in the worst cases. Only when the NP contribution to the tensor coefficients is very small ($|g_T| \ll 1$), the expressions work quite well, for example $\sim 5\%$ for $(R4)$.

- When we consider NP scenarios for the τ lepton with complex values for the Wilson Coefficients but without tensor contributions, i.e. $(C1) - (C4)$ and $(C6) - (C9)$, the expressions hold with errors at the percent level. This occurs even when we consider the expressions meant for real coefficients (Section 7.3.3). We stress again that this does not apply to scenarios with tensor contributions such as $(C0)$ and $(C5)$.

- We also tested the massless expressions in the case of NP scenarios affecting light leptons at the same level as the τ lepton. Such scenarios are ruled out by the current data, but they provide a further check of the robustness of our expressions. In these cases, the expressions that do not contain the angular coefficients containing imaginary parts of the amplitudes ($I_{7,8,9}$) (Section 7.3.2) are off by $\sim 20\%$ at worst. The agreement can be restored once we generalise the corresponding expressions so that they include these angular coefficients (Section 7.3.4), where we find a perfect agreement.

- In the first bin of most of the massless expressions, the relations are not completely fulfilled, with a difference up to 10% due to binning effects enhanced at the endpoint of the massless distribution.

This study shows that the expressions derived above under the assumption of no imaginary NP contributions and no tensor contributions in Sections 7.3.2 and 7.3.3 work very well even in the binned approximation. They are very accurate even in the presence of imaginary NP contributions. Their simple generalization including imaginary parts in Section 7.3.4 are as expected to be even more accurate also in the binned approximation. Finally, all relations fail in the presence of large tensor contributions.

7.3.6 Decision Tree

We have proposed different ways of determining $F_L^{D^*}$ (or $F_T^{D^*}$) which can be compared to the usual definition, based on the existing symmetries if additional assumptions are made about the nature of NP (no tensors, real contributions). One may then wonder how to interpret the situation when the determination of $F_T^{D^*}$ in a narrow bin in the case of the tau lepton yields different results from Eq. (7.69) and from the traditional determination. While we have provided different possible determinations we will focus on Eq. (7.69) because it includes pseudoscalar contributions and it is easily generalised in the presence of phases, see Eq. (7.73). There are three possible conclusions:

1) Our first hypothesis is the absence (or negligible size) of tensors. In the presence of tensors, there are no dependencies among the angular observables, and we cannot use Eq. (7.69) to determine $F_T^{D^*}$. This first hypothesis seems to be in agreement with the study in [166] that shows that tensors tend to substantially worsen the situation reducing even further the value of $F_L^{D^*}$ (or increasing $F_T^{D^*}$). If needed, this question can be tested by probing the relationships shown in Section 7.2 among the angular coefficients.

2) The second hypothesis is the absence of large imaginary parts. In this case one can generalise the expression Eq. (7.69) to the presence of imaginary parts to get Eq. (7.73), simply substituting:

$$(A\,I_3)^2 \to (A\,I_3)^2 + (A\,I_9)^2 \tag{7.97}$$

and similarly for the massless case. This simple substitution covers the presence of large phases but of course at the cost of measuring also I_9. Alternatively one can also measure $I_{7,8,9}$ which are sensitive to large imaginary parts and determine if they differ from zero in a significant way.

3) The third option is the presence of an experimental issue in the determination of $F_L^{D^*}$ in the traditional way for $B \to D^*\tau\nu$. The equivalences proposed here could help to determine the problem to be fixed and whether this second determination is also in disagreement not only with the SM but also with NP models.

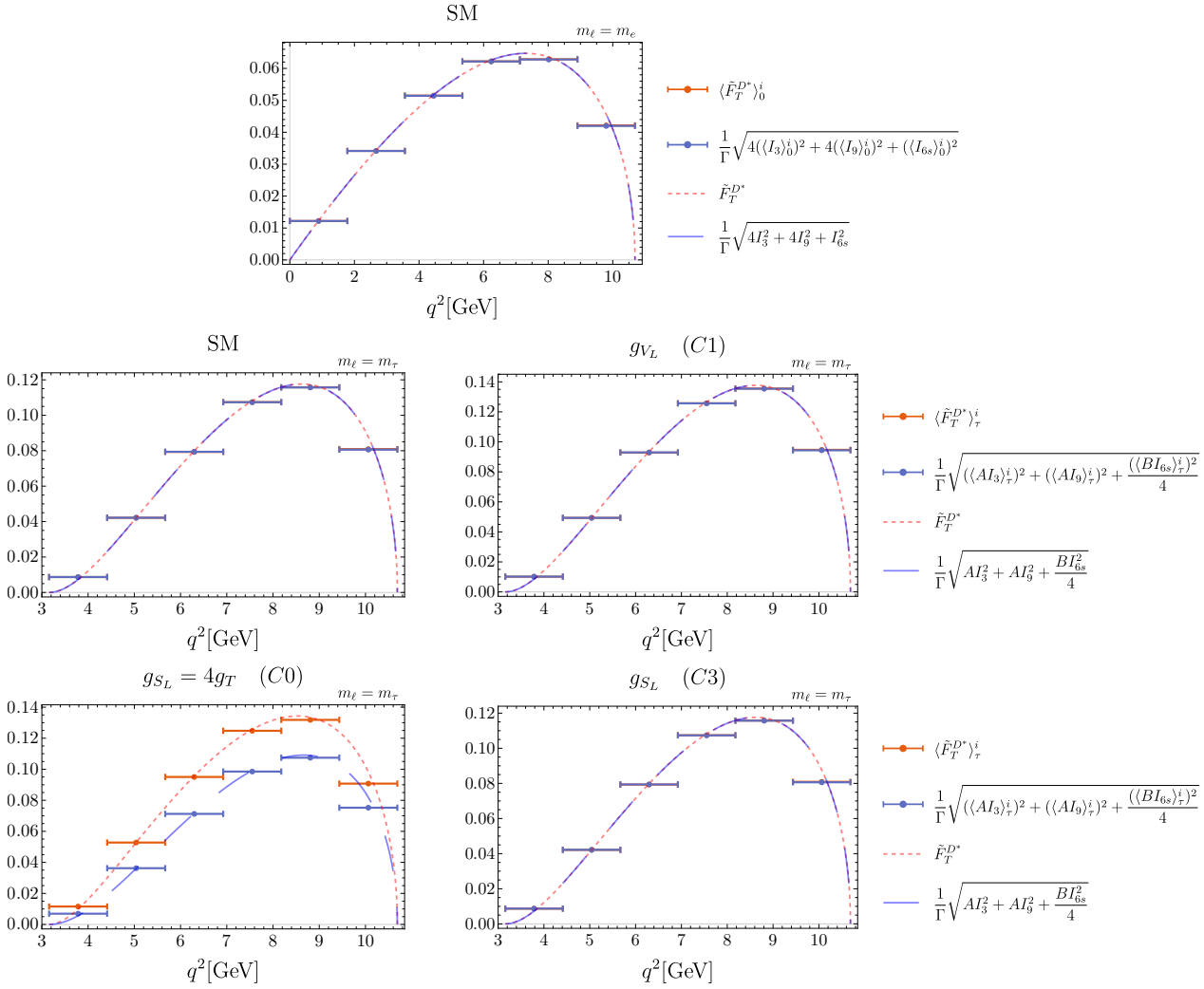

Figure 7.1: Illustration of the errors induced by binning on the relation in Eq. (7.77). The orange dashed curve corresponds to the standard definition of $\tilde{F}_T^{D^*}$, whereas the blue one corresponds to $\tilde{F}_T^{D^*\,\text{alt}}$. The orange bins in this plot are obtained using the binning form of the "standard" expression for $\tilde{F}_T^{D^*}$ while the blue ones are obtained using the approximate binned expression of $\tilde{F}_T^{D^*\,\text{alt}}$ in Eq. (7.77). The plots labelled SM correspond to the case $m_\ell = m_e$ and $m_\ell = m_\tau$ in the SM and the other plots correspond to $\tilde{F}_T^{D^*}$ in $B \to D^* \tau \nu$ in different NP scenarios described in the text. The differences come from the presence of tensor currents for $(C0)$ or from binning effects for the SM case.

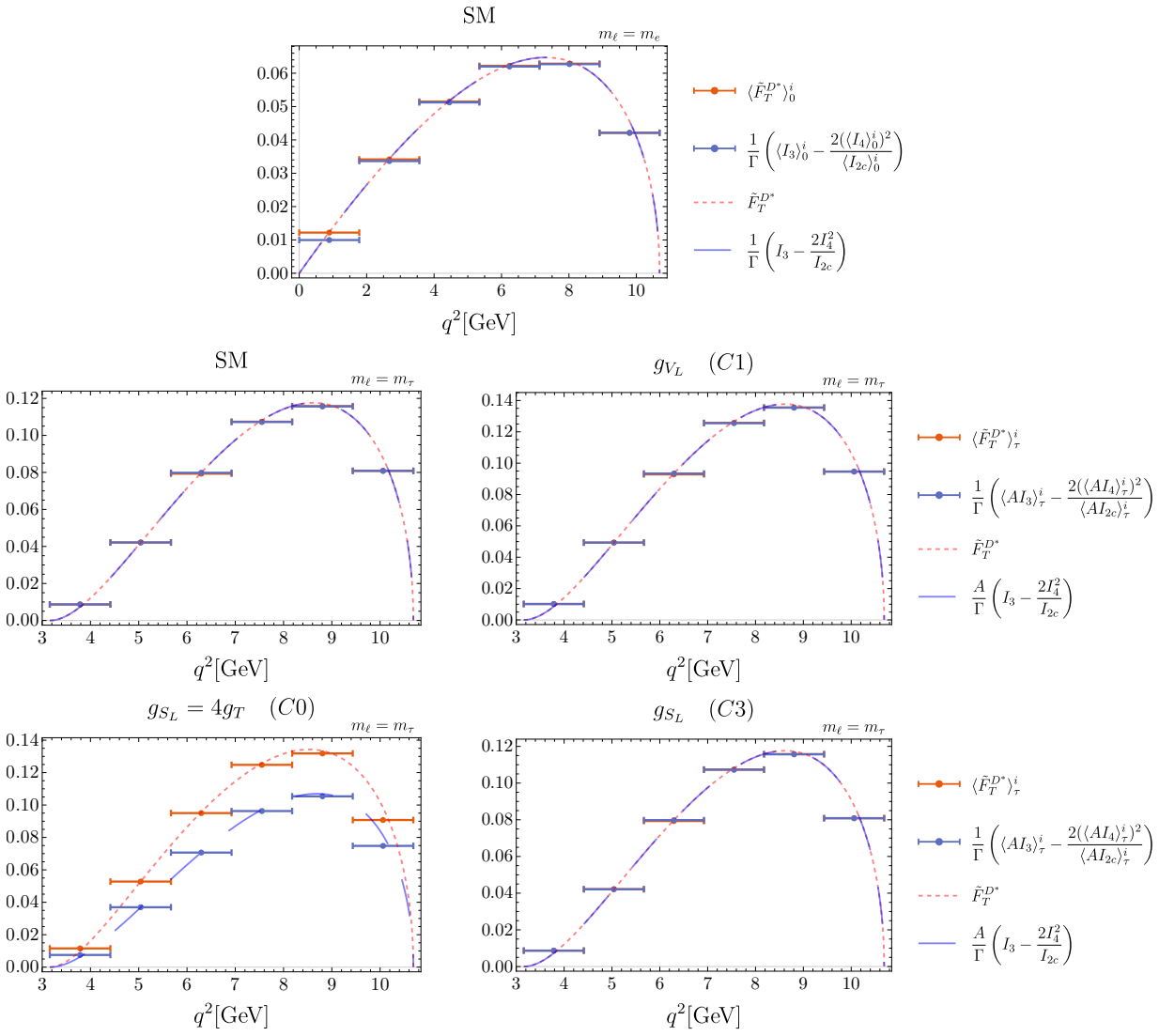

Figure 7.2: Same as Fig. 7.1 for Eq. (7.79).

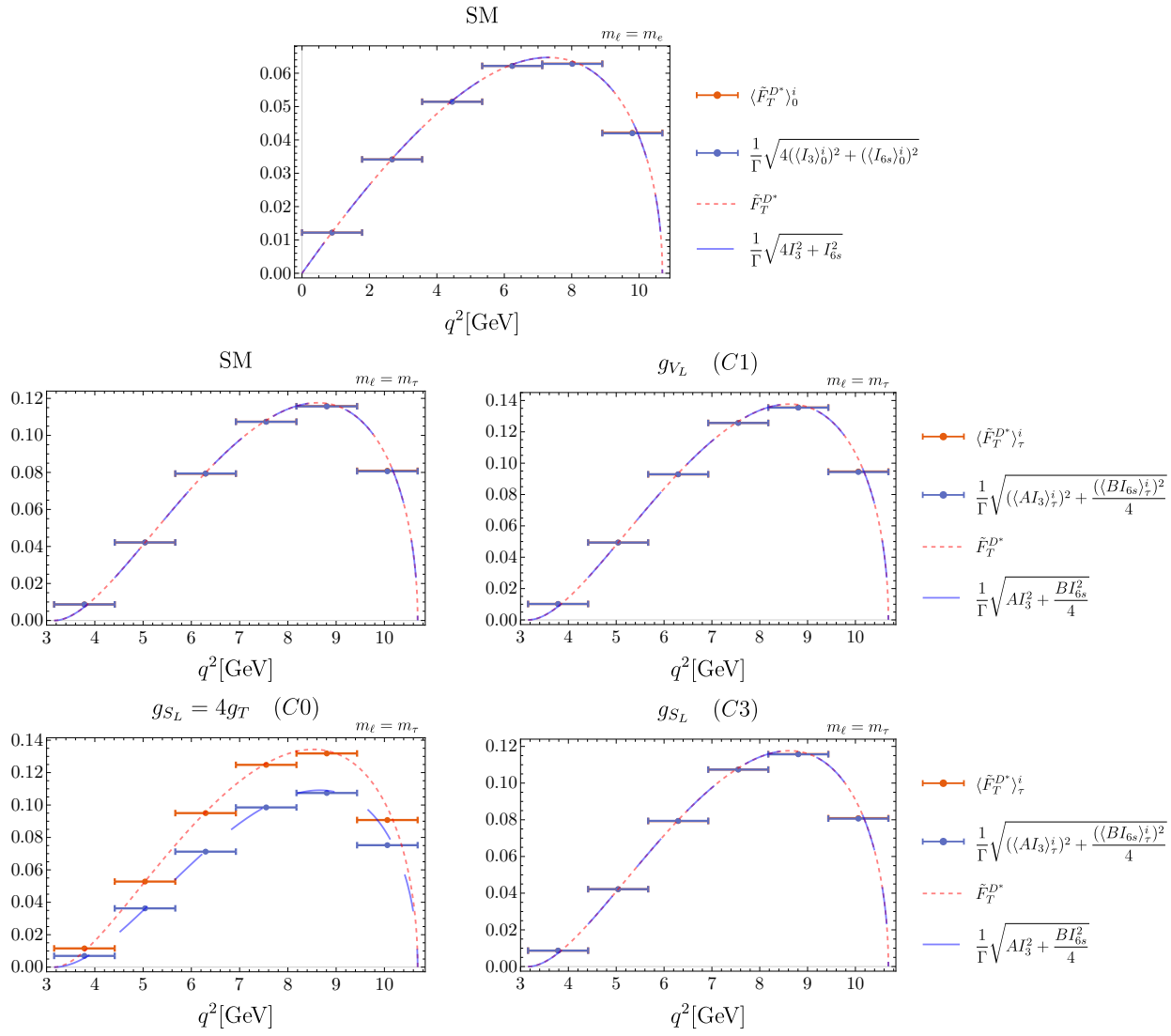

Figure 7.3: Same as Fig. 7.1 for Eq. (7.78).

7.4 Experimental sensitivity

Our analysis is based on the possibility of performing a full angular analysis of the $B \to D^* \ell \nu$ with a reasonable accuracy to check the relationships derived among angular observables. There is a major experimental challenge associated to the difficulty of measuring angular distributions of semitauonic decays due to the loss of the two neutrinos, one from the B decay and the other from the subsequent τ decay, making it difficult to reconstruct the τ direction. This problem arises both when the τ decays into a pion or a lepton [369, 370]. A novel approach [184] has been proposed using the three-prong $\tau^+ \to \pi^+\pi^+\pi^-\bar{\nu}_\tau$ decay instead of the muonic τ decay and a multidimensional template fit able to measure the coefficients of the angular distribution. We can use the numerical results from Ref. [184] to compare the expected experimental sensitivity of $F_L^{D^*}$ using the standard definition in Eq. (7.25) with the one using the equivalent expression in Eq. (7.69).[11]

Taking the results of the template fit for the 50 fb^{-1} collider scenario given in Tab. 11 and Fig. 10 of Ref. [184] and applying the transformation described in Eq. (7.75) we can obtain a rough estimate of the sensitivity of $\langle \tilde{F}_L^{D^* \, \rm alt} \rangle_\tau^{\rm I_9=0}$. Obtaining this estimate is not straightforward since $\langle \tilde{F}_L^{D^* \, \rm alt} \rangle_\tau^{\rm I_9=0}$ includes not only the angular observables I_3 and I_{6s} but also the kinematic factors A and B. As mentioned in Section 7.3.5, experimentalists can measure directly $A\,I_3$, and $B\,I_{6s}$ following the same binning as the angular observables arising in the differential branching ratio. In order to get a rough idea of these quantities in the absence of a dedicated experimental study including estimates of AI_3 and BI_{6s}, we study the ratios $\langle A\,I_3\rangle/\langle I_3\rangle$ and $\langle B\,I_{6s}\rangle/\langle I_{6s}\rangle$ and how they change in the presence of NP. Scanning the parameter space, we find these ratios to be rather independent of the NP considered. We find that $\langle A\,I_3\rangle/\langle I_3\rangle \approx 4.1$ and $\langle BI_{6s}\rangle/\langle I_{6s}\rangle \approx 2.4$, leading to our approximate determination of the binned observables

$$\langle A\,I_3\rangle_{\rm exp} \approx 4.1 \langle I_3\rangle_{\rm exp} \qquad \langle B\,I_{6s}\rangle_{\rm exp} \approx 2.4\ \langle I_{6s}\rangle_{\rm exp} \tag{7.98}$$

It is important to emphasise that this approximation would not be needed for future experimental measurements as long as $A\,I_3$, $A\,I_9$ and $B\,I_{6s}$ are measured directly.

Under these approximations and considering the uncertainties and correlations given for the 50 fb^{-1} collider scenario in Ref. [184], we obtain the following rough estimate for the alternative determination for the SM case considered in this reference

$$\langle \tilde{F}_L^{D^* \, \rm alt} \rangle_{50\ \rm fb^{-1}}^{\rm I_9=0} = 0.47 \pm 0.12 \tag{7.99}$$

to be compared with the standard determination

$$\langle \tilde{F}_L^{D^*} \rangle_{50\ \rm fb^{-1}} = 0.45 \pm 0.01 \tag{7.100}$$

The alternative determination suffers from the larger errors of the angular observables involved in its definition, in comparison with the standard determination which is dominated by I_{1s} with a smaller uncertainty than the other angular observables, as show in Fig. 10 of Ref. [184].

These uncertainties would be enough to identify discrepancies coming from tensor contributions, such as our scenario C5. The smaller differences between the two determinations coming from other types of scenarios (such as Wilson coefficients with imaginary parts) could not be distinguished and the two determinations should yield similar results. Conversely, it means that our relations will provide a non-trivial experimental cross-check of the angular analyses projected in Ref. [184], unless large tensor contributions are present.

7.5 Conclusions

As we discussed in Chapter 3, the charged-current $B \to D^* \ell \nu$ transition has been under scrutiny recently, as it exhibited a deviation from the SM in the LFUV ratio R_{D^*} comparing the branching ratios $\ell = \tau$ and lighter leptons. Moreover, the polarisation of both the D^* meson and the τ lepton have been measured for $B \to D^* \tau \nu$. If the latter agrees with the SM within large uncertainties, the Belle measurement of $F_L^{D^*}$ yields a rather high value compared to the SM prediction, which appears difficult to accommodate with NP scenarios.

We could understand better this situation by considering in more detail the angular observables that could be extracted from the differential decay rate, as described in Ref. [166]. We applied the formalism of amplitude symmetries of the angular distribution of the decays $B \to D^* \ell \nu$ for $\ell = e, \mu, \tau$. We showed that the set of angular observables used to describe the distribution of this class of decays are not independent in absence of NP contributing to tensor operators. We derived sets of relations among the angular coefficients of the decay distribution for the massless and massive lepton cases. These relations can be used to probe in a very general way the consistency among the angular observables and the underlying NP at work, and in particular whether it involves tensor operators or not.

[11] We refrain from using the more complete equivalent expression in Eq. (7.73) because the ratio $\langle A\,I_9\rangle/\langle I_9\rangle$ necessary to get the rough estimate described in the text is not properly defined in the SM.

We used these relations to access the integrated longitudinal polarisation fraction of the D^* using different angular coefficients from the ones used by Belle experiment. This in the near future can provide a measurement equivalent to $F_L^{D^*}$ for $B \to D^* \tau \nu$ to understand the relatively high value measured by Belle. We presented expressions in Eqs. (7.72) and (7.73) for the massless and massive case that cover the most general NP scenario including also pseudoscalars and imaginary contributions, with the only exception of tensor contributions.

We then studied the accuracy of these expressions if only binned observables are available, or if they are used in the case of scenarios beyond the assumptions made in their derivation (imaginary contributions, tensor contributions). We used several benchmark points corresponding to best-fit points from global fits to $b \to c\tau\nu$ observables, relying on a simple quark model for the hadronic form factors for this exploratory study. The expressions derived under the assumption of no imaginary NP contributions and no tensor contributions work very well even in the binned approximation. They are very accurate even in the presence of imaginary NP contributions. As expected, their generalisations, derived assuming the presence of imaginary contributions, are very well behaved also in the binned approximation. All relations fail in the presence of large tensor contributions, where no dependencies can be found among the angular observables.

Besides presenting the most general expressions for $F_L^{D^*}$ in the massless and massive case, we also derived a relation among observables ($\tilde{A}_{3,9,6s}$ and $F_L^{D^*}$) that are potentially interesting from the NP point of view if the deviation in $F_L^{D^*}$ is confirmed. Having specific model building predictions for these observables would be highly interesting. We also discussed the impact of the presence of light right-handed neutrinos. We showed that we could test their presence in some specific cases under the hypothesis that there are no tensor nor imaginary contributions, by comparing our two determinations of $F_L^{D^*}$. Moreover, under this hypothesis, the sign of the difference between the two determinations is fixed.

We have explored equivalences of $F_L^{D^*}$ based on our symmetries. In the absence of tensor contributions, these determinations based on other angular observables are fulfilled very accurately. This provides an important cross check for the experimental measurements: if our relations are not fulfilled by the experimental measurements, this would mean either a problem on the experimental side or the presence of large tensor contributions. Using recent projections on the experimental prospects for the measurements of angular observables, we find that these relations could be checked with an accuracy of 10% in the scenario of a 50 fb^{-1} hadron collider, which would be enough to spot a scenario with tensor contributions and would provide an interesting cross-check of the determination of the angular observables.

These additional measurements needed for this extraction make obviously this determination more challenging experimentally, but they can help to corner the kind of NP responsible for this high value or to understand the experimental problem responsible for this unexpected value of the D^* polarisation.

Appendices

7.A Explicit dependencies in the massive case

In this appendix we provide the detailed methodology followed and the full expressions of the dependencies among the angular coefficients in the massive case with no tensor contributions. It is useful to define the following four combinations in order to obtain compact expressions:

$$R_{s,d} = \mathrm{Re}(H_+) \pm \mathrm{Re}(H_-)\,, \quad I_{s,d} = \mathrm{Im}(H_+) \pm \mathrm{Im}(H_-) \tag{7.101}$$

One can solve the system of equations in terms of the variables defined above and find a twofold solution:

$$R_s = \frac{1}{H_0}\frac{I_4 q^2}{q^2 - m_\ell^2} \tag{7.102}$$

$$I_d = \frac{1}{H_0}\frac{I_8 q^2}{q^2 - m_\ell^2} \tag{7.103}$$

$$R_d = (-1)^n \frac{q^2\left(I_4 I_8 q^2 + H_0^2 I_9 (q^2 - m_\ell^2)\right)}{\sqrt{H_0^2(q^2-m_\ell^2)^2}\sqrt{-I_4^2 q^4 + H_0^2(m_\ell^2 - q^2)\left[(|H_-|^2 + |H_+|^2)(m_\ell^2 - q^2) + I_3 q^2\right]}} \tag{7.104}$$

$$I_s = (-1)^n \frac{\sqrt{-I_4^2 q^4 + H_0^2(m_\ell^2 - q^2)\left[(|H_-|^2 + |H_+|^2)(m_\ell^2 - q^2) + I_3 q^2\right]}}{\sqrt{H_0^2(q^2 - m_\ell^2)^2}} \tag{7.105}$$

with $n = 0, 1$. However, this sign ambiguity product of the twofold nature of the solution can be fixed, since physical combinations prevent interference terms that could be problematic. This set of solutions can be used to determine the square of the four amplitudes once H_0 is fixed to be real and positive through the symmetry of the angular distribution. One can also rewrite the real and imaginary parts of H_t in terms of the variables in Eq. (7.101) and H_0:

$$\mathrm{Re}(H_t) = -\frac{q^2\left[I_7\, I_s + I_5 R_d - 2H_0(I_s^2 + R_d^2)\right]}{2m_\ell^2\,(I_d I_s + R_s R_d)} \tag{7.106}$$

$$\mathrm{Im}(H_t) = \frac{q^2\left[-I_5 I_d + I_7 R_s + 2H_0(I_d R_d - R_s I_s)\right]}{2m_\ell^2\,(I_d I_s + R_s R_d)} \tag{7.107}$$

With these definitions, one can find the whole set of dependencies among angular coefficients. Besides the trivial dependency Eq. (7.54), there are four more relations which are obtained by taking combinations of the modulus of H_+, H_- and $\mathrm{Re}(H_t)$, $\mathrm{Im}(H_t)$.

The first non-trivial relation can be derived from the sum $|H_+|^2 + |H_-|^2$:

$$\begin{aligned} 0 = \frac{m_\ell^2 - q^2}{2a}\Big\{ &-4I_{1s}^2 I_{2c}(m_\ell^2 - q^2)^2 + 4I_{1s}(I_4^2 + I_8^2)(m_\ell^2 - q^2)(m_\ell^2 + 3q^2) \\ &+ \left[-2I_3 I_4^2 + 2I_3 I_8^2 - 4I_4 I_8 I_9 + I_{2c}(I_3^2 + I_9^2)\right](m_\ell^2 + 3q^2)^2\Big\} \end{aligned} \tag{7.108}$$

where

$$a = (m_\ell^2 - q^2)^2(m_\ell^2 + 3q^2)\left[2I_{1s}I_{2c}(m_\ell^2 - q^2) + (I_{2c}I_3 - 2I_4^2)(m_\ell^2 + 3q^2)\right] \tag{7.109}$$

From $|H_+|^2|H_-|^2$ one can obtain the second dependency:

$$0 = -I_3^2 - I_9^2 + \left(1 - \frac{m_\ell^2}{q^2}\right)^2\left[\left(\frac{2I_{1s}}{3 + m_\ell^2/q^2}\right)^2 - \frac{I_{6s}^2}{4}\right] \tag{7.110}$$

The third one follows from $[\mathrm{Re}(H_t)]^2$:

$$\begin{aligned} 0 = {} & \frac{8q^4}{a}\Big[2I_{1s}I_{2c}I_7(m_\ell^2 - q^2) + (I_{2c}I_3I_7 - 2I_4^2I_7 + 2I_4I_5I_8 - I_{2c}I_5I_9)(m_\ell^2 + 3q^2)\Big]^2 \\ & - \Big[\frac{I_{6s}I_{6c}}{2} - \frac{4q^4}{a}\Big(4I_{1s}^2I_{2c}^2(m_\ell^2 - q^2)^2 + 4I_{1s}I_{2c}(I_{2c}I_3 - 2I_4^2)(m_\ell^2 - q^2)(m_\ell^2 + 3q^2) \\ & + (4I_4^2(I_4^2 + I_8^2) - 4I_{2c}I_4(I_3I_4 + I_8I_9) + I_{2c}^2(I_3^2 + I_9^2))(m_\ell^2 + 3q^2)^2\Big)\Big]^2 \end{aligned} \tag{7.111}$$

with a defined in Eq. (7.109).

Finally, the last dependency is related to $[\mathrm{Im}(H_t)]^2$:

$$\begin{aligned} 0 = {} & 256I_{6s}^2(I_4I_7 - I_5I_8)^2(m_\ell^2 - q^2)^4q^{12} \\ & \times \left[I_{6c}^2(m_\ell^2 - q^2)^2 + 8I_{1c}I_{2c}m_\ell^2(-m_\ell^2 + q^2) + 8I_{2c}^2m_\ell^2(m_\ell^2 + q^2)\right] \\ & + \Big[64b - 64(I_4I_7 - I_5I_8)^2(m_\ell^2 - q^2)^2q^8 + I_{6s}^2(m_\ell^2 - q^2)^2q^4(I_{6c}^2(m_\ell^2 - q^2)^2 \\ & + 8I_{1c}I_{2c}m_\ell^2(-m_\ell^2 + q^2) + 8I_{2c}^2m_\ell^2(m_\ell^2 + q^2))\Big]^2 \end{aligned} \tag{7.112}$$

with

$$b = \frac{2q^{12}(2I_{1s}I_{2c}I_4(m_\ell^2 - q^2) + (-2I_4(I_4^2 + I_8^2) + I_{2c}(I_3I_4 + I_8I_9))(m_\ell^2 + 3q^2))^2}{(m_\ell^2 + 3q^2)(2I_{1s}I_{2c}(m_\ell^2 - q^2) + (I_{2c}I_3 - 2I_4^2)(m_\ell^2 + 3q^2))} \tag{7.113}$$

As a final comment, let us remark that these dependencies among angular coefficients yield Eqs. (7.55) to (7.58) when one considers only real Wilson coefficients, so that all imaginary contributions and $I_{7,8,9}$ can be neglected.

7.B Comparison of the binned expressions in benchmark NP scenarios

Following the setup of Section 7.3.5, we illustrate in Fig. 7.B.1 to Fig. 7.B.6 the errors induced on the binning by the approximation in Eq. (7.75) on relations derived using the amplitude symmetries under various assumptions on the NP scenario in the τ lepton case. We follow same convention as in Fig. 7.1.

We provide the relative errors for selected scenarios in Tables 7.B.1 and 7.B.2.

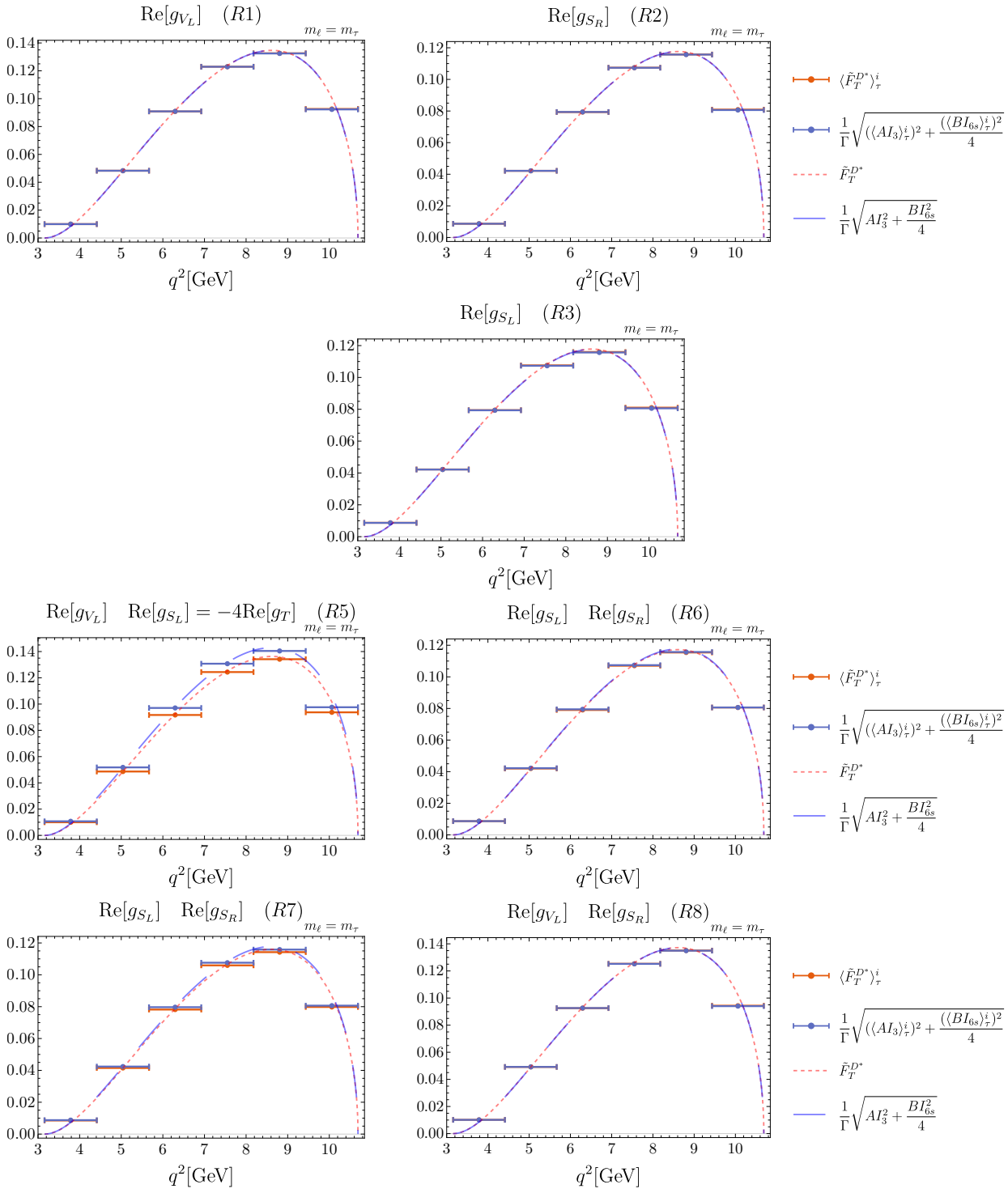

Figure 7.B.1: Study of binning effects for Eq. (7.78) for benchmark NP scenarios with real contributions.

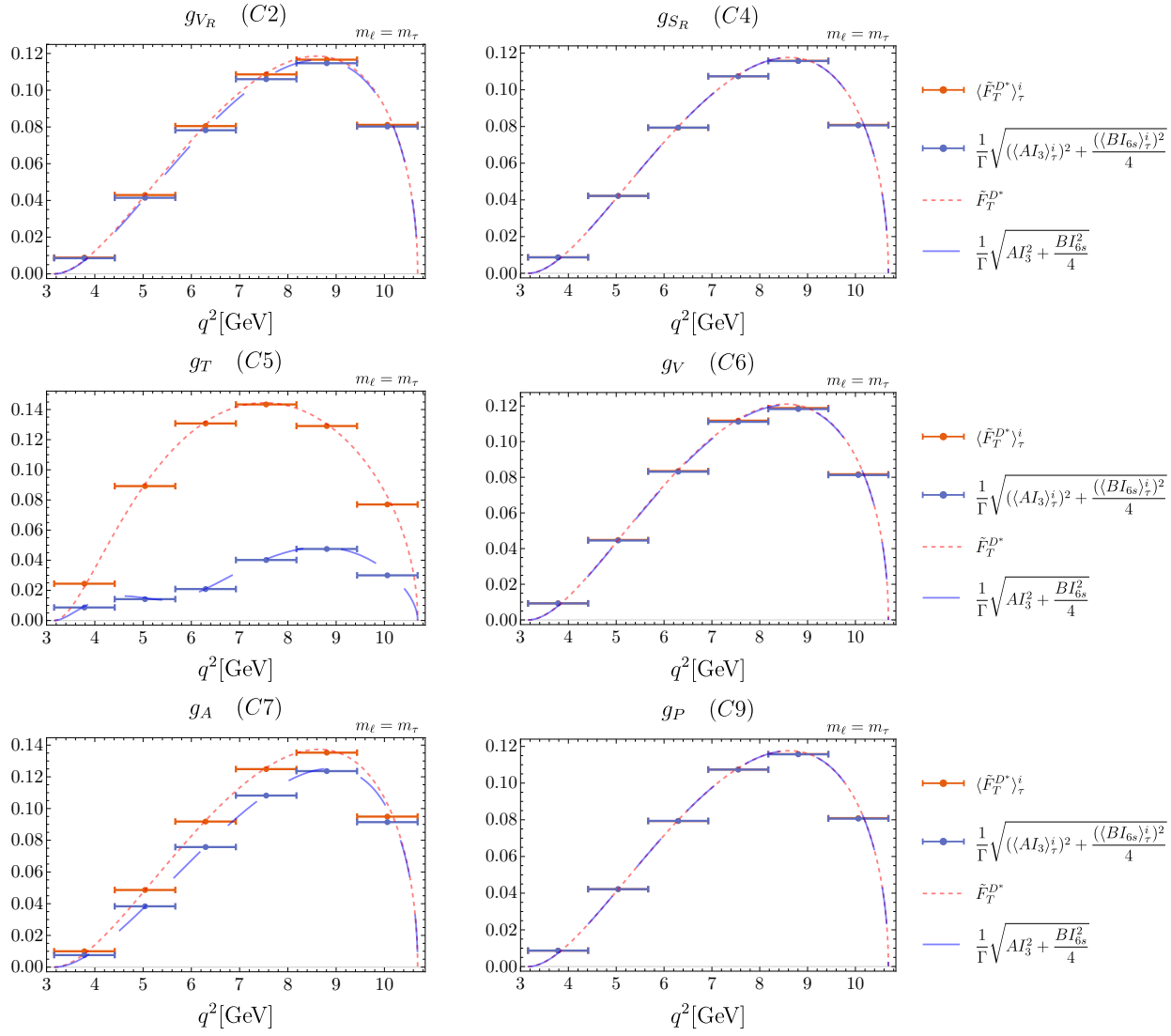

Figure 7.B.2: Study of binning effects for Eq. (7.78) for benchmark NP scenarios with complex contributions.

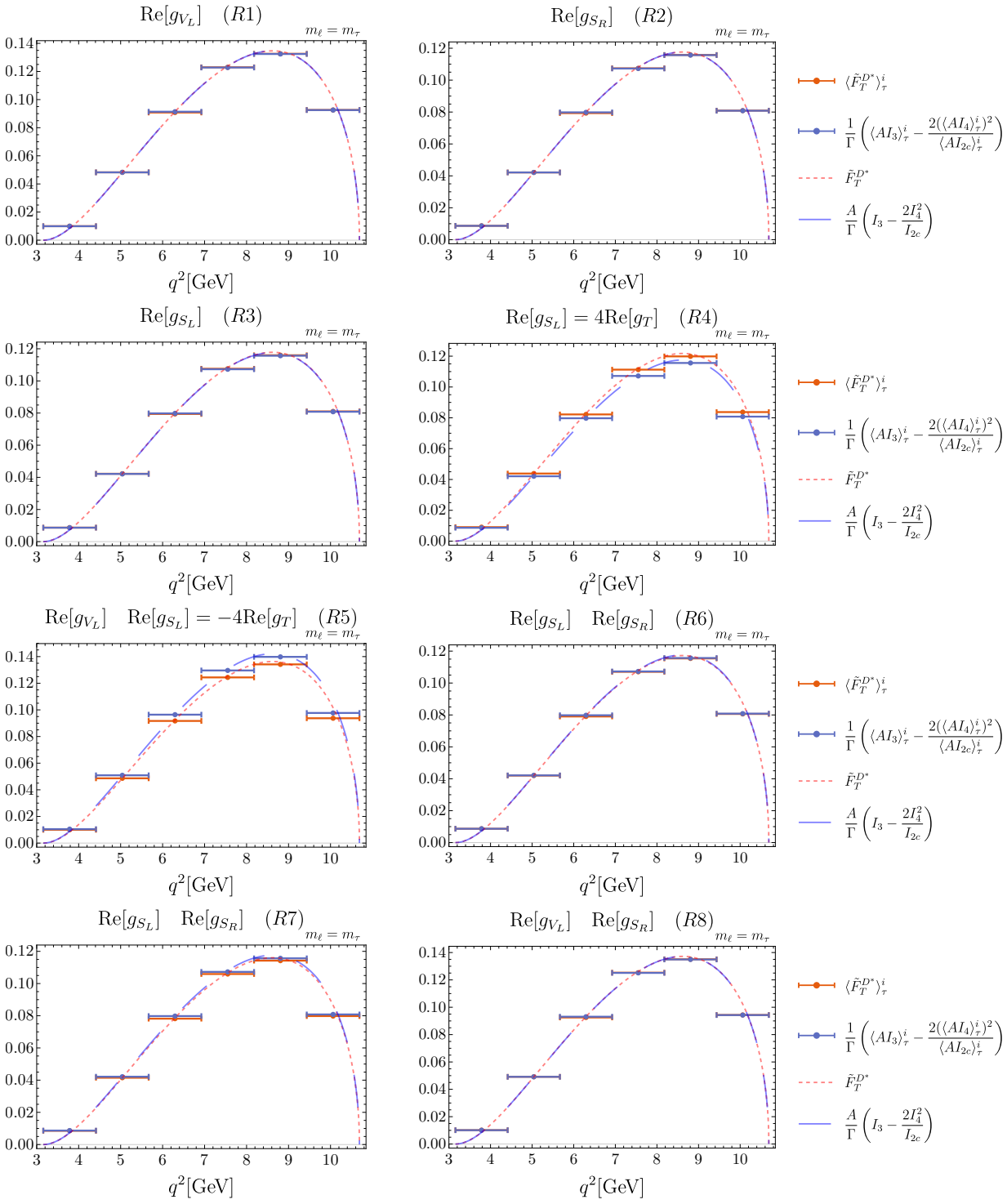

Figure 7.B.3: Study of binning effects for Eq. (7.79) for benchmark NP scenarios with real contributions.

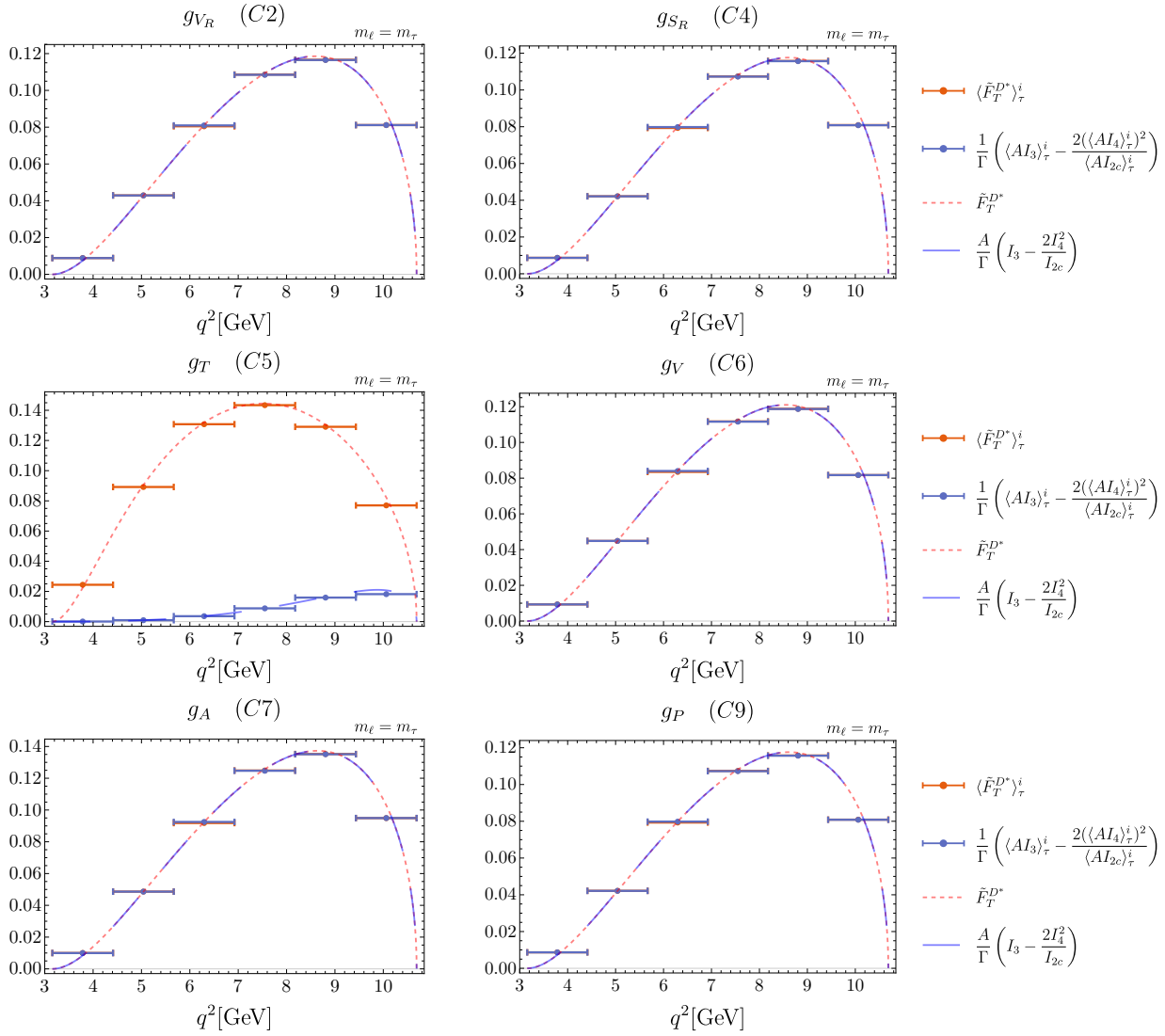

Figure 7.B.4: Study of binning effects for Eq. (7.79) for benchmark NP scenarios with complex contributions.

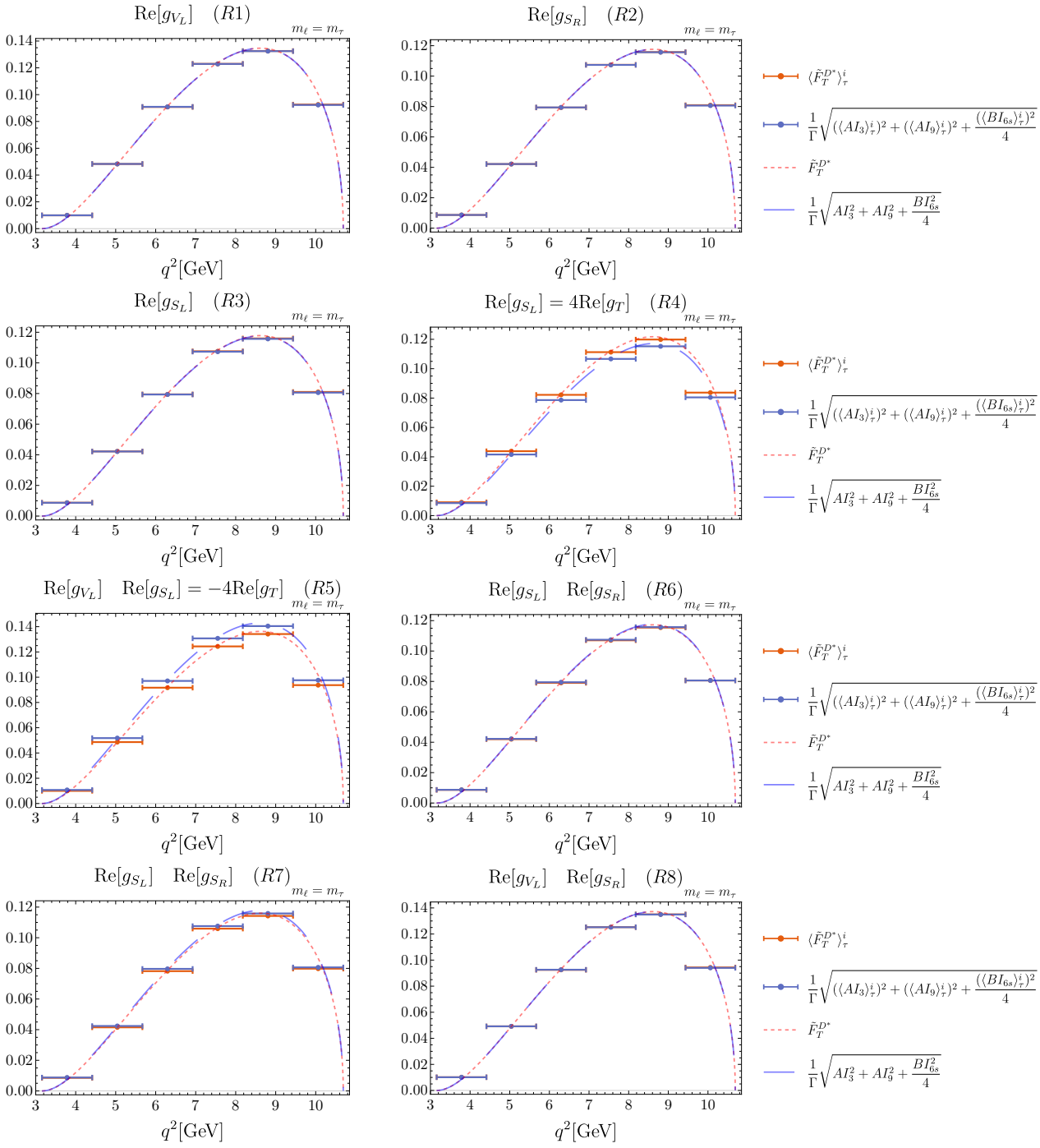

Figure 7.B.5: Study of binning effects for Eq. (7.77) for benchmark NP scenarios with real contributions.

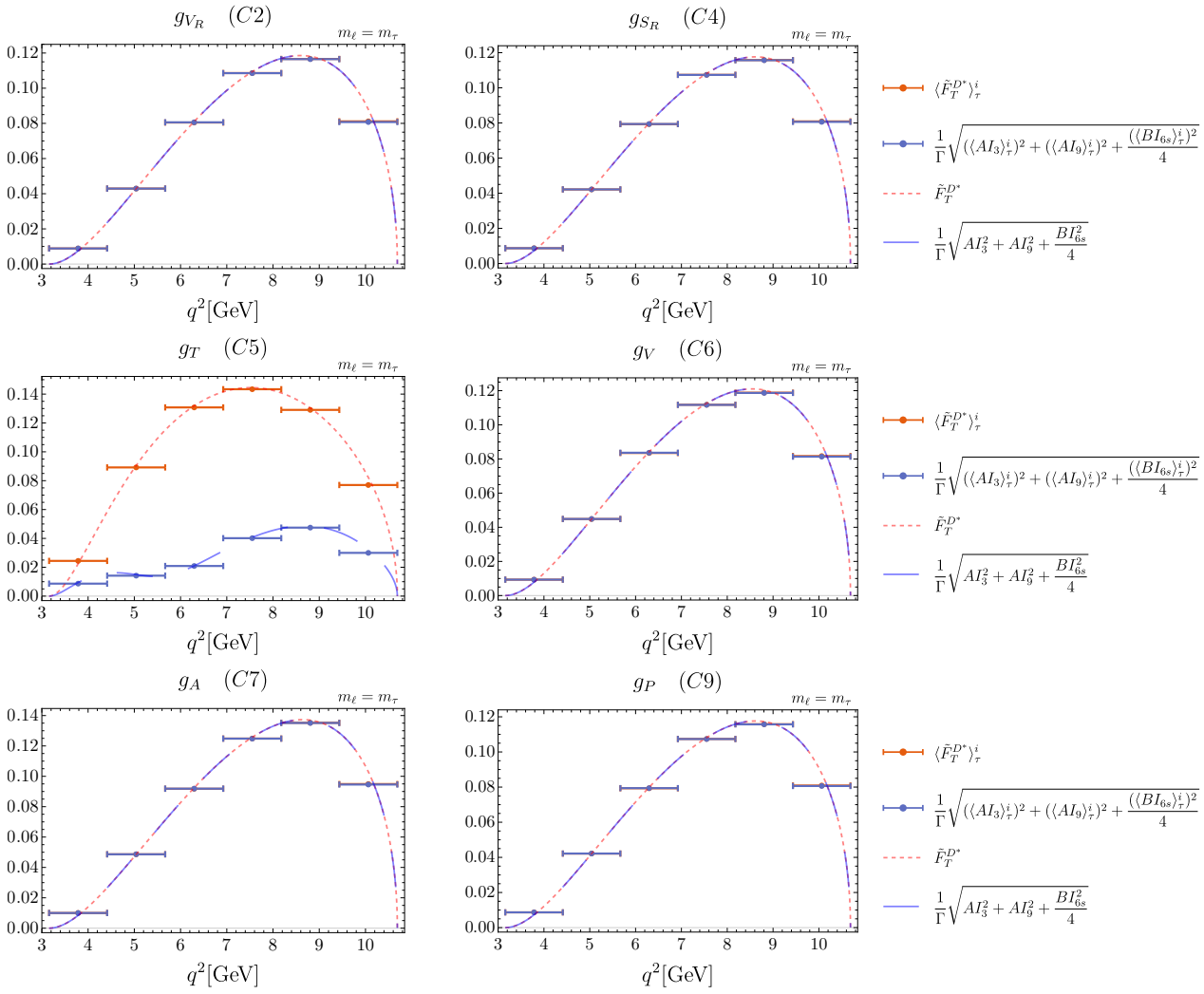

Figure 7.B.6: Study of binning effects for Eq. (7.77) for benchmark NP scenarios with complex contributions.

7.C Impact of the presence of light right-handed neutrinos

In this appendix we turn to the analysis of a case beyond the framework considered in Chapter 7, namely, the presence of light right-handed neutrinos (RHN) entering the decay $b \to c\tau\bar{\nu}$. The inclusion of light RHN was discussed in Refs. [187, 370, 386–394] as a way to obey all phenomenological constraints as well as cosmological and astrophysical limits. Here we will follow closely the recent discussion in Ref. [187] and we will use the results presented there to generalise our expressions.

If one neglects neutrino masses, the $b \to c\tau\bar{\nu}$ decay probability is given by an incoherent sum of the contributions from left- and right-handed neutrinos. This introduces a substantial change in the structure of the angular distribution, requiring a separate discussion.

The inclusion of RHN leads to a more general dimension-six effective Hamiltonian (see Ref. [187] for the definitions of the operators):

$$\mathcal{H}_{\text{eff}} = \frac{4G_F V_{cb}}{\sqrt{2}} \left(O_{LL}^V + \sum_{X=S,V,T}^{A,B=L,R} \mathcal{C}_{AB}^X \mathcal{O}_{AB}^X \right) \tag{7.114}$$

The Wilson coefficients are defined in such a way that $\mathcal{C}_{AB}^X = 0$ in the SM. Eq. (17) of Ref. [187] provides a translation table between our helicity basis and the transversity basis used in that reference.

The inclusion of RHN requires us to consider left and right chiralities of the leptonic current, while the hadronic current is not modified. Consequently the coefficients of the angular distribution get modified (see Ref. [187]):

$$I_j \to I_j(L) \pm I_j(R) \tag{7.115}$$

where the relative sign depends on the angular observable considered, and $I_j(L)$ and $I_j(R)$ involve different helicity amplitudes including $\mathcal{C}^L$ and $\mathcal{C}^R$ Wilson coefficients respectively. The total number of amplitudes entering the distribution gets thus enlarged from 7 to 14 (two of the helicity amplitudes always come in the same combination).

We can now discuss the impact of RHN on our previous discussion. Let us assume that there are neither tensor nor imaginary contributions, but that RHN are indeed present. We can compare the two determinations of $\tilde{F}_T^{D^*}$: the standard definition in Eq. (7.25) and the alternative determination in Eq. (7.69). The following relation holds:

$$\frac{\langle (\tilde{F}_T^{D^*})^2 - (\tilde{F}_T^{D^*\,\text{alt},\,\text{I}_9=0})^2 \rangle_\tau}{\langle (B\tilde{A}_{6s})^2 \rangle_\tau} = \Delta^F \equiv \frac{64}{729} \frac{(C_{LR}^V(1+C_{LL}^V) - C_{RL}^V C_{RR}^V)^2}{((1+C_{LL}^V)^2 - {C_{LR}^V}^2 - {C_{RL}^V}^2 + {C_{RR}^V}^2)^2} \tag{7.116}$$

where $\tilde{A}_{6s}$ refers to the observable including left and right components defined by

$$\langle \tilde{A}_{6s} \rangle_\tau = -\frac{27}{8} \frac{1}{\Gamma} \langle I_{6s} \rangle_\tau \tag{7.117}$$

In order that the previous expression becomes useful we have checked that Eq. (7.116) still holds in the following binned form:[12]

$$\frac{(\langle \tilde{F}_T^{D^*} \rangle_\tau)^2 - (\langle \tilde{F}_T^{D^*\,\text{alt}} \rangle_\tau^{\text{I}_9=0})^2}{\langle B\tilde{A}_{6s} \rangle_\tau^2} \simeq \Delta^F \tag{7.118}$$

Notice that given that Δ^F is always positive, Eq. (7.118) implies that an experimental determination using $\langle \tilde{F}_T^{D^*\,\text{alt}} \rangle_\tau^{\text{I}_9=0}$ should always be found equal or smaller than the "standard" $\langle \tilde{F}_T^{D^*} \rangle_\tau$ in absence of tensors and imaginary contributions.

We derived this expression assuming the hypotheses above and using the fact that Eq. (7.54) is valid in presence of RHN while Eq. (7.55) holds if the constraint

$$C_{LR}^V(1+C_{LL}^V) - C_{RL}^V C_{RR}^V = 0 \tag{7.119}$$

is imposed. In other words, only if this constraint is fulfilled, $\langle \tilde{F}_T^{D^*\,\text{alt}} \rangle_\tau$ can be interpreted as the physical transverse polarization fraction.

In Ref. [187] several interesting scenarios are identified which are able to fulfill the constraints from $\mathcal{B}_{B_c \to \tau\bar{\nu}}$, $\mathcal{R}_{D,D^*}$, $F_L^{D^*}$ and $\mathcal{P}_\tau^{D^*}$:

[12] We have scanned over a range of values of the RHN coefficients $C_{LL,LR,RL,RR}^V$ to compare Eqs. (7.116) and (7.118). The result of this test clearly indicates that for combinations of RHN resulting in reasonably small values of $\Delta_F < 1$, the two expressions agree up to $\mathcal{O}(10^{-3})$ corrections in all bins.

Scenario \ Bin	$[3.2, 4.4]$	$[4.4, 5.7]$	$[5.7, 6.9]$	$[6.9, 8.2]$	$[8.2, 9.4]$	$[9.4, 10.7]$	$[m_\tau^2, (m_B - m_{D^*})^2]$
SM	0.03%	0.03%	0.1%	0.04%	0.09%	0.4%	1%
C1	0.03%	0.03%	0.1%	0.04%	0.09%	0.4%	1%
C0	40%	30%	30%	20%	20%	20%	20%
C3	0.03%	0.03%	0.1%	0.04%	0.09%	0.4%	1%

Table 7.B.1: Relative difference in percent of the approximate binned expression of $\langle \tilde{F}_T^{D* \, \text{alt}} \rangle_\tau$ with respect to the "standard" $\langle \tilde{F}_T^{D*} \rangle_\tau$ for the SM and different NP scenarios. It corresponds to the relative difference in between the orange and blue bins displayed in Fig. 7.1 (normalised by the "standard" $\langle \tilde{F}_T^{D*} \rangle_\tau$ i.e. the orange bins). The bins in the first 6 columns correspond to the division of the kinematic range ($[m_\tau^2, (m_B - m_{D^*})^2]$) in 6 equally sized intervals. The last column corresponds to the whole kinematic range (not displayed in Fig. 7.1). Notice that, as expected, this approximation works better for smaller bins. The scenario $C0$ is displayed as an example of a scenario with tensor contributions where, as expected, the two determinations should yield different results.

Scenario \ Bin	$[0, 1.8]$	$[1.8, 3.6]$	$[3.6, 5.3]$	$[5.3, 7.1]$	$[7.1, 8.9]$	$[8.9, 10.7]$	$[0, (m_B - m_{D^*})^2]$
SM	0.08%	0.04%	0.1%	0.05%	0.1%	0.4 %	2%

Table 7.B.2: Relative difference in percent of the approximate binned expression of $\langle \tilde{F}_T^{D* \, \text{alt}} \rangle_0$ with respect to the "standard" $\langle \tilde{F}_T^{D*} \rangle_0$ for the SM. It corresponds to the relative difference in between the orange and blue bins displayed in Fig. 7.1 (normalised by the "standard" $\langle \tilde{F}_T^{D*} \rangle_0$ i.e. the orange bins). The bins in the first 6 columns correspond to the division of the kinematic range ($[m_\tau^2, (m_B - m_{D^*})^2]$) in 6 equally sized intervals. The last column corresponds to the whole kinematic range (not displayed in Fig. 7.1). Notice that, as expected, this approximation works better for smaller bins. The scenario $C0$ is displayed as an example of a scenario with tensor contributions where, as expected, the two determinations should yield different results.

1) The scenario with the highest pull_{SM} corresponds to scenario 3 (V_μ) with NP only in C^V_{RR}. Since $C^V_{LL} = C^V_{LR} = C^V_{RL} = 0$ in this scenario, Eq. (7.119) is fulfilled and $\Delta^F = 0$. However, in this scenario the NP contributions to $F_L^{D^*}$ cancel exactly and the tension with the experimental value is not relaxed.

2) A second interesting scenario is called 4b (Φ_b) in Ref. [187]. This scenario can be generated by a two Higgs doublet model and it yields non-zero values for C^S_X with $X = LL, LR, RL, RR$. Assuming $\mathcal{B}_{B_c\to\tau\bar{\nu}} < 30\%$, this scenario is able to relax the tensions of all observables including $F_L^{D^*}$. Since this scenario yields NP contributions only in C^S_i it fulfills automatically the constraint, leading to $\Delta^F = 0$.

3) In scenario 1 of Ref. [187], there are two solutions with non-vanishing values for $C^V_{LL,LR,RR}$ as well as $C^S_{LR,RR}$ and C^T_{RR}. One of the two solutions has a tensor contribution compatible with zero at 1σ. If we take this solution to remain under our initial hypothesis of the absence of tensor contributions we obtain $\Delta^F \sim 10^{-3}$ (central value of b.f.p) if $C^V_{RL} = 0$, which, obviously, cannot be detected. In Ref. [187] the coefficient C^V_{RL} is neglected because it is lepton-flavour universal within SMEFT and it cannot help to accommodate any of the deviations observed with LFUV observables. However, assuming the best-fit point of this scenario does not change when non-vanishing values of C^V_{RL} are allowed, we find that Δ^F can be much larger when C^V_{RL} approaches $\pm\sqrt{(1+C^V_{LL})^2 - {C^V_{LR}}^2 + {C^V_{RR}}^2}$, leading to a rather visible effect.

In summary, a difference between the two measurements of $F_T^{D^*}$ (or $F_L^{D^*}$) in absence of tensors and imaginary contributions could be attributed, barring experimental issues, to contributions coming from RHN. For some RHN scenarios, this would generate a non-zero value for Δ^F.

Chapter 8

Testing Lepton Flavour Universality in $\Upsilon(4S)$ Decays

In the previous chapter, we presented additional tests of the $b \to c\ell\bar{\nu}$ transitions at the level of the already measured angular distribution of $B \to D^*\ell\bar{\nu}$, providing tests of consistency among angular observables as well as potential indications about the nature of NP in case of discrepancies. Another possibility consists in considering new channels which have not been considered yet to probe NP, and in particular LFU violation, in $b \to c\ell\bar{\nu}$ transitions. Indeed, in light of the observations of hints of LFUV in the $b \to c\tau\bar{\nu}_\tau$ decays discussed in Chapter 3, several associated tests of LFU have been proposed, for instance, tests of LFU in $\Lambda_b \to \Lambda_c^{+(*)}$ decays [164, 335].

Following the proposal in Ref. [395], the BaBar collaboration has recently measured the lepton flavour universality (LFU) ratio in $\Upsilon(3S)$ decays [396]

$$R_{\tau/\mu}^{\Upsilon(3S)} \equiv \frac{\mathcal{B}(\Upsilon(3S) \to \tau^+\tau^-)}{\mathcal{B}(\Upsilon(3S) \to \mu^+\mu^-)} = 0.966 \pm 0.008 \pm 0.014\,, \tag{8.1}$$

where the first (second) uncertainty estimate is due to statistics (systematics). The measured value is within 1.8σ of the SM prediction $[R_{\tau/\mu}^{\Upsilon(3S)}]_{\rm SM} = 0.9948(1)$ [395]. This measurement is probing the $R_{D^{(*)}}$ LFU anomaly through $b\bar{b} \to \ell^+\ell^-$ transitions [397].

In the following we propose a related but potentially more direct test through inclusive di-leptonic $\Upsilon(4S)$ decays (see Fig. 8.1) by defining

$$\mathcal{B}_{\ell\ell'}^{\Upsilon(4S)} \equiv \mathcal{B}(\Upsilon(4S) \to \ell^+\ell'^-X)\,, \tag{8.2}$$

as the inclusive dileptonic branching fraction for $\Upsilon(4S)$ decays to a pair of opposite charged leptons of different flavours, where X denotes all the other (hadronic) activity and missing momentum in the event.

This fully inclusive measurement exploits several key capabilities of the Belle II experiment as well as some specific features of $\Upsilon(4S)$ and b-hadrons decays. On the experimental side, the excellent beam energy calibration of Super KEK-B can ensure that the $\Upsilon(4S)$ resonance is produced on shell even if its invariant mass is not reconstructed explicitly from the final state. This also allows the non-resonant background to be well estimated from sideband measurements. On the theory side, this inclusive decay is almost entirely saturated by decays into $B\bar{B}$ final states. Moreover, one can analyse the production of the leptons either from an initial b-quark decay or from subsequent parts of the decay chain in detail. All in all, ratios of the form

$$R_{\ell\ell'}^{\Upsilon(4S)} \equiv \frac{\mathcal{B}_{\ell''\ell}^{\Upsilon(4S)}}{\mathcal{B}_{\ell''\ell'}^{\Upsilon(4S)}}\,, \tag{8.3}$$

where ℓ, ℓ', ℓ'' are three different flavours of leptons e, μ, τ, provide a very interesting ground to probe lepton flavour universality with an inclusive measurement at Belle II[1], complementary to exclusive measurements accessible to both Belle II and LHCb experiments. In particular, under suitable experimental conditions one can relate

$$R_{\tau\ell}^{\Upsilon(4S)} = R(X)_{\tau\ell} + \ldots \tag{8.4}$$

where $\ell = e, \mu$ and $R(X)_{\tau\ell} \equiv \Gamma(B \to X\tau\nu)/\Gamma(B \to X\ell\nu)$ is the inclusive B decay LFU ratio, which can be precisely computed in the SM as $\mathcal{R}(X)_{\tau\ell} = 0.223(4)$ [398]. The dots denote corrections due to neutral B meson mixing effects and charm pollution. We propose to tame the first effect using a cut in the time difference between the two B-mesons decaying and we estimate the impact of this cut. The second effect is harder to mitigate

[1] In principle, a similar test could be envisioned using $\psi(3770)$ at BESIII since $\mathcal{B}(\psi(3770) \to D\bar{D}) \sim 93\%$ [6].

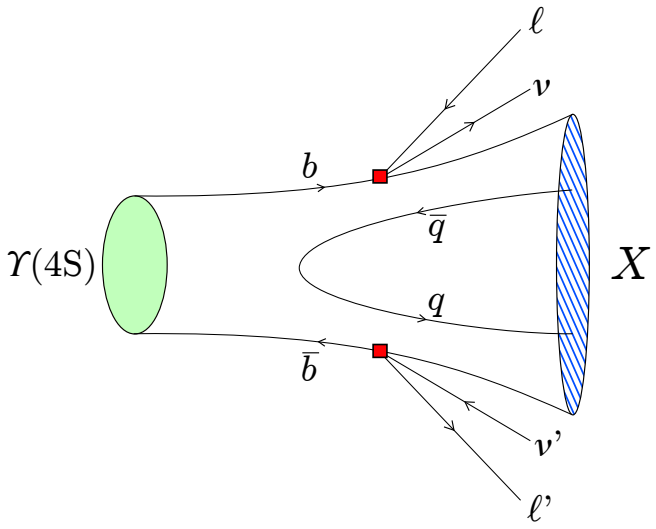

Figure 8.1: Diagram of inclusive di-leptonic $\Upsilon(4S)$ decays. The X represent all activity other than the lepton pair. Since the neutrinos go undetected, we will also consider them as part of X.

theoretically, and we will see that it requires additional experimental analyses to avoid a significant charm pollution.

This chapter is structured in the following way: In Section 8.1 we start by discussing the decays of the $\Upsilon(4S)$ meson into a $B\bar{B}$ pair. In Section 8.2 we discuss the subsequent decays of the $B\bar{B}$ system into lepton pairs and how they can be used to define the $R^{\Upsilon}(4S)$ LFU ratios. We then discuss the sources of possible contamination that these ratios can suffer that need to be dealt with experimentally. In Section 8.3 we discuss the $B-\bar{B}$ mixing effects, in Section 8.4 we discuss the pollution originated due to charm decays and in Section 8.5 we discuss the contamination of decays in which both leptons originate from a single B-meson. Lastly in Section 8.6, we finished the chapter with some conclusions regarding this analysis.

8.1 $\Upsilon(4S)$ decay

Let us start with the decay of the $\Upsilon(4S)$ resonance and estimate the amount of pollution from final states other than $B\bar{B}$. The $\Upsilon(4S)$ resonance overwhelmingly decays into $B\bar{B}$ final states. In particular, there is an experimental bound $\mathcal{B}(\Upsilon(4S)\to B\bar{B})>0.96$ [6] but $\mathcal{B}(\Upsilon(4S)\to B\bar{B})$ could actually be even much closer to one.

Indeed the dominant non-$B\bar{B}$ final states are expected to consist in light hadrons mediated by $\Upsilon(4S)\to 3g$ decays as well as decays to lighter bottomonium states, in particular, $\Upsilon(4S)\to(\Upsilon(n'S),h_b(n''P))(\pi\pi,\eta,\eta')$ with $n',''<4$.

Experimental measurements already exist for the latter contributions, in particular $\mathcal{B}(\Upsilon(4S)\to\Upsilon(1S)+X)<4\times10^{-3}$, $\mathcal{B}(\Upsilon(4S)\to\Upsilon(2S)\pi^+\pi^-)=8.2(8)\times10^{-5}$, $\mathcal{B}(\Upsilon(4S)\to h_b(1P)\eta)=2.18(21)\times10^{-3}$ with other known modes below the 10^{-4} level [6]. In total we thus estimate $\mathcal{B}(\Upsilon(4S)\to\text{bottomonia})<7\times10^{-3}$. On the other hand, the $\Upsilon(4S)\to 3g$ decay width can be estimated in NRQCD [399]. At leading order in velocity and QCD expansion, it is given by [400]

$$\Gamma(\Upsilon\to 3g)=0.0716\frac{\alpha_s^3\langle O_1\rangle_\Upsilon}{m_b^2}\,. \tag{8.5}$$

Both leading velocity and QCD corrections are of negative sign and thus serve to decrease the above estimate [400]. We thus take it as a conservative upper bound. Using $\alpha_s=0.22$, $m_b=4.6$ and the upper estimate on $\langle O_1\rangle_{\Upsilon(4S)}\lesssim\langle O_1\rangle_{\Upsilon(3S)}=1.279\,\text{GeV}^3$ [401] we obtain $\mathcal{B}(\Upsilon(4S)\to 3g)\lesssim 2\times10^{-3}$. In total we thus estimate that $\mathcal{B}(\Upsilon(4S)\to B\bar{B})\gtrsim 0.99$.

8.2 Lepton production

Having established that $\Upsilon(4S)$ decays almost only into pairs of B mesons, we consider their subsequent decays inclusively, focusing on final states containing leptons $\ell^{(\prime)}=e,\mu,\tau$ in the final state. We can differentiate between several measurable inclusive dilepton signatures such as

$$\Upsilon(4S)\to e^\pm\mu^\mp X\,,\quad \Upsilon(4S)\to\mu^\pm\tau^\mp_{\text{had}}X\,,\quad \Upsilon(4S)\to e^\pm\tau^\mp_{\text{had}}X\,, \tag{8.6}$$

where $\tau_{\rm had}$ denotes a τ lepton reconstructed from its hadronic decays (e.g. $\tau \to 3\pi\nu$)[2]. We will thus define

$$R^{\Upsilon(4S)}_{\tau_{\rm had}e} \equiv \frac{\mathcal{B}^{\Upsilon(4S)}_{\mu\tau_{\rm had}}}{\mathcal{B}^{\Upsilon(4S)}_{\mu e}} \qquad \text{and} \qquad R^{\Upsilon(4S)}_{\tau_{\rm had}\mu} \equiv \frac{\mathcal{B}^{\Upsilon(4S)}_{e\tau_{\rm had}}}{\mathcal{B}^{\Upsilon(4S)}_{\mu e}} \,. \tag{8.7}$$

To relate these ratios to inclusive B-decay LFU ratios, we need to isolate contributions where each of the two leptons is produced in a separate B-meson decay and suppress backgrounds where one or both leptons do not originate from a direct semileptonic B decay. Requiring different opposite-sign lepton flavour final states removes such contributions from $\Upsilon(4S) \to X + ((\bar{b}b) \to \ell^+\ell^-)$, $b \to q((c\bar{c}) \to \ell^+\ell^-)$ as well as from rare FCNC (semileptonic) B and charm decays.[3]

This approach is however not effective against contamination from $b \to q(c \to q'\ell^+\nu)(\bar{c} \to q''\ell'^-\nu)$ and $b \to (c \to q\ell^+\nu)\ell'^-\nu)$ transitions, which we will address in Section 8.5.

For the moment we assume that each of the two different lepton tags originates from a separate B-meson decay pattern. We will focus on $R^{\Upsilon(4S)}_{\tau_{\rm had}\mu}$ for the time being, but a very similar analysis can be performed for $R^{\Upsilon(4S)}_{\tau_{\rm had}e}$ swapping muons and electrons in the discussion. The single hadronic tau can be produced in the quark-level transition chains

$$\begin{aligned} &b \to q\tau\nu \,, \\ &b \to q\bar{q}'(c \to q''\tau\nu) \,. \end{aligned} \tag{8.8}$$

On the other hand a single muon (or equivalently electron) can originate from

$$\begin{aligned} &b \to q\mu\nu \,, \\ &b \to q\bar{q}'(c \to q''\mu\nu) \,, \\ &b \to q(\tau \to \mu\nu\nu)\nu \,, \\ &b \to q\bar{q}'(c \to q''(\tau \to \mu\nu\nu)\nu) \,. \end{aligned} \tag{8.9}$$

Inclusive semileptonic b-hadron decays (i.e. $b \to q\ell\nu$) are well under theoretical control and thus the associated rates can be well predicted, including possible effects of LFU violation [398]. The same cannot necessarily be said for inclusive semileptonic charm decays [403] , which thus represent a challenging background. One could imagine that the charge of the leptons could help us to disentangle the origin of the lepton, either from a b or from a c-quark. However, one should take into account that in approximately half of the cases, the $\Upsilon(4S)$ decays into neutral B mesons, which can oscillate and spoil the identification between the charge of initial quark and that of the lepton. We discuss strategies how to mitigate this effect next.

8.3 Mixing effects

We first define the amplitudes $A(B^0 \to \ell^- X), A(B^0 \to \ell^+ X), A(\bar{B}^0 \to \ell^+ X), A(\bar{B}^0 \to \ell^- X)$ embedding the complete meson decay chains (for instance it may contain $B \to D\pi$ followed by $D \to \ell X$), so that the lepton is not necessarily produced by the decay of the b-quark. However, it is not produced by the decay of the light quark in the B, which means that in the isospin limit, we have equalities of the type:

$$\begin{aligned} A(B^0 \to \ell^- X) &= A(B^+ \to \ell^- X) = A_{\ell^-} \\ A(\bar{B}^0 \to \ell^- X) &= A(B^- \to \ell^- X) = \bar{A}_{\ell^-} \\ &\vdots \end{aligned} \tag{8.10}$$

where the presence/absence of the bar indicates the charge of the b-quark inside the B-meson and the subscript denotes the charge and flavour of the lepton.

If we look for $\Upsilon(4S) \to \ell_1\ell_2 X$ (with 1 and 2 being different, either by flavour or charge) through an intermediate $B^0\bar{B}^0$ state, we can use the description introduced for the study of CP violation from the production of an intricated B-meson pair (sec 1.2.3 in Ref. [353]), leading to the time-dependent rate where one of the two B mesons decay into a state containing ℓ_1 at a time t_1 and the other one into a state containing ℓ_2 at a time t_2, leading to

$$R(t_1, t_2) = Ce^{-\Gamma(t_1+t_2)}\Big[\mathcal{I} - \cos(\Delta m(t_1 - t_2))\mathcal{C} + 2\sin(\Delta m(t_1 - t_2))\mathcal{S}\Big] \,, \tag{8.11}$$

[2] These hadronic tau lepton decays need to be efficiently disentangled from backgrounds like hadronic B decays involving three or more charged pions.

[3] The exceptions with $\ell^\pm = \tau^\pm$ where one of the taus decays leptonically and the other hadronically, leading to a final state with a hadronic tau and a lighter lepton, turn out to be numerically negligible as they are suppressed by small $\Upsilon(4S) \to X$+bottomonium, $B \to X$+charmonium [6], and $B \to X\tau^+\tau^-$ [402] branching ratios, respectively.

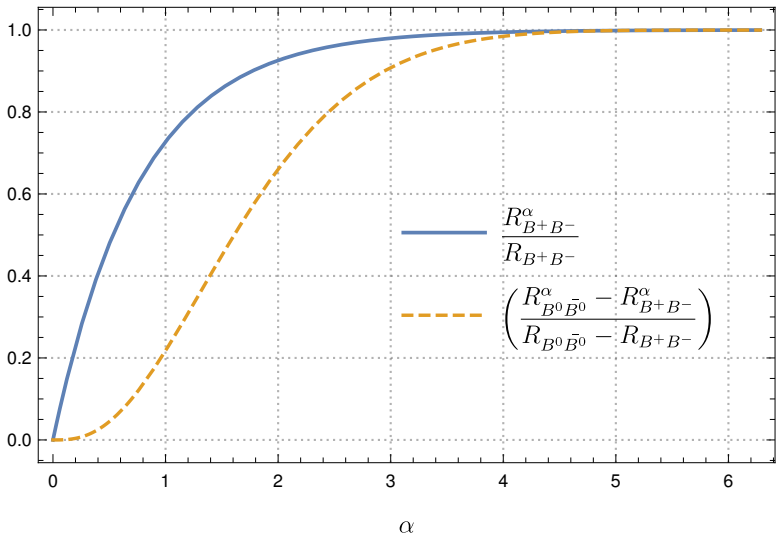

Figure 8.2: Relative branching fraction (blue solid) and mixing effect (yellow dashed) as a function of the cut parameter α.

where C is a normalisation coming from angular integration, Δm is the difference of mass between the two mass eigenstates, Γ is their average width, the approximations $|q/p| = 1$ and $\Delta\Gamma = 0$ have been used, and we have

$$\mathcal{I} = \left[(|A_1|^2 + |\bar{A}_1|^2)(|A_2|^2 + |\bar{A}_2|^2) - 4\mathrm{Re}\left(\frac{q}{p}A_1^*\bar{A}_1\right)\mathrm{Re}\left(\frac{q}{p}A_2^*\bar{A}_2\right)\right], \tag{8.12}$$

$$\mathcal{C} = \left[(|A_1|^2 - |\bar{A}_1|^2)(|A_2|^2 - |\bar{A}_2|^2) + 4\mathrm{Im}\left(\frac{q}{p}A_1^*\bar{A}_1\right)\mathrm{Im}\left(\frac{q}{p}A_2^*\bar{A}_2\right)\right], \tag{8.13}$$

$$\mathcal{S} = \left[\mathrm{Im}\left(\frac{q}{p}A_1^*\bar{A}_1\right)(|A_2|^2 - |\bar{A}_2|^2) + (|A_1|^2 - |\bar{A}_1|^2)\mathrm{Im}\left(\frac{q}{p}A_2^*\bar{A}_2\right)\right], \tag{8.14}$$

where $A_i \equiv A_{\ell_i}$ for $i = 1, 2$.

In order to prevent too large effects from mixing, one could consider cutting too large time differences $|t_1 - t_2|$, so that there has not been enough time for the evolution to take place. Cutting at $|t_1 - t_2| = \alpha/\Delta m$ (where α is the cut parameter) leads to

$$R^{\alpha}_{B^0\bar{B}^0} \equiv \int_{-\alpha/\Delta m}^{\alpha/\Delta m} R(t')\mathrm{d}t' = \frac{2C}{\Gamma^2}\left[(1 - e^{-\frac{\alpha}{x}})\mathcal{I} - \frac{1 - e^{-\frac{\alpha}{x}}(\cos\alpha - x\sin\alpha)}{1 + x^2}\mathcal{C}\right], \tag{8.15}$$

where $x = \Delta m/\Gamma \simeq 0.769$ [158]. In the case of B^+B^-, where no mixing is involved, we have

$$R^{\alpha}_{B^+B^-} \equiv \int_{-\alpha/\Delta m}^{\alpha/\Delta m} R(t')\Big|_{\Delta m=0}\mathrm{d}t' = \frac{2C}{\Gamma^2}(1 - e^{-\frac{\alpha}{x}})(\mathcal{I} - \mathcal{C})\,. \tag{8.16}$$

Denoting the result without cut in the time difference as $R_{BB} \equiv R^{\infty}_{BB}$, we see then that the effect of mixing corresponds to

$$R^{\alpha}_{B^0\bar{B}^0} - R^{\alpha}_{B^+B^-} = \left(1 - \frac{e^{-\frac{\alpha}{x}}(1 + x^2 - \cos\alpha + x\sin\alpha)}{x^2}\right)(R_{B^0\bar{B}^0} - R_{B^+B^-})\,, \tag{8.17}$$

whereas we have

$$R^{\alpha}_{B^+B^-} = (1 - e^{-\frac{\alpha}{x}})R_{B^+B^-}\,, \tag{8.18}$$

In Fig. 8.2, we illustrate the impact of the cut on the branching fraction of the decay into B^+B^- and on the mixing effect. We see that this cut can efficiently suppress the impact of mixing while keeping a large fraction of the B^+B^- signal.

We can study the impact of this cut on the $\Upsilon(4S)$ decay rate. Introducing $\rho = \mathcal{B}(\Upsilon(4S) \to B^+B^-) = 0.514 \pm 0.006$ [158], we have $\mathcal{B}(\Upsilon(4S) \to B^0\bar{B}^0) = 0.486 \pm 0.006 = 1 - \rho - \epsilon$ with $\epsilon < 0.01$ according to our estimates. We have then the total rate $R = \mathcal{B}(\Upsilon(4S) \to BB)$

$$R = \rho R_{B^+B^-} + (1 - \rho - \epsilon)R_{B^0\bar{B}^0} = (1 - \epsilon)R_{B^+B^-} + (1 - \rho - \epsilon)(R_{B^0\bar{B}^0} - R_{B^+B^-})\,, \tag{8.19}$$

where the first term corresponds to the rate without mixing (in the isospin limit) and the second term to the contamination due to mixing. Cutting $|t_1 - t_2| \leq \alpha/\Delta m$, we have

$$\begin{aligned} R^\alpha &= (1-\epsilon)R^\alpha_{B^+B^-} + (1-\rho-\epsilon)(R^\alpha_{B^0\bar{B}^0} - R^\alpha_{B^+B^-}) \\ &= (1-\epsilon)(1-e^{-\frac{\alpha}{x}})R_{B^+B^-} + (1-\rho-\epsilon)\left(1 - \frac{e^{-\frac{\alpha}{x}}(1+x^2-\cos\alpha + x\sin\alpha)}{x^2}\right)(R_{B^0\bar{B}^0} - R_{B^+B^-})\,. \end{aligned} \tag{8.20}$$

The first term in Eq. (8.20) goes like $O(\alpha)$ whereas the second term goes like $O(\alpha^3)$. Moreover, $(R_{B^0\bar{B}^0} - R_{B^+B^-})$ is equal to

$$R_{B^0\bar{B}^0} - R_{B^+B^-} = \frac{2C}{\Gamma^2}\frac{x^2}{1+x^2}\mathcal{C}\,, \tag{8.21}$$

so it goes like $O(x^2)$ and it is isospin suppressed. Then the second term in Eq. (8.20), corresponding to the mixing effects, is suppressed significantly.

From Fig. 8.2, we see that $\alpha = 0.53$ would ensure that the second contribution is $O(1\%)$ of $R_{B^+B^-}$, taking into account the suppressions by the α-dependent factor, by $x^2/(1+x^2)$ and by $1-\rho$ (but not taking into account the isospin suppression, which would further suppress this term). On the other hand, the first contribution in Eq. (8.20) would be half of $R_{B^+B^-}$ (essentially R without the effect of mixing in the isospin limit). More generally, a fit to R^α as a function of α would allow one to put a bound on $(R_{B^0\bar{B}^0} - R_{B^+B^-})$ and to extract $R_{B^+B^-}$ directly.

8.4 Charm pollution

As shown in the previous section, cutting on the time difference of the two decaying B mesons can suppress mixing effects and allow one to distinguish leptons originating from B and charm decays by charge. However, we still need to quantify the expected initial amount of charm contamination. Under the assumption that each tagged lepton originates from a separate B decay chain (which we will relax in the next section), the ratio $R^{\Upsilon(4S)}_{\tau_{\rm had}\mu}$ can be conveniently expressed in terms of

$$[R^{\Upsilon(4S)}_{\tau_{\rm had}\mu}]^{-1} = \frac{\mathcal{B}(B\to X\mu\nu) + \mathcal{B}(B\to X(h_c\to X'\mu\nu))}{\mathcal{B}(B\to X\tau_{\rm had}\nu) + \mathcal{B}(B\to X(h_c\to X'\tau_{\rm had}\nu))} + \frac{\mathcal{B}(\tau\to\mu\nu\bar{\nu})}{\mathcal{B}(\tau\to\tau_{\rm had})}\,, \tag{8.22}$$

where h_c denotes any weakly decaying charmed hadron, i.e. D^+, D^0, D_s, Λ_c and their charge conjugates. As discussed above, using charge ID, but also possibly a cut on leptons not originating from the secondary vertex (i.e. from B decays), it should be possible to suppress contributions where the leptons originate from secondary charm or, in the case of muons, tau decays, by efficiency factors $\epsilon^{(i)} \ll 1$. This allows us to simplify the above expression and write it in terms of the inverse of the inclusive ratio $R(X)_{\tau\mu}$. We obtain

$$\begin{aligned} [R^{\Upsilon(4S)}_{\tau_{\rm had}\mu_b}]^{-1} =& \Bigg\{ [R(X)_{\tau\mu}]^{-1}\left[1 - \epsilon^{(3)}\frac{\mathcal{B}(B\to X(h_c\to X'\tau\nu))}{\mathcal{B}(B\to X\tau\nu)}\right] \\ &+ \epsilon^{(1)}\mathcal{B}(\tau\to\mu\nu\bar{\nu}) + \epsilon^{(2)}\frac{\mathcal{B}(B\to X(h_c\to X'\mu\nu))}{\mathcal{B}(B\to X\tau\nu))}\Bigg\}[\mathcal{B}(\tau\to\tau_{\rm had})]^{-1}\,, \end{aligned} \tag{8.23}$$

where μ_b denotes muons consistent with originating from the secondary (i.e. b-decay) vertex and we have already used the fact that $\mathcal{B}(B\to X\tau\nu) \gg \mathcal{B}(B\to X(h_c\to X'\tau\nu))$, which we verify below.

We can estimate the size of all three corrections on the right-hand side of Eq. (8.23) (up to the $\epsilon^{(i)}$ efficiencies) based almost purely on experimental information. Starting with the $\epsilon^{(1)}$ term, $\mathcal{B}(\tau\to\mu\bar{\nu}\nu) = (17.39\pm0.04)\%$ [6] we see, that even without cuts (for $\epsilon^{(1)} \simeq 1$) it leads to an order 4% (computable) systematic effect in $\mathcal{R}(X)_{\tau\mu}$.

We estimate the second and third term thanks to the identity

$$\mathcal{B}(B\to X(h_c\to X'\ell\nu)) = \mathcal{B}(B\to X_c)\sum_i f(c\to h_c^{(i)})\mathcal{B}(h_c^{(i)}\to X\ell\nu)\,, \tag{8.24}$$

where the sum runs over all weakly decaying charmed hadrons and $f(c\to h_c^{(i)})$ are the corresponding fragmentation functions. We use Ref. [404] for the charm-inclusive decay branching ratio $\mathcal{B}(B\to X_c) = (97\pm4)\%$ and Ref. [405] for the charm fragmentation functions. Note that the above estimate relies on factorization of the inclusive B-decay amplitudes and is thus subject to related theoretical uncertainties. In addition, the application of charm fragmentation functions extracted from high energy e^+e^- and ep collision data to B decays carries further systematic errors. Consequently, our background evaluations should be taken as order-of-magnitude estimates,

which are however sufficient for our purpose. For $\mathcal{B}(D_s \to X\mu\nu)$ we use values measured by CLEO for the electron in the final state [406] $\mathcal{B}(D_s \to Xe\nu) = (6.52 \pm 0.39 \pm 0.15)\%$ which can serve as an effective upper bound on $\mathcal{B}(D_s \to X\mu\nu)$ assuming $e-\mu$ LFU in charm decays. We also use $\mathcal{B}(D^+ \to Xe\nu) = 0.1607 \pm 0.0030$ and $\mathcal{B}(D^0 \to Xe\nu) = 0.0649 \pm 0.0011$ [6]. Finally, we obtain

$$\begin{aligned}\mathcal{B}(B \to X(h_c \to X'\mu\nu)) &= \mathcal{B}(b \to X_c)\{f(c \to D^0)\mathcal{B}(D^0 \to X\mu\nu) + f(c \to D^+)\mathcal{B}(D^+ \to X\mu\nu) \\ &\quad + f(c \to D_s)\mathcal{B}(D_s \to X\mu\nu) + f(c \to \Lambda_c)\mathcal{B}(\Lambda_c \to X\mu\nu) + \ldots\} \lesssim 0.088\,, \qquad (8.25)\\ \mathcal{B}(B \to X(h_c \to X'\tau\nu)) &= \mathcal{B}(b \to X_c)\{f(c \to D^+)\mathcal{B}(D^+ \to \tau\nu) + f(c \to D_s)\mathcal{B}(D_s \to \tau\nu) + \ldots\} \\ &\quad \simeq 0.0067\,. \qquad (8.26)\end{aligned}$$

These values are to be compared with the LEP experimental determination of $\mathcal{B}(b \to q\tau\nu) \simeq \mathcal{B}(B \to X\tau\nu) = (2.41 \pm 0.23)\%$ [398]. In particular, before cuts and without lepton charge ID (for $\epsilon^{(2)} \simeq 1$) the second term in Eq. (8.23) would represent a dominant 80% systematic effect in the determination of $\mathcal{R}(X)_{\tau\mu}$. Finally, the effect of the $\epsilon^{(3)}$ term before cuts (for $\epsilon^{(3)} \simeq 1$) represents a relative 28% systematic effect on the determination of $\mathcal{R}(X)_{\tau\mu}$.

In summary, the term with $\epsilon^{(1)}$ is small thanks to the low value of $\mathcal{B}(\tau \to \mu\bar{\nu}\nu)$, whereas the factors of $\epsilon^{(2)}$ and $\epsilon^{(3)}$ have large values but are related to charm pollution, which (hopefully) can be reduced thanks to charge ID leading to small efficiencies $\epsilon^{(2,3)}$.

8.5 Leptons emitted from the same B-meson

Lastly we need to consider backgrounds where both leptons are of different charge and flavour, but originate from the same B-decay chain, corresponding to the parton-level chain

$$b \to q(c \to q'\ell^+\nu)(\bar{c} \to q''\ell'^-\nu) \quad \text{and} \quad b \to (c \to q\ell^+\nu)\ell'^-\nu\,. \qquad (8.27)$$

Denoting these processes collectively as $B \to X\ell\ell'$, and assuming they can be suppressed by cutting on leptons not originating from the secondary vertex (i.e. from b decays), we can again write the relative correction to Eq. (8.23) due to these contributions expanded to leading order in all $\epsilon^{(i)}$ as

$$\begin{aligned}[R^{\Upsilon(4S)}_{\tau_{\rm had}\mu_b}]^{-1} =& [R(X)_{\tau\mu}\mathcal{B}(\tau \to \tau_{\rm had})]^{-1} \\ &\times \left[1 - \epsilon^{(4)}\frac{\mathcal{B}(B \to X)\mathcal{B}(\bar{B} \to X\tau e)}{\mathcal{B}(B \to X\tau\nu)\mathcal{B}(\bar{B} \to Xe\nu)} + \epsilon^{(5)}\frac{\mathcal{B}(B \to X)\mathcal{B}(\bar{B} \to X\mu e)}{\mathcal{B}(B \to X\mu\nu)\mathcal{B}(\bar{B} \to Xe\nu)}\right] + \ldots \qquad (8.28)\end{aligned}$$

where the inclusive hadronic B-decay branching ratio is denoted as

$$\mathcal{B}(B \to X) \lesssim 1 - \sum_\ell \mathcal{B}(B \to X\ell\nu) \simeq 0.76\,, \qquad (8.29)$$

we take $\mathcal{B}(B \to X_c e\nu) \simeq \mathcal{B}(B \to X_c\mu\nu) \simeq 0.11$ [6], and the ellipsis denotes the remaining corrections on the right-hand side of Eq. (8.23). Using the numerical values given above we obtain for the relevant $b \to (c \to q\ell^+\nu)\ell'^-\nu$ transitions

$$\begin{aligned}&\mathcal{B}(B \to X(h_c \to X'e\nu)\tau\nu) = \\ &\quad \mathcal{B}(B \to X_c\tau\nu)[f(c \to D^0)\mathcal{B}(D^0 \to Xe\nu) + f(c \to D^+)\mathcal{B}(D^+ \to Xe\nu) \qquad (8.30)\\ &\qquad + f(c \to D_s)\mathcal{B}(D_s \to Xe\nu) + f(c \to \Lambda_c)\mathcal{B}(\Lambda_c \to Xe\nu) + \ldots] \simeq 0.0021\,,\end{aligned}$$

$$\mathcal{B}(B \to X(h_c \to X'\tau\nu)e\nu) = \mathcal{B}(B \to X_c e\nu)f(c \to D_s)\mathcal{B}(D_s \to \tau\nu) \simeq 0.00042\,, \qquad (8.31)$$

$$\begin{aligned}&\mathcal{B}(B \to X(h_c \to X'e\nu)\mu\nu) = \\ &\quad \mathcal{B}(B \to X_c\mu\nu)[f(c \to D^0)\mathcal{B}(D^0 \to Xe\nu) + f(c \to D^+)\mathcal{B}(D^+ \to Xe\nu) \qquad (8.32)\\ &\qquad + f(c \to D_s)\mathcal{B}(D_s \to Xe\nu) + f(c \to \Lambda_c)\mathcal{B}(\Lambda_c \to Xe\nu) + \ldots] \simeq 0.0095\end{aligned}$$

$$\begin{aligned}&\mathcal{B}(B \to X(h_c \to X'\mu\nu)e\nu) = \\ &\quad \mathcal{B}(B \to X_c e\nu)[f(c \to D^0)\mathcal{B}(D^0 \to X\mu\nu) + f(c \to D^+)\mathcal{B}(D^+ \to X\mu\nu) \qquad (8.33)\\ &\qquad + f(c \to D_s)\mathcal{B}(D_s \to X\mu\nu) + f(c \to \Lambda_c)\mathcal{B}(\Lambda_c \to X\mu\nu) + \ldots] \lesssim 0.010.\end{aligned}$$

Finally, for the decay chain $b \to qc\bar{c}(c \to q\ell\nu)(\bar{c} \to q'\ell'\nu)$, using $\mathcal{B}(B \to X_{c\bar{c}}) \simeq 22\%$ [407] and after including $c \to q\ell\nu$ and $\bar{c} \to q'\ell'\nu$ transition rates, we find

$$\begin{aligned}
&\mathcal{B}(B \to X(h_c \to X'e\nu)(h_{\bar{c}} \to X''\tau\nu)) = \\
&\quad \mathcal{B}(B \to X_{c\bar{c}}) f(\bar{c} \to \bar{D}_s)\mathcal{B}(\bar{D}_s \to \tau\nu) \\
&\quad \times \big[f(c \to D^0)\mathcal{B}(D^0 \to Xe\nu) + f(c \to D^+)\mathcal{B}(D^+ \to Xe\nu) \\
&\qquad + f(c \to D_s)\mathcal{B}(D_s \to Xe\nu) + f(c \to \Lambda_c)\mathcal{B}(\Lambda_c \to Xe\nu)\big] \simeq 0.0001\,,
\end{aligned} \tag{8.34}$$

$$\begin{aligned}
&\mathcal{B}(B \to X(h_c \to X'e\nu)(h_{\bar{c}} \to X''\mu\nu)) = \\
&\quad \mathcal{B}(B \to X_{c\bar{c}}) \big[f(c \to D^0)\mathcal{B}(D^0 \to X\mu\nu) + f(c \to D^+)\mathcal{B}(D^+ \to X\mu\nu) \\
&\qquad + f(c \to D_s)\mathcal{B}(D_s \to X\mu\nu) + f(c \to \Lambda_c)\mathcal{B}(\Lambda_c \to X\mu\nu)\big] \\
&\qquad \times \big[f(c \to D^0)\mathcal{B}(D^0 \to Xe\nu) + f(c \to D^+)\mathcal{B}(D^+ \to Xe\nu) \\
&\qquad + f(c \to D_s)\mathcal{B}(D_s \to Xe\nu) + f(c \to \Lambda_c)\mathcal{B}(\Lambda_c \to Xe\nu)\big] \simeq 0.0018\,.
\end{aligned} \tag{8.35}$$

Putting these values together we observe that these backgrounds are individually comparable in size to the signal (i.e. they would represent approximately 80% and 150% relative corrections, respectively) in absence of cuts to suppress them (for $\epsilon^{(4,5)} \simeq 1$). While they are similar in magnitude, they are highly correlated and contribute with opposite signs, so that they tend to cancel to a degree for $\epsilon^{(4)} \simeq \epsilon^{(5)}$. In fact, the two terms become exactly equal in the limit where one can neglect charm decays to muons and taus (in the ratio $R_{\tau e}^{\Upsilon(4S)}$ these would be charm decays to electrons and taus). On the other hand, contrary to the corrections outlined in Eq. (8.23), the corrections considered in this section cannot be suppressed using only lepton charge ID. This highlights the crucial importance of discriminating against leptons originating from the same B-decay chain, for instance through geometrical considerations. An alternative strategy could consist in discriminating leptons arising from the secondary (B-decay) vertices from those arising further down in the decay chains. A quantitative assessment of the feasibility of either of the two approaches through an appropriate experimental analysis would require a dedicated experimental study and is beyond the scope of this work.

8.6 Conclusions

Relying on the specific properties of B-factories and in particular the Belle II experiment, we have proposed to compare the inclusive rates of $\Upsilon(4S) \to e^\pm\mu^\mp X$, $\Upsilon(4S) \to \mu^\pm\tau_{\rm had}^\mp X$ and $\Upsilon(4S) \to e^\pm\tau_{\rm had}^\mp X$. This inclusive measurement can be related to the ratio $R(X)_{\tau\ell} \equiv \Gamma(b \to X\tau\nu)/\Gamma(b \to X\ell\nu)$ ($\ell = e$ or μ), once appropriate experimental cuts are applied to suppress the effects of neutral B mixing and leptons emitted from rare FCNC (semileptonic) B decays, as well as secondary charmonium, charm and tau decays. The feasibility of our proposal crucially assumes that hadronically decaying tau leptons originating from the B decay vertices can be efficiently disentangled from backgrounds (e.g. from hadronic B decays involving three or more charged pions) at Belle II. A dedicated experimental study of this is however beyond the scope of this work. Remarkably, this alternative determination of $R(X)_{\tau\ell}$ is a truly inclusive determination, contrary to the current one which corresponds to a sum of different exclusive modes.

We have focused on the case of $R_{\tau\mu}^{\Upsilon(4S)} \simeq R(X)_{\tau\mu}$, but our discussion applies equally well to the tau-electron combination, swapping the roles played by electrons and muons. The current deviations in $B \to D^*\ell\nu$ and $B \to D\ell\nu$ when τ channels are compared to electronic or muonic modes are at the level of 10% (for the LFU ratios of branching ratios) and provide a benchmark for the target sensitivity of our proposal. This is illustrated by the very simple case where NP mimics the $V-A$ structure of $b \to c\tau\nu$ currents in the SM, leading to a universal rescaling of all $b \to c\tau\nu$ branching ratios which would therefore impact the inclusive ratios $R(X)_{\tau\ell}$ in the same way as the exclusive measurements for R_D and R_D^*. Interestingly, the theoretical approach and the experimental environment are rather different in exclusive and inclusive measurements, and our proposal could provide very interesting cross-checks of the deviations currently seen in exclusive decays.

Given our estimates, the systematic uncertainties in the determination of $R(X)_{\tau\ell}$ from a measurement of $R_{\tau\ell}^{\Upsilon(4S)}$ could be brought below a given value ($\epsilon_{\rm sys}$) provided that (1) cuts on the $B-\bar{B}$ impact parameter difference can suppress the neutral B meson mixing effects below $\epsilon_{\rm sys}$ combined with an efficient lepton charge ID to suppress semileptonic charm-decay contamination; (2a) multiple leptons originating from the same B decay chain can be suppressed to better than $\epsilon_{\rm sys}$ or alternatively (2b) leptons arising from the secondary (B-decay) vertices can be discriminated against those arising further down in the decay chains to roughly better than $\epsilon_{\rm sys}$. Further dedicated experimental studies are needed to establish the actually attainable precision by Belle II. If this measurement turns out to be possible and accurate, one could imagine using the same OPE techniques as in the SM case to determine the sensitivity of the ratios $R(X)_{\tau\ell}$ to New Physics and to constrain the NP operators using this inclusive measurement.

In summary, we have proposed a novel method to test the persistent hints of violation of LFU observed in semileptonic B decays. This measurement would constitute an additional and potentially competitive probe of LFU violations in $b \to c\ell\nu$ transitions, complementary to exclusive measurements and accessible in the Belle II environment.

Part V

Connection to Other Modes

Chapter 9

Implications of the flavour anomalies in $B \to K^{(*)}\nu\bar{\nu}$ and $K \to \pi\nu\bar{\nu}$

In this chapter and in the following, we are going to look for potential implications of the $b \to s\ell^+\ell^-$ anomalies in other modes. We will keep the discussion at a general level, relying on EFT arguments, instead of discussing specific connections in New Physics models. In this chapter, we investigate the consequences of deviations from the Standard Model observed in $b \to s\mu^+\mu^-$ transitions for flavour-changing neutral-current processes involving down-type quarks and neutrinos, i.e. $b \to s\nu\bar{\nu}$ and $s \to d\nu\bar{\nu}$, under generic assumptions concerning the structure of NP. We derive the relevant Wilson coefficients within an effective field theory approach respecting the SM gauge symmetry, including right-handed currents, assuming a flavour structure based on approximate $U(2)$ symmetry, and considering only SM-like light neutrinos. We will discuss assumptions that can be made on the flavour structure of the theory to relate transitions among different families, to then discuss correlations among $B \to K^{(*)}\nu\bar{\nu}$ and $K \to \pi\nu\bar{\nu}$ branching ratios in the case of linear Minimal Flavour Violation and in a more general framework, highlighting in each case the role played by various New Physics scenarios proposed to explain $b \to s\mu^+\mu^-$ deviations.

As discussed in Chapter 3, recent experimental data in B physics hint towards deviations from Lepton Flavour Universality (LFU) in semi-leptonic b-quark decays. These deviations can be interpreted model-independently in terms of specific contributions to short-distance Wilson coefficients $\mathcal{C}_i$ of the weak effective Hamiltonian Eq. (2.35).

The global fits to $b \to s\ell^+\ell^-$ data (see Chapter 4) show that these deviations exhibit a consistent pattern favouring a significant additional New Physics (NP) contribution to $\mathcal{C}_9^\mu$ (of the order of 25% of the SM contribution) together with smaller contributions to $\mathcal{C}_{10}^\mu$ and/or $\mathcal{C}_{9'}^\mu$. Among the scenarios improving by over 6σ the description of the data compared to the SM, one can find the one-dimensional scenarios ($\mathcal{C}_9^{\mu,\mathrm{NP}}$, ($\mathcal{C}_9^{\mu,\mathrm{NP}} = -\mathcal{C}_{10}^{\mu,\mathrm{NP}}$) and ($\mathcal{C}_9^{\mu,\mathrm{NP}} = -\mathcal{C}_{9'}^{\mu,\mathrm{NP}}$) shown in Table 4.4. Two-dimensional scenarios achieving similarly high pulls with respect to the SM are obtained for NP contributions to ($\mathcal{C}_9^{\mu,\mathrm{NP}}, \mathcal{C}_{10}^{\mu,\mathrm{NP}}$) and ($\mathcal{C}_9^{\mu,\mathrm{NP}}, \mathcal{C}_{9'}^{\mu,\mathrm{NP}}$) with negative $\mathcal{C}_9^{\mu,\mathrm{NP}}$ and positive $\mathcal{C}_{10}^{\mu,\mathrm{NP}}$ and $\mathcal{C}_{9'}^{\mu,\mathrm{NP}}$ (see Table 4.5). Small contributions to electron operators $\mathcal{C}_{9(')10(')}^{e,\mathrm{NP}}$ are allowed by the data, but they are not required to achieve a good description. On other side, contributions to scalar and tensor operators do not enhance the description of the data [120, 128, 303, 408, 409].

9.1 Neutrino FCNCs

The SM neutrinos reside in the same leptonic weak doublets as the left-handed charged leptons. Therefore, FCNC decay modes with neutrinos in the final state offer complementary probes of NP in $b \to s\ell^+\ell^-$. However, FCNCs involving neutrinos bear important differences with their charged lepton equivalents.

We consider here only (SM-like) left-handed neutrinos, leading to only vector and axial structures for the lepton currents. Furthermore the charm loop contributions are very suppressed, since the coupling with the neutrinos is through a Z boson rather than a photon (see Fig. 9.1). Then, hadronic issues are limited to the question of form factors leading to very clean modes that can be predicted accurately.

9.1.1 B decays

In particular, decays $B \to h_s\nu\bar{\nu}$, with h_s standing for hadronic states of strangeness equal to 1, are known for their NP sensitivity [410].

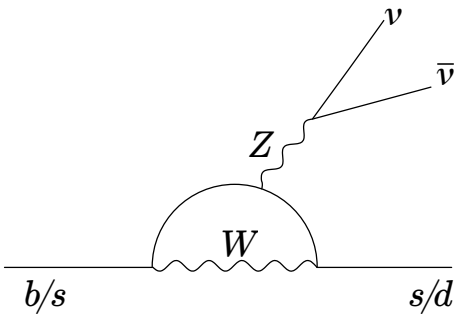

Figure 9.1: Penguin diagram for the flavour changing neutral currents in the SM into a pair of neutrinos. Opposed to the charged lepton case the coupling with the neutrinos is exclusively through a Z boson.

The effective Lagrangian for $b \to s\nu\bar{\nu}$ transitions can be written as [411]

$$\mathcal{L}_{\text{eff}}(b \to s\nu\bar{\nu}) = \frac{4G_F}{\sqrt{2}} V_{tb}^* V_{ts} \sum_{L,R} C_{L(R)}^{\nu_\alpha} \mathcal{O}_{L(R)}^{\nu_\alpha} \quad \text{with} \quad \alpha = e, \mu, \tau \,, \tag{9.1}$$

where the local operators are

$$\mathcal{O}_{L(R)}^{\nu_\alpha} = \frac{\alpha}{4\pi} (\bar{s}_{L(R)} \gamma_\mu b_{L(R)}) (\bar{\nu}^\alpha \gamma_\mu (1 - \gamma_5) \nu^\alpha) \tag{9.2}$$

and in the SM $C_R^{\nu_\alpha, \text{SM}}$ vanishes to a good approximation and $C_L^{\nu_\alpha, \text{SM}} = -\frac{X_t}{s_W^2} \approx -6.38$. s_W is given by the weak mixing angle

$$s_W \equiv \sin\theta_W \simeq 0.48 \,, \qquad c_W \equiv \cos\theta_W \,, \tag{9.3}$$

and X_i are defined in Ref. [412], numerically obtaining $X_t = 1.469(17)$ [412].

In the SM, branching ratios are found to be [413]

$$\mathcal{B}(B \to K^{(*)}\nu\bar{\nu})_{\text{SM}} = (9.6 \pm 0.9) \times 10^{-6} \,, \tag{9.4}$$

$$\mathcal{B}(B^+ \to K^+\nu\bar{\nu})_{\text{SM}} = (5.6 \pm 0.5) \times 10^{-6} \,. \tag{9.5}$$

The Belle collaboration has produced limits at 90% Confidence Level (CL)[414]

$$\mathcal{B}(B^0 \to K^{*0}\nu\bar{\nu})_{\text{exp}} < 1.8 \times 10^{-5} \,, \tag{9.6}$$

$$\mathcal{B}(B^+ \to K^{*+}\nu\bar{\nu})_{\text{exp}} < 6.1 \times 10^{-5} \,, \tag{9.7}$$

$$\mathcal{B}(B^+ \to K^+\nu\bar{\nu})_{\text{exp}} < 1.9 \times 10^{-5} \,. \tag{9.8}$$

The Belle II collaboration plans to observe these three decay modes with about 10 ab^{-1} of data, while the sensitivities to the SM branching ratio will reach a precision of about 10% with 50 ab^{-1} [413].

9.1.2 Kaon decays

In the kaon sector $K \to \pi\nu\bar{\nu}$ decays arguably offer the best sensitivity to NP [30], so we focus on these modes.

In the case of the $s \to d\nu\bar{\nu}$ transition, the effective Lagrangian can be written in a similar form to $b \to s\nu\bar{\nu}$

$$\mathcal{L}_{\text{eff}}(s \to d\nu\bar{\nu}) = \frac{4G_F}{\sqrt{2}} \sum_{L,R} C_{L(R),sd}^{\nu_\alpha} \frac{\alpha}{4\pi} (\bar{d}_{L(R)} \gamma_\mu s_{L(R)}) (\bar{\nu}^\alpha \gamma_\mu (1 - \gamma_5) \nu^\alpha) \tag{9.9}$$

where we absorb the CKM factor in the Wilson coefficient since both $V_{ts}V_{td}$ and $V_{cs}V_{cd}^*$ contribute. However, since we only look at decays of pseudoscalar mesons into pseudoscalar meson (i.e. $K \to \pi$), the only quark current allowed by parity is the vector current. This allows us to write the Wilson coefficients above as a single effective Wilson coefficient $C_{sd}^{\nu_\alpha} = C_{L,sd}^{\nu_\alpha} + C_{R,sd}^{\nu_\alpha}$. The SM value of this coefficient is $C_{sd}^{\nu_\alpha,\text{SM}} = V_{ts}V_{td}^* X_t + (X_c + \delta X_{c,u}) V_{cs}V_{cd}^*$ where $(X_c + \delta X_{c,u}) = 0.00106(6)$ [415, 416].

The experimental limits at 90% CL for the branching ratios were obtained by the E949 experiment [417, 418]

$$\mathcal{B}(K^+ \to \pi^+\nu\bar{\nu})_{\text{exp}} < 3.35 \times 10^{-10} \,, \tag{9.10}$$

while the NA62 collaboration has announced a 3.4σ evidence very recently for this decay [419]

$$\mathcal{B}(K^+ \to \pi^+\nu\bar{\nu})_{\text{exp}} = (1.06^{+0.40}_{-0.34} \pm 0.9) \times 10^{-10} \,. \tag{9.11}$$

On the other hand, KOTO [420] as set an upper limit [1] for the $K_L \to \pi^0\nu\bar{\nu}$ at 90% Confidence Level (CL)

$$\mathcal{B}(K_L \to \pi^0\nu\bar{\nu})_{\rm exp} < 4.9 \times 10^{-9}\,. \tag{9.13}$$

The corresponding SM values [422] are

$$\mathcal{B}(K^+ \to \pi^+\nu\bar{\nu})_{\rm SM} = (9.31 \pm 0.76) \times 10^{-11}\,, \tag{9.14}$$

and

$$\mathcal{B}(K_L \to \pi^0\nu\bar{\nu})_{\rm SM} = (3.74 \pm 0.72) \times 10^{-11}\,, \tag{9.15}$$

both in good agreement with the results from NA62 and KOTO.

We recall that these two branching ratios should obey the Grossman-Nir bound

$$\mathcal{B}(K_L \to \pi^0\nu\bar{\nu}) \leq 4.3\,\mathcal{B}(K^+ \to \pi^+\nu\bar{\nu})\,, \tag{9.16}$$

in which the numerical factor results from the difference in the total decay widths of K_L and K^+, isospin breaking effects, and QED radiative corrections [423]. In particular, the Grossman-Nir bound constitutes an additional very strong theoretical constraint on $\mathcal{B}(K_L \to \pi^0\nu\bar{\nu})$. The experiment NA62 is planning to eventually measure the rate of $K^+ \to \pi^+\nu\bar{\nu}$ with $O(10\%)$ precision [424]. For the neutral decay mode $K_L \to \pi^0\nu\bar{\nu}$ KOTO and KLEVER also aim at making significant progress [425].

Precise results for all these rare semileptonic $b \to s$ and $s \to d$ transitions will allow to get much better insight into possible NP effects observed in $R_{K^{(*)}}$. Particularly interesting is the question whether NP is only present in $b \to s$ transitions or also in other Flavour-Changing Neutral Currents (FCNC). The measurements of $s \to d\nu\bar{\nu}$ and $b \to s\nu\bar{\nu}$ rates should help to differentiate among NP models with different flavour and chiral structures in both the quark and lepton sectors. This issue has been already raised in many studies which mostly relied on particular models of NP [410, 426–429]. The main goal of our approach is to determine the impact of $R_{K^{(*)}}$ on future measurements of $B \to K^{(*)}\nu\bar{\nu}$ and $K \to \pi\nu\bar{\nu}$ in a general effective theory framework and to illustrate the potential correlations among these measurements.

9.2 EFT approach to NP in FCNC

9.2.1 NP in semileptonic FCNC decays

We will assume that the NP contributions will follow the symmetries of the SM in a similar approach to SMEFT. When considering $b \to s$ semileptonic FCNCs in general for both charged leptons and neutrinos, possible heavy NP contributions that respect the $SU(2)_L$ gauge symmetry should be written in terms of $SU(2)_L$ gauge invariant operators [249–251], e.g.

$$\begin{aligned}\mathcal{L}_{\rm eff.} = \mathcal{L}_{\rm SM} - \frac{1}{v^2}\lambda^q_{ij}\lambda^\ell_{\alpha\beta}\Big[&C_T\left(\bar{Q}^i_L\gamma_\mu\sigma^a Q^i_L\right)\left(\bar{L}^\alpha_L\gamma^\mu\sigma^a L^\beta_L\right)\\ &+ C_S\left(\bar{Q}^i_L\gamma_\mu Q^i_L\right)\left(\bar{L}^\alpha_L\gamma^\mu L^\beta_L\right) + C'_{RL}\left(\bar{d}^i_R\gamma_\mu d^i_R\right)\left(\bar{L}^\alpha_L\gamma^\mu L^\beta_L\right)\\ &+C'_{LR}\left(\bar{Q}^i_L\gamma_\mu Q^i_L\right)\left(\bar{\ell}^\alpha_R\gamma^\mu \ell^\beta_R\right) + C'_{RR}\left(\bar{d}^i_R\gamma_\mu d^i_R\right)\left(\bar{\ell}^\alpha_R\gamma^\mu \ell^\beta_R\right)\Big]\,,\end{aligned} \tag{9.17}$$

where we choose to write the operators in the down-quark and charged lepton mass basis (see Section 1.2)

$$Q^i_L = (V^{\rm CKM*}_{ji}u^j_L, d^i_L)^T\,, \qquad L^\alpha_L = (\nu^\alpha_L, \ell^\alpha_L)^T\,. \tag{9.18}$$

This Lagrangian, extending the one considered in Ref. [249] to include right-handed charged fermions, is chosen to reproduce the results of the global fits to $b \to s\ell^+\ell^-$ data discussed in Chapter 4. The latter favour scenarios limited to NP contributions to vector and axial operators $\mathcal{O}^\ell_{9(')10(')}$, without scalar or tensor contributions. If the purely left-handed operators proportional to C_S and C_T were not included, the Lagrangian would yield the scenario $\mathcal{C}^{\mu,\rm NP}_9 = \mathcal{C}^{\mu,\rm NP}_{10}$, see Eqs. (9.26) to (9.29) below, which is ruled out by the $b \to s\ell^+\ell^-$ data, as shown in Table 4.A.2 and in Fig. 4.2[2]. We have added right-handed operators compared to Ref. [249] to accommodate the NP scenarios involving right-handed currents also favoured in global fits.

The presence of operators with lepton doublets in Eq. (9.17) is the basis for the connection between flavour-changing neutral currents involving charged and neutral leptons that we explore in the following. Following Refs. [249, 426, 430] we assume that the same flavour structure encoded in λ^q_{ij} and $\lambda^\ell_{\alpha\beta}$ holds for all operators.

[1] Previous preliminary results from KOTO [421] indicated a value of

$$\mathcal{B}(K_L \to \pi^0\nu\bar{\nu})_{\rm exp} = 2.1^{+2.0(+4.1)}_{-1.1(-1.7)} \times 10^{-9}\,. \tag{9.12}$$

which would violate the Grossman-Nir bound in Eq. (9.16). However this result was finally attributed to background effects [420] that had been neglected, leading to a final result compatible with the Grossman-Nir bound.

[2] We explicitly checked that the updated analysis presented in Chapter 4 yields a pull of only 0.3 σ for the one-dimensional scenario $\mathcal{C}^{\mu,\rm NP}_9 = \mathcal{C}^{\mu,\rm NP}_{10}$ compared to the SM, with values for the NP contribution compatible with zero at 68% CL.

9.2.2 Flavour Structure in the quark sector

We need to connect the transitions among various quarks assuming a flavour structure for λ^q_{ij}. This can be done using flavour symmetries, generally inspired by the pattern of flavour symmetry breaking in the Standard Model. One can in particular consider that only the top-quark Yukawa is large and assume a U(2) symmetry preventing the first two generations from acquiring large Yukawas. In this case, we classify the NP flavour structures in terms of an approximate $\mathrm{U}(2)_{q=Q_L,D}$ flavour symmetry acting directly on the quark fields, under which two generations of quarks form doublets, while the third generation is invariant (see also [273, 431–435] for related work)

$$\mathbf{q} \equiv (q^1_L, q^2_L) \sim (\mathbf{2}, \mathbf{1})\,, \qquad \mathbf{d} \equiv (d^1_R, d^2_R) \sim (\mathbf{1}, \mathbf{2})\,, \qquad d^3_R, q^3_L \sim (\mathbf{1}, \mathbf{1})\,. \tag{9.19}$$

In the exact $U(2)_q$ limit only λ^q_{33} and $\lambda^q_{11} = \lambda^q_{22}$ in Eq. (9.17) are non-vanishing. Since a specific pattern of $U(2)_q$ breaking (by the SM Yukawas) is required to accommodate the first two generation quark masses and the CKM matrix, there is an ambiguity in the definition of the singlet field with respect to the down-quark mass basis, which, if chosen arbitrarily, may still result in unacceptably large mixing among generations. To avoid excessive effects in neutral kaon oscillation observables, we thus furthermore impose the *leading* NP $U(2)_q$ breaking to be aligned with the SM Yukawas, which is often referred to as a Minimal Flavour Violating (MFV) or General Minimal Flavour Violating (GMFV) [270] NP structure (see Section 3.3.3) Often the term MFV is used to refer to the limited case of linear MFV in which only first order terms on the Yukawa spurions are kept, we will use the term "(G)MFV" for the general type of MFV and the term "linear MFV" for the reduced one. In general, there is some arbitrariness in the choice of the $U(2)_q$ singlet, which can in principle mix the third generation singlet with the first and second generation doublets. In the case of (G)MFV and stopping at leading order in symmetry breaking, the form of the singlet is constrained to [249]

$$q^3_L = \begin{pmatrix} V^*_{jb} u^j_L \\ b_L \end{pmatrix} + \theta_q e^{i\phi_q} \left[V_{td} \begin{pmatrix} V^*_{jd} u^j_L \\ d_L \end{pmatrix} + V_{ts} \begin{pmatrix} V^*_{js} u^j_L \\ s_L \end{pmatrix} \right]. \tag{9.20}$$

where θ_q and ϕ_q are fixed but otherwise arbitrary numbers.[3] Therefore respecting the $U(2)_q$ symmetry with (G)MFV breaking, for the down-type quarks, one has

$$d^3_L = b_L + \theta_q e^{i\phi_q} \left(V_{td} d_L + V_{ts} s_L \right) . \tag{9.21}$$

The linear MFV limit [270] is recovered by taking $\theta_q = 1$ and $\phi_q = 0$. Note that within the linear MFV regime, owing to its rigid flavour breaking structure, the flavour construction in Eq. (9.17) does not imply extra assumptions, since any additional flavour re-scalings of individual operators can be absorbed into the definition of flavour universal C_i's. In (G)MFV, right-handed FCNCs among down-type quarks are suppressed so that we may set $C'_{RL} = C'_{RR} = 0$ then. Departures from the (G)MFV limit may manifest through additional explicit $U(2)_q$ breaking effects appearing as $\lambda^q_{i\neq j} \neq 0$ and we normalise such effects by the $U(2)_q$ symmetric (λ^q_{33}) contribution by defining $r_{ij} = \lambda^q_{ij}/\lambda^q_{33}$.

9.2.3 Flavour Structure in the lepton sector

For the lepton sector we assume an approximate $U(1)^3_\ell$ symmetry (broken only by the neutrino masses) yielding $\lambda^\ell_{i\neq j} \simeq 0$ as required by stringent limits on lepton flavour violation [6, 293, 436–443]. As already discussed, current (LFU) NP hints in rare semileptonic B decays only indicate significant non-standard effects in muonic final states. While a smaller effect in electrons is not excluded, $b \to s\tau^+\tau^-$ transitions are at present only poorly constrained and could in principle exhibit even much larger deviations than those observed in $R_{K^{(*)}}$ [295]. However, the corresponding neutrino flavours are not tagged in current and upcoming rare meson decay experiments. In order to correlate FCNC processes involving charged leptons and neutrinos we need to assume specific ratios of $U(1)^3_\ell$ charges (λ^ℓ). In the following we will consider three well known examples from the existing literature:

1. The simplest $\lambda^\ell_{ee} = \lambda^\ell_{\tau\tau} = 0$ scenario implies significant NP effects only in muonic final states. Correspondingly only a single neutrino flavour ν (e.g. in the sums of Eqs. (9.35) and (9.37)) receives NP effects. This is usually assumed in model-independent EFT analyses.

2. The anomaly-free assignment $\lambda^\ell_{\mu\mu} = -\lambda^\ell_{\tau\tau}$ and $\lambda^\ell_{ee} = 0$ allows for gauging of the leptonic flavour symmetry and is thus well suited for UV-complete model building [264, 444]. In this case two of the neutrino flavours in Eqs. (9.35) and (9.37) receive NP effects, equal in magnitude, but opposite in sign.

[3] Note that in general θ_q, ϕ_q could be operator specific. However in practice this does not lead to loss of generality of our main findings and results.

3. The hierarchical charge scenario $\lambda^\ell_{ee} \ll \lambda^\ell_{\mu\mu} \ll \lambda^\ell_{\tau\tau}$ is motivated by models of partial lepton compositeness and flavour models accounting for hierarchical charged lepton masses [255, 445]. In this case NP effects in Eqs. (9.35) and (9.37) are again dominated by a single (τ) neutrino flavour, however the effects can be much larger than indicated by the deviations in $R_{K^{(*)}}$. For concreteness in the following we consider $\lambda^\ell_{\tau\tau}/\lambda^\ell_{\mu\mu} = m_\tau/m_\mu$ and again neglect the small effects in λ^ℓ_{ee} for this scenario.

9.3 Matching

In order to relate the effective Lagrangian in Eq. (9.17) with the results of the $b \to s\ell^+\ell^-$ Global fits, we need to match the Wilson coefficients in Eq. (9.17) with the ones in Eq. (2.35). Similarly, in order to extract the observables for the $b \to s\nu\bar{\nu}$ and $s \to d\nu\bar{\nu}$ transitions, we match Eq. (9.17) with the effective Lagrangians commonly used to describe this transitions. For this we expand the left-handed doublet bilinears in Eq. (9.17) onto the relevant fields, leading to

$$\lambda^q_{ij}\left(\bar{Q}^i_L\gamma_\mu Q^i_L\right)\left(\bar{L}^\alpha_L\gamma^\mu L^\beta_L\right) \to \left(\lambda^q_{33}\theta_q e^{-i\phi_q}V^*_{ts}\bar{s}_L\gamma_\mu b_L + \lambda^q_{23}\bar{s}_L\gamma_\mu b_L + \lambda^q_{12}\bar{d}_L\gamma_\mu s_L + \lambda^q_{33}\theta^2_q V^*_{td}V_{ts}\bar{d}_L\gamma_\mu s_L\right)\times\left(\bar{\ell}^\alpha_L\gamma^\mu\ell^\beta_L + \bar{\nu}^\alpha_L\gamma^\mu\nu^\beta_L\right), \quad (9.22)$$

and

$$\lambda^q_{ij}\left(\bar{Q}^i_L\gamma_\mu\sigma^a Q^i_L\right)\left(\bar{L}^\alpha_L\gamma^\mu\sigma^a L^\beta_L\right) \to \left(\lambda^q_{33}\theta_q e^{-i\phi_q}V^*_{ts}\bar{s}_L\gamma_\mu b_L + \lambda^q_{23}\bar{s}_L\gamma_\mu b_L + \lambda^q_{12}\bar{d}_L\gamma_\mu s_L + \lambda^q_{33}\theta^2_q V^*_{td}V_{ts}\bar{d}_L\gamma_\mu s_L\right)\times\left(\bar{\ell}^\alpha_L\gamma^\mu\ell^\beta_L - \bar{\nu}^\alpha_L\gamma^\mu\nu^\beta_L\right), \quad (9.23)$$

whereas for the right-handed singlet

$$\lambda^q_{ij}\left(\bar{d}^i_R\gamma_\mu d^i_R\right)\left(\bar{L}^\alpha_L\gamma^\mu L^\beta_L\right) \to \left(\lambda^q_{23}\bar{s}_R\gamma_\mu b_R + \lambda^q_{12}\bar{d}_R\gamma_\mu s_R\right)\left(\bar{\ell}^\alpha_L\gamma^\mu\ell^\beta_L + \bar{\nu}^\alpha_L\gamma^\mu\nu^\beta_L\right). \quad (9.24)$$

9.3.1 $b \to s\mu^+\mu^-$

Expanding Eq. (9.17) and keeping only the terms relevant for $b \to s\ell^+\ell^-$ we obtain

$$\begin{aligned}\mathcal{L}_{\rm NP}(b\to s\mu^+\mu^-) = -\frac{\lambda^q_{33}\lambda^\ell_{\mu\mu}}{v^2}\Big\{&\left(\theta_q e^{-i\phi_q}V^*_{ts} + r_{23}\right)\\ &\times\left[(C_T+C_S)(\bar{s}_L\gamma_\mu b_L)(\mu_L\gamma_\mu\mu_L) + C'_{LR}(\bar{s}_L\gamma_\mu b_L)(\mu_R\gamma_\mu\mu_R)\right]\\ &+ r_{23}C'_{RL}(\bar{s}_R\gamma_\mu b_R)(\mu_L\gamma_\mu\mu_L) + r_{23}C'_{RR}(\bar{s}_R\gamma_\mu b_R)(\mu_R\gamma_\mu\mu_R)\Big\}.\end{aligned} \quad (9.25)$$

The matching of the Wilson coefficients of Eq. (2.35) and Eq. (9.17) is then, to linear order in $U(2)_q$ breaking, given by

$$\begin{aligned}\mathcal{C}^{\mu,\rm NP}_9 &= -\frac{\pi}{\alpha_{em}V_{tb}V^*_{ts}}\lambda^q_{33}\lambda^\ell_{\mu\mu}[V^*_{ts}\theta_q e^{-i\phi_q} + r_{23}]\\ &\quad\times(C_T + C_S + C'_{LR}),\end{aligned} \quad (9.26)$$

$$\begin{aligned}\mathcal{C}^{\mu,\rm NP}_{10} &= -\frac{\pi}{\alpha_{em}V_{tb}V^*_{ts}}\lambda^q_{33}\lambda^\ell_{\mu\mu}[V^*_{ts}\theta_q e^{-i\phi_q} + r_{23}]\\ &\quad\times(-C_T - C_S + C'_{LR}),\end{aligned} \quad (9.27)$$

$$\mathcal{C}^{\mu,\rm NP}_{9'} = -\frac{\pi}{\alpha_{em}V_{tb}V^*_{ts}}\lambda^q_{33}\lambda^\ell_{\mu\mu}r_{23}\left(C'_{RR} + C'_{RL}\right), \quad (9.28)$$

$$\mathcal{C}^{\mu,\rm NP}_{10'} = -\frac{\pi}{\alpha_{em}V_{tb}V^*_{ts}}\lambda^q_{33}\lambda^\ell_{\mu\mu}r_{23}\left(C'_{RR} - C'_{RL}\right), \quad (9.29)$$

where the SM component of the Wilson coefficients can be found in Table 2.1.

9.3.2 $b \to s\nu\bar{\nu}$

Expanding Eq. (9.17) and keeping only the terms relevant for $b \to s\nu\bar{\nu}$ we obtain

$$\begin{aligned}\mathcal{L}_{\rm NP}(b\to s\nu\bar{\nu}) = -\frac{\lambda^q_{33}\lambda^\ell_{\alpha\alpha}}{2v^2}\Big\{&\left(\theta_q e^{-i\phi_q}V^*_{ts} + r_{23}\right)(-C_T + C_S)(\bar{s}_L\gamma_\mu b_L)(\bar{\nu}^\alpha\gamma_\mu(1-\gamma_5)\nu^\alpha)\\ &+ r_{23}C'_{RL}(\bar{s}_R\gamma_\mu b_R)(\bar{\nu}^\alpha\gamma_\mu(1-\gamma_5)\nu^\alpha)\Big\}.\end{aligned} \quad (9.30)$$

The matching of the Wilson coefficients of Eq. (9.1) and Eq. (9.17) is then, including leading $U(2)_q$ breaking effects, given by

$$C_L^{\nu_\alpha,\mathrm{NP}} = -\frac{\pi}{\alpha_{em} V_{tb} V_{ts}^*} \lambda_{33}^q \lambda_{\alpha\alpha}^\ell [V_{ts}^* \theta_q e^{-i\phi_q} + r_{23}][C_S - C_T]\,, \tag{9.31}$$

$$C_R^{\nu_\alpha,\mathrm{NP}} = -\frac{\pi}{\alpha_{em} V_{tb} V_{ts}^*} \lambda_{33}^q \lambda_{\alpha\alpha}^\ell r_{23} C'_{RL}\,. \tag{9.32}$$

9.3.3 $s \to d\nu\bar{\nu}$

The expansion of Eq. (9.17) into the $s \to d\nu\bar{\nu}$ mode reads

$$\begin{aligned}\mathcal{L}_{\mathrm{NP}}(s \to d\nu\bar{\nu}) = -\frac{\lambda_{33}^q \lambda_{\alpha\alpha}^\ell}{2v^2} \Big\{ &\Big(\theta_q^2 V_{ts} V_{td}^* + r_{13}^* \theta_q e^{i\phi_q} V_{ts} + r_{23} \theta_q e^{-i\phi_q} V_{td}^* + r_{12}\Big) \\ &\times (-C_T + C_S)(\bar{s}_L \gamma_\mu b_L)(\bar{\nu}^\alpha \gamma_\mu (1-\gamma_5)\nu^\alpha) \\ &+ r_{12} C'_{RL} (\bar{d}_R \gamma_\mu s_R)(\bar{\nu}^\alpha \gamma_\mu (1-\gamma_5)\nu^\alpha)\Big\}\,,\end{aligned} \tag{9.33}$$

leading to the following effective NP Wilson coefficient

$$\begin{aligned}C_{sd}^{\nu_\alpha,\mathrm{NP}} = &\frac{\pi s_W^2}{\alpha_{em}} \lambda_{33}^q \lambda_{\alpha\alpha}^\ell [\theta_q^2 V_{ts} V_{td}^* (C_S - C_T) \\ &+ \theta_q (V_{ts} e^{i\phi_q} r_{13}^* + V_{td}^* e^{-i\phi_q} r_{23}) (C_S - C_T) \\ &+ r_{12} (C_S - C_T + C'_{RL})]\,.\end{aligned} \tag{9.34}$$

Since $s \to d$ transitions only appear at quadratic order in (G)MFV breaking of $U(2)_q$, in this case we have included up to quadratic $U(2)_q$ breaking terms, but at the same time kept only the linear $U(2)_q$ breaking contributions *beyond* (G)MFV, since these suffice for our following discussion.

9.4 Observables

9.4.1 $b \to s\nu\bar{\nu}$

The rare B decays $B \to K^{(*)}\nu\bar{\nu}$ can be conveniently expressed in presence of NP of the form in Eq. (9.17) as [410, 411]

$$\begin{aligned}\mathcal{B}(B \to K\nu\bar{\nu}) =&(4.5 \pm 0.7) \times 10^{-6} \frac{1}{3} \sum_\nu (1 - 2\eta_\nu)\epsilon_\nu^2\,, \\ \mathcal{B}(B \to K^*\nu\bar{\nu}) =&(6.8 \pm 1.1) \times 10^{-6} \frac{1}{3} \sum_\nu (1 + 1.31\eta_\nu)\epsilon_\nu^2\,, \\ \mathcal{B}(B \to X_s\nu\bar{\nu}) =&(2.7 \pm 0.2) \times 10^{-5} \frac{1}{3} \sum_\nu (1 + 0.09\eta_\nu)\epsilon_\nu^2\,, \\ \langle F_L \rangle =&(0.54 \pm 0.01) \frac{\sum_\nu (1 + 2\eta_\nu)\epsilon_\nu^2}{\sum_\nu (1 + 1.31\eta_\nu)\epsilon_\nu^2}\,,\end{aligned} \tag{9.35}$$

where 1.31 and 0.09 corresponds to an evaluation of the balance between helicities/states with different parities. $\langle F_L \rangle$ is the longitudinal K^* polarisation fraction in $B \to K^*\nu\bar{\nu}$ decays. For each flavour of neutrino $\nu = \nu_e, \nu_\mu, \nu_\tau$, the two NP parameters can in turn be expressed as

$$\epsilon_\nu = \frac{\sqrt{|C_L^\nu|^2 + |C_R^\nu|^2}}{|C_{\mathrm{SM}}^\nu|}\,, \quad \eta_\nu = \frac{-\mathrm{Re}(C_L^\nu C_R^{\nu *})}{|C_L^\nu|^2 + |C_R^\nu|^2}\,, \tag{9.36}$$

where $C_{L,R}^\nu = C_{L,R}^{\nu,\mathrm{SM}} + C_{L,R}^{\nu,\mathrm{NP}}$, $C_{L,R}^{\nu,\mathrm{NP}}$ are given in Eq. (9.31) and $C_L^{\nu,\mathrm{SM}} = -6.38$ and $C_R^{\nu,\mathrm{SM}} = 0$ at $\mu = m_b$.

Note that any deviations from SM in $\langle F_L \rangle$ or non-universal deviations in $\mathcal{B}(B \to (K, K^*, X_s)\nu\bar{\nu})/\mathcal{B}(B \to (K, K^*, X_s)\nu\bar{\nu})_{\mathrm{SM}}$ would signal the presence of right-handed quark currents ($C'_{RL} \neq 0$) and thus departures from the (G)MFV limit.

9.4.2 $s \to d\nu\bar{\nu}$

Similarly, the rare kaon decays $K^+ \to \pi^+\nu\bar{\nu}$ and $K_L \to \pi^0\nu\bar{\nu}$ can be conveniently expressed in presence of NP of the form in Eq. (9.17) as [427, 446]

$$\begin{aligned}\mathcal{B}(K^+ \to \pi^+\nu\bar{\nu}(\gamma)) &= (8.4 \pm 1.0) \times 10^{-11} \frac{1}{3} \sum_\nu \left| 1 + \frac{C_{sd}^{\nu,\mathrm{NP}}}{V_{ts}V_{td}^* X_t + (X_c + \delta X_{c,u}) V_{cs} V_{cd}^*} \right|^2 , \\ \mathcal{B}(K_L \to \pi^0\nu\bar{\nu}) &= (3.4 \pm 0.3) \times 10^{-11} \frac{1}{3} \sum_\nu \left[1 + \frac{\mathrm{Im}\left(C_{sd}^{\nu,\mathrm{NP}}\right)}{\mathrm{Im}\left(V_{ts}V_{td}^* X_t\right)} \right]^2 ,\end{aligned} \tag{9.37}$$

where $C_{sd}^{\nu,\mathrm{NP}}$ is given in Eq. (9.34)..

A short comment regarding the correlation in between $K_L \to \pi^0\nu\bar{\nu}$ and $K^+ \to \pi^+\nu\bar{\nu}$ is at hand. As it can be seen in Eq. (9.37), without CPV NP these modes are fully correlated. We note that new CP phases in $s \to d$ transitions, necessary to to break this correlation, only appear beyond the (G)MFV limit [270]. In the case of $K \to \pi\nu\bar{\nu}$ decays we can see this explicitly in Eq. (9.34) since only terms proportional to r_{ij} may carry additional phases. These terms should thus dominate over the first row indicating large departures from the (G)MFV limit. Unfortunately, little can be said about the implications of $b \to s\mu^+\mu^-$ data model independently in this part of parameter space. A potential future experimental confirmation of $\mathcal{C}_{9'}^{\mu,NP} \neq 0$ could at best provide circumstantial evidence for the presence of $U(2)_q$ breaking beyond (G)MFV.

9.5 Results in the linear MFV case

We first consider the limit of linear MFV in which $b \to s\nu\bar{\nu}$ and $s \to d\nu\bar{\nu}$ FCNC transitions are rigidly correlated via the corresponding CKM prefactors in Eqs. (9.31) and (9.34) and $C'_{RL} = C'_{RR} = 0$. Even before considering the implications of $R_{K^{(*)}}$, this immediately implies a very general correlation between $B \to h_s\nu\bar{\nu}$ and $K \to \pi\nu\bar{\nu}$ rates, driven by the combination of Wilson coefficients $C_S - C_T$ in Eq (9.17). For conciseness, we consider the branching ratios normalised to their SM values by introducing

$$R(i \to f) \equiv \mathcal{B}(i \to f)/\mathcal{B}(i \to f)_{\mathrm{SM}} \,. \tag{9.38}$$

The allowed region for these ratios is shown shaded in darker (2ν) and lighter (3ν) grey in Fig. 9.2, where arbitrary MFV NP effects in two (2ν) or three (3ν) neutrino flavours (with arbitrary varying $\lambda_{33}^q \lambda^\ell$) have been considered, respectively. The two ratios R are bounded by the same minimal value $(1 - N_\nu/3)$ where N_ν is the number of neutrino flavours affected by NP. Also shown are the present experimental constraints coming from NA62 [447, 448] and B-factories [414] respectively. An interesting observation is that a pair of future $B \to h_s\nu\bar{\nu}$ and $K \to \pi\nu\bar{\nu}$ rate measurements outside of this (albeit large) region would be a clear indication of non-MFV NP. On the same plot we also superimpose the three specific $U(1)_\ell^3$ scenarios (i.e. fixed $\lambda_{33}^q \lambda^\ell$).

In the $b \to s\ell^+\ell^-$ analysis, the (G)MFV limit corresponds to the $(\mathcal{C}_9^{\mu,\mathrm{NP}}, \mathcal{C}_{10}^{\mu,\mathrm{NP}})$ scenario. In terms of the EFT operator basis in Eq (9.17) $R_{K^{(*)}}$ measurements (and more generally $b \to s\ell^+\ell^-$ data) favour non-zero values for both $C_S + C_T$ and C'_{LR}. Since $B \to h_s\nu\bar{\nu}$ and $K \to \pi\nu\bar{\nu}$ depend on the orthogonal $C_S - C_T$ combination, interesting implications can only be derived in specific scenarios allowing us to convert the information from $b \to s\ell^+\ell^-$ observables into a constraint on C_S and C_T. The simplest possibilities ($C_S = 0$ or $C_T = 0$) are indicated in Fig. 9.2 for $U(1)_\ell^3$ scenarios 1 and 3 respectively. On the other hand, in scenario 2, no significant deviations are expected in either case. We observe that the pure $SU(2)$ triplet ($C_S = 0$) scenario 3 ($\lambda_{\tau\tau}^\ell / \lambda_{\mu\mu}^\ell = m_\tau/m_\mu$) was already close to being probed by searches for $B \to K^{(*)}\nu\bar{\nu}$ at the B-factories and that both pure $SU(2)$ triplet ($C_S = 0$) and singlet ($C_T = 0$) limits of scenario 3 are currently outside the 68% CL preferred region of the recent $\mathcal{B}(K^+ \to \pi^+\nu\bar{\nu})$ measurement. The final projected sensitivity of Belle II could be sufficient to eventually also distinguish between the pure $SU(2)$ triplet ($C_S = 0$) and singlet ($C_T = 0$) limits of scenario 1.

9.6 Results with right-handed currents

Beyond the MFV limit any correlation between $b \to s$ and $s \to d$ FCNCs is lost in general. Nonetheless, the potential presence of right-handed $b \to s$ FCNCs in the $(\mathcal{C}_9^{\mu,\mathrm{NP}}, \mathcal{C}_{9'}^{\mu,\mathrm{NP}})$ scenario[4] as well as the leptonic flavour structure of NP can both still be probed using correlations among two $B \to h_s\nu\bar{\nu}$ modes, as shown in Fig. 9.3

[4] Note that the additional inclusion of $\mathcal{C}_{10}^{\mu,\mathrm{NP}}$ to this NP scenario does not alter our conclusions, as it corresponds to the addition of C'_{LR} which is not involved in $b \to s\nu\bar{\nu}$.

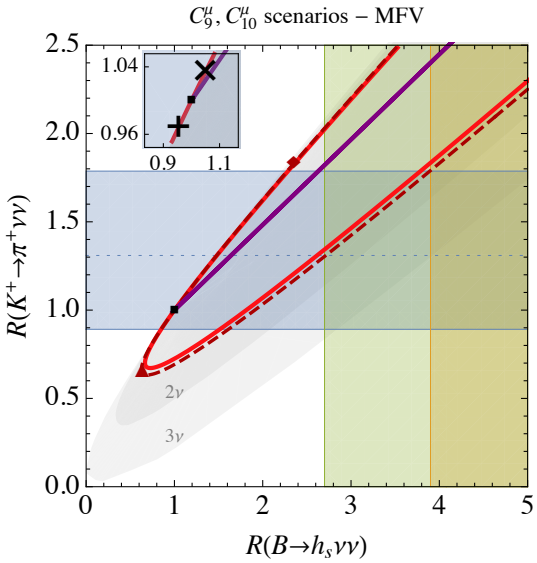

Figure 9.2: Correlation between the ratios $R(B \to h_s\nu\bar{\nu})$ ($h_s = K, K^*, X_s$) and $R(K^+ \to \pi^+\nu\bar{\nu})$ in the linear MFV limit. The SM value is represented by the black square. The region allowed for arbitrary NP effects in ν_μ and ν_τ only (all three neutrino flavours) is show in dark grey (light grey respectively). Curves are drawn for the specific $U(1)^3_\ell$ scenarios 1 (NP only in muons, red), 2 (opposite NP effects in muons and taus, purple) and 3 (hierarchical NP effects according to the generation, dashed brown). Scenarios with $C_S = 0$ or $C_T = 0$ are indicated as black $\times$ and $+$ respectively in the inset plot for scenario 1 and brown $\Diamond$ or $\triangle$ respectively for scenario 3. The vertical bands correspond to the 90 % CL limits on the observables for $R(B \to K^*\nu\bar{\nu})$ (green) and $R(B \to K\nu\bar{\nu})$ (orange) [414], while the horizontal blue region indicates the recent $\mathcal{B}(K^+ \to \pi^+\nu\bar{\nu})$ measurement [447, 448].

for the case $R(B \to K\nu\bar{\nu})$ vs. $R(B \to K^*\nu\bar{\nu})$. These results are obtained by varying all the relevant model parameters in Eqs. (9.26) and (9.28), while the different lepton flavour ($U(1)^3_\ell$ charge) assignments are shown in different contours.

First note that in the MFV limit relative NP effects in both modes are expected to be identical as indicated by the diagonal blue line. Beyond MFV however, any deviation from the diagonal would indicate the presence of right-handed currents and the amount of deviation from the diagonal would directly indicate the number of lepton flavours affected by NP.

In scenario 1 (where only muons couple significantly to NP) and scenario 2 (where muons and taus have opposite NP couplings) the $b \to s\ell^+\ell^-$ fit for $(\mathcal{C}_9^{\mu,\mathrm{NP}}, \mathcal{C}_{9'}^{\mu,\mathrm{NP}})$ (see Chapter 4) singles out a narrow region around the diagonal in this plane, whereas scenario 3 leaves a much larger region allowed. Conversely, a measurement of the two $b \to s\nu\bar{\nu}$ modes outside of the region for scenario 1 would indicate significant (right-handed FCNC) NP couplings to other neutrino species, e.g. ν_τ.

In absence of information on the size of the right-handed FCNCs from the $b \to s\mu^+\mu^-$ modes in principle the whole region within the grey 1ν contour could be accessible, with limits corresponding $\eta_\nu = -1/2$ and $+1/2$ (MFV corresponding to $\eta_\nu = 0$). In presence of significant couplings also to tau neutrinos as e.g. in scenario 3, the whole region within the grey dashed 2ν contour is possible, even when the existing constraints coming from $b \to s\mu^+\mu^-$ modes are taken into account.

Finally, in presence of significant right-handed FCNCs coupling to all three neutrino flavours the whole region within the grey dotted 3ν contour would be possible in principle.

9.7 Conclusions

In this chapter, we have investigated the consequences of deviations from the SM observed in $b \to s\mu^+\mu^-$ transitions for FCNC processes involving down-type quarks and neutrinos. Motivated by the results from the global fits to $b \to s\ell^+\ell^-$ observables as well as measurements and bounds on FCNC processes with neutrinos, we have considered a general EFT description of FCNC transitions in terms of $SU(2)_L$ gauge invariant operators including those with right-handed quarks and charged leptons. This allowed us to describe with the same short-distance Wilson coefficients $b \to s\mu^+\mu^-$, $b \to s\nu\bar{\nu}$ and $s \to d\nu\bar{\nu}$.

We have briefly touched upon the status of $K_L \to \pi^0\nu\bar{\nu}$ and its correlation with $K^+ \to \pi^+\nu\bar{\nu}$, which is only modified by CPV NP, which requires new flavour dynamics beyond (G)MFV. In this case, there is no clear

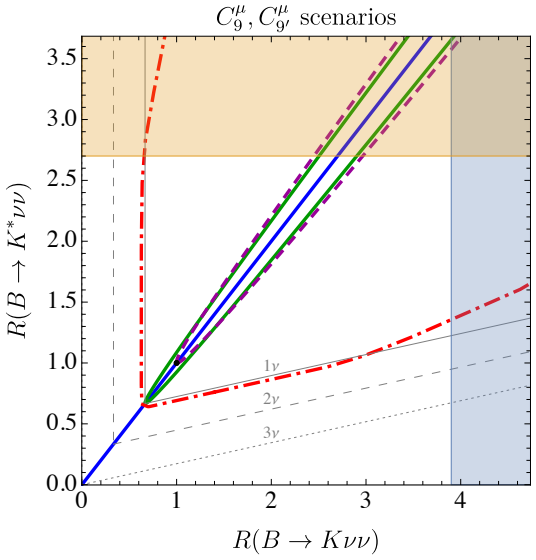

Figure 9.3: Correlation between the ratios $R(B \to K\nu\bar{\nu})$ and $R(B \to K^*\nu\bar{\nu})$ in the presence of NP in $b \to s\mu^+\mu^-$ transitions through $(\mathcal{C}_9^{\mu,\mathrm{NP}}, \mathcal{C}_{9'}^{\mu,\mathrm{NP}})$. The diagonal blue line corresponds to the (G)MFV case ($\mathcal{C}_{9'}^{\mu,\mathrm{NP}} = 0$). The 1 σ region allowed by $b \to s\mu^+\mu^-$ transitions yields an allowed region depending on the assumption on the couplings to leptons, inside the solid green line for scenario 1 (NP only in muons), dashed purple for scenario 2 (opposite NP effects in muons and taus) and dot-dashed red for scenario 3 (hierarchical NP effects according to the generation). Without information on the size of the right-handed FCNCs from $b \to s\mu^+\mu^-$, the allowed region assuming significant NP couplings to 1, 2, 3 neutrinos is above and on the right of the solid, dashed, dotted grey contours, respectively. The horizontal and vertical bands correspond to the 90 % CL limits on the observables for $R(B \to K^*\nu\bar{\nu})$ (orange) and $R(B \to K\nu\bar{\nu})$ (blue) [414].

correlation with the other FCNC modes discussed here. Assuming (G)MFV in the quark sector, we have studied the correlation between the branching ratios for $B \to h_s\nu\bar{\nu}$ and $K^+ \to \pi^+\nu\bar{\nu}$. Such a correlation is already present without assuming any definite structure for the neutrino NP couplings, but it can be made even more precise once particular NP scenarios assign specific values to these couplings. Moreover, for scenarios with no triplet ($C_T = 0$) or singlet ($C_S = 0$) contributions, the fits to $(\mathcal{C}_9^{\mu,\mathrm{NP}}, \mathcal{C}_{10}^{\mu,\mathrm{NP}})$ can be immediately converted into predictions for these two branching ratios in terms of

$$\mathbf{R}_{\nu\nu} \equiv [R(B \to h_s\nu\bar{\nu}), R(K^+ \to \pi^+\nu\bar{\nu})]\,. \tag{9.39}$$

In scenario 1 where NP couples only to muons, we find

$$\mathbf{R}_{\nu\nu} \simeq (0.95, 0.97) \quad \text{if} \quad C_S = 0\,, \tag{9.40}$$
$$\mathbf{R}_{\nu\nu} \simeq (1.05, 1.03) \quad \text{if} \quad C_T = 0\,. \tag{9.41}$$

In scenario 2 where muons and taus have opposite couplings, the values remain very close to the SM. In scenario 3 where NP hierarchical couplings proportional to the lepton mass are assumed, we find

$$\mathbf{R}_{\nu\nu} \simeq (0.64, 0.65) \quad \text{if} \quad C_S = 0\,, \tag{9.42}$$
$$\mathbf{R}_{\nu\nu} \simeq (2.40, 1.80) \quad \text{if} \quad C_T = 0\,. \tag{9.43}$$

Both limits are already in slight tension with the recent measurement of $\mathcal{B}(K^+ \to \pi^+\nu\bar{\nu})$.

Moving beyond the (G)MFV limit, we have investigated the correlation between $B \to K\nu\bar{\nu}$ and $B \to K^*\nu\bar{\nu}$, in particular showing that depending on the NP lepton couplings also the scenario with NP in $(\mathcal{C}_9^{\mu,\mathrm{NP}}, \mathcal{C}_{9'}^{\mu,\mathrm{NP}})$ can yield a tight correlation between the two modes when the $b \to s\ell^+\ell^-$ measurements are taken into account. For instance, in scenarios 1 and 2, the ratio $R(B \to K\nu\bar{\nu})/R(B \to K^*\nu\bar{\nu})$ cannot deviate from unity by more than 8%. More generally, such measurements could establish NP flavour breaking beyond (G)MFV as well indicate the number of lepton flavours affected by NP. For example, the measurements of the two ratios $R(B \to K\nu\bar{\nu})$ and $R(B \to K^*\nu\bar{\nu})$ outside the diagonal could be interpreted as the presence of right-handed currents in both $b \to s\nu\bar{\nu}$ and $b \to s\ell^+\ell^-$. Our work shows therefore that fairly general information on the pattern of NP could be obtained from the forthcoming measurements of $K \to \pi\nu\bar{\nu}$ and $B \to K^{(*)}\nu\bar{\nu}$.

Chapter 10

A new B-flavour anomaly in $B_{d,s} \to K^{*0}\bar{K}^{*0}$: anatomy and interpretation

If NP is indeed at the origin of the anomalies in semileptonic B decays, it is natural to expect signals in other observables involving $b \to s$ transitions (see Fig. 10.1 for instance). A natural place to explore the possible existence of these signals are non-leptonic B decays. This type of decays suffer from larger uncertainties compared to semileptonic B decays and are therefore more difficult to compute with a high accuracy. In particular, branching ratios and polarisation fractions receive contributions that suffer from large uncertainties due to power-suppressed but infrared-divergent weak annihilation and hard-spectator scattering [139, 149]. In this sense a deviation with respect to the SM prediction in non-leptonic B decays requires one to be much more conservative regarding these uncertainties than in the case of semileptonic B decays.

In this chapter, based on Ref. [449], we will follow a similar strategy to the one used in Refs. [87, 214] for semileptonic rare B decays. In $b \to s\ell\ell$ decays, one can build two different kinds of observables with a reduced sensitivity to hadronic uncertainties: on the one hand, angular observables from decays involving muons in the final state [87, 373] constructed exploiting heavy quark symmetry and on the other hand, ratios of branching ratios with muons versus electrons in the final state that test LFUV and where the dependence on the form factors cancels almost exactly in the SM [450]. There are tensions in observables involving leptons of the second family (for the former) and between the second and the first family of leptons (for the latter).

In this chapter we explore the parallel approach of using non-leptonic B decays rather than semileptonic ones, comparing quark transitions involving quarks of the second and first families instead of muons and electrons. More specifically, we compare transitions involving s-quarks and d-quarks to benefit from the approximate U-spin symmetry of the Standard Model in analogy with Lepton-Flavour Universality used to build the LFUV ratios in $b \to s\ell\ell$ decays. The analogy has evident limitations: since both symmetries are broken by fermion mass effects, the size of the corrections is easier to compute or estimate for LFU (involving mainly QED) than for U-spin (involving QCD). However, even in the nonleptonic case it is well known that ratios of this type offer many advantages in reducing hadronic uncertainties, explaining for instance the popularity of the ratio ξ to describe neutral-meson mixing in lattice QCD [59] and phenomenological studies of the CKM matrix [24, 151].

We may reach an even better control of hadronic uncertainties by combining several approaches. In Refs. [354, 451, 452] it was shown that the specific structure of penguin-mediated non-leptonic B-decays could lead

Figure 10.1: Diagrams of the $b \to s\ell\ell$ and $b \to sq\bar{q}$ contributions of a Z' NP model shown as an illustration of possible connections in between these modes.

to a better theoretical control on combinations of hadronic matrix elements within factorisation approaches. In the case of vector final states, it is also known that the decays into longitudinally polarised light mesons can be described more precisely than the transverse ones within these factorisation approaches, providing a further guide to build optimised observables (in analogy with the angular observables in semileptonic decays). Finally, if the B_d-meson decays have been studied at B-factories extensively, LHCb is now able to provide accurate measurements for many B_s-meson decays with the possibility to assess the correlation between B_d and B_s mesons decaying into the same final state [158].In particular, it is very interesting to notice the ratio of longitudinal polarisations [453, 454]

$$\frac{f_L(B_d \to K^{*0}\bar{K}^{*0})}{f_L(B_s \to K^{*0}\bar{K}^{*0})} = 0.33 \pm 0.06 \tag{10.1}$$

which is rather different from the U-spin expectation to be close to 1. With this particular decay in mind, we will consider a type of observables for penguin-mediated non-leptonic decays of B mesons into two vector particles, that we will refer as *L-observables*. These correspond essentially to the R_{sd} observable introduced in Ref. [354] in the case of $B_{d,s} \to K^{*0}\bar{K}^{*0}$ (up to a phase space). We present here a detailed and complete anatomy of this observable in the SM, updating the SM prediction and observing an increase in the tension with the experimental measurement compared to Ref. [354]. We then discuss NP explanations for the tension observed. We also point out possible improvements of the theoretical prediction of this observable.

In Section 10.1 we develop the theoretical framework that will be used to compute the L observable. We put a particular emphasis on the sources of hadronic uncertainties coming from infrared divergences that affect mostly branching ratios and polarisations. In Section 10.2 we construct this observable and we compute it. Then using the data of the previous section we determine its experimental value and the pull. In Section 10.3 we explore possible solutions in terms of NP shifts to Wilson coefficients in a model-independent EFT approach, before considering particular models illustrating the difficulty to explain this non-leptonic anomaly together with the $b \to s\ell\ell$ anomalies in Section 10.4. We finally conclude in Section 10.5.

Appendices 10.A to 10.C are devoted to a discussion of the QCD factorisation relevant elements, the semi-analyical description of relevant hadronic matrix elements, and complementary material concerning the sensitivity of L to different sources of NP.

10.1 Theoretical framework

10.1.1 Helicity amplitudes

We start by considering the theoretical description of $B_Q \to VV$ with $Q = d, s$ before focusing on $B_{d,s} \to K^{*0}\bar{K}^{*0}$ more specifically. Since the initial state has spin 0, the two vector mesons must have the same helicity, leading to a description of the decay in terms of three helicity amplitudes A^0, A^+ and A^-. In naive factorisation one expects a hierarchy of the type: $\bar{A}^0 > \bar{A}^- > \bar{A}^+$ for a $\bar{B} \to VV$ decay and $A^0 > A^+ > A^-$ for a $B \to VV$ decay. This hierarchy with a dominance of longitudinal amplitudes is easy to understand by means of the V-A structure of the SM [89]. Each amplitude is suppressed with respect to the previous one by $\mathcal{O}(\Lambda/m_b)$ due to helicity suppression [149]. The longitudinal amplitude in a $b \to s$ transition is dominant as compared to the positive helicity: the s quark is produced with an helicity $-1/2$ by weak interactions (in the limit $m_s \to 0$), which is not affected by the strong interactions, then the strange quark combines with the light spectator quark to form a V with a helicity which can reach 0 or -1 but not $+1$. In $\bar{A}^-$, a light-quark helicity flip is required to obtain both vector mesons with a negative helicity, whereas in $\bar{A}^+$, two helicity flips are required to reach a positive helicity for both vector mesons. Each of these helicity flips yields a suppression by a factor $\mathcal{O}(\Lambda/m_b)$, as expected in naive factorisation (see Section 2.8).

10.1.2 Hadronic matrix elements

For a $\bar{B}_Q$ meson decaying through a $b \to q$ penguin-mediated process into a V_1V_2 state with a definite polarisation, the decomposition

$$\bar{A}_f \equiv A(\bar{B}_Q \to V_1V_2) = \lambda_u^{(q)} T_q + \lambda_c^{(q)} P_q\,, \tag{10.2}$$

is always possible, with the CKM factors $\lambda_U^{(q)}$ defined in Eq. (1.42). We denote by T_q and P_q the matrix elements accompanying the $\lambda_u^{(q)}$ and $\lambda_c^{(q)}$ CKM factors respectively. In the SM, P_q is usually associated to penguin topologies, whereas T_q receives contributions from tree topologies (but it can also contain only penguin topologies in some decays). As discussed above, if we consider the longitudinal polarisation, T_q and P_q can be computed using factorisation approaches based on a $1/m_b$ expansion (see Appendix 10.A). In QCD factorisation [86], T_q and P_q are affected by possibly large long-distance $1/m_b$-suppressed effects that we discussed in Section 2.8. In

the case of penguin mediated decays like $B_{(d,s)} \to K^{*0}\bar{K}^{*0}$, it was observed [451, 452] that the same type of (long-distance) infrared divergences affect both P_q and T_q, so one can construct

$$\Delta_q = T_q - P_q\,, \tag{10.3}$$

free from these next-to-leading-order infrared divergences encoded in X_A and X_H (see Section 2.8).

Using the unitarity relation in Eq. (1.45), we can write Eq. (10.2) in terms of $\lambda_u^{(q)}$ and $\lambda_t^{(q)}$

$$\bar{A}_f = \lambda_u^{(q)}\,\Delta_q - \lambda_t^{(q)} P_q\,. \tag{10.4}$$

The weak phases in $\lambda_t^{(q)}$ are given by β_q, as defined in Eq. (1.42) whereas $\lambda_c^{(q)}$ is real to a very good approximation for both $q = d, s$, and $\lambda_u^{(q)} = -\lambda_c^{(q)} - \lambda_t^{(q)}$. The CP-conjugate amplitude is given by

$$A_{\bar{f}} = (\lambda_u^{(q)})^* T_q + (\lambda_c^{(q)})^* P_q = (\lambda_u^{(q)})^* \Delta_q - (\lambda_t^{(q)})^* P_q\,. \tag{10.5}$$

If $f = V_1V_2$ is a CP-eigenstate, note that $A_{\bar{f}}$ is different from $A = A(B \to V_1V_2)$, even though the two types of amplitudes are related:

$$\bar{A} = \bar{A}_f \qquad A = \eta_f A_{\bar{f}}\,, \tag{10.6}$$

where η_f is the CP-parity of the final state, given for $j = 0, ||, \perp$ respectively as $\eta, \eta, -\eta$ where $\eta = 1$ if V_1 is the charge conjugate of V_2 (this is the case for $K^{*0}\bar{K}^{*0}$).

10.2 The L-observable for $B_Q \to K^{*0}\bar{K}^{*0}$

10.2.1 Definition and experimental determination

The 2019 LHCb analysis with 3 fb^{-1} data measured the ratio of the untagged and time-integrated decay rates [454]

$$\frac{\mathcal{B}_{B_d\to K^{*0}\bar{K}^{*0}}}{\mathcal{B}_{B_s\to K^{*0}\bar{K}^{*0}}} = 0.0758 \pm 0.0057\,\text{stat} \pm 0.0025\,\text{syst} \pm 0.0016 \left(\frac{f_s}{f_d}\right), \tag{10.7}$$

The longitudinal polarisation of both modes has been measured as well. The average of $B_d \to K^{*0}\bar{K}^{*0}$ from LHCb [454] and BaBar [453]

$$f_L^{\text{LHCb}}(B_d \to K^{*0}\bar{K}^{*0}) = 0.724 \pm 0.051 \pm 0.016, \tag{10.8}$$

$$f_L^{\text{BaBar}}(B_d \to K^{*0}\bar{K}^{*0}) = 0.80^{+0.10}_{-0.12} \pm 0.06, \tag{10.9}$$

yields

$$f_L(B_d \to K^{*0}\bar{K}^{*0}) = 0.73 \pm 0.05, \tag{10.10}$$

whereas the polarisation for the $B_s \to K^{*0}\bar{K}^{*0}$ mode is [454]:

$$f_L(B_s \to K^{*0}\bar{K}^{*0}) = 0.240 \pm 0.031\,\text{stat} \pm 0.025\,\text{syst}\,. \tag{10.11}$$

Most of the experimental determinations are made assuming no direct CP-violation; however, the ones searching for CP violation found no hint in these decays [455].

One can notice already that the longitudinal polarisations are very different for these two modes, although they are related by U-spin symmetry in its most obvious form, i.e. the $d \leftrightarrow s$ exchange. In the SM, U-spin is broken only by the quark masses, and it is thus expected to be fairly well obeyed (up to a 20-30% correction). We propose to define an observable that will be sensitive to this effect but with a cleaner theoretical prediction:

$$L_{V_1V_2} = \frac{\mathcal{B}_{b\to s}}{\mathcal{B}_{b\to d}} \frac{g_{b\to d} f_L^{b\to s}}{g_{b\to s} f_L^{b\to d}} = \frac{|A_0^s|^2 + |\bar{A}_0^s|^2}{|A_0^d|^2 + |\bar{A}_0^d|^2}\,, \tag{10.12}$$

where $\mathcal{B}_{b\to q}$ ($f_L^{b\to q}$) refers to the branching ratio (longitudinal polarisation) of the $\bar{B}_Q \to V_1V_2$ decay governed by a $b \to q$ transition. A_0^q and $\bar{A}_0^q$ are the amplitudes for the B_Q and $\bar{B}_Q$ decays governed by $b \to q$ with final vector mesons being polarised longitudinally and

$$g_{b\to q} = \omega \sqrt{\left[M_{B_Q}^2 - \Sigma_{V_1V_2}\right]\left[M_{B_Q}^2 - \Delta_{V_1V_2}\right]}\,, \tag{10.13}$$

stands for the phase space factor involved in the corresponding branching ratio, with

$$\omega = \tau_{B_Q}/(16\pi M_{B_Q}^3)\,, \quad \Sigma_{ab} = (m_a + m_b)^2\,, \quad \Delta_{ab} = (m_a - m_b)^2\,, \tag{10.14}$$

and all quantities are CP-averaged.

This observable is defined such that the dependence on the troublesome transverse (parallel and perpendicular) amplitudes entering the branching ratio and longitudinal polarisation fraction cancel and it is close to the observable R_{sd} for the case of $B_{d,s} \to K^{*0}\bar{K}^{*0}$ up to a phase space factor [354].

Being purely sensitive to the longitudinal amplitudes, L is less affected by the hadronic uncertainties which impact the transverse polarisation amplitudes significantly and which are difficult to estimate within QCD Factorisation (see Section 2.8) or other approaches based on a $1/m_b$ expansion. The choice of this observable thus avoids the difficulties encountered in the interpretation of low longitudinal polarisation fractions observed in some non-leptonic modes [149]. We will now only focus on:

$$L_{K^*\bar{K}^*} = \frac{\mathcal{B}_{B_s\to K^{*0}\bar{K}^{*0}}}{\mathcal{B}_{B_d\to K^{*0}\bar{K}^{*0}}} \frac{g_{b\to d} f_L^{B_s}}{g_{b\to s} f_L^{B_d}} = \frac{|A_0^s|^2 + |\bar{A}_0^s|^2}{|A_0^d|^2 + |\bar{A}_0^d|^2}\,, \tag{10.15}$$

where the spectator quark Q of the initial b-flavoured meson and the quark q from the $b \to q$ transition coincide.

In the definition of $L_{K^*\bar{K}^*}$ and its connection with the longitudinal amplitudes $|A_0^q|^2$ in Eq. (10.15), we have not included the effect of B_s-meson mixing that arises in branching ratios when measured at hadronic machines. This effect of time integration at hadronic machines generates a correction of $\mathcal{O}(\Delta\Gamma/(2\Gamma))$ discussed in Refs. [354, 456], which would multiply the last term in Eq. (10.15) by:

$$\frac{1 + A^s_{\Delta\Gamma} y_s}{1 + A^d_{\Delta\Gamma} y_d} \frac{1 - y_d^2}{1 - y_s^2}, \tag{10.16}$$

where $y_q = \Delta\Gamma_{B_q}/(2\Gamma_{B_q})$ is well measured (y_d is negligible and $y_s \simeq 0.065$) and the asymmetries $-1 \le A^q_{\Delta\Gamma} \le 1$ combining CP violation in mixing and decay are difficult to estimate theoretically, leading to a correction of at most 7%.

Since we use the LHCb measurement Eq. (10.7) and since there are other sources of (theoretical and experimental) uncertainties, we treat Eq. (10.16) as a systematic uncertainty of 7% combined in quadrature with the other uncertainties, leading to the experimental value:

$$\text{Exp}: \qquad L_{K^*\bar{K}^*} = 4.43 \pm 0.92. \tag{10.17}$$

10.2.2 Theoretical prediction in the SM and comparison with data

On the theory side, we have

$$\begin{aligned} A_0^q &= (\lambda_c^{(q)*} + \lambda_u^{(q)*})\,[P_q + (\alpha^q)^* \Delta_q]\,, \\ \bar{A}_0^q &= (\lambda_c^{(q)} + \lambda_u^{(q)})\,[P_q + \alpha^q \Delta_q]\,, \end{aligned} \tag{10.18}$$

where $\alpha^q = \lambda_u^q/(\lambda_c^q + \lambda_u^q)$. We thus get

$$L_{K^*\bar{K}^*} = \kappa \left|\frac{P_s}{P_d}\right|^2 \left[\frac{1 + |\alpha^s|^2 \left|\frac{\Delta_s}{P_s}\right|^2 + 2\text{Re}\left(\frac{\Delta_s}{P_s}\right)\text{Re}(\alpha^s)}{1 + |\alpha^d|^2 \left|\frac{\Delta_d}{P_d}\right|^2 + 2\text{Re}\left(\frac{\Delta_d}{P_d}\right)\text{Re}(\alpha^d)}\right], \tag{10.19}$$

with the combinations of CKM factors (estimated using the summer 2019 CKMfitter update [24, 286, 457] (see Table 10.A.1):

$$\alpha^d = (-0.0136^{+0.0095}_{-0.0096}) + i(0.4181^{+0.0085}_{-0.0064}), \tag{10.20}$$

$$\alpha^s = (0.00863^{+0.00040}_{-0.00036}) + i(-0.01829^{+0.00037}_{-0.00042}), \tag{10.21}$$

$$\kappa = \left|\frac{\lambda_c^s + \lambda_u^s}{\lambda_c^d + \lambda_u^d}\right|^2 = 22.92^{+0.52}_{-0.30}. \tag{10.22}$$

From QCD factorisation (see Section 2.8 and Appendix 10.A) together with the WET (see Section 2.4) and the discussion in Section 10.1, we have

$$\frac{\Delta_d}{P_d} = (-0.16 \pm 0.15) + (0.23 \pm 0.20)i, \tag{10.23}$$

$$\frac{\Delta_s}{P_s} = (-0.15 \pm 0.22) + (0.23 \pm 0.25)i, \tag{10.24}$$

so that the brackets in Eq. (10.19) are very close to 1, with the main uncertainty of 1% from the term proportional to $|\alpha^d|^2$ (which will be included in the theoretical uncertainties below). The leading uncertainty in the theoretical evaluation of $L_{K^*\bar{K}^*}$ comes thus from the ratio $|P_s/P_d|$, which we can attempt to estimate in different ways. A naive SU(3) approach would consist in assuming

$$\text{naive SU(3)}: \left|\frac{P_s}{P_d}\right| = 1 \pm 0.3\,, \tag{10.25}$$

while a naive factorisation approach would rather yield

$$\text{fact SU(3)}: \left|\frac{P_s}{P_d}\right| = f = 0.91^{+0.20}_{-0.17}\,, \tag{10.26}$$

where the SU(3)-breaking ratio related to the form factors of interest is given by

$$f = \frac{A^s_{K^*\bar{K}^*}}{A^d_{K^*\bar{K}^*}} = \frac{m^2_{B_s} A_0^{B_s\to K^*}(0)}{m^2_{B_d} A_0^{B_d\to K^*}(0)}\,, \tag{10.27}$$

and we used the values of Ref. [278] for the form factors to estimate f. A last possibility amounts to using QCD factorisation. Using the same inputs as before, we obtain

$$\text{QCD fact}: \left|\frac{P_s}{P_d}\right| = 0.92^{+0.20}_{-0.18}\,. \tag{10.28}$$

The QCD factorisation-based prediction follows the theoretical computations of the different contributions to the amplitudes from Refs. [37, 139]. The numerical values of the input parameters used are updated with respect to the ones in Ref. [37] and can be found in Table 10.A.1 of Appendix 10.A.

Observable	1σ	2σ
$L_{K^*\bar{K}^*}$	$[12.7, 28.8]$	$[7.5, 43]$

Table 10.1: 1σ and 2σ confidence intervals for the SM prediction of $L_{K^*\bar{K}^*}$ within QCD factorisation.

We propagate the uncertainties by varying each input (given in Table 10.A.1) entering the penguin ratios in Eqs. (10.25), (10.26) and (10.28) and the CKM contribution κ following Eq. (10.22), using Gaussian distributions. We determine then the distribution of L in each case, leading to the 1σ ranges:

$$\text{naive SU(3)}: L_{K^*\bar{K}^*} = 23^{+16}_{-12} \qquad 1.9\sigma\,, \tag{10.29}$$

$$\text{fact SU(3)}: L_{K^*\bar{K}^*} = 19.2^{+9.3}_{-6.5} \qquad 3.0\sigma\,, \tag{10.30}$$

$$\text{QCD fact}: L_{K^*\bar{K}^*} = 19.5^{+9.3}_{-6.8} \qquad 2.6\sigma\,, \tag{10.31}$$

where we put the level of discrepancy with experiment, in units of σ. We stress that these discrepancies are obtained using symmetric confidence intervals and the whole distribution for L and not just the 1σ confidence intervals in the Gaussian approximation (see Table 10.1 for the 1 and 2σ confidence intervals). In Table 10.2 we present the error budget for $L_{K^*\bar{K}^*}$ in the SM. The comparison with the error budget of $|P_{d,s}|^2$ shows that the impact of X_A (X_H), introduced above Eq. (2.89), is reduced from 18% (2%) in $|P_{d,s}|^2$ to 4% (0.2%) in $L_{K^*\bar{K}^*}$. A similar reduction is observed for other inputs such as f_{K^*}, showing the benefit of defining the ratio $L_{K^*\bar{K}^*}$. It also indicates that the accuracy of the theoretical prediction of $L_{K^*\bar{K}^*}$ could be improved significantly by determining the correlations among the relevant $B \to K^*$ form factors in order to compute the associated SU(3) breaking. Moreover, the impact of the weak annihilation and hard-scattering divergences on the uncertainty is subdominant and would not be affected strongly by using a different approach for these power-suppressed infrared divergences.

From the comparison of the SM predictions in Eqs. (10.29) and (10.31) with the experimental result in Eq. (10.17), we see that all our theoretical estimates point towards a deficit in the $b \to s$ transition compared to the $b \to d$ one for these penguin-mediated modes, in analogy with the deficit observed in semileptonic decays to muons versus the decay to electrons in $b \to s\ell\ell$ decays.

10.3 Model-independent NP analysis

10.3.1 NP structures considered

Even though the deviation in $L_{K^*\bar{K}^*}$ is not yet at the level of a troublesome discrepancy with the SM, its potential connection with other B-flavour anomalies makes it interesting to investigate it further in terms

	Relative Error		
Input	$L_{K^*\bar{K}^*}$	$\lvert P_s\rvert^2$	$\lvert P_d\rvert^2$
f_{K^*}	$(-0.1\%, +0.1\%)$	$(-6.8\%, +7.1\%)$	$(-6.8\%, +7\%)$
$A_0^{B_d}$	$(-22\%, +32\%)$	–	$(-24\%, +28\%)$
$A_0^{B_s}$	$(-28\%, +33\%)$	$(-28\%, +33\%)$	–
λ_{B_d}	$(-0.6\%, +0.2\%)$	$(-4.6\%, +2.1\%)$	$(-4.1\%, +1.9\%)$
$\alpha_2^{K^*}$	$(-0.1\%, +0.1\%)$	$(-3.6\%, +3.7\%)$	$(-3.6\%, +3.6\%)$
X_H	$(-0.2\%, +0.2\%)$	$(-1.8\%, +1.8\%)$	$(-1.6\%, +1.6\%)$
X_A	$(-4.3\%, +4.4\%)$	$(-17\%, +19\%)$	$(-13\%, +14\%)$
κ	$(-1.4\%, +2.2\%)$	–	–
Others	$(-1.3\%, +1.1\%)$	$(-2.7\%, +2.5\%)$	$(-1.6\%, +1.6\%)$

Table 10.2: Error budget of $L_{K^*\bar{K}^*}$ and $|P_{d,s}|^2$. The relative error of each theoretical input is obtained by varying them individually. The main sources of uncertainty are the form factors, followed by weak annihilation at a significantly smaller level.

of possible SU(3)-breaking NP contributions. We may explore in a model-independent way how to explain this anomaly via contributions only to the Wilson coefficients of the $b \to s$ transition ($\mathcal{C}_{is}$), while keeping the corresponding $b \to d$ ($\mathcal{C}_{id}$) SM-like (or with opposite NP contributions).

This can be performed by using the weak effective theory introduced in Section 2.4. Note that in the presence of generic NP, the basis of operators must be extended since we expect this NP contribution to couple with different strength to different flavours (and in particular to d and s quarks), there is no a priori reason for it to yield "strong" and "electroweak" penguin operators with sums over all quark flavours following the same pattern as in the SM [458].

However, for simplicity, and in parallel with the results of the global fits for NP in $b \to s\ell\ell$ decays favouring SM operators or chirally-flipped versions of it, we consider here only NP entering the Wilson coefficients associated with the SM operators $\mathcal{O}_i$ or the chirally-flipped ones $\tilde{\mathcal{O}}_i$ as defined in Section 2.4.2 by exchanging P_L and P_R in all quark bilinears constituting the operators. These right-handed currents would modify the longitudinal amplitude by adding contributions that are functions of $\mathcal{C}_i^{\rm NP} - \tilde{\mathcal{C}}_i$ (where $\tilde{\mathcal{C}}_i$ is the coefficient of the chirally-flipped operator) leading to the structure $A_0[\mathcal{C}_i^{\rm SM}] + A_0[\mathcal{C}_i^{\rm NP} - \tilde{\mathcal{C}}_i]$. In practice this means that the NP contribution to each coefficient entering the longitudinal amplitude should be interpreted as stemming not only from the standard operators but also from the chirally flipped ones (with an opposite sign).

In this chapter, the Wilson coefficient basis differs slightly with the one in Section 2.4 by the exchange of $\mathcal{C}_{1s}$ and $\mathcal{C}_{2s}$. This is done to have a compatible convention with Refs. [37, 86, 139], from where QCDF results come from. The values of the SM values for the Wilson coefficients can be found in Table 10.A.1.

10.3.2 Sensitivity to individual Wilson coefficients

We consider the sensitivity of $L_{K^*\bar{K}^*}$ on each Wilson coefficient. We want to determine if there is a dominant operator that can naturally explain the low experimental value of $L_{K^*\bar{K}^*}$, as it happens for $b \to s\ell\ell$ with $\mathcal{O}_{9\ell}$. We assume that NP enters as described above with the further requirement that there are no additional NP phases, leading to real-valued Wilson coefficients. We can then compute the hadronic matrix elements within QCD factorisation exactly like in the SM. In Appendix 10.B we provide semi-analytical expressions for P_d and P_s, needed to compute $L_{K^*\bar{K}^*}$ in terms of Wilson coefficients. We provide the explicit dependence on the infrared divergences X_A and X_H although their numerical impact on the uncertainty is limited. Let us note in passing that the quantity Δ_q is still protected from infrared divergences in this NP extension: the structure of the longitudinal hadronic amplitudes T and P is unchanged, and only the numerical values of Wilson coefficients are modified compared to the SM (the protection of Δ from infrared divergences would not necessarily hold in more general NP extensions).

Considering the sensitivity of $L_{K^*\bar{K}^*}$ on each Wilson coefficient of the weak effective theory individually, we can determine the coefficients where a limited NP contribution would be sufficient to explain the discrepancy observed. We thus identify three dominant coefficients: $\mathcal{C}_{1q}^c$, $\mathcal{C}_{4q}$ and $\mathcal{C}_{8gq}^{\rm eff}$ (see Figs. 10.3 and 10.C.1 in Appendix 10.C). The strong dependence on these coefficients with respect to the others can be seen already in the explicit form of $P_{d,s}$:

$$P_s = (1.98 - 5.04i) + (2.37 - 1.65i)\mathcal{C}_{1s}^{c,\rm NP} + (9.98 + 148.76i)\mathcal{C}_{4s}^{\rm NP} - 7.98i\mathcal{C}_{8gs}^{\rm eff,NP} + \dots \tag{10.32}$$

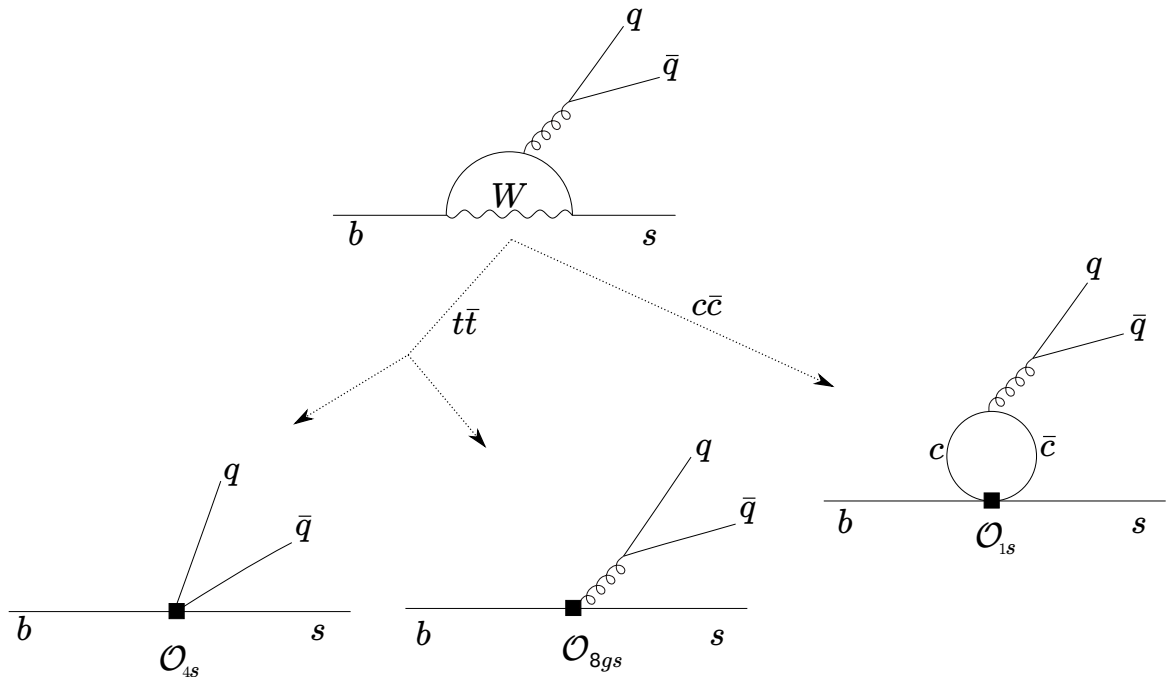

Figure 10.2: Reduction of the SM penguin $b \to sq\bar{q}$ into $\mathcal{O}_{1s,4s,8gs}$ in the WET.

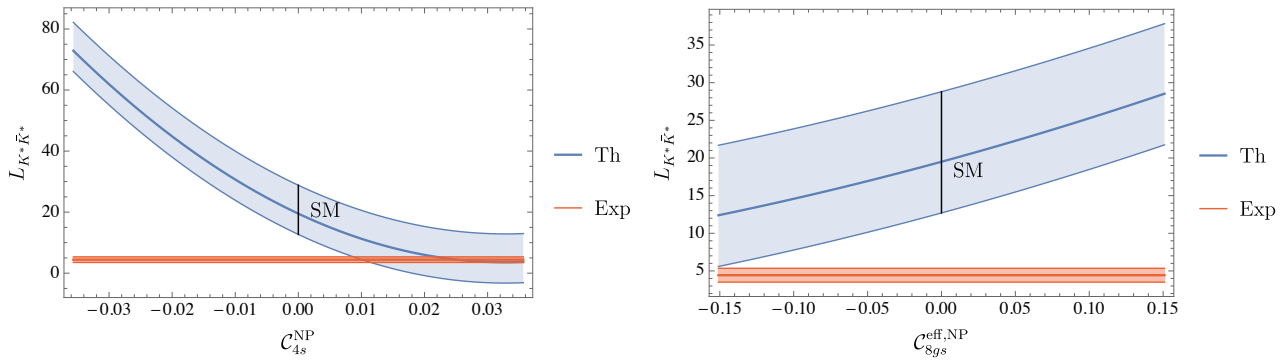

Figure 10.3: The tension between the theoretical prediction (blue) and the experimental value (orange) is reduced below 1σ for $\mathcal{C}_{4s}^{\rm NP} \simeq 0.25\mathcal{C}_{4s}^{\rm SM}$ (upper plot) or $\mathcal{C}_{8gs}^{\rm eff,NP} \simeq -\mathcal{C}_{8gs}^{\rm eff,SM}$ (lower plot). The predictions are given for $\mathcal{C}_{4s}^{\rm NP}$ and $\mathcal{C}_{8gs}^{\rm eff,NP}$ for a range corresponding to 100% of their respective SM values. The plots for the remaining Wilson coefficients can be found in Appendix 10.C.

$$P_d = (2.17 - 5.49i) + (2.60 - 1.80i)\mathcal{C}_{1d}^{c,\rm NP} + (10.95 + 161.74i)\mathcal{C}_{4d}^{\rm NP} - 8.76i\mathcal{C}_{8gd}^{\rm eff,NP} + \ldots \tag{10.33}$$

which translates into a dominant contribution for $L_{K^*\bar{K}^*}$ as well.

The reason behind this strong dependence on these coefficients can be understood in the following way. Let us consider a penguin-mediated decay, so that the SM tree-level operator $\mathcal{C}_{1s}^c$ contributes through a closed $c\bar{c}$ loop to the decay, putting its contribution at the same level as the "strong" penguin operators $i = 3\ldots6$ in the SM. A very similar contribution at the level of the underlying SM diagrams comes thus from both $\mathcal{C}_{1s}^c$ and $\mathcal{C}_{4s}$, as can be seen from the $V-A$ structure of the operators, which is also the case for $\mathcal{C}_{8gs}^{\rm eff}$ with the emission of a gluon coupling to a $q\bar{q}$ pair (see Fig. 10.2). The effect of the diagrams is similar in the SM, but the separation between long and short distances in the weak effective theory yields $\mathcal{C}_{4s}$ and $\mathcal{C}_{8gs}^{\rm eff}$ much smaller than $\mathcal{C}_{1s}^c$, which must be compensated by larger weights in Eqs. (10.32) and (10.33). The other penguin operators are suppressed either because of colour suppression ($\mathcal{C}_3$, thus associated with $1/N_c$ factors in the QCD factorisation formula) or helicity suppression ($\mathcal{C}_5$ and $\mathcal{C}_6$, which yield a vanishing contribution in the naive factorisation approach as they must be "Fierzed" into (pseudo)scalar operators with vanishing matrix elements). In the SM, the "electroweak" penguins $i = 7\ldots10$ are suppressed. Their contributions might be very significantly enhanced by NP which would not require such an electromagnetic suppression, although it would be difficult to obtain then "electroweak" operators at the m_b-scale since they involve explicitly the quark electric charges. If we nevertheless allowed for such very large contributions for the electroweak part (which we will discard in the following), the same argument

would apply as in the case of the "strong" penguins, so that the leading contribution from the "electroweak" penguins would be $\mathcal{C}_{10q}$.

As can be seen in Fig. 10.C.1, the coefficient $\mathcal{C}^c_{1s}$ requires a very large NP contribution w.r.t. the SM of order 60% to reduce this discrepancy at 1σ. We will not pursue the possibility of a contribution to $\mathcal{C}^c_{1q}$, as the size of the effect being so large at an absolute scale is in conflict with recent analyses of the global constraints on this coefficient [283] that suggest that the room for NP contributions is of $\mathcal{O}(10\%)$ of the SM. Dijet angular distributions [459], together with flavour bounds following from $\mathrm{SU}(2)_L$ gauge invariance, suggest bounds which are even tighter.

The penguin coefficient $\mathcal{C}_{4s}$ requires a NP contribution of order 25% (which is incidentally similar to the NP contribution needed in $\mathcal{C}_9$ for $b \to s\mu\mu$) in order to reduce the discrepancy in $L_{K^*\bar{K}^*}$ at 1σ. The NP contribution needed is thus quite large but not significantly constrained from other non-leptonic decays where many other coefficients enter [86].

Finally, $\mathcal{C}^{\text{eff}}_{8gs}$ would require a NP contribution of order 100% of the SM in order to obtain a similar reduction of the discrepancy. Although it might seem a large contribution, it is actually very difficult to obtain a precise bound on this effective coefficient which combines $\mathcal{C}_{8gs}$ with some Wilson coefficients of four-quark operators.

To sum up, in Fig. 10.5 we show the 1σ-range for the NP contribution to each Wilson coefficient that is able to explain the experimental value of $L_{K^*\bar{K}^*}$, normalised to its SM value.

Due to QCD loop effects, the constraint from $b \to s\gamma$ is actually on a linear combination of the Wilson coefficients $\mathcal{C}^{\text{eff}}_{7\gamma s}$ and $\mathcal{C}^{\text{eff}}_{8gs}$ at the scale μ_b [211]. Therefore, an effect in $\mathcal{C}^{\text{eff}}_{8gs}$ can always be cancelled by an effect in $\mathcal{C}^{\text{eff}}_{7\gamma s}$ so that the experimental bound from $b \to s\gamma$ is obeyed (the same is also true for $b \to d\gamma$ [460]). Even without such a cancellation from $\mathcal{C}^{\text{eff}}_{7\gamma s}$, the current measurements can accommodate a NP contribution to $\mathcal{C}^{\text{eff}}_{8gs}$ of the order of the SM. Another more direct bound on $\mathcal{C}^{\text{eff}}_{8gs}$ is provided by the $b \to sg$ contribution to inclusive non-leptonic charmless decays. The current bound on the $b \to sg$ branching ratio in Ref. [6] is at the level of 6.8%, whereas the SM contribution [461] is estimated at the level of 0.5%, leaving room for a NP contribution to $\mathcal{C}^{\text{eff}}_{8gs}$ up to three times as large as the SM one.

Naturally, in each case, if we allow for NP in both $\mathcal{C}_{is}$ and $\mathcal{C}_{id}$, we may get the same reduction of the discrepancy by assigning half of the NP contribution (with opposite signs) to both coefficients, as illustrated for $\mathcal{C}_4$ in Fig. 10.4. Thus, allowing NP in $b \to d$ transitions in addition to $b \to s$ transitions requires smaller NP contributions in each type of transition, and allows one to evade some of the bounds discussed above as they applied only to $b \to s$ transitions (e.g. $\mathcal{C}_{8gs}$). $\mathcal{C}_{8gd}$ is constrained from $b \to d\gamma$.

10.4 Simplified NP models

Our model-independent analysis showed that $L_{K^*\bar{K}^*}$ is mostly sensitive to colour-octet operators and to a lesser extent to the chromomagnetic operator. In the following, we will consider NP models able to generate such contributions, and for concreteness, present the formula for the case of $b \to s$ transitions.

Concerning $\mathcal{C}_{4s}$, it is natural to search for a tree-level explanation in terms of NP and a massive $\mathrm{SU}(3)_c$ octet vector particle, i.e. a Kaluza-Klein (KK) gluon [462], also called axi-gluon, comes naturally to mind. We parametrise its couplings to down quarks of different flavours as

$$\mathcal{L} = \Delta^L_{sb}\bar{s}\gamma^\mu P_L T^a b G^a_\mu + \Delta^R_{sb}\bar{s}\gamma^\mu P_R T^a b G^a_\mu \,. \tag{10.34}$$

with $\Delta^{L,R}_{sb}$ assumed real. We also define from Eq. (10.34) analogous flavour diagonal couplings which we will denote as $\Delta^{L,R}_{qq}$.

We may consider the constraints from neutral-meson mixing through the effective Hamiltonian of Ref. [463]

$$H^{\Delta F=2}_{eff} = \sum_{j=1}^{5} \mathcal{C}_j^{B_s\bar{B}_s}\mathcal{O}_j^{B_s\bar{B}_s} + \sum_{j=1}^{3} \tilde{\mathcal{C}}_j^{B_s\bar{B}_s}\tilde{\mathcal{O}}_j^{B_s\bar{B}_s} \,, \tag{10.35}$$

$$\mathcal{O}_1^{B_s\bar{B}_s} = [\bar{s}_\alpha\gamma^\mu P_L b_\alpha]\,[\bar{s}_\beta\gamma_\mu P_L b_\beta] \,, \tag{10.36}$$

$$\mathcal{O}_4^{B_s\bar{B}_s} = [\bar{s}_\alpha P_L b_\alpha]\,[\bar{s}_\beta P_R b_\beta] \,, \tag{10.37}$$

$$\mathcal{O}_5^{B_s\bar{B}_s} = [\bar{s}_\alpha P_L b_\beta]\;[\bar{s}_\beta P_R b_\alpha] \,, \tag{10.38}$$

where only the operators relevant for the discussion are displayed and where the operators with a tilde are obtained by exchanging the chirality projectors P_L and P_R. We get the matching contributions

$$\mathcal{C}_1^{B_s\bar{B}_s} = \frac{1}{2m^2_{KK}}\left(\Delta^L_{sb}\right)^2 \frac{1}{2}\left(1 - \frac{1}{N_C}\right) \,, \tag{10.39}$$

$$\tilde{\mathcal{C}}_1^{B_s\bar{B}_s} = \frac{1}{2m_{KK}^2}\left(\Delta_{sb}^R\right)^2 \frac{1}{2}\left(1-\frac{1}{N_C}\right), \tag{10.40}$$

$$\mathcal{C}_4^{B_s\bar{B}_s} = -\frac{1}{m_{KK}^2}\Delta_{sb}^L\Delta_{sb}^R, \tag{10.41}$$

$$\mathcal{C}_5^{B_s\bar{B}_s} = \frac{1}{N_C m_{KK}^2}\Delta_{sb}^L\Delta_{sb}^R, \tag{10.42}$$

where m_{KK} is the mass of the KK gluon. Using the two-loop Renormalisation Group Equations of Refs. [464, 465] and the bag factors of Ref. [59] this translates to

$$\frac{\Delta M_{B_s}^{\rm NP}}{\Delta M_{B_s}^{\rm SM}} \times 10^{-10} = \left(1.1(\mathcal{C}_1^{B_s\bar{B}_s} + \tilde{\mathcal{C}}_1^{B_s\bar{B}_s}) + 8.4\mathcal{C}_4^{B_s\bar{B}_s} + 3.1\mathcal{C}_5^{B_s\bar{B}_s}\right) \text{GeV}^2, \tag{10.43}$$

for a NP scale around 5 TeV. This has to be compared with the outcome of global fits allowing for NP in mixing [466, 467], favouring a value slightly above 1 for the ratio $\Delta M_{B_s}^{\rm exp}/\Delta M_{B_s}^{\rm SM}$. Encompassing the results obtained from these recent fits in a conservative manner, we consider here

$$\frac{\Delta M_{B_s}^{\rm exp}}{\Delta M_{B_s}^{\rm SM}} = 1.11 \pm 0.09\,. \tag{10.44}$$

We obtain the allowed region shown in blue in Fig. 10.6 for real values of the Wilson coefficients and neglecting the bag factor uncertainties related to $\mathcal{C}_{4,5}^{B_s\bar{B}_s}$.

Assuming that the KK gluon has universal flavour-diagonal coupling to the first two generations of quarks, which is also needed to avoid unacceptably large effects in $K-\bar{K}$ and/or $D^0-\bar{D}^0$ mixings [468], our model generates [1] a NP contribution to $\mathcal{C}_{4s}$ given at the matching scale by

$$\mathcal{C}_{4s} = -\frac{1}{4}\frac{\Delta_{sb}^L\Delta_{qq}^L}{\sqrt{2}G_F V_{tb}V_{ts}^* m_{KK}^2}, \tag{10.45}$$

(and similarly for $\tilde{\mathcal{C}}_{4s}$ with L replaced by R). The couplings $\Delta_{sb}^{L,R}$ are defined in Eq. (10.34) while $\Delta_{qq}^{L,R}$ stand for the corresponding flavour-diagonal couplings to up and down quarks of the first two generations.

However, couplings of first generation quarks to KK gluons are strongly constrained by di-jet searches [469]: $(\Delta_{qq}^L/m_{KK})^2 < (2.2/(10\,\text{TeV}))^2$. Allowing for NP also in $b\to d$ transitions could increase the effect in $L_{K^*\bar{K}^*}$, but since here the effect is bounded by $B_d-\bar{B}_d$ mixing, whose constraints are of the same order as $B_s-\bar{B}_s$ mixing, one can only gain a factor ≈ 2. Using this maximal coupling for the Δ_{qq}^L couplings and setting the Δ_{qq}^R couplings to zero, we can see from Fig. 10.6 that a significant amount of fine-tuning is needed to account for $L_{K^*\bar{K}^*}$.

Alternatively, one could try to explain $L_{K^*\bar{K}^*}$ with a NP contribution in the chirally-flipped coefficient $\tilde{\mathcal{C}}_{4s}$, given by Eq. (10.45) with the Δ_{sb}^L and Δ_{qq}^L couplings replaced by Δ_{sb}^R and Δ_{qq}^R, respectively. In principle, one could exploit the fact that the couplings do not have to respect an $U(2)$ flavour symmetry (since up- and down-type quark couplings are not related via $\text{SU}(2)_L$), so that couplings to first-generation quarks could be avoided, which would relax LHC bounds and reduce the fine-tuning needed in $B_s-\bar{B}_s$ mixing. However, as in the previous case, flavour universality for diagonal couplings to quarks is needed to be able to make use of our expressions for $L_{K^*\bar{K}^*}$. Moreover, according to QCD factorisation, the dominant leading-order effect in $L_{K^*\bar{K}^*}$ originates from the term in $\mathcal{O}_{4s}$ with down quarks in the bilinear summed over flavours. Therefore, (dominant) right-handed couplings cannot be used to evade LHC bounds and still fine-tuning in $B_s-\bar{B}_s$ mixing, like in the case of left-handed couplings, is needed.

As indicated earlier, one could also try to explain $L_{K^*\bar{K}^*}$ with the Wilson coefficient of the chromomagnetic operator $\mathcal{O}_{8gs}$. Here an effect of the order of the SM contribution is required. $\mathcal{C}_{8gs}$ can only be generated at the loop level and involves necessarily coloured particles for which strong LHC limits exist. Therefore, a value of the order of the SM contribution can only be obtained thanks to chiral enhancement.

A simplified model fulfilling these requirements features two vector-like quarks, one $\text{SU}(2)_L$ doublet and one $\text{SU}(2)_L$ singlet (with a large coupling λ to the SM Higgs doublet) and an additional neutral scalar particle [470]. In this setup, $\mathcal{C}_{8gs}$ receives a contribution which scales like $\lambda/(m_b/v)\times v^2/M^2$ w.r.t. the SM, where M is the NP scale. Inevitably an effect in $\mathcal{C}_{7\gamma s}$ is generated at the matching scale M which however has free sign and magnitude as it depends on the (not necessarily quantized) electric charges of the new fermions and scalar inside the loop. Therefore, the electric charges of the new particles can be chosen in such a way that in $\mathcal{C}_{7\gamma s}$ (at the m_b

[1] Note that our model is only flavour universal with respect to four but not five flavours and does not fulfill the requirements of Section 10.3. However, the effect of bottom quarks within the $\mathcal{O}_{4s}$ operator in $L_{K^*\bar{K}^*}$ is $\mathcal{O}(\alpha_s)$-suppressed within QCD factorisation and thus the impact of our model on $L_{K^*\bar{K}^*}$ can be mimicked by a shift in $\mathcal{C}_{4s}$ to a good approximation.

scale) the NP contributions to $\mathcal{C}_{7\gamma s}$ and $\mathcal{C}_{8gs}$ (taken at the matching scale) cancel. As we need a NP contribution to $\mathcal{C}_{8gs}$ of the order of the SM one, and $\mathcal{C}_{7\gamma s}$ at the low scale is known at the 5% level, a tuning of the order of 1/20 is necessary here.

Both simplified models allow for the possibility of a connection with the $b \to s\ell^+\ell^-$ anomalies. On the one hand, the KK gluon may be part of the particle spectrum of a composite/extra-dimensional model and is then accompanied by a Z' boson. This could explain $b \to s\ell^+\ell^-$ without violating LHC di-lepton bounds [471] due to the large sb coupling of the Z' needed to explain $L_{K^*\bar{K}^*}$, leading to NP contributions with the correct sign in both types of anomalies. On the other hand, the model generating a large effect in $\mathcal{C}_{8g}$ could easily be extended by a vector-like lepton in order to account for $b \to s\ell^+\ell^-$ [470].

10.5 Conclusions

We have analysed the non-leptonic penguin decays $B_d \to K^{*0}\bar{K}^{*0}$ and $B_s \to K^{*0}\bar{K}^{*0}$, where recent LHCb results indicate striking differences in the longitudinal polarisation of these two modes. This is unexpected since they are related by U-spin and should thus have a similar QCD and EW dynamics (up to tiny corrections due to the down and strange quark masses).

We introduced the L-observable as a combination of polarisation fractions and branching ratios in order to compare the longitudinal amplitudes in both modes, as they can be computed with better theoretical control in a $1/m_b$ expansion such as QCD factorisation. We exploited the fact that these penguin-mediated decays exhibit very similar hadronic matrix elements for the "tree" and "penguin" contributions in the usual decomposition based on CKM factors, so that these contributions are very strongly correlated. This means that the L-observable is a measure of U-spin breaking between the penguin contributions to B_d and B_s decays, with a deviation from the SM expectation between 2σ and 3σ depending on the specific theoretical framework considered. This observation reinforces and puts on a firmer ground the hint for NP already suspected by considering the difference between the longitudinal polarisation fractions in these two modes. We performed a detailed error budget analysis for $L_{K^*\bar{K}^*}$ and we found a relatively small impact of infrared divergences coming from weak annihilation and hard-spectator scattering, compared to observables like branching ratios or polarisation fractions involving troublesome transverse amplitudes.

We then interpreted this deviation in a model-independent approach using the weak effective theory. For simplicity, we allowed NP only in SM Wilson coefficients or their chirally-flipped counterparts. We identified three operators which could accommodate the deviation with NP contributions at most as large as the SM. While $\mathcal{C}_{1q}$ is already very significantly constrained by other nonleptonic modes and LHCb bounds (up to the point of excluding this solution), the situation is less constrained for the strong penguin coefficient $\mathcal{C}_{4q}$ and the chromomagnetic one $\mathcal{C}_{8gq}^{\text{eff}}$ where NP contributions of a similar size to the SM one are allowed and could explain the deviation in $L_{K^*\bar{K}^*}$. We discussed examples of simplified NP models that could provide large contributions, at the price of accepting fine tuning to accommodate the bounds on $B_s - \bar{B}_s$ mixing and $b \to s\gamma$. Interestingly, within a general composite or extra-dimensional model [472], the Kaluza-Klein gluon contribution to the $b \to s$ amplitude in $B_s \to K^{*0}\bar{K}^{*0}$ has the same sign as the Z' contribution to $b \to s\ell^+\ell^-$ w.r.t the SM. Therefore, if one accepts the fine-tuning in $B_s - \bar{B}_s$ mixing, such models can provide a common explanation of $L_{K^*\bar{K}^*}$ and $b \to s\ell^+\ell^-$ data.

This hint of NP in $L_{K^*\bar{K}^*}$ could be sharpened with a precise estimate of U-spin breaking in the form factors involved, as they drive the theoretical uncertainty of the SM prediction and their correlation is not known precisely. A comparison of the theoretical and experimental information on the polarisations in $B_s \to K^*\phi$ and $B_d \to K^*\phi$ could also be valuable to check whether a similar tension arises. Complementary information could be obtained also from pseudoscalar-vector and pseudoscalar-pseudoscalar penguin-mediated modes [158, 354, 451, 452] ($K^0\bar{K}^{*0}$ and $K^0\bar{K}^0$). Moreover, if the same source of NP is responsible for the suppression of $b \to sq\bar{q}$ versus $b \to dq\bar{q}$ and $b \to s\mu^+\mu^-$ versus $b \to se^+e^-$, it would be certainly interesting to perform a thorough study of $b \to d\ell^+\ell^-$ modes compared to $b \to s\ell^+\ell^-$ ones, which should be accessible with more data from the LHCb and Belle II experiments.

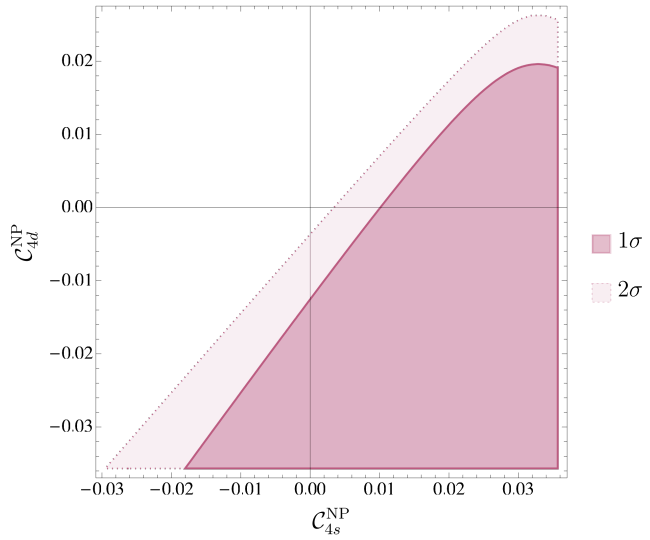

Figure 10.4: 1σ and 2σ CL regions from $L_{K^*\bar{K}^*}$ allowing NP contributions to both $\mathcal{C}_{4s}$ and $\mathcal{C}_{4d}$.

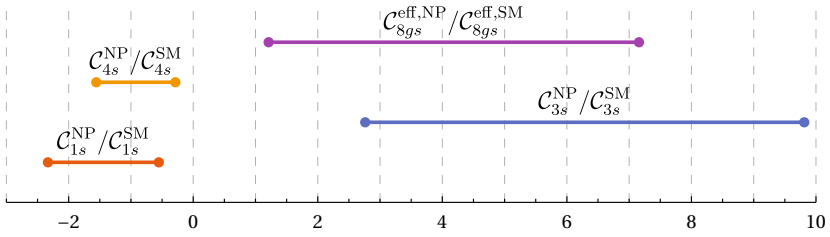

Figure 10.5: 1σ intervals for the NP contribution to Wilson coefficients needed to explain $L_{K^*\bar{K}^*}$, normalised to their SM value.

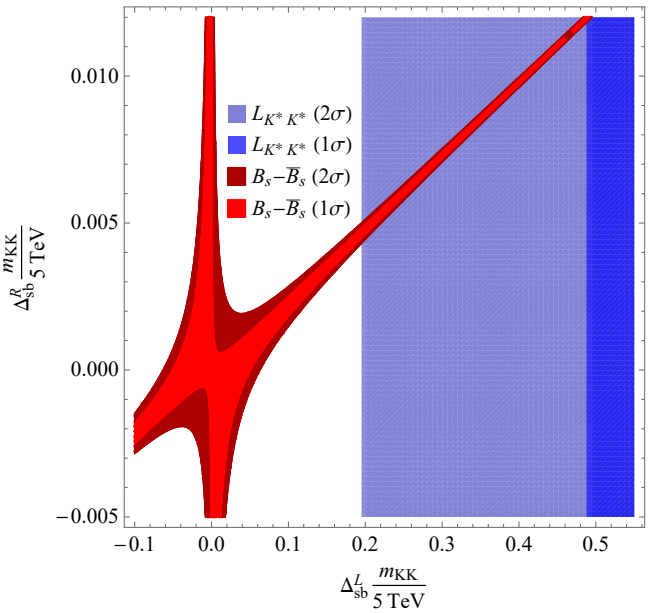

Figure 10.6: Preferred regions from $B_s - \bar{B}_s$ mixing (red) and $L_{K^*\bar{K}^*}$ (blue) for $\Delta_{qq}^R = 0$ and the maximal value of Δ_{qq}^L compatible with LHC searches assuming real couplings. Note that explaining $L_{K^*\bar{K}^*}$ requires some fine-tuning in Δ_{sb}^L vs Δ_{sb}^R.

Appendices

10.A QCD factorisation for $B_{d,s} \to \bar{K}^{*0} K^{*0}$

As discussed in Section 2.8, QCD factorisation relies on the weak effective theory to compute non-leptonic B-decay hadronic matrix elements, by performing a further separation of scales between m_b and the typical QCD scale, later reinterpreted in terms of a Soft-Collinear Effective Theory (SCET). Following Refs. [37, 139] and using the same notation as in this reference, we have for the vector modes for a given polarisation:

$$\begin{aligned}
T(\bar{B}_d \to \bar{K}^{*0} K^{*0}) &= A_{\bar{K}^* K^*}[\alpha_4^u - \frac{1}{2}\alpha_{4,EW}^u + \beta_3^u + \beta_4^u - \frac{1}{2}\beta_{3,EW}^u - \frac{1}{2}\beta_{4,EW}^u] \\
&\quad + A_{K^* \bar{K}^*}[\beta_4^u - \frac{1}{2}\beta_{4,EW}^u]\,, \\
P(\bar{B}_d \to \bar{K}^{*0} K^{*0}) &= A_{\bar{K}^* K^*}[\alpha_4^c - \frac{1}{2}\alpha_{4,EW}^c + \beta_3^c + \beta_4^c - \frac{1}{2}\beta_{3,EW}^c - \frac{1}{2}\beta_{4,EW}^c] \\
&\quad + A_{K^* \bar{K}^*}[\beta_4^c - \frac{1}{2}\beta_{4,EW}^c]\,, \\
T(\bar{B}_s \to \bar{K}^{*0} K^{*0}) &= A_{\bar{K}^* K^*}[\beta_4^u - \frac{1}{2}\beta_{4,EW}^u] \\
&\quad + A_{K^* \bar{K}^*}[\alpha_4^u - \frac{1}{2}\alpha_{4,EW}^u + \beta_3^u + \beta_4^u - \frac{1}{2}\beta_{3,EW}^u - \frac{1}{2}\beta_{4,EW}^u]\,, \\
P(\bar{B}_s \to \bar{K}^{*0} K^{*0}) &= A_{\bar{K}^* K^*}[\beta_4^c - \frac{1}{2}\beta_{4,EW}^c] \\
&\quad + A_{K^* \bar{K}^*}[\alpha_4^c - \frac{1}{2}\alpha_{4,EW}^c + \beta_3^c + \beta_4^c - \frac{1}{2}\beta_{3,EW}^c - \frac{1}{2}\beta_{4,EW}^c]\,.
\end{aligned} \tag{10.46}$$

The coefficients α and β are a parametrisation of the different QCDF contributions. They correspond to a convolution of the hard scattering kernels and the mesons DAs and form factors multiplied by the corresponding Wilson coefficient. The contributions of the hard scattering kernels $T_{ij}^I(u)$ and $T_{ij}^I I(\xi, u, v)$ (introduced in Section 2.8), are contained in α and β respectively. The difference between α_i^u and α_i^c occurs from the $\mathcal{O}(\alpha_s)$ penguin contractions in P_4^p and P_6^p, and specifically from the loops with u or c quarks and a W exchange (so that these contributions come with factors $\alpha_s/(4\pi)$ and $\mathcal{C}_1^c$). This comes from the fact that the effective Hamiltonian has a specific structure in the SM: only two types of four-fermion operators O_1^p and O_2^p ($p = u, c$) involve explicitly different $\lambda_p^{(q)}$, whereas the other operators treat all quarks on the same footing, they come from top loops and are accompanied with a CKM term $\lambda_t^{(q)} = -\lambda_u^{(q)} - \lambda_c^{(q)}$ leading to an identical contribution to T and P.

As discussed in Refs. [354, 451, 452], this explains why the quantity Δ defined in Eq. (10.3) can be computed safely within QCD factorisation for penguin mediated decays because of the cancellation of long-distance contributions. As a consequence of this cancellation, only penguin contractions contribute to Δ, as can be seen by inspection of the formulae above, leading to the following very simple expression within QCD factorisation:

$$\Delta = A_{M_1 M_2}^Q \frac{C_F \alpha_s}{4\pi N} \mathcal{C}_1 [\bar{G}_{M_2}(m_c^2/m_b^2) - \bar{G}_{M_2}(0)]\,, \tag{10.47}$$

where the normalisation $A_{M_1 M_2}^Q$ is defined as:

$$A_{M_1 M_2}^Q = \frac{G_F}{\sqrt{2}} m_{B_q}^2 f_{M_2} A^{B_q \to M_1}(0)\,, \tag{10.48}$$

and $\bar{G}_{M_2}$ is the penguin function defined in Ref. [451].

10.B Semi-analytical expressions

In the following we provide the key elements to construct a semi-analytical expression of $L_{K^* \bar{K}^*}$. Specifically we give P_s and P_d in terms of Wilson coefficients and the parameters X_H and X_A. κ is given in Eq. (10.22) and

$B_{d,s}$ Distribution Amplitudes (at $\mu = 1$ GeV) [473, 474]		
λ_{B_d} [GeV]	$\lambda_{B_s}/\lambda_{B_d}$	σ_B
0.383 ± 0.153	1.19 ± 0.14	1.4 ± 0.4

K^* Distribution Amplitudes (at $\mu = 2$ GeV) [475]			
$\alpha_1^{K^*}$	$\alpha_{1,\perp}^{K^*}$	$\alpha_2^{K^*}$	$\alpha_{2,\perp}^{K^*}$
0.02 ± 0.02	0.03 ± 0.03	0.08 ± 0.06	0.08 ± 0.06

Decay Constants (at $\mu = 2$ GeV) [59, 278, 476]			
f_{B_d}	f_{B_s}/f_{B_d}	f_{K^*}	$f_{K^*}^{\perp}/f_{K^*}$
0.190 ± 0.0013	1.209 ± 0.005	0.204 ± 0.007	0.712 ± 0.012

$B_{d,s} \to K^*$ form factors [278] and B-meson lifetimes (ps)			
$A_0^{B_s}(q^2 = 0)$	$A_0^{B_d}(q^2 = 0)$	τ_{B_d}	τ_{B_s}
0.314 ± 0.048	0.356 ± 0.046	1.519 ± 0.004	1.515 ± 0.004

Wolfenstein parameters [24]			
A	λ	$\bar{\rho}$	$\bar{\eta}$
$0.8235^{+0.0056}_{-0.0145}$	$0.22484^{+0.00025}_{-0.00006}$	$0.1569^{+0.0102}_{-0.0061}$	$0.3499^{+0.0079}_{-0.0065}$

QCD scale and masses [GeV]					
$\bar{m}_b(\bar{m}_b)$	m_b/m_c	m_{B_d}	m_{B_s}	m_{K^*}	$\Lambda_{\rm QCD}$
4.2	4.577 ± 0.008	5.280	5.367	0.892	0.225

SM Wilson Coefficients (at $\mu = 4.2$ GeV)					
$\mathcal{C}_1$	$\mathcal{C}_2$	$\mathcal{C}_3$	$\mathcal{C}_4$	$\mathcal{C}_5$	$\mathcal{C}_6$
1.082	-0.191	0.013	-0.036	0.009	-0.042
$\mathcal{C}_7/\alpha_{em}$	$\mathcal{C}_8/\alpha_{em}$	$\mathcal{C}_9/\alpha_{em}$	$\mathcal{C}_{10}/\alpha_{em}$	$\mathcal{C}_{7\gamma}^{\rm eff}$	$\mathcal{C}_{8g}^{\rm eff}$
-0.011	0.058	-1.254	0.223	-0.318	-0.151

Table 10.A.1: Input parameters used to determine the SM predictions. The SM Wilson Coefficients are compatibles with the NLO results of Ref. [86], whit only slight numerical differences. We insist on the fact that the basis of Wilson coefficients in this chapter differs of the basis given in Section 2.4 by an exchange of $\mathcal{C}_{1s}$ and $\mathcal{C}_{2s}$ in order to be compatible with the convention of Ref. [86]. The slightly different values for the SM Wilson coefficients with respect to Table 2.1 comes from the different choice of renormalisation scale $\mu = 4.2\,\text{GeV}$ and because in this chapter we omit NNLO corrections for simplicity, as we explicitly vary the scale μ when performing the error budget.

the last bracket in Eq. (10.19) has a negligible impact and can be taken to be conservative 0.99 ± 0.01. We have followed the corrected expression of Ref. [477] for the modelling of the weak annihilation in terms of X_A.

$$
\begin{aligned}
10^7 \times P_d = {} & i0.076\mathcal{C}_{7\gamma}^{\rm eff} - i8.8\mathcal{C}_{8g}^{\rm eff} + ((2.6 - i1.8) + i0.13X_A - i0.041X_A^2 - i0.025X_H)\mathcal{C}_1^c \\
& + ((-0.045 + i0.39) - i0.61X_A + i0.16X_A^2 + i0.035X_H)\mathcal{C}_2^c \\
& + ((15.5 + i38.9) + i0.31X_A + i0.25X_A^2 + i3.8X_H)\mathcal{C}_3 \\
& + ((11.0 + i156.9) + i0.25X_A + i0.96X_A^2 - i0.54X_H)\mathcal{C}_4 \\
& + ((-7.4 - i7.2) + i9.2X_A - i3.3X_A^2 + i0.11X_H)\mathcal{C}_5 \\
& + ((11.0 - i19.9) + i27.7X_A - 8.9X_A^2 + i0.24X_H)\mathcal{C}_6 \\
& + ((3.7 + i3.8) - i4.7X_A + i1.7X_A^2 + i0.00042X_H)\mathcal{C}_7 \\
& + ((i6.9) - i15.7X_A + i5.0X_A^2 - i0.008X_H)\mathcal{C}_8 \\
& + ((-6.4 - i19.4) - i0.55X_A - i0.041X_A^2 - i1.9X_H)\mathcal{C}_9 \\
& + (-i81.9 - 1.4X_A - i0.15X_A^2 + i0.32X_H)\mathcal{C}_{10}\,,
\end{aligned}
\tag{10.49}
$$

$$
\begin{aligned}
10^7 \times P_s = {} & i0.069\mathcal{C}_{7\gamma}^{\text{eff}} - i8.0\mathcal{C}_{8g}^{\text{eff}} + ((2.4 - i1.7) + i0.16X_A - i0.049X_A^2 - i0.026X_H)\mathcal{C}_1^c \\
& + ((-0.041 + i0.45) - i0.74X_A + i0.1X_A^2 + i0.037X_H)\mathcal{C}_2^c \\
& + ((14.2 + i36.4) + i0.37X_A + i0.3X_A^2 + i3.9X_H)\mathcal{C}_3 \\
& + ((10.0 + i142.7) + i0.31X_A + i1.2X_A^2 - i0.56X_H)\mathcal{C}_4 \\
& + ((-6.7 - i7.7) + i11.1X_A - i3.9X_A^2 + i0.11X_H)\mathcal{C}_5 \\
& + ((10.0 - i21.7) + i33.5X_A - 10.8X_A^2 + i0.25X_H)\mathcal{C}_6 \\
& + ((3.4 + i4.0) - i5.7X_A + i2.0X_A^2 + i0.00043X_H)\mathcal{C}_7 \\
& + ((i8.3) - i19.0X_A + i6.0X_A^2 - i0.008X_H)\mathcal{C}_8 \\
& + ((-5.8 - i18.1) - i0.66X_A - i0.049X_A^2 - i2.0X_H)\mathcal{C}_9 \\
& + (-i74.3 - 1.7X_A - i0.18X_A^2 + i0.33X_H)\mathcal{C}_{10}\,.
\end{aligned}
\tag{10.50}
$$

10.C Sensitivity to New Physics

We show how NP contributions can help to reduce the tension between theory and experiment for $L_{K^*\bar{K}^*}$, completing the results shown in Fig. 10.3 discussed in Section 10.3.

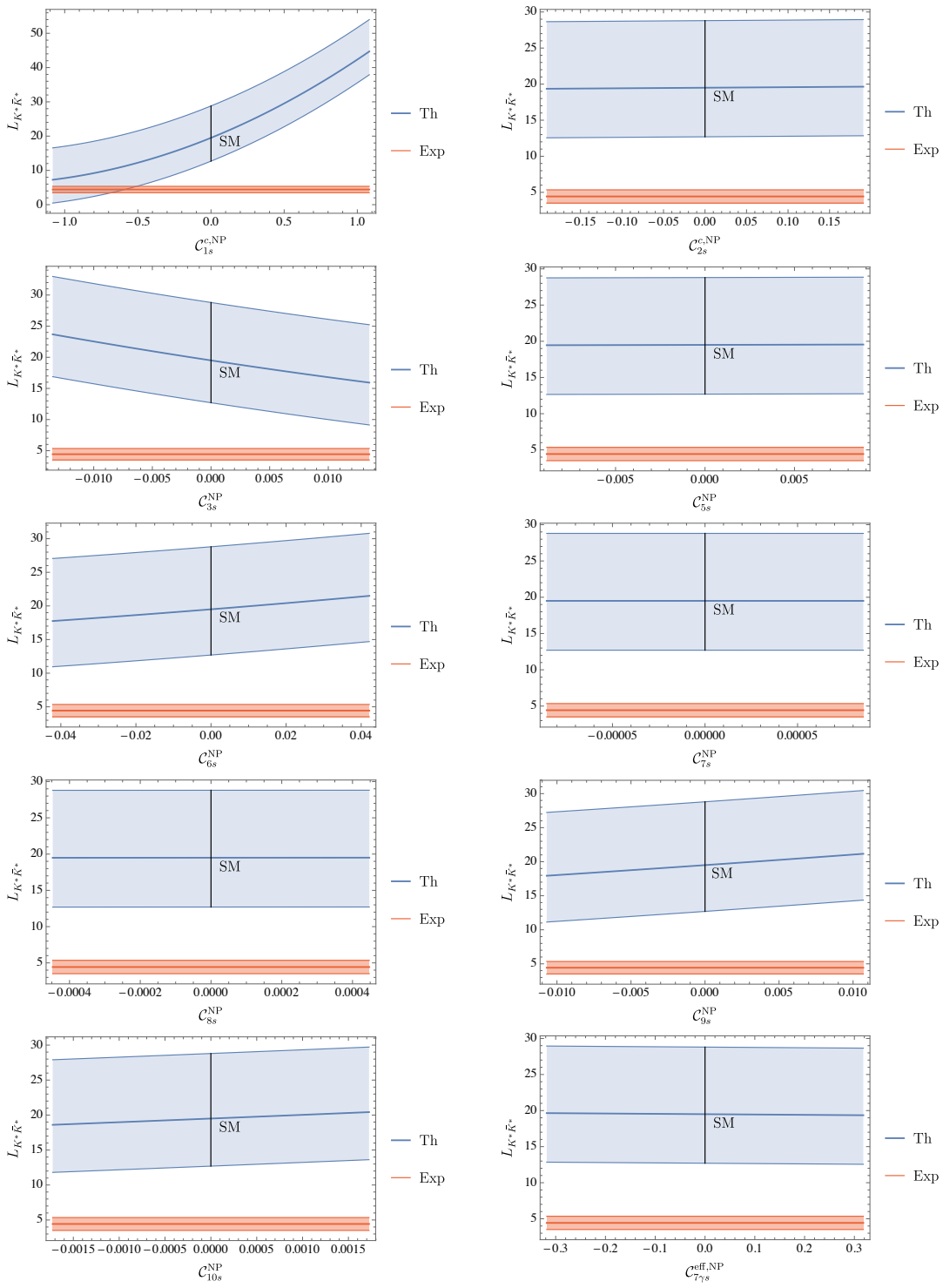

Figure 10.C.1: Sensitivity of $L_{K^*\bar{K}^*}$ to individual contributions of NP in all different $\mathcal{C}_{is}^{\mathrm{NP}}$. For each coefficient, the range of variation considered for the NP contribution corresponds to 100% of its SM value.

Conclusion

In this manuscript we carefully discussed the flavour anomalies observed in the semileptonic b decays $b \to s\ell^+\ell^-$ and $b \to c\ell\bar{\nu}$. We first introduced the necessary framework for this analysis, then we discussed the current status of the experimental measurements and the related theoretical predictions with a brief explanation of the overall framework and the hadronic inputs required for these predictions. Furthermore we analysed these decays in the model-independent framework of Effective Field Theories (EFTs) which allowed us to constrain the different potential New Physics (NP) scenarios that can be behind the deviations in the two kinds of decays. Subsequently, we studied new observables and new modes that could be measured in the future for each of these transitions. Finally, we discussed other related modes involving other quarks and/or leptons, which could be expected to exhibit related deviations in simple NP models and which are worth investigating both theoretically and experimentally.

We specially focused on the $b \to s\ell^+\ell^-$ mode, in which deviations do not appear only in a single or a few observables but as a set of coherent deviations. This showed the need of new modes and new observables to further reinforce the conclusions of the current global analyses and to better constrain the EFT parameter space, which is still unconstrained in several directions. Indeed we expect that different modes give new information, either through different systematics that will allow to see the coherence of these flavour anomalies or through different NP sensitivity that will help to better pinpoint the NP structure. We thus proposed the study of the baryonic $\Lambda_b \to \Lambda^*\ell^+\ell^-$ mode leading to angular observables that we analysed in detail, assessing their theoretical uncertainties, showing their sensitivity to right handed currents and discussing their measurement in upcoming LHCb runs. Similarly, we proposed to perform a time-dependent analysis of $B_d \to K_S\mu^+\mu^-$, with additional observables probing interferences between mixing and decay. These observables are free from hadronic contributions in the Standard Model (SM) and several NP scenarios and can strongly help to constrain the CP-violating (complex) NP contributions to Wilson coefficients and in a smaller degree the scalar and tensor NP currents. Due to the potential of $b \to s\ell^+\ell^-$ transitions to open windows of the physics beyond the Standard Model, it is clear that the determination and measurement of new observables will remain a topic of intense discussion both experimentally and theoretically in the coming years, and we hope that $\Lambda_b \to \Lambda^*\ell^+\ell^-$ and $B_d \to K_S\mu^+\mu^-$ (and similar B_s decays) will contribute to the field in a useful manner.

We then considered $b \to c\ell\bar{\nu}$ transitions. Using symmetries of its angular distribution, we provided relations between the angular observables of the $B \to D^*\ell\bar{\nu}$ decay that asses the presence of possible NP with tensor-like couplings and at the same time test the coherence of the experimental measurements. We checked that even binned observables must fulfil these very general relations. We expect that the results of Chapter 7 will be of particular interest once the LHCb and Belle II experiments are able to analyse the $B \to D^*\ell\bar{\nu}$ decays in more detail. We then proposed a new method for the measurement of the inclusive Lepton Flavour Universality (LFU) ratios $R(X)_{\tau\ell}$ through the direct use of $\Upsilon(4S)$ decays. We showed that one can systematically suppress the pollution induced by $B - \bar{B}$ mixing by cutting on the time difference between the B-meson decays. We factorised the different contributions from charm decays that can affect this measurement and estimate them to be either smaller or of the same order of magnitude than the signal indicating that additional experimental cuts must be applied and studied in detail. If they are efficient enough, this could provide an alternative, truly inclusive determination of LFU in $b \to c\ell\bar{\nu}$, as opposed to the current one which relies on the sum of different exclusive modes.

We finally looked at other modes that may be closely related to the semileptonic $b \to s\ell^+\ell^-$ mode as illustrated by many NP models. On one side we studied how we can correlate the anomalies that we see in the charged lepton mode $b \to s\ell^+\ell^-$ with the neutrino modes $b \to s\nu\bar{\nu}$ and $s \to d\nu\bar{\nu}$ finding that under simple and motivated assumptions on the New Physics flavour structure we can correlate these modes. Through these correlation we can find bounds for the branching fractions of these modes that are currently being probed by B-factories and Kaon experiments. Our results strengthen the case for more accurate measurements of $b \to s\nu\bar{\nu}$ and $s \to d\nu\bar{\nu}$ modes, in order to determine which direction should be followed to develop viable NP models describing the deviations in $b \to s\mu^+\mu^-$ and providing a connection with other quark generations at the same time. On the other side we studied the non-leptonic $B_{d(s)} \to K^{*0}\bar{K}^{*0}$ modes which present strong deviations

from naive SU(3) expectations concerning their longitudinal polarisations. We introduced the $L_{K^*\bar{K}^*}$ observable, protected from long-distance hadronic uncertainties and built using the longitudinal polarisation amplitudes leading to a tension of 2.6σ with the experimental measurements. We could not easily explain this tension with simplified NP models without significant fine tuning. The interplay between non-leptonic and semileptonic rare decays could prove highly beneficial to identify new B-flavour anomalies and understand their actual origin in terms of physics beyond the SM.

After these illustrations of various avenues to exploit the b-quark anomalies currently observed, it is worth discussing problems that could become relevant in a near future. The question of the statistical significance of the anomalies and their interpretation are still relatively open questions that might change the picture in the next few years. It is important to clarify the criteria under which the SM hypothesis will be considered statistically as unable to explain the data on the basis of indirect measurements as no clear consensus exist on this subject at the moment. Other important step related to the statistical treatment might be the proper inclusion of non-gaussianities and correlations in both experimental data and theoretical predictions, which are often neglected nowadays but might become important as more precise data is available. Ideally, collaborations should provide the full likelihood obtained through their measurements and the global fit analyses should be able to take into account these elements of information as well as assess the impact of the treatment of systematic uncertainties.

In the near future, new information should be available: LHCb will keep on taking data and exploring these transitions, CMS is expected to explot their so called "parked data" soon and Belle II will provide new insight on several modes, including $b \to s\ell^+\ell^-$ and $b \to c\ell\bar{\nu}$ but also the neutrino modes $b \to s\nu\bar{\nu}$ with completely different systematics in particular for LFU measurements due to its methods for lepton identification totally different from the LHCb case. This additional data should be matched with an improvement in theoretical uncertainties as the future experimental precision will require more precise determinations of form factors, a better understanding of hadronic non-factorisable corrections and of electromagnetic corrections. Concerning the form factors we can expect new and more precise theoretical predictions from Lattice QCD, which continue to evolve due to the growth of computational power. Additionally a better understanding of the systematics of Light Cone Sum Rules, which are far from being as well understood as the uncertainties in Lattice QCD, will be required. Furthermore, the charm loop contributions need to still be studied in further detail, an improvement in the computation of this effect is essential to reduce its uncertainties and assess more precisely the systematics attached to the computations : this is a question for the computation using light-cone sum rules, but also for the models used to extrapolate or interpolate the results obtained in the large-recoil region to the whole q^2 range.

In the years to come this new experimental and theoretical information should provide a better understanding of the anomalies, for instance, excluding some of the NP scenarios currently allowed by the data and providing constraints on complex CP-violating NP contributions. Presumably, we should see a better connection with specific NP models that can explain these anomalies, which are constrained by direct searches from LHC and can lead to connections with other modes involving up-type quark decays and Flavour Changing Neutral Currents into τ leptons, allowing us to close in on the nature of these deviations. Potential links with other flavour anomalies (like $(g-2)_\mu$ or $|V_{ud}|$) should also be very active research fields, using specific models or in EFT approaches. The inclusion of these related new modes requires the use of a broader framework than the Weak Effective Theory, namely the treatment in the Standard Model Effective Field Theory framework. This long-term effort of both experimental and theoretical communities will hopefully help us to understand better the true nature of these tantalising deviations, with the hope to identify the next step to take, beyond the Standard Model, and thus to determine the New Physics behind the b-quark anomalies.

List of Publications

This manuscript is based on the following publications that have been developed in collaboration with Yasmine Ahmis, Marcel Algueró, Bernat Capdevila, Andreas Crivellin, Sébastien Descotes-Genon, Svjetlana Fajfer, Jernej F. Kamenik, Carla Marin Benito, Pere Masjuan, Joaquim Matias, Marie-Hélène Schune, Javier Virto and K. Keri Vos.

Journal Publications

1. Sébastien Descotes-Genon et al. "Testing lepton flavor universality in $\Upsilon(4S)$ decays". In: *Phys. Rev. D* 103.11 (2021), p. 113009. DOI: 10.1103/PhysRevD.103.113009. arXiv: 2104.06842 [hep-ph]

2. Marcel Algueró et al. "A new B-flavour anomaly in $B_{d,s} \to K^{*0}\bar{K}^{*0}$: anatomy and interpretation". In: *JHEP* 04 (2021), p. 066. DOI: 10.1007/JHEP04(2021)066. arXiv: 2011.07867 [hep-ph]

3. Sébastien Descotes-Genon, Martín Novoa-Brunet, and K. Keri Vos. "The time-dependent angular analysis of $B_d \to K_S\ell\ell$, a new benchmark for new physics". In: *JHEP* 02 (2021), p. 129. DOI: 10.1007/JHEP02(2021)129. arXiv: 2008.08000 [hep-ph]

4. Yasmine Amhis et al. "Prospects for New Physics searches with $\Lambda_b^0 \to \Lambda(1520)\ell^+\ell^-$ decays". In: *Eur. Phys. J. Plus* 136.6 (2021), p. 614. DOI: 10.1140/epjp/s13360-021-01194-5. arXiv: 2005.09602 [hep-ph]

5. Sébastien Descotes-Genon et al. "Implications of $b \to s\mu\mu$ anomalies for future measurements of $B \to K^{(*)}\nu\bar{\nu}$ and $K \to \pi\nu\bar{\nu}$". In: *Phys. Lett. B* 809 (2020), p. 135769. DOI: 10.1016/j.physletb.2020.135769. arXiv: 2005.03734 [hep-ph]

6. Marcel Algueró et al. "Symmetries in $B \to D^*\ell\nu$ angular observables". In: *JHEP* 06 (2020), p. 156. DOI: 10.1007/JHEP06(2020)156. arXiv: 2003.02533 [hep-ph]

7. Marcel Algueró et al. "Emerging patterns of New Physics with and without Lepton Flavour Universal contributions". In: *Eur. Phys. J. C* 79.8 (2019). [Addendum: Eur.Phys.J.C 80, 511 (2020)], p. 714. DOI: 10.1140/epjc/s10052-019-7216-3. arXiv: 1903.09578 [hep-ph]

8. S. Descotes-Genon and Martín Novoa-Brunet. "Angular analysis of the rare decay $\Lambda_b \to \Lambda(1520)(\to NK)\ell^+\ell^-$". In: *JHEP* 06 (2019). [Erratum: JHEP 06, 102 (2020)], p. 136. DOI: 10.1007/JHEP06(2019)136. arXiv: 1903.00448 [hep-ph]

Conference Proceedings

9. M. Algueró et al. "Anatomy of a new anomaly in non-leptonic B decays". In: *55th Rencontres de Moriond on QCD and High Energy Interactions*. May 2021. arXiv: 2105.11837 [hep-ph]

10. Sébastien Descotes-Genon et al. "Implications of $b \to s\ell^+\ell^-$ constraints on $b \to s\nu\bar{\nu}$ and $s \to d\nu\bar{\nu}$". In: *55th Rencontres de Moriond on Electroweak Interactions and Unified Theories*. May 2021. arXiv: 2105.09693 [hep-ph]

11. Marcel Algueró et al. "$b \to s\ell\ell$ global fits after Moriond 2021 results". In: *55th Rencontres de Moriond on QCD and High Energy Interactions*. Apr. 2021. arXiv: 2104.08921 [hep-ph]

Résumé en français

La situation actuelle de la physique des particules est assez particulière. Depuis des nombreuses années, les expérimentateurs sont à l'affût de ce qui pourrait être la prochaine étape dans la détermination des constituants fondamentaux de la matière et de leurs interactions. Cette recherche de l'étape suivante s'est faite en ayant certaines directives de l'expérience sur ce qu'il faut chercher (en termes d'énergie et de processus), car les phénomènes observés n'étaient pas bien expliqués avec les particules et les interactions déjà connues. C'était le cas, par exemple, de la diffusion inélastique profonde, qui a permis de sonder la théorie des interactions fortes et de confirmer l'existence physique des quarks et des gluons, que l'on a ensuite recherchés dans les événements de jet des collisions e^+e^-. De même, les courants neutres changeant de saveur (FCNC) ont fourni un test pour la structure des interactions électrofaibles et une indication pour les bosons vectoriels qui ont été, plus tard, recherchés par production directe dans les collisions $p\bar{p}$. Cependant, depuis la découverte du boson de Higgs en 2012, le modèle standard (SM) est désormais "complet", c'est-à-dire qu'il est très bien compris et bien testé à toutes les échelles et dans tous les secteurs, ce qui rend la prochaine étape peu claire.

Plusieurs raisons nous amènent à penser que le SM n'est pas la réponse finale, la plus évidente étant que la gravité ne s'explique pas par lui et qu'il n'est pas facile de la réconcilier avec lui. Cela implique l'effondrement du SM et de la relativité générale, au moins lorsque des énergies proches de la masse de Planck sont atteintes. Cependant, il existe plusieurs problèmes plus subtils du SM et des indices de Nouvelle Physique (NP) qui suggèrent que nous pouvons nous attendre à trouver de nouvelles particules à une échelle inférieure. Par exemple, certains de ces indices sont liés aux observations astrophysiques et cosmologiques, qui suggèrent l'existence de la matière noire sans laquelle la formation et la dynamique des structures à grande échelle (galaxies, amas) ne peuvent être expliquées de manière satisfaisante. De plus, de nouvelles sources de violation de CP sont nécessaires pour atteindre l'asymétrie des baryons nécessaire pour expliquer les données cosmologiques qui est beaucoup plus grande que celle prédite par le SM. En outre, si aucune nouvelle particule n'est présente à proximité de l'échelle électrofaible, des niveaux élevés de réglage fin sont nécessaires pour expliquer la masse du boson de Higgs, ce que l'on appelle souvent le problème de la hiérarchie.

Malheureusement, aucune nouvelle particule n'a encore été découverte par recherche directe au Grand collisionneur de hadrons, ce qui indique que l'énergie de ces nouvelles particules pourrait être trop élevée ou que leurs couplages aux particules SM sont trop faibles pour être détectés par les expériences actuelles. En outre, ces particules devraient en principe apparaître dans les recherches indirectes si celles-ci sont suffisamment précises, car elles induiraient des corrections quantiques aux prédictions SM de nombreux processus. En fait, les recherches indirectes à des énergies plus basses ont prédit dans le passé l'existence de particules plus lourdes, par exemple, le quark charmé a été prédit par le mécanisme de Glashow-Iliopoulos-Maiani dans le mélange de kaons, et la masse du quark top a également été limitée par le mélange $B - \bar{B}$.

La prochaine étape peut être difficile à identifier actuellement, mais il existe quelques indices expérimentaux qui méritent d'être pris en compte. C'est notamment le cas des anomalies dites du quark b (ou anomalies de saveur) qui constituent l'une des rares déviations des prédictions du SM qui aient été observées. Ces anomalies, qui affectent deux transitions différentes, $b \to c\ell\bar{\nu}$ et $b \to s\ell^+\ell^-$, ont commencé avec la mesure d'un excès dans le rapport de branchement $B \to D^*\tau\bar{\nu}$ par BaBar en 2012 et avec la mesure de déviations dans les observables angulaires de $B \to K^*\mu^+\mu^-$ par LHCb en 2013, déclenchant depuis lors une activité intense à la fois dans la communauté théorique et dans plusieurs collaborations expérimentales. Aujourd'hui, ces déviations apparaissent dans une série d'observables mesurées à la fois dans les usines à B, Belle et BaBar, et dans les expériences du Large Hadron Collider, LHCb, CMS et ATLAS, montrant des déviations assez cohérentes dans les désintégrations semi-leptoniques du quark b.

Cadre théorique

Dans la première partie du manuscrit, nous présentons les principaux concepts et outils nécessaires à la description des désintégrations semi-leptoniques du quark b. Nous commençons par décrire le SM et discutons de la rupture de la symétrie électrofaible et de ses conséquences. L'une des conséquences de la rupture de la symétrie électrofaible

est le mélange entre les différentes générations qui sont à l'origine des courants dits de changement de saveur. Dans le cas des courants chargés, nous discutons brièvement de la structure et de l'impact des matrices de mélange de générations, en nous concentrant sur la matrice de mélange des quarks de Cabibbo-Kobayashi-Maskawa qui est bien contrainte par divers tests expérimentaux. Dans le cas des courants neutres, nous verrons qu'il n'y a pas de mélange entre les générations dans le SM et qu'ils sont générés uniquement au niveau de boucle. Cela indique que les deux transitions sont des tests intéressants du SM.

Nous discutons ensuite du potentiel de ces courants en tant que sondes NP et tests du SM, qui est au centre du manuscrit. Nous discutons des détails importants de la QCD et de ses éléments non perturbatifs, qui jouent un rôle important dans l'étude des courants à changement de saveur. Cela indique que les transitions de changement de saveur impliquant à la fois les quarks et les leptons peuvent fournir un environnement très intéressant pour tester le SM, car elles peuvent être testées dans divers environnements hadroniques avec un contrôle théorique raisonnable des effets non perturbatifs de la QCD. De plus, l'universalité des couplages dans le SM peut être sondée en particulier par des tests de l'universalité de la saveur des leptons. Nous établissons ensuite le cadre théorique pour étudier les courants de changement de saveur dans les désintégrations des hadrons lourds. Ces désintégrations sont assez complexes car elles impliquent à la fois l'interaction électrofaible et la chromodynamique quantique qui nécessitent des traitements différents. Cette complexité nécessite une séparation des différentes échelles d'énergie du problème. Cela nécessite une factorisation de ces processus et l'introduction de plusieurs théories de champ effectives grâce auxquelles nous sommes en mesure de comprendre ces désintégrations. Cette approche effective permet en outre une approche indépendante du modèle pour les analyses NP, ce qui est fondamental pour l'étude des anomalies de saveur.

Anomalies de saveur

Dans la partie suivante de ce manuscrit, nous discutons en détail des anomalies de saveur actuelles : les différentes observables qui peuvent être mesurées, leurs principales incertitudes théoriques, et leurs déterminations expérimentales actuelles. Les anomalies de saveur observées dans les désintégrations semi-leptoniques des mésons B constituent l'un des indices les plus prometteurs de NP découverts au LHC et dans les usines à B. Les plus robustes de ces déviations se situent dans les rapports d'universalité de la saveur des leptons, $R_{D^{(*)}}$ qui compare le rapport de branchement de $B \to D^{(*)}\ell\bar{\nu}$ pour le lepton τ et les leptons légers et $R_{K^{(*)}}$ qui compare le rapport de branchement de $B \to K^{(*)}\ell^+\ell^-$ pour les muons et les électrons, présentant des tensions de plus de 3σ des deux côtés. D'autres déviations ont été observées pour les rapports de branchement et les observables angulaires de plusieurs modes de désintégration avec une sensibilité différente à la NP, ce qui conduit à une image globale de NP violant la saveur du lepton affectant ces désintégrations.

Nous présentons ensuite une analyse globale des données expérimentales des transitions $b \to s\ell^+\ell^-$ et des anomalies dites b en termes de la théorie effective faible (WET). Nous discutons les différents éléments entrant dans les prédictions théoriques pour les modes considérés et la procédure utilisée pour évaluer les différentes hypothèses de NP et contraindre leurs paramètres, c'est-à-dire les contributions de NP aux coefficients de Wilson de la WET.

Nos résultats montrent que la NP peut expliquer les anomalies $b \to s\ell^+\ell^-$, où les contributions de NP aux coefficients de Wilson du mode muon sont nécessaires pour expliquer les données. Les contributions universelles à la saveur lepton (ou les contributions de NP dans le mode électron), bien que non requises, sont autorisées.

En outre, plusieurs scénarios peuvent expliquer les données, etant

$$\mathcal{C}_{9\mu}^{\rm NP}, \qquad \mathcal{C}_{9\mu}^{\rm NP} = -\mathcal{C}_{10\mu}^{\rm NP}, \qquad (\mathcal{C}_{9\mu}^{\rm NP}, \mathcal{C}_{9'\mu}^{\rm NP} = -\mathcal{C}_{10\mu}^{\rm NP}) \quad \text{et} \quad (\mathcal{C}_9^V = -\mathcal{C}_{10}^V, \mathcal{C}_{9\mu}^U)$$

les plus favorisés. Une caractéristique commune de ces scénarios est la présence dans tous d'une contribution de NP significative à $\mathcal{C}_{9\mu}^{\rm NP}$ (environ 1/4 de la contribution SM).

Des analyses globales ont également été réalisées dans le cas de la transition $b \to c\ell\bar{\nu}$. Les deux analyses globales montrent une cohérence entre les différentes observables étudiées et une tendance suggérant la présence d'une nouvelle physique violant l'universalité de la saveur du lepton avec des couplages de type vectoriel, cependant les contraintes actuelles ne sont pas suffisantes pour déterminer la nature de la NP qui pourrait être à l'origine de ces anomalies. Dans le cas de $b \to c\ell\bar{\nu}$, seulement quelques mesures expérimentales sont disponibles, ce qui rend difficile la détermination de la nature de la NP en jeu. Dans le cas de $b \to s\ell^+\ell^-$, davantage de mesures expérimentales sont disponibles, mais les prédictions théoriques souffrent d'incertitudes légèrement plus importantes. De plus, les phases complexes des coefficients de Wilson décrivant la transition $b \to s\ell^+\ell^-$ ne sont pas encore bien contraintes.

Il est donc particulièrement important de sonder ces transitions (à la fois $b \to c\ell\bar{\nu}$ et $b \to s\ell^+\ell^-$) avec une plus grande précision expérimentale et théorique, mais aussi de fournir de nouveaux modes et observables contraignant les scénarios de NP de différentes manières. Nous discutons ensuite des modèles spécifiques de NP qui pourraient être à la source des anomalies de quark b, en constatant que des modèles simples peuvent

expliquer chacune de ces anomalies. En fait, certains modèles simplifiés qui peuvent expliquer ces anomalies (séparément ou ensemble), incluent généralement de nouveaux bosons vectoriels, des leptoquarks scalaires ou des leptoquarks vectoriels. Ces modèles simplifiés nécessitent toutefois d'être intégrés dans un modèle plus large, complet dans l'ultraviolet, ce qui ouvre la possibilité d'explorer expérimentalement un nouveau secteur.

Nouveaux tests de la physique à l'oeuvre dans $b \to s\ell^+\ell^-$

L'idéal serait de pouvoir démêler les différents scénarios de NP afin de trouver une solution de NP unique. Cependant, les données actuelles ne nous permettent pas encore de démêler tous les scénarios possibles, en partie parce que les observables les plus précises sont sensibles aux mêmes combinaisons de coefficients de Wilson et que les observables qui pourraient démêler cela ne sont pas encore assez précises. L'étude de nouvelles observables et la mesure d'observables déjà proposées qui n'ont pas encore été mesurées pourraient améliorer la situation. Nous discutons les différentes observables qui peuvent aider à ce démêlage de NP étant P_5', Q_5' et R_K complémentaires dans cette tâche dans le cas de coefficients de Wilson réels.

Il est clair que des modes et des observables supplémentaires seraient utiles pour progresser dans ce domaine. D'une part, les modes baryoniques ne sont pas très représentés bien qu'ils soient accessibles à LHCb. D'autres observables seraient également nécessaires pour étudier correctement la possibilité de coefficients de Wilson complexes. En effet, les parties imaginaires des coefficients de Wilson ne sont encore que faiblement contraintes, donc la mesure de nouvelles observables pour contraindre ces phases complexes est fondamentale pour comprendre la structure de NP qui pourrait être derrière les anomalies de saveur.

Par conséquent, nous présentons de nouveaux repères pour étudier la transition $b \to s\ell^+\ell^-$, à la fois dans le mode actuellement mesuré $B \to K\ell^+\ell^-$ par une analyse en fonction du temps qui repose sur le mélange $B - \bar{B}$ et $K - \bar{K}$ et dans le nouveau mode baryonique $\Lambda_b \to \Lambda^*\ell^+\ell^-$ par une analyse angulaire complète de ce mode. Ces résultats fournissent des observables intéressants qui pourraient contraindre la structure complexe des NP possibles derrière les anomalies.

Analyse angulaire de $\Lambda_b \to \Lambda^*(\to pK)\ell^+\ell^-$

Les modèles persistants d'écarts par rapport aux attentes du SM dans les désintégrations $b \to s\mu^+\mu^-$ et les indices de violation de l'universalité des saveurs leptoniques entre les électrons et les muons dans ces modes incitent fortement à chercher des confirmations en utilisant d'autres modes avec des incertitudes théoriques et expérimentales différentes. Nous étudions la désintégration rare $\Lambda_b \to \Lambda^*(\to N\bar{K})\ell^+\ell^-$ comme une nouvelle source d'information, en plus des canaux mésoniques déjà étudiés dans les usines à B et au LHC. Nous donnons une description détaillée de la cinématique de la désintégration et mettons l'accent sur les questions liées à la propagation et à la désintégration forte du baryon Λ^* de spin 3/2. Nous calculons le taux de désintégration dans le cadre de l'approche hamiltonienne effective, en ne considérant que les opérateurs SM et à chiralité inversée, en prenant l'approximation de largeur étroite pour le baryon Λ^*. L'implication des états de spin 1/2 et de spin 3/2 donne un taux de désintégration différentiel assez compliqué qui est exprimé en termes de 12 observables angulaires qui dépendent de la masse invariante du dilepton q^2. Chaque observable peut être considérée comme la somme des termes d'interférence entre 12 amplitudes d'hélicité, qui peuvent être exprimées en termes de coefficients de Wilson à courte distance et de facteurs de forme de transition hadronique définis dans une base d'hélicité. Nous vérifions que notre résultat est en accord avec les attentes générales du formalisme de l'amplitude d'hélicité, et nous vérifions également que nos expressions présentent le comportement attendu dans la limite de photons réels $q^2 \to 0$ afin de récupérer le rapport de branchement pour $\Lambda_b \to \Lambda^*\gamma$.

Nous discutons des simplifications qui apparaissent dans la limite d'un quark b infiniment lourd : en fonction de la cinématique (faible ou grand recul de Λ^*, c'est-à-dire grand ou petit q^2), la théorie effective du quark lourd (HQET) et la théorie effective molle et colinéaire (SCET) peuvent être utilisées pour exprimer tous les facteurs de forme en termes de facteurs de forme réduits 2 ou 1 à l'ordre principal (c'est-à-dire jusqu'à des corrections d'ordre α_s et $\Lambda_{\rm QCD}/m_b$). Comme il n'y a actuellement aucune détermination des facteurs de forme sur tout l'ensemble des valeurs de q^2 disponible à partir de simulations sur reseaux ou de règles de somme sur le cône de lumière, nous effectuons une première illustration de la sensibilité des observables aux contributions NP en utilisant des entrées hadroniques provenant de modèles de quark. Nous considérons plusieurs scénarios NP favorisés par les anomalies observées récemment dans les modes de désintégration $b \to s\ell^+\ell^-$ et nous comparons les résultats obtenus en utilisant l'ensemble des facteurs de forme ou en exploitant les relations HQET/SCET entre les facteurs de forme. Nous discutons des conséquences phénoménologiques pour certaines observables. Nous avons remarqué que le taux de désintégration différentiel est assez sensible au scénario NP spécifique considéré, à la fois pour les faibles et les grands reculs. D'autre part, les coefficients angulaires normalisés à ce taux de désintégration montrent moins de variations. En effet, dans le cas de scénarios NP avec des contributions modérées à $\mathcal{C}_{9\mu}^{\rm NP}$ et/ou $\mathcal{C}_{10\mu}^{\rm NP}$, les quatre amplitudes numériquement significatives ($A_{\perp,||}^L$) sont dominées par une

seule combinaison de coefficients de Wilson qui s'annulent entre le numérateur et le dénominateur des coefficients angulaires S normalisés par rapport au rapport de branchement. Dans la région de grand recul, l'interférence avec le pôle du photon permet une certaine discrimination entre les scénarios NP pour certaines des observables. D'autre part, ces coefficients angulaires s'avèrent assez sensibles à la présence de contributions droites $\mathcal{C}_{9'\mu}^{\rm NP}$ qui affectent différemment les diverses amplitudes de transversalité dominantes.

Nous présentons ensuite les perspectives d'analyses angulaires des désintégrations $\Lambda_b \to \Lambda^* \ell^+\ell^-$, motivées en particulier par les résultats récents sur l'universalité de la saveur leptonique dans $\Lambda_b \to pK^-\ell^+\ell^-$ au LHCb. En utilisant le rendement attendu des données qui seront collectées par l'expérience LHCb dans un avenir proche, nous présentons des études de sensibilité afin de déterminer la précision expérimentale sur les observables angulaires liées à la distribution leptonique et leur potentiel d'identification des NP. Nous étudions l'impact des effets d'acceptation sur l'extraction de ces observables angulaires en utilisant les données LHCb publiées ainsi que le logiciel de simulation rapide `RapidSim`. L'asymétrie avant-arrière des leptons A_{FB}^{ℓ} semble particulièrement prometteuse : en fonction des progrès réalisés dans la réduction des incertitudes sur les prédictions de la théorie, à un moment donné entre le Run 3 et le Upgrade 2, on pourrait utiliser cette observable à faible masse invariante des dileptons pour distinguer entre le SM et un scénario avec des contributions NP à $\mathcal{C}_{9\mu}^{\rm NP}$ soutenu par les données actuelles de $b \to s\ell^+\ell^-$. Nous avons vérifié que nos conclusions n'étaient pas biaisées par les simplifications importantes de la distribution angulaire que nous avons proposées sur la base de la limite des quarks lourds et soutenues par les estimations phénoménologiques. La distribution angulaire se factorise alors en un produit de deux termes, à savoir une dépendance triviale de l'angle décrivant l'état final hadronique et une dépendance non triviale de l'angle décrivant l'état final leptonique. Les trois observables peuvent être réexprimées comme le rapport de branchement, l'asymétrie avant-arrière des leptons et une troisième observable angulaire S_{1cc}. Les deux premières observables présentent une certaine sensibilité aux contributions des NP au coefficient de Wilson à courte distance $\mathcal{C}_{9\mu}^{\rm NP}$ pour les transitions $b \to s\mu^+\mu^-$.

Les futures informations expérimentales sur ces observables pourraient donc fournir des informations complémentaires à la recherche en cours de nouvelle physique pour les transitions $b \to s\ell^+\ell^-$. Cependant, plusieurs questions doivent être résolues avant que ce mode puisse être comparé de manière compétitive aux désintégrations $B \to K^{(*)}\ell^+\ell^-$ et même $\Lambda_b \to \Lambda(\to N\pi)\ell^+\ell^-$. En effet, la détermination théorique des contributions hadroniques, locales (facteurs de forme) et non-locales (boucles de charme) doit être effectuée avec précision. En principe, on pourrait également exploiter la polarisation de l'état initial et de l'état final pour construire d'autres observables, de manière similaire aux etudes realisés sur la transition $\Lambda_b \to \Lambda\ell^+\ell^-$. Ces aspects devraient être étudiés et résolus (partiellement ou totalement) à l'avenir. Cela ouvrirait la possibilité d'une étude de $\Lambda_b \to \Lambda^*(\to N\bar{K})\ell^+\ell^-$ au LHC qui pourrait compléter d'autres modes dans la quête actuelle de NP dans les transitions $b \to s\ell^+\ell^-$.

Analyse angulaire en fonction du temps de $B_d \to K_S\ell^+\ell^-$

Une façon intéressante de sonder davantage les transitions $b \to s\mu^+\mu^-$ consiste à utiliser le mélange de mésons neutres et l'analyse en fonction du temps afin de définir de nouvelles observables pour les désintégrations B_d et B_s. Ceci a déjà été appliqué à $B_d \to K^*\mu\mu$ et $B_s \to \phi\mu\mu$ dans le passé. Nous considérons la même idée dans le cas plus simple de $B_d \to K_S\mu\mu$. Le mode chargé $B^\pm \to K^\pm\mu\mu$ a une structure angulaire beaucoup plus simple, avec seulement trois observables qui fournissent des contraintes intéressantes mais limitées sur les contributions scalaires et tensorielles. Les entrées hadroniques (facteurs de forme et contributions de la boucle de charme) sont également beaucoup plus simples à manipuler et à analyser. Nous avons discuté des avantages d'une analyse angulaire en fonction du temps de ce mode.

Après avoir rappelé le formalisme en l'absence de mélange (cas chargé), nous nous sommes intéressés au cas neutre. Cela a nécessité une définition minutieuse de la cinématique du mode pour connecter les désintégrations CP-conjuguées qui sont maintenant liées par le mélange de $B - \bar{B}$. Une analyse angulaire dépendant du temps conduit à 6 nouvelles observables, mesurant la violation de CP dans l'interférence entre la désintégration et le mélange. Trois de ces observables, notées $s_{0,1,2}$, semblent plutôt prometteuses, et elles peuvent également être obtenues à partir d'observables angulaires intégrées dans le temps en comparant les modes neutres et chargés dans les machines hadroniques si le étiquetage de la saveur de l'état initial est disponible. Ces 3 observables $s_{0,1,2}$ ont des expressions simples en termes d'amplitudes de transversalité. Elles peuvent être combinées avec les observables angulaires habituelles pour $B \to K\ell^+\ell^-$ pour obtenir les observables $\sigma_{0,1,2}$, ρ_2 et $R_{S,T_t,W}$.

De manière très intéressante, nous montrons que σ_0 et ρ_2 sont très précisément connus dans le SM et dans les scénarios de NP avec des contributions réelles aux opérateurs SM et chiralement retournés. Ils ne dépendent que de l'angle de mélange B_d, c'est-à-dire de l'angle CKM β, et ils sont valables pour toute valeur de la masse invariante du dilepton q^2. Nous soulignons que ces prédictions sont très robustes, car elles sont valables quelles que soient les hypothèses sur les facteurs de forme et les contributions de la boucle de charme. Par conséquent, elles constituent des tests très puissantes des scénarios NP actuellement favorisés par les ajustements globaux aux données de la transition $b \to s\ell^+\ell^-$.

Nous étudions ensuite deux cas de NP où ces prédictions sont modifiées. Nous montrons que R_S, R_T et R_W peuvent sonder d'autres scénarios NP, à savoir des opérateurs scalaires et tenseurs (avec des contributions réelles) et des contributions NP complexes entrant avec une phase CP-impair "faible". La sensibilité de ces observables à chaque scénario est différente, et les incertitudes théoriques attachées aux prédictions théoriques sont faibles, ce qui nous permet de fournir une référence des scénarios NP reposant sur les mesures de $s_{0,1,2}$. Nous discutons également brièvement de modes de désintégration B_s similaires tels que $B_s \to f_0\mu\mu$, $B_s \to \eta\mu$ et $B_s \to \eta'\mu$.

En conclusion, la simplicité de la désintégration sous-jacente $B \to K\mu\mu$ nous a permis de fournir une analyse détaillée de l'analyse en fonction du temps de $B_d \to K_S\mu\mu$ avec étiquetage de la saveur. Ces nouvelles observables fournissent de puissantes vérifications croisées des différentes hypothèses de NP. Elles peuvent également contribuer de manière utile aux ajustements globaux de $b \to s\ell^+\ell^-$, en fournissant des contraintes d'un type différent sur la physique à courte distance encodée dans les coefficients de Wilson.

Nouveaux tests de la physique à l'oeuvre dans $b \to c\ell\bar{\nu}$

Nous présentons également de nouveaux repères pour étudier la transition $b \to c\ell\bar{\nu}$. Dans le premier cas, nous considérons la distribution angulaire de $B \to D^*\ell\bar{\nu}$ et nous proposons des verifications intéressantes des mesures expérimentales des observables angulaires et différentes manières de sonder la NP en s'appuyant sur les symétries de la distribution angulaire. Dans le deuxième cas, nous fournissons de nouveaux moyens de sonder les rapports inclusifs d'universalité de la saveur des leptons $R(X)_{\tau\ell}$ par l'utilisation directe des désintégrations du meson $\Upsilon(4S)$, ce qui, contrairement aux méthodes précédentes, se fait par une méthode véritablement inclusive.

Symétries dans les observables angulaires de $B \to D^*\ell\bar{\nu}$

Nous appliquons le formalisme des symétries d'amplitude de la distribution angulaire des désintégrations $B \to D^*\ell\nu$ pour $\ell = e, \mu, \tau$. Nous montrons que l'ensemble des observables angulaires utilisées pour décrire la distribution de cette classe de désintégrations ne sont pas indépendantes en l'absence de NP contribuant aux opérateurs tensoriels. Nous dérivons des ensembles de relations entre les coefficients angulaires de la distribution des désintégrations pour les cas de leptons massifs et non massifs. Ces relations peuvent être utilisées pour sonder d'une manière très générale la cohérence entre les observables angulaires et la NP sous-jacente à l'oeuvre, et en particulier si elle implique des opérateurs tenseurs ou non.

Nous utilisons ensuite ces relations pour accéder à la fraction de polarisation longitudinale intégrée du D^* en utilisant des coefficients angulaires différents de ceux utilisés par l'expérience Belle. Dans un futur proche, cela peut fournir une mesure équivalente à $F_L^{D^*}$ pour $B \to D^*\tau\nu$ afin de comprendre la valeur relativement élevée mesurée par Belle. Nous présentons des expressions pour le cas massif et sans masse qui couvrent le scénario le plus général de NP incluant également les pseudoscalaires et les contributions imaginaires, avec la seule exception des contributions tensorielles.

Nous étudions ensuite la précision de ces expressions si seules des observables binées sont disponibles, ou si elles sont utilisées dans le cas de scénarios dépassant les hypothèses faites dans leur dérivation (contributions imaginaires, contributions tensorielles). Nous utilisons plusieurs points de référence correspondant aux points les mieux ajustés des ajustements globaux aux observables $b \to c\tau\nu$, en nous appuyant sur un modèle simple de quark pour les facteurs de forme hadroniques pour cette étude exploratoire. Les expressions dérivées sous l'hypothèse de l'absence de contributions imaginaires NP et de contributions tensorielles fonctionnent très bien, même dans l'approximation binée. Elles sont très précises même en présence de contributions NP imaginaires. Comme prévu, leurs généralisations, dérivées en supposant la présence de contributions imaginaires, se comportent très bien également dans l'approximation binée. Toutes les relations échouent en présence de grandes contributions tensorielles, où aucune dépendance ne peut être trouvée parmi les observables angulaires.

En plus de présenter les expressions les plus générales de $F_L^{D^*}$ dans le cas massif et sans masse, nous dérivons également une relation entre les observables ($\tilde{A}_{3,9,6s}$ et $F_L^{D^*}$) qui sont potentiellement intéressantes du point de vue de la NP si la déviation de $F_L^{D^*}$ est confirmée. Avoir des prédictions spécifiques de construction de modèle pour ces observables serait très intéressant. Nous discutons également de l'impact de la présence de neutrinos légers droitiers. Nous montrons que nous pouvons tester leur présence dans certains cas spécifiques sous l'hypothèse qu'il n'y a pas de contributions tensorielles ou imaginaires, en comparant nos deux déterminations de $F_L^{D^*}$. De plus, sous cette hypothèse, le signe de la différence entre les deux déterminations est fixé.

En utilisant des projections récentes sur les perspectives expérimentales pour les mesures des observables angulaires, nous trouvons que ces relations pourraient être vérifiées avec une précision de 10% dans le scénario d'un collisionneur de hadrons de 50 fb^{-1}, ce qui serait suffisant pour repérer un scénario avec des contributions tensorielles et fournirait une contre-vérification intéressante de la détermination des observables angulaires.

Ces mesures supplémentaires nécessaires pour cette extraction rendent évidemment cette détermination plus difficile expérimentalement, mais elles peuvent aider à coincer le type de NP responsable de cette valeur élevée

ou à comprendre le problème expérimental responsable de cette valeur inattendue de la polarisation du D^*.

Tester l'universalité des saveurs de lepton avec les désintégrations du meson $\Upsilon(4S)$

En nous appuyant sur les propriétés spécifiques des usines à B et en particulier sur l'expérience Belle II, nous proposons de comparer les taux inclusifs de $\Upsilon(4S) \to e^{\pm}\mu^{\mp}X$, $\Upsilon(4S) \to \mu^{\pm}\tau^{\mp}_{\rm had}X$ et $\Upsilon(4S) \to e^{\pm}\tau^{\mp}_{\rm had}X$. Cette mesure inclusive peut être reliée au rapport $R(X)_{\tau\ell} \equiv \Gamma(b \to X\tau\nu)/\Gamma(b \to X\ell\nu)$ ($\ell = e$ ou μ), une fois que les coupures expérimentales appropriées sont appliquées pour supprimer les effets du mélange de B neutre et des leptons émis par les désintégrations FCNC (semileptoniques) rares de B, ainsi que les désintégrations secondaires du charmonium, du charme et du tau. La faisabilité de notre proposition suppose de manière cruciale que les leptons tau à désintégration hadronique provenant des sommets de désintégration B peuvent être efficacement démêlés du bruit de fond (par exemple, des désintégrations B hadroniques impliquant trois pions chargés ou plus) à Belle II. Une étude expérimentale dédiée à ce sujet dépasse toutefois le cadre de ce travail. Il est remarquable que cette détermination alternative de $R(X)_{\tau\ell}$ soit une détermination réellement inclusive, contrairement à la détermination actuelle qui correspond à une somme de différents modes exclusifs.

Nous nous sommes concentrés sur le cas de $R^{\Upsilon(4S)}_{\tau\mu} \simeq R(X)_{\tau\mu}$, mais notre discussion s'applique tout aussi bien à la combinaison tau-électron, en intervertissant les rôles joués par les électrons et les muons. Les déviations actuelles de $B \to D^*\ell\nu$ et de $B \to D\ell\nu$ lorsque les canaux τ sont comparés aux modes électroniques ou muoniques sont de l'ordre de 10% (pour les rapports LFU des rapports de branchement) et fournissent un point de référence pour la sensibilité cible de notre proposition. Ceci est illustré par le cas très simple où la NP imite la structure $V-A$ des courants $b \to c\tau\nu$ dans le SM, conduisant à une remise à l'échelle universelle de tous les rapports de branchement $b \to c\tau\nu$ qui aurait donc un impact sur les rapports inclusifs $R(X)_{\tau\ell}$ de la même manière que les mesures exclusives pour R_D et R^*_D. Il est intéressant de noter que l'approche théorique et l'environnement expérimental sont assez différents dans les mesures exclusives et inclusives, et notre proposition pourrait fournir des contre-vérifications très intéressantes des déviations actuellement observées dans les désintégrations exclusives.

Compte tenu de nos estimations les incertitudes systématiques dans la détermination de $R(X)_{\tau\ell}$ à partir d'une mesure de $R^{\Upsilon(4S)}_{\tau\ell}$ pourraient être ramenées en dessous d'une valeur donnée ($\epsilon_{\rm sys}$) à condition que (1) les coupures sur la différence de paramètre d'impact $B-\bar{B}$ peuvent supprimer les effets de mélange des mésons neutres B en dessous de $\epsilon_{\rm sys}$, combinés à une ID de charge leptonique efficace pour supprimer la contamination par désintégration semi-leptonique du charme; (2a) les leptons multiples provenant de la même chaîne de désintégration B peuvent être supprimés à un niveau supérieur à $\epsilon_{\rm sys}$ ou alternativement (2b) les leptons provenant des sommets secondaires (désintégration B) peuvent être distingués de ceux provenant des chaînes de désintégration inférieures à un niveau à peu près supérieur à $\epsilon_{\rm sys}$. D'autres études expérimentales dédiées sont nécessaires pour établir la précision réellement atteignable par Belle II. Si cette mesure s'avère possible et précise, on pourrait imaginer utiliser les mêmes techniques OPE que dans le cas du SM pour déterminer la sensibilité des rapports $R(X)_{\tau\ell}$ au NP et contraindre les opérateurs NP à l'aide de cette mesure inclusive.

En résumé, nous avons proposé une nouvelle méthode pour tester les indices persistants de violation du LFU observés dans les désintégrations semi-leptoniques de B. Cette mesure constituerait une sonde supplémentaire et potentiellement compétitive des violations de l'universalité de la saveur leptonique dans les transitions $b \to c\ell\nu$, complémentaire aux mesures exclusives et accessible dans l'environnement Belle II.

Autres modes associés

Dans la dernière partie de ce manuscrit, nous discutons des connexions possibles des anomalies du quark b avec d'autres modes étroitement liés sous des hypothèses assez générales, à savoir les modes de neutrino $b \to s\nu\bar{\nu}$ et $s \to d\nu\bar{\nu}$; et le mode non-leptonique $B_{d(s)} \to K^{*0}\bar{K}^{*0}$. Dans le premier cas, nous obtenons des limites pour ces modes grâce à des principes simples de violation minimale de la saveur (MFV) et, dans le second, nous trouvons une nouvelle anomalie potentielle dans les modes hadroniques.

Implications des anomalies de saveur dans $B \to K^{(*)}\nu\bar{\nu}$ et $K \to \pi\nu\bar{\nu}$

Nous étudions les conséquences des déviations du SM observées dans les transitions $b \to s\mu^+\mu^-$ pour les processus FCNC impliquant des quarks et des neutrinos de type down. Motivés par les résultats des ajustements globaux aux observables $b \to s\mu^+\mu^-$ ainsi que par les mesures et les limites des processus FCNC avec des neutrinos, nous considérons une description EFT générale des transitions FCNC en termes d'opérateurs invariants de jauge $SU(2)_L$, y compris ceux avec des quarks droitiers et des leptons chargés. Cela nous permet de décrire avec les mêmes coefficients de Wilson à courte distance $b \to s\mu^+\mu^-$, $b \to s\nu\bar{\nu}$ et $s \to d\nu\bar{\nu}$.

Nous abordons brièvement le statut de $K_L \to \pi^0\nu\nu$ et sa corrélation avec $K^+ \to \pi^+\nu\nu$, qui est seulement modifié par la NP si elle comporte des nouvelles sources de violation de CP, ce qui nécessite une nouvelle

dynamique des saveurs au-delà de MFV. Dans ce cas, il n'y a pas de corrélation claire avec les autres modes FCNC discutés ici. En supposant MFV dans le secteur des quarks, nous étudions la corrélation entre les rapports de branchement pour $B \to h_s \nu\bar{\nu}$ et $K^+ \to \pi^+ \nu\bar{\nu}$. Une telle corrélation est déjà présente sans supposer une structure définie pour les couplages NP des neutrinos, mais elle peut être rendue encore plus précise une fois que des scénarios NP particuliers attribuent des valeurs spécifiques à ces couplages.

Au-delà de la limite MFV, nous étudions la corrélation entre $B \to K\nu\bar{\nu}$ et $B \to K^*\nu\bar{\nu}$, en montrant notamment que, selon les couplages leptoniques NP, le scénario avec NP dans $(\mathcal{C}_9^{\mu,\mathrm{NP}}, \mathcal{C}_{9'}^{\mu,\mathrm{NP}})$ peut donner une corrélation étroite entre les deux modes lorsque les mesures $b \to s\ell^+\ell^-$ sont prises en compte. Ces mesures pourraient établir la rupture de saveur NP au-delà de MFV et indiquer le nombre de saveurs de leptons affectées par la NP. Par exemple, les mesures des deux rapports $R(B \to K\nu\bar{\nu})$ et $R(B \to K^*\nu\bar{\nu})$ en dehors de la diagonale pourraient être interprétées comme la présence de courants droitiers dans $b \to s\nu\bar{\nu}$ et $b \to s\ell^+\ell^-$. Notre travail montre donc que des informations assez générales sur le modèle de NP pourraient être obtenues à partir des mesures à venir de $K \to \pi\nu\bar{\nu}$ et $B \to K^{(*)}\nu\bar{\nu}$.

Une nouvelle anomalie de saveur B dans $B_{d,s} \to K^{*0}\bar{K}^{*0}$: anatomie et interprétation

Nous analysons ensuite les désintégrations pingouines non leptoniques $B_d \to K^{*0}\bar{K}^{*0}$ et $B_s \to K^{*0}\bar{K}^{*0}$, où les récents résultats du LHCb indiquent des différences frappantes dans la polarisation longitudinale de ces deux modes. Ceci est inattendu puisqu'ils sont liés par le U-spin et devraient donc avoir des dynamiques QCD et electrofaible similaires (jusqu'à d'infimes corrections dues aux masses des quark down et strange).

Nous introduisons l'observable L comme une combinaison de fractions de polarisation et de rapports de branchement afin de comparer les amplitudes longitudinales dans les deux modes, car elles peuvent être calculées avec un meilleur contrôle théorique dans une expansion $1/m_b$ telle que la factorisation QCD. Nous exploitons le fait que ces désintégrations médiées par les pingouins présentent des éléments de matrice hadroniques très similaires pour les contributions "arbre" et "pingouin" dans la décomposition habituelle basée sur les facteurs CKM, de sorte que ces contributions sont très fortement corrélées. Cela signifie que l'observable L est une mesure de la rupture de U-spin entre les contributions pingouins aux désintégrations B_d et B_s, avec une déviation par rapport à l'attente SM entre 2σ et 3σ selon le cadre théorique spécifique considéré. Cette observation renforce et met sur une base plus solide l'indice de NP déjà suspecté en considérant la différence entre les fractions de polarisation longitudinale dans ces deux modes. Nous effectuons une analyse détaillée du budget d'erreur pour $L_{K^*\bar{K}^*}$ et ne trouvons qu'un impact relativement faible des divergences infrarouges provenant de l'annihilation faible et de la diffusion de spectateurs durs, par rapport à des observables comme les rapports de branchement ou les fractions de polarisation impliquant des amplitudes transversales gênantes.

Nous interprétons ensuite cette déviation dans une approche indépendante du modèle en utilisant la théorie effective faible. Pour des raisons de simplicité, nous n'autorisons la NP que dans les coefficients de Wilson de la SM ou leurs contreparties chirales. Nous avons identifié trois opérateurs qui pourraient accommoder la déviation avec des contributions de NP au plus aussi importantes que celles du SM. Alors que $\mathcal{C}_{1q}$ est déjà très fortement contraint par d'autres modes nonleptoniques et par les limites du LHCb (au point d'exclure cette solution), la situation est moins contrainte pour le coefficient pingouin $\mathcal{C}_{4q}$ et le coefficient chromomagnétique $\mathcal{C}_{8gq}^{\mathrm{eff}}$ où des contributions NP d'une taille similaire à celle du SM sont autorisées et pourraient expliquer la déviation dans $L_{K^*\bar{K}^*}$. Nous discutons des exemples de modèles NP simplifiés qui pourraient fournir de grandes contributions, au prix de l'acceptation d'un réglage fin pour tenir compte des limites sur le mélange $B_s - \bar{B}_s$ et $b \to s\gamma$. Il est intéressant de noter que dans un modèle composite ou extradimensionnel général, la contribution du gluon de Kaluza-Klein à l'amplitude $b \to s$ dans $B_s \to K^{*0}\bar{K}^{*0}$ a le même signe que la contribution Z' à $b \to s\ell^+\ell^-$ par rapport au SM. Par conséquent, si l'on accepte le réglage fin du mélange $B_s - \bar{B}_s$, de tels modèles peuvent fournir une explication commune des données de $L_{K^*\bar{K}^*}$ et de $b \to s\ell^+\ell^-$.

Ce soupçon de NP dans $L_{K^*\bar{K}^*}$ pourrait être affiné avec une estimation précise de la rupture de U-spin dans les facteurs de forme impliqués, car ils sont à l'origine des incertitudes théoriques de la prédiction SM et leur corrélation n'est pas connue précisément. Une comparaison des informations théoriques et expérimentales sur les polarisations dans $B_s \to K^*\phi$ et $B_d \to K^*\phi$ pourrait également être utile pour vérifier si une tension similaire apparaît. Des informations complémentaires pourraient également être obtenues à partir des modes manchots à médiation pseudoscalaire-vecteur et pseudoscalaire-pseudoscalaire ($K^0\bar{K}^{*0}$ et $K^0\bar{K}^0$). De plus, si la même source de NP est responsable de la suppression de $b \to sq\bar{q}$ par rapport à $b \to dq\bar{q}$ et de $b \to s\mu^+\mu^-$ par rapport à $b \to se^+e^-$, il serait certainement intéressant de réaliser une étude approfondie des modes $b \to d\ell^+\ell^-$ par rapport aux modes $b \to s\ell^+\ell^-$, ce qui devrait être accessible avec davantage de données provenant des expériences LHCb et Belle II.

Perspective

Nous conclurons enfin ce manuscrit en donnant une perspective des directions que ces anomalies pourraient prendre dans le futur, des nouveaux résultats qui pourraient aider à les démêler, et des études contribuant à rendre cette image encore plus robuste.

Après ces illustrations des différentes voies d'exploitation des anomalies du quark b actuellement observées, il convient de discuter des problèmes qui pourraient devenir pertinents dans un avenir proche. La question de la signification statistique des anomalies et leur interprétation sont encore des questions relativement ouvertes qui pourraient changer la donne dans les prochaines années. Il est important de clarifier les critères selon lesquels l'hypothèse SM sera considérée statistiquement comme incapable d'expliquer les données sur la base de mesures indirectes, car il n'existe pas de consensus clair sur ce sujet pour le moment. Une autre étape importante liée au traitement statistique pourrait être la prise en compte correcte des non-gaussianités et des corrélations dans les données expérimentales et les prédictions théoriques, qui sont souvent négligées de nos jours mais pourraient devenir importantes à mesure que des données plus précises sont disponibles. Idéalement, les collaborations devraient fournir toute la vraisemblance obtenue par leurs mesures et les analyses d'ajustement global devraient pouvoir prendre en compte ces éléments d'information ainsi qu'évaluer l'impact du traitement des incertitudes systématiques.

Dans un avenir proche, de nouvelles informations devraient être disponibles : LHCb continuera à recueillir des données et à explorer ces transitions, CMS devrait bientôt publier ses données dites "parquées" et Belle II fournira de nouvelles informations sur plusieurs modes, y compris les modes $b \to s\ell^+\ell^-$ et $b \to c\ell\bar{\nu}$ mais aussi les modes neutrinos $b \to s\nu\bar{\nu}$ avec des systématiques complètement différentes, en particulier pour les mesures de l'universalité de la saveur leptonique en raison de ses méthodes d'identification des leptons qui sont totalement différentes de celles de LHCb. Ces données supplémentaires devraient être assorties d'une amélioration des incertitudes théoriques, car la précision expérimentale future nécessitera des déterminations plus précises des facteurs de forme, une meilleure compréhension des corrections hadroniques non factorisables et des corrections électromagnétiques. En ce qui concerne les facteurs de forme, nous pouvons nous attendre à de nouvelles prédictions théoriques plus précises de la QCD sur reseaux, qui continuent d'évoluer en raison de la croissance de la puissance de calcul. En outre, une meilleure compréhension de la systématique des règles de somme sur le cône de lumière, qui sont loin d'être aussi bien comprises que les incertitudes de la QCD sur reseaux, sera nécessaire. En outre, les contributions de la boucle de charme doivent encore être étudiées plus en détail, une amélioration du calcul de cet effet est essentielle pour réduire ses incertitudes et évaluer plus précisément les systématiques attachées aux calculs : c'est une question pour le calcul utilisant les règles de la somme du cône de lumière, mais aussi pour les modèles utilisés pour extrapoler ou interpoler les résultats obtenus dans la région de grand recul à tout l'ensemble des valeurs de q^2.

Dans les années à venir, ces nouvelles informations expérimentales et théoriques devraient permettre de mieux comprendre les anomalies, par exemple en excluant certains des scénarios de NP actuellement autorisés par les données et en fournissant des contraintes sur les contributions complexes de NP violant CP. Vraisemblablement, nous devrions voir une meilleure connexion avec des modèles NP spécifiques qui peuvent expliquer ces anomalies, qui sont contraintes par des recherches directes du LHC et peuvent conduire à des connexions avec d'autres modes impliquant des désintégrations de quark de type up et des courants neutres changeant de saveur dans des leptons τ, nous permettant de nous rapprocher de la nature de ces déviations. Les liens potentiels avec d'autres anomalies de saveur (comme $(g-2)_\mu$ ou $|V_{ud}|$) devraient également être des domaines de recherche très actifs, en utilisant des modèles spécifiques ou dans des approches EFT. L'inclusion de ces nouveaux modes associés nécessite l'utilisation d'un cadre plus large que la théorie effective faible, à savoir le traitement dans le cadre de la théorie effective des champs du SM (SMEFT). Cet effort à long terme des communautés expérimentale et théorique nous aidera, nous l'espérons, à mieux comprendre la véritable nature de ces déviations, dans l'espoir d'identifier la prochaine étape à franchir, au-delà de la SM, et donc de déterminer la NP derrière les anomalies du quark b.

Bibliography

[1] S. L. Glashow. "Partial Symmetries of Weak Interactions". In: *Nucl. Phys.* 22 (1961), pp. 579–588. DOI: 10.1016/0029-5582(61)90469-2 (cit. on p. 7).

[2] Steven Weinberg. "A Model of Leptons". In: *Phys. Rev. Lett.* 19 (1967), pp. 1264–1266. DOI: 10.1103/PhysRevLett.19.1264 (cit. on p. 7).

[3] Abdus Salam. "Weak and Electromagnetic Interactions". In: *Conf. Proc. C* 680519 (1968), pp. 367–377. DOI: 10.1142/9789812795915_0034 (cit. on p. 7).

[4] Gerard 't Hooft and M. J. G. Veltman. "Regularization and Renormalization of Gauge Fields". In: *Nucl. Phys. B* 44 (1972), pp. 189–213. DOI: 10.1016/0550-3213(72)90279-9 (cit. on p. 7).

[5] Wikipedia Commons. *Standard Model of Elementary Particles*. 2020. URL: https://commons.wikimedia.org/wiki/File:Standard_Model_of_Elementary_Particles.svg (cit. on p. 8).

[6] Particle Data Group et al. "Review of Particle Physics". In: *Progress of Theoretical and Experimental Physics* 2020.8 (Aug. 2020). 083C01. ISSN: 2050-3911. DOI: 10.1093/ptep/ptaa104. eprint: https://academic.oup.com/ptep/article-pdf/2020/8/083C01/34673722/ptaa104.pdf. URL: https://doi.org/10.1093/ptep/ptaa104 (cit. on pp. 8, 10, 16, 17, 20, 22, 23, 58, 78, 82, 84, 105, 148, 151, 153, 154, 193–195, 197, 198, 206, 220).

[7] Christopher Smith. *Minimal Flavor Violation*. Sept. 2016 (cit. on pp. 9, 69, 73).

[8] Michael E. Peskin. "Beyond the standard model". In: *The 1996 European School of High-Energy Physics (formerly CERN / JINR School of Physics)*. May 1997. arXiv: hep-ph/9705479 (cit. on p. 10).

[9] Steven Weinberg. "General Theory of Broken Local Symmetries". In: *Phys. Rev. D* 7 (1973), pp. 1068–1082. DOI: 10.1103/PhysRevD.7.1068 (cit. on p. 10).

[10] Peter W. Higgs. "Broken Symmetries and the Masses of Gauge Bosons". In: *Phys. Rev. Lett.* 13 (1964). Ed. by J. C. Taylor, pp. 508–509. DOI: 10.1103/PhysRevLett.13.508 (cit. on p. 10).

[11] Peter W. Higgs. "Broken symmetries, massless particles and gauge fields". In: *Phys. Lett.* 12 (1964), pp. 132–133. DOI: 10.1016/0031-9163(64)91136-9 (cit. on p. 10).

[12] F. Englert and R. Brout. "Broken Symmetry and the Mass of Gauge Vector Mesons". In: *Phys. Rev. Lett.* 13 (1964). Ed. by J. C. Taylor, pp. 321–323. DOI: 10.1103/PhysRevLett.13.321 (cit. on p. 10).

[13] G. S. Guralnik, C. R. Hagen, and T. W. B. Kibble. "Global Conservation Laws and Massless Particles". In: *Phys. Rev. Lett.* 13 (1964). Ed. by J. C. Taylor, pp. 585–587. DOI: 10.1103/PhysRevLett.13.585 (cit. on p. 10).

[14] Peter W. Higgs. "Spontaneous Symmetry Breakdown without Massless Bosons". In: *Phys. Rev.* 145 (1966), pp. 1156–1163. DOI: 10.1103/PhysRev.145.1156 (cit. on p. 10).

[15] T. W. B. Kibble. "Symmetry breaking in nonAbelian gauge theories". In: *Phys. Rev.* 155 (1967). Ed. by J. C. Taylor, pp. 1554–1561. DOI: 10.1103/PhysRev.155.1554 (cit. on p. 10).

[16] G. Aad et al. "The ATLAS Experiment at the CERN Large Hadron Collider". In: *JINST* 3 (2008), S08003. DOI: 10.1088/1748-0221/3/08/S08003 (cit. on p. 12).

[17] S. Chatrchyan et al. "The CMS Experiment at the CERN LHC". In: *JINST* 3 (2008), S08004. DOI: 10.1088/1748-0221/3/08/S08004 (cit. on p. 12).

[18] Vardan Khachatryan et al. "Precise determination of the mass of the Higgs boson and tests of compatibility of its couplings with the standard model predictions using proton collisions at 7 and 8 TeV". In: *Eur. Phys. J. C* 75.5 (2015), p. 212. DOI: 10.1140/epjc/s10052-015-3351-7. arXiv: 1412.8662 [hep-ex] (cit. on p. 12).

[19] Johannes Haller et al. "Update of the global electroweak fit and constraints on two-Higgs-doublet models". In: *Eur. Phys. J. C* 78.8 (2018), p. 675. DOI: 10.1140/epjc/s10052-018-6131-3. arXiv: 1803.01853 [hep-ph] (cit. on p. 13).

[20] Makoto Kobayashi and Toshihide Maskawa. "CP Violation in the Renormalizable Theory of Weak Interaction". In: *Prog. Theor. Phys.* 49 (1973), pp. 652–657. DOI: 10.1143/PTP.49.652 (cit. on p. 14).

[21] Ling-Lie Chau and Wai-Yee Keung. "Comments on the Parametrization of the Kobayashi-Maskawa Matrix". In: *Phys. Rev. Lett.* 53 (1984), p. 1802. DOI: 10.1103/PhysRevLett.53.1802 (cit. on p. 14).

[22] Lincoln Wolfenstein. "Parametrization of the Kobayashi-Maskawa Matrix". In: *Phys. Rev. Lett.* 51 (1983), p. 1945. DOI: 10.1103/PhysRevLett.51.1945 (cit. on p. 15).

[23] Andrzej J. Buras, Markus E. Lautenbacher, and Gaby Ostermaier. "Waiting for the top quark mass, K+ —> pi+ neutrino anti-neutrino, B(s)0 - anti-B(s)0 mixing and CP asymmetries in B decays". In: *Phys. Rev. D* 50 (1994), pp. 3433–3446. DOI: 10.1103/PhysRevD.50.3433. arXiv: hep-ph/9403384 (cit. on p. 15).

[24] J. Charles et al. "CP violation and the CKM matrix: Assessing the impact of the asymmetric B factories". In: *Eur. Phys. J. C* 41.1 (2005), pp. 1–131. DOI: 10.1140/epjc/s2005-02169-1. arXiv: hep-ph/0406184. URL: http://ckmfitter.in2p3.fr (cit. on pp. 15, 16, 148, 213, 216, 226).

[25] C. Jarlskog. "Commutator of the Quark Mass Matrices in the Standard Electroweak Model and a Measure of Maximal CP Violation". In: *Phys. Rev. Lett.* 55 (1985), p. 1039. DOI: 10.1103/PhysRevLett.55.1039 (cit. on p. 15).

[26] Simone Bifani et al. "Review of Lepton Universality tests in B decays". In: *J. Phys.* G46.2 (2019), p. 023001. DOI: 10.1088/1361-6471/aaf5de. arXiv: 1809.06229 [hep-ex] (cit. on pp. 16, 47, 48, 50).

[27] S. L. Glashow, J. Iliopoulos, and L. Maiani. "Weak Interactions with Lepton-Hadron Symmetry". In: *Phys. Rev. D* 2 (1970), pp. 1285–1292. DOI: 10.1103/PhysRevD.2.1285 (cit. on p. 17).

[28] Gerhard Buchalla, Andrzej J. Buras, and Markus E. Lautenbacher. "Weak decays beyond leading logarithms". In: *Rev. Mod. Phys.* 68 (1996), pp. 1125–1144. DOI: 10.1103/RevModPhys.68.1125. arXiv: hep-ph/9512380 (cit. on pp. 17, 34–36, 38, 39, 49, 54).

[29] Michael E. Peskin and Daniel V. Schroeder. *An Introduction to quantum field theory*. Reading, USA: Addison-Wesley, 1995. ISBN: 978-0-201-50397-5 (cit. on pp. 19, 26, 27, 150).

[30] Andrzej J. Buras. "Weak Hamiltonian, CP violation and rare decays". In: *Les Houches Summer School in Theoretical Physics, Session 68: Probing the Standard Model of Particle Interactions*. June 1998, pp. 281–539. arXiv: hep-ph/9806471 (cit. on pp. 19, 36, 38, 39, 204).

[31] David J. Gross and Frank Wilczek. "Ultraviolet Behavior of Nonabelian Gauge Theories". In: *Phys. Rev. Lett.* 30 (1973). Ed. by J. C. Taylor, pp. 1343–1346. DOI: 10.1103/PhysRevLett.30.1343 (cit. on p. 20).

[32] H. David Politzer. "Reliable Perturbative Results for Strong Interactions?" In: *Phys. Rev. Lett.* 30 (1973). Ed. by J. C. Taylor, pp. 1346–1349. DOI: 10.1103/PhysRevLett.30.1346 (cit. on p. 20).

[33] Yoshiaki Koma and Miho Koma. "Spin-dependent potentials from lattice QCD". In: *Nucl. Phys. B* 769 (2007), pp. 79–107. DOI: 10.1016/j.nuclphysb.2007.01.033. arXiv: hep-lat/0609078 (cit. on p. 22).

[34] Kenneth G. Wilson. "Confinement of Quarks". In: *Phys. Rev. D* 10 (1974). Ed. by J. C. Taylor, pp. 2445–2459. DOI: 10.1103/PhysRevD.10.2445 (cit. on p. 21).

[35] Alexander Khodjamirian. *Hadron Form Factors: From Basic Phenomenology to QCD Sum Rules*. Boca Raton, FL, USA: CRC Press, Taylor & Francis Group, 2020. ISBN: 978-1-138-30675-2, 978-1-315-14200-5 (cit. on pp. 22, 26–28).

[36] M. Beneke et al. "QCD Factorization for $B \to \pi\pi$ Fecays: Strong Phases and CP Violation in the Heavy Quark Limit". In: *Phys. Rev. Lett.* 83 (1999), pp. 1914–1917. DOI: 10.1103/PhysRevLett.83.1914. arXiv: hep-ph/9905312 (cit. on pp. 23, 51).

[37] Martin Beneke and Matthias Neubert. "QCD factorization for B —> PP and B —> PV decays". In: *Nucl. Phys. B* 675 (2003), pp. 333–415. DOI: 10.1016/j.nuclphysb.2003.09.026. arXiv: hep-ph/0308039 (cit. on pp. 23, 52, 53, 217, 218, 225).

[38] M. Beneke and T. Feldmann. "Symmetry breaking corrections to heavy to light B meson form-factors at large recoil". In: *Nucl. Phys. B* 592 (2001), pp. 3–34. DOI: 10.1016/S0550-3213(00)00585-X. arXiv: hep-ph/0008255 (cit. on pp. 24, 46, 79, 91, 124).

[39] Nico Gubernari, Ahmet Kokulu, and Danny van Dyk. "$B \to P$ and $B \to V$ Form Factors from B-Meson Light-Cone Sum Rules beyond Leading Twist". In: *JHEP* 01 (2019), p. 150. DOI: 10.1007/JHEP01(2019)150. arXiv: 1811.00983 [hep-ph] (cit. on pp. 24, 44, 64, 79, 147, 148, 174).

[40] Thorsten Feldmann and Matthew W. Y. Yip. "Form factors for $\Lambda_b \to \Lambda$ transitions in the soft-collinear effective theory". In: *Phys. Rev. D* 85 (2012). [Erratum: Phys.Rev.D 86, 079901 (2012)], p. 014035. DOI: 10.1103/PhysRevD.85.014035. arXiv: 1111.1844 [hep-ph] (cit. on pp. 26, 46, 64, 109, 111, 115–117, 122–124).

[41] William Rarita and Julian Schwinger. "On a theory of particles with half integral spin". In: *Phys. Rev.* 60 (1941), p. 61. DOI: 10.1103/PhysRev.60.61 (cit. on pp. 26, 113).

[42] Lonnie Mott and Winston Roberts. "Rare dileptonic decays of Λ_b in a quark model". In: *Int. J. Mod. Phys. A* 27 (2012), p. 1250016. DOI: 10.1142/S0217751X12500169. arXiv: 1108.6129 [nucl-th] (cit. on pp. 26, 115–117, 123–128, 131, 142).

[43] J. D. Bjorken. "Asymptotic Sum Rules at Infinite Momentum". In: *Phys. Rev.* 179 (1969), pp. 1547–1553. DOI: 10.1103/PhysRev.179.1547 (cit. on p. 27).

[44] Richard A. Brandt and Giuliano Preparata. "Operator product expansions near the light cone". In: *Nucl. Phys. B* 27 (1971), pp. 541–567. DOI: 10.1016/0550-3213(71)90265-3 (cit. on p. 27).

[45] Y. Frishman. "Scale invariance and current commutators near the light cone". In: *Phys. Rev. Lett.* 25 (1970), pp. 966–969. DOI: 10.1103/PhysRevLett.25.966 (cit. on p. 27).

[46] Y. Frishman. "Operator products at almost light like distances". In: *Annals Phys.* 66 (1971), pp. 373–389. DOI: 10.1016/0003-4916(71)90195-3 (cit. on p. 27).

[47] Patricia Ball et al. "Higher twist distribution amplitudes of vector mesons in QCD: Formalism and twist - three distributions". In: *Nucl. Phys. B* 529 (1998), pp. 323–382. DOI: 10.1016/S0550-3213(98)00356-3. arXiv: hep-ph/9802299 (cit. on pp. 27, 28).

[48] Patricia Ball and Vladimir M. Braun. "Handbook of higher twist distribution amplitudes of vector mesons in QCD". In: *3rd Workshop on Continuous Advances in QCD (QCD 98)*. Apr. 1998. arXiv: hep-ph/9808229 (cit. on pp. 27, 28).

[49] Patricia Ball, V. M. Braun, and A. Lenz. "Higher-twist distribution amplitudes of the K meson in QCD". In: *JHEP* 05 (2006), p. 004. DOI: 10.1088/1126-6708/2006/05/004. arXiv: hep-ph/0603063 (cit. on pp. 28, 29).

[50] Patricia Ball and Vladimir M. Braun. "Higher twist distribution amplitudes of vector mesons in QCD: Twist - 4 distributions and meson mass corrections". In: *Nucl. Phys. B* 543 (1999), pp. 201–238. DOI: 10.1016/S0550-3213(99)00014-0. arXiv: hep-ph/9810475 (cit. on p. 28).

[51] Patricia Ball, V. M. Braun, and A. Lenz. "Twist-4 distribution amplitudes of the K* and phi mesons in QCD". In: *JHEP* 08 (2007), p. 090. DOI: 10.1088/1126-6708/2007/08/090. arXiv: 0707.1201 [hep-ph] (cit. on p. 28).

[52] Vladimir M. Braun et al. "Baryon distribution amplitudes in QCD". In: *Nucl. Phys. B* 553 (1999), pp. 355–426. DOI: 10.1016/S0550-3213(99)00265-5. arXiv: hep-ph/9902375 (cit. on p. 28).

[53] V. Braun et al. "Higher twist distribution amplitudes of the nucleon in QCD". In: *Nucl. Phys. B* 589 (2000). [Erratum: Nucl.Phys.B 607, 433–433 (2001)], pp. 381–409. DOI: 10.1016/S0550-3213(00)00516-2. arXiv: hep-ph/0007279 (cit. on p. 28).

[54] V. M. Braun, G. P. Korchemsky, and Dieter Müller. "The Uses of conformal symmetry in QCD". In: *Prog. Part. Nucl. Phys.* 51 (2003), pp. 311–398. DOI: 10.1016/S0146-6410(03)90004-4. arXiv: hep-ph/0306057 (cit. on p. 28).

[55] Gunnar S. Bali et al. "Light-cone distribution amplitudes of pseudoscalar mesons from lattice QCD". In: *JHEP* 08 (2019). [Addendum: JHEP 11, 037 (2020)], p. 065. DOI: 10.1007/JHEP08(2019)065. arXiv: 1903.08038 [hep-lat] (cit. on pp. 28, 29).

[56] Nathan Isgur et al. "Semileptonic B and D Decays in the Quark Model". In: *Phys. Rev. D* 39 (1989), pp. 799–818. DOI: 10.1103/PhysRevD.39.799 (cit. on p. 28).

[57] N. Barik and P. C. Dash. "Exclusive semileptonic decay of D and B mesons in the independent quark model". In: *Phys. Rev. D* 53 (1996), pp. 1366–1377. DOI: 10.1103/PhysRevD.53.1366 (cit. on p. 28).

[58] Daryl Scora and Nathan Isgur. "Semileptonic meson decays in the quark model: An update". In: *Phys. Rev. D* 52 (1995), pp. 2783–2812. DOI: 10.1103/PhysRevD.52.2783. arXiv: hep-ph/9503486 (cit. on p. 28).

[59] S. Aoki et al. "FLAG Review 2019: Flavour Lattice Averaging Group (FLAG)". In: *Eur. Phys. J. C* 80.2 (2020), p. 113. DOI: 10.1140/epjc/s10052-019-7354-7. arXiv: 1902.08191 [hep-lat] (cit. on pp. 29, 213, 221, 226).

[60] Laurent Lellouch et al., eds. *Modern perspectives in lattice QCD: Quantum field theory and high performance computing. Proceedings, International School, 93rd Session, Les Houches, France, August 3-28, 2009*. 2011 (cit. on p. 29).

[61] Thomas DeGrand. "Lattice methods for students at a formal TASI". In: *Theoretical Advanced Study Institute in Elementary Particle Physics: The Many Dimensions of Quantum Field Theory*. July 2019. arXiv: 1907.02988 [hep-th] (cit. on p. 29).

[62] Christof Gattringer and Christian B. Lang. *Quantum chromodynamics on the lattice*. Vol. 788. Berlin: Springer, 2010. ISBN: 978-3-642-01849-7, 978-3-642-01850-3. DOI: 10.1007/978-3-642-01850-3 (cit. on p. 29).

[63] Mikhail A. Shifman, A. I. Vainshtein, and Valentin I. Zakharov. "QCD and Resonance Physics. Theoretical Foundations". In: *Nucl. Phys. B* 147 (1979), pp. 385–447. DOI: 10.1016/0550-3213(79)90022-1 (cit. on p. 30).

[64] V. L. Chernyak and I. R. Zhitnitsky. "B meson exclusive decays into baryons". In: *Nucl. Phys. B* 345 (1990), pp. 137–172. DOI: 10.1016/0550-3213(90)90612-H (cit. on p. 30).

[65] I. I. Balitsky, Vladimir M. Braun, and A. V. Kolesnichenko. "Radiative Decay Sigma+ —> p gamma in Quantum Chromodynamics". In: *Nucl. Phys. B* 312 (1989), pp. 509–550. DOI: 10.1016/0550-3213(89)90570-1 (cit. on p. 30).

[66] Vladimir M. Braun and I. E. Filyanov. "QCD Sum Rules in Exclusive Kinematics and Pion Wave Function". In: *Z. Phys. C* 44 (1989), p. 157. DOI: 10.1007/BF01548594 (cit. on p. 30).

[67] Fulvia De Fazio, Thorsten Feldmann, and Tobias Hurth. "Light-cone sum rules in soft-collinear effective theory". In: *Nucl. Phys. B* 733 (2006). [Erratum: Nucl.Phys.B 800, 405 (2008)], pp. 1–30. DOI: 10.1016/j.nuclphysb.2008.03.022. arXiv: hep-ph/0504088 (cit. on pp. 30, 46).

[68] Fulvia De Fazio, Thorsten Feldmann, and Tobias Hurth. "SCET sum rules for B —> P and B —> V transition form factors". In: *JHEP* 02 (2008), p. 031. DOI: 10.1088/1126-6708/2008/02/031. arXiv: 0711.3999 [hep-ph] (cit. on pp. 30, 46).

[69] J. Gasser and H. Leutwyler. "Chiral Perturbation Theory to One Loop". In: *Annals Phys.* 158 (1984), p. 142. DOI: 10.1016/0003-4916(84)90242-2 (cit. on p. 30).

[70] Estia Eichten and Brian Russell Hill. "An Effective Field Theory for the Calculation of Matrix Elements Involving Heavy Quarks". In: *Phys. Lett. B* 234 (1990), pp. 511–516. DOI: 10.1016/0370-2693(90)92049-0 (cit. on p. 30).

[71] Howard Georgi. "An Effective Field Theory for Heavy Quarks at Low-energies". In: *Phys. Lett. B* 240 (1990), pp. 447–450. DOI: 10.1016/0370-2693(90)91128-X (cit. on p. 30).

[72] Christian W. Bauer et al. "Hard scattering factorization from effective field theory". In: *Phys. Rev. D* 66 (2002), p. 014017. DOI: 10.1103/PhysRevD.66.014017. arXiv: hep-ph/0202088 (cit. on pp. 30, 44).

[73] Christian W. Bauer, Dan Pirjol, and Iain W. Stewart. "Soft collinear factorization in effective field theory". In: *Phys. Rev. D* 65 (2002), p. 054022. DOI: 10.1103/PhysRevD.65.054022. arXiv: hep-ph/0109045 (cit. on pp. 30, 44).

[74] Christian W. Bauer and Iain W. Stewart. "Invariant operators in collinear effective theory". In: *Phys. Lett. B* 516 (2001), pp. 134–142. DOI: 10.1016/S0370-2693(01)00902-9. arXiv: hep-ph/0107001 (cit. on pp. 30, 44).

[75] Christian W. Bauer et al. "An Effective field theory for collinear and soft gluons: Heavy to light decays". In: *Phys. Rev. D* 63 (2001), p. 114020. DOI: 10.1103/PhysRevD.63.114020. arXiv: hep-ph/0011336 (cit. on pp. 30, 44).

[76] Christian W. Bauer, Sean Fleming, and Michael E. Luke. "Summing Sudakov logarithms in B —> X(s gamma) in effective field theory". In: *Phys. Rev. D* 63 (2000), p. 014006. DOI: 10.1103/PhysRevD.63.014006. arXiv: hep-ph/0005275 (cit. on pp. 30, 44).

[77] Joseph Polchinski. "Effective field theory and the Fermi surface". In: *Theoretical Advanced Study Institute (TASI 92): From Black Holes and Strings to Particles*. June 1992. arXiv: hep-th/9210046 (cit. on p. 33).

[78] Matthias Neubert. "Effective field theory and heavy quark physics". In: *Theoretical Advanced Study Institute in Elementary Particle Physics: Physics in $D \geqq 4$*. Dec. 2005. DOI: 10.1142/9789812773579_0004. arXiv: hep-ph/0512222 (cit. on pp. 33, 43).

[79] Benjamin Grinstein, Roxanne P. Springer, and Mark B. Wise. "Effective Hamiltonian for Weak Radiative B Meson Decay". In: *Phys. Lett. B* 202 (1988), pp. 138–144. DOI: 10.1016/0370-2693(88)90868-4 (cit. on p. 34).

[80] Matthias Neubert. "Renormalization Theory and Effective Field Theories". In: (Jan. 2019). Ed. by Sacha Davidson et al. DOI: 10.1093/oso/9780198855743.003.0001. arXiv: 1901.06573 [hep-ph] (cit. on p. 36).

[81] Andrzej J. Buras, Katrin Gemmler, and Gino Isidori. "Quark flavour mixing with right-handed currents: an effective theory approach". In: *Nucl. Phys. B* 843 (2011), pp. 107–142. DOI: 10.1016/j.nuclphysb.2010.09.021. arXiv: 1007.1993 [hep-ph] (cit. on p. 37).

[82] Monika Blanke et al. "Impact of polarization observables and $B_c \to \tau\nu$ on new physics explanations of the $b \to c\tau\nu$ anomaly". In: *Phys. Rev. D* 99.7 (2019), p. 075006. DOI: 10.1103/PhysRevD.99.075006. arXiv: 1811.09603 [hep-ph] (cit. on pp. 37, 61, 63, 72, 168, 174).

[83] Monika Blanke et al. "Addendum to Impact of polarization observables and $B_c \to \tau\nu$ on new physics explanations of the $b \to c\tau\nu$ anomaly"". In: (May 2019). [Addendum: Phys.Rev.D 100, 035035 (2019)]. DOI: 10.1103/PhysRevD.100.035035. arXiv: 1905.08253 [hep-ph] (cit. on pp. 37, 61–63, 72, 168, 174).

[84] Martín González-Alonso, Jorge Martin Camalich, and Kin Mimouni. "Renormalization-group evolution of new physics contributions to (semi)leptonic meson decays". In: *Phys. Lett. B* 772 (2017), pp. 777–785. DOI: 10.1016/j.physletb.2017.07.003. arXiv: 1706.00410 [hep-ph] (cit. on pp. 37, 174).

[85] Andrzej J. Buras, Paolo Gambino, and Ulrich A. Haisch. "Electroweak penguin contributions to nonleptonic Delta F = 1 decays at NNLO". In: *Nucl. Phys. B* 570 (2000), pp. 117–154. DOI: 10.1016/S0550-3213(99)00810-X. arXiv: hep-ph/9911250 (cit. on p. 39).

[86] M. Beneke et al. "QCD factorization in B —> pi K, pi pi decays and extraction of Wolfenstein parameters". In: *Nucl. Phys. B* 606 (2001), pp. 245–321. DOI: 10.1016/S0550-3213(01)00251-6. arXiv: hep-ph/0104110 (cit. on pp. 39, 51, 214, 218, 220, 226).

[87] Sebastien Descotes-Genon et al. "Optimizing the basis of $B \to K^*ll$ observables in the full kinematic range". In: *JHEP* 05 (2013), p. 137. DOI: 10.1007/JHEP05(2013)137. arXiv: 1303.5794 [hep-ph] (cit. on pp. 39, 65, 123, 167, 213).

[88] Thomas Blake, Gaia Lanfranchi, and David M. Straub. "Rare B Decays as Tests of the Standard Model". In: *Prog. Part. Nucl. Phys.* 92 (2017), pp. 50–91. DOI: 10.1016/j.ppnp.2016.10.001. arXiv: 1606.00916 [hep-ph] (cit. on pp. 39, 40, 48).

[89] Alexander L. Kagan. "Right-handed currents, CP violation, and B —> VV". In: (July 2004). arXiv: hep-ph/0407076 (cit. on pp. 40, 53, 214).

[90] Matthias Neubert. "Heavy quark symmetry". In: *Phys. Rept.* 245 (1994), pp. 259–396. DOI: 10.1016/0370-1573(94)90091-4. arXiv: hep-ph/9306320 (cit. on p. 43).

[91] Nathan Isgur and Mark B. Wise. "Weak Decays of Heavy Mesons in the Static Quark Approximation". In: *Phys. Lett. B* 232 (1989), pp. 113–117. DOI: 10.1016/0370-2693(89)90566-2 (cit. on pp. 43, 57, 174).

[92] Nathan Isgur and Mark B. Wise. "WEAK TRANSITION FORM-FACTORS BETWEEN HEAVY MESONS". In: *Phys. Lett. B* 237 (1990), pp. 527–530. DOI: 10.1016/0370-2693(90)91219-2 (cit. on pp. 43, 57, 174).

[93] Matthias Neubert and Volker Rieckert. "New approach to the universal form-factors in decays of heavy mesons". In: *Nucl. Phys. B* 382 (1992), pp. 97–119. DOI: 10.1016/0550-3213(92)90080-U (cit. on p. 43).

[94] Nathan Isgur and Mark B. Wise. "Relationship Between Form-factors in Semileptonic $\bar{B}$ and D Decays and Exclusive Rare $\bar{B}$ Meson Decays". In: *Phys. Rev. D* 42 (1990), pp. 2388–2391. DOI: 10.1103/PhysRevD.42.2388 (cit. on p. 43).

[95] Christoph Bobeth et al. "The Decay $B \to K\ell^+\ell^-$ at Low Hadronic Recoil and Model-Independent $\Delta B = 1$ Constraints". In: *JHEP* 01 (2012), p. 107. DOI: 10.1007/JHEP01(2012)107. arXiv: 1111.2558 [hep-ph] (cit. on p. 43).

[96] Alexander Khodjamirian and Aleksey V. Rusov. "$B_s \to K\ell\nu_\ell$ and $B_{(s)} \to \pi(K)\ell^+\ell^-$ decays at large recoil and CKM matrix elements". In: *JHEP* 08 (2017), p. 112. DOI: 10.1007/JHEP08(2017)112. arXiv: 1703.04765 [hep-ph] (cit. on pp. 44, 64, 147).

[97] Benjamin Grinstein and Dan Pirjol. "Exclusive rare $B \to K^*\ell^+\ell^-$ decays at low recoil: Controlling the long-distance effects". In: *Phys. Rev. D* 70 (2004), p. 114005. DOI: 10.1103/PhysRevD.70.114005. arXiv: hep-ph/0404250 (cit. on pp. 43, 49, 81).

[98] Christoph Bobeth, Gudrun Hiller, and Danny van Dyk. "The Benefits of $\bar{B}- > \bar{K}^*l^+l^-$ Decays at Low Recoil". In: *JHEP* 07 (2010), p. 098. DOI: 10.1007/JHEP07(2010)098. arXiv: 1006.5013 [hep-ph] (cit. on p. 43).

[99] Joanne L. Hewett et al., eds. *The Discovery potential of a Super B Factory. Proceedings, SLAC Workshops, Stanford, USA, 2003*. Dec. 2004. arXiv: hep-ph/0503261 (cit. on p. 43).

[100] Benjamin Grinstein and Dan Pirjol. "Symmetry breaking corrections to heavy meson form-factor relations". In: *Phys. Lett. B* 533 (2002), pp. 8–16. DOI: 10.1016/S0370-2693(02)01601-5. arXiv: hep-ph/0201298 (cit. on p. 43).

[101] Michael J. Dugan and Benjamin Grinstein. "QCD basis for factorization in decays of heavy mesons". In: *Phys. Lett. B* 255 (1991), pp. 583–588. DOI: 10.1016/0370-2693(91)90271-Q (cit. on p. 44).

[102] J. Charles et al. "Heavy to light form-factors in the heavy mass to large energy limit of QCD". In: *Phys. Rev. D* 60 (1999), p. 014001. DOI: 10.1103/PhysRevD.60.014001. arXiv: hep-ph/9812358 (cit. on pp. 44, 46).

[103] Christopher Balzereit, Thomas Mannel, and Wolfgang Kilian. "Evolution of the light cone distribution function for a heavy quark". In: *Phys. Rev. D* 58 (1998), p. 114029. DOI: 10.1103/PhysRevD.58.114029. arXiv: hep-ph/9805297 (cit. on p. 44).

[104] Ugo Aglietti and Giulia Ricciardi. "Matching of the shape function". In: *Phys. Lett. B* 466 (1999), p. 313. DOI: 10.1016/S0370-2693(99)01103-X. arXiv: hep-ph/9907501 (cit. on p. 44).

[105] Bjorn O. Lange and Matthias Neubert. "Factorization and the soft overlap contribution to heavy to light form-factors". In: *Nucl. Phys. B* 690 (2004). [Erratum: Nucl.Phys.B 723, 201–202 (2005)], pp. 249–278. DOI: 10.1016/j.nuclphysb.2005.06.019. arXiv: hep-ph/0311345 (cit. on p. 44).

[106] M. Beneke et al. "Soft collinear effective theory and heavy to light currents beyond leading power". In: *Nucl. Phys. B* 643 (2002), pp. 431–476. DOI: 10.1016/S0550-3213(02)00687-9. arXiv: hep-ph/0206152 (cit. on pp. 44, 46).

[107] Richard J. Hill and Matthias Neubert. "Spectator interactions in soft collinear effective theory". In: *Nucl. Phys. B* 657 (2003), pp. 229–256. DOI: 10.1016/S0550-3213(03)00116-0. arXiv: hep-ph/0211018 (cit. on p. 44).

[108] Sébastien Descotes-Genon et al. "Global analysis of $b \to s\ell\ell$ anomalies". In: *JHEP* 06 (2016), p. 092. DOI: 10.1007/JHEP06(2016)092. arXiv: 1510.04239 [hep-ph] (cit. on pp. 47, 50, 77, 80, 81, 85).

[109] Nico Gubernari, Danny van Dyk, and Javier Virto. "Non-local matrix elements in $B_{(s)} \to \{K^{(*)}, \phi\}\ell^+\ell^-$". In: *JHEP* 02 (2021), p. 088. DOI: 10.1007/JHEP02(2021)088. arXiv: 2011.09813 [hep-ph] (cit. on pp. 47, 49, 50, 63, 64, 79–81, 90, 124).

[110] A. J. Buras et al. "Theoretical uncertainties and phenomenological aspects of B —> X(s) gamma decay". In: *Nucl. Phys. B* 424 (1994), pp. 374–398. DOI: 10.1016/0550-3213(94)90299-2. arXiv: hep-ph/9311345 (cit. on p. 49).

[111] M. Beneke, T. Feldmann, and D. Seidel. "Systematic approach to exclusive $B \to Vl^+l^-$, $V\gamma$ decays". In: *Nucl. Phys. B* 612 (2001), pp. 25–58. DOI: 10.1016/S0550-3213(01)00366-2. arXiv: hep-ph/0106067 (cit. on pp. 49, 80, 124).

[112] Christoph Bobeth et al. "Long-distance effects in $B \to K^*\ell\ell$ from analyticity". In: *Eur. Phys. J. C* 78.6 (2018), p. 451. DOI: 10.1140/epjc/s10052-018-5918-6. arXiv: 1707.07305 [hep-ph] (cit. on pp. 49, 50, 63, 80, 90, 91, 111, 124).

[113] M. Beylich, G. Buchalla, and T. Feldmann. "Theory of $B \to K^{(*)}\ell^+\ell^-$ decays at high q^2: OPE and quark-hadron duality". In: *Eur. Phys. J. C* 71 (2011), p. 1635. DOI: 10.1140/epjc/s10052-011-1635-0. arXiv: 1101.5118 [hep-ph] (cit. on pp. 50, 81, 124).

[114] James Lyon and Roman Zwicky. "Resonances gone topsy turvy - the charm of QCD or new physics in $b \to s\ell^+\ell^-$?" In: (June 2014). arXiv: 1406.0566 [hep-ph] (cit. on pp. 50, 82, 124).

[115] A. Khodjamirian et al. "Charm-loop effect in $B \to K^{(*)}\ell^+\ell^-$ and $B \to K^*\gamma$". In: *JHEP* 09 (2010), p. 089. DOI: 10.1007/JHEP09(2010)089. arXiv: 1006.4945 [hep-ph] (cit. on pp. 50, 63, 79–81, 91, 111, 124).

[116] A. Khodjamirian, Th. Mannel, and Y. M. Wang. "$B \to K\ell^+\ell^-$ decay at large hadronic recoil". In: *JHEP* 02 (2013), p. 010. DOI: 10.1007/JHEP02(2013)010. arXiv: 1211.0234 [hep-ph] (cit. on pp. 50, 63, 81, 111, 124, 159).

[117] Marcin Chrzaszcz et al. "Prospects for disentangling long- and short-distance effects in the decays $B \to K^*\mu^+\mu^-$". In: *JHEP* 10 (2019), p. 236. DOI: 10.1007/JHEP10(2019)236. arXiv: 1805.06378 [hep-ph] (cit. on p. 50).

[118] Nicola Serra, Rafael Silva Coutinho, and Danny van Dyk. "Measuring the breaking of lepton flavor universality in $B \to K^*\ell^+\ell^-$". In: *Phys. Rev. D* 95.3 (2017), p. 035029. DOI: 10.1103/PhysRevD.95.035029. arXiv: 1610.08761 [hep-ph] (cit. on p. 50).

[119] T. Hurth, F. Mahmoudi, and S. Neshatpour. "Implications of the new LHCb angular analysis of $B \to K^* \mu^+ \mu^-$: Hadronic effects or new physics?" In: *Phys. Rev. D* 102.5 (2020), p. 055001. DOI: 10.1103/PhysRevD.102.055001. arXiv: 2006.04213 [hep-ph] (cit. on pp. 50, 80, 89).

[120] A. Arbey et al. "Update on the $b \to s$ anomalies". In: *Phys. Rev. D* 100.1 (2019), p. 015045. DOI: 10.1103/PhysRevD.100.015045. arXiv: 1904.08399 [hep-ph] (cit. on pp. 50, 155, 203).

[121] Tobias Hurth et al. "New global fits to $b \to s$ data with all relevant parameters". In: *Nucl. Part. Phys. Proc.* 303-305 (2018). Ed. by Giulia Ricciardi et al., pp. 2–7. DOI: 10.1016/j.nuclphysbps.2019.03.002. arXiv: 1812.07602 [hep-ph] (cit. on p. 50).

[122] T. Hurth et al. "Lepton nonuniversality in exclusive $b \to s\ell\ell$ decays". In: *Phys. Rev. D* 96.9 (2017), p. 095034. DOI: 10.1103/PhysRevD.96.095034. arXiv: 1705.06274 [hep-ph] (cit. on p. 50).

[123] V. G. Chobanova et al. "Large hadronic power corrections or new physics in the rare decay $B \to K^* \mu^+ \mu^-$?" In: *JHEP* 07 (2017), p. 025. DOI: 10.1007/JHEP07(2017)025. arXiv: 1702.02234 [hep-ph] (cit. on pp. 50, 80, 89).

[124] T. Hurth, F. Mahmoudi, and S. Neshatpour. "Global fits to $b \to s\ell\ell$ data and signs for lepton non-universality". In: *JHEP* 12 (2014), p. 053. DOI: 10.1007/JHEP12(2014)053. arXiv: 1410.4545 [hep-ph] (cit. on p. 50).

[125] Marco Ciuchini et al. "Hadronic uncertainties in semileptonic $B \to K^* \mu^+ \mu^-$ decays". In: *PoS* BEAUTY2018 (2018). Ed. by Robert Fleischer et al., p. 044. DOI: 10.22323/1.326.0044. arXiv: 1809.03789 [hep-ph] (cit. on p. 50).

[126] Marco Ciuchini et al. "On Flavourful Easter eggs for New Physics hunger and Lepton Flavour Universality violation". In: *Eur. Phys. J. C* 77.10 (2017), p. 688. DOI: 10.1140/epjc/s10052-017-5270-2. arXiv: 1704.05447 [hep-ph] (cit. on pp. 50, 124).

[127] Marco Ciuchini et al. "$B \to K^* \ell^+ \ell^-$ decays at large recoil in the Standard Model: a theoretical reappraisal". In: *JHEP* 06 (2016), p. 116. DOI: 10.1007/JHEP06(2016)116. arXiv: 1512.07157 [hep-ph] (cit. on pp. 50, 80, 89).

[128] Jason Aebischer et al. "B-decay discrepancies after Moriond 2019". In: *Eur. Phys. J. C* 80.3 (2020), p. 252. DOI: 10.1140/epjc/s10052-020-7817-x. arXiv: 1903.10434 [hep-ph] (cit. on pp. 50, 93, 203).

[129] Wolfgang Altmannshofer et al. "Status of the $B \to K^* \mu^+ \mu^-$ anomaly after Moriond 2017". In: *Eur. Phys. J. C* 77.6 (2017), p. 377. DOI: 10.1140/epjc/s10052-017-4952-0. arXiv: 1703.09189 [hep-ph] (cit. on p. 50).

[130] Wolfgang Altmannshofer and David M. Straub. "Implications of $b \to s$ measurements". In: *50th Rencontres de Moriond on EW Interactions and Unified Theories*. Mar. 2015. arXiv: 1503.06199 [hep-ph] (cit. on p. 50).

[131] Wolfgang Altmannshofer and David M. Straub. "New physics in $b \to s$ transitions after LHC run 1". In: *Eur. Phys. J. C* 75.8 (2015), p. 382. DOI: 10.1140/epjc/s10052-015-3602-7. arXiv: 1411.3161 [hep-ph] (cit. on p. 50).

[132] Marcel Algueró et al. "Emerging patterns of New Physics with and without Lepton Flavour Universal contributions". In: *Eur. Phys. J. C* 79.8 (2019). [Addendum: Eur.Phys.J.C 80, 511 (2020)], p. 714. DOI: 10.1140/epjc/s10052-019-7216-3. arXiv: 1903.09578 [hep-ph] (cit. on pp. 50, 77, 85, 87–91, 154, 231).

[133] Marcel Algueró et al. "What R_K and Q_5 can tell us about New Physics in $b \to s\ell\ell$ transitions?" In: *JHEP* 07 (2019), p. 096. DOI: 10.1007/JHEP07(2019)096. arXiv: 1902.04900 [hep-ph] (cit. on pp. 50, 86, 88).

[134] Marcel Algueró et al. "Are we overlooking lepton flavour universal new physics in $b \to s\ell\ell$?" In: *Phys. Rev. D* 99.7 (2019), p. 075017. DOI: 10.1103/PhysRevD.99.075017. arXiv: 1809.08447 [hep-ph] (cit. on pp. 50, 77, 85–89).

[135] Bernat Capdevila et al. "Patterns of New Physics in $b \to s\ell^+\ell^-$ transitions in the light of recent data". In: *JHEP* 01 (2018), p. 093. DOI: 10.1007/JHEP01(2018)093. arXiv: 1704.05340 [hep-ph] (cit. on pp. 50, 77, 78, 85, 88).

[136] Bernat Capdevila et al. "Assessing lepton-flavour non-universality from $B \to K^* \ell\ell$ angular analyses". In: *JHEP* 10 (2016), p. 075. DOI: 10.1007/JHEP10(2016)075. arXiv: 1605.03156 [hep-ph] (cit. on pp. 50, 65).

[137] Sébastien Descotes-Genon et al. "On the impact of power corrections in the prediction of $B \to K^* \mu^+ \mu^-$ observables". In: *JHEP* 12 (2014), p. 125. DOI: 10.1007/JHEP12(2014)125. arXiv: 1407.8526 [hep-ph] (cit. on pp. 50, 79, 80).

[138] M. Beneke et al. "QCD factorization for exclusive, nonleptonic B meson decays: General arguments and the case of heavy light final states". In: *Nucl. Phys. B* 591 (2000), pp. 313–418. DOI: 10.1016/S0550-3213(00)00559-9. arXiv: hep-ph/0006124 (cit. on pp. 51, 52).

[139] Martin Beneke, Johannes Rohrer, and Deshan Yang. "Branching fractions, polarisation and asymmetries of B —> VV decays". In: *Nucl. Phys. B* 774 (2007), pp. 64–101. DOI: 10.1016/j.nuclphysb.2007.03.020. arXiv: hep-ph/0612290 (cit. on pp. 51, 53, 54, 213, 217, 218, 225).

[140] N. Cabibbo and L. Maiani. "Two-Body Decays of Charmed Mesons". In: *Phys. Lett. B* 73 (1978). [Erratum: Phys.Lett.B 76, 663 (1978)], p. 418. DOI: 10.1016/0370-2693(78)90754-2 (cit. on p. 51).

[141] Dotcho Fakirov and Berthold Stech. "F and D Decays". In: *Nucl. Phys. B* 133 (1978), pp. 315–326. DOI: 10.1016/0550-3213(78)90306-1 (cit. on p. 51).

[142] A. V. Efremov and A. V. Radyushkin. "Factorization and Asymptotical Behavior of Pion Form-Factor in QCD". In: *Phys. Lett. B* 94 (1980), pp. 245–250. DOI: 10.1016/0370-2693(80)90869-2 (cit. on p. 51).

[143] G. Peter Lepage and Stanley J. Brodsky. "Exclusive Processes in Perturbative Quantum Chromodynamics". In: *Phys. Rev. D* 22 (1980), p. 2157. DOI: 10.1103/PhysRevD.22.2157 (cit. on p. 51).

[144] Guido Bell et al. "Two-loop non-leptonic penguin amplitude in QCD factorization". In: *JHEP* 04 (2020), p. 055. DOI: 10.1007/JHEP04(2020)055. arXiv: 2002.03262 [hep-ph] (cit. on pp. 52, 53).

[145] Christian W. Bauer, Ira Z. Rothstein, and Iain W. Stewart. "SCET analysis of B —> K pi, B —> K anti-K, and B —> pi pi decays". In: *Phys. Rev. D* 74 (2006), p. 034010. DOI: 10.1103/PhysRevD.74.034010. arXiv: hep-ph/0510241 (cit. on p. 53).

[146] M. Beneke et al. "Comment on 'B —> M(1)M(2): Factorization, charming penguins, strong phases, and polarization"'. In: *Phys. Rev. D* 72 (2005), p. 098501. DOI: 10.1103/PhysRevD.72.098501. arXiv: hep-ph/0411171 (cit. on p. 53).

[147] Christian W. Bauer et al. "B —> M(1) M(2): Factorization, charming penguins, strong phases, and polarization". In: *Phys. Rev. D* 70 (2004), p. 054015. DOI: 10.1103/PhysRevD.70.054015. arXiv: hep-ph/0401188 (cit. on p. 53).

[148] Christian W. Bauer, Dan Pirjol, and Iain W. Stewart. "A Proof of factorization for B —> D pi". In: *Phys. Rev. Lett.* 87 (2001), p. 201806. DOI: 10.1103/PhysRevLett.87.201806. arXiv: hep-ph/0107002 (cit. on p. 53).

[149] Alexander L. Kagan. "Polarization in B —> VV decays". In: *Phys. Lett. B* 601 (2004), pp. 151–163. DOI: 10.1016/j.physletb.2004.09.030. arXiv: hep-ph/0405134 (cit. on pp. 53, 213, 214, 216).

[150] Marzia Bordone, Martin Jung, and Danny van Dyk. "Theory determination of $\bar{B} \to D^{(*)}\ell^-\bar{\nu}$ form factors at $\mathcal{O}(1/m_c^2)$". In: *Eur. Phys. J. C* 80.2 (2020), p. 74. DOI: 10.1140/epjc/s10052-020-7616-4. arXiv: 1908.09398 [hep-ph] (cit. on pp. 57, 58, 60).

[151] Sébastien Descotes-Genon and Patrick Koppenburg. "The CKM Parameters". In: *Ann. Rev. Nucl. Part. Sci.* 67 (2017), pp. 97–127. DOI: 10.1146/annurev-nucl-101916-123109. arXiv: 1702.08834 [hep-ex] (cit. on pp. 58, 63, 213).

[152] Andreas Crivellin. "Effects of right-handed charged currents on the determinations of |V(ub)| and |V(cb)|". In: *Phys. Rev. D* 81 (2010), p. 031301. DOI: 10.1103/PhysRevD.81.031301. arXiv: 0907.2461 [hep-ph] (cit. on p. 58).

[153] Pietro Colangelo and Fulvia De Fazio. "Tension in the inclusive versus exclusive determinations of $|V_{cb}|$: a possible role of new physics". In: *Phys. Rev. D* 95.1 (2017), p. 011701. DOI: 10.1103/PhysRevD.95.011701. arXiv: 1611.07387 [hep-ph] (cit. on p. 58).

[154] Florian U. Bernlochner et al. "Combined analysis of semileptonic B decays to D and D^*: $R(D^{(*)})$, $|V_{cb}|$, and new physics". In: *Phys. Rev. D* 95.11 (2017). [Erratum: Phys.Rev.D 97, 059902 (2018)], p. 115008. DOI: 10.1103/PhysRevD.95.115008. arXiv: 1703.05330 [hep-ph] (cit. on pp. 58, 174).

[155] Martin Jung and David M. Straub. "Constraining new physics in $b \to c\ell\nu$ transitions". In: *JHEP* 01 (2019), p. 009. DOI: 10.1007/JHEP01(2019)009. arXiv: 1801.01112 [hep-ph] (cit. on p. 58).

[156] Christoph Bobeth et al. "Lepton-flavour non-universality of $\bar{B} \to D^*\ell\bar{\nu}$ angular distributions in and beyond the Standard Model". In: (Apr. 2021). arXiv: 2104.02094 [hep-ph] (cit. on pp. 58, 61).

[157] E. Waheed et al. "Measurement of the CKM matrix element $|V_{cb}|$ from $B^0 \to D^{*-}\ell^+\nu_\ell$ at Belle". In: *Phys. Rev. D* 100.5 (2019). [Erratum: Phys.Rev.D 103, 079901 (2021)], p. 052007. DOI: 10.1103/PhysRevD.100.052007. arXiv: 1809.03290 [hep-ex] (cit. on p. 58).

[158] Yasmine Sara Amhis et al. "Averages of b-hadron, c-hadron, and τ-lepton properties as of 2018". In: *Eur. Phys. J. C* 81.3 (2021), p. 226. DOI: 10.1140/epjc/s10052-020-8156-7. arXiv: 1909.12524 [hep-ex] (cit. on pp. 58, 60, 67, 93, 151, 196, 214, 222).

[159] Judd Harrison, Christine T. H. Davies, and Andrew Lytle. "$R(J/\psi)$ and $B_c^- \to J/\psi\ell^-\bar{\nu}_\ell$ Lepton Flavor Universality Violating Observables from Lattice QCD". In: *Phys. Rev. Lett.* 125.22 (2020), p. 222003. DOI: 10.1103/PhysRevLett.125.222003. arXiv: 2007.06956 [hep-lat] (cit. on pp. 58, 59).

[160] R. Aaij et al. "Measurement of the ratio of branching fractions $\mathcal{B}(B_c^+ \to J/\psi\tau^+\nu_\tau)/\mathcal{B}(B_c^+ \to J/\psi\mu^+\nu_\mu)$". In: *Phys. Rev. Lett.* 120.12 (2018), p. 121801. DOI: 10.1103/PhysRevLett.120.121801. arXiv: 1711.05623 [hep-ex] (cit. on pp. 58, 60).

[161] E. McLean et al. "$B_s \to D_s\ell\nu$ Form Factors for the full q^2 range from Lattice QCD with non-perturbatively normalized currents". In: *Phys. Rev. D* 101.7 (2020), p. 074513. DOI: 10.1103/PhysRevD.101.074513. arXiv: 1906.00701 [hep-lat] (cit. on pp. 58, 59).

[162] Judd Harrison and Christine T. H. Davies. "$B_s \to D_s^*$ Form Factors for the full q^2 range from Lattice QCD". In: (May 2021). arXiv: 2105.11433 [hep-lat] (cit. on pp. 58, 59).

[163] William Detmold, Christoph Lehner, and Stefan Meinel. "$\Lambda_b \to p\ell^-\bar{\nu}_\ell$ and $\Lambda_b \to \Lambda_c\ell^-\bar{\nu}_\ell$ form factors from lattice QCD with relativistic heavy quarks". In: *Phys. Rev. D* 92.3 (2015), p. 034503. DOI: 10.1103/PhysRevD.92.034503. arXiv: 1503.01421 [hep-lat] (cit. on pp. 58, 59).

[164] Alakabha Datta et al. "Phenomenology of $\Lambda_b \to \Lambda_c\tau\overline{\nu}_\tau$ using lattice QCD calculations". In: *JHEP* 08 (2017), p. 131. DOI: 10.1007/JHEP08(2017)131. arXiv: 1702.02243 [hep-ph] (cit. on pp. 58, 59, 193).

[165] Clara Murgui et al. "Global fit to $b \to c\tau\nu$ transitions". In: *JHEP* 09 (2019), p. 103. DOI: 10.1007/JHEP09(2019)103. arXiv: 1904.09311 [hep-ph] (cit. on pp. 58, 60–62, 72).

[166] Damir Beirevi et al. "Lepton Flavor Universality tests through angular observables of $\overline{B} \to D^{(*)}\ell\overline{\nu}$ decay modes". In: (July 2019). arXiv: 1907.02257 [hep-ph] (cit. on pp. 59, 61, 63, 72, 165–167, 169, 171, 174, 175, 179).

[167] Damir Beirevi et al. "New Physics effects in leptonic and semileptonic decays". In: *JHEP* 05 (2021), p. 175. DOI: 10.1007/JHEP05(2021)175. arXiv: 2012.09872 [hep-ph] (cit. on p. 59).

[168] Svjetlana Fajfer, Jernej F. Kamenik, and Ivan Nisandzic. "On the $B \to D^*\tau\bar{\nu}_\tau$ Sensitivity to New Physics". In: *Phys. Rev. D* 85 (2012), p. 094025. DOI: 10.1103/PhysRevD.85.094025. arXiv: 1203.2654 [hep-ph] (cit. on p. 59).

[169] Philipp Böer et al. "Angular Analysis of \boldmath $\Lambda_b \to \Lambda_c(\to \Lambda\pi)\ell\bar{\nu}$". In: *JHEP* 12 (2019), p. 082. DOI: 10.1007/JHEP12(2019)082. arXiv: 1907.12554 [hep-ph] (cit. on p. 59).

[170] Stefan Meinel and Gumaro Rendon. "$\Lambda_b \to \Lambda_c^*(2595, 2625)\ell^-\bar{\nu}$form factors from lattice QCD". In: *Phys. Rev. D* 103.9 (2021), p. 094516. DOI: 10.1103/PhysRevD.103.094516. arXiv: 2103.08775 [hep-lat] (cit. on p. 59).

[171] C. McNeile et al. "Heavy meson masses and decay constants from relativistic heavy quarks in full lattice QCD". In: *Phys. Rev. D* 86 (2012), p. 074503. DOI: 10.1103/PhysRevD.86.074503. arXiv: 1207.0994 [hep-lat] (cit. on p. 59).

[172] B. Colquhoun et al. "B-meson decay constants: a more complete picture from full lattice QCD". In: *Phys. Rev. D* 91.11 (2015), p. 114509. DOI: 10.1103/PhysRevD.91.114509. arXiv: 1503.05762 [hep-lat] (cit. on p. 59).

[173] Yasmine Amhis et al. "Prospects for $B_c^+ \to \tau^+\nu_\tau$ at FCC-ee". In: (May 2021). arXiv: 2105.13330 [hep-ex] (cit. on p. 59).

[174] J. P. Lees et al. "Evidence for an excess of $\bar{B} \to D^{(*)}\tau^-\bar{\nu}_\tau$ decays". In: *Phys. Rev. Lett.* 109 (2012), p. 101802. DOI: 10.1103/PhysRevLett.109.101802. arXiv: 1205.5442 [hep-ex] (cit. on p. 60).

[175] J. P. Lees et al. "Measurement of an Excess of $\bar{B} \to D^{(*)}\tau^-\bar{\nu}_\tau$ Decays and Implications for Charged Higgs Bosons". In: *Phys. Rev. D* 88.7 (2013), p. 072012. DOI: 10.1103/PhysRevD.88.072012. arXiv: 1303.0571 [hep-ex] (cit. on p. 60).

[176] M. Huschle et al. "Measurement of the branching ratio of $\bar{B} \to D^{(*)}\tau^-\bar{\nu}_\tau$ relative to $\bar{B} \to D^{(*)}\ell^-\bar{\nu}_\ell$ decays with hadronic tagging at Belle". In: *Phys. Rev. D* 92.7 (2015), p. 072014. DOI: 10.1103/PhysRevD.92.072014. arXiv: 1507.03233 [hep-ex] (cit. on p. 60).

[177] Roel Aaij et al. "Measurement of the ratio of branching fractions $\mathcal{B}(\bar{B}^0 \to D^{*+}\tau^-\bar{\nu}_\tau)/\mathcal{B}(\bar{B}^0 \to D^{*+}\mu^-\bar{\nu}_\mu)$". In: *Phys. Rev. Lett.* 115.11 (2015). [Erratum: Phys.Rev.Lett. 115, 159901 (2015)], p. 111803. DOI: 10.1103/PhysRevLett.115.111803. arXiv: 1506.08614 [hep-ex] (cit. on p. 60).

[178] S. Hirose et al. "Measurement of the τ lepton polarization and $R(D^*)$ in the decay $\bar{B} \to D^* \tau^- \bar{\nu}_\tau$". In: *Phys. Rev. Lett.* 118.21 (2017), p. 211801. DOI: 10.1103/PhysRevLett.118.211801. arXiv: 1612.00529 [hep-ex] (cit. on p. 60).

[179] S. Hirose et al. "Measurement of the τ lepton polarization and $R(D^*)$ in the decay $\bar{B} \to D^* \tau^- \bar{\nu}_\tau$ with one-prong hadronic τ decays at Belle". In: *Phys. Rev. D* 97.1 (2018), p. 012004. DOI: 10.1103/PhysRevD.97.012004. arXiv: 1709.00129 [hep-ex] (cit. on p. 60).

[180] R. Aaij et al. "Measurement of the ratio of the $B^0 \to D^{*-} \tau^+ \nu_\tau$ and $B^0 \to D^{*-} \mu^+ \nu_\mu$ branching fractions using three-prong τ-lepton decays". In: *Phys. Rev. Lett.* 120.17 (2018), p. 171802. DOI: 10.1103/PhysRevLett.120.171802. arXiv: 1708.08856 [hep-ex] (cit. on p. 60).

[181] R. Aaij et al. "Test of Lepton Flavor Universality by the measurement of the $B^0 \to D^{*-} \tau^+ \nu_\tau$ branching fraction using three-prong τ decays". In: *Phys. Rev. D* 97.7 (2018), p. 072013. DOI: 10.1103/PhysRevD.97.072013. arXiv: 1711.02505 [hep-ex] (cit. on p. 60).

[182] A. Abdesselam et al. "Measurement of $\mathcal{R}(D)$ and $\mathcal{R}(D^*)$ with a semileptonic tagging method". In: (Apr. 2019). arXiv: 1904.08794 [hep-ex] (cit. on p. 60).

[183] A. Abdesselam et al. "Measurement of the D^{*-} polarization in the decay $B^0 \to D^{*-} \tau^+ \nu_\tau$". In: *10th International Workshop on the CKM Unitarity Triangle*. Mar. 2019. arXiv: 1903.03102 [hep-ex] (cit. on pp. 60, 61).

[184] Donal Hill et al. "Model-independent method for measuring the angular coefficients of $B^0 \to D^{*-} \tau^+ \nu_\tau$ decays". In: *JHEP* 11 (2019), p. 133. DOI: 10.1007/JHEP11(2019)133. arXiv: 1908.04643 [hep-ph] (cit. on pp. 60, 166, 179).

[185] Xin-Qiang Li, Ya-Dong Yang, and Xin Zhang. "Revisiting the one leptoquark solution to the R(D$^{(*)}$) anomalies and its phenomenological implications". In: *JHEP* 08 (2016), p. 054. DOI: 10.1007/JHEP08(2016)054. arXiv: 1605.09308 [hep-ph] (cit. on pp. 60, 61).

[186] Rodrigo Alonso, Benjamín Grinstein, and Jorge Martin Camalich. "Lifetime of B_c^- Constrains Explanations for Anomalies in $B \to D^{(*)} \tau \nu$". In: *Phys. Rev. Lett.* 118.8 (2017), p. 081802. DOI: 10.1103/PhysRevLett.118.081802. arXiv: 1611.06676 [hep-ph] (cit. on pp. 60, 61, 72).

[187] Rusa Mandal et al. "The role of right-handed neutrinos in $b \to c\tau\bar{\nu}$ anomalies". In: *JHEP* 08.08 (2020), p. 022. DOI: 10.1007/JHEP08(2020)022. arXiv: 2004.06726 [hep-ph] (cit. on pp. 61, 72, 189, 191).

[188] Damir Becirevic et al. "Angular distributions of $\bar{B} \to D^{(*)} \ell \bar{\nu}_\ell$ decays and search of New Physics". In: *Nucl. Phys. B* 946 (2019), p. 114707. DOI: 10.1016/j.nuclphysb.2019.114707. arXiv: 1602.03030 [hep-ph] (cit. on pp. 61, 166).

[189] Pietro Colangelo and Fulvia De Fazio. "Scrutinizing $\overline{B} \to D^* (D\pi) \ell^- \overline{\nu}_\ell$ and $\overline{B} \to D^* (D\gamma) \ell^- \overline{\nu}_\ell$ in search of new physics footprints". In: *JHEP* 06 (2018), p. 082. DOI: 10.1007/JHEP06(2018)082. arXiv: 1801.10468 [hep-ph] (cit. on pp. 61, 167).

[190] A. G. Akeroyd and Chuan-Hung Chen. "Constraint on the branching ratio of $B_c \to \tau \bar{\nu}$ from LEP1 and consequences for $R(D^{(*)})$ anomaly". In: *Phys. Rev. D* 96.7 (2017), p. 075011. DOI: 10.1103/PhysRevD.96.075011. arXiv: 1708.04072 [hep-ph] (cit. on p. 61).

[191] Admir Greljo, Jorge Martin Camalich, and José David Ruiz-Álvarez. "Mono-τ Signatures at the LHC Constrain Explanations of B-decay Anomalies". In: *Phys. Rev. Lett.* 122.13 (2019), p. 131803. DOI: 10.1103/PhysRevLett.122.131803. arXiv: 1811.07920 [hep-ph] (cit. on p. 61).

[192] Damir Beirevi et al. "Scalar leptoquarks from grand unified theories to accommodate the B-physics anomalies". In: *Phys. Rev. D* 98.5 (2018), p. 055003. DOI: 10.1103/PhysRevD.98.055003. arXiv: 1806.05689 [hep-ph] (cit. on pp. 63, 168).

[193] Chris Bouchard et al. "Rare decay $B \to K \ell^+ \ell^-$ form factors from lattice QCD". In: *Phys. Rev. D* 88.5 (2013). [Erratum: Phys.Rev.D 88, 079901 (2013)], p. 054509. DOI: 10.1103/PhysRevD.88.054509. arXiv: 1306.2384 [hep-lat] (cit. on pp. 64, 79).

[194] Jon A. Bailey et al. "$B \to K l^+ l^-$ Decay Form Factors from Three-Flavor Lattice QCD". In: *Phys. Rev. D* 93.2 (2016), p. 025026. DOI: 10.1103/PhysRevD.93.025026. arXiv: 1509.06235 [hep-lat] (cit. on p. 64).

[195] Ronald R. Horgan et al. "Lattice QCD calculation of form factors describing the rare decays $B \to K^* \ell^+ \ell^-$ and $B_s \to \phi \ell^+ \ell^-$". In: *Phys. Rev. D* 89.9 (2014), p. 094501. DOI: 10.1103/PhysRevD.89.094501. arXiv: 1310.3722 [hep-lat] (cit. on pp. 64, 79, 81).

[196] Thomas Gutsche et al. "Rare baryon decays $\Lambda_b \to \Lambda l^+ l^- (l = e, \mu, \tau)$ and $\Lambda_b \to \Lambda \gamma$: differential and total rates, lepton- and hadron-side forward-backward asymmetries". In: *Phys. Rev. D* 87 (2013), p. 074031. DOI: 10.1103/PhysRevD.87.074031. arXiv: 1301.3737 [hep-ph] (cit. on p. 64).

[197] Philipp Böer, Thorsten Feldmann, and Danny van Dyk. "Angular Analysis of the Decay $\Lambda_b \to \Lambda(\to N\pi)\ell^+\ell^-$". In: *JHEP* 01 (2015), p. 155. DOI: 10.1007/JHEP01(2015)155. arXiv: 1410.2115 [hep-ph] (cit. on pp. 64, 66, 115–117, 122).

[198] Shibasis Roy, Ria Sain, and Rahul Sinha. "Lepton mass effects and angular observables in $\Lambda_b \to \Lambda(\to p\pi)\ell^+\ell^-$". In: *Phys. Rev. D* 96.11 (2017), p. 116005. DOI: 10.1103/PhysRevD.96.116005. arXiv: 1710.01335 [hep-ph] (cit. on p. 64).

[199] Diganta Das. "On the angular distribution of $\Lambda_b \to \Lambda(\to N\pi)\tau^+\tau^-$ decay". In: *JHEP* 07 (2018), p. 063. DOI: 10.1007/JHEP07(2018)063. arXiv: 1804.08527 [hep-ph] (cit. on p. 64).

[200] Diganta Das. "Model independent New Physics analysis in $\Lambda_b \to \Lambda\mu^+\mu^-$ decay". In: *Eur. Phys. J. C* 78.3 (2018), p. 230. DOI: 10.1140/epjc/s10052-018-5731-2. arXiv: 1802.09404 [hep-ph] (cit. on p. 64).

[201] Thomas Blake and Michal Kreps. "Angular distribution of polarised Λ_b baryons decaying to $\Lambda\ell^+\ell^-$". In: *JHEP* 11 (2017), p. 138. DOI: 10.1007/JHEP11(2017)138. arXiv: 1710.00746 [hep-ph] (cit. on pp. 64, 66, 112, 137, 139).

[202] Srimoy Bhattacharya et al. "Detailed study of the $\Lambda_b \to \Lambda\ell^+\ell^-$ decays in the standard model". In: *Phys. Rev. D* 101.7 (2020), p. 073006. DOI: 10.1103/PhysRevD.101.073006. arXiv: 1912.06148 [hep-ph] (cit. on p. 64).

[203] William Detmold and Stefan Meinel. "$\Lambda_b \to \Lambda\ell^+\ell^-$ form factors, differential branching fraction, and angular observables from lattice QCD with relativistic b quarks". In: *Phys. Rev. D* 93.7 (2016), p. 074501. DOI: 10.1103/PhysRevD.93.074501. arXiv: 1602.01399 [hep-lat] (cit. on pp. 64, 95).

[204] Marzia Bordone, Gino Isidori, and Andrea Pattori. "On the Standard Model predictions for R_K and R_{K^*}". In: *Eur. Phys. J. C* 76.8 (2016), p. 440. DOI: 10.1140/epjc/s10052-016-4274-7. arXiv: 1605.07633 [hep-ph] (cit. on p. 64).

[205] Bernat Capdevila et al. "Hadronic uncertainties in $B \to K^*\mu^+\mu^-$: a state-of-the-art analysis". In: *JHEP* 04 (2017), p. 016. DOI: 10.1007/JHEP04(2017)016. arXiv: 1701.08672 [hep-ph] (cit. on pp. 64, 89, 109, 124).

[206] Roel Aaij et al. "Search for lepton-universality violation in $B^+ \to K^+\ell^+\ell^-$ decays". In: *Phys. Rev. Lett.* 122.19 (2019), p. 191801. DOI: 10.1103/PhysRevLett.122.191801. arXiv: 1903.09252 [hep-ex] (cit. on pp. 64, 66).

[207] R. Aaij et al. "Test of lepton universality with $B^0 \to K^{*0}\ell^+\ell^-$ decays". In: *JHEP* 08 (2017), p. 055. DOI: 10.1007/JHEP08(2017)055. arXiv: 1705.05802 [hep-ex] (cit. on pp. 64, 66, 78, 84, 104).

[208] Martin Beneke, Christoph Bobeth, and Robert Szafron. "Power-enhanced leading-logarithmic QED corrections to $B_q \to \mu^+\mu^-$". In: *JHEP* 10 (2019), p. 232. DOI: 10.1007/JHEP10(2019)232. arXiv: 1908.07011 [hep-ph] (cit. on p. 64).

[209] Christoph Bobeth et al. "$B_{s,d} \to l^+l^-$ in the Standard Model with Reduced Theoretical Uncertainty". In: *Phys. Rev. Lett.* 112 (2014), p. 101801. DOI: 10.1103/PhysRevLett.112.101801. arXiv: 1311.0903 [hep-ph] (cit. on p. 64).

[210] Kristof De Bruyn et al. "Probing New Physics via the $B_s^0 \to \mu^+\mu^-$ Effective Lifetime". In: *Phys. Rev. Lett.* 109 (2012), p. 041801. DOI: 10.1103/PhysRevLett.109.041801. arXiv: 1204.1737 [hep-ph] (cit. on p. 64).

[211] M. Misiak, Abdur Rehman, and Matthias Steinhauser. "Towards $\overline{B} \to X_s\gamma$ at the NNLO in QCD without interpolation in m_c". In: *JHEP* 06 (2020), p. 175. DOI: 10.1007/JHEP06(2020)175. arXiv: 2002.01548 [hep-ph] (cit. on pp. 65, 220).

[212] Ayan Paul and David M. Straub. "Constraints on new physics from radiative B decays". In: *JHEP* 04 (2017), p. 027. DOI: 10.1007/JHEP04(2017)027. arXiv: 1608.02556 [hep-ph] (cit. on pp. 65, 69, 96).

[213] Christoph Bobeth, Gudrun Hiller, and Giorgi Piranishvili. "Angular distributions of $\bar{B} \to \bar{K}\ell^+\ell^-$ decays". In: *JHEP* 12 (2007), p. 040. DOI: 10.1088/1126-6708/2007/12/040. arXiv: 0709.4174 [hep-ph] (cit. on pp. 65, 147).

[214] Joaquim Matias et al. "Complete Anatomy of $\bar{B}_d - > \bar{K}^{*0}(- > K\pi)l^+l^-$ and its angular distribution". In: *JHEP* 04 (2012), p. 104. DOI: 10.1007/JHEP04(2012)104. arXiv: 1202.4266 [hep-ph] (cit. on pp. 65, 123, 145, 167, 168, 213).

[215] Christoph Bobeth, Gudrun Hiller, and Danny van Dyk. "Angular analysis of $B \to V(\to P_1P_2) + \bar{\ell}\ell$ decays". In: *J. Phys. Conf. Ser.* 335 (2011). Ed. by Antonio Di Domenico et al., p. 012038. DOI: 10.1088/1742-6596/335/1/012038. arXiv: 1105.2659 [hep-ph] (cit. on p. 65).

[216] Christoph Bobeth, Gudrun Hiller, and Danny van Dyk. "General analysis of $\bar{B} \to \bar{K}^{(*)}\ell^+\ell^-$ decays at low recoil". In: *Phys. Rev. D* 87.3 (2013), p. 034016. DOI: 10.1103/PhysRevD.87.034016. arXiv: 1212.2321 [hep-ph] (cit. on p. 65).

[217] Sébastien Descotes-Genon and Javier Virto. "Time dependence in $B \to V\ell\ell$ decays". In: *JHEP* 04 (2015). [Erratum: JHEP 07, 049 (2015)], p. 045. DOI: 10.1007/JHEP04(2015)045. arXiv: 1502.05509 [hep-ph] (cit. on pp. 65, 145, 149–153, 157).

[218] R Aaij et al. "Measurements of the $\Lambda_b^0 \to J/\psi\Lambda$ decay amplitudes and the Λ_b^0 polarisation in pp collisions at $\sqrt{s} = 7$ TeV". In: *Phys. Lett. B* 724 (2013), pp. 27–35. DOI: 10.1016/j.physletb.2013.05.041. arXiv: 1302.5578 [hep-ex] (cit. on pp. 66, 115).

[219] A. Abdesselam et al. "Test of lepton flavor universality in $B \to K^*\ell^+\ell^-$ decays at Belle". In: (Apr. 2019). arXiv: 1904.02440 [hep-ex] (cit. on pp. 66, 78, 104).

[220] S. Choudhury et al. "Test of lepton flavor universality and search for lepton flavor violation in $B \to K\ell\ell$ decays". In: *JHEP* 03 (2021), p. 105. DOI: 10.1007/JHEP03(2021)105. arXiv: 1908.01848 [hep-ex] (cit. on pp. 66, 78, 99, 104, 157).

[221] J. P. Lees et al. "Measurement of Branching Fractions and Rate Asymmetries in the Rare Decays $B \to K^{(*)}l^+l^-$". In: *Phys. Rev. D* 86 (2012), p. 032012. DOI: 10.1103/PhysRevD.86.032012. arXiv: 1204.3933 [hep-ex] (cit. on pp. 66, 68).

[222] Johannes Albrecht, Danny van Dyk, and Christoph Langenbruch. "Flavour anomalies in heavy quark decays". In: *Prog. Part. Nucl. Phys.* 120 (2021), p. 103885. DOI: 10.1016/j.ppnp.2021.103885. arXiv: 2107.04822 [hep-ex] (cit. on pp. 66, 68, 70).

[223] Roel Aaij et al. "Test of lepton universality with $\Lambda_b^0 \to pK^-\ell^+\ell^-$ decays". In: *JHEP* 05 (2020), p. 040. DOI: 10.1007/JHEP05(2020)040. arXiv: 1912.08139 [hep-ex] (cit. on pp. 67, 78, 109, 111, 131–133).

[224] R. Aaij et al. "Differential branching fractions and isospin asymmetries of $B \to K^{(*)}\mu^+\mu^-$ decays". In: *JHEP* 06 (2014), p. 133. DOI: 10.1007/JHEP06(2014)133. arXiv: 1403.8044 [hep-ex] (cit. on pp. 67, 68, 84, 99, 103).

[225] Roel Aaij et al. "Branching fraction measurements of the rare $B_s^0 \to \phi\mu^+\mu^-$ and $B_s^0 \to f_2'(1525)\mu^+\mu^-$ decays". In: (May 2021). arXiv: 2105.14007 [hep-ex] (cit. on pp. 67, 68, 78).

[226] Roel Aaij et al. "Differential branching fraction and angular analysis of $\Lambda_b^0 \to \Lambda\mu^+\mu^-$ decays". In: *JHEP* 06 (2015). [Erratum: JHEP 09, 145 (2018)], p. 115. DOI: 10.1007/JHEP06(2015)115. arXiv: 1503.07138 [hep-ex] (cit. on pp. 67, 68, 78, 95, 112, 139).

[227] Thomas Blake, Stefan Meinel, and Danny van Dyk. "Bayesian Analysis of $b \to s\mu^+\mu^-$ Wilson Coefficients using the Full Angular Distribution of $\Lambda_b \to \Lambda(\to p\,\pi^-)\mu^+\mu^-$ Decays". In: *Phys. Rev. D* 101.3 (2020), p. 035023. DOI: 10.1103/PhysRevD.101.035023. arXiv: 1912.05811 [hep-ph] (cit. on pp. 67, 68, 95).

[228] Roel Aaij et al. "Measurements of the S-wave fraction in $B^0 \to K^+\pi^-\mu^+\mu^-$ decays and the $B^0 \to K^*(892)^0\mu^+\mu^-$ differential branching fraction". In: *JHEP* 11 (2016). [Erratum: JHEP 04, 142 (2017)], p. 047. DOI: 10.1007/JHEP11(2016)047. arXiv: 1606.04731 [hep-ex] (cit. on pp. 68, 84, 102).

[229] Roel Aaij et al. "Angular analysis and differential branching fraction of the decay $B_s^0 \to \phi\mu^+\mu^-$". In: *JHEP* 09 (2015), p. 179. DOI: 10.1007/JHEP09(2015)179. arXiv: 1506.08777 [hep-ex] (cit. on pp. 68, 84, 103, 104, 151).

[230] Vardan Khachatryan et al. "Angular analysis of the decay $B^0 \to K^{*0}\mu^+\mu^-$ from pp collisions at $\sqrt{s} = 8$ TeV". In: *Phys. Lett. B* 753 (2016), pp. 424–448. DOI: 10.1016/j.physletb.2015.12.020. arXiv: 1507.08126 [hep-ex] (cit. on pp. 68, 101, 102).

[231] J. -T. Wei et al. "Measurement of the Differential Branching Fraction and Forward-Backword Asymmetry for $B \to K^{(*)}\ell^+\ell^-$". In: *Phys. Rev. Lett.* 103 (2009), p. 171801. DOI: 10.1103/PhysRevLett.103.171801. arXiv: 0904.0770 [hep-ex] (cit. on p. 68).

[232] T. Aaltonen et al. "Observation of the Baryonic Flavor-Changing Neutral Current Decay $\Lambda_b \to \Lambda\mu^+\mu^-$". In: *Phys. Rev. Lett.* 107 (2011), p. 201802. DOI: 10.1103/PhysRevLett.107.201802. arXiv: 1107.3753 [hep-ex] (cit. on p. 68).

[233] "Combination of the ATLAS, CMS and LHCb results on the $B_{(s)}^0 \to \mu^+\mu^-$ decays." In: (Aug. 2020). URL: http://cds.cern.ch/record/2728059 (cit. on pp. 67, 69).

[234] Bernard Aubert et al. "Measurement of Branching Fractions and CP and Isospin Asymmetries in $B \to K^*(892)\gamma$ Decays". In: *Phys. Rev. Lett.* 103 (2009), p. 211802. DOI: 10.1103/PhysRevLett.103.211802. arXiv: 0906.2177 [hep-ex] (cit. on p. 67).

[235] T. Horiguchi et al. "Evidence for Isospin Violation and Measurement of CP Asymmetries in $B \to K^*(892)\gamma$". In: *Phys. Rev. Lett.* 119.19 (2017), p. 191802. DOI: 10.1103/PhysRevLett.119.191802. arXiv: 1707.00394 [hep-ex] (cit. on p. 67).

[236] D. Dutta et al. "Search for $B_s^0 \to \gamma\gamma$ and a measurement of the branching fraction for $B_s^0 \to \phi\gamma$". In: *Phys. Rev. D* 91.1 (2015), p. 011101. DOI: 10.1103/PhysRevD.91.011101. arXiv: 1411.7771 [hep-ex] (cit. on p. 67).

[237] R Aaij et al. "Measurement of the ratio of branching fractions $BR(B_0 \to K^{\star 0}\gamma)/BR(B_{s0} \to \phi\gamma)$ and the direct CP asymmetry in $B_0 \to K^{\star 0}\gamma$". In: *Nucl. Phys. B* 867 (2013), pp. 1–18. DOI: 10.1016/j.nuclphysb.2012.09.013. arXiv: 1209.0313 [hep-ex] (cit. on p. 67).

[238] Roel Aaij et al. "Angular analysis of charged and neutral $B \to K\mu^+\mu^-$ decays". In: *JHEP* 05 (2014), p. 082. DOI: 10.1007/JHEP05(2014)082. arXiv: 1403.8045 [hep-ex] (cit. on pp. 67, 145, 157).

[239] Roel Aaij et al. "Angular analysis of the $B^0 \to K^{*0}\mu^+\mu^-$ decay using 3 fb^{-1} of integrated luminosity". In: *JHEP* 02 (2016), p. 104. DOI: 10.1007/JHEP02(2016)104. arXiv: 1512.04442 [hep-ex] (cit. on pp. 67, 70, 133).

[240] Roel Aaij et al. "Angular analysis of the $B^+ \to K^{*+}\mu^+\mu^-$ decay". In: (Dec. 2020). arXiv: 2012.13241 [hep-ex] (cit. on pp. 67, 70, 84, 102, 103).

[241] Roel Aaij et al. "Strong constraints on the $b \to s\gamma$ photon polarisation from $B^0 \to K^{*0}e^+e^-$ decays". In: *JHEP* 12 (2020), p. 081. DOI: 10.1007/JHEP12(2020)081. arXiv: 2010.06011 [hep-ex] (cit. on pp. 68, 104).

[242] S. Wehle et al. "Lepton-Flavor-Dependent Angular Analysis of $B \to K^*\ell^+\ell^-$". In: *Phys. Rev. Lett.* 118.11 (2017), p. 111801. DOI: 10.1103/PhysRevLett.118.111801. arXiv: 1612.05014 [hep-ex] (cit. on pp. 68, 70, 78, 84, 103, 104).

[243] Roel Aaij et al. "Angular analysis of the rare decay $B_s^0 \to \phi\mu^+\mu^-$". In: (July 2021). arXiv: 2107.13428 [hep-ex] (cit. on pp. 68, 78).

[244] R Aaij et al. "Differential branching fraction and angular analysis of the decay $B_s^0 \to \phi\mu^+\mu^-$". In: *JHEP* 07 (2013), p. 084. DOI: 10.1007/JHEP07(2013)084. arXiv: 1305.2168 [hep-ex] (cit. on p. 68).

[245] Albert M Sirunyan et al. "Measurement of angular parameters from the decay $B^0 \to K^{*0}\mu^+\mu^-$ in proton-proton collisions at $\sqrt{s} = 8$ TeV". In: *Phys. Lett. B* 781 (2018), pp. 517–541. DOI: 10.1016/j.physletb.2018.04.030. arXiv: 1710.02846 [hep-ex] (cit. on pp. 70, 101).

[246] Morad Aaboud et al. "Angular analysis of $B_d^0 \to K^*\mu^+\mu^-$ decays in pp collisions at $\sqrt{s} = 8$ TeV with the ATLAS detector". In: *JHEP* 10 (2018), p. 047. DOI: 10.1007/JHEP10(2018)047. arXiv: 1805.04000 [hep-ex] (cit. on pp. 70, 84, 100, 101).

[247] Roel Aaij et al. "Angular moments of the decay $\Lambda_b^0 \to \Lambda\mu^+\mu^-$ at low hadronic recoil". In: *JHEP* 09 (2018), p. 146. DOI: 10.1007/JHEP09(2018)146. arXiv: 1808.00264 [hep-ex] (cit. on pp. 68, 78, 95, 112, 139).

[248] M. Ablikim et al. "Complete Measurement of the Λ Electromagnetic Form Factors". In: *Phys. Rev. Lett.* 123.12 (2019), p. 122003. DOI: 10.1103/PhysRevLett.123.122003. arXiv: 1903.09421 [hep-ex] (cit. on pp. 68, 95).

[249] Dario Buttazzo et al. "B-physics anomalies: a guide to combined explanations". In: *JHEP* 11 (2017), p. 044. DOI: 10.1007/JHEP11(2017)044. arXiv: 1706.07808 [hep-ph] (cit. on pp. 70–72, 205, 206).

[250] G. D'Ambrosio et al. "Minimal flavor violation: An Effective field theory approach". In: *Nucl. Phys. B* 645 (2002), pp. 155–187. DOI: 10.1016/S0550-3213(02)00836-2. arXiv: hep-ph/0207036 (cit. on pp. 70, 73, 205).

[251] Tobias Hurth et al. "Constraints on New Physics in MFV models: A Model-independent analysis of Δ F = 1 processes". In: *Nucl. Phys.* B808 (2009), pp. 326–346. DOI: 10.1016/j.nuclphysb.2008.09.040. arXiv: 0807.5039 [hep-ph] (cit. on pp. 70, 205).

[252] G. C. Branco et al. "Theory and phenomenology of two-Higgs-doublet models". In: *Phys. Rept.* 516 (2012), pp. 1–102. DOI: 10.1016/j.physrep.2012.02.002. arXiv: 1106.0034 [hep-ph] (cit. on pp. 71, 72).

[253] I. Dorner et al. "Physics of leptoquarks in precision experiments and at particle colliders". In: *Phys. Rept.* 641 (2016), pp. 1–68. DOI: 10.1016/j.physrep.2016.06.001. arXiv: 1603.04993 [hep-ph] (cit. on p. 71).

[254] David B. Kaplan, Howard Georgi, and Savas Dimopoulos. "Composite Higgs Scalars". In: *Phys. Lett. B* 136 (1984), pp. 187–190. DOI: 10.1016/0370-2693(84)91178-X (cit. on p. 71).

[255] Christoph Niehoff, Peter Stangl, and David M. Straub. "Violation of lepton flavour universality in composite Higgs models". In: *Phys. Lett. B* 747 (2015), pp. 182–186. DOI: 10.1016/j.physletb.2015.05.063. arXiv: 1503.03865 [hep-ph] (cit. on pp. 71, 207).

[256] Jogesh C. Pati and Abdus Salam. "Lepton Number as the Fourth Color". In: *Phys. Rev. D* 10 (1974). [Erratum: Phys.Rev.D 11, 703–703 (1975)], pp. 275–289. DOI: 10.1103/PhysRevD.10.275 (cit. on p. 71).

[257] R. Barbier et al. "R-parity violating supersymmetry". In: *Phys. Rept.* 420 (2005), pp. 1–202. DOI: 10.1016/j.physrep.2005.08.006. arXiv: hep-ph/0406039 (cit. on p. 71).

[258] Andrei Angelescu et al. "On the single leptoquark solutions to the B-physics anomalies". In: (Mar. 2021). arXiv: 2103.12504 [hep-ph] (cit. on pp. 71, 72).

[259] A. Angelescu et al. "Closing the window on single leptoquark solutions to the B-physics anomalies". In: *JHEP* 10 (2018), p. 183. DOI: 10.1007/JHEP10(2018)183. arXiv: 1808.08179 [hep-ph] (cit. on p. 72).

[260] Andrzej J. Buras et al. "The Anatomy of Quark Flavour Observables in 331 Models in the Flavour Precision Era". In: *JHEP* 02 (2013), p. 023. DOI: 10.1007/JHEP02(2013)023. arXiv: 1211.1237 [hep-ph] (cit. on p. 72).

[261] Andrzej J. Buras, Fulvia De Fazio, and Jennifer Girrbach. "331 models facing new $b \to s\mu^+\mu^-$ data". In: *JHEP* 02 (2014), p. 112. DOI: 10.1007/JHEP02(2014)112. arXiv: 1311.6729 [hep-ph] (cit. on p. 72).

[262] Andrzej J. Buras and Fulvia De Fazio. "331 Models Facing the Tensions in $\Delta F = 2$ Processes with the Impact on ε'/ε, $B_s \to \mu^+\mu^-$ and $B \to K^*\mu^+\mu^-$". In: *JHEP* 08 (2016), p. 115. DOI: 10.1007/JHEP08(2016)115. arXiv: 1604.02344 [hep-ph] (cit. on p. 72).

[263] Sofiane M. Boucenna et al. "Phenomenology of an $SU(2) \times SU(2) \times U(1)$ model with lepton-flavour non-universality". In: *JHEP* 12 (2016), p. 059. DOI: 10.1007/JHEP12(2016)059. arXiv: 1608.01349 [hep-ph] (cit. on p. 72).

[264] Wolfgang Altmannshofer et al. "Quark flavor transitions in $L_\mu - L_\tau$ models". In: *Phys. Rev. D* 89 (2014), p. 095033. DOI: 10.1103/PhysRevD.89.095033. arXiv: 1403.1269 [hep-ph] (cit. on pp. 72, 92, 206).

[265] Admir Greljo, Gino Isidori, and David Marzocca. "On the breaking of Lepton Flavor Universality in B decays". In: *JHEP* 07 (2015), p. 142. DOI: 10.1007/JHEP07(2015)142. arXiv: 1506.01705 [hep-ph] (cit. on pp. 72, 93).

[266] Darius A. Faroughy, Admir Greljo, and Jernej F. Kamenik. "Confronting lepton flavor universality violation in B decays with high-p_T tau lepton searches at LHC". In: *Phys. Lett. B* 764 (2017), pp. 126–134. DOI: 10.1016/j.physletb.2016.11.011. arXiv: 1609.07138 [hep-ph] (cit. on p. 72).

[267] Wolfgang Altmannshofer and Peter Stangl. "New Physics in Rare B Decays after Moriond 2021". In: (Mar. 2021). arXiv: 2103.13370 [hep-ph] (cit. on pp. 72, 94–97).

[268] Pere Arnan et al. "Two Higgs doublet models and $b \to s$ exclusive decays". In: *Eur. Phys. J. C* 77.11 (2017), p. 796. DOI: 10.1140/epjc/s10052-017-5370-z. arXiv: 1703.03426 [hep-ph] (cit. on p. 72).

[269] Andreas Crivellin, Dario Müller, and Christoph Wiegand. "$b \to s\ell^+\ell^-$ transitions in two-Higgs-doublet models". In: *JHEP* 06 (2019), p. 119. DOI: 10.1007/JHEP06(2019)119. arXiv: 1903.10440 [hep-ph] (cit. on pp. 72, 87, 93).

[270] Alexander L. Kagan et al. "General Minimal Flavor Violation". In: *Phys. Rev. D* 80 (2009), p. 076002. DOI: 10.1103/PhysRevD.80.076002. arXiv: 0903.1794 [hep-ph] (cit. on pp. 73, 74, 206, 209).

[271] Riccardo Barbieri et al. "Flavour physics from an approximate $U(2)^3$ symmetry". In: *JHEP* 07 (2012), p. 181. DOI: 10.1007/JHEP07(2012)181. arXiv: 1203.4218 [hep-ph] (cit. on p. 74).

[272] Gianluca Blankenburg, Gino Isidori, and Joel Jones-Perez. "Neutrino Masses and LFV from Minimal Breaking of $U(3)^5$ and $U(2)^5$ flavor Symmetries". In: *Eur. Phys. J. C* 72 (2012), p. 2126. DOI: 10.1140/epjc/s10052-012-2126-7. arXiv: 1204.0688 [hep-ph] (cit. on p. 74).

[273] Riccardo Barbieri et al. "Anomalies in B-decays and $U(2)$ flavour symmetry". In: *Eur. Phys. J. C* 76.2 (2016), p. 67. DOI: 10.1140/epjc/s10052-016-3905-3. arXiv: 1512.01560 [hep-ph] (cit. on pp. 74, 206).

[274] R Aaij et al. "Measurement of Form-Factor-Independent Observables in the Decay $B^0 \to K^{*0}\mu^+\mu^-$". In: *Phys. Rev. Lett.* 111 (2013), p. 191801. DOI: 10.1103/PhysRevLett.111.191801. arXiv: 1308.1707 [hep-ex] (cit. on p. 77).

[275] Marcel Algueró et al. "$b \to s\ell\ell$ global fits after Moriond 2021 results". In: *55th Rencontres de Moriond on QCD and High Energy Interactions*. Apr. 2021. arXiv: 2104.08921 [hep-ph] (cit. on pp. 77, 85, 231).

[276] Albert M Sirunyan et al. "Angular analysis of the decay $B^+ \to K^*(892)^+\mu^+\mu^-$ in proton-proton collisions at $\sqrt{s} = 8$ TeV". In: (Oct. 2020). arXiv: 2010.13968 [hep-ex] (cit. on pp. 78, 103).

[277] Roel Aaij et al. "Test of lepton universality in beauty-quark decays". In: (Mar. 2021). arXiv: 2103.11769 [hep-ex] (cit. on pp. 78, 84, 104).

[278] Aoife Bharucha, David M. Straub, and Roman Zwicky. "$B \to V\ell^+\ell^-$ in the Standard Model from light-cone sum rules". In: *JHEP* 08 (2016), p. 098. DOI: 10.1007/JHEP08(2016)098. arXiv: 1503.05534 [hep-ph] (cit. on pp. 79, 94, 95, 217, 226).

[279] S. Jäger and J. Martin Camalich. "On $B \to V\ell\ell$ at small dilepton invariant mass, power corrections, and new physics". In: *JHEP* 05 (2013), p. 043. DOI: 10.1007/JHEP05(2013)043. arXiv: 1212.2263 [hep-ph] (cit. on p. 79).

[280] Sebastian Jäger and Jorge Martin Camalich. "Reassessing the discovery potential of the $B \to K^*\ell^+\ell^-$ decays in the large-recoil region: SM challenges and BSM opportunities". In: *Phys. Rev. D* 93.1 (2016), p. 014028. DOI: 10.1103/PhysRevD.93.014028. arXiv: 1412.3183 [hep-ph] (cit. on p. 79).

[281] M. Beneke, Th. Feldmann, and D. Seidel. "Exclusive radiative and electroweak $b \to d$ and $b \to s$ penguin decays at NLO". In: *Eur. Phys. J. C* 41 (2005), pp. 173–188. DOI: 10.1140/epjc/s2005-02181-5. arXiv: hep-ph/0412400 (cit. on pp. 80, 91).

[282] Marco Ciuchini et al. "$B \to K^*\ell^+\ell^-$ in the Standard Model: Elaborations and Interpretations". In: *PoS* ICHEP2016 (2016), p. 584. DOI: 10.22323/1.282.0584. arXiv: 1611.04338 [hep-ph] (cit. on pp. 80, 89).

[283] Alexander Lenz and Gilberto Tetlalmatzi-Xolocotzi. "Model-independent bounds on new physics effects in non-leptonic tree-level decays of B-mesons". In: *JHEP* 07 (2020), p. 177. DOI: 10.1007/JHEP07(2020)177. arXiv: 1912.07621 [hep-ph] (cit. on pp. 82, 220).

[284] G. Cowan. *Statistical data analysis*. 1998. ISBN: 978-0-19-850156-5 (cit. on p. 82).

[285] S. S. Wilks. "The Large-Sample Distribution of the Likelihood Ratio for Testing Composite Hypotheses". In: *Annals Math. Statist.* 9.1 (1938), pp. 60–62. DOI: 10.1214/aoms/1177732360 (cit. on pp. 83, 96).

[286] Jérôme Charles et al. "Modeling theoretical uncertainties in phenomenological analyses for particle physics". In: *Eur. Phys. J. C* 77.4 (2017), p. 214. DOI: 10.1140/epjc/s10052-017-4767-z. arXiv: 1611.04768 [hep-ph] (cit. on pp. 84, 216).

[287] Roel Aaij et al. "Measurement of CP-Averaged Observables in the $B^0 \to K^{*0}\mu^+\mu^-$ Decay". In: *Phys. Rev. Lett.* 125.1 (2020), p. 011802. DOI: 10.1103/PhysRevLett.125.011802. arXiv: 2003.04831 [hep-ex] (cit. on pp. 84, 99, 100, 134).

[288] Sebastien Descotes-Genon, Joaquim Matias, and Javier Virto. "Understanding the $B \to K^*\mu^+\mu^-$ Anomaly". In: *Phys. Rev. D* 88 (2013), p. 074002. DOI: 10.1103/PhysRevD.88.074002. arXiv: 1307.5683 [hep-ph] (cit. on p. 86).

[289] Christoph Bobeth et al. "Patterns of Flavour Violation in Models with Vector-Like Quarks". In: *JHEP* 04 (2017), p. 079. DOI: 10.1007/JHEP04(2017)079. arXiv: 1609.04783 [hep-ph] (cit. on pp. 87, 93).

[290] Alejandro Celis et al. "Gauge-invariant implications of the LHCb measurements on lepton-flavor nonuniversality". In: *Phys. Rev. D* 96.3 (2017), p. 035026. DOI: 10.1103/PhysRevD.96.035026. arXiv: 1704.05672 [hep-ph] (cit. on p. 88).

[291] Andreas Crivellin et al. "Importance of Loop Effects in Explaining the Accumulated Evidence for New Physics in B Decays with a Vector Leptoquark". In: *Phys. Rev. Lett.* 122.1 (2019), p. 011805. DOI: 10.1103/PhysRevLett.122.011805. arXiv: 1807.02068 [hep-ph] (cit. on pp. 89, 92, 93).

[292] A. Arbey et al. "Hadronic and New Physics Contributions to $b \to s$ Transitions". In: *Phys. Rev. D* 98.9 (2018), p. 095027. DOI: 10.1103/PhysRevD.98.095027. arXiv: 1806.02791 [hep-ph] (cit. on pp. 90, 91, 124).

[293] Rodrigo Alonso, Benjamín Grinstein, and Jorge Martin Camalich. "Lepton universality violation and lepton flavor conservation in B-meson decays". In: *JHEP* 10 (2015), p. 184. DOI: 10.1007/JHEP10(2015)184. arXiv: 1505.05164 [hep-ph] (cit. on pp. 93, 206).

[294] Lorenzo Calibbi, Andreas Crivellin, and Toshihiko Ota. "Effective Field Theory Approach to $b \to s\ell\ell^{(')}$, $B \to K^{(*)}\nu\overline{\nu}$ and $B \to D^{(*)}\tau\nu$ with Third Generation Couplings". In: *Phys. Rev. Lett.* 115 (2015), p. 181801. DOI: 10.1103/PhysRevLett.115.181801. arXiv: 1506.02661 [hep-ph] (cit. on p. 93).

[295] Bernat Capdevila et al. "Searching for New Physics with $b \to s\tau^+\tau^-$ processes". In: *Phys. Rev. Lett.* 120.18 (2018), p. 181802. DOI: 10.1103/PhysRevLett.120.181802. arXiv: 1712.01919 [hep-ph] (cit. on pp. 93, 206).

[296] Monika Blanke and Andreas Crivellin. "B Meson Anomalies in a Pati-Salam Model within the Randall-Sundrum Background". In: *Phys. Rev. Lett.* 121.1 (2018), p. 011801. DOI: 10.1103/PhysRevLett.121.011801. arXiv: 1801.07256 [hep-ph] (cit. on p. 93).

[297] Luca Di Luzio, Admir Greljo, and Marco Nardecchia. "Gauge leptoquark as the origin of B-physics anomalies". In: *Phys. Rev. D* 96.11 (2017), p. 115011. DOI: 10.1103/PhysRevD.96.115011. arXiv: 1708.08450 [hep-ph] (cit. on p. 93).

[298] Lorenzo Calibbi, Andreas Crivellin, and Tianjun Li. "Model of vector leptoquarks in view of the B-physics anomalies". In: *Phys. Rev. D* 98.11 (2018), p. 115002. DOI: 10.1103/PhysRevD.98.115002. arXiv: 1709.00692 [hep-ph] (cit. on p. 93).

[299] Marzia Bordone et al. "A three-site gauge model for flavor hierarchies and flavor anomalies". In: *Phys. Lett. B* 779 (2018), pp. 317–323. DOI: 10.1016/j.physletb.2018.02.011. arXiv: 1712.01368 [hep-ph] (cit. on p. 93).

[300] David M. Straub. "flavio: a Python package for flavour and precision phenomenology in the Standard Model and beyond". In: (Oct. 2018). arXiv: 1810.08132 [hep-ph] (cit. on pp. 94–96).

[301] Ashutosh Kumar Alok et al. "Continuing search for new physics in $b \to s\mu\mu$ decays: two operators at a time". In: *JHEP* 06 (2019), p. 089. DOI: 10.1007/JHEP06(2019)089. arXiv: 1903.09617 [hep-ph] (cit. on pp. 95, 97).

[302] J. Bhom et al. "A model-independent analysis of $b \to s\mu^+\mu^-$ transitions with GAMBIT's FlavBit". In: (June 2020). arXiv: 2006.03489 [hep-ph] (cit. on pp. 95, 97).

[303] Aritra Biswas et al. "New physics in $b \to s\ell\ell$ decays with complex Wilson coefficients". In: (Apr. 2020). arXiv: 2004.14687 [hep-ph] (cit. on pp. 95, 97, 156, 203).

[304] Danny van Dyk et al. *eos/eos: EOS Version 0.3.1*. Version v0.3.1. Dec. 2019. DOI: 10.5281/zenodo.3569692. URL: https://doi.org/10.5281/zenodo.3569692 (cit. on p. 95).

[305] Stefan Meinel and Danny van Dyk. "Using $\Lambda_b \to \Lambda\mu^+\mu^-$ data within a Bayesian analysis of $|\Delta B| = |\Delta S| = 1$ decays". In: *Phys. Rev. D* 94.1 (2016), p. 013007. DOI: 10.1103/PhysRevD.94.013007. arXiv: 1603.02974 [hep-ph] (cit. on p. 95).

[306] J. De Blas et al. "`HEPfit`: a code for the combination of indirect and direct constraints on high energy physics models". In: *Eur. Phys. J. C* 80.5 (2020), p. 456. DOI: 10.1140/epjc/s10052-020-7904-z. arXiv: 1910.14012 [hep-ph] (cit. on p. 96).

[307] Davide Lancierini et al. "On the significance of new physics in $b \to s\ell^+\ell^-$ decays". In: (Apr. 2021). arXiv: 2104.05631 [hep-ph] (cit. on p. 97).

[308] Albert M Sirunyan et al. "Angular analysis of the decay $B^+ \to K^+\mu^+\mu^-$ in proton-proton collisions at $\sqrt{s} = 8$ TeV". In: *Phys. Rev. D* 98.11 (2018), p. 112011. DOI: 10.1103/PhysRevD.98.112011. arXiv: 1806.00636 [hep-ex] (cit. on p. 99).

[309] Serguei Chatrchyan et al. "Angular Analysis and Branching Fraction Measurement of the Decay $B^0 \to K^{*0}\mu^+\mu^-$". In: *Phys. Lett. B* 727 (2013), pp. 77–100. DOI: 10.1016/j.physletb.2013.10.017. arXiv: 1308.3409 [hep-ex] (cit. on pp. 101, 102).

[310] Federica Legger and Thomas Schietinger. "Photon helicity in $\Lambda_b \to pK\gamma$ decays". In: *Phys. Lett. B* 645 (2007). [Erratum: Phys.Lett.B 647, 527–528 (2007)], pp. 204–212. DOI: 10.1016/j.physletb.2006.12.011. arXiv: hep-ph/0605245 (cit. on pp. 109, 110, 121, 143).

[311] G. Hiller et al. "Photon polarization from helicity suppression in radiative decays of polarized Lambda(b) to spin-3/2 baryons". In: *Phys. Lett. B* 649 (2007), pp. 152–158. DOI: 10.1016/j.physletb.2007.03.056. arXiv: hep-ph/0702191 (cit. on pp. 109, 121, 143, 144).

[312] Roel Aaij et al. "Observation of the decay $\Lambda_b^0 \to pK^-\mu^+\mu^-$ and a search for CP violation". In: *JHEP* 06 (2017), p. 108. DOI: 10.1007/JHEP06(2017)108. arXiv: 1703.00256 [hep-ex] (cit. on p. 109).

[313] Roel Aaij et al. "Observation of $J/\psi p$ Resonances Consistent with Pentaquark States in $\Lambda_b^0 \to J/\psi K^-p$ Decays". In: *Phys. Rev. Lett.* 115 (2015), p. 072001. DOI: 10.1103/PhysRevLett.115.072001. arXiv: 1507.03414 [hep-ex] (cit. on pp. 110, 133).

[314] Stefan Meinel and Gumaro Rendon. "$\Lambda_b \to \Lambda^*(1520)\ell^+\ell^-$ form factors from lattice QCD". In: *Phys. Rev. D* 103.7 (2021), p. 074505. DOI: 10.1103/PhysRevD.103.074505. arXiv: 2009.09313 [hep-lat] (cit. on pp. 109, 123, 125, 132).

[315] Stefan Meinel and Gumaro Rendon. "$\Lambda_c \to \Lambda^*(1520)$ form factors from lattice QCD and improved analysis of the $\Lambda_b \to \Lambda^*(1520)$ and $\Lambda_b \to \Lambda_c^*(2595, 2625)$ form factors". In: (July 2021). arXiv: 2107.13140 [hep-lat] (cit. on p. 109).

[316] Nils Offen. "Light-cone sum rule approach for Baryon form factors". In: *Few Body Syst.* 57.10 (2016), pp. 975–983. DOI: 10.1007/s00601-016-1135-8. arXiv: 1607.01227 [hep-ph] (cit. on p. 109).

[317] Thomas Blake et al. "An empirical model to determine the hadronic resonance contributions to $\overline{B}^0 \to \overline{K}^{*0}\mu^+\mu^-$ transitions". In: *Eur. Phys. J. C* 78.6 (2018), p. 453. DOI: 10.1140/epjc/s10052-018-5937-3. arXiv: 1709.03921 [hep-ph] (cit. on pp. 111, 124).

[318] Yu-Ming Wang and Yue-Long Shen. "Perturbative Corrections to $\Lambda_b \to \Lambda$ Form Factors from QCD Light-Cone Sum Rules". In: *JHEP* 02 (2016), p. 179. DOI: 10.1007/JHEP02(2016)179. arXiv: 1511.09036 [hep-ph] (cit. on pp. 111, 124).

[319] S. Descotes-Genon and Martín Novoa-Brunet. "Angular analysis of the rare decay $\Lambda_b \to \Lambda(1520)(\to NK)\ell^+\ell^-$". In: *JHEP* 06 (2019). [Erratum: JHEP 06, 102 (2020)], p. 136. DOI: 10.1007/JHEP06(2019)136. arXiv: 1903.00448 [hep-ph] (cit. on pp. 111, 231).

[320] Yasmine Amhis et al. "Prospects for New Physics searches with $\Lambda_b^0 \to \Lambda(1520)\ell^+\ell^-$ decays". In: *Eur. Phys. J. Plus* 136.6 (2021), p. 614. DOI: 10.1140/epjp/s13360-021-01194-5. arXiv: 2005.09602 [hep-ph] (cit. on pp. 111, 231).

[321] James Gratrex, Markus Hopfer, and Roman Zwicky. "Generalised helicity formalism, higher moments and the $B \to K_{J_K}(\to K\pi)\bar{\ell}_1\ell_2$ angular distributions". In: *Phys. Rev. D* 93.5 (2016), p. 054008. DOI: 10.1103/PhysRevD.93.054008. arXiv: 1506.03970 [hep-ph] (cit. on pp. 112, 113, 121, 139, 141, 146, 147, 150).

[322] C. Patrignani et al. "Review of Particle Physics". In: *Chin. Phys. C* 40.10 (2016), p. 100001. DOI: 10.1088/1674-1137/40/10/100001 (cit. on p. 112).

[323] Howard E. Haber. "Spin formalism and applications to new physics searches". In: *21st Annual SLAC Summer Institute on Particle Physics: Spin Structure in High-energy Processes (School: 26 Jul - 3 Aug, Topical Conference: 4-6 Aug) (SSI 93)*. Apr. 1994. arXiv: hep-ph/9405376 (cit. on pp. 113, 139).

[324] Shi-Zhong Huang et al. "Solution to the Rarita-Schwinger equations". In: *Eur. Phys. J. C* 26 (2003), pp. 609–623. DOI: 10.1140/epjc/s2002-01026-1 (cit. on pp. 114, 140).

[325] Matthew D. Schwartz. *Quantum Field Theory and the Standard Model*. Cambridge University Press, Mar. 2014. ISBN: 978-1-107-03473-0 (cit. on p. 114).

[326] M. Benmerrouche, R. M. Davidson, and N. C. Mukhopadhyay. "Problems of Describing Spin 3/2 Baryon Resonances in the Effective Lagrangian Theory". In: *Phys. Rev. C* 39 (1989), pp. 2339–2348. DOI: 10.1103/PhysRevC.39.2339 (cit. on p. 114).

[327] Kenneth Johnson and E. C. G. Sudarshan. "Inconsistency of the local field theory of charged spin 3/2 particles". In: *Annals Phys.* 13 (1961), pp. 126–145. DOI: 10.1016/0003-4916(61)90030-6 (cit. on p. 114).

[328] G. Velo and D. Zwanziger. "Noncausality and other defects of interaction lagrangians for particles with spin one and higher". In: *Phys. Rev.* 188 (1969), pp. 2218–2222. DOI: 10.1103/PhysRev.188.2218 (cit. on p. 114).

[329] M. Kobayashi and Y. Takahashi. "The Rarita-schwinger Paradoxes". In: *J. Phys. A* 20 (1987), p. 6581. DOI: 10.1088/0305-4470/20/18/053 (cit. on p. 114).

[330] V. Pascalutsa. "Quantization of an interacting spin - 3 / 2 field and the Delta isobar". In: *Phys. Rev. D* 58 (1998), p. 096002. DOI: 10.1103/PhysRevD.58.096002. arXiv: hep-ph/9802288 (cit. on p. 114).

[331] L. M. Nath, B. Etemadi, and J. D. Kimel. "Uniqueness of the interaction involving spin 3/2 particles". In: *Phys. Rev. D* 3 (1971), pp. 2153–2161. DOI: 10.1103/PhysRevD.3.2153 (cit. on p. 114).

[332] Albert M Sirunyan et al. "Measurement of the Λ_b polarization and angular parameters in $\Lambda_b \to J/\psi\,\Lambda$ decays from pp collisions at $\sqrt{s} = 7$ and 8 TeV". In: *Phys. Rev. D* 97.7 (2018), p. 072010. DOI: 10.1103/PhysRevD.97.072010. arXiv: 1802.04867 [hep-ex] (cit. on p. 115).

[333] Wolfgang Altmannshofer et al. "Symmetries and Asymmetries of $B \to K^*\mu^+\mu^-$ Decays in the Standard Model and Beyond". In: *JHEP* 01 (2009), p. 019. DOI: 10.1088/1126-6708/2009/01/019. arXiv: 0811.1214 [hep-ph] (cit. on pp. 115, 143).

[334] Stefan Meinel and Gumaro Rendon. "Lattice QCD calculation of form factors for $\Lambda_b \to \Lambda(1520)\ell^+\ell^-$ decays". In: *PoS* LATTICE2016 (2016), p. 299. DOI: 10.22323/1.256.0299. arXiv: 1608.08110 [hep-lat] (cit. on pp. 116, 117).

[335] Philipp Böer et al. "Testing lepton flavour universality in semileptonic $\Lambda_b \to \Lambda_c^*$ decays". In: *JHEP* 06 (2018), p. 155. DOI: 10.1007/JHEP06(2018)155. arXiv: 1801.08367 [hep-ph] (cit. on pp. 116, 117, 193).

[336] Diganta Das and Jaydeb Das. "The $\Lambda_b \to \Lambda^*(1520)(\to N\bar{K})\ell^+\ell^-$ decay at low-recoil in HQET". In: *JHEP* 07 (2020), p. 002. DOI: 10.1007/JHEP07(2020)002. arXiv: 2003.08366 [hep-ph] (cit. on pp. 121, 123, 131).

[337] Thomas Mannel, Winston Roberts, and Zbigniew Ryzak. "Baryons in the heavy quark effective theory". In: *Nucl. Phys. B* 355 (1991), pp. 38–53. DOI: 10.1016/0550-3213(91)90301-D (cit. on pp. 122, 123).

[338] Thomas Mannel and Yu-Ming Wang. "Heavy-to-light baryonic form factors at large recoil". In: *JHEP* 12 (2011), p. 067. DOI: 10.1007/JHEP12(2011)067. arXiv: 1111.1849 [hep-ph] (cit. on pp. 122, 123).

[339] R. R. Horgan et al. "Moving NRQCD for heavy-to-light form factors on the lattice". In: *Phys. Rev. D* 80 (2009), p. 074505. DOI: 10.1103/PhysRevD.80.074505. arXiv: 0906.0945 [hep-lat] (cit. on p. 123).

[340] Marzia Bordone. "Heavy Quark Expansion of $\Lambda_b \to \Lambda^*$ (1520) Form Factors beyond Leading Order". In: *Symmetry* 13.4 (2021), p. 531. DOI: 10.3390/sym13040531. arXiv: 2101.12028 [hep-ph] (cit. on pp. 123, 131).

[341] Danny van Dyk. "Is there a road to $\Lambda_b \to \Lambda\mu^+\mu-$ at small q^2?" *b*- Baryon Fest. 2020. URL: https://indico.in2p3.fr/event/20198/contributions/87860/ (cit. on p. 124).

[342] Gudrun Hiller and Roman Zwicky. "Endpoint Relations for Baryons". In: (July 2021). arXiv: 2107.12993 [hep-ph] (cit. on p. 131).

[343] Roel Aaij et al. "Physics case for an LHCb Upgrade II - Opportunities in flavour physics, and beyond, in the HL-LHC era". In: (2016). arXiv: 1808.08865 [hep-ex] (cit. on p. 132).

[344] G. A. Cowan, D. C. Craik, and M. D. Needham. "RapidSim: an application for the fast simulation of heavy-quark hadron decays". In: *Comput. Phys. Commun.* 214 (2017), pp. 239–246. DOI: 10.1016/j.cpc.2017.01.029. arXiv: 1612.07489 [hep-ex] (cit. on p. 133).

[345] R. Aaij et al. "Differential branching fraction and angular analysis of the decay $B^0 \to K^{*0}\mu^+\mu^-$". In: *JHEP* 08 (2013), p. 131. DOI: 10.1007/JHEP08(2013)131. arXiv: 1304.6325 [hep-ex] (cit. on p. 139).

[346] Christoph Bobeth, Gudrun Hiller, and Giorgi Piranishvili. "CP Asymmetries in bar $B \to \bar{K}^*(\to \bar{K}\pi)\bar{\ell}\ell$ and Untagged $\bar{B}_s$, $B_s \to \phi(\to K^+K^-)\bar{\ell}\ell$ Decays at NLO". In: *JHEP* 07 (2008), p. 106. DOI: 10.1088/1126-6708/2008/07/106. arXiv: 0805.2525 [hep-ph] (cit. on pp. 145, 151).

[347] Sébastien Descotes-Genon, Martín Novoa-Brunet, and K. Keri Vos. "The time-dependent angular analysis of $B_d \to K_S\ell\ell$, a new benchmark for new physics". In: *JHEP* 02 (2021), p. 129. DOI: 10.1007/JHEP02(2021)129. arXiv: 2008.08000 [hep-ph] (cit. on pp. 145, 231).

[348] Damir Becirevic et al. "Complementarity of the constraints on New Physics from $B_s \to \mu^+\mu^-$ and from $B \to Kl^+l^-$ decays". In: *Phys. Rev. D* 86 (2012), p. 034034. DOI: 10.1103/PhysRevD.86.034034. arXiv: 1205.5811 [hep-ph] (cit. on p. 147).

[349] Jon A. Bailey et al. "$|V_{ub}|$ from $B \to \pi\ell\nu$ decays and (2+1)-flavor lattice QCD". In: *Phys. Rev. D* 92.1 (2015), p. 014024. DOI: 10.1103/PhysRevD.92.014024. arXiv: 1503.07839 [hep-lat] (cit. on p. 147).

[350] Isard Dunietz et al. "How to extract CP violating asymmetries from angular correlations". In: *Phys. Rev. D* 43 (1991), pp. 2193–2208. DOI: 10.1103/PhysRevD.43.2193 (cit. on p. 150).

[351] Isard Dunietz, Robert Fleischer, and Ulrich Nierste. "In pursuit of new physics with B_s decays". In: *Phys. Rev. D* 63 (2001), p. 114015. DOI: 10.1103/PhysRevD.63.114015. arXiv: hep-ph/0012219 (cit. on p. 151).

[352] Ulrich Nierste. "Three Lectures on Meson Mixing and CKM phenomenology". In: *Helmholz International Summer School on Heavy Quark Physics*. Mar. 2009. arXiv: 0904.1869 [hep-ph] (cit. on p. 151).

[353] D. Boutigny et al. *The BABAR physics book: Physics at an asymmetric B factory*. Oct. 1998 (cit. on pp. 152, 195).

[354] Sebastien Descotes-Genon, Joaquim Matias, and Javier Virto. "An analysis of $B_{d,s}$ mixing angles in presence of New Physics and an update of $B_s \to \bar{K}^{0*}anti - K^{0*}$". In: *Phys. Rev. D* 85 (2012), p. 034010. DOI: 10.1103/PhysRevD.85.034010. arXiv: 1111.4882 [hep-ph] (cit. on pp. 152, 213, 214, 216, 222, 225).

[355] Damir Beirevi et al. "Enhanced CP asymmetries in $B \to K\mu^+\mu^-$". In: *Eur. Phys. J. C* 80.10 (2020), p. 940. DOI: 10.1140/epjc/s10052-020-08518-2. arXiv: 2008.09064 [hep-ph] (cit. on p. 156).

[356] Pietro Colangelo, Fulvia De Fazio, and Wei Wang. "$B_s \to f_0(980)$ form factors and B_s decays into $f_0(980)$". In: *Phys. Rev. D* 81 (2010), p. 074001. DOI: 10.1103/PhysRevD.81.074001. arXiv: 1002.2880 [hep-ph] (cit. on p. 160).

[357] Goran Duplancic and Blazenka Melic. "Form factors of B, $B_s \to \eta^{(\prime)}$ and D, $D_s \to \eta^{(\prime)}$ transitions from QCD light-cone sum rules". In: *JHEP* 11 (2015), p. 138. DOI: 10.1007/JHEP11(2015)138. arXiv: 1508.05287 [hep-ph] (cit. on p. 160).

[358] Blaenka Meli and Goran Duplani. private communication. 2020 (cit. on p. 160).

[359] Shan Cheng and Jian-Ming Shen. "$\bar{B}_s \to f_0(980)$ form factors and the width effect from light-cone sum rules". In: *Eur. Phys. J. C* 80.6 (2020), p. 554. DOI: 10.1140/epjc/s10052-020-8124-2. arXiv: 1907.08401 [hep-ph] (cit. on p. 161).

[360] Marcel Algueró et al. "Symmetries in $B \to D^* \ell\nu$ angular observables". In: *JHEP* 06 (2020), p. 156. DOI: 10.1007/JHEP06(2020)156. arXiv: 2003.02533 [hep-ph] (cit. on pp. 165, 231).

[361] Ulrik Egede et al. "New physics reach of the decay mode $\bar{B} \to \bar{K}^{*0}\ell^+\ell^-$". In: *JHEP* 10 (2010), p. 056. DOI: 10.1007/JHEP10(2010)056. arXiv: 1005.0571 [hep-ph] (cit. on pp. 165, 168).

[362] Joaquim Matias and Nicola Serra. "Symmetry relations between angular observables in $B^0 \to K^*\mu^+\mu^-$ and the LHCb P_5' anomaly". In: *Phys. Rev. D* 90.3 (2014), p. 034002. DOI: 10.1103/PhysRevD.90.034002. arXiv: 1402.6855 [hep-ph] (cit. on pp. 165, 168).

[363] Lars Hofer and Joaquim Matias. "Exploiting the symmetries of P and S wave for B $\to$K $\mu^+\mu$ ". In: *JHEP* 09 (2015), p. 104. DOI: 10.1007/JHEP09(2015)104. arXiv: 1502.00920 [hep-ph] (cit. on pp. 165, 168).

[364] P. Colangelo, F. De Fazio, and F. Loparco. "Probing New Physics with $\bar{B} \to \rho(770)\,\ell^-\bar{\nu}_\ell$ and $\bar{B} \to a_1(1260)\,\ell^-\bar{\nu}_\ell$". In: *Phys. Rev. D* 100.7 (2019), p. 075037. DOI: 10.1103/PhysRevD.100.075037. arXiv: 1906.07068 [hep-ph] (cit. on p. 165).

[365] "Measurement of the P_1 and P_5' angular parameters of the decay $B^0 \to K^{*0}\mu^+\mu^-$ in proton-proton collisions at $\sqrt{s} = 8$ TeV". In: (2017) (cit. on p. 165).

[366] Pietro Biancofiore, Pietro Colangelo, and Fulvia De Fazio. "On the anomalous enhancement observed in $B \to D^{(*)}\tau\bar{\nu}_\tau$ decays". In: *Phys. Rev. D* 87.7 (2013), p. 074010. DOI: 10.1103/PhysRevD.87.074010. arXiv: 1302.1042 [hep-ph] (cit. on p. 165).

[367] Murugeswaran Duraisamy and Alakabha Datta. "The Full $B \to D^*\tau^-\bar{\nu_\tau}$ Angular Distribution and CP violating Triple Products". In: *JHEP* 09 (2013), p. 059. DOI: 10.1007/JHEP09(2013)059. arXiv: 1302.7031 [hep-ph] (cit. on p. 166).

[368] Murugeswaran Duraisamy, Preet Sharma, and Alakabha Datta. "Azimuthal $B \to D^*\tau^-\bar{\nu_\tau}$ angular distribution with tensor operators". In: *Phys. Rev. D* 90.7 (2014), p. 074013. DOI: 10.1103/PhysRevD.90.074013. arXiv: 1405.3719 [hep-ph] (cit. on p. 166).

[369] Rodrigo Alonso, Andrew Kobach, and Jorge Martin Camalich. "New physics in the kinematic distributions of $\bar{B} \to D^{(*)}\tau^-(\to \ell^-\bar{\nu}_\ell\nu_\tau)\bar{\nu}_\tau$". In: *Phys. Rev. D* 94.9 (2016), p. 094021. DOI: 10.1103/PhysRevD.94.094021. arXiv: 1602.07671 [hep-ph] (cit. on pp. 166, 179).

[370] Zoltan Ligeti, Michele Papucci, and Dean J. Robinson. "New Physics in the Visible Final States of $B \to D^{(*)}\tau\nu$". In: *JHEP* 01 (2017), p. 083. DOI: 10.1007/JHEP01(2017)083. arXiv: 1610.02045 [hep-ph] (cit. on pp. 166, 179, 189).

[371] Jason Aebischer, Thomas Kuhr, and Kilian Lieret. "Clustering of $\bar{B} \to D^{(*)}\tau^-\bar{\nu}_\tau$ kinematic distributions with ClusterKinG". In: *JHEP* 04 (2020). [Erratum: JHEP 05, 147 (2021)], p. 007. DOI: 10.1007/JHEP04(2020)007. arXiv: 1909.11088 [hep-ph] (cit. on p. 166).

[372] Bhubanjyoti Bhattacharya et al. "CP Violation in $\bar{B}^0 \to D^{*+}\mu^-\bar{\nu}_\mu$". In: *JHEP* 05 (2019), p. 191. DOI: 10.1007/JHEP05(2019)191. arXiv: 1903.02567 [hep-ph] (cit. on p. 167).

[373] Sebastien Descotes-Genon et al. "Implications from clean observables for the binned analysis of $B- > K*\mu^+\mu^-$ at large recoil". In: *JHEP* 01 (2013), p. 048. DOI: 10.1007/JHEP01(2013)048. arXiv: 1207.2753 [hep-ph] (cit. on pp. 167, 213).

[374] Minoru Tanaka and Ryoutaro Watanabe. "New physics in the weak interaction of $\bar{B} \to D^{(*)}\tau\bar{\nu}$". In: *Phys. Rev. D* 87.3 (2013), p. 034028. DOI: 10.1103/PhysRevD.87.034028. arXiv: 1212.1878 [hep-ph] (cit. on p. 168).

[375] Ulrik Egede, Mitesh Patel, and Konstantinos A. Petridis. "Method for an unbinned measurement of the q^2 dependent decay amplitudes of $\overline{B}^0 \to K^{*0}\mu^+\mu^-$ decays". In: *JHEP* 06 (2015), p. 084. DOI: 10.1007/JHEP06(2015)084. arXiv: 1504.00574 [hep-ph] (cit. on p. 173).

[376] Adam F. Falk and Matthias Neubert. "Second order power corrections in the heavy quark effective theory. 1. Formalism and meson form-factors". In: *Phys. Rev. D* 47 (1993), pp. 2965–2981. DOI: 10.1103/PhysRevD.47.2965. arXiv: hep-ph/9209268 (cit. on p. 174).

[377] Benjamin Grinstein and Zoltan Ligeti. "Heavy quark symmetry in $_{B\to D(*)l\bar{\nu}}$ spectra". In: *Phys. Lett. B* 526 (2002). [Erratum: Phys.Lett.B 601, 236–237 (2004)], pp. 345–354. DOI: 10.1016/S0370-2693(01)01517-9. arXiv: hep-ph/0111392 (cit. on p. 174).

[378] C. Glenn Boyd, Benjamin Grinstein, and Richard F. Lebed. "Model independent extraction of |V(cb)| using dispersion relations". In: *Phys. Lett. B* 353 (1995), pp. 306–312. DOI: 10.1016/0370-2693(95)00480-9. arXiv: hep-ph/9504235 (cit. on p. 174).

[379] Irinel Caprini, Laurent Lellouch, and Matthias Neubert. "Dispersive bounds on the shape of anti-B —> D(*) lepton anti-neutrino form-factors". In: *Nucl. Phys. B* 530 (1998), pp. 153–181. DOI: 10.1016/S0550-3213(98)00350-2. arXiv: hep-ph/9712417 (cit. on p. 174).

[380] Paolo Gambino, Thomas Mannel, and Nikolai Uraltsev. "B -> D* at zero recoil revisited". In: *Phys. Rev. D* 81 (2010), p. 113002. DOI: 10.1103/PhysRevD.81.113002. arXiv: 1004.2859 [hep-ph] (cit. on p. 174).

[381] Paolo Gambino, Thomas Mannel, and Nikolai Uraltsev. "B-> D* Zero-Recoil Formfactor and the Heavy Quark Expansion in QCD: A Systematic Study". In: *JHEP* 10 (2012), p. 169. DOI: 10.1007/JHEP10(2012)169. arXiv: 1206.2296 [hep-ph] (cit. on p. 174).

[382] C. Bernard et al. "The $\bar{B} \to D^* \ell \bar{\nu}$ form factor at zero recoil from three-flavor lattice QCD: A Model independent determination of $|V_{cb}|$". In: *Phys. Rev. D* 79 (2009), p. 014506. DOI: 10.1103/PhysRevD.79.014506. arXiv: 0808.2519 [hep-lat] (cit. on p. 174).

[383] Jon A. Bailey et al. "Update of $|V_{cb}|$ from the $\bar{B} \to D^* \ell \bar{\nu}$ form factor at zero recoil with three-flavor lattice QCD". In: *Phys. Rev. D* 89.11 (2014), p. 114504. DOI: 10.1103/PhysRevD.89.114504. arXiv: 1403.0635 [hep-lat] (cit. on p. 174).

[384] Judd Harrison, Christine Davies, and Matthew Wingate. "$|V_{cb}|$ from the $\bar{B}^0 \to D^{*+} \ell^- \bar{\nu}$ zero-recoil form factor using $2+1+1$ flavour HISQ and NRQCD". In: *PoS* LATTICE2016 (2017), p. 287. DOI: 10.22323/1.256.0287. arXiv: 1612.06716 [hep-lat] (cit. on p. 174).

[385] D. Melikhov and B. Stech. "Weak form-factors for heavy meson decays: An Update". In: *Phys. Rev. D* 62 (2000), p. 014006. DOI: 10.1103/PhysRevD.62.014006. arXiv: hep-ph/0001113 (cit. on p. 174).

[386] Pouya Asadi, Matthew R. Buckley, and David Shih. "Its all right(-handed neutrinos): a new W model for the $R_{D^{(*)}}$ anomaly". In: *JHEP* 09 (2018), p. 010. DOI: 10.1007/JHEP09(2018)010. arXiv: 1804.04135 [hep-ph] (cit. on p. 189).

[387] Admir Greljo et al. "R(D$^{()}$) from W and right-handed neutrinos". In: *JHEP* 09 (2018), p. 169. DOI: 10.1007/JHEP09(2018)169. arXiv: 1804.04642 [hep-ph] (cit. on p. 189).

[388] Dean J. Robinson, Bibhushan Shakya, and Jure Zupan. "Right-handed neutrinos and R(D$^{()}$)". In: *JHEP* 02 (2019), p. 119. DOI: 10.1007/JHEP02(2019)119. arXiv: 1807.04753 [hep-ph] (cit. on p. 189).

[389] Aleksandr Azatov et al. "Combined explanations of B-physics anomalies: the sterile neutrino solution". In: *JHEP* 10 (2018), p. 092. DOI: 10.1007/JHEP10(2018)092. arXiv: 1807.10745 [hep-ph] (cit. on p. 189).

[390] Julian Heeck and Daniele Teresi. "Pati-Salam explanations of the B-meson anomalies". In: *JHEP* 12 (2018), p. 103. DOI: 10.1007/JHEP12(2018)103. arXiv: 1808.07492 [hep-ph] (cit. on p. 189).

[391] Pouya Asadi, Matthew R. Buckley, and David Shih. "Asymmetry Observables and the Origin of $R_{D^{(*)}}$ Anomalies". In: *Phys. Rev. D* 99.3 (2019), p. 035015. DOI: 10.1103/PhysRevD.99.035015. arXiv: 1810.06597 [hep-ph] (cit. on p. 189).

[392] K. S. Babu, Bhaskar Dutta, and Rabindra N. Mohapatra. "A theory of R(D*, D) anomaly with right-handed currents". In: *JHEP* 01 (2019), p. 168. DOI: 10.1007/JHEP01(2019)168. arXiv: 1811.04496 [hep-ph] (cit. on p. 189).

[393] Debjyoti Bardhan and Diptimoy Ghosh. "B -meson charged current anomalies: The post-Moriond 2019 status". In: *Phys. Rev. D* 100.1 (2019), p. 011701. DOI: 10.1103/PhysRevD.100.011701. arXiv: 1904.10432 [hep-ph] (cit. on p. 189).

[394] John D. Gómez, Néstor Quintero, and Eduardo Rojas. "Charged current $b \to c\tau\bar{\nu}_\tau$ anomalies in a general W' boson scenario". In: *Phys. Rev. D* 100.9 (2019), p. 093003. DOI: 10.1103/PhysRevD.100.093003. arXiv: 1907.08357 [hep-ph] (cit. on p. 189).

[395] Daniel Aloni et al. "Υ and ψ leptonic decays as probes of solutions to the $R_D^{(*)}$ puzzle". In: *JHEP* 06 (2017), p. 019. DOI: 10.1007/JHEP06(2017)019. arXiv: 1702.07356 [hep-ph] (cit. on p. 193).

[396] J. P. Lees et al. "Precision measurement of the $\mathcal{B}(\Upsilon(3S) \to \tau^+\tau^-)/\mathcal{B}(\Upsilon(3S) \to \mu^+\mu^-)$ ratio". In: *Phys. Rev. Lett.* 125 (2020), p. 241801. DOI: 10.1103/PhysRevLett.125.241801. arXiv: 2005.01230 [hep-ex] (cit. on p. 193).

[397] Cristian H. García-Duque et al. "Extra gauge bosons and lepton flavor universality violation in Υ and B meson decays". In: *Phys. Rev. D* 103.7 (2021), p. 073003. DOI: 10.1103/PhysRevD.103.073003. arXiv: 2103.00344 [hep-ph] (cit. on p. 193).

[398] Marat Freytsis, Zoltan Ligeti, and Joshua T. Ruderman. "Flavor models for $\bar{B} \to D^{(*)}\tau\bar{\nu}$". In: *Phys. Rev. D* 92.5 (2015), p. 054018. DOI: 10.1103/PhysRevD.92.054018. arXiv: 1506.08896 [hep-ph] (cit. on pp. 193, 195, 198).

[399] Geoffrey T. Bodwin, Eric Braaten, and G. Peter Lepage. "Rigorous QCD analysis of inclusive annihilation and production of heavy quarkonium". In: *Phys. Rev. D* 51 (1995). [Erratum: Phys.Rev.D 55, 5853 (1997)], pp. 1125–1171. DOI: 10.1103/PhysRevD.55.5853. arXiv: hep-ph/9407339 (cit. on p. 194).

[400] Wen-Long Sang, Feng Feng, and Yu Jia. "$\mathcal{O}(\alpha_s v^2)$ corrections to the hadronic decay of vector quarkonia". In: *Phys. Rev. D* 102.9 (2020), p. 094021. DOI: 10.1103/PhysRevD.102.094021. arXiv: 2010.11896 [hep-ph] (cit. on p. 194).

[401] Hee Sok Chung, Jungil Lee, and Chaehyun Yu. "NRQCD matrix elements for S-wave bottomonia and $\Gamma[\eta_b(nS) \to \gamma\gamma]$ with relativistic corrections". In: *Phys. Lett. B* 697 (2011), pp. 48–51. DOI: 10.1016/j.physletb.2011.01.033. arXiv: 1011.1554 [hep-ph] (cit. on p. 194).

[402] J. F. Kamenik et al. "Lepton polarization asymmetries in rare semi-tauonic $b \to s$ exclusive decays at FCC-ee". In: *Eur. Phys. J. C* 77.10 (2017), p. 701. DOI: 10.1140/epjc/s10052-017-5272-0. arXiv: 1705.11106 [hep-ph] (cit. on p. 195).

[403] Paolo Gambino and Jernej F. Kamenik. "Lepton energy moments in semileptonic charm decays". In: *Nucl. Phys. B* 840 (2010), pp. 424–437. DOI: 10.1016/j.nuclphysb.2010.07.019. arXiv: 1004.0114 [hep-ph] (cit. on p. 195).

[404] Bernard Aubert et al. "Study of inclusive B- and anti-B0 decays to flavor-tagged D, D(s) and Lambda+(c)". In: *Phys. Rev. D* 75 (2007), p. 072002. DOI: 10.1103/PhysRevD.75.072002. arXiv: hep-ex/0606026 (cit. on p. 197).

[405] Mykhailo Lisovyi, Andrii Verbytskyi, and Oleksandr Zenaiev. "Combined analysis of charm-quark fragmentation-fraction measurements". In: *Eur. Phys. J. C* 76.7 (2016), p. 397. DOI: 10.1140/epjc/s10052-016-4246-y. arXiv: 1509.01061 [hep-ex] (cit. on p. 197).

[406] D. M. Asner et al. "Measurement of absolute branching fractions of inclusive semileptonic decays of charm and charmed-strange mesons". In: *Phys. Rev. D* 81 (2010), p. 052007. DOI: 10.1103/PhysRevD.81.052007. arXiv: 0912.4232 [hep-ex] (cit. on p. 198).

[407] D. Abbaneo et al. "Combined results on b hadron production rates and decay properties". In: (June 2001). arXiv: hep-ex/0112028 (cit. on p. 199).

[408] Marco Ciuchini et al. "New Physics in $b \to s\ell^+\ell^-$ confronts new data on Lepton Universality". In: *Eur. Phys. J. C* 79.8 (2019), p. 719. DOI: 10.1140/epjc/s10052-019-7210-9. arXiv: 1903.09632 [hep-ph] (cit. on p. 203).

[409] Srimoy Bhattacharya et al. "Exhaustive model selection in $b \to s\ell\ell$ decays: Pitting cross-validation against the Akaike information criterion". In: *Phys. Rev. D* 101.5 (2020), p. 055025. DOI: 10.1103/PhysRevD.101.055025. arXiv: 1908.04835 [hep-ph] (cit. on p. 203).

[410] Wolfgang Altmannshofer et al. "New strategies for New Physics search in $B \to K^*\nu\bar{\nu}$, $B \to K\nu\bar{\nu}$ and $B \to X_s\nu\bar{\nu}$ decays". In: *JHEP* 04 (2009), p. 022. DOI: 10.1088/1126-6708/2009/04/022. arXiv: 0902.0160 [hep-ph] (cit. on pp. 203, 205, 208).

[411] Andrzej J. Buras et al. "$B \to K^{(*)}\nu\bar{\nu}$ decays in the Standard Model and beyond". In: *JHEP* 02 (2015), p. 184. DOI: 10.1007/JHEP02(2015)184. arXiv: 1409.4557 [hep-ph] (cit. on pp. 204, 208).

[412] Joachim Brod, Martin Gorbahn, and Emmanuel Stamou. "Two-Loop Electroweak Corrections for the $K \to \pi\nu\bar{\nu}$ Decays". In: *Phys. Rev. D* 83 (2011), p. 034030. DOI: 10.1103/PhysRevD.83.034030. arXiv: 1009.0947 [hep-ph] (cit. on p. 204).

[413] W. Altmannshofer et al. "The Belle II Physics Book". In: *PTEP* 2019.12 (2019). Ed. by E. Kou and P. Urquijo. [Erratum: PTEP 2020, 029201 (2020)], p. 123C01. DOI: 10.1093/ptep/ptz106. arXiv: 1808.10567 [hep-ex] (cit. on p. 204).

[414] J. Grygier et al. "Search for $\boldsymbol{B \to h\nu\bar{\nu}}$ decays with semileptonic tagging at Belle". In: *Phys. Rev.* D96.9 (2017). [Addendum: Phys. Rev.D97,no.9,099902(2018)], p. 091101. DOI: 10.1103/PhysRevD.97.099902, 10.1103/PhysRevD.96.091101. arXiv: 1702.03224 [hep-ex] (cit. on pp. 204, 209–211).

[415] Gino Isidori, Federico Mescia, and Christopher Smith. "Light-quark loops in $Kto\pi\nu\bar{\nu}$". In: *Nucl. Phys.* B718 (2005), pp. 319–338. DOI: 10.1016/j.nuclphysb.2005.04.008. arXiv: hep-ph/0503107 [hep-ph] (cit. on p. 204).

[416] Joachim Brod and Martin Gorbahn. "Electroweak Corrections to the Charm Quark Contribution to $K^+ \to \pi^+ \nu\bar{\nu}$". In: *Phys. Rev. D* 78 (2008), p. 034006. DOI: 10.1103/PhysRevD.78.034006. arXiv: 0805.4119 [hep-ph] (cit. on p. 204).

[417] A. V. Artamonov et al. "New measurement of the $K^+ \to \pi^+ \nu\bar{\nu}$ branching ratio". In: *Phys. Rev. Lett.* 101 (2008), p. 191802. DOI: 10.1103/PhysRevLett.101.191802. arXiv: 0808.2459 [hep-ex] (cit. on p. 204).

[418] A. V. Artamonov et al. "Study of the decay $K^+ \to \pi^+ \nu\bar{\nu}$ in the momentum region $140 < P_\pi < 199$ MeV/c". In: *Phys. Rev.* D79 (2009), p. 092004. DOI: 10.1103/PhysRevD.79.092004. arXiv: 0903.0030 [hep-ex] (cit. on p. 204).

[419] Eduardo Cortina Gil et al. "Measurement of the very rare $K^+ \to \pi^+ \nu\bar{\nu}$ decay". In: *JHEP* 06 (2021), p. 093. DOI: 10.1007/JHEP06(2021)093. arXiv: 2103.15389 [hep-ex] (cit. on p. 204).

[420] J. K. Ahn et al. "Study of the $K_L \to \pi^0 \nu\bar{\nu}$ Decay at the J-PARC KOTO Experiment". In: *Phys. Rev. Lett.* 126.12 (2021), p. 121801. DOI: 10.1103/PhysRevLett.126.121801. arXiv: 2012.07571 [hep-ex] (cit. on p. 205).

[421] S. Shinohara. "Search for the rare decay $K_L \to \pi^0 \nu\bar{\nu}$ at J-PARC KOTO experiment". In: *J. Phys. Conf. Ser.* 1526.1 (2020). Ed. by Patrizia Cenci and Mauro Piccini, p. 012002. DOI: 10.1088/1742-6596/1526/1/012002 (cit. on p. 205).

[422] Andrzej J. Buras et al. "$K^+ \to \pi^+ \nu\bar{\nu}$ and $K_L \to \pi^0 \nu\bar{\nu}$ in the Standard Model: status and perspectives". In: *JHEP* 11 (2015), p. 033. DOI: 10.1007/JHEP11(2015)033. arXiv: 1503.02693 [hep-ph] (cit. on p. 205).

[423] Yuval Grossman and Yosef Nir. "$K_L \to \pi^0$ neutrino anti-neutrino beyond the standard model". In: *Phys. Lett.* B398 (1997), pp. 163–168. DOI: 10.1016/S0370-2693(97)00210-4. arXiv: hep-ph/9701313 [hep-ph] (cit. on p. 205).

[424] Giuseppe Ruggiero. "Status of the CERN NA62 Experiment". In: *J. Phys. Conf. Ser.* 800.1 (2017), p. 012023. DOI: 10.1088/1742-6596/800/1/012023 (cit. on p. 205).

[425] Richard Keith Ellis et al. "Physics Briefing Book". In: (2019). arXiv: 1910.11775 [hep-ex] (cit. on p. 205).

[426] Marzia Bordone et al. "Probing Lepton Flavour Universality with $K \to \pi\nu\bar{\nu}$ decays". In: *Eur. Phys. J.* C77.9 (2017), p. 618. DOI: 10.1140/epjc/s10052-017-5202-1. arXiv: 1705.10729 [hep-ph] (cit. on p. 205).

[427] Jernej F. Kamenik, Yotam Soreq, and Jure Zupan. "Lepton flavor universality violation without new sources of quark flavor violation". In: *Phys. Rev.* D97.3 (2018), p. 035002. DOI: 10.1103/PhysRevD.97.035002. arXiv: 1704.06005 [hep-ph] (cit. on pp. 205, 209).

[428] S. Fajfer, N. Konik, and L. Vale Silva. "Footprints of leptoquarks: from $R_{K^{(*)}}$ to $K \to \pi\nu\bar{\nu}$". In: *Eur. Phys. J.* C78.4 (2018), p. 275. DOI: 10.1140/epjc/s10052-018-5757-5. arXiv: 1802.00786 [hep-ph] (cit. on p. 205).

[429] Jason Aebischer et al. "Quark-lepton connections in Z? mediated FCNC processes: gauge anomaly cancellations at work". In: *JHEP* 02 (2020), p. 183. DOI: 10.1007/JHEP02(2020)183. arXiv: 1912.09308 [hep-ph] (cit. on p. 205).

[430] Claudia Cornella, Javier Fuentes-Martin, and Gino Isidori. "Revisiting the vector leptoquark explanation of the B-physics anomalies". In: *JHEP* 07 (2019), p. 168. DOI: 10.1007/JHEP07(2019)168. arXiv: 1903.11517 [hep-ph] (cit. on p. 205).

[431] Riccardo Barbieri et al. "$U(2)$ and Minimal Flavour Violation in Supersymmetry". In: *Eur. Phys. J.* C71 (2011), p. 1725. DOI: 10.1140/epjc/s10052-011-1725-z. arXiv: 1105.2296 [hep-ph] (cit. on p. 206).

[432] Riccardo Barbieri et al. "B-decay CP-asymmetries in SUSY with a $U(2)^3$ flavour symmetry". In: *Eur. Phys. J. C* 71 (2011), p. 1812. DOI: 10.1140/epjc/s10052-011-1812-1. arXiv: 1108.5125 [hep-ph] (cit. on p. 206).

[433] Andrzej J. Buras, Dario Buttazzo, and Robert Knegjens. "$K \to \pi\nu\bar{\nu}$ and ϵ'/ϵ in simplified new physics models". In: *JHEP* 11 (2015), p. 166. DOI: 10.1007/JHEP11(2015)166. arXiv: 1507.08672 [hep-ph] (cit. on p. 206).

[434] Andreas Crivellin, Giancarlo D'Ambrosio, and Julian Heeck. "Addressing the LHC flavor anomalies with horizontal gauge symmetries". In: *Phys. Rev. D* 91.7 (2015), p. 075006. DOI: 10.1103/PhysRevD.91.075006. arXiv: 1503.03477 [hep-ph] (cit. on p. 206).

[435] Lorenzo Calibbi et al. "Z' models with less-minimal flavour violation". In: *Phys. Rev. D* 101.9 (2020), p. 095003. DOI: 10.1103/PhysRevD.101.095003. arXiv: 1910.00014 [hep-ph] (cit. on p. 206).

[436] Sacha Davidson and Federica Palorini. "Various definitions of Minimal Flavour Violation for Leptons". In: *Phys. Lett. B* 642 (2006), pp. 72–80. DOI: 10.1016/j.physletb.2006.09.016. arXiv: hep-ph/0607329 (cit. on p. 206).

[437] Sheldon L. Glashow, Diego Guadagnoli, and Kenneth Lane. "Lepton Flavor Violation in B Decays?" In: *Phys. Rev. Lett.* 114 (2015), p. 091801. DOI: 10.1103/PhysRevLett.114.091801. arXiv: 1411.0565 [hep-ph] (cit. on p. 206).

[438] Roel Aaij et al. "Search for the lepton flavour violating decay $B^+ \to K^+\mu^-\tau^+$ using B^{*0}_{s2} decays". In: *JHEP* 06 (2020), p. 129. DOI: 10.1007/JHEP06(2020)129. arXiv: 2003.04352 [hep-ex] (cit. on p. 206).

[439] Roel Aaij et al. "Search for Lepton-Flavor Violating Decays $B^+ \to K^+\mu^\pm e^\mp$". In: *Phys. Rev. Lett.* 123.24 (2019), p. 241802. DOI: 10.1103/PhysRevLett.123.241802. arXiv: 1909.01010 [hep-ex] (cit. on p. 206).

[440] Roel Aaij et al. "Search for the lepton-flavour-violating decays $B^0_s \to \tau^\pm\mu^\mp$ and $B^0 \to \tau^\pm\mu^\mp$". In: *Phys. Rev. Lett.* 123.21 (2019), p. 211801. DOI: 10.1103/PhysRevLett.123.211801. arXiv: 1905.06614 [hep-ex] (cit. on p. 206).

[441] Roel Aaij et al. "Search for the lepton-flavour violating decays $\mathrm{B}^0_{(s)} \to e^\pm\mu^\mp$". In: *JHEP* 03 (2018), p. 078. DOI: 10.1007/JHEP03(2018)078. arXiv: 1710.04111 [hep-ex] (cit. on p. 206).

[442] Bernard Aubert et al. "Measurements of branching fractions, rate asymmetries, and angular distributions in the rare decays $B \to K\ell^+\ell^-$ and $B \to K^*\ell^+\ell^-$". In: *Phys. Rev. D* 73 (2006), p. 092001. DOI: 10.1103/PhysRevD.73.092001. arXiv: hep-ex/0604007 (cit. on p. 206).

[443] A. Abdesselam et al. "Search for lepton-flavor-violating tau decays to $\ell\gamma$ modes at Belle". In: (Mar. 2021). arXiv: 2103.12994 [hep-ex] (cit. on p. 206).

[444] Andreas Crivellin et al. "Lepton Flavor Non-Universality in B decays from Dynamical Yukawas". In: *Phys. Lett. B* 766 (2017), pp. 77–85. DOI: 10.1016/j.physletb.2016.12.057. arXiv: 1611.02703 [hep-ph] (cit. on p. 206).

[445] Michele Redi and Andreas Weiler. "Flavor and CP Invariant Composite Higgs Models". In: *JHEP* 11 (2011), p. 108. DOI: 10.1007/JHEP11(2011)108. arXiv: 1106.6357 [hep-ph] (cit. on p. 207).

[446] Andrzej J. Buras, Fulvia De Fazio, and Jennifer Girrbach. "The Anatomy of Z' and Z with Flavour Changing Neutral Currents in the Flavour Precision Era". In: *JHEP* 02 (2013), p. 116. DOI: 10.1007/JHEP02(2013)116. arXiv: 1211.1896 [hep-ph] (cit. on p. 209).

[447] Eduardo Cortina Gil et al. "An investigation of the very rare $K^+ \to \pi^+\nu\bar{\nu}$ decay". In: (July 2020). arXiv: 2007.08218 [hep-ex] (cit. on pp. 209, 210).

[448] Radoslav Marchevski. "New result on the search for the $K^+ \to \pi^+\nu\bar{\nu}$ decay at the NA62 experiment at CERN". In: *PoS* ICHEP2020 (2021), p. 398. DOI: 10.22323/1.390.0398 (cit. on pp. 209, 210).

[449] Marcel Algueró et al. "A new B-flavour anomaly in $B_{d,s} \to K^{*0}\bar{K}^{*0}$: anatomy and interpretation". In: *JHEP* 04 (2021), p. 066. DOI: 10.1007/JHEP04(2021)066. arXiv: 2011.07867 [hep-ph] (cit. on pp. 213, 231).

[450] Gudrun Hiller and Frank Kruger. "More model-independent analysis of $b \to s$ processes". In: *Phys. Rev. D* 69 (2004), p. 074020. DOI: 10.1103/PhysRevD.69.074020. arXiv: hep-ph/0310219 (cit. on p. 213).

[451] Sebastien Descotes-Genon, Joaquim Matias, and Javier Virto. "Exploring B(d,s) —> KK decays through flavour symmetries and QCD-factorisation". In: *Phys. Rev. Lett.* 97 (2006), p. 061801. DOI: 10.1103/PhysRevLett.97.061801. arXiv: hep-ph/0603239 (cit. on pp. 213, 215, 222, 225).

[452] Sebastien Descotes-Genon, Joaquim Matias, and Javier Virto. "Penguin-mediated $B_{d,s} \to VV$ decays and the $B_s - \bar{B}_s$ mixing angle". In: *Phys. Rev. D* 76 (2007). [Erratum: Phys.Rev.D 84, 039901 (2011)], p. 074005. DOI: 10.1103/PhysRevD.76.074005. arXiv: 0705.0477 [hep-ph] (cit. on pp. 213, 215, 222, 225).

[453] Bernard Aubert et al. "Observation of $B^0 \to$ K*0 $\bar{K}$* 0 and search for $B^0 \to$ K*0 K*0". In: *Phys. Rev. Lett.* 100 (2008), p. 081801. DOI: 10.1103/PhysRevLett.100.081801. arXiv: 0708.2248 [hep-ex] (cit. on pp. 214, 215).

[454] Roel Aaij et al. "Amplitude analysis of the $B^0_{(s)} \to K^{*0}\overline{K}^{*0}$ decays and measurement of the branching fraction of the $B^0 \to K^{*0}\overline{K}^{*0}$ decay". In: *JHEP* 07 (2019), p. 032. DOI: 10.1007/JHEP07(2019)032. arXiv: 1905.06662 [hep-ex] (cit. on pp. 214, 215).

[455] Roel Aaij et al. "First measurement of the CP-violating phase $\phi_s^{d\bar{d}}$ in $B^0_s \to (K^+\pi^-)(K^-\pi^+)$ decays". In: *JHEP* 03 (2018), p. 140. DOI: 10.1007/JHEP03(2018)140. arXiv: 1712.08683 [hep-ex] (cit. on p. 215).

[456] Kristof De Bruyn et al. "Branching Ratio Measurements of B_s Decays". In: *Phys. Rev. D* 86 (2012), p. 014027. DOI: 10.1103/PhysRevD.86.014027. arXiv: 1204.1735 [hep-ph] (cit. on p. 216).

[457] Sébastien Descotes-Genon and Patrick Koppenburg. "The CKM Parameters". In: *Ann. Rev. Nucl. Part. Sci.* 67 (2017), pp. 97–127. DOI: 10.1146/annurev-nucl-101916-123109. arXiv: 1702.08834 [hep-ex] (cit. on p. 216).

[458] Yuval Grossman, Matthias Neubert, and Alexander L. Kagan. "Trojan penguins and isospin violation in hadronic B decays". In: *JHEP* 10 (1999), p. 029. DOI: 10.1088/1126-6708/1999/10/029. arXiv: hep-ph/9909297 (cit. on p. 218).

[459] Albert M Sirunyan et al. "Search for new physics in dijet angular distributions using protonproton collisions at $\sqrt{s} = 13$ TeV and constraints on dark matter and other models". In: *Eur. Phys. J. C* 78.9 (2018), p. 789. DOI: 10.1140/epjc/s10052-018-6242-x. arXiv: 1803.08030 [hep-ex] (cit. on p. 220).

[460] Andreas Crivellin and Lorenzo Mercolli. "$B- > X_d\gamma$ and constraints on new physics". In: *Phys. Rev. D* 84 (2011), p. 114005. DOI: 10.1103/PhysRevD.84.114005. arXiv: 1106.5499 [hep-ph] (cit. on p. 220).

[461] Christoph Greub and Patrick Liniger. "Calculation of next-to-leading QCD corrections to b —> sg". In: *Phys. Rev. D* 63 (2001), p. 054025. DOI: 10.1103/PhysRevD.63.054025. arXiv: hep-ph/0009144 (cit. on p. 220).

[462] Kaustubh Agashe, Gilad Perez, and Amarjit Soni. "Flavor structure of warped extra dimension models". In: *Phys. Rev. D* 71 (2005), p. 016002. DOI: 10.1103/PhysRevD.71.016002. arXiv: hep-ph/0408134 (cit. on p. 220).

[463] D. Becirevic et al. "$B_d - \bar{B}_d$ mixing and the $B_d \to J/\psi K_s$ asymmetry in general SUSY models". In: *Nucl. Phys. B* 634 (2002), pp. 105–119. DOI: 10.1016/S0550-3213(02)00291-2. arXiv: hep-ph/0112303 (cit. on p. 220).

[464] Marco Ciuchini et al. "Next-to-leading order QCD corrections to Delta F = 2 effective Hamiltonians". In: *Nucl. Phys. B* 523 (1998), pp. 501–525. DOI: 10.1016/S0550-3213(98)00161-8. arXiv: hep-ph/9711402 (cit. on p. 221).

[465] Andrzej J. Buras, Mikolaj Misiak, and Jorg Urban. "Two loop QCD anomalous dimensions of flavor changing four quark operators within and beyond the standard model". In: *Nucl. Phys. B* 586 (2000), pp. 397–426. DOI: 10.1016/S0550-3213(00)00437-5. arXiv: hep-ph/0005183 (cit. on p. 221).

[466] M. Bona et al. "Model-independent constraints on $\Delta F = 2$ operators and the scale of new physics". In: *JHEP* 03 (2008), p. 049. DOI: 10.1088/1126-6708/2008/03/049. arXiv: 0707.0636 [hep-ph] (cit. on p. 221).

[467] Jérôme Charles et al. "New physics in B meson mixing: future sensitivity and limitations". In: *Phys. Rev. D* 102.5 (2020), p. 056023. DOI: 10.1103/PhysRevD.102.056023. arXiv: 2006.04824 [hep-ph] (cit. on p. 221).

[468] Lorenzo Calibbi et al. "Z' models with less-minimal flavour violation". In: *Phys. Rev. D* 101.9 (2020), p. 095003. DOI: 10.1103/PhysRevD.101.095003. arXiv: 1910.00014 [hep-ph] (cit. on p. 221).

[469] Albert M Sirunyan et al. "Search for new physics with dijet angular distributions in proton-proton collisions at $\sqrt{s} = 13$ TeV". In: *JHEP* 07 (2017), p. 013. DOI: 10.1007/JHEP07(2017)013. arXiv: 1703.09986 [hep-ex] (cit. on p. 221).

[470] Pere Arnan et al. "Generic Loop Effects of New Scalars and Fermions in $b \to s\ell^+\ell^-$, $(g-2)_\mu$ and a Vector-like 4^{th} Generation". In: *JHEP* 06 (2019), p. 118. DOI: 10.1007/JHEP06(2019)118. arXiv: 1904.05890 [hep-ph] (cit. on pp. 221, 222).

[471] Georges Aad et al. "Search for new non-resonant phenomena in high-mass dilepton final states with the ATLAS detector". In: *JHEP* 11 (2020). [Erratum: JHEP 04, 142 (2021)], p. 005. DOI: 10.1007/JHEP11(2020)005. arXiv: 2006.12946 [hep-ex] (cit. on p. 222).

[472] Roberto Contino et al. "Warped/composite phenomenology simplified". In: *JHEP* 05 (2007), p. 074. DOI: 10.1088/1126-6708/2007/05/074. arXiv: hep-ph/0612180 (cit. on p. 222).

[473] Alexander Khodjamirian, Rusa Mandal, and Thomas Mannel. "Inverse moment of the B_s-meson distribution amplitude from QCD sum rule". In: *JHEP* 10 (2020), p. 043. DOI: 10.1007/JHEP10(2020)043. arXiv: 2008.03935 [hep-ph] (cit. on p. 226).

[474] Patricia Ball and Roman Zwicky. "$|V_{td}/V_{ts}|$ from $B \to V\gamma$". In: *JHEP* 04 (2006), p. 046. DOI: 10.1088/1126-6708/2006/04/046. arXiv: hep-ph/0603232 (cit. on p. 226).

[475] Patricia Ball and G. W. Jones. "Twist-3 distribution amplitudes of K* and phi mesons". In: *JHEP* 03 (2007), p. 069. DOI: 10.1088/1126-6708/2007/03/069. arXiv: hep-ph/0702100 (cit. on p. 226).

[476] C. Allton et al. "Physical Results from 2+1 Flavor Domain Wall QCD and SU(2) Chiral Perturbation Theory". In: *Phys. Rev. D* 78 (2008), p. 114509. DOI: 10.1103/PhysRevD.78.114509. arXiv: 0804.0473 [hep-lat] (cit. on p. 226).

[477] Matthaus Bartsch, Gerhard Buchalla, and Christina Kraus. "B —> V(L) V(L) Decays at Next-to-Leading Order in QCD". In: (Oct. 2008). arXiv: 0810.0249 [hep-ph] (cit. on p. 226).

[478] Joshua Ellis. "TikZ-Feynman: Feynman diagrams with TikZ". In: *Comput. Phys. Commun.* 210 (2017), pp. 103–123. DOI: 10.1016/j.cpc.2016.08.019. arXiv: 1601.05437 [hep-ph].

[479] Sébastien Descotes-Genon et al. "Testing lepton flavor universality in $\Upsilon(4S)$ decays". In: *Phys. Rev. D* 103.11 (2021), p. 113009. DOI: 10.1103/PhysRevD.103.113009. arXiv: 2104.06842 [hep-ph] (cit. on p. 231).

[480] Sébastien Descotes-Genon et al. "Implications of $b \to s\mu\mu$ anomalies for future measurements of $B \to K^{(*)}\nu\bar{\nu}$ and $K \to \pi\nu\bar{\nu}$". In: *Phys. Lett. B* 809 (2020), p. 135769. DOI: 10.1016/j.physletb.2020.135769. arXiv: 2005.03734 [hep-ph] (cit. on p. 231).

[481] M. Algueró et al. "Anatomy of a new anomaly in non-leptonic B decays". In: *55th Rencontres de Moriond on QCD and High Energy Interactions*. May 2021. arXiv: 2105.11837 [hep-ph] (cit. on p. 231).

[482] Sébastien Descotes-Genon et al. "Implications of $b \to s\ell^+\ell^-$ constraints on $b \to s\nu\bar{\nu}$ and $s \to d\nu\bar{\nu}$". In: *55th Rencontres de Moriond on Electroweak Interactions and Unified Theories*. May 2021. arXiv: 2105.09693 [hep-ph] (cit. on p. 231).

université PARIS-SACLAY

ÉCOLE DOCTORALE
Particules, hadrons, énergie et noyau : instrumentation, imagerie, cosmos et simulation (PHENIICS)

Titre: Nouvelle physique dans les désintégrations rares du quark b : contraintes théoriques et conséquences phénoménologiques

Mots clés: Physique des saveurs, Theorie effective des champs, Anomalies du quark b, Nouvelle Physique, Factorisation QCD, Desintegrations rares

Résumé: Ces dernières années, des écarts par rapport aux prévisions du modèle standard sont apparus dans les désintégrations semi-leptoniques des mésons b, entre lesquels, plusieurs indices de violation de l'universalité de la saveur leptonique (LFU). Ces déviations, appelées anomalies du quark b, sont apparues de manière prédominante dans deux types différents de transitions, $b \to c\ell\bar{\nu}$ et $b \to s\ell\ell$.

Le traitement de ces désintégrations se fait dans le cadre des théories effectives des champs ou plus précisément, dans le cadre du hamiltonien effectif faible. Dans ce cadre, les contributions de nouvelle physique se reflètent dans les changements des coefficients de Wilson de courte distance. Dans ce manuscrit, nous analysons ces écarts des points de vue théorique et phénoménologique.

Après avoir résumé les caractéristiques importantes du modèle standard, nous introduisons le cadre théorique pertinent des théories effectives des champs et les résultats expérimentaux associés à ces désintégrations semileptoniques.

Nous effectuons d'abord une analyse globale de la transition $b \to s\ell\ell$ où nous ajustons les coefficients de Wilson du hamiltonien effectif faible aux données expérimentales. Nous étudions la signification statistique de ces écarts, illustrant la cohérence globale des scénarios de Nouvelle Physique émergeant de cette analyse indépendante du modèle.

Nous présentons ensuite plusieurs nouveaux tests de la physique à l'oeuvre pour les transitions $b \to s\ell\ell$. Tout d'abord, nous discutons de l'analyse angulaire de la transition $\Lambda_b \to \Lambda(1520)(\to pK)\ell\ell$ du point de vue théorique, et nous donnons des projections quant à la sensibilité attendue de l'expérience LHCb. Deuxièmement, nous discutons du potentiel d'une analyse angulaire dépendante du temps du mode $B \to K_S\ell\ell$, qui offre des sondes intéressantes des contributions complexes de la Nouvelle Physique aux coefficients de Wilson.

Nous discutons aussi des tests de Nouvelle Physique pour les transitions $b \to c\ell\bar{\nu}$. Tout d'abord, nous mettons en évidence l'utilisation des symétries entre les observables angulaires de la désintégration $B \to D^*\ell\bar{\nu}$, conduisant à des relations entre ces observables qui testent les contributions tensorielles. Nous proposons ensuite un nouveau test d'universalité de la saveur leptonique à travers les désintégrations de $\Upsilon(4S)$ dans les usines à B, à condition que la pollution par le charme puisse être contrôlée expérimentalement.

Enfin, nous étudions les connexions potentielles des anomalies du quark b avec d'autres modes. D'une part, en utilisant des hypothèses minimales sur les symétries de saveur auxquelles la Nouvelle Physique doit obéir, nous connectons ces anomalies aux désintégrations $b \to s\nu\bar{\nu}$ et $s \to d\nu\bar{\nu}$ avec des perspectives expérimentales prometteuses. D'autre part, nous étudions les modes non-leptonique de type pingouins $B_{d/s} \to K^{*0}K^{*0}$ qui pourraient être reliés aux modes $b \to s\ell\ell$ dans des modèles spécifiques de la nouvelle physique et nous discutons d'une éventuelle nouvelle anomalie de saveur de l'ordre de 2,6 écarts-type par rapport aux données de LHCb.

Université Paris-Saclay
Espace Technologique / Immeuble Discovery
Route de l'Orme aux Merisiers RD 128 / 91190 Saint-Aubin, France

université PARIS-SACLAY

ÉCOLE DOCTORALE
Particules, hadrons, énergie et noyau : instrumentation, imagerie, cosmos et simulation (PHENIICS)

Title: New physics in rare b-decays: theoretical constraints and phenomenological consequences

Keywords: Flavour physics, Effective field theory, b-anomalies, QCD factorisation, New Physics, Rare decays

Abstract: In recent years, deviations from Standard Model predictions have appeared in b-meson semileptonic decays, with several hints of violation of Lepton Flavour Universality (LFU). These deviations, usually called the b-anomalies, have appeared prominently in two different types of transitions, $b \to c\ell\bar{\nu}$ and $b \to s\ell\ell$.

The treatment of these decays is done in the context of Effective Field Theories or more precisely, in the framework of the Weak Effective Hamiltonian. In this framework, New physics contributions are reflected in changes in the short distance Wilson coefficients. In this manuscript, we analyse these deviations from the theoretical and phenomenological points of view.

After summarising important features of the Standard Model, we introduce the relevant theoretical framework of effective field theories and the experimental results associated with these semileptonic decays.

We first perform a global analysis of the $b \to s\ell\ell$ transition where we fit the Wilson coefficients of the Weak Effective Hamiltonian to the experimental data. We study the statistical significance of these deviations, illustrating the global consistency of the pattern of New Physics emerging from this model-independent analysis.

We then present several New physics benchmarks for $b \to s\ell\ell$ transitions. First, we discuss the angular analysis of the $\Lambda_b \to \Lambda(1520)(\to pK)\ell\ell$ transition from the theoretical point of view, and we give projections for the sensitivity of the LHCb experiment. Secondly, we discuss the potential of a time-dependent angular analysis of the $B \to K_S\ell\ell$ mode offering interesting probes of complex New Physics contributions to Wilson Coefficients.

We discuss also probes of New Physics for the $b \to c\ell\bar{\nu}$ transitions. First, we highlight the use of symmetries between the angular observables of the $B \to D^*\ell\bar{\nu}$ decay, leading to relations among these observables, which probe tensor contributions. We then propose a new test of lepton flavour universality through $\Upsilon(4S)$ decays at B-factories, provided that charm pollution can be controlled experimentally.

Finally, we study the potential connections of these b-anomalies with other modes. On one hand, using minimal assumptions on flavour symmetries obeyed by New Physics, we connect these anomalies to $b \to s\nu\bar{\nu}$ and $s \to d\nu\bar{\nu}$ decays with promising experimental prospects. On the other hand, we study the non-leptonic penguin modes $B_{d/s} \to K^{*0}K^{*0}$ which could be connected to $b \to s\ell\ell$ modes in specific New Physics models, and we discuss a possible new flavour anomaly at the order of 2.6 standard deviations from the LHCb data.

Université Paris-Saclay
Espace Technologique / Immeuble Discovery
Route de l'Orme aux Merisiers RD 128 / 91190 Saint-Aubin, France